

**SELF-ASSEMBLING PEPTIDE/AMINO ACID
BASED FUNCTIONAL GELS AND COPPER
NANOCLUSTERS: FROM FORMATION TO
APPLICATIONS**

**THESIS SUBMITTED FOR THE DEGREE OF
DOCTOR OF PHILOSOPHY (SCIENCE)
OF
JADAVPUR UNIVERSITY**




BIPLAB MONDAL
School of Biological Sciences,
Indian Association for the Cultivation of Science, Jadavpur,
Kolkata -700032, India
January, 2023

CERTIFICATE FROM THE SUPERVISOR

This is to certify that the thesis entitled “Self-Assembling Peptide/Amino Acid Based Functional Gels and Copper Nanoclusters: From Formation to Applications” submitted by **Sri Biplab Mondal**, who got his name registered on 30.08.2018 for the award of Ph. D. (Science) Degree of Jadavpur University, is absolutely based upon his own work under the supervision of **Prof. Arindam Banerjee** and that neither this thesis nor any part of it has been submitted for any degree/diploma or any other academic award anywhere before.

A. Banerjee
30.01.2023
Prof. Arindam Banerjee

 प्रो. अरिंदम बनर्जी / Prof. Arindam Banerjee
वरिष्ठ प्रध्यापक / Senior Professor
जैविक विज्ञान शाखा / School of Biological Sciences
इण्डियन एसोसियेशन फॉर द कल्चिवेशन ऑफ साइन्स
Indian Association for the Cultivation of Science
यादवपुर, कोलकाता - 700032 / Jadavpur, Kolkata - 700032, INDIA

[Signature of the Supervisor(s) & date with official seal]

DECLARATION

The research work embodied in this thesis entitled “**Self-Assembling Peptide/Amino Acid Based Functional Gels and Copper Nanoclusters: From Formation to Applications**” being submitted to Jadavpur University, Kolkata, has been carried out at the **Indian Association for the Cultivation of Science**, Jadavpur, under the supervision of **Prof. Arindam Banerjee**, Senior Professor, School of Biological Sciences, Indian Association for the Cultivation of Science. This work is original and has not been submitted in part or in full, for any degree or diploma to this or any other university.

BIPLAB MONDAL

Index No: **142/18/Chem./26**

*Dedicated to
All of My Family Members,
Friends and Teachers.....*

Table of Contents

| | |
|---|------------------|
| <i>Abstract</i> | xiii |
| <i>Preface</i> | xv |
| <i>Acknowledgement</i> | xix |
| <i>Abbreviations</i> | xxv |
| <i>Chapter 1: General Introduction</i> | 1–139 |
| 1.1. Supramolecular Chemistry: Discovery and Development..... | 3 |
| 1.2. Self-Assembly and Its Role in Supramolecular Architecture..... | 3 |
| 1.2.1. Non-Covalent Interactions as Major Driving Force for the Process of Self-Assembly..... | 6 |
| 1.2.2. Nature of Self-Assembly: Static vs. Dynamic..... | 8 |
| 1.3. Amino Acids and Peptides in Supramolecular Systems..... | 10 |
| 1.3.1. Building Blocks..... | 10 |
| 1.3.2. Secondary Structure of Peptide and Protein..... | 13 |
| 1.3.3. Amino Acids and Peptides Based Supramolecular Architectures and Their Implications..... | 16 |
| 1.4. Low Molecular Weight Gelators..... | 23 |
| 1.4.1. Characterisation of Gel at the Molecular Level..... | 24 |
| 1.4.2. Classification of Low Molecular Weight Gels..... | 28 |
| 1.5. Amino Acid and Peptide Based Small Molecule Gelators: From Soft Matter to Functional Materials..... | 33 |
| 1.5.1. Simple Designing Strategy of Amino Acid/Peptide Based Gels..... | 34 |
| 1.5.2. Various Approach Towards Gelation of Amino Acid/Peptide Based Materials..... | 41 |
| 1.6. Amino Acids and Peptides as Functional Bio-materials..... | 46 |
| 1.6.1. Amino Acid and Peptide Based Hydrogels for Antibacterial Activity..... | 47 |
| 1.6.2. Amino Acid and Peptide Based Hydrogel in Drug Delivery..... | 52 |
| 1.6.3. Amino Acid and Peptide Based Hydrogels in Tissue Engineering..... | 55 |
| 1.7. Peptide or Amino Acids Based Gels in Environmental Remediation..... | 58 |
| 1.7.1. Removal of Toxic Organic Dyes..... | 59 |
| 1.7.2. Removal of Toxic Metal Ions..... | 61 |
| 1.7.3. Oil Spill Recovery..... | 62 |
| 1.8. Some Other Applications of Amino Acids/ Peptide Based Materials..... | 66 |
| 1.8.1. Gels for Making Optoelectronic Devices..... | 66 |
| 1.8.2. Gels as Catalysts..... | 66 |
| 1.8.3. Pesticidal Activity..... | 68 |
| 1.8.4. Fungicidal Activity..... | 69 |
| 1.8.5. Herbicidal Activity..... | 70 |
| 1.9. Nanomaterial's: Development and Significance..... | 71 |
| 1.9.1. Brief History: Early Identification..... | 71 |

| | |
|--|----------------|
| 1.9.2. Nano: the Size..... | 72 |
| 1.9.3. Nanomaterial and Nanoparticle: Definition..... | 73 |
| 1.9.4. Development in Metallic Nanostructures Field..... | 74 |
| 1.10. Nanoclusters vs Nanocrystals..... | 75 |
| 1.11. Nanoclusters: Importance and Scope..... | 78 |
| 1.12. Fluorescent Copper Nanoclusters..... | 79 |
| 1.13. Fluorescent Properties of the CuNCs..... | 80 |
| 1.14. Synthesis of Metal Quantum Clusters..... | 81 |
| 1.14.1. Synthesis of Copper Nanoclusters..... | 82 |
| 1.15. Various Methods for the Synthesis of Metal Nanoclusters..... | 83 |
| 1.15.1. Synthetic Methods for Gold Nanoclusters..... | 83 |
| 1.15.2. Synthetic Methods for Silver Nanoclusters..... | 90 |
| 1.15.3. Synthetic Methods for Copper Nanoclusters..... | 93 |
| 1.16. Applications of Au, Ag and Cu Nanoclusters..... | 99 |
| 1.16.1. Metals (Au, Ag, Cu) Nanoclusters as Sensor..... | 100 |
| 1.16.2. Metals (Au, Ag, Cu) Nanoclusters as Imaging Materials..... | 104 |
| 1.16.3. Metals (Au, Ag, Cu) Nanoclusters as Catalysts..... | 108 |
| 1.17. References..... | 112 |
| Chapter 2: Materials and Methods | 141–145 |
| 2.1. Introduction..... | 143 |
| 2.2. Source of Chemicals..... | 143 |
| 2.3. Experimental Procedures..... | 143 |
| 2.4. Spectroscopic Measurements..... | 144 |
| 2.5. Microscopic Studies..... | 145 |
| 2.6. Rheological Study..... | 145 |
| 2.7. References..... | 145 |
| Chapter 3: Peptide-Based Gel in Environmental Remediation: Removal of Toxic Organic Dyes and Hazardous Pb²⁺ and Cd²⁺ Ions from Wastewater and Oil Spill Recovery..... | 147–190 |
| 3.1. Introduction..... | 149 |
| 3.2. Experimental Section..... | 153 |
| 3.2.1. Materials..... | 153 |
| 3.2.2. Methods..... | 153 |
| 3.2.3. Synthesis of Gelator Peptide P1..... | 155 |
| 3.2.4. Instrumentation..... | 164 |
| 3.3. Results and Discussion..... | 165 |
| 3.3.1. Gelation Study..... | 165 |
| 3.3.2. Morphological Study..... | 166 |
| 3.3.3. FTIR Analysis..... | 167 |
| 3.3.4. Rheological Study..... | 168 |
| 3.3.5. XRD Analysis..... | 170 |

| | |
|---|----------------|
| 3.3.6. SAXS Analysis..... | 171 |
| 3.3.7. Dye Adsorption Study..... | 172 |
| 3.3.8. Metal Ions Removal Study..... | 177 |
| 3.3.9. Oil Spill Recovery..... | 177 |
| 3.4. Conclusion..... | 180 |
| 3.5. References..... | 180 |
| <i>Chapter 4: Amino Acid Containing Amphiphilic Hydrogelators with Antibacterial and Antiparasitic Activities</i> | <i>191–246</i> |
| 4.1. Introduction..... | 193 |
| 4.2. Experimental Section..... | 195 |
| 4.2.1. Materials..... | 195 |
| 4.2.2. Methods..... | 196 |
| 4.2.3. Synthesis Details of Peptide Amphiphiles (P1–P4)..... | 200 |
| 4.2.4. Instrumentation..... | 223 |
| 4.3. Results and Discussion..... | 224 |
| 4.3.1. Gelation Study..... | 224 |
| 4.3.2. Thermal Stability of Gels..... | 225 |
| 4.3.3. Rheological Study..... | 225 |
| 4.3.4. Morphological Study..... | 227 |
| 4.3.5. FTIR Analysis..... | 228 |
| 4.3.6. XRD Analysis..... | 228 |
| 4.3.7. SAXS Analysis..... | 229 |
| 4.3.8. Antibacterial Study..... | 231 |
| 4.3.9. MTT Assay Study..... | 234 |
| 4.3.10. ROS Generation Study..... | 237 |
| 4.3.11. AFM Image Analysis for Antiparasitic Study..... | 238 |
| 4.4. Conclusion..... | 241 |
| 4.5. References..... | 242 |
| <i>Chapter 5: Copper Nanoclusters for Catalytic Carbon–Carbon and Carbon–Nitrogen Bond Formations</i> | <i>247–308</i> |
| 5.1. Introduction..... | 249 |
| 5.2. Experimental Section..... | 252 |
| 5.2.1. Materials..... | 252 |
| 5.2.2. Methods..... | 252 |
| 5.2.3. Synthesis Details..... | 252 |
| 5.2.4. Computational Details..... | 271 |
| 5.2.5. Instrumentation..... | 284 |
| 5.3. Results and Discussion..... | 285 |
| 5.3.1. Synthesis Protocol of Copper Nanoclusters and UV-vis Studies..... | 285 |
| 5.3.2. Fluorescence Spectroscopic Study..... | 286 |
| 5.3.3. XPS Analysis..... | 287 |
| 5.3.4. MALDI-TOF MS Analysis..... | 288 |
| 5.3.5. MALDI-TOF Analysis for the Reaction Intermediates..... | 288 |
| 5.3.6. UHR-FEG-TEM Study..... | 290 |
| 5.3.7. Structural Investigation of CuNCs Using DFT..... | 291 |
| 5.3.8. C–C and C–N Bond Formation Using CuNCs as a Catalyst..... | 292 |
| 5.3.9. Mechanistic Elucidation Based on DFT Study..... | 294 |

| | |
|---|----------------|
| 5.4. Conclusion..... | 301 |
| 5.5. References..... | 302 |
| <i>Chapter 6: Atomically Precise Red Emitting Copper Nanoclusters Containing Hydrogel as a Potential Fluorescent Ink.....</i> | <i>309–330</i> |
| 6.1. Introduction..... | 311 |
| 6.2. Experimental Section..... | 312 |
| 6.2.1. Materials..... | 312 |
| 6.2.2. Methods..... | 313 |
| 6.2.3. Synthesis of Gelator Peptide G1..... | 315 |
| 6.2.4. Instrumentation..... | 315 |
| 6.3. Results and Discussion..... | 316 |
| 6.3.1. Synthesis of Stable Red Emitting CuNCs in the Hydrogel Matrix..... | 316 |
| 6.3.2. UV–vis Spectroscopic Analysis..... | 317 |
| 6.3.3. FTIR Analysis..... | 318 |
| 6.3.4. XPS Analysis..... | 319 |
| 6.3.5. MALDI–TOF MS Analysis..... | 320 |
| 6.3.6. UHR-FEG-TEM Studies..... | 321 |
| 6.3.7. Fluorescence Spectroscopy Study..... | 322 |
| 6.3.8. Time-Dependent Change in Fluorescence Study..... | 323 |
| 6.3.9. CuNCs Containing Gel as an Anti-counterfeiting Fluorescent Ink..... | 324 |
| 6.4. Conclusion..... | 325 |
| 6.5. References..... | 325 |
| <i>List of Publications.....</i> | <i>331</i> |

Abstract

Index No: **142/18/Chem./26**

Thesis title: **SELF-ASSEMBLING PEPTIDE/AMINO ACID BASED FUNCTIONAL GELS AND COPPER NANOCLUSTERS: FROM FORMATION TO APPLICATION**

Submitted by: **Biplab Mondal**

Now a days, peptide based soft functional materials have drawn increasing attention due to their cheap process-ability and biocompatibility. A simple peptide based amphiphilic ambidextrous gelator molecule [Myristyl-L-tryptophan-L-phenyl alanine] has been designed and synthesized and this can form gel in both aqueous and organic solvents starting from n-hexane to aqueous buffer solution at pH 7.46. The gelator has been successfully utilized for the removal of toxic organic dyes, metal ions, and spilled oil from waste water. Moreover, this gelator molecule shows highly selectivity towards cationic organic dyes in presence of organic anionic dyes. A series of peptide amphiphiles containing L-phenyl alanine and L-tryptophan as residues have been studied for anti-bacterial and antiparasitic studies. The peptide amphiphiles with the amino acid L-phenyl alanine shows both anti-bacterial and anti-parasitic activity. Highly stable blue emitting copper nanoclusters (CuNCs) has been synthesised and found to be used as an active catalyst for $C(sp^2)-C(sp^2)$ and $C(sp^2)-N(sp^3)$ bond forming reaction. Moreover, a red emitting CuNCs was synthesised in gel medium and these clusters are found to be highly stable in gel medium as well as in solid state (xerogel stae) form. This red emitting CuNCs hydrogel can be used as a potential fluorescent ink and the solid state material can be used as a fingerprinting material in future.

Preface

The research embodied in the present thesis entitled “**SELF-ASSEMBLING PEPTIDE/AMINO ACID BASED FUNCTIONAL GELS AND COPPER NANOCLUSTERS: FROM FORMATION TO APPLICATION**” deals with the synthesis, characterization and gelation study of several synthetic self-assembling short-peptides and copper nanoclusters formation to their various applications.

Investigations described in this thesis have been carried out by the author in the School of Biological Sciences, **Indian Association for the Cultivation of Science**, Jadavpur, Kolkata 700 032, India during the period of **2016–2022** under the supervision of *Prof. Arindam Banerjee*. The entire work has been described and summarized within six chapters in this thesis.

Chapter 1 is the general introduction which provides the comprehensive literature survey on low molecular weight supramolecular gels, a special class of soft materials. This chapter highlights structural and features of amino acid and peptide based supramolecular hydrogels and their different applications. Particularly, different biological applications of amino acid and peptide based hydrogels have been discussed in details. At the end of this chapter, synthesis of fluorescent noble metal nanoclusters and their different applications have been reviewed.

Chapter 2 describes the reagents and instruments used, and the experimental procedures followed to perform the entire work embodied in this thesis.

Chapter 3 discusses a dipeptide-based synthetic amphiphile bearing a myristyl chain has been found to form hydrogels in the pH range 6.9–8.5 and organogels in various organic solvents including petroleum ether, diesel, kerosene, and petrol. These organogels and hydrogels have been thoroughly studied and characterized by different techniques including high-resolution transmission electron microscopy, X-ray diffraction, Fourier-transform infrared spectroscopy, and rheology. It has been found that the xerogel obtained from the peptide gelator can trap various toxic organic dyes from wastewater efficiently. Moreover, the hydrogel has been used to remove toxic heavy metal ions Pb^{2+} and Cd^{2+} from wastewater. Dye adsorption kinetics has been studied, and it has been fitted by

using the Freundlich isotherm equation. Interestingly, the gelator amphiphilic peptide gels fuel oil, kerosene, diesel, and petrol in a biphasic mixture of salt water and oil within a few seconds. This indicates that these gels not only may find application in oil spill recovery but also can be used to remove toxic organic dyes and hazardous toxic metal ions from wastewater. Moreover, the gelator can be recycled several times without significant loss of activity, suggesting the sustainability of this new gelator. This holds future promise for environmental remediation by using peptide-based gelators.

Chapter 4 describes a nanoscale self-assembly of peptide constructs represent a promising means to present bioactive motifs to develop new functional materials. Here we present a series of peptide amphiphiles which form hydrogels based on β -sheet nanofibril networks, several of which have very promising anti-microbial and anti-parasitic activities, in particular against multiple strains of *Leishmania* including drug-resistant ones. Aromatic amino acid based amphiphilic supramolecular gelators C_{14} -Phe-CONH-(CH₂)_n-NH₂ (n=6 for **P1** and n=2 for **P3**) and C_{14} -Trp-CONH-(CH₂)_n-NH₂ (n=6 for **P2** and n=2 for **P4**) have been synthesized, characterized, and their self-assembly and gelation behaviour has been investigated in the presence of ultrapure water (**P1**, **P2**, **P4**) or 2% DMSO (v/v) in ultrapure water (**P3**). The rheological, morphological and structural properties of the gels have been comprehensively examined. The amphiphilic gelators (**P1** and **P3**) were found to be active against both Gram-positive bacteria *B. subtilis* and Gram-negative bacteria *E. coli* and *P. aeruginosa*. Interestingly, amphiphiles **P1** and **P3** containing L-phenylalanine residue show both antibacterial and antiparasitic activity. Herein, we report that synthetic amphiphiles with an amino acid residue exhibit a potent anti-protozoan activity and are cytotoxic towards a wide array of protozoal parasites, which includes Indian varieties of *Leishmania donovani* and also kill resistant parasitic strains including BHU575, MIL^R and CPT^R cells. These gelators are highly cytotoxic to promastigotes of *Leishmania* and trigger apoptotic-like events inside the parasite. The mechanism of killing the parasite is shown and these gelators are non-cytotoxic to host macrophage cells indicating a potential use of these gels as therapeutic agents against multiple forms of leishmaniasis in the near future.

Chapter 5 describes a newly synthesized blue-emitting few-atom copper nanoclusters (CuNCs) have been successfully utilized for catalysing

C(sp²)-C(sp²) and C(sp²)-N(sp³) bond formations. Various substituted biphenyls and 2° aromatic amines have been synthesized in good yield using this copper catalyst at facile reaction conditions in dimethyl sulfoxide. The amount of required nanocatalysts is as low as merely 2 mol % for carrying out these reactions. These types of copper nanoclusters are promising as potential and cheap catalysts for replacing conventional metal nanoparticles and heavy-metal-ion-based organic catalysts. The optimized structure of Cu₆(GS)₂ [GS = C₁₀H₁₆N₃O₆S] from computational studies revealed the perfect arrangements of Cu atoms in CuNCs and their interactions with stabilizing ligands. It is evident from the structure that some free Cu sites are available in the nanocluster species. These kinds of coordinatively unsaturated sites are highly active toward the catalytic reactions. Matrix-assisted laser desorption ionization–time-of-flight (MALDI–TOF) analysis also supports the computational hypothesis. Interestingly, matrix-assisted laser desorption ionization–time-of-flight mass spectrometry (MALDI–TOF MS) and computational studies revealed the formation of several reaction key intermediates in catalyzing C(sp²)-C(sp²) bond formation.

Chapter 6 describes the synthesis of stable red fluorescent copper nanoclusters by using a suitable method. In this regard, four approaches have been made to make a stable red fluorescent copper nanoclusters (CuNCs). To make these red fluorescent copper nanoclusters, Copper acetate monohydrate [Cu(CH₃COO)₂.H₂O]₂ has been used as a metal precursor, 4-mercaptobenzoic acid (4-MBA) as a stabilizing ligand, and L-ascorbic acid as a reducing agent. The presence of the thiol group in 4-MBA can easily stabilize the CuNCs as it can easily cap the nascent CuNCs. In the first two approaches, the solution phase, i.e., in DMSO and DMF solvent medium synthesis of CuNCs was performed. But the DMSO and DMF solvent-mediated cluster was not so stable and underwent decomposition after 24–72 h. A different approach has been made to make this cluster stable, i.e., the gel-mediated synthesis and stabilization of Cu-nanoclusters studies have been performed. The amphiphilic gelator **G1** [(S)-N-(1-((2-aminoethyl)amino)-1-oxo-3-phenylpropan-2-yl)tetradecanamide] containing L-phenylalanine as a natural amino acid has been used as a template for synthesizing Cu-nanoclusters by the co-solvent induced gelation method. In our third approach, when 5 % DMSO was used as a co-solvent, the formation of an

uncontrolled synthesis of red fluorescent copper nanoclusters was observed. On the other hand, in the final fourth approach, CuNCs formed in 5–10 % DMF show high stability in the co-solvent induced gel state and xerogel (dried gel) state. The CuNCs form in DMF takes place slowly in a controlled manner 12 h to 24 h with very high stability. All the CuNCs formed very rapidly can be considered an uncontrolled synthesis. The controlled way of synthesizing CuNCs has been characterized by various techniques like UV-vis, PL, XPS, UHR-FEG-TEM, and MALDI-TOF MS spectrometric analysis. As the gel phase synthesized CuNCs are responsible for the fluorescent nature of the gel, it has the potential to be used as a fluorescent ink. The dried gel can also be used as a fingerprinting material.

Each chapter from chapter 3 to 6 begins with a short ‘Introduction’ followed by ‘Experimental Section’, ‘Results and discussion’ and ‘Conclusion’. For convenience, ‘References’ are given at the end of each chapter. List of publications has been appended at the end of the thesis.

Acknowledgement

First and foremost, I would like to express my deep sense of gratefulness, pranam, and thanks to my Ph.D. supervisor Prof. Arindam Banerjee, who allowed me to join his lab as a Ph.D. student and navigated my research work for the entire tenure. During the days of doctoral studies, many ups and downs happened to my research, but he was there with me in every uphill moment. I got his soulful support and help during data assembling, systematically explaining them, and writing scientific reports. Mainly, his vision and guidance throughout the complete tenure made the completion of this thesis possible.

I sincerely acknowledge the University Grand Commission (UGC), India, for taking care of my doctoral fellowship for the last five years.

I do not have words to express my thanks to the four internet giants, Google, Wikipedia, Grammarly, and Sci-Finder, as I cannot dream of compiling my research work without them. They not only ease the pressure of searching and gaining knowledge about several matters related to my research, but they also provide me a window to the outside world from my lab day in and day out.

The laboratory and other instrumental facilities, along with the friendly and cordial surroundings, rank the Indian Association for the Cultivation of Science (IACS) among the best in the country to enroll as a Ph.D. scholar. So, I am deeply fortunate to work at this institute and have an opportunity to interact with the members of the IACS family.

I also want to thank Jadavpur University and its Department of Chemistry for allowing me to get registered as a Ph.D. student.

During Ph.D. every day, we mainly spend the lion's part of a day in the laboratory; therefore lab is like our second home. Thus, lab mates played a vital role during these years of my research work. Therefore, I gratefully acknowledge all my past and present lab members, Dr. Abhishek Baral, Dr. Kingshuk Basu, Dr. Nibedita Nandi, Dr. Subir Paul, Dr. Kousik Gayen, Dipayan Bairagi, Biswanath Hansda, Soumyajit Hazra, Niladri Hazra, Purnadas Ghosh, Tanushree Mondal, Swapnendu Deb, and Supratim Bose for their support and help during the different phases of my research work. In this regard, I want to express my special thanks to Kingshuk Da, who mentored my early-day research in every way, from the beginning of my work in the lab to assembling results and writing

scientific articles. I also want to say special thanks to Biswanath and Tanushree for their incredible help and support throughout my tenure of research work for my Ph.D. degree. Without such unconditional support from past and present lab mates, it would be almost impossible for me to complete my work smoothly.

I would also like to thank our extended lab family members Miss. Asmita Banerjee and Mrs. Tulika Banerjee, for their support.

School of Biological Sciences was my extended family, where I got encouragement from various faculty, students, and staff members. I want to acknowledge our current school chair, Prof. P. K. Das, along with other faculty members, Prof. R. Mukhopadhyay, Prof. S. S. Jana, Prof. P. Sen, Prof. D. K. Sinha, Prof. B. B. Das, and Dr. R. R. Pal.

Thanks to our school staff, Mr. Sovan Mallick, Mr. Gour Chandra Bairadi, Mr. Prasenjit Ghosh, Mr. Ashoke Kumar, and Mr. Chanchal Banerjee, for their cordial help.

Apart from my lab, I gratefully acknowledge some other lab seniors, friends, and juniors; Hiya Di, Jayita Di, Debduitta Di, Tanushree Di, Deep Da, Krishnendu Da, Pritam Da, Saheli Di, Soumik Da, Debayan, Deblina, Anup, Monalisa, Aftab, Aparajita Di, Kathakoli, Sudeshna, Afrin, Suvendu Da, Arijit Da, Srijita, Sangheeta, Subhasis, Aparna, Joy, Samprita, Indranil, Kumarjit, Ditipriya, Budhaditya, Tamal Da, Sidhu Da, Deba Da, Subir Da, Debobrata Da, Shridhar Da, Debabrata, Arka Da, Subhasis Da, Manotosh, Bhaskar, Jayanta, Ishita, Ujjwal, Madhab Da, Dipankar Da, Goutam, Arnab, Sanjay Da, Dinesh Da, Subhra, Saily, Radhakanta Da, Debasish, Tathagata Da, Ranajit, Rajesh, Arnab, Ishita, Saidul, Ambreen, Parijat, Subhamay, Sanu, and others of our school and other schools for their scientific help and support.

Collaborators played a vital role in my doctoral research projects. Thus, my sincere gratitude goes to Prof. Ian W. Hamley, Dr. Valeria Castelletto, Dr. Charlotte JC Edwards-Gayle, (University of Reading, UK), Prof. Ayan Datta, Rajkumar Jana, Partha Mondal (School of Chemical Sciences, IACS, India) and Prof. Parasuraman Jaisankar, Vivek Kumar Gupta, Arpita Bhoumik, Prof. Hemanta K. Majumder (Indian Institute of Chemical Biology, India). They not only provide experimental facilities but also provide me the opportunity to learn many things beyond the scope of my lab.

My research involves a lot of instrumental techniques. Thus, the technical help from Mr. Arunim Paul, Mr. Supriya Chakraborty, Mr. Sanjoy Sarkar, Mrs. Chapma Bag, Dr. Sasanka Majhi, Mr. Chinmoy Chakraborty, Mr. Arup Das, Mr. Chanchal Kumar Das, Dr. Bholanath Mondal, Mr. S. K. Sarkar, Mr. Goutam Biswas, Mr. Sumit Roy, Mr. Sachin Roy, Mr. Nirmalya Dutta, as well as help from glassware, electrical and engineering section is deeply acknowledged.

Other than our school, other persons from different schools of IACS helped me to use their facility. Again it is not easy to remember all the names, but I am deeply grateful to all of those people. Special thanks to Prof. Suhrit Ghosh and his scholar Dr. Anurag Mukherjee for their help in fluorescence studies. Thanks to Prof. P. Dastidar and his group for gifting us various bacteria. Thanks to Prof. Sougata Ray and his scholar, Sambhu for the ICP-MS study. I want to acknowledge Dr. Biswajit Biswas for his help in fluorescence studies. Special thanks to Prof. Surajit Sinha for his valuable suggestions regarding my research work. I gratefully acknowledge Dr. Amit Majumdar and his students, Dr. Suman Khatua, Dr. Nabendu Pal, Dr. Manish Jana, Dr. Tilak Naskar, Dr. Tuhin Ganguly, Dr. Ayan Das, Sayan, and Kamal, for allowing us to use their lab facilities.

Other than our institute, others from the different institutes also help me with various experiments, such as photoluminescence studies and AAS studies. In this regard, I want to express my special thanks to Manisha Karmakar and Pranab Chandra Saha for their incredible help.

I gratefully acknowledge Dr. Sudin Pal, and Dr. Nirmalya Pradhan for their help and encouragement to join this lab after my MSc.

I gratefully acknowledge my roommate Dr. Rajib Ghosh and other messmates, Dr. Rajesh Bera, Sourav Dutta, Sourav Singha, and ranni mashi maa (Sova Mallik) for their unconditional support, love, and inspiration.

I gratefully acknowledge all my MSc roommates, Anubhab, Partha, Avijit, and other batchmates, Manas, Ranjan, Debashis, Puspendu, Sanjib, Nirmalya, Dipankar, and others for their encouragement.

Special thanks to my best friend, Ananda Naskar (the most kind-hearted person I have ever met), and his wife Barnali Naskar for their kindness, support, and valuable suggestion.

My academic journey would not even be possible without having great teachers throughout the stages of this part. I want to thank all of my teachers, especially Manoranjan Tanti and others (Primary), Late Sasodhar Maity, Late Bishnupada Sanfui, Late Anupam Sanpui, Suchismita Sanpui (Halder), Bapi Maity, Biswajit Biswas, Sudhyana Mondal, Kajoli Biswas, Goutam Pramanik, Raja Bose and others (Madhyamik), Biswajit Roy, Laxman Saha, Madan da, Samir Da (HS), Dr. Sunanda Achariya, Dr. Subrata Maji, Rakesh Chatterjee, Dr. Sujay Pattanayak, Swapan Sir, Arijit Sir, Kunal Sir, Dipankar Sir and others (BSc) for their trust.

The Chemistry Department of Ramakrishna Mission Residential College, Narendrapur boosted my motivation of doing Ph.D. So, the contribution from my teachers Dr. Prasanta Ghosh, Dr. Pulak Gangopadhyay, Dr. Bikas Baran Ghosh, Dr. Rathindranath Ghosh, Dr. Arogya Varam Saha, Prof. Tarun Kumar Sarkar, Dr. Bimal Kumar Sadhukhan, Dr. Sanjib Bagchi, and others are deeply acknowledged.

My pranam and special thanks to principal Maharaj, Swami Bhudebananda, and other Maharaj and Sanyasis of Narendrapur Ramakrishna Mission Residential College (Autonomous) for giving me the opportunity to complete my MSc almost free, as without this opportunity it was impossible for me to come at this point.

During the last few years away from home, my elder sister, Nilima Mondal (Pishimaar Meye), and brother-in-law, Nilratan Mondal, made me an integral part of any occasions that ensured I never felt away from my near ones. Even they never give me a chance to miss my home and home food as well.

Special thanks to my uncle, Srikanta Mondal (mejo jethu) and aunty Anima Mondal (Mejo jathima) for taking care of my early day's education along with my mother Ganga Mondal. Also, special thanks to my elder brother, Mathur Mondal (Baro jethu's elder son) for his incredible help in every part of my life.

Special thanks to my brother Bivas Mondal to take care of our family and taking responsibility of our family from the very early days of his life along with my father Sripati Mondal. Special thanks to my two sisters Tapati Mondal and Tanushree Mondal for their love, support, and inspiration throughout my life. Thanks to my brother-in-law, Subhankar Haldar (Tapati's husband) for his support.

Most importantly, this acknowledgement is just worthless without expressing my love to my parents. I want to thank the two persons for whom today I am writing my thesis. My first teachers, first guides and my first friends, were my parents, Ganga Mondal (Maa) and Sripati Mondal (Baba). Special thanks to my parents, Ganga Mondal (Maa) and Sripati Mondal (Baba), for their prayer, moral support, love and sacrifices which motivate me to remain focused towards achieving various milestones of my journey. But, they never demanded anything from me. My gratitude is not enough to cover their kindness. If I get a Doctoral Degree all of its credit goes to them.

Finally, my pranam and thanks to the almighty God for giving me everything.

Indian Association for the
Cultivation of Science
Kolkata
Date:

Biplab Mondal

Abbreviations

Abbreviations used for amino acids, peptides, derivatives, substituent, reagents, experimental tools, etc. are largely in accordance with the recommendations of the IUPAC-IUB commission on Biochemical Nomenclature, 1974, *Pure and Applied Chemistry*, **40**, 315–331. Other symbols, nomenclature, etc. are based on the list in *J. Biol. Chem.*, 1989, 669–671. Protein amino acids are of L-configuration unless otherwise indicated. Standard three letter coding is used for all amino acids. Additional abbreviations used in this thesis are listed below.

| | |
|----------|---|
| AAS | Atomic absorption spectroscopy |
| AFM | Atomic force Microscopy |
| AU | Absorbance units |
| a.u. | Arbitrary units |
| Boc | Tertiary butyloxycarbonyl |
| CCCP | Carbonyl cyanide m-chloro-phenylhydrazone |
| CPT | Camptothecin |
| CuNCs | Copper nanoclusters |
| δ | Chemical shift |
| d | Doublet |
| DCC | N,N'-dicyclohexylcarbodiimide |
| DCU | N,N'-dicyclohexylurea |
| DMF | Dimethyl formamide |
| DMSO | Dimethyl sulfoxide |
| ESI | Electro spray ionization |
| FEG-TEM | Field emission gun transmission electron microscope |
| FICT | Fluorescein isothiocyanate |
| FL | Fluorescence |
| FT-IR | Fourier transform-Infra red |
| GSH | Glutathione |
| HCOOH | Formic acid |
| h | Hours |
| HR | High resolution |
| ICP-MS | Inductively coupled plasma mass spectrometry |
| IR | Infrared |
| J | Coupling constant |
| LVE | Linear viscoelastic region |

| | |
|--------|--|
| M | Molar |
| m | Multiplate |
| Me | Methyl |
| MeOH | Methanol |
| MHz | Megahertz |
| MIC | Minimum inhibitory concentration |
| mM | Milimolar |
| MS | Mass spectrometry |
| NAC | N-acetyl cystine |
| nm | Nanometer |
| NMR | Nuclear magnetic resonance |
| PCD | Programmed cell death |
| Ph | Phenyl |
| pH | The negative logarithm hydrogen-ion activity (-log ₁₀ [H ₃ O ⁺]) |
| Phe | Phenyl alanine |
| PL | Photoluminescence |
| PXRD | Powder X-Ray Diffraction |
| q | Quartet |
| ROS | Reactive oxygen species |
| s/ sec | Seconds |
| s | Singlet (in NMR) |
| SAXRD | Small angle X-ray diffraction |
| SAXS | Small angle X-ray scattering |
| t | Triplet |
| TEM | Transmission electron microscope |
| TFA | Trifluoroacetic acid |
| TLC | Thin layer chromatography |
| TMS | Tetramethylsilane |
| UV-vis | Ultraviolet-visible |
| WAXS | Wide angle X-ray scattering |
| XRD | X-ray diffraction |
| Trp | Tryptophan |
| ZOI | Zone of inhibition |

Chapter 1

General Introduction



Chapter 1

1. General Introduction

1.1. Supramolecular Chemistry: Discovery and Development

The term “supramolecular chemistry” introduced by Jean-Marie Lehn, who won the Nobel Prize for his work in the area in 1987, is “chemistry beyond the molecule”,¹⁻³ which takes into account the chemistry of molecular assemblies using non-covalent bonds. This definition points to the relationship between molecular and supramolecular chemistry in structure and function. The breakthrough in supramolecular chemistry came in the 1960s when Charles J. Pedersen synthesized crown ether. Following the work of Pederson, other researchers such as Donald J. Cram and Jean-Marie Lehn synthesized shape- and ion-selective receptors. Furthermore, in the 1980s, significant knowledge was gathered regarding mechanically-interlocked molecular architectures. In the 1990s, another scientist James Fraser Stoddart developed molecular machinery and highly complex self-assembled structures, and Itamar Willner developed sensors and methods of electronic and biological interfacing.

Self-assembly is a process in which pre-existing disordered components form ordered arrangement structure (supramolecular architecture) by non-covalent interactions. So, keeping in mind the importance of self-assembly in supramolecular chemistry, I would like to say something about self-assembly and its role in supramolecular architecture in the next topic of my thesis.

1.2. Self-Assembly and Its Role in Supramolecular Architectures

Scientists across the world starting from pre-historic age to the recent times have tried to understand the basic functioning unit of natural systems. In this way they have developed direct and indirect tools to “see” the basic building blocks of natures, the atoms and the molecules. However, natural systems mostly deal with a group of molecules, where

they undergo extensive interactions with each other. This kind of aggregation or assembly is termed as molecular self-assembly or self-aggregation. A beautiful example of self-assembly in living systems (Figure 1.1) is the cell membrane, which consists mainly of lipids, proteins and carbohydrates. The self-assembly of lipids into a stable bilayer membrane is governed by hydrophobic interactions between the lipid chains. This is a direct consequence of the fact that lipid-lipid interactions (Figure 1.1) are energetically more favorable than lipid-water interactions. Importantly, cell membranes confine the constituents of cells within a small volume. As a result, reactions are performed in bulk will show different reaction rates and equilibrium constants as compared to the cellular reaction. The differences in rate constants are due to a higher collision rate between the reactant molecules within a confined space. This macromolecular crowding has been shown to enhance natural processes such as gene expression and it is involved in directing the kinetics of natural processes. Furthermore, cell membranes also supply cells with mechanisms to actively import and export molecules to and from the cell and allows for communication between cells. Protein molecules are formed by assembly of small peptides and together they behave like molecular machines and do all sorts of biological activity. Medicines bind with proper receptors to show their respective actions. Muscles are moved by well-orchestrated mechanism of motor proteins. Therefore, it is clear that, the nature always deals with an ensemble of molecules rather than one single molecule (Figure 1.1). Figure 1.1 shows the difference in self-assembly in nature vs synthetic system. In this regard, another question comes automatically, whether a bunch of molecules behaves just like their monomers? The answer is no way simple. A single molecule of benzene is obviously gaseous however bulk benzene is a liquid at normal temperature and atmospheric pressure. A pair of Na^+ and Cl^- ions neutralizes each other in water, however when these ions are assemble and packed within a lattice they form a hard solid structure. A single molecule of phospholipid is not useful until or unless at least few thousands of them assembled together to form a bi-layer like structure and finally able to encapsulate a number of organelles inside them to give birth of a cell. A single DNA molecule is not stable until

they form hydrogen bonding with another complementary strand and finally undergo supercoiling to get packed inside a chromosome. Here we come with a new term “Self-assembly”. Prof. Whiteside have defined self-assembly as, “*Self-assembly is the autonomous organization of components into patterns or structures without human intervention.*”⁴ Processes from the non-covalent association of organic molecules in solution to the growth of semiconductor quantum dots on solid substrates have been called self-assembly and nature of this process is not same for every system, which make the definition of “self-assembly” elastic. The process is basically formation of ordered structures out of chaotic motion of monomers. The interactions working within the self-assembled molecules are generally weaker compared to the covalent interactions and delicate balance between attractive and repulsive forces imparts a reversible nature to these types of interactions. Before going to the discussion about the self-assembly and their consequences I should say something about “Non-Covalent Interactions”.

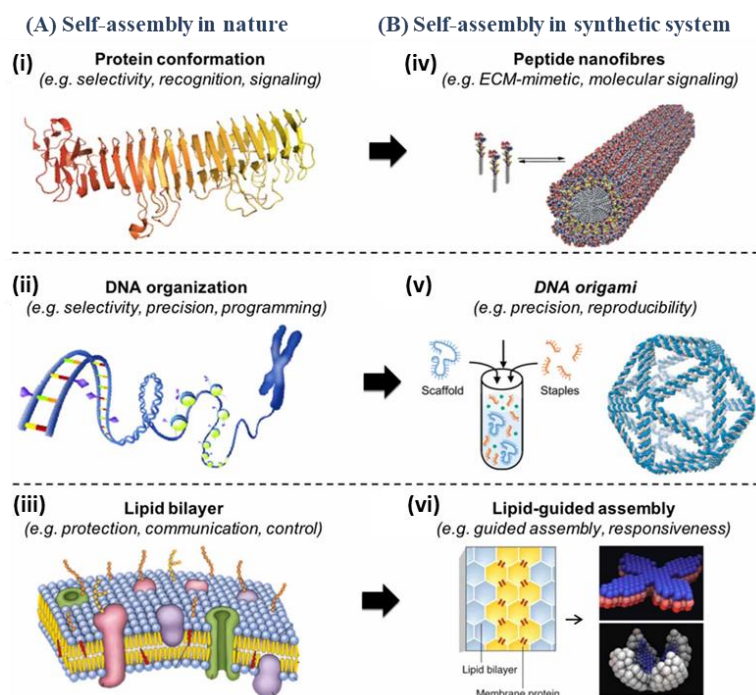


Figure 1.1. Self-assembly in nature and synthetic systems. Illustrations of (A) three examples of self-assembling systems found in nature including (i) protein conformation, (ii) DNA double helical organisation, and (iii) cell lipid bilayer membrane, and (B) three examples of how these systems inspire synthetic self-assembling ones including (iv) self-assembling peptide nanofibres, (v) DNA origami, and (vi) lipid-guided assembly (adapted from, C. L. Hedegaard and A. Mata, *Biofabrication*, 2020, **12**, 032002).

1.2.1. Non-Covalent Interactions as Major Driving Force for the Process of Self-Assembly

Rigid three dimensional structures are formed by atoms through sharing electron pairs to form covalent bond(s). However, sometimes weak interactions take place between them without sharing an electron pair. These interactions are basically through space interactions and much weaker than the covalent interactions therefore they are called non-covalent interactions. The existence of intermolecular forces was first postulated by Johannes Diderik van der Waals in 1873. However, it is with Nobel laureate Hermann Emil Fischer that supramolecular chemistry has its philosophical roots. In 1890, Fischer suggested that enzyme-substrate interactions take the form of a "lock and key", pre-empting the concepts of molecular recognition and host-guest chemistry. In the early twentieth century non-covalent bonds were understood in gradually more detail, with the hydrogen bond being described by Latimer and Rodebush in 1920. The term "non-covalent"⁵ contains an enormous range of intermolecular interactions. The non-covalent forces are in the order of decreasing energies are given in Table 1. Among all the non-covalent interaction ion-ion interaction is the strongest one having energy comparable to the covalent bond energy. Ion-ion interactions from the interaction of the opposite charges become strongest when charges can come close to each other. Example of ion-ion interactions are NaCl crystal and the interaction of tris (diazabicyclooctane) host with anions such as $[\text{Fe}(\text{CN})_6]^{3-}$. Ion-dipole interaction is seen in both solid and solution state.

Table 1.1. Various non-covalent interactions with corresponding interaction energy values.

| Interactions | Energy (kJM^{-1}) |
|---------------------------|------------------------------|
| Ion-Ion | 50–350 |
| Ion-Dipole | 50–200 |
| Hydrogen bonding | 4–120 |
| Cation- π | 5–80 |
| Dipole-Dipole | 5–50 |
| π - π stacking | 0–50 |
| Solvent effect | 4–40 |
| van der Waals interaction | < 5 |

When NaCl is dissolved in water, the interaction of the Na^+ with the polar molecule H_2O is an example of the ion-dipole interaction. Alignment of two adjacent dipoles gives rise to significant attractive interaction known as dipole-dipole interaction. Hydrogen bonding is a kind of dipole-dipole interaction where the hydrogen atom linked with an electronegative atom attracts the lone pair of the neighbouring electronegative atom. Cations of the transition metals are known to form complex with olefinic and aromatic hydrocarbon. For example, Fe^{2+} and Pt(II) form π complex in ferrocene $[\text{Fe}(\text{C}_5\text{H}_5)_2]$ and Zeise's salt $[\text{PtCl}_3(\text{C}_2\text{H}_4)]^-$ respectively. π - π stacking interaction is a very weak electrostatic interaction between two aromatic rings.⁶ In general four types of π -stacking are possible like, (a) face to face, (b) parallel-displaced, (c) edge to face and (d) T-shaped C-H... π . DNA double helix nucleobase pairs give face to face π -stacking to stabilize the helix. In edge to face interaction electron deficient hydrogen atoms interact with the π -cloud of another aromatic ring. The molecules which are weakly solvated in the polar solvent like H_2O are excluded from the solvent and this phenomenon is known as hydrophobic effect. Hydrophobic effect is an important effect for binding organic molecules in the hydrophobic core of a micelle or vesicle in H_2O medium. Sometimes organic molecules are attracted by the H_2O molecule by hydrophilic interaction. van der Waals interactions are very weak and non-directional electrostatic attraction. In the field of supramolecular chemistry van der Waals interactions come into the consideration during the formation of the inclusion complex in which small organic compounds are loosely incorporated within the molecular cavity. Although a single interaction is generally much weaker than a covalent bond, the cooperative action of many of such interactions leads to a thermodynamically and kinetically more stable architecture under various conditions. Now-a-days, the area of supramolecular chemistry is very broad as it stretches from molecular recognition in natural and artificial complexes to applications in new materials, in biotechnology and in nanotechnology.^{7,8}

1.2.2. Nature of Self-Assembly: Static vs. Dynamic

Properly designed synthetic pathway leads to desired molecules; self-assembly makes ordered ensembles of as-synthesized molecules (or ordered forms of macromolecules). The structures generated in molecular self-assembly are generally stays in equilibrium states (or at least in their metastable states of assembly).⁹ Depending on the nature of association self-assembly can be classified as, static and dynamic self-assembly.⁴ Molecular self-assembly is an unavoidable phenomenon in chemistry, materials science, and biology and has been so long before self-assembly emerged as a discrete field of study and as a synthetic strategy. Depending upon the nature and thermodynamics of self-assembly, it can be broadly classified as (a) static and (b) dynamic self-assembly. Static self-assemblies are kinetic or thermodynamically trapped aggregated states. Molecular crystals, most of the folded proteins are examples of static self-assembly. Concept of self-assembly is basically concerned about molecules, chemists try to manipulate the properties of self-assembled materials at molecular level. However, with a huge development in the field now people are now changing their approach and focusing on sizes larger than molecules. Grossly, there are now three ranges of sizes of components for which self-assembly is important: molecular, nanoscale (colloids, nanowires and nanospheres, and related structures), and meso- to macroscopic (objects with dimensions from microns to centimeters). The general rules are mostly same for all three size regimes but not identical, because the size is highly important for microelectronics, photonics and near field optics.¹⁰⁻¹⁴

Most of these well-defined nanostructured materials are examples of static self-assembly where the assembled microphases have reached their most stable (or at least metastable) state of equilibrium. Much works are available in literature regarding these materials and their functional uses. Much of the scientific endeavour till now has been put for the study of static self-assembly. However, dynamic self-assembly is still an unknown phenomenon for scientist. This field has tremendous scope because only dynamic self-assembly can solve the riddle of chemical evolution of a cell. The components of a cell replicate and assemble into another cell

during mitosis. Life is, however, a dynamic: you just stop the flux of energy through the cell and it dies. In dynamic self-assembly continuous dissipation of energy is required to retain the self-assembled structures stable and active. From this point of view the exchange of energy between cell and the outer environment give rise to basic vital force in nature. Examples of dynamic self-assemblies also includes non-living chemical processes like, oscillatory reactions in solution and on the surface of catalysts, Rayleigh-Bernard convection cells, patterns that form in fluidized beds of particles, and storm cells in the atmosphere are all examples pattern formation in oscillatory reactions (Figure 1.2). These kind of far from equilibrium systems are still a less studied subject of science.¹⁵

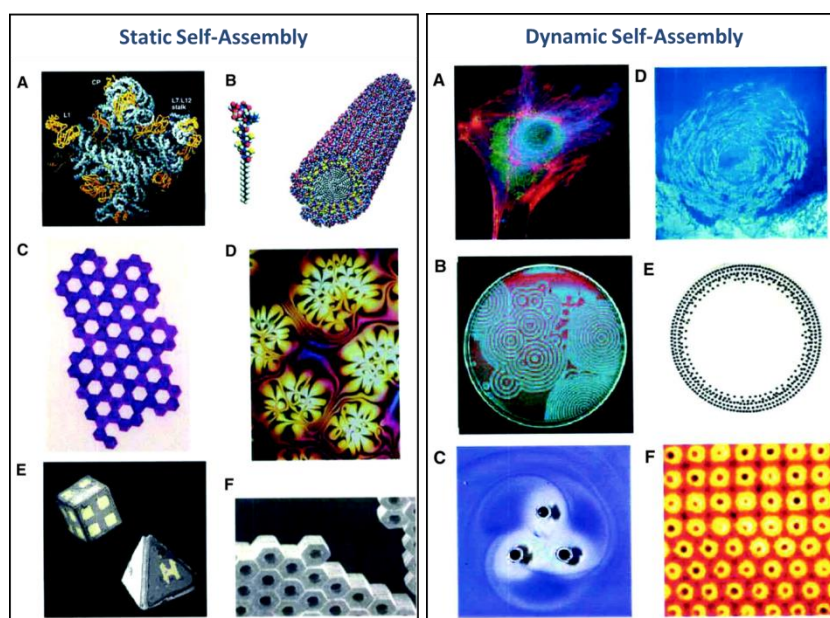


Figure 1.2. Examples of static and dynamic self-assembly, under static self-assembly (left box) various stable (both kinetically and thermodynamically) nanostructures have been shown, (A) Crystal structure of a ribosome. (B) Self-assembled peptide-amphiphile nanofibers. (C) An array of millimetre sized polymeric plates assembled at a water/perfluorodecalin interface by capillary interactions. (D) Thin film of a nematic liquid crystal on an isotropic substrate. (E) Micrometer sized metallic polyhedral folded from planar substrates. (F) A three-dimensional aggregate of micrometer plates assembled by capillary forces. Under dynamic self-assembly static image of changing events have been shown, (A) An optical micrograph of a cell with fluorescently labeled cytoskeleton and nucleus; microtubules (~24 nm in diameter) are colored red. (B) Reaction-diffusion waves in a Belousov-Zhabotinski reaction in a 3.5-inch Petri dish. (C) A simple aggregate of three millimeter-sized, rotating, magnetized disks interacting with one another via vortex-vortex interactions. (D) A school of fish. (E) Concentric rings formed by charged metallic beads 1 mm in diameter rolling in circular paths on a dielectric support. (F) Convection cells formed above a micro-patterned metallic support. The distance between the centers of the cells is ~2 mm (adapted from, G. M. Whiteside and B. Grzybowski, *Science*, 2012, **295**, 2418-2421).

In this thesis, my main focus is the synthesis of low molecular weight supramolecular gelators by using amino acid residue(s). Various applications of these supramolecular gels have been tried to explore. Natural amino acids (L-phenylalanine and L-tryptophan) containing amphiphilic peptide-based ambidextrous gelator has also been developed to get a trifunctional application, namely removal of toxic dyes from the wastewater, removal of metal ions from wastewater, and recovery of spilled oil from the ocean bed. Also, single amino acids (L-phenylalanine and L-tryptophan) based amphiphilic gelators have been developed for extensive biological applications. Among them, only L-phenylalanine containing gelator amphiphiles show very good antibacterial activity towards Gram-positive and Gram-negative bacteria and antiparasitic activity towards drug-resistant, multi-drug resistant, and wild-type of *Leishmania donovani* strains.

This thesis is concerned about amino acids and peptide based nano structured materials, therefore a brief insight of amino acids and peptide based supramolecular interactions are given in the next topic of discussion.

1.3. Amino Acids and Peptides in Supramolecular Systems

1.3.1. Building Blocks

Amino acids having both amino and carboxylic acid functionalities provide a wonderful moiety for synthesizing peptides having multiple amino acid residues useful for designing supramolecular architectures. There are 20 natural α -amino acids and all are in L-configuration (Figure 1.3).¹⁶ In α -amino acids, the two functional groups (carboxyl and amino) are linked to a common tetrahedral carbon centre, the α -carbon atom. Peptide bonds that are composed of L- α -amino acid residues are cleavable by proteolytic enzymes. A proteolytic enzyme is any enzyme that conducts proteolysis, i.e. it begins protein catabolism by hydrolysis of the peptide bonds that link amino acids together in the polypeptide chain.¹⁷ The only difference between individual natural amino acids lies in the side-chains (Figure 1.3). However, wide variation in the functionality of the side-chains makes amino acids one of the basic

building blocks of any living systems. These side chains can be classified according to their functional groups and they are usually defined as hydrophobic or polar amino acids. As the α -carbon has four different functional groups attached, α -amino acids are chiral (with the exception of glycine, where the side chain is a hydrogen atom) (Figure 1.3). For designing biomaterials for application in living systems proteolytic instability of α -amino acid containing peptides sometimes become a serious problem. To overcome this, proteolytic stability of the peptide bonds can be enhanced by using D- α -amino acid instead of L- α -amino acid.^{18,19}

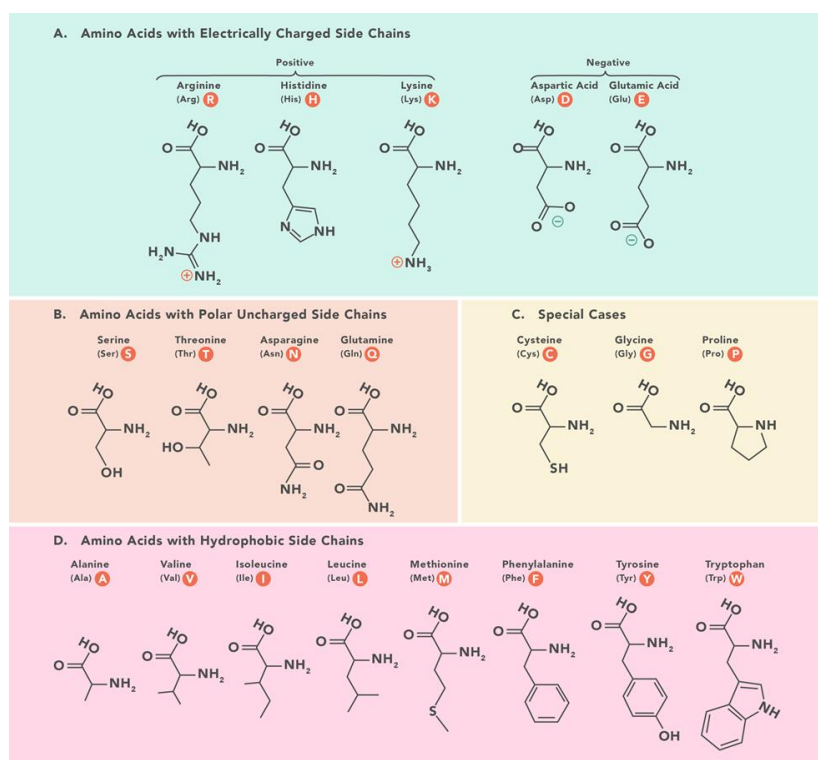


Figure 1.3. The list of 20 proteinaceous α -amino acids with their names and abbreviations, grouped according to their side-chains chemical structures (adapted from Google images).

Although nature adopts α -amino acids as the chief building block for making majority of the structures for living systems, it has some limitations. Thus, the amino acids that possess two functional groups (carboxyl and amino) separated by variable number of polymethylene units becomes significant. The use of α -amino acids in peptide design is extremely important due to its ability to increase the flexibility (additional methylene groups) of the peptide backbone and to provide

proteolytic resistance to bioactive peptide sequences.^{20,21} α -Alanine (α -Ala), γ -amino butyric acid (γ -Abu), and δ -amino valeric acid (δ -Ava) are consecutive members of a homologous series of ω -amino acids (Figure 1.4). β -Alanine (β -Ala) is the only naturally occurring β -amino acid, whose role in different biological processes is significant. It is believed to be a neurotransmitter in the central nervous system, binding to receptor sites common to glycine and γ -amino butyric acid (γ -Abu), and acting in the visual system. β -Ala is one of the constituents of the naturally occurring dipeptides anserine (β -alanyl-N-methyl-L-histidine) and carnosine (β -alanyl-L-histidine).²²⁻²⁶ Both of these dipeptides are predominantly localized in that part of the muscle, which is in contact with the post-synaptic membrane. They are involved in the transmission of nerve impulse to the muscle and in muscular metabolism. β -Ala is also a constituent of the vitamin B₅ (panthothenic acid). γ -aminobutyric acid (γ -Abu) is found in the mammalian brain,²⁷ where it is enzymatically produced and it acts as a neurotransmitter.²⁸ Isolation of δ -amino valeric acid (δ -Ava) derived from rumen ciliate protozoa has also been documented in the literature.²⁹ The Gly–Gly segment in bovine pancreatic trypsin inhibitor has been replaced by δ -Ava using semisynthesis, resulting in diminished inhibition of trypsin.³⁰ This is a fascinating example of increasing proteolytic stability of a bioactive peptide by incorporation of a non-proteinaceous (unusual) amino acid residue.

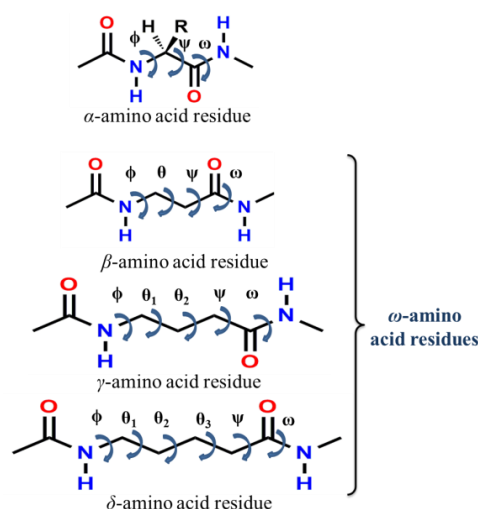


Figure 1.4. α and ω -amino acid residues and their important torsional angles (adapted from, A. Banerjee and P. Balaram, *Curr. Sci.*, 1997, **73**, 1067–1077).

Moreover, a recent study illustrates how biologically active tripeptide glutathione (GSH), having an unusual γ -peptide linkage (in place of α -linkage of glutamic acid), can be a “prebiotic answer” to the α -peptide based life.³¹ Molecular biological studies have already showed that the presence of nonregular peptide bond prevents GSH from being degraded by the peptidases.³² Thus they concluded that not only the γ -peptide bond ensures GSH’s role as the key antioxidant agent in living systems today but also it can be assumed that the chemistry of its formation is responsible for its appearance in living organisms in the first place.³¹ Inspired by this tactics employed by nature many functional supramolecular systems have been designed with ω -amino acids to achieve proteolytic stable biomaterials.³³ Moreover, ω -amino acids containing large number of methylene units like 11-aminoundecanoic acid have been used to make flexible soft materials.³⁴

1.3.2. Secondary Structure of Peptide and Protein

The regular folding patterns along a peptide chain in a protein are known as secondary structures (Figure 1.5). Important, abundant and recognizable secondary structures found in proteins are helices, β -strands and reverse turns.

Helices: Helices are predominant, recurring form of secondary structures. Helices are very well studied structural elements among the protein structural elements. There are various types of helices in the literature.^{35,36}

β - Strands and Sheets: The β -strand is the second major structural element found in proteins. The β -strand are usually 5 to 10 residues long and are in almost fully extended conformation with ϕ , ψ angles close to -120° , 140° within the broad structurally allowed region in the upper left quadrant of the Ramachandran plot.³⁷ The extended nature of the polypeptide chain causes the side chains of consecutive residues to position in opposite directions. There are no intra-strand hydrogen bonds and van der Waals interactions between atoms of neighboring residues in particular strand, a common feature in case of α -helices. Here, hydrogen bonding occurs between neighboring polypeptide chains. Several such adjacent β -strands associate to form either parallel or antiparallel β -sheets

Chapter 1

with C^α atoms successively a little above and below the plane of the β -sheets (Figure 1.6).

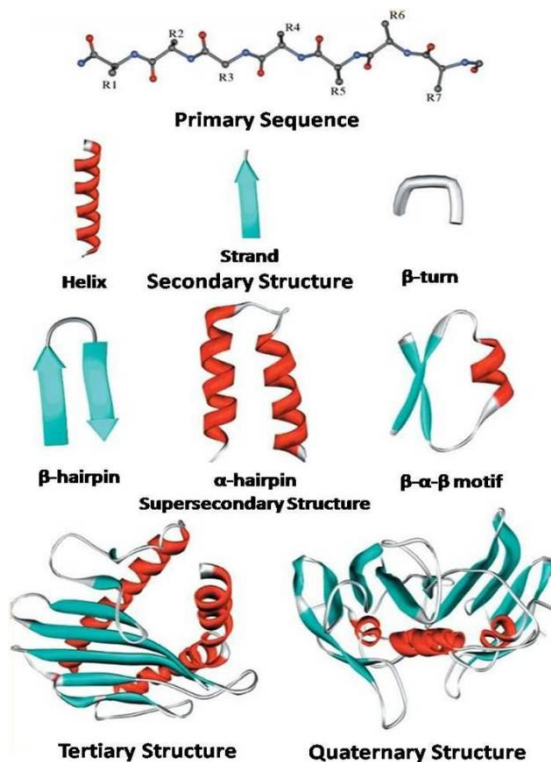


Figure 1.5. Various levels of structural organizations observed in protein structures (adapted from, D. Voet and J. G. Voet, Biochemistry, J. Wiley and Sons, 4rd edition, 2011).

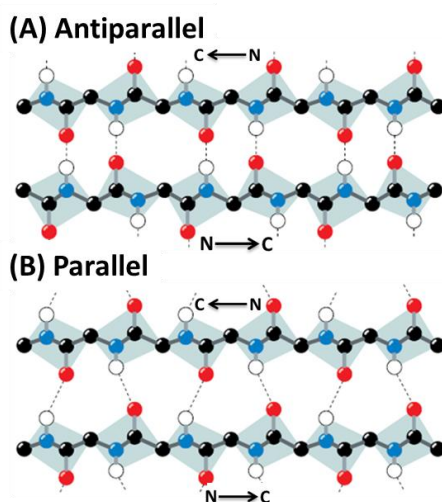


Figure 1.6. Structure of the parallel and antiparallel β -sheet segments. The picture shows the hydrogen bonding patterns in parallel and anti-parallel β -sheet structure (C= black, N= blue, O= red an H= white). It is evident that hydrogen bonds are more linear in the antiparallel sheet (adapted from, Google Images).

The amino acids in the aligned β -strands can run in the same direction to form the parallel β -pleated sheets (Figure 1.6) or the amino acid residues in successive strands can run through in opposite direction to produce the antiparallel β -pleated sheets (Figure 1.6). The antiparallel β -sheet is thought to be intrinsically more stable than a parallel β -sheet structure due to more optimal orientation of the inter-strand hydrogen bonds and minimum peptide bond dipole. The peptide chain within a β -pleated sheet is fully extended maintaining a distance of 0.35 nm between the neighbouring C^α atoms. β -sheets are slightly curved and sometimes assemble to form a β -barrel. The β -polypeptide conformation is a characteristic feature of the pathological amyloid fiber aggregates (Figure 1.7) associated with various neurodegenerative diseases, including Alzheimer's, Huntington's and Parkinson's, as well as systemic amyloidoses.³⁸ Amyloid fibrils contain bundles of β -sheets with backbones oriented perpendicular to the direction of fiber propagation in the so-called “cross- β ” structure. The characteristic features in an X-ray scattering pattern of the cross- β structure are a 4.7 Å meridional reflection corresponding to the spacing between peptide backbones and an equatorial reflection at 8–12 Å, which is broader and this corresponds to the stacking periodicity of the β -sheets (the range of values reflects different side-chain dimensions).^{39,40}

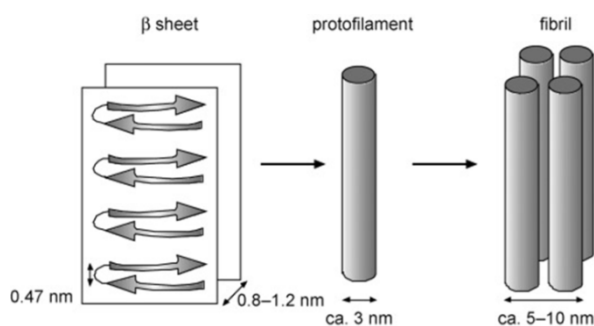


Figure 1.7. Hierarchical structure of amyloid fibrils (adapted from, I. W. Hamley, *Angew. Chem. Int. Ed.*, 2007, **46**, 8128-8147).

Self-assembly of short model peptides with appropriate backbone conformations that can form supramolecular β -sheet structure through various non-covalent interactions, is very important for their numerous applications in biological and material sciences. The model β -sheet design is very difficult due to its higher aggregation propensity to form

high molecular weight β -sheet quaternary structure. Nowick et al. introduced a unique amino acid that can readily be incorporated into peptides to make them fold into β -sheet-like structures that dimerize through β -sheet interactions.^{41,42} Our group has been deeply involved in design and synthesis of acyclic peptide based supramolecular β -sheet structures utilizing backbone hydrogen-bonding functionalities and other non-covalent interactions.⁴³⁻⁴⁵

1.3.3. Amino Acids and Peptides Based Supramolecular Architectures and Their Implications

Amino acids and peptides are building blocks of most of the living beings in this world. The supramolecular chemistry community, since the last two three decades, has found that rules from natural systems can be implemented in the design of peptidic supramolecular functional materials. A wide range of architectures is accessible through peptide based materials including cages, spheres, tubes, fiber-like morphologies, tapes, and larger extended sheet-like arrays (Figure 1.8). The building blocks either can be adapted from biology (e.g., collagens,⁴⁶ elastins,⁴⁷ β -sheet systems,⁴⁸ α helices/coiled-coils,⁴⁹ or are obtained using new design strategies based on cyclic, aliphatic and aromatic amphiphiles, or dendritic oligopeptides. Synthetic strategies of oligopeptide-based one-dimensional supramolecular polymers and understanding the mechanism

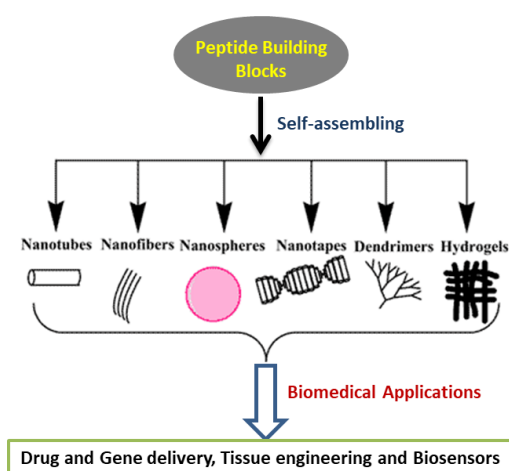


Figure 1.8. Schematic representations of various nanostructures formed by selfassembly of peptide-based building blocks and their potential applications (adapted from, P. P. Sharma, B. Rathi, J. Rodrigues and N. Y. Gorobets, *Curr Top Med Chem.*, 2015, **15**, 1268-1289).

of supramolecular assembly are important for design of new functional materials using peptides as building blocks. Some important applications include stimuli-responsive properties in soft materials^{50,51} biomedical applications in regenerative medicine.^{52,53}

Cyclic Peptides and Peptide Conjugates: Use of oligopeptide building blocks as supramolecular synthons is catching researchers' eye due to their capacity to selectively form ordered nanostructures. Pioneering work of Ghadiri has led to the design of cyclic oligopeptides with alternating D- and L-amino acids that self-assemble into hydrogen-bonded one-dimensional nanotubes in water.^{50,54,55} The earliest system was based on the cyclic octapeptide cyclo[-(^DAla-^LGlu-^DAla-^LGln-)₂], where FT-IR and electron diffraction analysis suggested an antiparallel β -sheet formation (Figure 1.9). The backbone amide groups lie nearly perpendicular to the plane of the peptide ring, while the amino acid side chains occupy equatorial positions along the ring's edge.^{54,56,57} The authors proposed a cooperative formation of highly stable and long tubes, whereby pre-organization of the hydrogen-bonding motif and the multiple supramolecular interactions involved were at the origin for the cooperative nature of the self-assembly mechanism.⁵⁸ Ghadiri also prepared cyclic tetrapeptides, composed of alternating α - and 1,4-substituted ϵ -amino acids, that in organic solvents gave rise to a rarely observed anti-cooperative polymerization mechanism.⁵⁹

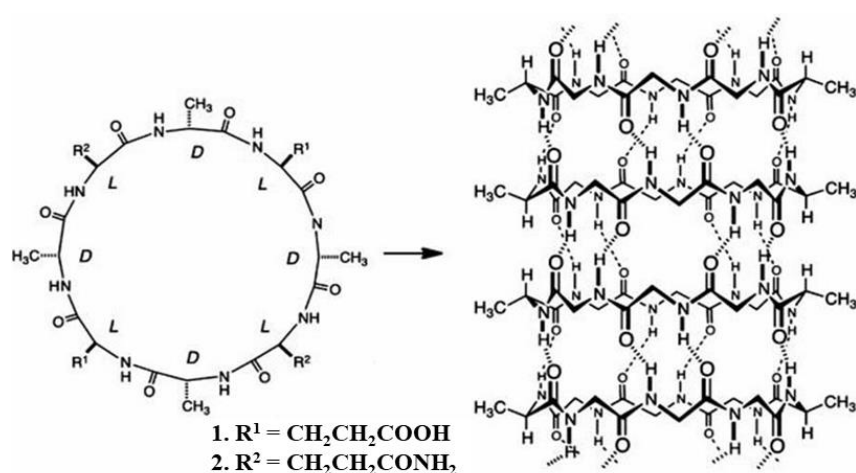


Figure 1.9. Molecular structure (left) and self-assembled nanotubular structure (right) of the cyclic octapeptide **1** and **2** (only the peptidic backbone is represented) (adapted from, J. Montenegro, M. R. Ghadiri and J. R. Granja, *Acc. Chem. Res.*, 2013, **46**, 2955–2965).

Incorporation of hydrophobic tryptophan and leucine residues in the cyclic octapeptides results in formation of nanotubes that can partition into the lipid bilayer of vesicles and form transmembrane channels with high ion transport activities.⁵⁴ Since then, large variety of structural motifs have been reported for applications not only as ion channels but also as antimicrobial agents and artificial photosynthetic systems.⁶⁰⁻⁶² More recently, a series of strategies have been developed to prepare cyclic peptide-polymer conjugates that are able to self-assemble into 1D core-shell tubular morphologies.⁶³⁻⁶⁵ In a recent report, Joliffe and Perrier investigated a series of cyclic peptide conjugates with hydrophobic and hydrophilic polyacrylates and acylamides of controlled molecular weight and low polydispersity, highlighting a clear correlation between the lipophilicity of the polymers expressed as the partition coefficient log P and the proton transport activity of the peptide-polymer conjugates forming trans-bilayer channels.⁶⁶ The assay was based on calcein and carboxy fluorescein entrapped in large unilamellar vesicles (LUVs), that suggested that proton transfer occurs through unimeric nanotube channels, rather than “clustered” barrels stave or carpet-like bilayer disruption. Experiments with thermoresponsive poly(N-isopropylacrylamide) conjugates lead to temperature-induced channel formation and allow for thermal gating of proton efflux properties. Otto and his research group have recently disclosed a series of reports on self-synthesizing macrocyclic molecules in water. The strategy was based on reversible dynamic covalent chemistry using dithiol building blocks. Under oxidative conditions the dithiols form an equilibrating mixture of disulfide-linked macrocycles, referred to as dynamic combinatorial library (DCL).⁶⁷ Usually the distribution of the library members in DCLs can be shifted by the external addition of template molecules, which amplifies the formation of members with a high affinity to the template at the expense of weaker binders. Otto and colleagues have now showed that the library distribution can be shifted if one of the macrocycles is able to recognize itself through self-assembly of β -sheet encoded GLKLK peptide side chains (Figure 1.10).⁶⁷ This induced shift of the library composition toward the self-assembling macrocycle gives rise to a self-replicating material.⁶⁸

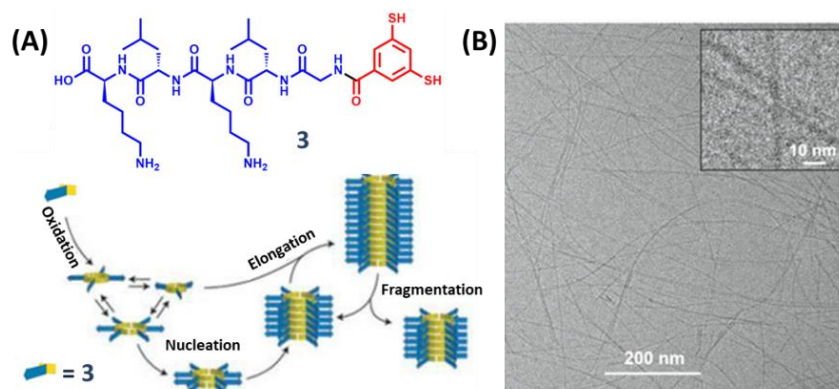


Figure 1.10. Thiol-functionalized GLKLK peptide (**3**) building block forms a DCL of disulfide-linked macrocycles. (A) Schematic representation of the hexamer macrocycle that nucleates and elongates into supramolecular fibers, and (B) cryo-TEM image of the fibre (adapted from, J. M. A. Carnall, C. A. Waudby, A. M. Belenguer, M. C. A. Stuart, J. J.-P. Peyralans and S. Otto, *Science*, 2010, **327**, 1502–1506).

Ashkenasy earlier reported linear amphiphilic peptides with up to 12 amino acids, including a $-(FE)_n-$ repeat domain, that form soluble 1D β -sheet aggregates in water.⁶⁹ These were able to act as templates for self-replication using native chemical ligation of an electrophile thioester and a nucleophilic N-terminal cysteine.

In a recent study Otto and co-authors confirm that the hydrophobicity of the peptide building block, in combination with multivalent effects, determines which of several potential self-replicating materials emerges from a DCL.⁷⁰

Aliphatic and Peptide Amphiphiles: A widely applicable and important set of building blocks for the design of self-assembled and functional soft matter in water is based on amphiphilic fatty acid conjugated oligopeptides.^{50,71} Peptides with N or C terminal protection with long alkyl chains shows very good amphiphilic character and has myriads of applications. Peptide/ amino acid based amphiphiles are also good candidates for gelation. My research works (chapter 3 and 4) are mainly on peptide/ amino acid based amphiphiles on material and biological applications. Therefore, I will discuss this topic “peptide amphiphile” and their application in biological and material field in the introduction section “1.6. Amino Acids and Peptides as Functional Bio-materials” and “1.7. Peptide or Amino acid Based Gels in Environmental Remediation”.

Samuel I. Stupp and his co-workers have contributed immensely in this regard. They demonstrated the supramolecular polymerization of the peptide amphiphiles into very long 1D nanorods and fibers in aqueous buffer.^{72,73} The general design of the building block combines an aliphatic hydrocarbon chain (domain I) with a peptide block that contains a hydrophobic sheet-forming sequence (domain II), water solubilizing charged amino acids (domain III), and a bioactive signalling epitope (domain IV) (Figure 1.11). The morphology of the nanofibers has usually been determined using cryo-TEM, but the internal structure was characterized using transmission infrared (IR) spectroscopy and polarization modulation infrared reflection-absorption spectroscopy (PMIRRAS): the β -sheet is oriented parallel to the long axis of the nanofiber. The internal order is highly dependent on peptide sequence and morphology,^{74,75} also supported by CD investigations.⁷⁶ Molecular dynamics simulation studies by De la Cruz group indicates that self-assembly is governed by an intricate balance between desolvation and van der Waal interactions in the hydrophobic alkyl tails with a network of hydrogen bonding between the peptide segments.⁷⁷ This leads to formation of different morphologies like single and stacked parallel β -sheets, spherical micelles, micelles with β -sheets in the corona or long cylindrical fibers.⁷⁷ Schatz, in his simulation studies with palmitoyl-conjugated amphiphiles found that , cylindrical configurations are most stable, resulting in nanofiber formation.⁷⁸ Recent work by Stupp and Meijer on self-assembly of peptide amphiphiles, palmitoyl-V₃A₃E₃-NH₂ also highlighted the impact of the assembly pathway on the produced supramolecular morphology.⁷⁹ The Stupp lab has also disclosed a report on hexahistidine based self-assembling peptide amphiphiles, whereby the shape of the pH-responsive nanostructures can be controlled via molecular design.⁸⁰

Banerjee and co-workers have discussed a peptide based amphiphilic hydrogel which forms helical fibers upon self-assembly, with different helical pitch length for different fibers. However, upon aging the pitch length of all fibers becomes uniform in nature. A macroscopic change was also observed for the gel, the transparent gel becomes opaque upon standing for several hours. X-ray diffraction and scattering experiment

shows, upon aging the molecules come closer to each other and forms more interdigitated networks.⁸¹

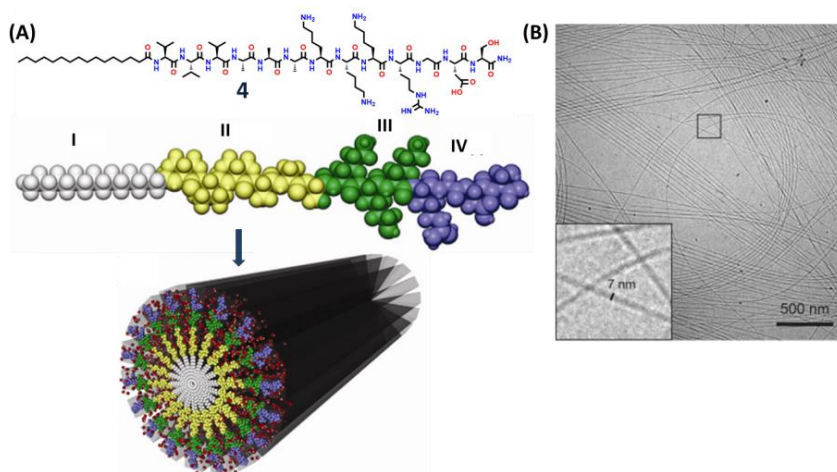


Figure 1.11. (A) Chemical structure and space-filling model of the peptide amphiphile palmitoyl-V₃A₃K₃-RGDS-NH₂ (**4**), highlighting the four structural domains (I–IV), and a schematic representation of the self-assembly into a nanofiber, with red spheres representing water molecules (adapted from, J. B. Matson, R. H. Zha and S. I. Stupp, *Curr Opin Solid State Mater Sci.*, 2011, **15**, 225–235). (B) Cryo-TEM micrograph of the peptide amphiphiles palmitoyl-V₂A₂E₂-NH₂ in water, revealing high aspect ratio nanofibers with diameters of about 7 nm (adapted from, J. H. Ortony, C. J. Newcomb, J. B. Matson, L. C. Palmer, P. E. Doan, B. M. Hoffman and S. I. Stupp, *Nat. Mater.*, 2014, **13**, 812–816).

The group of Goldberger investigated the fine tuning of the pH transition in switchable amphiphiles–micelle–nanofiber morphologies within a building block consisting of palmitoyl-XA₃E₄-NH₂ where the XA₃ block is a known β -sheet-forming domain (X is any amino acid with a hydrophobic side chain), and the four glutamic acids linked on the C-terminus ensures water solubility.⁸²

The interplay between attractive and repulsive intermolecular interactions has been one of the key conditions for supramolecular self-assembly.

This has been utilized to design an elegant strategy by the Hartgerink research lab in order to produce objects of finite size instead of fibers of micrometer scale usually associated with amphiphilic peptide.⁸³ Here, a library of nine peptides with a triblock A-B-A oligopeptide was prepared. The A blocks contain variable length of oligo-lysines while the middle B block possess alternating glutamine-leucine encoded to form β -sheets (Figure 1.12). Here, the concept of molecular frustration was introduced as a means to hamper the attractive forces from the middle block with repulsive electrostatic forces from the charged oligo-lysines in the periphery to yield finitely sized nanofibers with a length of 150 ± 45 nm

in the case of $K_2(QL)_6K_2$ at a particular pH. Thereafter, increasing pH will cause deprotonation of the lysine side-chain amino groups resulting in the screening of repulsive forces. This facilitates supramolecular polymerization that will increase the length of the fibers.

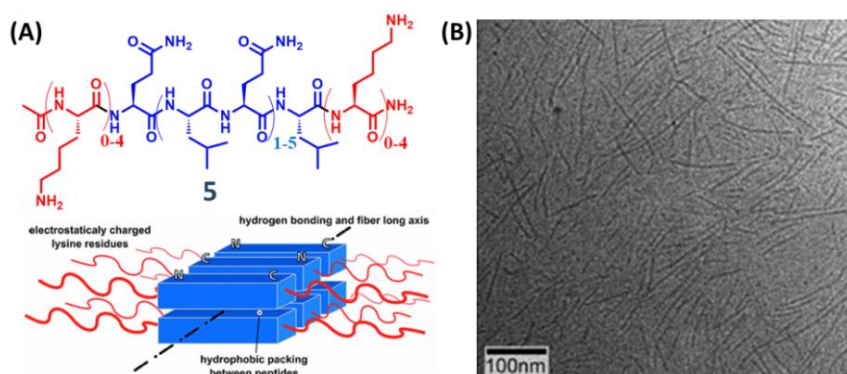


Figure 1.12. (a) Chemical structure of the $K_x(QL)_yK_x$ series of peptides (**5**) ($x = 0-4$, $y = 2-6$), and the proposed model of nanofiber formation, indicating the hydrophobic packing region (in blue), the axis of hydrogen bonding, and the repulsive positive charges (in red). (b) Cryo-TEM micrograph of the peptide $K_2(QL)_6K_2$ in 10 mM Tris buffer at pH 7.4 with 150 mM NaCl (adapted from, H. Dong, S. E. Paramonov, L. Aulisa, E. L. Bakota, and J. D. Hartgerink, *J. Am. Chem. Soc.*, 2007, **129**, 12468–12472).

Aromatic Oligo-peptides and Peptide Conjugates: Gazit and his coworkers report a key work in the self-assembly of aromatic peptides when they found a small peptide made of aromatic building blocks, diphenylalanine (FF) self-assembling into extremely stable, stiff, and micrometer-long rod and tube-like morphologies.⁸⁴ It has potential applications, for example, in optoelectronic and piezoelectric devices, sensors, or super- hydrophobic surfaces.⁸⁴⁻⁸⁶ Micrometer-long fibers tend to entangle at higher concentrations to form physical networks and strong self-supporting hydrogels, which occupies a key position in present day soft materials research important for solving several real problems in today's world. Design of this supramolecular hydrogels is in fact one of the objectives of this thesis works (chapters 3, 4) and will be discussed in more detail later in this chapter.

1.4. Low Molecular Weight Gelators

So far we have mostly discussed about self-assembled supramolecular materials with an emphasis over peptide based materials. Upon discussing the topic we have encountered a term “gel”. Now what is gel? In our daily life we use different types of gel or gel-like materials, starting from the table jam to pain relieving gels. Now, how can we describe gel in terms of science? A gel is a solid jelly-like material that can have properties ranging from soft and weak to hard and tough. Gels are defined as a substantially dilute cross-linked system, which exhibits no flow when in the steady-state.⁸⁷ By weight, gels are mostly liquid, yet they behave like solids due to a three-dimensional cross-linked network within the liquid. It is the crosslinking within the fluid that gives a gel its structure (hardness) and contributes to the adhesive stick (tack). In this way gels are a dispersion of molecules of a liquid within a solid in which liquid particles are dispersed in the solid medium. The word gel was coined by 19th-century Scottish chemist Thomas Graham by clipping from gelatine. Self-assembly is one of the important processes in gelation. From molecular point of view, gels can be visualized as: molecules associate among themselves through physical or chemical interactions to form a three-dimensional network which finally encapsulate solvent molecules within the interstitial space to form gel.

In this aspect low molecular weight gelators (LMWGs) are important. Small molecules associate or rather self-assemble into long anisotropic 3D networked structures to encapsulate huge amount of solvent within interstitial spaces. These gels differ permanently from covalently cross-linked polymer gels because the cross-linking can be reversed by the input of energy, for example, by heating. Such usefulness has made LMWGs important candidates of industrial uses, though such industrial applications are less encountered in academic literature. In addition to the industrial applications, fiber formation is a result of molecular stacking and these fibres can be useful for optoelectronic applications. Gels are now used as cell payloads. Stimuli responsive LMWG based gels are useful for application in tissue engineering, where the tissue containing

gels can be directly implanted in the patient's body. However, such processes are yet to be optimized for clinical applications (Figure 1.13).

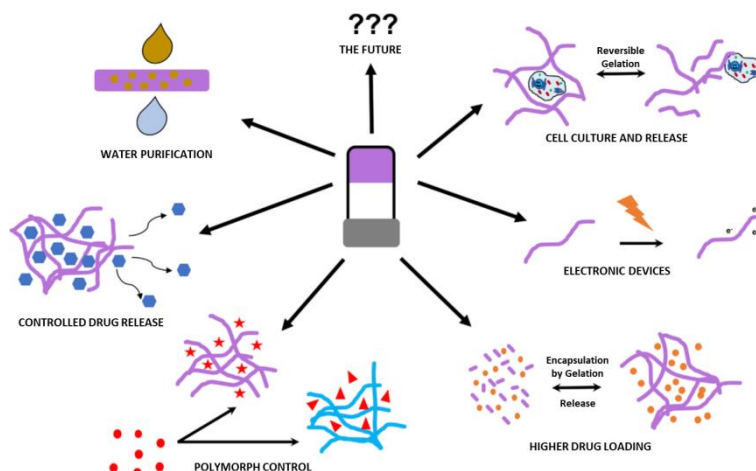


Figure 1.13. Cartoon showing some the potential uses of low-molecular-weight gelators, including cell culture and differentiation with non-harmful release from the gelled material, photoresponsive semiconducting gel fibers, high loading of a drug particle with a targeted release, slow and controlled drug release upon addition of a stimulus, water purification by the removal of heavy metals, and the control of polymorph by changing the gel network (adapted from, E. R. Draper and D. J. Adams, *Chem*, 2017, **3**, 390-410).

1.4.1. Characterisation of Gel at the Molecular Level

The study of gel phase with all sorts of molecular interactions (solute-solute as well as solvent-solute) is not a very easy task. The gels arise from assembly across many length scales, and understanding all of these is difficult. At the molecular level, the molecules must interact in a manner that leads to the formation of suitable aggregates that can eventually entangle. Thus, one-dimensional growth must be favoured. From this perspective, it is very frustrating that it is often extremely difficult to predict whether a molecule will form a gel or not; indeed, gelation has been described as an empirical science. Structurally similar small molecules can exhibit extremely different propensity to form gels. A number of methods have been attempted to overcome this.^{88, 89} A numbers of people have attempted to link gelation to crystal structures.⁹⁰⁻⁹² In many ways, this seems surprising. It is not at all clear that there is (or even that there has to be) a link between the interactions that lead to crystallization in some situations and gelation in others. Indeed, although it has been widely assumed that there is a link, there are a number of examples that now specifically show that packing is different in the gel phase and crystals grown even from the same solvent.⁹³⁻⁹⁵ As a specific

example, Adams and co-workers showed that fiber X-ray diffraction data from the gel phase did not match the crystal structure of a crystal grown directly from the gel phase.⁹³ It is necessary to note, how does the self-assembly of gelator molecules change from one solvent to the other. In some cases crystalline has been found within gel phase,⁹⁶ but it is not clear how these data can be shown to not arise from simply some (possibly a very small amount of) crystallization within an amorphous gel phase.

Other methods that have been used to tackle this inability to predict gelation include using computational study on a library of gelator molecules. The library approach simply involves generating a large number of similar molecules and then determining which form gels.⁹⁷⁻⁹⁹ This brute force approach is often successful in finding gelators, but it is less effective in explaining why some molecules can form gels and others cannot. This happens because it is difficult to vary only one parameter at a time. For example, changing one functional group to another will result in a change in the steric bulk of the molecule, the ability to pack, possibly the number of hydrogen bond donors or acceptors, the absolute solubility in a particular solvent, etc. Hence, simple lists of gelators and their efficiency often do not capture the complexity of the system. Recent advances in computational approaches have been successful in predicting gelators.

Tuttle's group has effectively predicted tripeptide-based gelators,¹⁰⁰ and we have recently been successful in generating a descriptor-based approach that can be used to predict new gelators.¹⁰¹ However, in both cases the methods again do not explain why some molecules form gels and others do not. One important thing that should be remembered regarding LMWGs, they can form gel only with a few specific solvents. Recently this fact has been quantitatively demonstrated using Hansen solubility parameters. It has been found that, a particular LMWG is able to form gel within a particular range of Hansen space. (Figure 1.14)

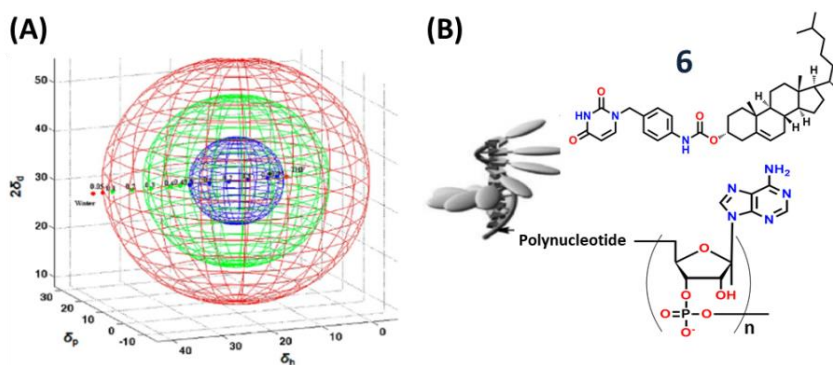


Figure 1.14. (A) Plot of solubility data for a specific molecule in Hansen space; blue shows where the molecule is soluble, green shows where a gel is formed, and red shows where the molecule is insoluble; (B) Schematic illustration of a polynucleotide interacting with a gel fiber formed by the gelator 6 (adapted from, E. R. Draper and D. J. Adams, *Chem*, 2017, **3**, 390-410).

A particular gelator can form gel only above a particular concentration called, minimum gelator concentration (mgc). Though sometimes it is assumed that, the molecular packing and supramolecular aggregates are the same above and below the mgc, this is rarely proven. Temperature is another key condition to induce a phase transfer process in gelation. People often specify it as T_{gel} in literature. Most of the LMWGs show gelation ability within a fixed temperature range. Additives are also useful to promote gelation in some cases. It has been found that some salt additive can promote gelation in the basis of Hofmeister series.¹⁰² Some polymer additives also have been found to promote gelation process [Figure 1.14 (B)] above.¹⁰³

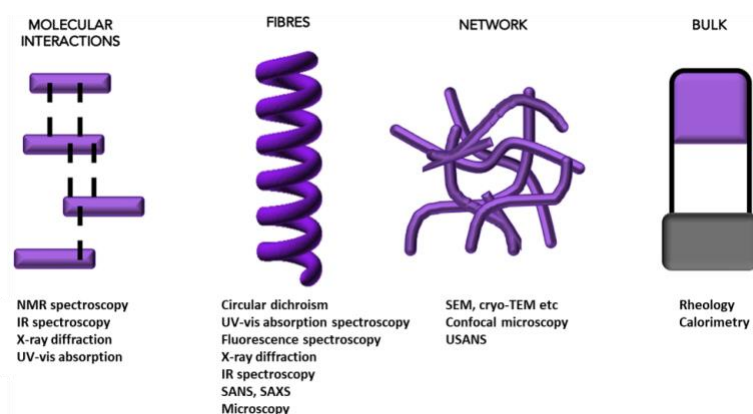


Figure 1.15. Hierarchical assembly across length scales. Low-molecular-weight gels form as a result of assembly across a range of length scales; different techniques are appropriate for analyzing the structures formed at each length scale (adapted from, E. R. Draper and D. J. Adams, *Chem.*, 2017, **3**, 390-410).

Now let's return to the previous topic of characterising gel. Hence, to attempt to understand gelation, a wide range of skills and techniques need

to be used (Figure 1.15). Molecules interact with each other through various weak interactions. These interactions obviously change the electron density profiles of the corresponding molecules which can be characterized by different spectroscopic techniques like, nuclear magnetic resonance (NMR) spectroscopy, infrared spectroscopy, circular dichroism, fluorescence, and X-ray diffraction studies and others.^{104, 105}

Though there are different kinds of bottlenecks are associated with each type of spectroscopic technique. For circular dichroism the concentration of the gelator molecule should be low enough, sometimes it lies below the mgc value. In such a low concentration it is not always safe to assume that the packing pattern is same for both gel phase and dilute phase. X-ray diffraction makes the assumption that the diffraction (if any is observed) is from the gel phase as opposed to crystalline impurities. Nonetheless, such techniques can be hugely informative. For example, NMR spectroscopy can be used to both probe the rate of assembly and to infer information about the molecular interactions leading to assembly. Likewise, infrared spectroscopy can be used to show that specific hydrogen bonding is occurring on assembly.

At the next level of hierarchy, the nature of the fibers is usually probed by microscopy or by small-angle scattering. Any electron microscopy image can only represent a tiny fraction of the sample. Also, unless cryo-transmission electron microscopy (TEM) is used, there could be drying artifacts in the sample preparation. However, in general, microscopy most often shows the presence of long fibers, commonly entangled or branched. In the gel phase, this network structure always is in three dimensions, but collapses to two dimensions when it is examined by microscopy. Three dimensional imaging can be captured by confocal microscopic studies. Although there are significant advances in this area, most examples have relatively low resolution. Nonetheless, confocal imaging can provide useful information on the microstructure and distribution of the fibers in space. Small-angle X-ray or neutron scattering are hugely powerful techniques for imaging gels; the imaging can be done in situ.¹⁰⁶ Although access to a beamline at a facility is usually required, the quality of more accessible lab-based X-ray equipment is improving constantly to allow access to good-quality data. The scattering

data of course have to be fitted to a model, but the advantages are that these are bulk measurements, representing the sample as a whole.

Finally, the mechanical properties of the gels can be measured by techniques such as rheology.¹⁰⁷ A range of different measurements are possible and are able to inform on the gel networks. A typical LMWG will have a storage and a loss modulus (G' and G'' , respectively), which are frequency independent, and will break at relatively low strain. Often simple vial inversion is used as a means of proving gelation, despite the concern that this does not necessarily demonstrate that a gel has been formed; viscous liquids can also be stable to inversion, albeit for a relatively short time.¹⁰⁸ It is also apparent to the careful reader that some of the inverted samples seem to be in the process of flowing. From the rheological data, different behaviour is often shown, which implies that there are different underlying networks, although significantly more work needs to be done here to understand this.

1.4.2. Classification of Low Molecular Weight Gels

Gels can be classified¹⁰⁹ in various modes depending upon their origin, the nature of solvents, gelator and intermolecular interactions (Figure 1.16). Depending upon the medium of the gel formation, gelator molecule can be classified into three sections: organogel, hydrogel and aerogel/xerogel. However, it is not yet possible to select a molecule that can gelify definitively a selected liquid.

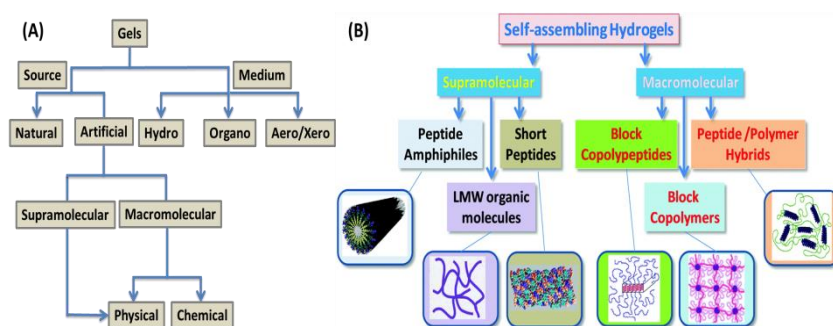


Figure 1.16. (A) Classification of gels (adapted from, N. M. Sangeetha and U. Maitra, *Chem. Soc. Rev.*, 2005, **34**, 821) and (B) classification of self-assembling hydrogels (adapted from, C. Chassenieux and C. Tsitsilianis, *Soft Matter*, 2016, **12**, 1344-1359).

The most fascinating fact associated with the LMWGs is they can respond to the external stimuli. These external stimuli are like physical or chemical perturbations, e.g. heat, light, sonication (or ultra-sonic sound) metal-ions, pH and many other things. Now, there is now straight-forward rule to design gelators, till now it is generally obtained by serendipity. Maitra and Sangeetha have judiciously summarized diverse types of LMWGs in a single figure in order to realize underlying rational of designing LMWGs (Figure 1.17).

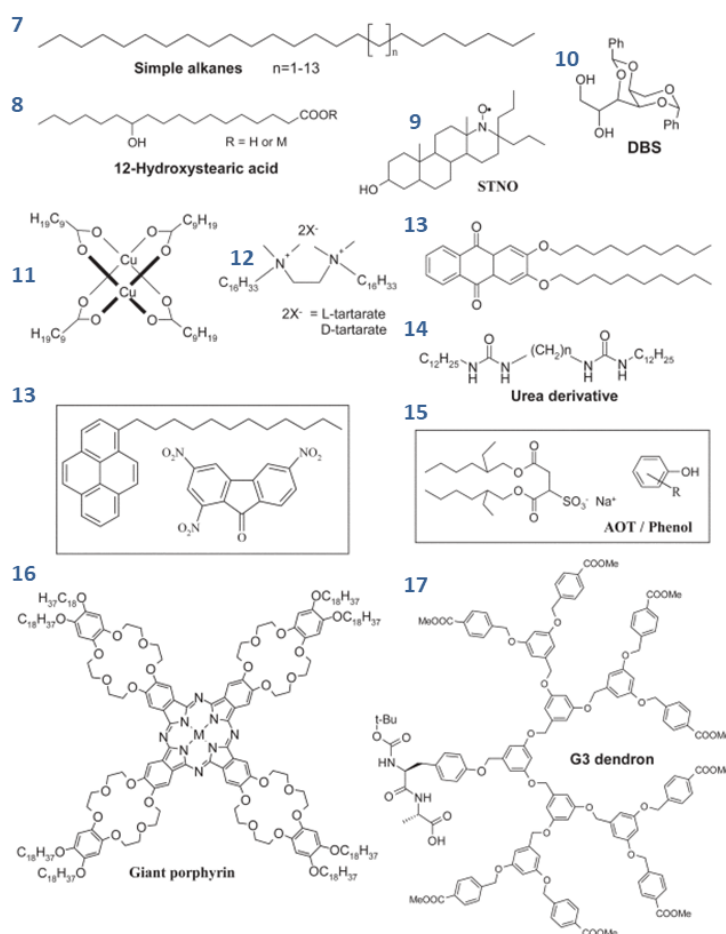


Figure 1.17. Chemical structures of different LMWGs (adapted from, N. Sangeetha and U. Maitra, *Chem. Soc. Rev.*, 2005, **34**, 821-836).

I must discuss about salient features of LMWGs by discussing a few examples of them. Many scientists worldwide have developed this field by introducing structurally and functionally diverse LMWGs and hence it is not possible to encompass all the work within this short introduction.

Terech and co-workers developed chiral and racemic 12-hydroxyoctadecanoic acid based LMWGs in early 90's and also

elucidated the packing pattern of the molecule in gel state using scattering experiments (Figure 1.18).¹¹⁰

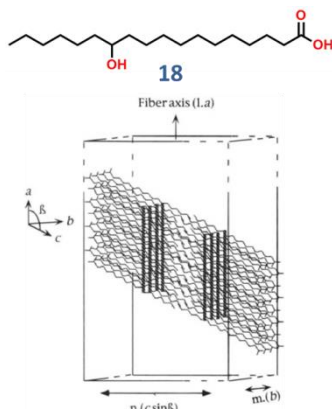


Figure 1.18. Structural model of the fibrillar or ribbon like aggregates in organic solvents formed by gelator 12-hydroxyoctanoic acid (**18**). The crystallographic axis and the fiber geometry are indicated. The dimensions are proportional to the crystallographic cell parameters as shown (adapted from, P. Terech, V. Rodriguez, J. D. Barnes and G. B. McKenna, *Langmuir* 1994, 10, 3406-3418).

Natural hydrocarbons such as sterols are good candidates for LMWGs. Shinkai and co-workers developed light responsive cholesterol based gelators with on-off properties, i.e. for them light act's as stimuli.¹¹¹ Latter on Maitra and co-workers devoted much endeavour to develop cholesterol based gelators. They developed cholesterol based tripodal gelators that have a hydrophobic pocket within the hydrophilic outer sphere.¹¹² Cholestol gels has good advantage of huge hydrophobicity therefore, incorporating metal-binding and photo-responsive motifs into the structure enhances stimuli responsiveness of these gels (Figure 1.19).¹¹³⁻¹¹⁵

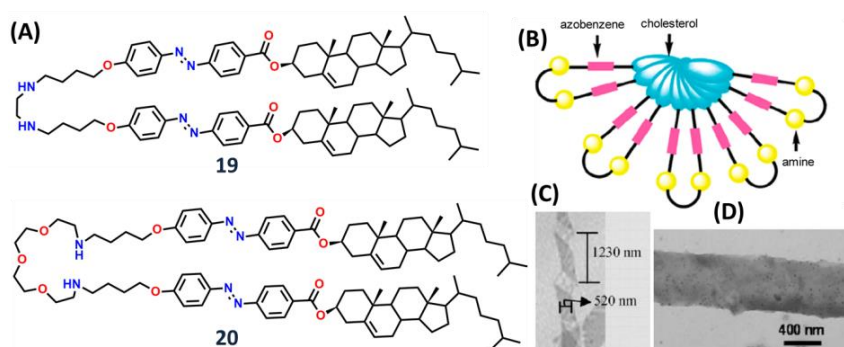


Figure 1.19. (A) The structure of gelators **19** and **20** having metal binding and photo-responsive motifs (B) Schematic representation of 1D molecular stacking of **19**. TEM images of (C) helical ribbon and (D) tubular structure of self-assembled **20** in the absence and presence of Pd metal ion (adapted from, S. S. Babu, V. Praveen and A. Ajayaghosh, *Chem. Rev.*, 2014, **114**, 1973–2129.)

Shinkai and co-workers developed azobenzene containing sugar based bola amphiphilic molecules, gelators can be found by combinatorial screening of the appropriate sugar groups from a carbohydrate family. Sol to gel transfer and vesicle to fiber transformation was modulated by incorporation of a boronic acid moiety, **25** (Figure 1.20).¹¹⁶

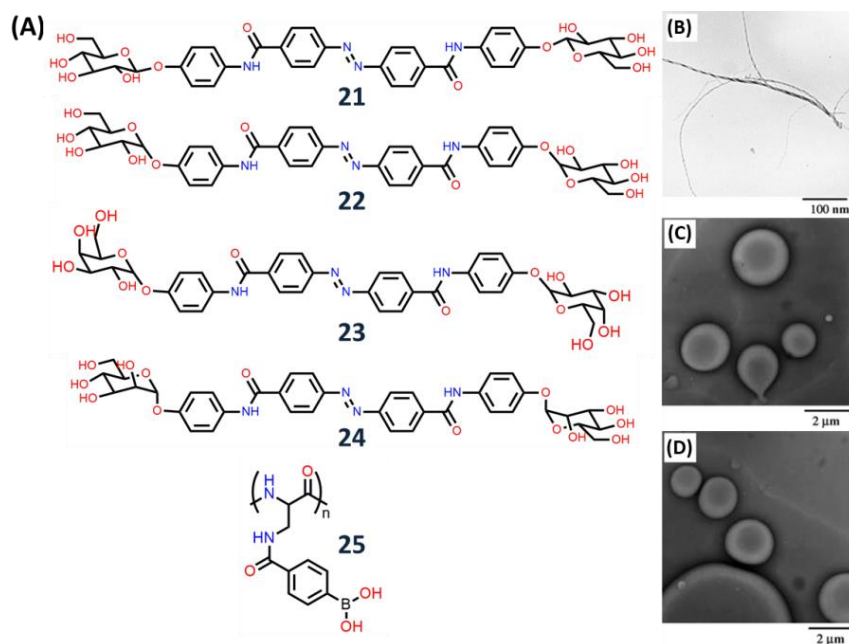


Figure 1.20. (A) Molecular structures of sugar based bola-amphiphiles (**21-24**) and a boronic acid containing poly-L-Lysine (**25**). TEM images of (B) **22**, (C) **23** and (D) **24** in 1:1 (v/v) DMSO-water mixtures. The sample for **22** ($6.4 \times 10^{-3} \text{ mol dm}^{-3}$) was prepared by pouring the gel into acetone. The TEM image of **21** (not shown here) was basically similar to that of **22**. The samples for **23** and **24** ($6.4 \times 10^{-3} \text{ mol dm}^{-3}$ each) were prepared from the top clear part of their precipitate mixtures. The samples were stained with uranyl acetate (2.0% aqueous solution) (adapted from, H. Kobayashi, K. Koumoto, J. H. Junga and S. Shinkai, *J. Chem. Soc., Perkin Trans.*, **2**, 2002, 1930–1936).

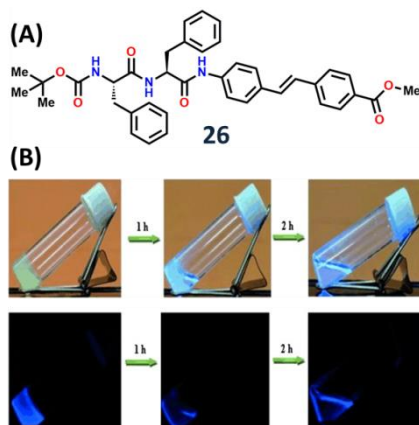


Figure 1.21. (A) Chemical structure of gelator molecule **26**. (B) UV-light-responsive nature of the organogel in *n*-octanol (adapted from, D. K. Maiti and A. Banerjee, *Chem. Asian J.*, 2013, **8**, 113-120).

Aromatic moieties with C=C, double bonds shows cis-trans isomerisation upon photo-irradiation. Molecules containing these groups have been successfully utilized as photoresponsive gelators. Many groups have reported gelators with such functionalities.^{117, 118} Banerjee and co-workers developed stilbene based unnatural amino acid containing gelator with photoresponsive nature (Figure 1.21).¹¹⁹

Porphyrines containing large π -surface are efficient motifs for gelation. Nolte and co-workers developed a tetra(thiafulvalene-crown-ether) phthalocyanine that, self-assembles into helical tapes (Figure 1.22) nanometers wide and micrometers long.¹²⁰

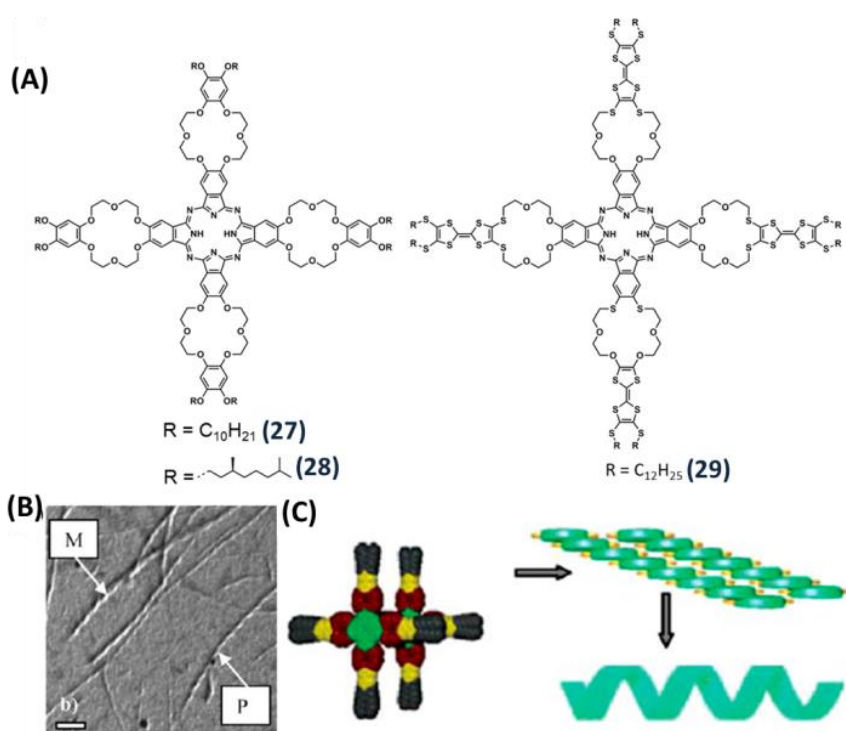


Figure 1.22. (A) Chemical structures of tetra(thiafulvalene-crown-ether) phthalocyanines (27-29). (B) TEM image of the gel fibers of showing an equal distribution of both left and right helical structures (scale bar = 200 nm). (C) Molecular model (phthalocyanine moiety in green, crown-ether in red, TTF in yellow, alkyl chains in gray) showing the stacking mode of the molecules (adapted from, S. S. Babu, V. Praveen and A. Ajayaghosh, *Chem. Rev.*, 2014, **114**, 1973–2129).

Ajayaghosh and his group first developed oligo-p-phenylenevinylene (OPV) containing π -gelators.¹²¹ They made a self-supporting soft solid from aliphatic hydrocarbon solvents such as hexane, cyclohexane, decane, dodecane, petrol, diesel, and kerosene, when dissolved in small quantities (<2 mM) at room temperature (Figure 1.23).

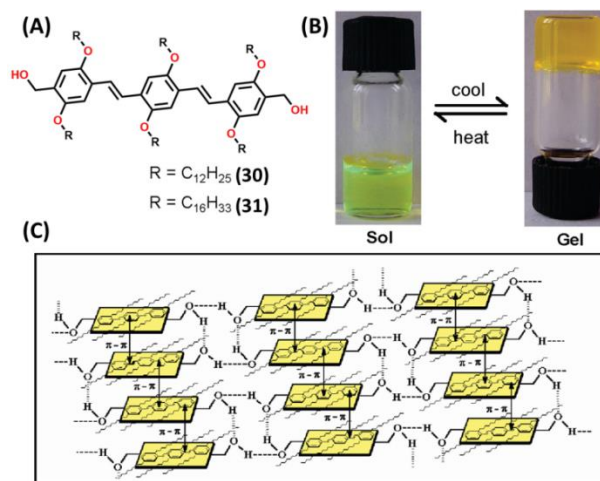


Figure 1.23. (A) Structures of the gel-forming OPVs (**30** and **31**). (B) Photograph of OPV **30** in cyclohexane before and after gelation (critical gelator concentration, CGC = 1.1 mM). (C) Probable self-assembly of OPVs, depicting the H-bond and π -stack induced three dimensional network formations (adapted from, A. Ajayaghosh and V. K. Praveen, *Acc. Chem. Res.*, 2007, **40**, 644-656).

The above stated examples were a few tricks for designing LMGs. As stated previously, this thesis is mainly concerned about peptide and amino acid containing materials. Therefore, in this point I am switching to my old topic of peptide based self-assembly and gelation. It is not very easy to summarize or explain all the features of peptide based gels, because it is an emerging field of research and new methods are coming routinely to characterize and utilize these materials for future uses.

1.5. Amino Acid and Peptide Based Small Molecule Gelators: From Soft Matter to Functional Materials

Peptide and amino acid based small gelator molecules have been attracting the attention of the researchers since last few decades. These soft materials have many fold functional applications in different fields of material sciences. Amino acid and peptides are natural molecules with diverse functionalities that are coded within their structures. People from different corners of the world have exploited the key features of amino acids and peptides to form self-assembled soft materials. Interestingly, the first reported supramolecular hydrogel was an amino acid containing gel dibenzo-L-cystine, which formed gel when benzylation of cysteine was carried out.^{122, 123} After that, myriads of peptide and amino acid based gels have been developed by different research groups throughout the world within last few decades.

1.5.1. Simple Designing Strategy of Amino Acid/Peptide Based Gels

An interesting debate in the field of low molecular weight gelator is, “Can we design a gelator?”¹²⁴ The answer is in no way straightforward. By investigating different known gelator molecules reported in literature, one can only get a vague idea about the possible way of designing molecules that may subsequently form a gel in a particular solvent, but it is still a trial and error. Balance of various supramolecular interactions (i.e. H-bonding interactions, van der Waals’ forces, hydrophobic interactions, π - π interactions, salivation interactions, columbic interactions and many others) between a group of molecules as well as solvent sometimes leads to gelation. Therefore interplay between these complex parameters sometimes can be simulated or evaluated by theoretical approach. Another possible approach is to study structure property relationship by varying functional group of a self-assembling molecule and to optimize minimum criteria of gelation.

Short Peptides: Short peptides with both hydrophilic and hydrophobic residues show amphiphilic behavior. They are generally composed of charged head group containing a few charged peptide sequence and a tail group containing neutral amino acid sequence.¹²⁵ Amyloids are naturally occurring fibrous proteins which are the major cause of neurodegenerative diseases like Alzheimer's, Parkinson's and Huntington's diseases. They are generally borne out by irregular folding and aggregation of proteins in human body. Amyloids are good examples of peptide amphiphiles and many studies have been done to study their aggregation behavior. It has been found that, A β (16–20), i.e., KLVFF is the key sequence of fibrillization and it forms β -sheet like arrangement upon aggregation in aqueous environment. Pochan and co-workers have demonstrated the gelation behavior of KLVFF in phosphate buffer saline.¹²⁶ Even a simple dipeptide Phe-Phe which is the key motif of the above sequence is able to form robust self-assembled higher-order nanostructures.¹²⁷ Replacing the first Phe residue with Ile yields hydrogel with a fine networked nanostructure.¹²⁸ Replacing the Phe residue of Ile-Phe with, conformationally rigid α , β -dehydrophenylalanine (Δ Phe) yield stronger hydrogel at physiological condition with injectable applications.¹²⁹ Recently the long sequence A β ₁₋₄₀ has been also found to

form hydrogel.¹³⁰ Another interesting example of naturally occurring self-assembling peptide is collagens. Collagens are found in connective tissues, cartilage, vitreous humor, skin, lung, vascular system, basement membranes and serve as extracellular matrix in animal body.¹³¹ Among 29 kinds of collagen only type I, II, III, V and XI has an ability to form fibers. They generally contain a repetitive sequence of -Gly-X-Y- with X and Y, proline and hydroxyproline respectively to form a triple helix structure.^{132, 133} This triple helical conformation places the amino acid residues X and Y on the surface of the molecule. This kind of functional group disposition forces these helical strands to further self-assemble into like fibers.¹³¹ Due to its extracellular matrix like behavior, collagen has been used as a good bio-material for wound healing, 3D tissue scaffold, regenerative medicine and many others.¹³³ Hence, collagen can be a good biomolecule to be mimicked to obtain hydrogels. Yamazaki *et al.* have designed gelator peptides with alternative -Gly-Pro-Hyp- sequences and disulphide bridges.¹³⁴ Longtelechelic polypeptides with (Pro-Gly-Pro)₉ end block has also been designed and synthesized by genetically modified yeast (*Pichia pastoris*) and found to be aggregated to form hydrogel. The gelation is expected to the formation of triple helical knot structure by three intertwining (Pro-Gly-Pro)₉ domains.¹³⁵ Recently Hartgerink and co-workers have given a nice example of collagen mimetic gelator peptide with following sequence: (Pro-Lys-Gly)₄(Pro-Hyp-Gly)₄(Asp-Hyp-Gly)₄. (Also show the image)¹³⁶ The peptide forms a strong gel with high mechanical strength by sticky end interaction between Lysine and Aspartate residues. Simple tri and tetra peptide molecules are also found to form stable gel upon sheet like assembly. Linear peptides with hydrophobic residues like, Phe, Ala, Ile, Leu are found to form hydrogel at physiological pH by forming an antiparallel β -sheet like structure upon self-assembly (Figure 1.24).¹³⁷ Peptides with alternative hydrophilic and hydrophobic residues are prone to form antiparallel β -sheet structure upon self-assembly in water.¹³⁸ Due to this kind of structural arrangement the self-assembled sheet has two distinct faces, one hydrophobic and another hydrophilic. The hydrophobic face invariably try to hide itself from water by burring itself in the core of fibers and the resulting charged fibers further entangled to form gel in

aqueous media.^{139, 140} Pochan and Schneider have investigated another class of amphiphilic peptides with β -hairpin like structure showing folding dependent gelation due to intramolecular folding pattern. A peptide molecule (MAX) consisting of alternative valine and lysine residues at the two arms of the hairpin and a D-proline residue at the central position undergoes gelation only in presence of certain folding condition. It forms pH triggered stable hydrogel upon folding.¹⁴¹⁻¹⁴³ They have designed another type of β -hairpin with dissimilar arm length with an exchangeable β -strand region that can enjoy swapping with another exchangeable β -strand of another peptide.¹⁴⁴

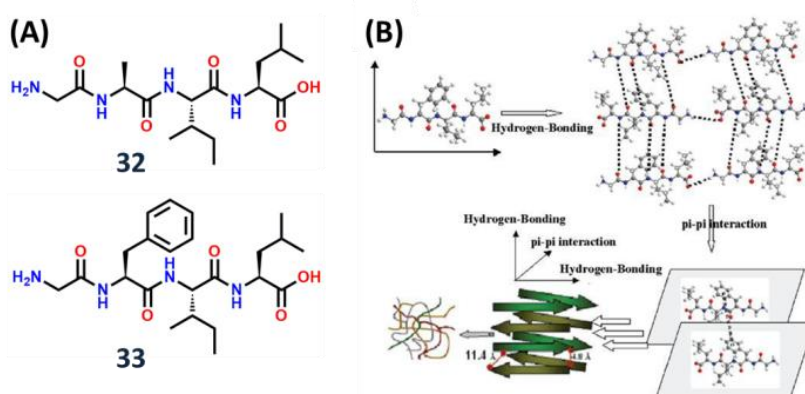


Figure 1.24. (A) Tetra-peptide gelators **32** and **33** (Gly-Ala-Ile-Leu and Gly-Phe-Ile-Leu) and (B) their mode of packing in gel phase (adapted from, J. Naskar, G. Palui and A. Banerjee, *J. Phys. Chem. B*, 2009, **113**, 11787-11792).

Protection of Terminal Positions: An N-terminal protecting group can be introduced within a peptide molecule to minimize the repulsive effect of the amine groups and introduce some more H-bonding, π -stacking and hydrophobic interactions into the molecules. Gelation properties of peptides and amino acids have been tuned by judicious modification of these moieties. Banerjee and his group has reported the effect of different types of substitution on the gelation ability of a model tripeptide system. Simple aromatic protecting group, benzoylcarbonyl promotes gelation, when attached to the N-terminus.¹⁴⁵ Their mode of assembly have been shown in Figure 1.25. Bola-amphiphilic amino acid based molecules with benzoylcarbonyl N-terminus protection was been found to form organogels.¹⁴⁶ Hexafluoro derivative of the benzoylcarbonyl derivative is even a better motif for gelation when a phenyl alanine residue is present in the N-terminus of the peptide and such kind of peptides show sequence specific gelation.¹¹⁶ Pyrene, a fluorescent polyaromatic hydrocarbon, can

be a good candidate to induce enough hydrophobicity in peptides and amino acid to trigger their self-assembly.^{148, 149}

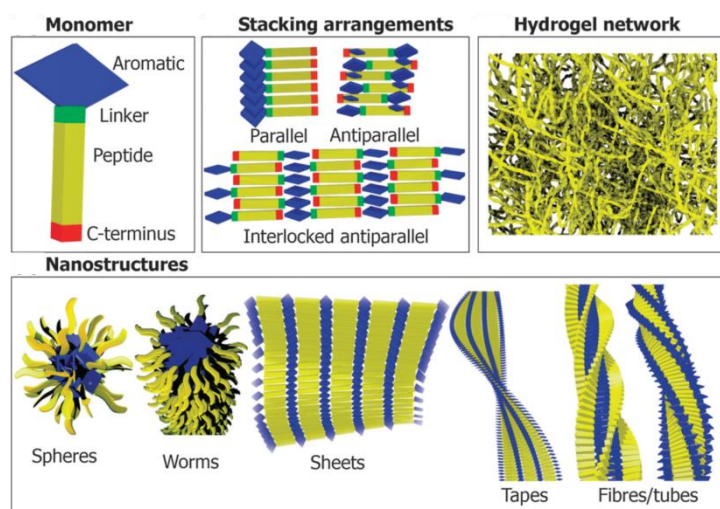


Figure 1.25. Schematic representation of aromatic peptide amphiphile self-assembly (clock wise) a simplified model of aromatic peptide amphiphile; some possible elementary stacking arrangements; a nanofibrous hydrogel network; mechanism behind the formation supramolecular nanostructures (adapted from, S. Fleming and R. V. Ulijn, *Chem. Soc. Rev.*, 2014, **43**, 8150-8177).

N-terminally capped pyrene containing tripeptide Phe-Phe-Ala-OMe (X) was found to form organogel upon sonication and it can immobilize graphene nanosheets inside the entangled network.¹⁵⁰ Attachment of pyrene to simple amino acids like Phe, Trp leads to gelation and as prepared gels sometime show pH dependent morphological changes.^{151, 152} An unnatural amino acid, 11-aminoundecanoic acid undergoes gelation upon covalent attachment of pyrene moiety with it. The gel shows self-healing property which can be enhanced by incorporation of carbon based nanomaterials.¹⁵³ However, sometimes pyrene moiety becomes hydrophobic enough to inhibit gelation of a peptide.¹⁵⁴ 9-fluorenylmethoxycarbonyl (Fmoc) is a protecting group generally used during the synthesis of peptides. It has an aromatic core and an oxycarbonyl moiety for π -stacking and hydrogen bonding interactions respectively. Fmoc when attached to the amino acids has been reported as gelators. Fmoc-Phe is a well-known gelator which yields strong hydrogels with different applications. Modification on the phenylalanine ring by incorporating fluorine (F) substitution(s) in the phenyl ring leads to better gelation ability due to better hydrogen bonding interactions.¹⁵⁵⁻¹⁵⁷ Gazit and his co-workers have described a novel strategy to design

peptide based strong hydrogel by capping a simple dipeptide, diphenylalanine with an aromatic protecting group, 9-fluorenylmethoxycarbonyl (Fmoc-) moiety.¹⁵⁸ In this context, it is important to note that, the linker distance between the aromatic group and the peptide segment sometimes play a very crucial role. Changing in the linker distance between fluorene group and YL peptide moiety has been found to influence gelation. More rigid structure with a shorter linker was found to promote efficient gelation.¹⁵⁹ Xu and co-workers have reported several examples of naphthalene and pyrene containing peptide based gelators and their potential applications as biomaterials. Sometimes naphthalene is a preferred protecting group over Fmoc to get a more rigid gel.¹⁶⁰ A $\text{O-CH}_2\text{-(C=O)-}$ linker between naphthalene ring and the peptide was found to promote gelation of a number of dipeptide based gelator.¹⁶¹ Various substitutions (like bromo or cyano group) in the naphthalene moiety was also found to enhance the gelation property.¹⁶² Another advantage of these aromatic group is that one can incorporate various acceptor chromophore inside the gel matrix to construct charge transfer complexes inside the gels.¹⁶³ These kind of charge transfer phenomena sometimes strongly influences the selectivity of formation of a single gelator peptide in a dynamic combinatorial system.¹⁶⁴ Another important class of N-terminal protecting group is electron deficient naphthalenediimide (NDI) and perylenediimide (PDI) about which we will discuss later, they are also able furnish a π -surface in a peptide based molecule to promote its' gelation. NDI and PDI molecule has two anhydride groups in their both ends and they are able to form bola-amphiphilic fluorescent gelator systems. NDI containing peptide based molecule can also form charge transfer gels in aqueous media with dialkoxy/dihydroxy naphthalene molecule.¹⁶⁵ In a recent review Ulijn and Fleming have nicely surveyed the examples of aromatic protecting group containing peptides.¹⁶⁶ Redox responsive and photo responsive aromatic moieties have been attached to the N-terminus to get redox and photo responsive gels which I will discuss later.¹⁶⁷ Nucleobases are very intriguing motifs prone to form H-bonding interactions to facilitate DNA/RNA helices. Protecting the N-terminus of peptide with nucleobases yield strong hydrogels, and relatively strong gel was found

upon attachment of Purine bases to the aromatic dipeptides probably due to better Hoogsteen base pair interactions than the pyrimidine analogues.¹⁶⁸ Whereas, two different non-gelator peptides with two different kind nucleic base (complementary two each other) were found to form hydrogel gel upon mixing. In this study the heterodimers were found to form a Watson-Crick type interaction and the hydrogel shows enhanced stability towards protease enzymes with respect to the component peptides.¹⁶⁹ Functionalizing the C-terminus of a peptide with another important class of biomolecules, saccharides yields stable hydrogel¹⁷⁰ endowed with anti-microbial properties.¹⁷¹ Attachment of glycopeptides into Fmoc-Phe-Phe-Asp moiety have been found to form a gel which can stop postoperative fibrosis in rabbit eyes.¹⁷² Bing Xu and co-workers have series of peptides appended with nucleobases at the N-terminus and carbohydrates at the C-terminus¹⁷³ to make a “Molecular Trinity” which form biocompatible gels and have been used for DNA delivery.¹⁷⁴

A peptide or amino acid based hydrogel that contains a free C-terminus is highly sensitive to the pH of the medium and just by changing pH, gel to sol transition can be triggered.^{175, 176} Generally pKa of the terminal COOH group strongly dictates its solubility at a given pH. However, upon molecular association, pKa of the corresponding group changes drastically due to the presence of hydrophobic environment.¹⁷⁷ Saiani and co-workers have shown that, aromatic dipeptide Fmoc-Phe-Phe-COOH has two pKa values and upon self-assembly they form an antiparallel β -sheet at pH range 10.2-9.5 with a charged fibrillar structure. Upon further neutralization of the surface charge at a pH range around, 9.5 to 6.2 the fibrils undergo assembly to form ribbon and finally below pH 6.2 the β -sheet arrangement disrupts completely to form precipitate.¹⁷⁸ Apart from this type of change in fibrillar association, morphological transition of self-assembled peptide with a change in pH is also a common phenomena.¹⁷⁹ Banerjee and co-workers have shown morphological transition of a pyrene linked amino acid based gelator Y upon varying the pH. Gelator **34** and **35** can form hydrogel within a wide range of pH, 7.46 to 14. However, gels within pH range 7.46 to 10.5 shows thixotropic property. Moreover, upon increasing the pH the helical gel fibers

transforms into straight fibers as observed from the scanning electron microscopy (SEM) (Figure 1.26).¹⁵¹

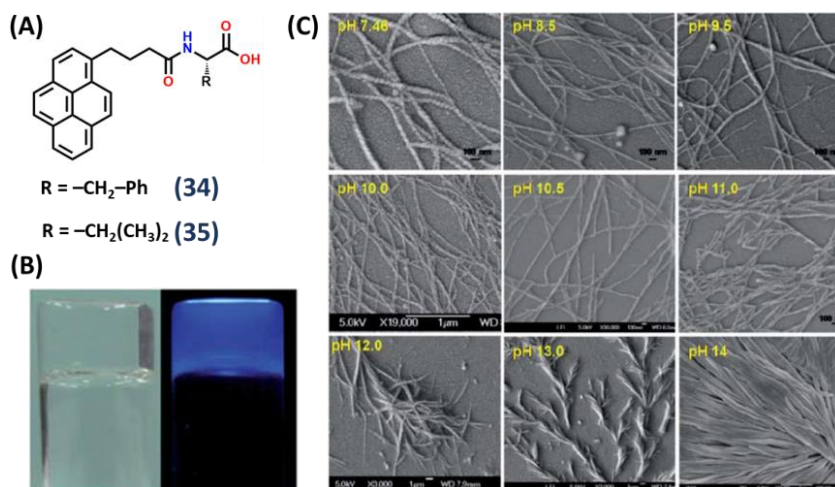


Figure 1.26. (A) Molecular structure of pyrene amino acid conjugate; (B) hydrogel obtained from gelator **34** in gel vial in daylight and under UV-irradiation; (C) FE-SEM images of the hydrogels at different pH showing a pH-dependent change in morphology (adapted from, J. Nanda, A. Biswas and A. Banerjee, *Soft Matter*, 2013, **9**, 4198-4208).

The molecules that contains COOH group are soluble at higher pH due to formation of COO^- group, then upon lowering the pH they sometimes form gel.¹⁷⁸ A series of Fmoc protected dipeptides initially soluble at higher pH have been found to undergo gelation upon switching to the lower pH value.¹⁸⁰ Glucono- δ -lactone (GDL) is a small molecule that undergoes slow hydrolysis in neutral aqueous medium, as a result, pH of the medium falls slowly and homogenously. Therefore, it acts as a pH switch for the gelation of peptides which are soluble in higher pH but immediately forms gel upon the subtle decrement of the pH. Decreasing pH with GDL ensures, the pH of the medium is decreasing slowly and homogenously. Therefore the gel strength and gelation kinetics can be manipulated precisely by changing the amount of GDL involved in gelation.^{181, 175} Anhydrides upon dissociation also lowers the pH of the medium and it has been found that, acetic anhydride, maleic anhydride, diglycolic anhydride and glutaral anhydride are also good triggers for self- assembly of a β -naphthol based gelator. Mechanical property of the gel can be tuned by changing the trigger.¹⁸²

Peptide Amphiphiles: Already discussed elaborately into the section “1.3.3. Amino Acids and Peptides Based Supramolecular Architectures and Their Implications” of my thesis.

1.5.2. Various Approach Towards Gelation of Amino Acid/Peptide Based Materials

Theoretical Approach Towards Gelation of Peptides: Non-covalent interactions present in supramolecular assembly of peptides can simply be varied by changing the amino acid sequence. Researchers from different corners of the world have paid considerable attention to figure out the basic structural requirements of peptides that can form gel in a suitable solvent. A peptide should have the criteria to be self-assembled to form a supramolecular network structure. Tuttle and Ulijn have used theoretical tricks to predict gelation ability of a series of peptides.¹⁸³ They have successfully introduced a scoring method for self-assembly measured based on MARTINI force field for bio-molecular simulations. In MARTINI force field, several atoms of a particular peptide or amino acid are considered as a “virtual” bead that interacts through an effective potential. This is an improved version of Coarse Grained simulation which takes care of the polarity, shape, and non-bonded interaction potential of the amino acids, implicitly without going into the structural details.¹⁸⁴ Aggregation propensities of 400 dipeptides were measured and they have been marked as AP score. (Figure 1.27) Peptides with AP score higher than 2 have been subjected for farther scanning. In a latter work the same group have extended the principle for tripeptides. In this context a huge number of peptides (203 = 8000) have been studied with such computational method. By this study a set of design rules that promote aggregation has been described: To attain maximum aggregation propensity score (a) The aromatic amino acid residue should be placed at the 2 or 3 position of the peptide (b) The hydrogen-bonding residues should be placed at position 1 (N-terminus) and (c) negative residues at position 3 (C-terminus). Experimental finding also matches well with the theoretical prediction, unprotected tripeptides with KYF, KYY, KFF and KYW have been found to form hydrogels in absence of any organic solvents.¹⁸³

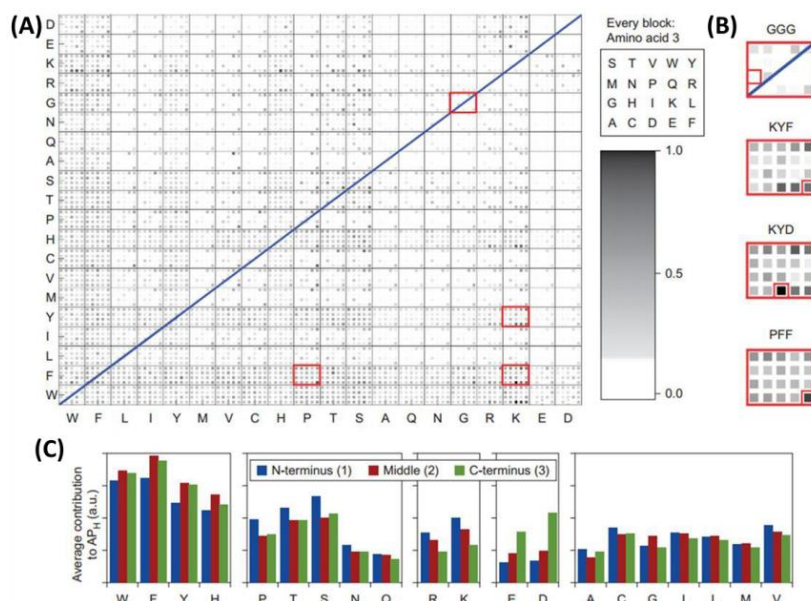


Figure 1.27. From screening to design rules. (A) Normalized APH score for all 8,000 combinations of three amino acids after a 50 ns simulation. Within every rectangle, the third amino acid is represented by the position of the coloured square at the locations indicated in the legend on the right. A darker shade indicates a larger degree of aggregation. An equivalent graph with amino acids 2 and 3 on the x- and y-axes is provided in Supplementary Fig. 3. (B) Expansion of the highlighted areas in a with the four peptide entries indicated. (C) Average APH scores of tripeptides with the specific amino acid on the x-axis in the N-terminal (blue), middle (red) and C-terminal (green) positions. A higher score indicates a higher propensity to aggregate. Amino acids are grouped by aromatic, hydrophilic, cationic, anionic and small/hydrophobic side chains (adapted from, W. J. M. FrederixPim, G. G. Scott, Y. M. Abul-Haija, D. Kalafatovic, C. G. Pappas, N. Javid, N. T. Hunt, R. V. Ulijn, and T. Tuttle, *Nat. Chem.*, 2015, **7**, 30-37).

Enzyme Assisted Gelation: Enzymes are basic molecular catalysts of life. Specific enzyme can be used for removal of a selective group of a peptide and after removal of that particular group that peptide can self-assemble into gel. The enzymes that assist peptide bond cleavage are generally called hydrolase. During the mid of last century it has been found that the hydrolysing protein can act in reverse way under some specific circumstances i.e. they can assist peptide bond formation also. It is still difficult to synthesize natural polypeptides by a chemoenzymatic approach; however, chemoenzymatic synthesis offers a flexible and more specific method for peptide synthesis.¹⁸⁵ Enzymes have recently emerged as tools to achieve this by converting non-assembling peptide precursors into self-assembling building blocks under stable pH, ionic strength and temperature condition. Peptide based systems that are responsive to enzymes can make them useful in biological situations, for example taking advantage of an early enzyme in blood clotting. It may help prevent blood loss, if a liquid can be switched to a gel. Enzyme-assisted

self-assembly can be achieved either by catalysing the synthesis of a self-assembly molecule, or by removing a blocking group from a molecule to facilitate assembly.

Another example of an enzyme assisted self-assembly system is reversed hydrolysis. In that case, a protease was used to drive the self-assembly of peptide hydrogelators via coupling of non-assembling precursors. A range of Fmoc-amino acids and FF or LL were used to synthesise Fmoc-tripeptide derivatives.¹⁸⁶ This method relies on an enzymatic step that is thermodynamically 'up-hill', which is driven thermodynamically by the self-assembly process. It is thought that the fully reversible nature of this method will help prevent formation of kinetic aggregates and favour the thermodynamically stable assembly, thereby paving the way to a self-assembled structure with fewer defects.

There is an example of an enzyme assisted conformational transformation from a O-acyl to N-acyl conversion through a peptide cleavage. In this system a β -sheet forming peptide sequence have been attached to a side chain of serine, threonine or cysteine and a short capping peptide is attached to the amino group. This capping peptide is designed to be cleaved off by a specific protease. Once this occurs, a chemical rearrangement happens that repositions the desired peptide chain onto the amino group leaving the normal serine, threonine or cysteine side chain present. Due to this chemical rearrangement after the action of the protease the process is irreversible.¹⁸⁷ A reversible system using two enzymes that catalyse opposite reactions (phosphorylation/dephosphorylation) was demonstrated to control the gel-sol transition of a peptide in a highly controlled manner. The peptide used is naphthalene linked to FFGEY, this peptide is a gel in water (Figure 1.28), in the presence of adenosine triphosphate, kinase adds a phosphate group to the tyrosine residue, resulting in a transition to a solution. The further addition of a phosphatase results in the removal of the phosphate and to trigger gelation.¹⁸⁸ The use of enzymes in self-assembly (Figure 1.29) adds a level of control over the self-assembly process and is therefore expected to play a key role in the future development of more complex structures with fewer defects.

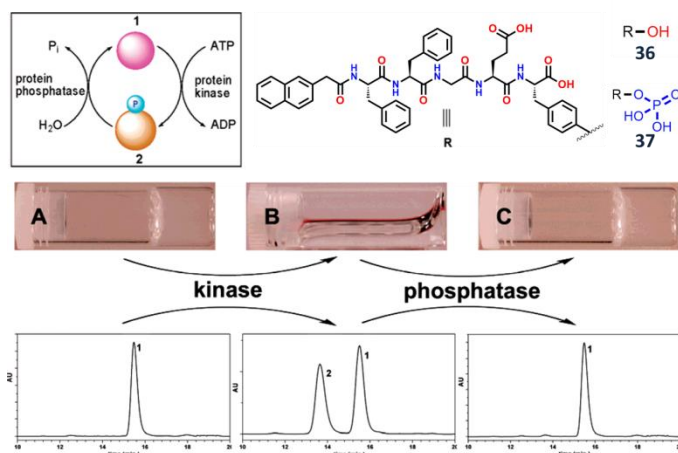


Figure 1.28. Reversible modification of the subunits of a gel by a phosphatase/kinase reaction where the addition of a phosphate group to the tyrosine of the molecule causes the gel to disassemble, addition of a phosphatase removes the phosphate group and triggers gelation again (adapted from, Z. M. Yang, G. L. Liang, L. Wang and B. Xu, *J. Am. Chem. Soc.*, 2006, **128**, 3038-3043).

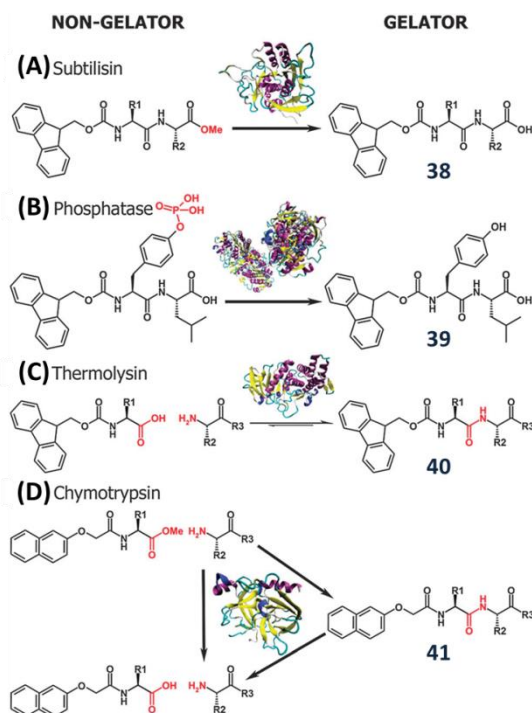


Figure 1.29. Summary of reported enzyme responsive hydrogelation examples including: (A) subtilisin methyl ester cleavage; (B) phosphatase phosphate cleavage; (C) thermolysin amide bond cleavage and (D) chymotrypsin non-equilibrium (temporary) assembly (adapted from, S. Fleming and R. V. Ulijn, *Chem. Soc. Rev.*, 2014, **43**, 8150-8177).

Metal Assisted Gelation: Metals are good candidates for triggering self-assembly process of peptides. Ghadiri and co-workers have designed and developed a 15-residue amphiphilic peptide with a 2,2'-bipyridine functionality at the N-terminus and it has been shown to undergo spontaneous self-assembly, in the presence of transition metal ions, to

form a 45-residue triple-helical coiled-coil metalloprotein.¹⁸⁹ Similarly, a number of techniques have been developed to make peptide based metal ion assisted gel. Recently, Xu and co-workers have reported that a tripeptide derivative (A) (Figure 1.31), that was a versatile self-assembly motif and it forms hydrogel.¹⁹⁰ Incorporation of the bipyridine motif into the hydrogelator formed compound (B) which has the lack of ability to form hydrogel. Surprisingly, compound (B) formed nanofibers with a ruthenium-(II)tris(bipyridine) complex (C) (Figure 1.30) that leads to a hydrogel.¹⁹¹ The ruthenium complex offers a geometrical control to prearrange the peptide prior to the self-assembly. This metallo-hydrogelator not only formed a hydrogel but also exhibits gel-sol transition upon oxidation of the metal centre. The metal complex imparted optical, electronic, redox, or magnetic properties to supramolecular hydrogels.

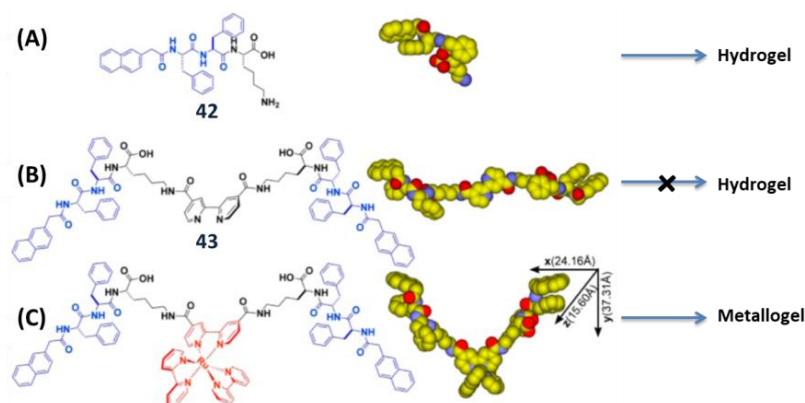


Figure 1.30. Incorporation of metal ion binding motif into peptide to form redox responsive metallogel (adapted from, Y. Gao, Y. Kuang, Z. -F. Guo, Z. Guo, I. J. Krauss and B. Xu, *J. Am. Chem. Soc.*, 2009, **131**, 13576–13577; Y. Zhang, B. Zhang, Y. Kuang, Y. Gao, J. Shi, X. X. Zhang, and B. Xu, *J. Am. Chem. Soc.*, 2013, **135**, 5008–5011).

Peptide Amphiphiles on Metal Assisted Gelation: Banerjee and co-workers has reported a series of amphiphilic tyrosine based self-healable, multi-stimuli responsive metallo-hydrogels. Formation of these hydrogels is highly selective to Ni^{2+} ions. (Figure 1.31) The self-healing property and the stiffness of these metallo-hydrogels can be tuned by varying the chain length of the corresponding gelator amphiphile.¹⁹²

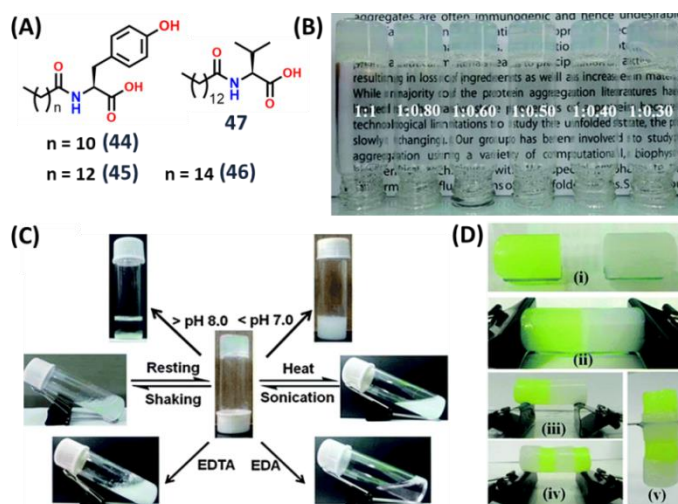


Figure 1.31. (A) Chemical structures of various amphiphiles (**44–47**). (B) Pictures of glass vials containing metallo-hydrogels obtained from different proportions of the gelator **46** and nickel salt (NiCl₂). (C) Multi-stimuli responsiveness shown by the hydrogel obtained from **46**. (D) Illustration of self-healing behavior (i–v) shown by the metallo-hydrogel obtained from **46** (adapted from, S. Basak, J. Nanda and A. Banerjee, *Chem. Commun.*, 2014, **50**, 2356-2359).

1.6. Amino Acids and Peptides as Functional Bio-materials

Increased understanding of protein functions from cell biology and structural biology leads to considerable efforts on the incorporation of peptide epitopes as the functional motifs on supramolecular hydrogelators for a wide range of biological applications.^{193,194} These endeavors also stimulated the quest for determination of the protein targets of supramolecular hydrogels.^{195,196}

Stupp and his research group has disclosed a number of reports on peptide amphiphiles as promising materials for biomedical applications.^{50,71} Scaffold materials derived from self-assembled nanofibers support cells and on derivatization with bioactive ligands or epitopes, can signal cells for differentiation.¹⁹⁷ In vivo studies have revealed the potential of bioactive supports in spinal cord injury,¹⁹⁸ the formation of blood vessels,¹⁹⁹ and regeneration of bone^{200,201} and cartilage.²⁰² β -Sheet oligopeptide-directed nanofibers have also been reported as efficient scaffolds for RNA and DNA complexation and gene transfer.²⁰³⁻²⁰⁵ As research on self-assembly of supramolecular polymers continues to unravel newer strategies day by day, the community has grown quickly in realizing that molecular self-assembly is a viable

nanotechnological route to create supramolecular biomaterials via a 'bottom-up' approach.⁵⁰

Hydrogels in general, are excellent materials for biomedical applications as most of the requirement for a good biomaterial like multiple functionalities of a hydrogel network and dynamic interactions between the surrounding matrixes and cells are fulfilled by the hydrogels. It has found applications in inhibition or selective binding of cancer cells,^{206,207} 3D cellculture^{208,209} or in cell adhesion to hydrogel matrix.^{210,211} The hydrogels' range of utility covers its use as a platform for chemosensor,²¹² biosensor like detection and inhibition of bacteria²¹³ or as a dye absorbing agent that can absorb toxic dyes from polluted water.²¹⁴

As one of the objectives of this thesis work is to search for new peptide based hydrogels for antibacterial activity (chapter 4), we will now give a brief review on this topic.

1.6.1. Amino Acid and Peptide Based Hydrogels for Antibacterial Activity

Infectious disease remains a major threat to public health, and new antimicrobial agents is an utmost priority to fight against the multi-drug resistant bacteria. The discovery of antimicrobial peptides has stimulated the use of self-assembly of peptide amphiphiles to develop antibacterial hydrogels.

Schneider, Pochan and their co-workers reported a series of β -sheet peptide-based hydrogels,²¹⁵ among which the surface of **48** (Figure 1.32) is inherently antibacterial and exhibits broad-spectrum activity against both Gram-negative (*Klebsiella pneumonia* and *E. coli*) and Gram-positive (*Staphylococcus epidermidis*, *Staphylococcus aureus* and *Streptococcus pyogenes*) bacteria without incorporating exogenous antimicrobial agents. Using the LIVE/DEAD assays by laser scanning confocal microscopy (LSCM), they found that the surface of the hydrogel of 2% (w/v) **48** displays broad-spectrum antibacterial activity when incubated with bacterial solutions. On the basis of the β -galactosidase leakage experiments, they suggested that the surface of the **48** hydrogel likely causes inner and outer membrane disruption and controls the release of β -galactosidase from the cytoplasm of lactose permease-

deficient *E. coli* ML-35, resulting in cell death upon cellular contact with the surface of the hydrogel.²¹⁵ Laverty *et al.* reported a series of cationic, naphthalene derivatized self-assembling ultrashort peptides, among which the peptide, 2-Naphthyl-FFKK self-assembles to form hydrogels with a β -sheet structure at a concentration of 1% (w/v) and pH of 7.4 in water. The authors found that the hydrogel at 2% (w/v) significantly reduces the viable *S. epidermidis* biofilm by 94% while exhibiting little haemolytic side effect towards human red blood cells (hRBCs) and murine fibroblast (NCTC 929) cell lines, thereby indicating the hydrogel's biocompatibility.²¹⁶ Das and his group designed and synthesized several dipeptide-based cationic amphiphiles with different head group structures by varying the combinations of L-amino acid residues. Among all the dipeptide derivatives, **49** (Figure 1.32) inhibits the growth of several Gram-positive (MIC = 0.1–0.5 $\mu\text{g/mL}$) and Gram-negative (MIC = 5–10 $\mu\text{g/mL}$) bacteria as well as fungi (MIC = 1–5 $\mu\text{g/mL}$). Moreover, the authors reported that **49** is compatible with different mammalian cell lines such as Hep G2, HeLa, and SiHa.²¹⁷

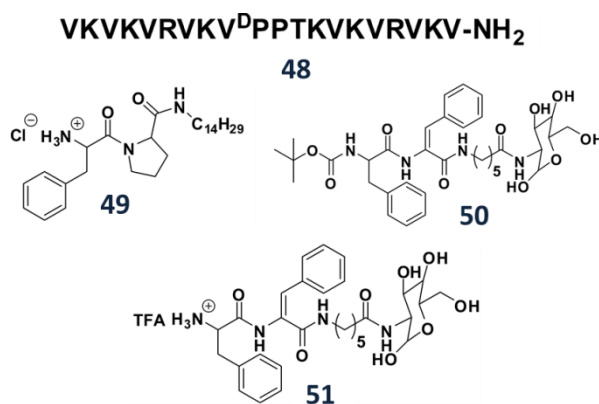


Figure 1.32. Chemical structures of some peptide based antibacterial hydrogelators (**48–51**) (adapted from, X. Du, J. Zhou, J. Shi and B. Xu, *Chem. Rev.*, 2015, **115**, 13165–13307).

Sharma *et al.* synthesized two self-assembled amphiphilic α , β -dehydrophenylalanine-containing small glyco-dehydropeptides, **50** and **51** (Figure 1.32), with glucosamine attached at the C-terminal through a 6-aminocaproic acid linker. The authors observed that **50** and **51** give hydrogels in methanol-water mixture at 0.1% (w/v). The authors used a disk diffusion assay to test the antimicrobial activity of the peptides **50** and **51**, and found that the peptides display antimicrobial activity against *Micrococcus flavus*, *Bacillus subtilis*, and *P. aeruginosa*.¹⁷¹

Yang, Yi and co-workers designed and synthesized a unique hydrogelator **52** (Figure 1.33) based on (–)-menthol and a lysine that self-assembles to form an opaque hydrogel at 0.83% (w/v) concentration. Interestingly, the hydrogelators form the 3D multiporous networks through acid–base interactions and strong double hydrogen bonding between amino acids for encapsulating some known antibacterial agents such as Zn^{2+} and a series of water-soluble organic antibiotic medicines such as lincomycin, amoxicillin etc. The authors found that the antimicrobial susceptibility of the hydrogels loaded with Zn^{2+} or lincomycin was much more effective than that of the corresponding aqueous solution when they were incubated with *E. coli* and *S. epidermidis*. Moreover, the **52** hydrogel is innocuous to mammalian HeLa cells thus enhancing its applicability as a

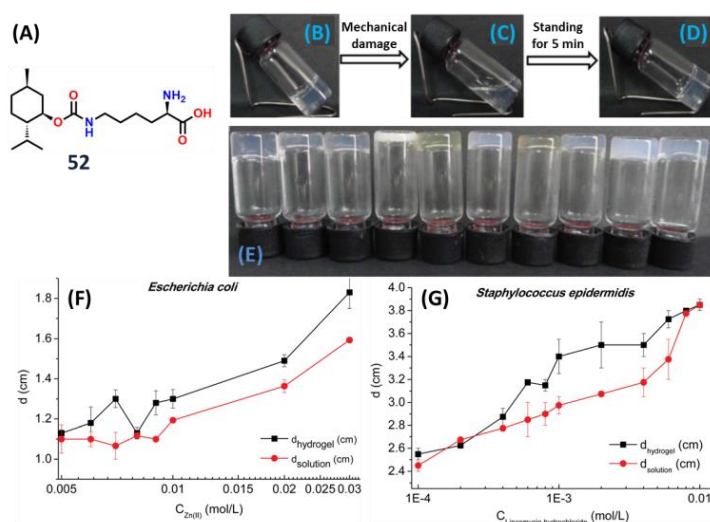


Figure 1.33. (A) Chemical structure of the hydrogelator **52**. (B–D) The self-repairing phenomenon of hydrogel **52** (B, original gel; C, after mechanical damage and D, following 5 min standing at room temperature). (E) The pictures of the hydrogels with different antibiotics, from left to right, **52**, **52** + Zn^{2+} , **52** + lincomycin, **52** + streptomycin sulphate, **52** + amoxicillin, **52** + penicillin sodium (800,000 IU), **52** + ceftiofur sodium, **52** + vancomycin hydrochloride, **52** + kanamycin, **52** + ampicillin, respectively. The concentrations of **52** for the hydrogel are 1.9% for pure **52**, 3.25% for **52** + Zn^{2+} and **52** + lincomycin, 2.3% for the others. The concentrations are 0.001 M for lincomycin and 0.01 M for the others. The changes on the bacteriostatic circle diameter with addition of (F) Zn^{2+} in different concentrations from 0.005 to 0.03 M, and (g) lincomycin hydrochloride in different concentrations from 0.0001 to 0.01 M in hydrogel of **52** and aqueous solution (adapted from, Y. Li, F. Zhou, Y. Wen, K. Liu, L. Chen, Y. Mao, S. Yang and T. Yi, *Soft Matter*, 2014, **10**, 3077–3085).

universal antibacterial carrier (Figure 1.33).²¹⁸ Chen and Li *et al.* reported the preparation of biocompatible hydrogels with antimicrobial activity against Gram-positive bacteria by taking advantage of the intermolecular aromatic–aromatic interactions of Fmoc and the phenyl group. They

generated a hydrogel based on the co-assembly of Fmoc-Phe and Fmoc-Leu and found that the co-assembled (Fmoc-Phe + Fmoc-Leu) supramolecular hydrogel is bactericidal against Gram-positive bacteria via a mechanism involving cell wall and membrane disruption (Figure 34). As the hydrogel is biocompatible with normal mammalian cells, the authors suggested that this type of antibacterial hydrogel can potentially serve as an antimicrobial coating in clinical devices and wound dressings or a topical agent for the treatment of clinical skin and wound infections mainly caused by Gram-positive bacteria such as *S. aureus*.²¹⁹

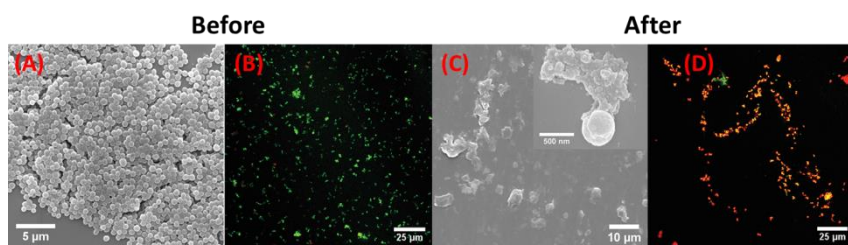


Figure 1.34. (A and C) Representative SEM images and (B and D) overlapping fluorescence images for the LIVE/DEAD bacterial staining assay of *S. aureus* before and after contact with the co-assembled (Fmoc-Phe + Fmoc-Leu) hydrogel for 2 h. Two fluorescent dyes were used in LIVE/DEAD staining in which SYTO 9 with green color labeled both live and dead bacteria while propidium iodide with red color stained only dead bacteria. Adapted from, I. Irwansyah, Y.-Q. Li, W. Shi, D. Qi, W. R. Leow, M. B. Y. Tang, S. Li and X. Chen, *Adv. Mater.*, 2015, **27**, 648–654).

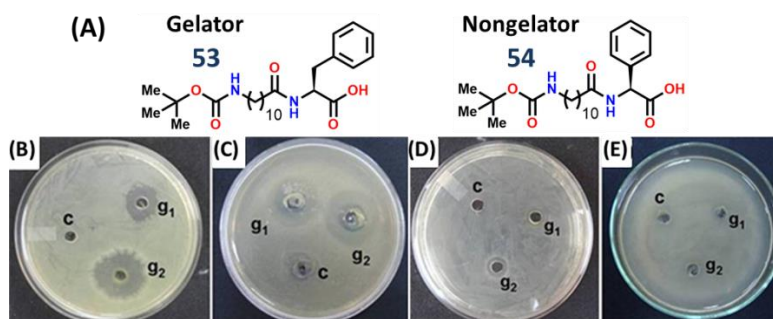


Figure 1.35. (A) Chemical structures of the peptides 53 and 54. (B-D) Determination of the effect of hydrogel on Gram-negative and Gram-positive bacteria by agar-diffusion assay method of various bacteria: (B) *Escherichia coli*, (C) *Pseudomonas aeruginosa*, (D) *Staphylococcus aureus*, and (E) *Bacillus subtilis* were spread on an Agar plate. In each case, two different amounts of 1% (w/v) 53 hydrogel (g1 (10 μ L/well) and g2 (20 μ L/well)) were added to the wells (adapted from, A. Baral, S. Roy, S. Ghosh, D. Hermida-Merino, I. W. Hamley and A. Banerjee, *Langmuir*, 2016, **32**, 1836–1845).

Baral *et al.* reported that an N-Boc protected dipeptide **53** (Figure 1.35) shows remarkable antibacterial activity towards Gram-negative bacteria *E. coli* and *P. aeruginosa*. It is also observed that a simple change in the gelator molecule **53** turns the gelator molecule into a nongelator molecule

54 (Figure 1.35) which also shows a negative impact on the Gram-negative bacteria *E. coli* and *P. aeruginosa*.²²⁰

Banerjee and co-workers also reported a series of single amino acid based amphiphilic hydrogelators **55–59** (Figure 1.36). The variation of the long chain at the N-terminal position shows that gelators **58** and **59** with the higher long chains show highly antibacterial activity against Gram-positive bacteria *S. aureus*, *B. subtilis*, and Gram-negative bacteria *Escherichia coli* (Figure 1.36). The hemolysis study shows that at the minimum inhibitory concentration (MIC) almost nonsignificant or very little hemolysis was observed for human erythrocyte cells.²²¹

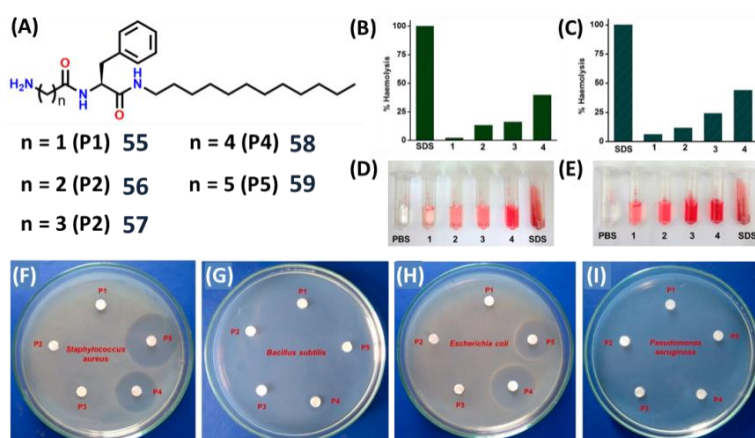


Figure 1.36. (A) Molecular structures of amino acid based gelator amphiphiles **55** to **59**. (B and C) Dose–response plot for the hemolysis of human red blood cells by hydrogels formed by gelator **58** and **59**. (D and E) Dose–response images for the hemolysis of human red blood cells by hydrogel formed by gelator **58** and **59** respectively. Concentrations of the hydrogels: (1) 50, (2) 100, (3) 200, and (4) 500 µg/mL. (F–I) Effect of hydrogel on Gram-positive and Gram-negative bacteria (F) *S. aureus*, (G) *B. subtilis*, (H) *E. coli*, and (I) *P. aeruginosa* by agar-diffusion assay method keeping concentration of the hydrogelators 500 µg/mL for all cases (adapted from, N. Nandi, K. Gayen, S. Ghosh, D. Bhunia, S. Kirkham, S. K. Sen, S. Ghosh, I. W. Hamley and A. Banerjee, *Biomacromolecules*, 2017, **18**, 3621–3629).

Antimicrobial hydrogels are excellent materials for use as fillers or wound dressings. As hydrogels are very rich in water content, it provides a moist and heavily hydrated environment to the wound area. This hydrated environment facilitates cellular immunological activity crucial to the wound healing process. However, the hydrated environment of the hydrogel is also able to promote microbial infection. Thus, hydrogels having an antimicrobial activity to serve their primary functional role such as wound healing, drug delivery, etc. are desirable.

Apart from the antibacterial study, there are other biological applications of the low molecular weight gelators. Some of the biological applications will be given into the next topic of introduction.

1.6.2. Amino Acid and Peptide Based Hydrogel in Drug Delivery

Several interesting architectures from amino acid and peptide based self-assembled molecules can be utilized for drug delivery applications. One of them is vesicles. Vesicles can be considered to be an important delivery vehicle to carry drugs and other bioactive molecules inside cells. Vesicles offer interesting functions including encapsulation and sustained release of drugs and other biologically important molecules.^{222,223} Pramanik and co-workers developed a set of molecules that includes isolucine, γ -amino butyric acid and proline based nanovesicles that can encapsulate dye molecules which can be released by the addition of an acid.²²⁴ Verma and co-workers designed a dihistidine conjugate which self-assemble to form nanospheres that interact with ATP to form doughnut shaped microspheres. This can be used for transport of small molecules, as they disintegrate upon exposure to cations that can be used as a delivery vehicle for transport of small molecules, as they disintegrate upon exposure to cations.²²⁵

Apart from nanovesicles, supramolecular hydrogels are one of the most important drug delivery systems because the majority of the volume of supramolecular hydrogels is micropores filled with water. These interstices allow the hydrogels to serve as a carrier or medium for other bioactive molecules.²²⁶⁻²²⁸ These molecules can be delivered by the hydrogels at desired sites of human (or other animal) body for drug delivery applications.²²⁹⁻²³¹

Das and co-workers reported ten structurally correlated amino acid-based amphiphiles for screening hydrogelators, and found three of them to confer pH-responsive hydrogels at room temperature. The hydrogel **60** (Figure 1.37), with an MGC of 4% (w/v), exhibits remarkable sensitivity to pH, which makes the hydrogels suitable for the release of vitamin B₁₂ and cytochrome c. The authors found that, at pH 7.4, all three hydrogelators form suitable hydrogels to release the entrapped biomolecules via diffusion. At endosomal pH (~5.5) or a further lower

pH, the release rate of biomolecules from the hydrogel of **552** increases by about 10-fold compared to that observed at pH 7.4, largely due to the dissociation of the gels.²³² Schneider and Pochan have designed a class of self-assembling peptides that undergo triggered hydrogelation in response to physiological pH and in salt conditions (pH 7.4, 150 mM NaCl) to form mechanically rigid, viscoelastic hydrogels.²²⁹ Among the β -hairpin peptides, **62** (Figure 1.32) and **61** (Figure 1.37) are two peptide sequences with different charge states for directly encapsulating and controllably releasing model fluorescein isothiocyanate (FITC)-dextran macromolecules of varying size and hydrodynamic diameters.²³³ The authors also reported that the mobility of the macromolecules or the probes within and release of these hydrogels depended on the sizes of the probes, the peptide sequences, and the mesh size of the hydrogel.²³⁴

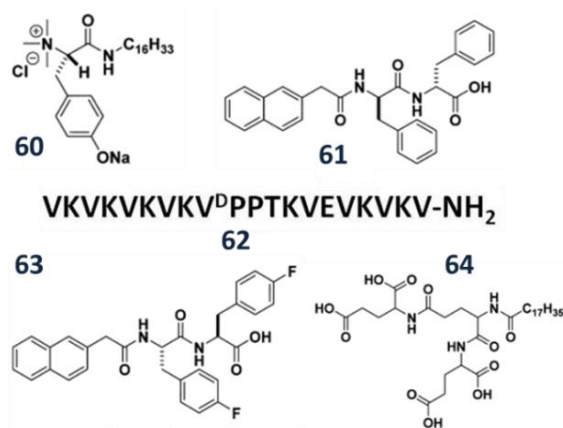


Figure 1.37. Chemical structures of some peptide based hydrogelators that can encapsulate drugs (adapted from, X. Du, J. Zhou, J. Shi and B. Xu, *Chem. Rev.*, 2015, **115**, 13165–13307).

Xu *et al.* reported the first *in vivo* imaging for investigating the drug release properties of the supramolecular hydrogel formed by hydrogelators **62** and **63** (Figure 1.37) consisting of naphthalene (Nap) and a D-peptide of diphenylalanine. The incorporation of D-peptide ensures that the hydrogels resist hydrolysis catalyzed by proteinase K and offer long-term biostability. This makes the **63** hydrogel suitable for controlled release of drugs *in vivo*.¹⁹

Adams *et al.* reported the hydrogels of Fmoc-Phe and Fmoc-Tyr formed hydrogel after adjusting the pH of the solution using GdL. They found that the hydrogels of Fmoc-Phe and Fmoc-Tyr entrap and release certain dye molecules under the control of Fickian diffusion. Interestingly, on the

basis of the similar diffusion coefficients of the dyes of different radii from the hydrogel of Fmoc-Phe, the authors concluded that the networks in the hydrogel of Fmoc-Phe only restrict molecules larger than 5 nm.²³⁵

Liu and co-workers designed a supramolecular hydrogel based on a peptide Dendron **64** (Figure 1.37) and found that metal ions can trigger a continuous shrinkage after the gels have been annealed for several hours. It is reported that the metal ions (e.g., Mg^{2+} , Cu^{2+}) significantly promote the gelation capacity, and decrease the MGC from 0.3 to 0.08% (w/v) or below. In addition, the reversible shrinkage property of the hydrogels allows the controlled release of small molecules such as vitamin B₁ after addition of divalent metal ions like Mg^{2+} into the gel.^{236,237}

Our group has reported two N-terminally protected β -amino acid containing dipeptides (**65** and **66** (Figure 1.38)) with that form hydrogels at physiological pH (7.46) and temperature (37 °C). The hydrogels having nanofibrillar network, can encapsulate and sustainably release vitamin B₂ and vitamin B₁₂ over 3 days.³³ The same group has also reported two synthetic self-assembling tetrapeptides GAIL and GFIL, that form thermoreversible and pH-sensitive hydrogels consisting of long, interconnected nanofibrillar network with fiber diameters of 15–30 and 10–25 nm, respectively. These hydrogels entrap doxorubicin to allow its slow release at physiological pH, and achieve almost 85% (for GAIL) and 90% (for GFIL) release of the drug molecules after 45 h (Figure 1.38).¹³⁷

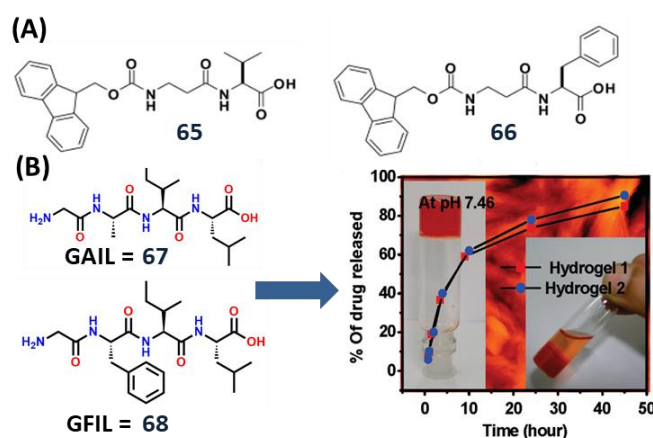


Figure 1.38. (A) Chemical structures of the hydrogelators **65** and **66** (adapted from, J. Nanda and A. Banerjee, *Soft Matter*, 2012, **8**, 3380–3386). (B) Hydrogelators GAIL and GFIL and release of the anticancer drug doxorubicin from the corresponding self-supporting hydrogels (adapted from, J. Naskar, G. Palui and A. Banerjee, *J. Phys. Chem. B*, 2009, **113**, 11787–11792).

1.6.3. Amino Acid and Peptide Based Hydrogels in Tissue Engineering

It is not hard to realize that we are primarily constructed of soft tissues. Because of the remarkable similarity between hydrogels and soft tissues, supramolecular hydrogels are excellent materials in tissue engineering.²³⁸⁻²⁴³ Over the past two decades, hydrogels have been used as the most common scaffolds in tissue engineering due to their ability to maintain a distinct 3D structure. This provides mechanical support for the cells in tissue engineering. The hydrogel is very high in water content. So, it can deliver an ideal environment for cell survival. Hydrogel systems have been serving as a supportive matrix for cell immobilization and growth factor delivery.

Li and co-workers developed an N-terminal protected short peptide derivative containing halogenated phenylalanine and reported that the presence of halogenated peptide exhibits better gelation properties than the gelator Fmoc-Phe in aqueous solutions.²⁴⁴ They found that the fluorinated gelator Fmoc-4-fluorophenylalanine is the most efficient gelator than Fmoc-Phe that gels PBS buffer solution at an MGC of 0.15 wt %. Based on this observation, the authors designed and synthesized a Fmoc-peptide **69** (Figure 1.39) and utilized the peptidic hydrogel to culture NIH/3T3 cells. The authors reported that the 20% DMSO containing co-solvent induced hydrogel could efficiently stimulate the adhesion and proliferation of NIH/3T3 cells.²⁴⁴

Tirrell and co-workers reported a peptide amphiphile (**70**) that forms a hydrogel upon changing the pH from acidic to neutral. The hydrogel can achieve a storage modulus of 10 kPa at a 1% (w/v) of gelator **70**. The viscoelastic properties of the hydrogels can be regulated by modulating the concentration of gelator **70**. This broadens their versatility for complying with the mechanical requirement of a wide range of tissues. The authors examined the culture of NIH/3T3 fibroblast cells on the hydrogel formed by the gelators **70** for evaluating the biocompatibility of the hydrogel (Figure 1.39).²⁴⁵

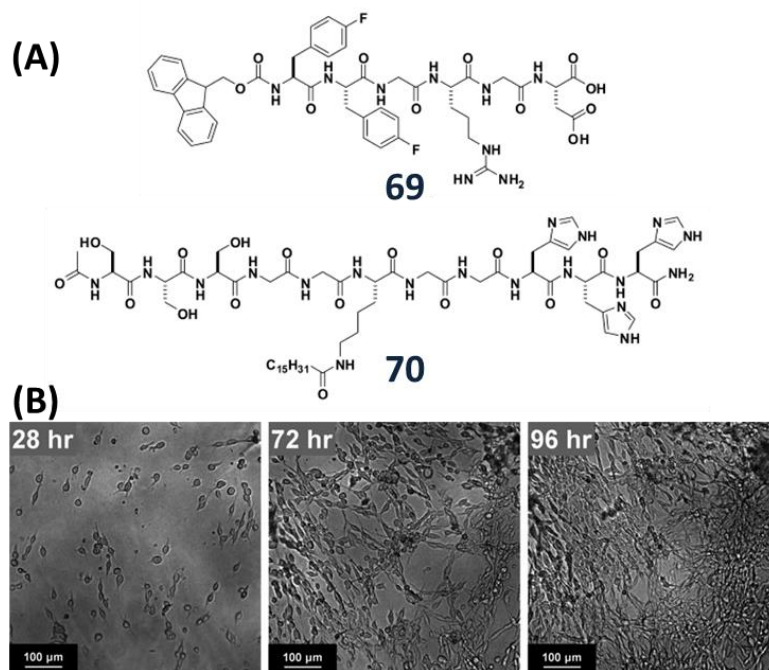


Figure 1.39. (A) Chemical structures of some peptide based hydrogelators **69** and **70** that can be used in tissue engineering (adapted from, X. Du, J. Zhou, J. Shi and B. Xu, *Chem. Rev.*, 2015, **115**, 13165–13307). (B) Nanofibrous hydrogels formed by gelator **70** were compatible with NIH 3T3 fibroblasts. In the presence of serum, fibroblasts spread by 28 hours. At 72 hours, spreading appeared to be spindle-like, resembling the natural morphology of the cell type. The fibroblasts proliferated for a minimum of 96 hours. These images are from a single hydrogel (adapted from, B. F. Lin, K. A. Megley, N. Viswanathan, D. V. Krogstad, L. B. Drews, M. J. Kade, Y. Qian and M. V. Tirrell, *J. Mater. Chem.*, 2012, **22**, 19447–19454).

Luis *et al.* reported that octapeptide **71** (Figure 1.40), which can make a biodegradable 3D scaffold to aid the regeneration of bone tissues.²⁴⁶ The 3D scaffold formed by the self-assembly of octapeptide **71**, can produce a profitable microenvironment for homogeneous cell distribution and uphold the cell viability of human mesenchymal stem cells (hMSCs). A considerable population of hMSCs stayed alive for over 12 days (Figure 1.40), and clear *in vitro* extracellular matrix (ECM) production (collagen-1, alkaline phosphatase, osteocalcin) was observed within this scaffold, suggesting successful bone formation. Being a simple composition, low cost, and good *in vivo* performance of the hydrogel formed by the gelator **71**, this system can be a profitable bone engineering material for translation into clinical usefulness.^{246,247} Yao *et al.* further utilize this peptide (**71**) hydrogel as a coating on polycaprolactone (PCL) scaffolds for demonstrating the advancement of dual regeneration of articular cartilage and subchondral bone together.²⁴⁸

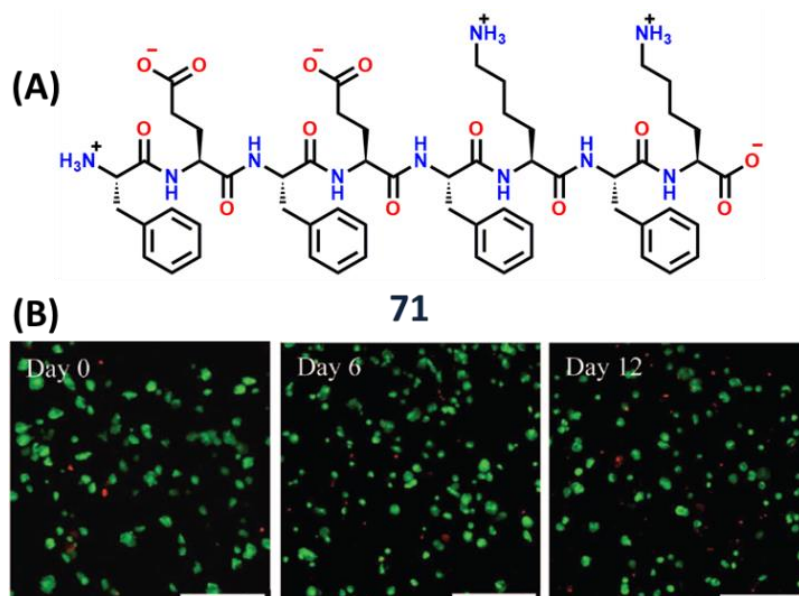


Figure 1.40. (A) Chemical structures of gelator peptide **71** and, (B) Live/dead assay showing viable (green) and non-viable (red) hMSCs within the **71** gel over 12 days of cell culture. Magnification = 20 \times . Scale bars = 250 μ m (adapted from, L. A. Castillo Diaz, M. Elsaywy, A. Saiani, J. E. Gough, A. F. Miller, *J. Tissue Eng.*, 2016, **7**, 1–15).

The slow progress in the field of “tissue engineering” is due to the complexity of the biological process. Also, most of the short peptide-based supramolecular hydrogels consist of only one or two amino acid residues which limit their roles in the biological process. Despite these challenges scientists throughout the world are working in this field to meet the challenges ahead. One of the most common challenges is the healing of wounded tissue in the field of tissue engineering, as the invasion of microorganisms can infect the wounded tissues, especially in diabetic wounds.

Apart from the biological applications, peptide-based hydrogel can be used in other fields of research work as well. As one of my research work is related to peptide based gel in environmental remediation (chapter 3), I will give a brief description on this topic. However, it is very difficult to discuss every detail of the applications of amino acid/peptide-based soft materials in this short introduction section of my thesis. But some of them will be discussed in the later section of my thesis introduction.

1.7. Peptide or Amino Acids Based Gels in Environmental Remediation

The current industrial world produces millions of tons of heavy metals, dyes, pharmaceuticals, petroleum products, pesticides, and fertilizer wastes daily. The resulting impacts have seriously impaired global environmental water quality. When these pollutants are discharged as untreated effluent into rivers, lakes, and oceans, they affect aquatic life and the food chain and also predispose people to health-related problems, including vomiting, cancer, neurological damage, liver failure, and cognitive dysfunction. As such, both biological and physicochemical methods have been devised to combat with water pollution. Generally, the dissolved organic/inorganic pollutants are adsorbed onto solid materials. The process has a few advantages: simplicity, ease of operation and handling, regeneration, near-complete removal of pollutants, and economic feasibility.^{249, 250} The use of commercial activated carbon and other non-conventional adsorbents such as zeolites, chitosans, mineral clays, sawdust, and waste biomatter to remove dyes and heavy metals from water is common practice. However, they have a few drawbacks like lack of selectivity, generation of large amounts of toxic sludge, low pollutant uptake, and costly regeneration processes. This means there is still significant interest in developing innovative materials with applications in environmental remediation.

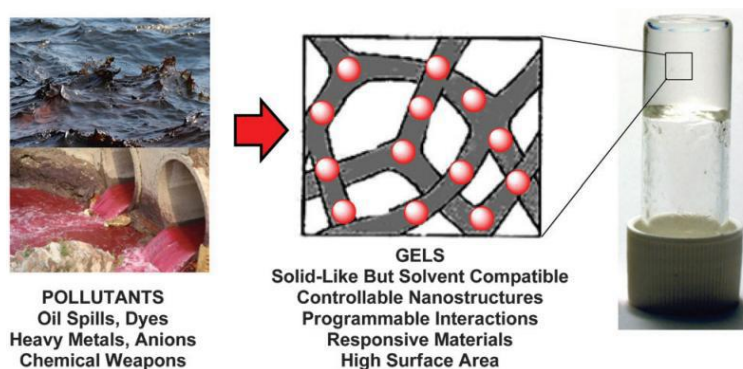


Figure 1.41. Self-assembled gel-phase soft materials for environmental remediation (adapted from, B. O. Okesola and D. K. Smith, *Chem. Soc. Rev.*, 2016, **45**, 4226–4251).

Gels are colloidal soft matter systems, usually consisting of a sample-spanning nanoscale (or sometimes microscale) solid-like network within a liquid-like medium. The gels exhibit viscoelastic behavior, which

means they have elasticity like solid, and under a definite amount of strain, they exhibit viscosity like a fluid. As such, they can potentially be manipulated as solids while simultaneously bringing their structuring into intimate contact with liquid environmental phases, maintaining high surface areas and rapid internal diffusion kinetics. Clearly, nano-structured gels would be preferential to microstructured gels in this regard. The low cost and biocompatibility make the gel a very good candidate for environmental remediation (Figure 1.41).

1.7.1. Removal of Toxic Organic Dyes

Dyes are not only valuable for the textile industry but also in paints, plastics, rubbers, printing, drugs, food, paper, and cosmetics. Most dyes are non-biodegradable, with significant discharges into the aquatic environment.²⁵¹ Even at low concentrations, dyes have harmful effects on environmental quality, as they have potential toxic effects. Therefore, eliminating dyes from the ecological biosphere is an important goal. Unlike remediation of oil spills, where the pollutant becomes the solvent phase of an organogel, in this case, the pollutant dyes will be typically dissolved in water, which should be removed. Gels based on LMWGs can be easily made and modified; their high nanoscale surface areas are the potential for direct interactions with solvated dyes, while their reversibility and responsiveness give the potential for recycling and reuse. They are highly solvent compatible, allowing effective contact between the polluted aqueous phase and the self-assembled nanofibres. Furthermore, they can be applied either in the solvated state (as gels) or in the dried state (as xerogels), leaving the inherent gel-phase nanostructuring intact. Gels are often amphiphilic, and this also assists them in forming interactions with dye molecules.²⁵²

In one of the earliest reports of amino acid-based gel for dye removal, in 2007, Banerjee and co-workers reported the synthesis of phenylalanine-based bolaamphiphilic hydrogelator **72** (Figure 1.42) that formed hydrogels in the presence of divalent metals within the physiological pH range (6.5–7.2).²¹⁴ The dried metallated xerogels demonstrated some uptake of crystal violet (a cationic dye), naphthol blue black (an anionic

dye), and pyrene (a non-ionic dye). Ionic dyes were taken up more effectively than non-ionic, and the maximum uptake was 84 mg g^{-1} . Although the pH range in which gels formed was somewhat limited, this study was a significant pioneering step into the field. Furthermore, pH variation enabled the conversion of the gels into a precipitate or a sol (at low and high pH, respectively), and was used to demonstrate controlled entrapment and release of a biological molecule, vitamin B₁₂, suggesting further scope for controlled pollutant uptake and drug release.²¹⁴



Figure 1.42. Chemical structure of phenylalanine-based Bola **1** which forms hydrogels in the presence of divalent metals, and a photograph of copper(II)-modified xerogelator removing crystal violet from aqueous solution (adapted from, S. Ray, A. K. Das and A. Banerjee, *Chem. Mater.*, 2007, **19**, 1633–1639).

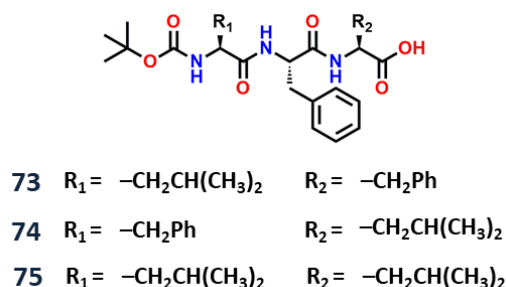


Figure 1.43. Structures of phenylalanine-based tripeptide gelators (adapted from, B. Adhikari, G. Palui and A. Banerjee, *Soft Matter*, 2009, **5**, 3452–3460).

A family of dipeptide organogelators which selectively gelled aromatic organic solvents in the presence of water was reported by Das and co-workers.²⁵³ A library of tripeptide-based hydrogelators **73–75** (Figure 1.43) was reported by Banerjee and co-workers, and in this case, the ability of their wet hydrogels to capture and remove rhodamine B, reactive blue 4, and direct red 80 from the water were studied.²⁵⁴ Unlike the pH-responsive metallo-hydrogels reported earlier by these authors,²¹⁴ the tripeptides formed thermoreversible hydrogels at basic pH values (11.5–13.5). Below pH 11.5 the gelators were insoluble. The hydrogels of gelator **74** demonstrated some removal of the dyes from water over extended periods. The spent gelators could be regenerated by drop wise

addition of 1 (M) HCl, with the peptides precipitating out at pH 7.5, leaving behind the organic dyes in the aqueous medium; the gelator was then filtered off, repeatedly washed with deionized water, and dried. Although somewhat complex, this demonstrates some potential for recyclability and subsequent reuse.

1.7.2. Removal of Toxic Metal Ions

Heavy metal ions are a problem for water bodies due to their ability to bind to biomolecules and modify/prevent their normal modes of action, leading to significant toxicity. Cd, Pb, Hg, etc., are highly toxic to the environment. The industries release these toxic metals and steadily come into the ecosystem and cause various diseases. We know the miserable instants of Minamata and Itai-itai.

Schneider and co-workers designed a metal-binding hairpin peptide (VKVKVKV-CGPKECVKVKVKV-NH₂) which was capable of forming hydrogel on complexation with monomethyl arsenous acid (MMA), ZnCl₂, CdCl₂, HgCl₂ or Pb(NO₃)₂.²⁵⁵ The addition of stoichiometric amounts of metal ion to the peptide solution leads to metal coordination, and this yielded an amphiphilic β -hairpin that then self-assembled into rigid self-supporting hydrogels. Self-assembly is therefore predicated on the folding of the peptide triggered by the chelation of heavy metal ion to the two free cysteinyl thiols flanking the β -turn. Circular dichroism and mass spectrometry were used to confirm 1 : 1 metal-peptide stoichiometry and TEM imaging showed that the hydrogels formed in the presence of MMA and Zn²⁺ are composed of elongated, and twisted fibrils with high-order laminates. This is a very elegant approach to metal-triggered self-assembly. Still, given this peptide's laborious processes and synthetic costs, it is important to reiterate that low-cost materials are required for sustainable water purification.

Banerjee and co-workers developed a simple N-terminally open dipeptide supergelator, and the gels can absorb both toxic dyes and metal ions. The dual-purpose gel was used to remove four toxic dyes: Brilliant Blue, Congo Red, Malachite Green, Rhodamine B, and two metal ions, Ni²⁺ and Co²⁺, from water (Figure 1.44).²⁵⁶ Recently, they have reported a

self-shrinking gel that is able to rove both toxic dyes and Pb^{2+} from wastewater.²⁵⁷ Elemental mapping has shown that the metal ions are trapped inside the interstitial spaces of the gel fibers.

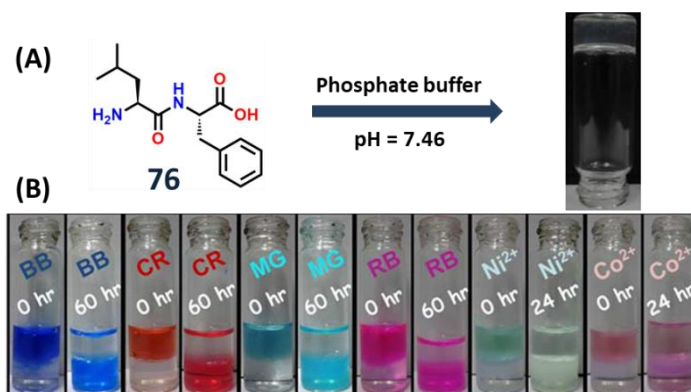


Figure 1.44. (A) The chemical structure of the peptide **76** and the photograph of the hydrogel from peptide **76** at 0.1% (w/v). (B) The photographs of the hydrogels before and after absorption of the dyes Brilliant Blue (BB), Congo Red (CR), Malachite Green (MG), Rhodamine B (RB), and the metal ions nickel(II) (Ni^{2+}), cobalt(II) (Co^{2+}). The concentration of hydrogels was 0.1% (w/v) for all these cases. (Adapted from, N. Nandi, A. Baral, K. Basu, S. Roy and A. Banerjee, *Peptide Science*, 2017, **108**: e22915).

1.7.3. Oil Spill Recovery

Accidental or intentional discharge of crude oil and petrochemicals is a severe environmental problem that causes marine pollution. Waterways have witnessed alarming oil spills, for example, the 5 billion barrels of crude oil released in the Gulf of Mexico in 2010.²⁵⁸ This is problematic from both an economic perspective through wastage of valuable non-renewable oil, as well as the potential impacts on human health through consumption of sea foods obtained from oil-polluted seas, impacts on climate as a result of the accumulation of volatile hydrocarbons in the stratosphere, and devastating effects on the delicate balance of the marine ecosystem.²⁵⁹ Conventional methods for remediating oil spills include absorption, dispersion, bioremediation, and solidification.^{260, 261} Sorbents are solids that absorb the oil, dispersants emulsify the oil, and solidifiers are polymeric materials that gel the oil. However, these approaches are often either inefficient, not economically viable for large-scale application, or can themselves leave behind toxic residues which bioaccumulate through food cycles. Low molecular weight organogelators have potential application for congealing oil spills, in particular in cases where the gelator has the following key properties: (i) simple, low-cost

synthesis, (ii) environmental compatibility, (iii) thermoreversibility facilitating oil recovery, and (iv) recyclability and reusability.

Interestingly, the use of LMWGs with oil slicks has been known since the 1970s; however, these early industrial examples are rarely cited in the more recent, academically driven literature. For instance, in 1971, in situ formation of colloidal gel-forming ureas by reaction of amines and isocyanates was explored as a technology for oil-spill immobilization, although a practical solution to the problem was not found at this point using this approach.²⁶² Another early example of gelling oils with small organic molecules was demonstrated in the patent of Saito et al. from 1976.²⁶³ In the original patent, derivatives of N-acetyl amino acids were ad-mixed with nonpolar organic solvents such as kerosene and stirred at elevated temperatures (120 °C). A stable gel was then formed within 2 min as the solution cooled to room temperature. As a proof of principle for oil-spill remediation, an explanation of N-lauroylglutamic acid- α , γ -di-n-acrylamide (1 g) dissolved in benzene (5 mL) selectively gelled a heavy oil suspension (25 g) within 20 min in the presence of seawater. The benzene was also entrapped along with a small amount of water. The solidified oil was filtered off through wire gauze in order to separate it from the bulk seawater. It should be noted that in this early work, the requirement of 4 wt% gelators is not ideal; indeed, more recent work has highlighted that LMWGs can be effective at concentrations well below 1 wt%.

Amino acid-based gelator for the recovery of the marine oil spill was first described by Bhattacharya and Krishnan-Ghosh. They used a simple amino acid amphiphile, N-lauroyl-(L)-alanine **77** (Figure 1.45), to selectively gel aromatic and aliphatic hydrocarbons as well as commercial oils such as kerosene, petrol, and paraffin in biphasic oil-water mixtures.²⁶⁴ A requisite amount (typically 0.1% wt/vol) of the gelator was added to the biphasic oil-water mixture either by dissolving the gelator in the solvent mixture by heating or by adding it as a solution in ethanol. The oil phase was selectively gelled, leaving the aqueous phase unaffected, with the gels remaining stable for one week. Moreover, the presence of NaCl, CuSO₄, KMnO₄, and other potentially competitive

impurities had no significant effect on gelation, indicative of effective self-assembly. Self-assembly of **77** is evident from SEM studies, as shown in Figure 1.45. In water, due to the presence of a lipophilic alkyl chain, **1** exerts a hydrophobic effect and excludes water. Additional stabilization of such aggregates most likely originates from Van der Waals contacts of the polymethylene chains.

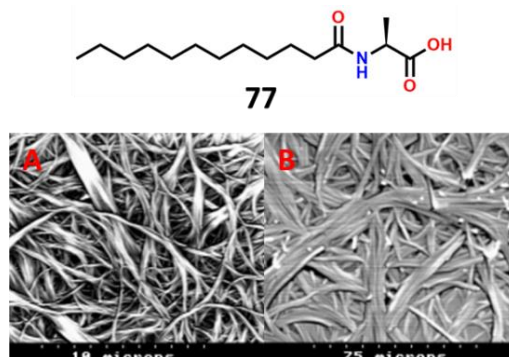


Figure 1.45. SEM of gels of (A) *n*-heptane and (B) toluene with **77** (adapted from, S. Bhattacharya and Y. Krishnan-Ghosh, *Chem. Commun.*, 2001, 185–186).

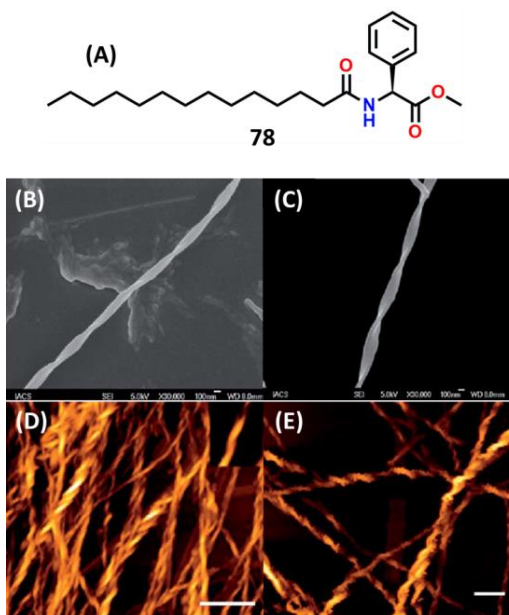


Figure 1.46. (A) Chemical structure of gelator **78**, (B) and (C) FE-SEM images of **78** in *n*-heptane and *n*-octane solvents, respectively, (E) and (F) AFM images of **78** in *n*-heptane and *n*-octane solvents respectively (scale bar 1 μ m). Both microscopy studies show right-handed twisted ribbons (adapted from, S. Basak, J. Nanda and A. Banerjee, *J. Mater. Chem.*, 2012, **22**, 11658–11664).

Basak *et al.* synthesized an aromatic amino acid-based gelator molecule **78** (Figure 1.46) which can gelate spilled oil within a very short period of 90 sec. Organogels have been well characterized morphologically by field emission scanning electron microscopy (FE-SEM) and atomic force

microscopy (AFM). Morphological studies of these xerogels have revealed the presence of fascinating right-handed twisted nanoribbons (in n-heptane and n-octane).²⁶⁵

Yu *et al.* have demonstrated phenylalanine containing C_2 symmetric gelator molecule for oil spill remediation (Figure 1.47). Spectroscopic and microscopic experiments confirmed a β -turn arrangement and a fibrous structure of the gelators, which is formed through hydrogen bonding, π - π stacking, and van der Waals interactions.²⁶⁶

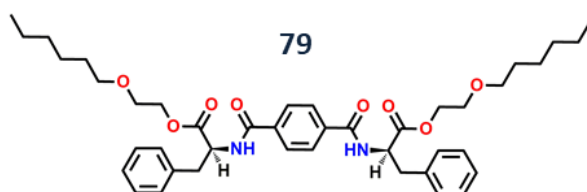


Figure 1.47. 1,4-Bi(phenylalanineethylene glycol monohexyl ether)-benzene (**79**) for oil spill recovery (adapted from, S.-L. Yu, X. -Q. Dou, D. -H. Qu and C. -L. Feng, *J. Mol. Liq.*, 2014, **190**, 94-98).

Recently, Banerjee and co-workers develop an ambidextrous gelator (**80**) which has potential to gelify the aqueous as well as organic solvent. In this work, the gel formed in phosphate buffer (pH 7.46) was used for the removal of toxic organic dyes. The gelator molecule can also selectively gelify the organic solvent such as petroleum ether, diesel, petrol, kerosene, etc. Moreover, this peptide has the potential to be reused further for several times without loss of its any activity (Figure 1.48).²⁶⁷

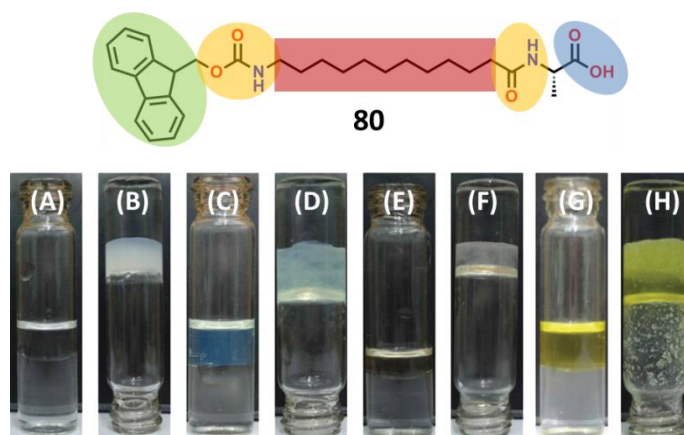


Figure 1.48. Gelator molecule **80** with various zones of interactions like π - π interactions (green), hydrogen-bonding sites (yellow), van der Waals interactions (red) and the polar head group (blue) and its gelation of oil from biphasic mixtures of different oils and water: (A) and (B) with petroleum ether; (C) and (D) with diesel; (E) and (F) with petrol; (G) and (H) with pump oil. (Adapted from, K. Basu, N. Nandi, B. Mondal, A. Dehsorkhi, I. W. Hamley and A. Banerjee, *Interface Focus*, **7**: 20160128).

1.8. Some Other Applications of Amino Acids/ Peptide Based Materials

1.8.1. Gels for Making Optoelectronic Devices

Peptides are generally nonconducting materials to be used as optoelectronic devices, however when they are attached with some organic semiconducting molecules they extensively dictate the assembly and arrangement of fluorophores which ultimately triggers the formation of properly stacked superstructure. These structures eventually help proper orientations of charge hopping sites in a self-assembled material and good current response is achieved. Under the section “Rylene dye containing gelators” I have discussed a few examples of them. However, other than those, Trover and his group have developed peptide based gelator molecules containing oligo-thiophene and oligo-p-phenylenevinylene (OPV) moieties to get good current voltage response upon shear-thinning (Figure 1.49).²⁶⁸

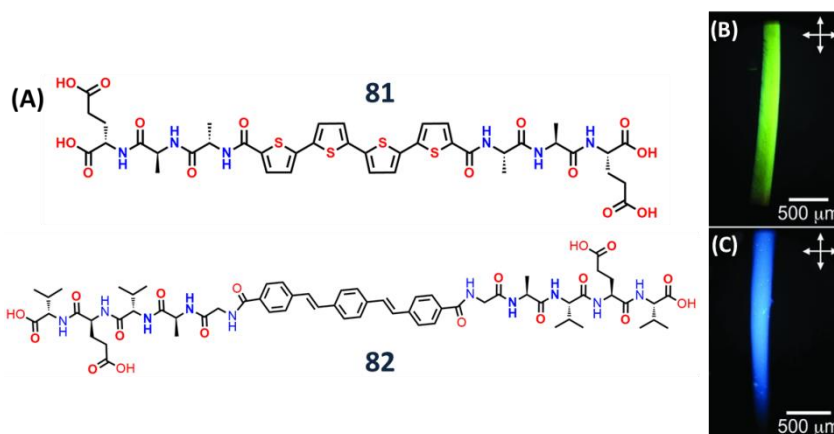


Figure 1.49. (A) Molecular structures of thiophene and OPV containing peptide gelators. **81** (B) and **82** (C) as seen under crossed polarizers. The colors presented were obtained directly from microscopy and result from the interaction of the polarized light with the anisotropic orientation (adapted from, B. D. Wall, S. R. Diegelmann, S. Zhang, T. J. Dawidczyk, W. L. Wilson, H. E. Katz, H.-Q. Mao, J. D. Tovar, *Adv. Mater.*, 2011, **23**, 5009–5014).

1.8.2. Gels as Catalysts

In nature proteins that we call enzymes catalyze reactions which are seemingly impossible to be done by synthetic chemists at laboratory temperature. Active sites in such proteins bring the reaction centers closer to each other and that makes the reaction facile by formation of a reactive intermediates. Short peptides with rational design have been developed to

be used in catalyzing various reactions like natural enzymes.²⁶⁹ Peptide based hydrogels are highly ordered arrays of peptide amphiphile molecules, scientists have used these materials in catalyzing various typical organic reactions.²⁷⁰⁻²⁷⁴ They have developed a series of short peptides possessing the sequence (FE)_n or (EF)_n and bearing L-proline at their N-terminus that self-assemble into high aspect ratio aggregates and hydrogels (Figure 1.50). They have shown that only upon assembly the peptide can catalyze aldol reaction, however, the non-assembled counterparts are catalytically inactive.²⁷⁵

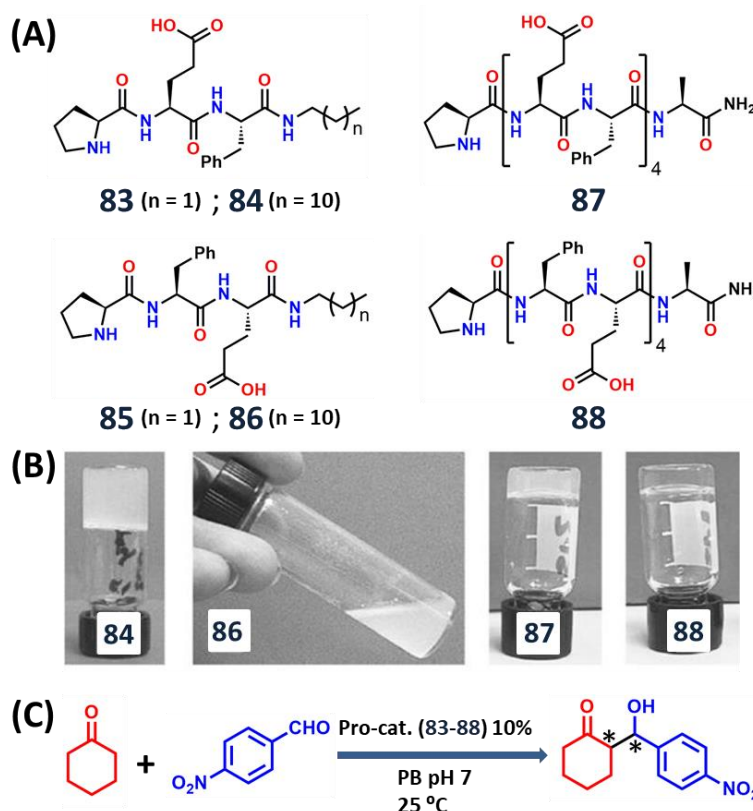


Figure 1.50. (A) Structures of peptides with (FE)_n or (EF)_n sequence. (B) Gel/aggregates formed by peptide **84**, **86**, **87** and **88**. (C) Catalyzing the asymmetric aldol reactions (adapted from, M. Tena-Solsona, J. Nanda, S. Díaz-Oltra, A. Chotera, G. Ashkenasy and B. Escuder, *Chem. Eur. J.*, 2016, **22**, 6687–6694).

Recently, Banerjee and co-workers developed a histidine containing amphiphile **89** which gives metallo-hydrogels in presence of Fe³⁺ and Hg²⁺ metal ions. Moreover, the amphiphile, **89** and metallo-hydrogel of Fe³⁺ and Hg²⁺, all of them are able to show catalytic activity for the hydrolysis of p-nitrophenyl esters to p-nitrophenol and acetyl, n-butyl and n-octyl acids. But the ferric ion containing metallo-hydrogel shows very

high catalytic activity for the hydrolysis of p-nitrophenyl esters (Figure 1.51).²⁷⁶

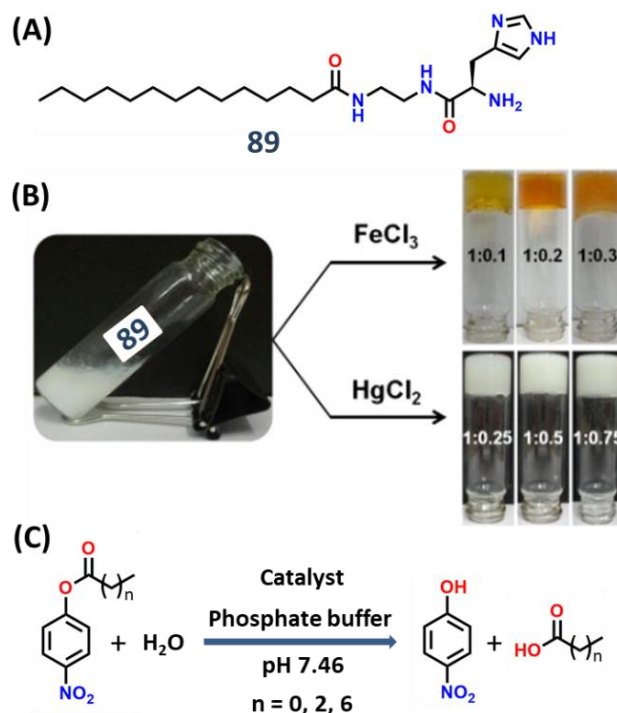


Figure 1.51. (A) Chemical structure of amphiphile **89**; (B) FeCl₃ and HgCl₂-induced hydrogel of compound **89**; (C) Hydrolysis reaction of p-nitrophenyl esters ($n = 0$ for p-nitrophenyl acetate [PNPA], $n = 2$ for butyrate [PNPB] and $n = 6$ for octanoate [PNPO]) catalyzed by aggregated **89**/Fe³⁺ ion-induced hydrogel of **89** (adapted from, K. Gayen, K. Basu, D. Bairagi, V. Castelletto, I. W. Hamley and A. Banerjee, *ACS Appl. Bio Mater.*, 2018, **1**, 1717–1724).

1.8.3. Pesticidal Activity

Pesticides are innovative compounds for crop blossoming and storage via controlling pests in commercial agriculture.^{277, 278} Organophosphorus pesticides (OPs) are the most widely utilized pesticides worldwide due to their moderately high efficacy and low persistence.^{279, 280} However, their excess use for crop protection has increased very high safety concerns. The inaccurate use, improper dumping, and residues of OPs result in contamination of agricultural products into the surface and groundwater of the environment.^{281, 282} In particular, OPs function as a neurotoxin by hampering cholinesterase activity at low concentrations, causing damage to human health or even deadly consequences.^{283, 284} The amino acid base peptides have very high biocompatibility and biodegradability. So, the use of amino acid-based derivatives as substituents can increase the pesticide's attractiveness.

Recently, multiple teams of EU (European Union) researchers have developed peptide-based highly selective eco-friendly pest controllers. The new class of peptide-based biopesticides will reduce the risk of pesticide use in sustainable crop protection, which is not harmful to the environment and human health.²⁸⁵

1.8.4. Fungicidal Activity

Fungicides are biological microorganisms or chemical compounds, which can kill parasitic fungi or their spores.²⁸⁶ Fungi can cause serious damage to agricultural products. So, this damage can result in critical losses of yield, quality, and profit. Fungicides are used to fight against both agricultural and animal fungal infections.²⁸⁷ The use of sulphur as a major component makes fungicides very toxic. So, excessive use of sulphur components may be very dangerous for human health.²⁸⁸ The amino acids

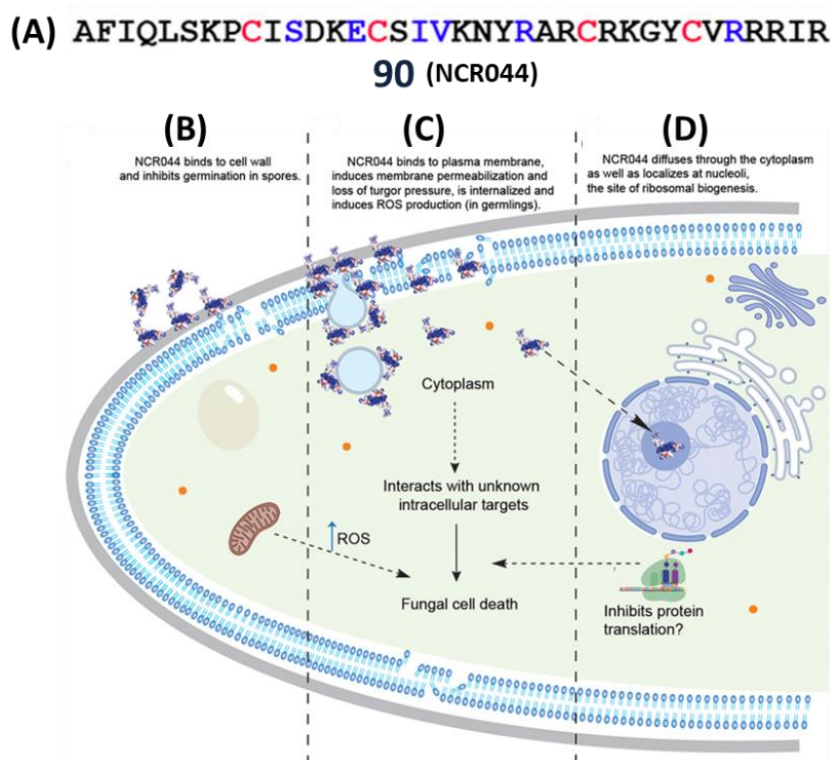


Figure 1.52. (A) Primary amino acid sequences peptide **90** (NCR044) with 36 residues in length. Conserved cysteine residues are highlighted in red and six nonconserved residues are highlighted in blue. Proposed multistep model for the antifungal action of **90** against *B. cinerea*. (B) **90** binds to cell wall and inhibits germination in spores. (C) **90** binds to plasma membrane, induces membrane permeabilization and loss of turgor pressure, is internalized, and induces ROS production (in germlings). (D) **90** diffuses through the cytoplasm as well as localizes at nucleoli, the site of ribosomal biogenesis (adapted from, S. L. S. Velivelli, K. J. Czymmek, H. Li, J. B. Shaw, G. W. Buchko and D. M. Shah, *Proc. Natl. Acad. Sci.*, 2020, **117**, 16043–16054).

containing derivatives such as cystine-containing molecules not only make the peptide biodegradable and nontoxic but also can be used as an antifungal agent.

Velivelli *et al.* reported that the NCR044 symbiotic peptide **90**, which contains 36 natural amino acids, shows antifungal activity. Based on the results, they also reported a multistep model for the antifungal action of **90** (NCR044) against *B. cinerea* (Figure 1.52).²⁸⁹

1.8.5. Herbicidal Activity

The herbicides are commonly known as weedkillers. These are the substance that controls the growth and development of undesired plants. There are two types of herbicides, selective and non-selective herbicides. The selective herbicides damage the specific weed species keeping the desired weeds unharmed. Non-selective herbicides (total killer) are used to clean the waste ground as it kills every plant with which they come in contact.

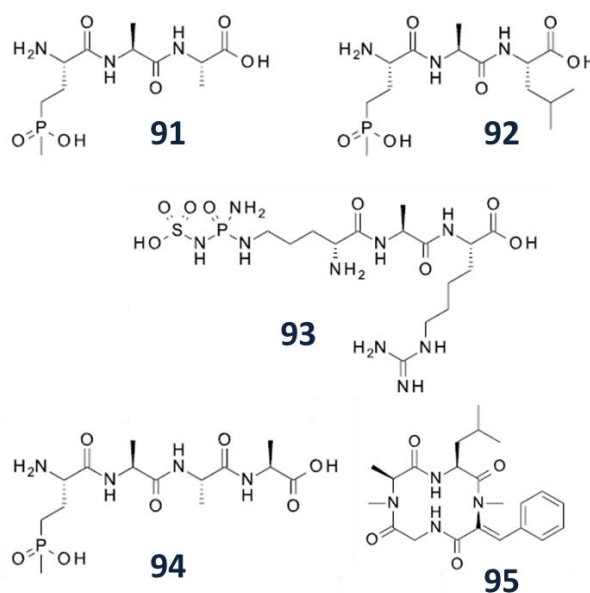


Figure 1.53. Chemical structure of some peptide based naturally synthesis derivatives (**91–95**) with herbicidal property (adapted from, C. Lamberth, Amino Acids., 2016, **48**, 929–940).

There are some naturally synthesized amino acids based peptide herbicides (**91–95**), but among them, **91–94**, all are non-selective. The herbicide **95** (tentoxin), the cyclic peptide shows quite selectivity towards corn and soybean weeds without affecting the corresponding crops (Figure 1.53).²⁹⁰ So, there is a real need for synthesizing amino acid-

based selective herbicides, which will be very low in cost and environment friendly.

Future Prospects

Nowadays, different scientific groups and institutions across the globe are trying to use gel-based materials in diverse fields of science. From the view of a chemist, it is very much fascinating to check and manipulate the molecular interactions on the nanoscale. Peptide-based gels and soft materials have a promising future in this regard, and it is essential to explore their material applications for obtaining new biological applications for them. Peptides are natural building blocks, and therefore it is expected that they should have little or no detrimental effect on the environment, and they will be green and clean sources for future material research in our society.

1.9. Nanomaterial's: Development and Significance

1.9.1. Brief History: Early Identification

The earliest use of metal nanoparticles dates back to the ancient history of Roman, Egyptian, and Chinese civilizations, although nanoparticles were not identified then. Gold and silver nanoparticles were used to stain glasses for cathedrals and other decorative purposes. The application, though, was not just restricted to decoration. In ancient India, metal nanoparticles had been used in medicinal applications to cure arthritis and had a high cosmetic value. Despite these common applications, their size range was unknown due to the unavailability of nanoscale imaging techniques. The most significant scientific experiment came forward in the mid-nineteenth century when Michael Faraday reported the synthesis of gold colloid by reducing gold salt with white phosphorus in a two-phase system. Faraday believed that the particles of his colloid were of dimensions smaller than the wavelength of visible light.²⁹¹ The ruby red color of gold colloid stimulated much interest in scientific research. After half a century, Gustov Mie solved the Maxwell equation in 1908 and successfully modeled the optical spectra of gold colloids. This was the first study of the interaction of light with nanoparticles (gold), and it explained the absorption and scattering properties of gold nanoparticles.

1.9.2. Nano: the Size

After identifying the existence of a gold particle that behaves differently than its larger counterparts in interacting with lights, the major challenge is determining its size. The invention of transmission electron microscopy (TEM) by Knoll and Raska in 1931 was an important asset, as the size of the synthesized nanoparticles could be precisely measured. J. Turkevich, in a pioneering work,²⁹² synthesized gold nanoparticles by employing citrate ions and gold salt in an aqueous solution. TEM imaging of these gold nanoparticles suggests that the size of the synthesized gold particles was 10-20 nm.²⁹²

Thus, the word "Nano," from the Greek "Nanos" (or Latin "nanus"), has become the key to modern science to which everyone is looking up. "Nano" refers to the 10^{-9} power, or one billionth. In these terms, it refers to a meter, or a nanometer, on the scale of an atomic diameter. A typical carbon-carbon bond length, or the spacing between these atoms in a molecule, is in the range of 0.12–0.15 nm. Also, ten hydrogen atoms are about 1 nm, a DNA double-helix has a diameter of around 2 nm, a cell membrane is about 9 nm thick, a virus is about 70 nm long, and a red blood cell is 5000 nm in diameter. A single particle of smoke is in the order of 1000 nm. A human hair is about 50,000–1,00,000 nm across (Figure 1.54). A sheet of paper is about 100,000 nm thick. Figure 1.55 describes the size variation from a single atom to a human being. The evolution of atoms to humans can be seen via an electron microscope, light microscope, and naked eyes. Generally, nanoscale refers to measurements of 1–100 nm.

Now, after getting the idea of the size, the critical question is what is unique in size and why it is essential. When objects are below 100 nm in size, they can exhibit unexpected chemical and physical properties. The optical, electrical, mechanical, magnetic, and chemical properties can be systematically manipulated by adjusting this class of materials' size, composition, and shape on the sub-100 nm length scale. For example, if a block of gold is cut into smaller and smaller pieces, it would still have the same color, melting temperature, etc. But at specific ranges of the nanoscale, gold particles behave differently.²⁹³ The properties of materials with nanometric dimensions are significantly different from the

bulk materials due to the increase in surface area/volume ratio (Figure 1.56). Nanomaterials' optical and electronic properties would differ from their bulk counterpart. In nanomaterials, the catalytic property is also enhanced than their bulk counterpart due to greater surface area. The catalytic efficiency of nano-dimensional materials increases because more surface area ensures greater contact with the substrate molecules.



Figure 1.54. Comparison between nanofibres with a single human hair (adapted from Google images).

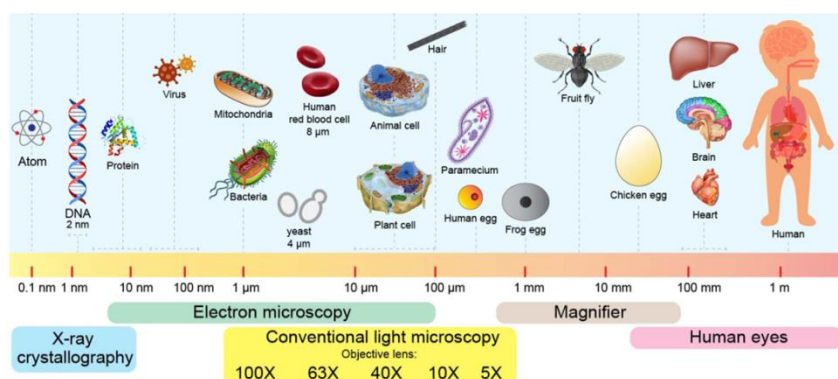


Figure 1.55. Different dimensions: from atom to human beings (adapted from Google Images).

1.9.3. Nanomaterial and Nanoparticle: Definition

Nanomaterial is a research area that takes a material science-based approach to nanotechnology. It deals with the material having morphological features within the range nanoscale. The European Commission approved the following definition of a nanomaterial: “A natural, incidental or manufactured material containing particles, in an unbound state or as an aggregate or as an agglomerate and where, for 50% or more of the particles in the number size distribution, one or more external dimensions is in the size range 1 nm–100 nm.”

In nanotechnology, a particle is defined as a nanoparticle whose size remains between 1 and 100 nm. Nanoparticle research is currently an area of immense scientific interest due to various potential biomedical, optical, and electronic applications.

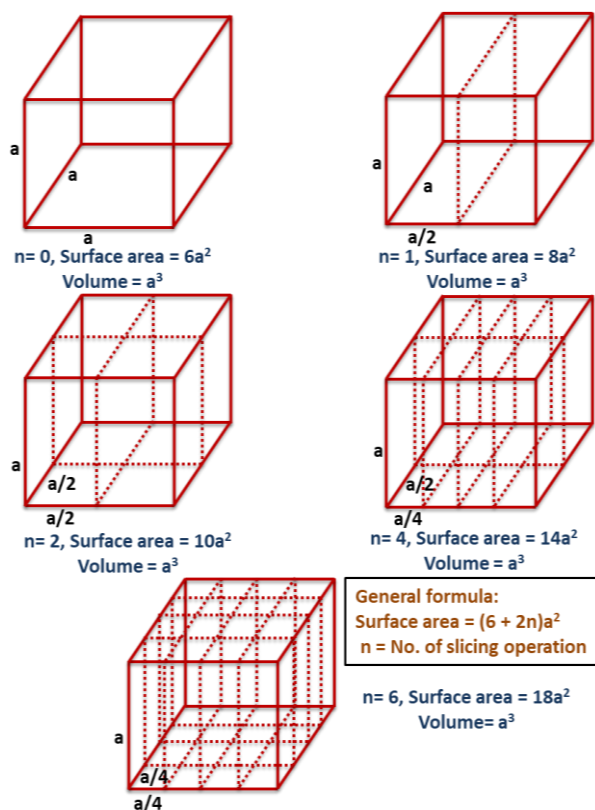


Figure 1.56. Surface area/volume ratio increases respectively when no of slices increases.

1.9.4. Development in Metallic Nanostructures Field

J. Turkevich²⁹² developed a method for synthesizing gold nanoparticles using citrate as a reducing and stabilizing agent, which G. Frens further modified. It has since become a standard method for preparing citrate-capped gold nanoparticles of >10 nm diameter.^{294, 295} The early synthesis of some of the metal nanoparticles followed this approach of using some stabilizer to prevent the nanoparticles from aggregation due to collisions in the solution state. Some common stabilizers are surfactants, amphiphilic polymers, ligands, and even solvent molecules if they can bind to nanoparticle surfaces.²⁹⁶ An early example of producing magnetic nanoparticles was proposed by Hess *et al.* to prepare a Co-colloid of 10-100 nm. In this method, $\text{Co}_2(\text{CO})_8$ was heated to a high temperature in the presence of dispersant polymer.²⁹⁷ The generation of metal nanoparticles

by thermal decomposition of metal-organic precursor in the presence of a stabilizer became a common approach for synthesizing Fe, Co, Ni, and Cd metal nanoparticles.²⁹⁸⁻³⁰⁰ Better size control of metal nanoparticles was achieved using another process where a high concentration of reducing agents like citrate or sodium borohydride were used. Schmid *et al.* developed the synthesis of phosphine-protected gold nanoparticles by using excess NaBH_4 , where the size of gold nanoparticles was ~ 1.4 nm.³⁰¹ “B Brust-Schiffin method” reported a popular method for synthesizing gold nanoparticles in 1994. This method was motivated by the thiol self-assembled- monolayer (SAM) on metal surfaces.³⁰²⁻³⁰⁴ This was the first report of using thiol as a capping ligand for synthesizing gold nanoparticles. Brust’s method involves two steps; the first step involves the phase transfer of gold salt using a phase transfer agent (surfactant). Subsequently, NaBH_4 reduced the Au(I) thiolate polymer to form nanoparticles. The excess reducing agent (typically ten times the gold salt) helped narrow the size distribution. This nanoparticle system was highly stable due to the strong interaction of thiol with the gold surface and the van der Waals interactions. The nanoparticle size can be effectively controlled by the ratio of precursor gold salt to alkane thiol. Due to their extraordinary stability, these thiol-protected nanoparticles can be isolated, stored in powder form, and further re-dispersed in any desired solvent. This was in strong contrast to the behavior of the earlier mentioned gold colloid in the solution that was stabilized by charge stabilization.³⁰⁵⁻³⁰⁷

1.10. Nanoclusters vs Nanocrystals

The term “nanoclusters” refers to ultrasmall nanoparticles (e.g., <2 nm). On the other hand, the term “nanocrystals” refers to crystalline nanoparticles, while nanoparticles refer to entities that are not necessarily crystalline (e.g., polymer nanoparticles). Whetten and co-workers synthesized ultrasmall gold nanoparticles with a narrow size distribution. They employed solvent-based precipitation where a typical selective size can be precipitated using solvents with different polarities.^{308, 309} They also isolated Au nanocrystals in size range of 1.5–3.5 nm, estimated to have ~ 100 to ~ 1300 gold atoms. LDI-MS (Laser Desorption Ionization

Mass Spectrometry) further analyzed these isolated fractions. These fractionated nanoparticles were readily forming superlattices, which indicated their high monodispersity.³⁰⁸⁻³¹⁰ The LDI-MS revealed several critical sizes of Au nanocrystals, including 27-29 k, 45-46 k, 57 k, and 92-93 k species ($k = 1000$ a.m.u. units). Figure 1.57 shows the eight isolated fractions of gold nanocrystals with their core diameters and masses determined by LDI-MS. HR-TEM study of the 92 k species revealed an fcc lattice arrangement. Theoretical calculations suggested the optimum size of the Au core to be Au_{459} (92 k, 2.5 nm), Au_{314} (57 k, 2.1 nm), Au_{225} (45 k, 2 nm), and Au_{140} (28 k, 1.7 nm) species.³¹¹ Murray and co-workers also reported Au nanocrystals with a core diameter of ~ 1.5 nm and estimated it to be $\sim \text{Au}_{400}$.³¹² In all these cases, even if the reported size was less than 2 nm, the nanoparticles still showed surface plasmon resonance (SPR) which is surprising.

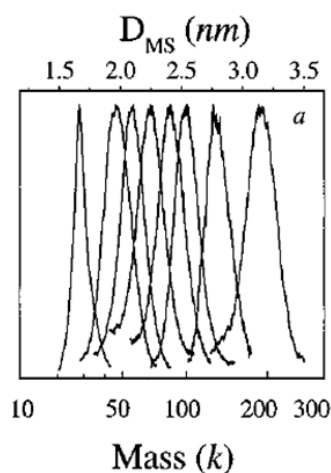


Figure 1.57. Sizing of the nanocrystal gold molecule fractions by mass spectrometry where the principal peaks from the mass spectra are displayed versus mass (in $k = 1000$ amu units, lower axis, cube-root scale) and versus equivalent diameter (D_{MS} , upper axis, linear scale): (a) 3.2, 2.7, 2.5, 2.4, 2.2, 2.1, 2.0, and 1.7 nm (using hexyl thiolate as passivant) (adapted from, M. M. Alvarez, J. T. Khoury, T. G. Schaaff, M. N. Shafigullin, R. L. Whetten and I. Vezmar, *J. Phys. Chem. B*, 1997, **101**, 3706–3712).

Gold nanoparticles generally show a distinct SPR band between 500–570 nm depending upon their size (for spherical particles), while silver shows SPR in the 430–460 nm range. The SPR of gold or silver nanoparticles also depends upon the particle-particle interaction, the capping ligand, and the dielectric medium around the nanoparticle. The surface plasmon for gold nanoparticles is well defined when nanoparticle size varies between 2–100 nm. An increase in size causes inhomogeneous polarization of nanoparticles by the incident light resulting in retardation

of the electromagnetic field around the nanoparticle. This inhomogeneous polarisation causes plasmon broadening and a substantial red shift of the peak wavelength.³¹³ However, if the size decreases below 2 nm, the plasmon properties disappear, and the quantum confinement plays a vital role in the spectral properties.

Thus, the SPR of particles below 2 nm is surprising because of the purity of the isolated nanoparticles. The high molar absorptivity coefficient of plasmonic nanoparticles will dominate the spectral feature of smaller nanoparticles. So the intriguing question is how the spectral properties of nanoparticle changes when their size is smaller than 2 nm? When the size of nanoparticles is below 2 nm, the metal core possesses only a countable number of atoms (up to ~200). Such ultra-small particles behave as clusters of atoms or like molecules. The properties of such nanoclusters differ from the bulk metal and their larger counterparts (i.e., conventional nanoparticles). Some clusters are also called ‘superatom’, as they show some of the properties of ordinary atoms. It would be interesting to know at what size (i.e., the precise number of atoms) the gold nanoparticles start showing quantum confinement.

The free electron model throws light on determining the limiting size of the nanoclusters as the quantum size regime can be estimated using this model. As the particle size becomes smaller, the electronic energy levels’ average spacing (δ) becomes considerable and δ increases with decreasing size. The average spacing (δ) can be roughly expressed as-

$$\delta = \frac{E_f}{N}$$

where E_f refers to the Fermi energy, and N is the number of metal atoms since N can be expressed as $\propto d^3$ (d is the nanoparticle diameter). So the spacing is inversely proportional to the cube of particle diameter. If room temperature thermal energy ($k_B T$) is used as a criterion for considering quantum confinement, then the following relation is obtained:

$$\delta = k_B T$$

after substituting the value of Fermi energy for gold, $E_f = 5.5$ eV, into the equation, we can get the critical number of gold atoms to be 220. The number of gold atoms and the particle volume is related as

$$N = (59 \text{ nm}^{-3}) \cdot V$$

This gives the value of equivalent diameter to ~2 nm. Thus, for gold nanoparticles below 2 nm, the electronic energy quantization will dominate, and the collective plasmon mode will no longer be supported. They are often called nanoclusters to differentiate such ultrasmall particles from conventional plasmonic nanoparticles. When the particle's size is decreased to a few atoms, the size approaches the Fermi wavelength of electrons, leading to the break-up of the continuous density of states into discrete energy levels, which leads to dramatically different optical, electrical and chemical properties compared to larger nanoparticles.

1.11. Nanoclusters: Importance and Scope

In the smallest size regime, metal clusters become “molecular species”,³¹⁴⁻³¹⁷ and discrete states with strong fluorescence can be observed.³¹⁸⁻³²²

These molecule-like properties of such a few atom metal clusters are the primary topic of this thesis. In this thesis, I have attempted to answer some questions regarding these molecular clusters by creating a series of fluorescent gold clusters and investigating their photophysical properties. Providing the “missing link” between atomic and nanoparticle behavior in noble metals, these highly fluorescent noble metal nanoclusters smoothly link the optical and electronic structure transitions from atoms to nanoparticles with observable free electron behavior and also offer new opportunities for creating new biological labels, energy transfer pairs, and other light-emitting sources in nanoscale electronics. As the size of the nanocluster is confined within the quantum regime, they are often called quantum clusters. Sub-nanometer-sized metal nanoclusters (gold/silver/platinum) display molecule-like properties and they have discrete size-dependent electronic state.³²³ Their distinct molecule-like electronic transition resulted in exciting properties, including fluorescence,³²⁴⁻³²⁷ redox-like charging behavior,³²⁸ ferromagnetism,³²⁹ and unique size- and shape-dependent catalytic, optical, electrical, magnetic, and chemical properties that are often different from their bulk (Figure 1.58).³³⁰⁻³³⁴ They found prospective applications in bioassays and

bio-labeling,³³⁵⁻³³⁸ sensing,³³⁹⁻³⁴³ single molecular spectroscopy,³⁴⁴ catalysis,³⁴⁵⁻³⁴⁸ and nanoelectronics.³²³

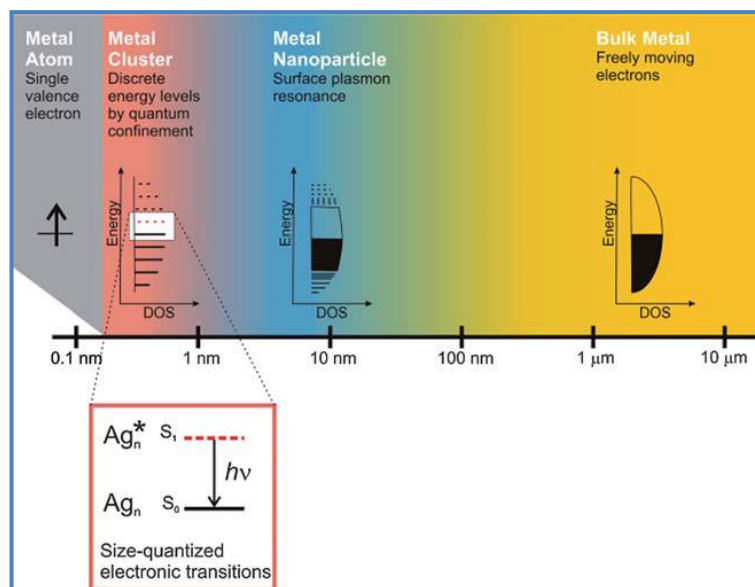


Figure 1.58. The effect of size on metals. Whereas bulk metal and metal nanoparticles have a continuous band of energy levels, the limited number of atoms in metal nanoclusters results in discrete energy levels, allowing interaction with light by electronic transitions between energy levels. Metal nanoclusters bridge the gap between single atoms and nanoparticles (adapted from, I. Diez and R. H. A. Ras, *Nanoscale*, 2011, **3**, 1963–1970).

A strong fluorescent emission can often be observed upon excitation of these nanoclusters in the UV–visible range. They also exhibit size dependent, ligand-dependent, solvent-dependent and temperature dependent fluorescence properties.

A part of this thesis deals with the synthesis and characterization of copper nanoclusters using peptide and aromatic acid having thiol groups as stabilizing agents in Chapters 5 and 6. So I will discuss more details about fluorescent copper nanoclusters in the next topic of discussion.

1.12. Fluorescent Copper Nanoclusters

Fluorescent copper nanoclusters (CuNCs) have gradually become an active research area due to their low cost, good water solubility, wide availability and excellent optical properties.³⁴⁹ The biggest advantage of CuNCs is their low-cost and tunable fluorescence properties compared to fluorescent gold and silver nanoparticles, resulting in the extensive synthesis and wide applications of CuNCs. Before 2010, few reports about CuNCs have been published as they are easily oxidised and

difficult to be prepared. However, considerable efforts have been devoted to explore the preparation and applications of CuNCs with different emissions and good biocompatibility since 2010 and a great progress has been achieved since last few years.

1.13. Fluorescent Properties of the CuNCs

Like other metal Nanoclusters fluorescent properties of the CuNCs are one of the key features of them. Recently, lots of efforts have been devoted to prepare various water-soluble CuNCs with different emissions from blue to red (Figure 1.59).³⁵⁰ The fluorescence of CuNCs is generally attributed to the electronic transitions between the occupied d bands and states above the Fermi level (ca. sp bands) or the electronic transitions between the highest occupied molecular orbital (HOMO) and the lowest unoccupied molecular orbital (LUMO).^{351, 352}

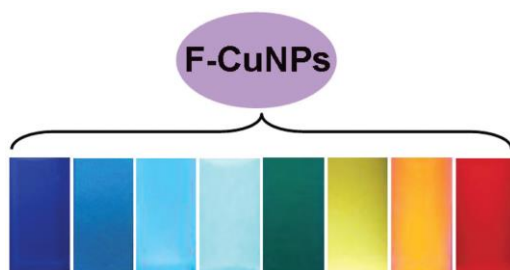


Figure 1.59. CuNCs with different emissions from blue light to red light (adapted from, Y. Guo, F. Cao, X. Lei, L. Mang, S. Cheng and J. Song, *Nanoscale*, 2016, **8**, 4852–4863).

The ligands show a significant effect on the fluorescence properties of CuNCs. For example, CuNCs stabilized by double-stranded DNA (dsDNA) exhibit bright fluorescence at 587–600 nm under excitation at 340 nm.^{353, 354} However, poly (thymine) stabilized CuNCs emit red fluorescence around 615 nm with excitation at 340 nm ultraviolet (UV) light. The fluorescence intensity increases with the length of the poly T segment within single-stranded DNA (ssDNA).³⁵⁴ Moreover, the synthetic method also significantly affects the fluorescence properties of CuNCs. For example, the bovine serum albumin (BSA)-templated CuNCs can exhibit blue and red emission due to different synthetic methods.^{355, 356}

Two-photon fluorescence properties have received much attention as two-photon fluorescence imaging possesses the advantages of larger penetration depth, minimized tissue auto-fluorescence background, and

reduced photodamage in biotissues and higher spatial resolution when compared with that of the one-photon counterparts.³⁵⁷ Similarly, bifunctional peptide stabilized CuNCs show both one-photon and two-photon fluorescence properties. The CuNCs show blue emission centered at 418 nm under excitation at 365 nm, and the two photon fluorescence emission wavelength is located at 460 nm with excitation at a femtosecond laser at 750 nm. And the F-CuNPs can be used to label the nuclei of HeLa and A549 cells.³⁵⁸

Aggregation-induced emission (AIE) is an interesting phenomenon occurring in some organic molecules, which is rarely found in fluorescent nanomaterials.³⁵⁹ However, Wang's group has recently found that some CuNCs exhibit AIE fluorescence properties. Namely, the aggregated CuNPs emit stronger fluorescence than that in a dispersed state. The glutathione (GSH)-stabilized CuNCs prepared by the etching method in aqueous solution exhibit weak emission centered at 620 nm. While a strong emission peak at 600 nm and a minor emission peak at 426 nm are observed upon the addition of ethanol that can cause the aggregation of the GSH-stabilized CuNCs. The AIE effect of CuNCs may be ascribed to the restriction of intramolecular motion in the aggregates. In the aggregates of CuNCs, the restricted intramolecular motions block the non-radiative path and activate radiative decay, resulting in a long fluorescence lifetime and enhanced emission efficiency. However, the molecular motions of the dispersed CuNCs in aqueous solution are not restricted, accelerating the non-radiative deactivation. As a result, the dispersed CuNCs exhibit a shorter fluorescence lifetime and lower quantum yield (QY).³⁶⁰ Moreover, D-penicillamine (DPA)-capped F-CuNPs and L-cysteine (L-Cys)-stabilized F-CuNPs also display AIE properties.^{361, 362}

1.14. Synthesis of Metal Quantum Clusters

Different synthetic approaches have been adopted by researchers around the globe to prepare different sized few atom metal (Au, Ag and Cu) quantum clusters (Figure 1.60).³⁶³⁻³⁶⁶

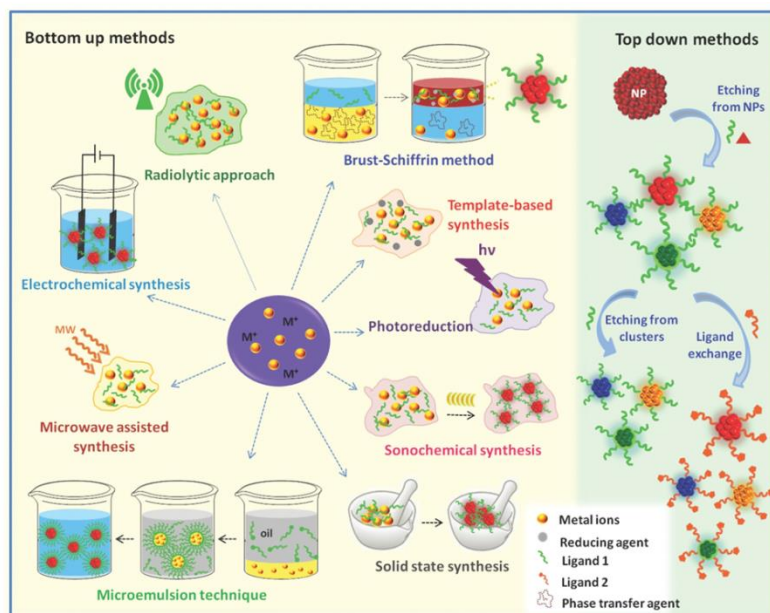


Figure 1.60. Various routes for the synthesis of atomically precise, sub-nanometer-sized, noble metal quantum clusters (adapted from, A. Mathew and T. Pradeep, *Part. Part. Syst. Charact.*, 2014, **31**, 1017–1053).

Important parameters for controlling the size, structure, oxidation state, and surface properties of metal QCs and thus their optical properties include the species and concentration of chemicals (ligands) or templates, the concentration of metal ions, the species and concentration of reducing agents, the pH of the solution, as well as reaction temperature and time. Stable and highly fluorescent metal QCs can be prepared only in presence of different capping agents like peptides, polymers, and proteins. As this thesis (chapters 5 and 6) discusses synthesis of fluorescent copper nanoclusters, a brief discussion on the synthesis of copper nanoclusters are discussed in the next topic of my thesis introduction section.

1.14.1. Synthesis of Copper Nanoclusters

Stabilization of CuNCs continues to be an enigma to the scientists. The lower redox stability of Cu(0) with its lower standard reduction potential ($E^0_{\text{Cu}^{2+}/\text{Cu(s)}} = +0.377 \text{ V}$) compared to other members of Group 11 noble metals, like Ag and Au ($E^0_{\text{Ag}^+/\text{Ag(s)}} = +0.799$ and $E^0_{\text{Au}^{3+}/\text{Au(s)}} = +1.5 \text{ V}$) makes such tiny sized particles very much reactive towards environmental conditions.³⁶⁷ However, high costs of Ag and Au noble metal precursors limit their large scale production, therefore synthesis of CuNCs is not only challenging but also interesting research field for both

scientific and industrial researchers. Recently, various synthetic techniques have been developed to prepare water-soluble CuNCs with different emissions from blue to red (Figure 1.59). Generally, CuNCs are formed by the reduction of Cu^{2+} in the presence of suitable reducing agents and stabilizing agents, which can markedly affect their properties. Moreover, the stabilizing agents of CuNCs are responsible for their fluorescence emission and their sizes. Therefore, we will discuss various methods for the CuNCs synthesis as well as the synthesis of Au and Ag NCs in the next topic of discussion.

1.15. Various Methods for the Synthesis of Metal Nanoclusters

1.15.1. Synthetic Methods for Gold Nanoclusters

Chemical Reduction: Stable AuQCs are commonly prepared through the reduction of Au^{3+} to Au in the presence of reducing and capping agents. Thiol compounds occupy a key position among capping agents for its ability to form strong Au-S bonding with Au atoms/ions. Common reducing agents used to prepare AuQCs in the presence of thiol compounds are sodium borohydride (NaBH_4) and tetrakis-(hydroxymethyl) phosphonium chloride (THPC). Stable glutathione-stabilized AuQCs (GSH-AuQCs) have been prepared from Au^{3+} in the presence of glutathione (GSH) using NaBH_4 as a reducing agent.³⁶⁶ After purification and separation, different sizes of GSH–AuQCs with quantum yields (QYs) of <0.1% can be obtained that can emit from visible to NIR region.^{366, 386} By adapting a similar approach, many other thiols such as tiopronin,³⁶⁹ phenylethylthiolate,³⁷⁰ polyethylene glycol appended lipoic acid, and thiolate³⁷¹ cyclodextrin³⁷² have been used to prepare monolayer-stabilized AuQCs. The particle size and the QY of the thiol-stabilized AuQCs usually decrease upon increasing the molar ratio of thiol to-Au ions. Unfortunately, all of the prepared thiol-stabilized AuQCs have low QYs. Among thiol stabilized AuQCs, GSH has been widely used as capping and reducing agent to prepare highly fluorescent QCs. Under neutral conditions, GSH acts as a weak reducing agent but a strong capping agent that allows incomplete reduction of Au^{3+} to Au to form the

AuQC core, each of which is stabilized with a monolayer of thiolate-Au⁺ complexes.^{373, 374}

Xie and co-workers reported a GSH stabilized fluorescent Au@Au⁺-thiolate core-shell QCs (QY of ~15%) with a relatively low thiol-to-Au molar ratio (1.5:1). Here, the core-shell QCs were prepared through the controlled aggregation of the thiolate-Au⁺ complex on the *in situ* generated Au cores (Figure 1.61).³⁷⁴

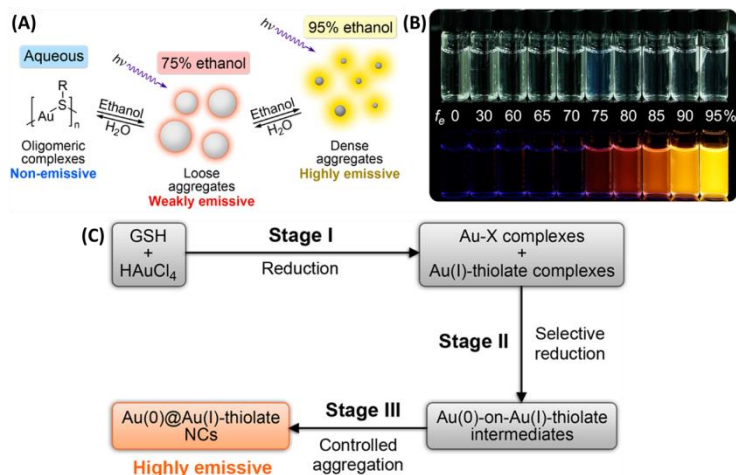


Figure 1.61. (A) Schematic illustration of solvent-induced AIE properties of oligomeric Au(I)-thiolate complexes. (B) Digital photos of Au(I)-thiolate complexes in mixed solvents of ethanol and water with different f_e (v ethanol/ v ethanol+water) under visible (top row) and UV (bottom row) light. (C) Schematic of synthesis of highly luminescent Au(0)@Au(I)-thiolate NCs. X in the Au(I)-X complexes can be any non-thiolate functional group in the reaction mixture (adapted from, Z. Luo, X. Yuan, Y. Yu, Q. Zhang, D. T. Leong, J. Y. Lee and J. Xie, *J. Am. Chem. Soc.*, 2012, **134**, 16662–16670).

In addition to small thiol compounds, polymers such as poly(amidoamine) (PAMAM) dendrimers can be used as a template to prepare highly fluorescent AuQCs. Through the complex coordination between Au³⁺ ions and the amino or carboxylic groups of PAMAM, PAMAM-stabilized AuNCs were prepared through a chemical reduction using NaBH₄ as a reducing agent.³⁷⁵ Dickson and co-workers have utilized second and fourth generation OH-terminated PAMAM to stabilize and solubilize gold nanoclusters in both aqueous and methanol solutions.³⁷⁵ The synthesized gold cluster is actually Au₈ nanodots that show strong size-specific emission, with a quantum yield of ~41% in aqueous solution (Figure 1.62). By varying the molar ratio of PAMAM to Au ions from 1:1 to 1:15, the same group has also prepared different sizes of AuQCs, including Au₅, Au₈, Au₁₃, Au₂₃, and Au₃₁ were prepared. The

PAMAM stabilized Au NCs emit at wavelengths from the UV to near infrared (NIR) region, with QYs ranging from 10% to 70%.³⁷⁶

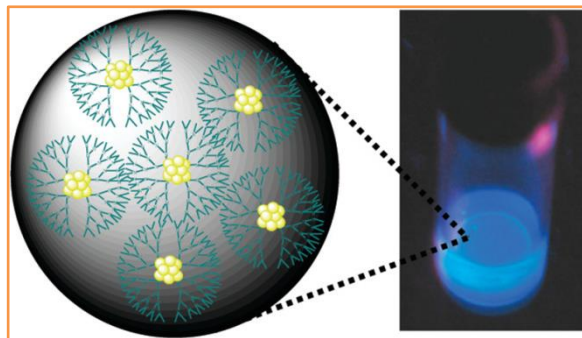


Figure 1.62. Emission from Au nanodots under long-wavelength UV lamp irradiation (366 nm) (adapted from, J. Zheng, J. T. Petty and R. M. Dickson, *J. Am. Chem. Soc.*, 2003, **125**, 7780–7781).

Kawasaki and co-workers have also demonstrated the synthesis of dimethylformamide (DMF)-protected gold nanoclusters using a surfactant-free DMF reduction method.³⁷⁷ DMF-protected AuQCs are obtained without the formation of gold nanoparticles and bulk metals as by-products using a hot injection process for the homogeneous reduction. The as-prepared DMF-protected AuQCs were a mixture of various-sized AuQCs with a cluster number of less than 20 including at least Au₈ and Au₁₃. The photoluminescence emission from Au₈ and Au₁₃ was confirmed in the photoluminescence spectra. Mattoussi and his co-workers have developed a new set of highly fluorescent gold nanoclusters (AuQCs) by using one-step aqueous reduction of a gold precursor salt in the presence of bidentate ligands composed of lipoic acid anchoring groups, appended with either a poly(ethylene glycol) short chain or a zwitterion group.³⁷⁸ The AuQCs fluoresce in the red to near-infrared region of the optical spectrum with emission centered at ~750 nm and a quantum yield of ~10 to 14%, and they exhibit long fluorescence lifetimes (up to ~300 ns). Dispersions of these AuNCs exhibit great long-term colloidal stability, over a wide range of pHs (2 to 13) and in the presence of high electrolyte concentrations, and a strong resistance to reducing agents such as glutathione.³⁷⁸ Biomolecules including peptides, proteins, DNA have been evolved as structure-defined scaffolds to induce the nucleation and growth of Au NCs. BSA is the most commonly used protein for the preparation of Au NCs.³⁷⁹

Photochemical Reduction: The common reducing agent used for chemical reduction is NaBH_4 which is a hazardous substance. To avoid this, photoreduction can be an alternative approach for the preparation of AuQCs.^{380, 381} Tan and co-workers used tridentate thioether terminated polymers, including poly(methyl methacrylate), poly(n-butyl methacrylate), and poly(tert-butyl methacrylate), to synthesize fluorescent Au QCs through photoreduction.³⁸¹ These Au NCs exhibit blue emission with QYs of 3.8%, 14.3%, and 20.1%, respectively. The size and QYs of these Au NCs are dependent on the nature of the polymers and can be controlled by varying the molar ratio of polymer to Au ions. Chang and co-workers have developed mannose modified gold nanodots (Man–AuNDs) through the reaction of 2.9 nm-diameter gold nanoparticles (AuNPs) with 11-mercapto-3,6,9-trioxaundecyl- α -D-mannopyranoside (Man-RSH) under irradiation by a green light emitting diode (LED) within 8 hours.³⁸² They have found that the irradiation enhances the quantum yield ($\sim 11\%$), alters the emission wavelength and lifetimes, and shortens the preparation time.

pH of the Medium: Solution pH is an important parameter in controlling the reducing strength, protein conformation, and capping capability of the protein, and thus various sizes of Au NCs can be prepared at various pH values. Porcine pepsin with strong pH-dependent conformational states presents a good example for the preparation of various sizes of AuNCs.³⁸³ Pradeep and co-workers have successfully utilized a synthetic route for the synthesis of highly luminescent, water soluble gold quantum clusters (QCs), which are stabilized by an iron binding transferrin family protein, lactoferrin (Lf) using 1 M NaOH.³⁸⁴ They have found that two distinct cluster cores by mass spectrometry and sub-nanometre cores were observed in TEM. Kawasaki and co-workers have demonstrated the first pH-dependent synthesis of pepsin mediated AuQCs with blue-, green-, and red-fluorescent emission from Au_5 (Au_8), Au_{13} , and Au_{25} , respectively at different pHs (Figure 1.63).³⁸⁵ Tseng and co-workers have developed a one-pot approach for preparing highly fluorescent Au_8 clusters by reacting the Au^{III} precursor solution with lysozyme type VI (Lys VI) at pH 3.³⁸⁶

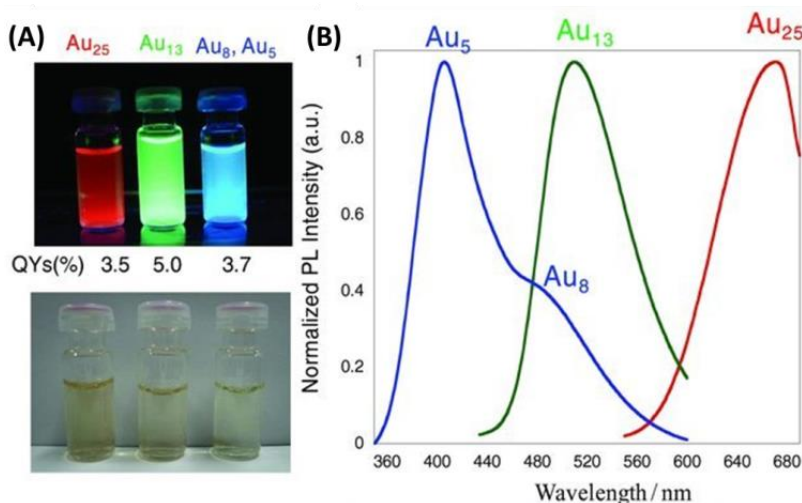


Figure 1.63. (A) Pepsin-mediated AuNCs with red, green, and blue emission under UV light (above) or visible light (below) in aqueous solutions. (B) Fluorescence spectra of aqueous solutions of pepsin-mediated AuNCs with red (sample I, Au₂₅) at pH 12, green (sample II, Au₁₃) at pH 1, and blue (sample III, Au₅ and Au₈) emission at pH 9 (adapted from, H. Kawasaki, K. Hamaguchi, I. Osaka and R. Arakawa, *Adv. Funct. Mater.*, 2011, **21**, 3508–3515).

The fluorescence band of (Lys VI)-stabilized Au₈ clusters is centred at 455 nm on the excitation at 380 nm. This blue-emitting Au₈ clusters have a high quantum yield ($\sim 56\%$), two fluorescence lifetimes, and a rare amount of Au^I on the surface of the Au core. They have converted Au₈ clusters to Au₂₅ clusters upon sudden increase of pH from 3 to 12. This conversion is also observed in the case of (Lys VI)-directed synthesis of Au₂₅ clusters at pH 12.

Core-Etching: AuQCs can be prepared from larger AuNPs with a core size of 2–4 nm through the ligand-induced etching method using excess ligands. Au NPs which are prepared under alkaline conditions from Au³⁺ using THPC as capping and reducing agent, can be used to prepare AuQCs using thiol ligands like 11-mercaptoundecanoic acid (11-MUA) as an etching agent. At such a high pH value (>12.0), 11-MUA provides strong etching ability to etch the surface Au atoms and provide strong coordination ability to form stable 11-MUA–Au complexes on the surface of each Au core to stabilize it, yielding fluorescent 11-MUA capped AuNCs (11-MUA–AuQCs) with a QY of 3.1%.³³⁹ One feature of this approach is that the size of AuQCs and thus their optical properties can be controlled by using different thiol compounds. Alkanethiol-bound AuQCs prepared by using different chain lengths of alkanethiols as

ligands have the emission wavelengths within the range of 501–613 nm, with QYs ranging from 0.0062 to 3.1%.³³⁹ Different sizes of AuQCs that emit different colors have also been prepared by using Al₂O₃ NPs as supports in the presence of HAuCl₄ and 6-mercaptohexanol.³⁸⁷ Penicillamine (PA) adsorbed on the surfaces of Al₂O₃ reduces Au³⁺ ions to Au⁺ ions that are further reduced to form small AuNPs by THPC. The as-formed AuNPs are further etched by 6-mercaptohexanol under irradiation of blue light-emitting diode (LED). Stronger fluorescent AuQCs can be prepared much more rapidly under LED irradiation than in the day light (4 h vs 3 days).

These fluorescent AuQCs exhibit a number of attractive optical properties: tunable fluorescent wavelength, long lifetime (>200 ns), and large Stokes shift (>100 nm). These properties provide the feasibility for sensing proteins in biological samples and metal ions in environmental samples.^{339, 365, 387-389} Nie and co-workers have developed a new method for preparing highly fluorescent and water-soluble metal nanoclusters based on the use of multivalent coordinating polymers to etch preformed high-quality gold nanocrystals (Figure 1.64).³⁹⁰ They have used polyethylenimine stabilized gold nanoclusters using sodium borohydride as a reducing agent. Martinez and co-workers have reported a new method for preparing fluorescent and water-soluble Au nanoclusters using small molecules as reducing agents and stabilizing ligands.³⁹¹ They showed that the reaction proceeds by first forming irregularly shaped nanoparticles, which are subsequently etched by excess ligands to produce fluorescent nanoclusters. These reaction mixtures yield fluorescent species with sizes consistent with gold cores of a few atoms and have large effective quantum yields with nanosecond fluorescence lifetimes.³⁹¹

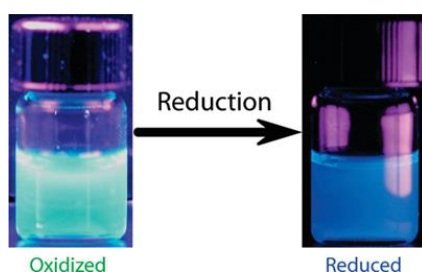


Figure 1.64. Color photographs of the original Au nanocrystals (adapted from, H. Duan and S. Nie, *J. Am. Chem. Soc.*, 2007, **129**, 2412-2413).

Pradeep and co-workers have revolutionized the field of core-etching approaches by using different synthetic procedure for the synthesis and stabilization of gold nanoclusters using NaBH_4 as a reducing agent (Figure 1.65).³⁹² They have developed two fluorescent quantum clusters of gold, namely Au_{25} and Au_8 from mercaptosuccinic acid-protected gold nanoparticles of 4-5 nm core diameters by etching with excess glutathione. While etching at pH ~ 3 yielded Au_{25} , that at pH 7-8 yielded Au_8 . This simple method makes it possible to synthesize well-defined clusters in gram quantities.

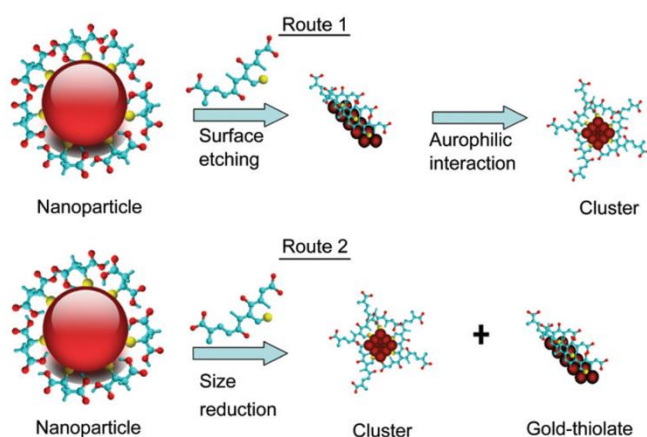


Figure 1.65. Schematic representation of two possible routes for the formation of clusters from Au@MSA nanoparticles (adapted from, M. A. H. Muhammed, S. Ramesh, S. S. Sinha, S. K. Pal and T. Pradeep, *Nano Res.*, 2008, **1**, 333–340).

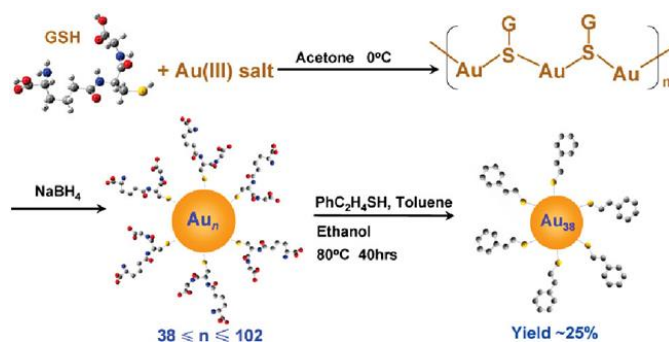


Figure 1.66. A two-step procedure for synthesizing monodisperse $\text{Au}_{38}(\text{SC}_2\text{H}_4\text{Ph})_{24}$ clusters in high yield (adapted from, H. Qian, Y. Zhu and R. Jin, *ACS Nano*, 2009, **3**, 3795–3803).

Jin and his co-workers have developed a facile, high yielding synthetic method for preparing truly monodisperse $\text{Au}_{38}(\text{SC}_2\text{H}_4\text{Ph})_{24}$ nanoclusters (Figure 1.66).³⁹³ They showed that the synthetic approach involves two main steps: first, glutathionate (-SG) protected polydisperse $(\text{Au})_n$ clusters (n ranging from 38 to ~ 102) were synthesized by reducing Au(I)-SG in acetone; subsequently, the size-mixed Au_n clusters react with

excess phenylethylthiol ($\text{PhC}_2\text{H}_4\text{SH}$) for ~40 h at 80 °C, which leads to $\text{Au}_{38}(\text{SC}_2\text{H}_4\text{Ph})_{24}$ clusters of molecular purity. Our group has also reported a dipeptide Cys-Cys stabilized blue AuQC with high quantum yield (~41%) synthesized by a sulfur etching process from large plasmonic AuNPs.³⁹⁴ Pradeep and co-workers have also synthesized fluorescent, porphyrin-anchored Au_{22} clusters in a single step, starting from well-characterized Au_{25} clusters protected with glutathione (-SG) by a combined core reduction/ligand exchange protocol, at a liquid-liquid interface by using tetraphenylporphyrinithiol ($\text{H}_2\text{TPPOASH}$) (Figure 1.67).³⁹⁵

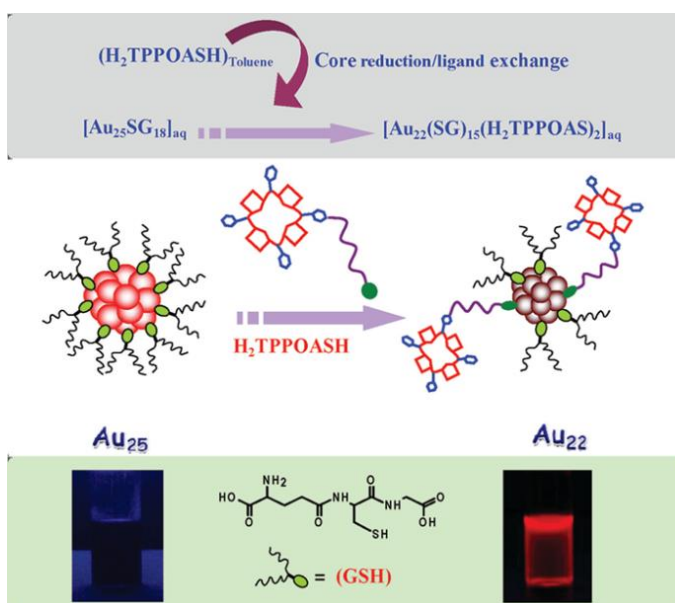


Figure 1.67. Schematic Representation of the Formation of NIR-Emitting Au_{22} clusters from parent Au_{25} by simultaneous Core Reduction and Ligand Exchange (adapted from, E. S. Shibu, R. Radha, P. K. Verma, P. Bhyrappa, G. U. Kulkarni, S. K. Pal and T. Pradeep, *ACS Appl. Mater. Interfaces*, 2009, 1, 2199–2210).

1.15.2. Synthetic Methods for Silver Nanoclusters

Chemical Reduction: Silver ions (in presence of a proper stabilizing agent) are rapidly reduced by strong reducing agents (like sodium borohydride) to form fluorescent silver nanoclusters. DNA oligonucleotides are often used as a stabilizing agent as silver ions can interact strongly with DNA. Previously, Dickson and his co-workers used DNA as a template for the synthesis of water-soluble fluorescent Ag NCs using NaBH_4 as a reducing agent.³⁹⁶ Ag(I) ions have a strong interaction with single-stranded DNA, and upon the addition of NaBH_4 , Ag nanoclusters are formed. The mass spectrometric study confirmed that

small Ag nanoclusters are formed with 2–4 atoms, and these are bonded to the DNA template. The obtained Ag nanoclusters have discrete absorption and fluorescence property. Later some groups used single-stranded DNA consisting of 12 cystine to make strongly emissive near-IR emitted Ag nanoclusters.³⁹⁷ Ag nanoclusters prepared in this method have a fluorescence quantum yield of 17% and these Ag nanoclusters exhibit excellent properties including good photostability and high quantum efficiency.

Dickson and co-workers have made fluorescent Ag NCs with discrete emissions ranging from blue to NIR using DNA microarrays of 12-mer oligonucleotide strands. They have tried to find out optimal sequences for Ag NC formation. However, the synthesis of each specific NCs did not follow a general procedure.³⁹⁸ These Ag NCs are reported to have very high quantum yields ranging from 16% to 34%. It can be mentioned that the yellow, red, and NIR-emitting clusters have exhibited greatly reduced bleaching and blinking. O'Neill and co-workers have demonstrated the loop-dependent synthesis of fluorescent Ag NCs using DNA hairpins with having 3–12 cytosines in the loop.³⁹⁹

Deng and co-workers have reported oligonucleotide stabilized fluorescent Ag NCs. They have estimated the quantum yield of the silver nanoclusters at room temperature is $28 \pm 1\%$.⁴⁰⁰

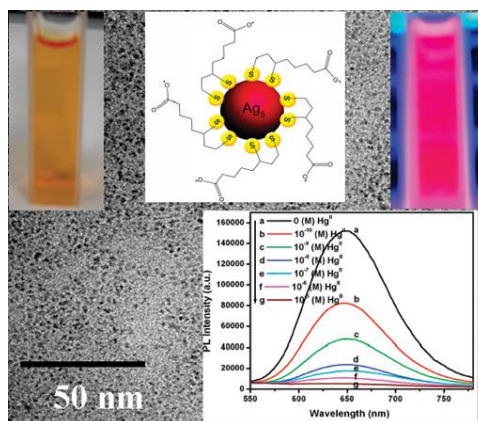


Figure 1.68. Fluorescent silver nanoclusters containing five atoms showing two different color in visible light and in presence of UV-light (adapted from, B. Adhikari and A. Banerjee, *Chem. Mater.* 2010, **22**, 4364–4371).

Banerjee and co-workers have developed dihydro lipoic acid stabilized highly fluorescent silver nanoclusters (Figure 1.68) using sodium borohydride as a reducing agent in a water medium. The author showed

mass spectrometrically the presence of a few atoms in nanoclusters containing only Ag₄ and Ag₅. The reported fluorescent Ag nanoclusters with excellent optical properties, including a narrow emission profile, larger Stokes shift (more than 200 nm), and good photostability.⁴⁰¹

Photochemical Reduction: In a pioneering work, Dickson and co-workers made fluorescent Ag nanoclusters using the photoirradiation approach in AgO films in the year 2001.⁴⁰² The obtained fluorescent silver nanoclusters consist of 2–8 Ag atoms. In the first report of water-soluble fluorescent Ag nanoclusters,⁴⁰³ Dickson and co-workers utilized a similar photoreduction of polymers with abundant carboxylic acid groups that were identified as promising templates for synthesizing highly fluorescent, water-soluble Ag NCs using a photoreduction approach.

Kumacheva and co-workers have reported the successful photogeneration of fluorescent Ag nanoclusters in poly(N-isopropyl acrylamide-acrylic acid-2-hydroxyethyl acetate) copolymer-based hydrogel microspheres by UV irradiation (Figure 1.69).⁴⁰⁴ The fluorescent property of Ag nanoclusters formed within the polymer microgels can be finely controlled by UV-irradiation time. Moreover, the fluorescent microgels show stimuli responsiveness including pH and temperature.

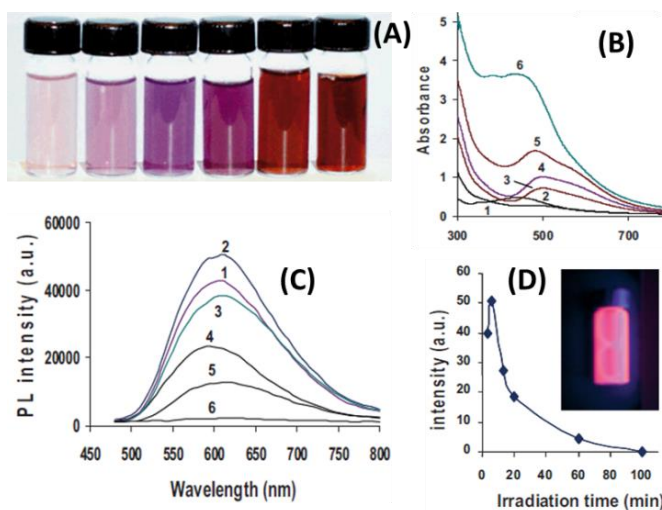


Figure 1.69. Ag nanoclusters stabilized in microgel dispersions. (A) Photograph under day light; (B) UV-vis spectra of poly(N-isopropyl acrylamide-acrylic acid-2-hydroxyethyl acetate) microgel dispersion formed after mixing with Ag⁺ ions and UV-irradiation (365 nm) for different time intervals: (1) 3 min, (2) 6 min, (3) 13 min, (4) 20 min, (5) 40 min and (6) 100 min. (A) Shows the same times of irradiation from left to right. Evolution of (C) photoluminescence spectra and (D) photoluminescence intensity ($\lambda_{\text{ex}} = 450$ nm) of Ag nanoclusters photogenerated in microgel vs. duration of irradiation. The inset in (D) shows a photoluminescent hybrid microgel obtained after 10 min UV irradiation (adapted from, J. Zhang, S. Xu and E. Kumacheva, *Adv. Mater.*, 2005, **17**, 2336).

Core-Etching: Pradeep and co-workers have made an outstanding contribution in this field. They have designed a method for gram-scale synthesis of two luminescent silver nanoclusters, Ag₇ having blue emission and Ag₈ having red/NIR emission.⁴⁰⁵ The nanoclusters exhibit two emission bands at 440 nm and 650 nm corresponding to Ag₇ and Ag₈ nanoclusters respectively. They have prepared this nanocluster by etching large silver nanoparticles at the interface of several aqueous/organic biphasic systems using a thiol-containing small molecule, mercaptosuccinic acid as a template. The fluorescence quantum yield can be increased up to 9% with decreasing temperature for Ag₈ clusters (Figure 1.70). Ag₈ clusters can selectively adsorb on metal oxides including Al₂O₃, TiO₂, and MgO and this suggests the potential application of these clusters as a catalyst.

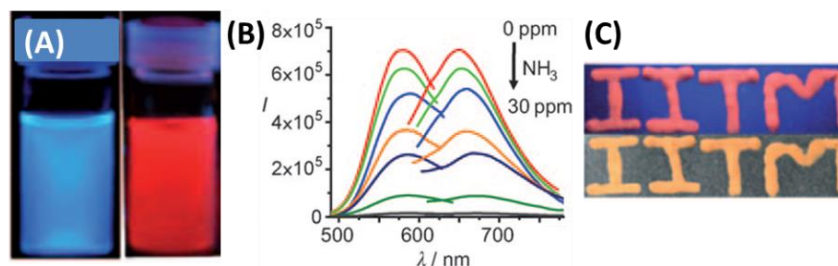


Figure 1.70. (A) Photograph of Ag₇ and Ag₈ clusters samples under UV-light; (B) fluorescence quenching by addition of NH₃; (C) photograph of Ag₈-loaded alumina at 0.5 wt% under UV-light (top) and under visible light (bottom) at room temperature (adapted from, T. U. B. Rao and T. Pradeep, *Angew. Chem. Int. Ed.*, 2010, **49**, 3925–3929).

1.15.3. Synthetic Methods for Copper Nanoclusters

Chemical Reduction: Currently, a variety of small molecules have been employed as stabilizers or reducers to synthesize CuNCs. These small molecule-functionalized CuNCs are generally divided into two main types: thiol- and non-thiol-functionalized CuNCs.

Thiols are commonly used to prepare lots of fluorescent metal nanoparticles since thiols exhibit good reducibility to metallic salts and affinity to metal nanoparticles. D-penicillamine (DPA) recently has been used as capping and reducing agent to fabricate CuNCs with AIE properties via simple mixing of DPA with Cu²⁺ at room temperature.³⁶¹ With the aid of NaOH, L-Cys can also serve as the capping and reducing agent for the synthesis of CuNCs with different emissions (Figure 1.71).⁴⁰⁶ Zhang's group has recently developed a simple method for the in

situ synthesis of red emissive CuNCs in supramolecular hydrogels via employing a series of bile acid derivatives (BAs) as pregelators. The work shows that Cu^{2+} could interact with a series of BAs to form supramolecular hydrogels, and excess L-Cys can diffuse into the gels to generate the CuNCs with red emission at 615 nm. The formation of the CuNCs is attributed to the fact that excess Cys could reduce and decompose the partial Cys- Cu^+ coordination polymers formed by the coordination of Cu^{2+} to produce the red emissive CuNCs with the QY of 0.1%.⁴⁰⁷ Chang's group recently prepared CuNCs stabilized by three isomers of mercaptobenzoic acids and found that the structure of mercaptobenzoic acids exhibits a great effect on the synthesis and fluorescence properties of CuNCs. Among the three kinds of CuNCs, 2-mercaptobenzoic acid-CuNC (2-MBA-CuNC) aggregates with blue emission show the strongest fluorescence, 4-MBA-CuNC aggregates emitting red fluorescence exhibit an interesting AIE effect, and 3-MBA-CuNC aggregates show weakly red fluorescence (Figure 1.72).⁴⁰⁸ Now, great efforts have been devoted to enhancing the fluorescence emission of CuNCs. Wu *et al.* have demonstrated the fluorescence enhancement of CuNCs via a self-assembly strategy. The original non-fluorescent 1-dodecanethiol capped CuNCs are self-assembled into the compact and ordered self-assembly architectures exhibiting mechanochromic and thermochromic fluorescence properties. The high compactness reinforces the cuprophilic interactions of F-CuNPs, and suppresses the intramolecular vibration and rotation of the capping ligands, resulting in the fluorescence enhancement of the as-prepared CuNCs. Meanwhile, the strategy can tune the regularity of the assemblies of CuNCs, producing different emissions (Figure 1.73).⁴⁰⁹

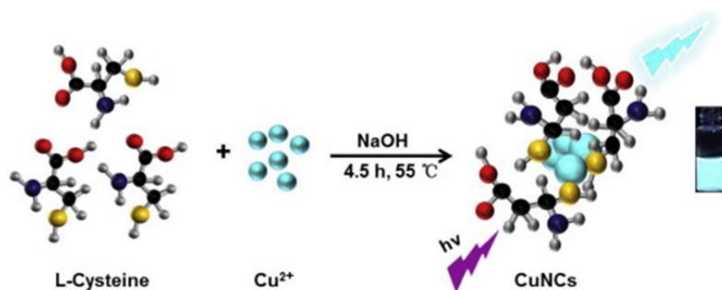


Figure 1.71. Synthetic approach of F-CuNPs stabilized by L-Cys (adapted from, X. Yang, Y. Feng, S. Zhu, Y. Luo, Y. Zhuo and Y. Dou, *Anal. Chim. Acta*, 2014, **847**, 49–54).

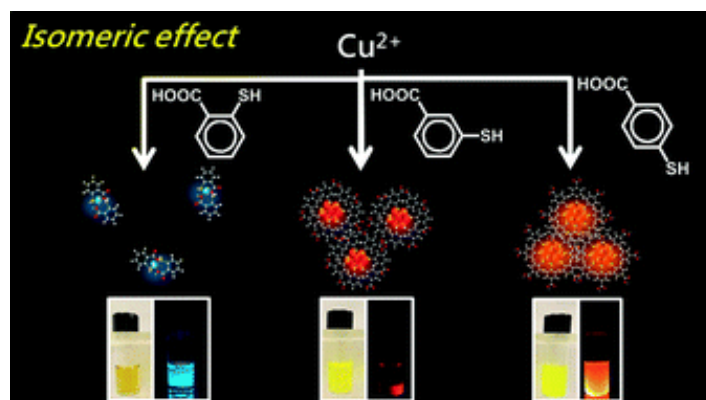


Figure 1.72. The change in fluorescence due to the isomeric effect of different mercaptobenzoic acid (adapted from, Y.-J. Lin, P.-C. Chen, Z. Yuan, J.-Y. Ma and H.-T. Chang, *Chem. Commun.*, 2015, **51**, 11983–11986).

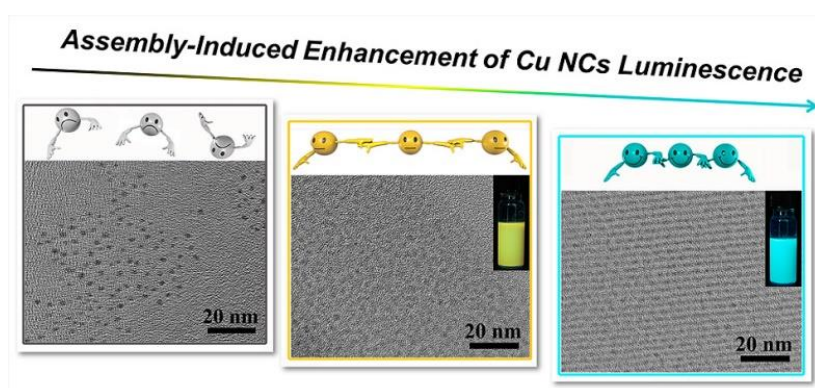


Figure 1.73. Illustration of the assembly-induced fluorescent enhancement of F-CuNCs (adapted from, Z. Wu, J. Liu, Y. Gao, H. Liu, T. Li, H. Zou, Z. Wang, K. Zhang, Y. Wang, H. Zhang, and B. Yang, *J. Am. Chem. Soc.*, 2015, **137**, 12906–12913).

The chemical reduction method has been used to prepare thiol-stabilized CuNCs. Wei *et al.* have recently prepared stable CuNCs (Cu_n , $n \leq 8$) via a one-pot chemical reduction method with 2-mercapto-5-n-propylpyrimidine as the protecting ligand and NaBH_4 as the reducing agent. The resultant CuNCs are soluble in nonpolar solvents such as toluene, hexane, and chloroform. The solution of the CuNCs in CHCl_3 shows an orange color under UV light ($\lambda_{\text{ex}} = 365 \text{ nm}$). The CuNCs exhibit apparent luminescence with dual emissions at 425 and 593 nm and high electrocatalytic activity in the electroreduction of oxygen.⁴¹⁰ Dihydrolipoic acid-functionalized CuNCs with red emission have been fabricated by using ascorbic acid and dihydrolipoic acid as the reducing agents in the presence of polyvinylpyrrolidone. The CuNCs in the solid form are stable and retain their optical properties for a month, and the CuNCs exhibit pH-tunable reversible optical properties in an aqueous solution.⁴¹¹

The chemical reduction can be used to prepare CuNCs stabilized by nonthiols. Isomura *et al.* have recently synthesized a kind of surfactant-free CuNCs under reflux at 140 °C via the DMF reduction method. The resulting CuNCs with a size of about 2.0 nm exhibit the maximum emission wavelength at around 420 nm with the excitation at 350 nm.⁴¹² Histidine has been used both as a stabilizer and reducer to fabricate CuNCs with blue emission under refluxing at 70 °C.⁴¹³ At the same time, tannic acid,⁴¹⁴ linoleic acid,⁴¹⁵ 1,10-phenanthroline,⁴¹⁶ Ethanol,³⁵¹ etc. have been employed to prepare CuNCs.

Polymers have been directly utilized as the template to prepare CuNCs because of the presence of multiple binding sites. Lipoic acid-modified poly(ethylene glycol) (LA-PEG₇₅₀-OCH₃) has been employed as the stabilizer for synthesizing water-soluble CuNCs with the size of 2.5 nm based on the direct metal reduction by NaBH₄ under reflux. The CuNCs with a QY of 3.6% exhibit blue emission at 416 nm and high photostability.⁴¹⁷ More recently, polyethyleneimine (PEI) has been used as a stabilizing agent to prepare PEI-stabilized CuNCs with N₂H₄·H₂O to reduce Cu²⁺ at 95 °C. The PEI-stabilized CuNCs with the size of 1.8 nm exhibit blue emission centered at 480 nm and the QY in ethanol is 3.8%. Similarly, formaldehyde and ascorbic acid have been utilized as reducing agents to prepare PEI-stabilized CuNCs.^{418, 419}

A solid-state synthesis method is a newly emerged green method, which has been widely used in organic synthesis without the extensive use of toxic solvents.^{420, 421} Ganguly *et al.* have recently prepared a kind of CuNCs protected with phenylethanethiol using NaBH₄ as the reducing agent in an agate mortar. However, the as-made CuNCs are unstable and decompose in about 2 h at room temperature. More efforts are needed to improve atmospheric stability.⁴²²

Photochemical Reduction: The photoreduction method is a clean, non-toxic, and less time-consuming approach for the synthesis of various nanomaterials without the use of additional reducing agents. Similarly, Tan's group has recently synthesized CuNCs via a photoreduction method in the presence of poly(methacrylic acid) functionalized with pentaerythritol tetrakis 3-mercaptopropionate (PTMP-PMAA). They used a UV light source (8 W, wavelength = 365 nm) to irradiate the solution of

$\text{Cu}(\text{NO}_3)_2$ in the presence of PTMP-PMAA. The irradiation of UV light for 1.5 h leads to the formation of CuNCs, which show the maximum emission peak at 630 nm when excited at 360 nm. The size of the obtained CuNCs is 0.7 ± 0.3 nm, and the QY is 2.2%. MALDI-TOF indicates that Cu_5 is the actual cluster formed in the solution. The optimal pH value for the formation of CuNCs is 3.4. It should be notified that the stability of the as-prepared CuNCs is not good because the CuNCs powder does not show fluorescence, and thus much work is needed to improve the performance of the CuNCs. More interestingly, this photo-reduction method has also been successfully used to prepare fluorescent gold and silver nanoparticles in the presence of PTMP-PMAA (Figure 1.74).³⁸⁰ The polymer-stabilized CuNCs needed to be further investigated.

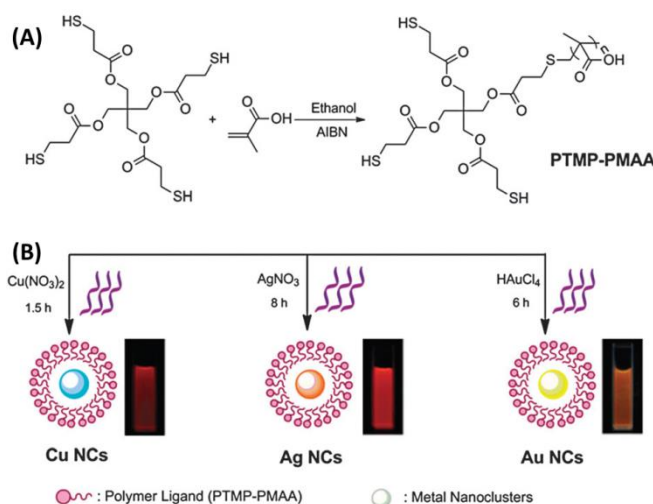


Figure 1.74. (A) Scheme for the synthesis of polymer PTMP-PMAA. (B) Preparation of CuNCs functionalized by polymers (adapted from, H. Zhang, X. Huang, L. Li, G. Zhang, I. Hussain, Z. Li and B. Tan, *Chem. Commun.*, 2012, **48**, 567–569).

Core-Etching: The etching method is another method for the synthesis of F-CuNPs. In the process of the etching method, the nonfluorescent nanoparticles are first prepared and the subsequent etching of the nonfluorescent metal nanoparticles with suitable ligands can produce fluorescent metal nanoparticles. Recently, Yuan *et al.* have synthesized F-CuNPs with the etching method by electrostatically induced reversible phase transfer. Using GSH as a model ligand, the F-CuNPs show two emission peaks at 412 and 438 nm upon excitation at 378 nm. Intriguingly, the approach can also be used to synthesize fluorescent gold,

silver, and platinum nanoparticles. At the same time, the fluorescent metal nanoparticles with desired functionalities can be fabricated by using simple custom-designed peptides, which may contribute to the wide applications of the fluorescent metal nanoparticles.⁴²³ More recently, Wang's group has proposed a facile method for synthesizing CuNCs with 1.3 ± 0.4 nm via surface etching from nonfluorescent Cu nanocrystals with the size of 4.2 ± 1.1 nm using GSH. Interestingly, the as-prepared CuNCs show amazing AIE enhancement effects. The possible route for the formation of CuNCs is "*surface etching*". Excess GSH interacts with Cu(I) to form the Cu(I)-GSH complex, which can remove Cu atoms from the surface of the Cu nanocrystals and tends to generate Cu₂ clusters due to the Cu⁺...Cu⁺ cuprophilic interactions. Intriguingly, other CuNCs with different surface functionalities can also be prepared with the designed thiol ligands.³⁶⁹ This approach provides a versatile method for synthesizing CuNCs with different surface properties.³⁶²

Microwave Irradiation: Non-thiols can also be employed to stabilize CuNCs via different approaches. Microwave irradiation is a widely accepted new processing technology because of its environmental friendliness and low energy consumption. Microwave irradiation can offer rapid and uniform heating of solvents, reagents, and intermediates, which can provide uniform nucleation and growth conditions for nanomaterials.^{424, 425} The microwave-assisted method has been recently utilized to synthesize CuNCs in ethylene glycol solution without using additional protective and reducing agents. The obtained CuNCs with an average size of 2.3 ± 0.25 nm can be dispersed again in a variety of polar solvents, including ethylene glycol, N, N-dimethylformamide (DMF), ethanol, and water. The CuNCs in ethanol shows blue emission centered at 475 nm under excitation at 350 nm, and the QY for the CuNCs in EG solution is 0.65%. The formation of CuNCs is related to the high reaction temperature and the addition of NaOH.⁴²⁶

Microemulsion: The microemulsion method is a general method for preparing various nanoparticles due to the precise control of the size and shape of nanoparticles.⁴²⁷ The microemulsion is formed by mixing a surfactant, a cosurfactant, an organic solvent, and water. The metal salt is

introduced in water, and the addition of the reducing agent can lead to the formation of monodisperse nanoparticles with a precisely controlled size because the surfactant can well control the growth of nanoparticles. CuNCs can be prepared via the microemulsion method by using sodium dodecyl sulfate as the surfactant; isopentanol as the cosurfactant; cyclohexane as the oily phase, and CuSO_4 solution as the aqueous phase to form a microemulsion. It is found that low percentages of NaBH_4 (<10%) can create CuNCs with the maximum fluorescence emission at 330 nm when excited at 290 nm. The CuNCs show good stability and mainly constitute Cu_{13} .⁴²⁸

Electrochemical: The electrochemical method is an efficient method for synthesizing various functional nanoparticles because of its simplicity.⁴²⁹ The electrochemical route mainly consists of electrolysis and electrodeposition. In the electrolysis method, CuNCs are produced in solution by the electrolysis of a Cu anode. The electrodeposition method is used to prepare CuNCs deposited on a solid electrode. Vilar-Vidal and co-workers have synthesized tetrabutylammonium nitrate (TBAN)-stabilized CuNCs with blue emission at 410 nm by a simple electrochemical method under galvanostatic conditions. The synthesis procedure is based on the reduction of Cu^{2+} generated during the electrolysis from the soluble Cu anode in a thermostated three-electrode conventional electrochemical cell. The TBAN-stabilized CuNCs are mainly formed from Cu_{14} , and the QY is 13%. The TBAN-stabilized CuNCs are highly stable and can be dispersed in both polar and nonpolar solvents.⁴³⁰

1.16. Applications of Au, Ag and Cu Nanoclusters

The unique optical and luminescence properties of noble metal nanoclusters make them highly appropriate for various applications such as sensing,^{431, 432} catalysis,^{433, 434} optics, imaging,⁴³⁵ and biolabeling.⁴³⁶⁻⁴³⁹ Mathew and Pradeep⁴⁴⁰ have addressed the applications of noble metal nanoclusters in detail in their review article. Some intriguing examples of study with monolayer protected nanoclusters are summarized below in Figure 1.75.

1.16.1. Metals (Au, Ag, Cu) Nanoclusters as Sensor

Au and Ag Nanoclusters Based Sensors

100 | Page

Sensing of different molecules or biomolecules or ions including hazardous ions (such as Hg^{2+}) using nanomaterials have now become an interesting topic in materials science.⁴⁴¹⁻⁴⁴³ In most of the cases, luminescence quenching is primarily utilized. Most of the literature on sensors is focused on the detection of Hg^{2+} and Cu^{2+} ions. For example, gold and silver clusters have a strong tendency to sense Cu^{2+} , as can be seen from the case of Au_{15} clusters reported by Shibu *et al.*⁴⁴⁴ This cluster was fabricated with chitosan to make a composite whose intense red luminescence was quenched upon addition of Cu^{2+} or on dipping the composite in Cu^{2+} solution.⁴⁴⁵ The composite film exhibited visual sensitivity to Cu^{2+} , up to 1 ppm, below the permissible limit (1.3 ppm) in drinking water [by the Environmental Protection Agency (EPA)]. Although the limit of detection for toxic metal ions reached below the parts per billion level in a few reports,⁴⁴⁶ the underlying mechanism was not identified.

Chang and his co-workers have shown that 11-mercaptoundecanoic acid-capped fluorescent AuQCs are able to detect Hg^{2+} ions based on Hg^{2+} induced aggregation of AuQCs.³⁵¹ The limit of detection (LOD) are measured to be 5.0 nM. Ying and his co-workers have reported BSA-templated fluorescent Au and Ag QCs for the selective and sensitive detection of Hg^{2+} ions.³⁴¹ The sensing mechanism is based on the high-affinity metallophilic $\text{Hg}^{2+}\text{--Au}^+$ or $\text{Hg}^{2+}\text{--Ag}^+$ interactions and this can efficiently quench the fluorescence property of Au and Ag QCs (Figure 1.76).³⁴¹

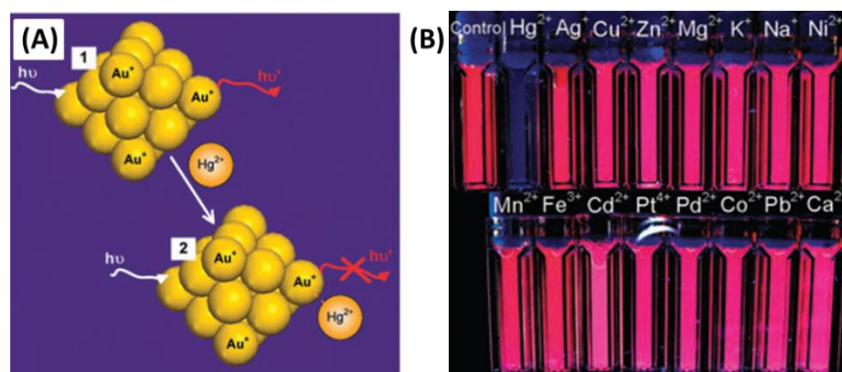


Figure 1.76. (A) Schematic representation of Hg^{2+} sensing based on fluorescence quenching of AuNCs resulting from high-affinity metallophilic $\text{Hg}^{2+}\text{--Au}^+$ bonds. (B) Photographs of aqueous BSA-AuNCs solutions in the presence of various metal ions under UV light (adapted from, J. Xie, Y. Zheng and J.Y. Ying, *Chem. Commun.*, 2010, **46**, 961-963).

Banerjee and his group have reported an easy way of synthesizing blue fluorescent gold nanoclusters from gold nanorods. These gold nanoclusters can selectively sense Fe(III) in water in presence of other metal ions. They also determined Fe(III) / Fe(II) ratio in real water samples.⁴⁴⁷ Based on the fluorescence quenching of the cluster, Zhu and co-workers reported a fluorescent silver nanocluster probe for detecting Cr^{3+} ions with high sensitivity and selectivity. The detection limit of Cr^{3+} ions was $28 \times 10^{-9} \text{ M}$.⁴⁴⁸

Sensing of Biomolecules: In a different work Chen and co-workers used a Au@GSH clusters initially quenched by Fe(III) as a sensing probe for phosphate-containing metabolites.⁴⁴⁹ Jin *et al.* have reported a cholic acid stabilized Au nanoclusters for detection of creatinine. Upon addition of creatinine the nanoclusters started glowing in green fluorescence under UV-light irradiation.

Xie and co-workers presented a simple method for sensing cystine (Cys) biomolecule using GSH-protected silver nanoclusters combining the thiol-silver chemistry and steric hindrance of the ligand shell protecting the cluster surface. Thiol containing Cys shows very high selectivity towards the Ag nanoclusters compared to the other 19 non-thiol natural amino acids (Figure 1.77) due to the specific thiol–Ag interaction.⁴³¹

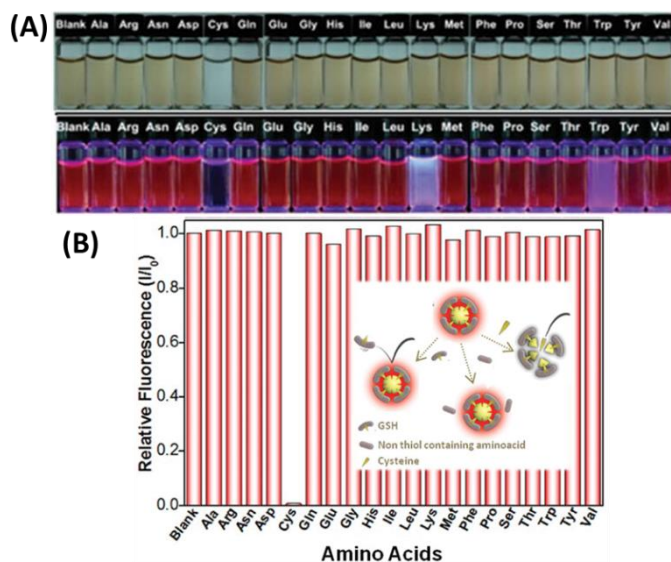


Figure 1.77. (A) Photographs of the Ag@GSH cluster solution in presence of different amino acids, under visible (top panel) and UV (bottom panel) light. (B) Relative fluorescence intensities of the corresponding solutions are shown. Schematic of the sensing mechanism is also shown (adapted from, X. Yuan, Y. Tay, X. Dou, Z. Luo, D. T. Leong and J. Xie, *Anal. Chem.*, 2013, **85**, 1913–1919).

Copper Nanoclusters Based Sensors

Sensing of Metal Ions: CuNCs exhibiting unique physicochemical properties and easy fabrication have increasingly been captivating the attention of scientists. Various applications of CuNCs in different fields have been well investigated over the past few years. Wang's group has recently proposed a facile fluorescence turnon nanosensor for Hg^{2+} by utilization of dsDNA-specific CuNCs. The presence of Hg^{2+} can induce the formation of a complementary primer-template complex and subsequent primer-extension reaction, which can provide the template for the formation CuNCs after the addition of Cu^{2+} and ascorbate. The dsDNA stabilized CuNCs have good selectivity for Hg^{2+} due to the specific interaction between Hg^{2+} and the thymine of the dsDNA (Figure 1.78). Intriguingly, the proposed approach has also been used to assay other targets, such as polymerase and nucleic acid.⁴⁵⁰

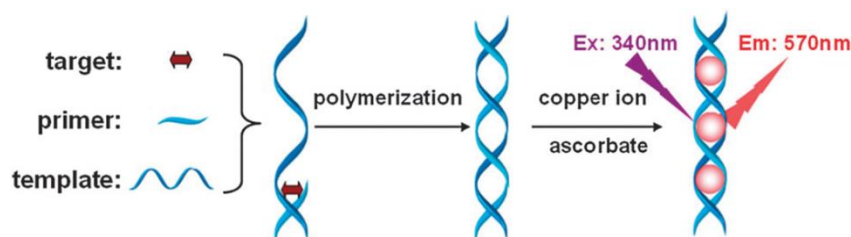


Figure 1.78. Schematic representation of polymerization-mediated biochemical analysis with dsDNA-specific CuNCs (adapted from, Z. Qing, T. Qing, Z. Mao, X. He, K. Wang, Z. Zou, H. Shi and D. He, *Chem. Commun.*, 2014, **50**, 12746–12748).

Sensitive detection of Pb^{2+} with CuNCs can also be achieved. BSA-protected F-CuNPs with the maximum emission of 410 nm have been synthesized for the detection of Pb^{2+} at part-per-million concentrations without any interference from other metal ions. The fluorescence turn-off detection of Pb^{2+} can be realized based on the aggregation of F-CuNPs caused by Pb^{2+} .³⁵⁵

Sensing of Biomolecules: Wang and his group have recently shown that, fluorescence of DNA-hosted copper nanoclusters are very much sensitive to the base types located in the major grooves. They have exploited this property in detecting single mismatch in DNA structures (Figure 1.79).⁴⁵¹

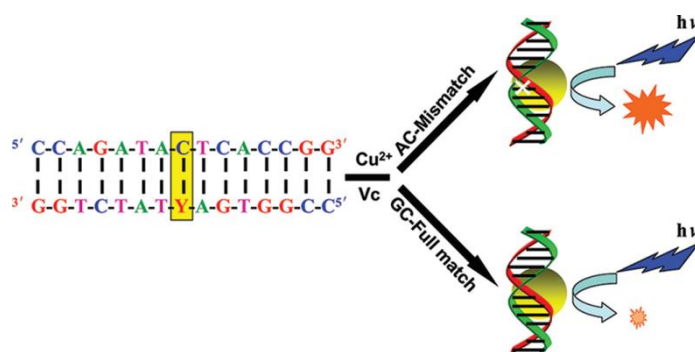


Figure 1.79. Schematic representation of detection DNA-single mismatch (Y: Single nucleotide polymorphisms site) (adapted from, X. Jia, J. Li, L. Han, J. Ren, X. Yang and E. Wang, *ACS Nano*, 2012, **6**, 3311-3317).

1.16.2. Metals (Au, Ag, Cu) Nanoclusters as Imaging Materials

Metal Nanoclusters are basically synthetically derived fluorescent probes. Like other organic dyes like DAPY, FITC noble metal Nanoclusters have been extensively used for imaging of biological samples both in-vitro and in-vivo.

Au and Ag-Nanoclusters as Imaging Materials: Protein-stabilized Au and Ag QCs are particularly important among various types of Au and Ag QCs, as they are especially suitable for cell imaging and therapy.⁴⁵² This is because of their unique functionality, ease in conjugation, biocompatibility, large Stoke shift, long lifetime, as well as photo and chemical stability. Advanced techniques in imaging have shown that multifunctional AuQCs/composites are practical for *in vivo* imaging and efficient therapy of various diseases. However, to make AuQCs ideal candidates for imaging, some important issues like affinity toward specific cells or organs, stability during delivery, and cell penetration have to be considered carefully. Modification of AuQCs with recognition molecules has attracted sincere efforts from researchers to recent years to enhance their performance in tumor diagnosis and therapy. Recognition elements can be conjugated to protein-stabilized AuQCs through their reactions with thiol, amino, and carboxyl residues on proteins. For instance, cancer cell recognized molecules (e.g, folic acid and herceptin) have been intensely used to functionalize BSA–AuQCs by using the conventional 1-ethyl-3-(3-(dimethylamino)propyl)carbodiimide (EDC) coupling chemistry.⁴⁵³⁻⁴⁵⁵ Cells labeled with these functionalized BSA-AuQCs can be clearly imaged with the NIR-emitting fluorescence

(emission wavelengths 700–800 nm) when excited at the wavelengths over 480–550 nm, with minimum interference from autofluorescence of biological matrixes.

Human transferrin-stabilized AuQCs and insulin-stabilized AuQCs can directly target transferrin receptor overexpressed cells (e.g. A549 cells) and insulin receptor overexpressed cells (e.g. C2C12 cells), respectively.^{456, 453}

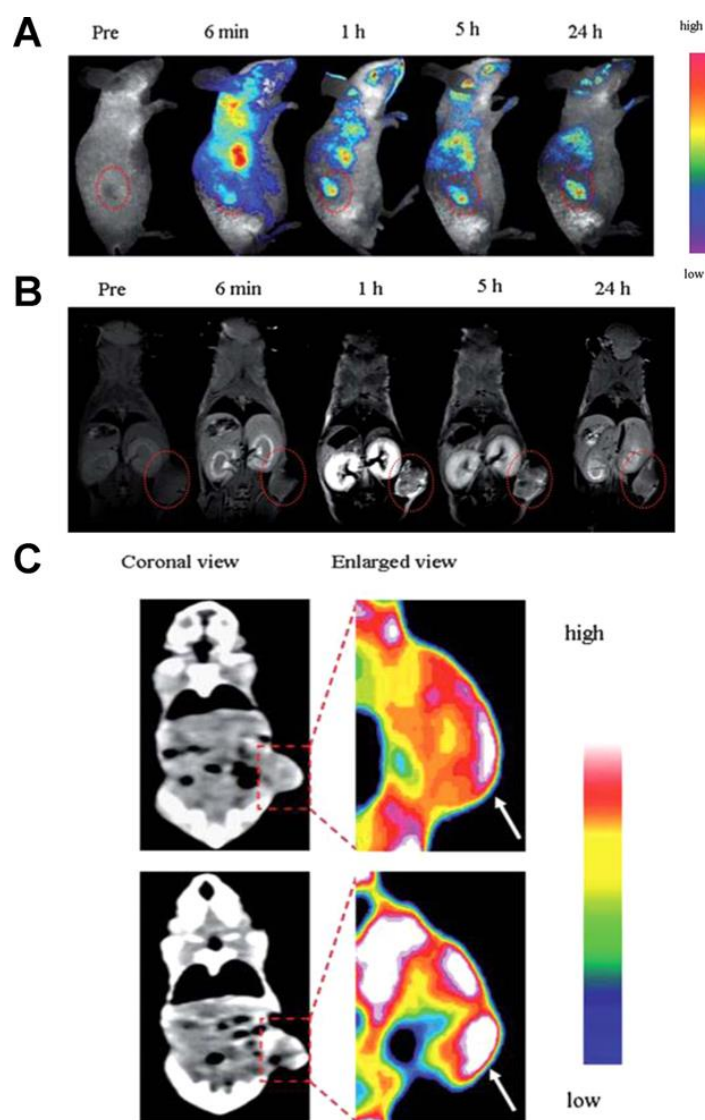


Figure 1.80. In vivo (A) fluorescence, (B) MRI, and (C) CT imaging of tumor bearing mice after the tail injection of BSA-AuQCs based multimodal imaging probe (adapted from, D.-H. Hu, Z.-H. Sheng, P.-F. Zhang, D.-Z. Yang, S.-H. Liu, P. Gong, D.-Y. Gao, S.-T. Fang, Y.-F. Ma and L.-T. Cai, *Nanoscale*, 2013, **5**, 1624–1628).

Gold QCs have also been used for *in vivo* live animal imaging. For example, BSA-AuQCs have been used for *in vivo* imaging.⁴⁵⁷ Gadolinium(III) functionalized BSA-AuQCs have been synthesized by

Cai and his group as fluorescence/MRI/CT-based multimodal imaging probes for *in vivo* tumor-bearing mice.⁴⁵⁸ The fluorescence, CT, and T1-weighted MRI signal derived from gadolinium(III) functionalized BSA-AuQCs were all very distinguishable in the tumor region from other tissues, indicating a significant accumulation of the probe in tumor tissues through the enhanced permeation and retention effect and a reduced clearance from the tumor (Figure 1.80).⁴⁵⁸

A number of studies have reported biological-imaging applications based on fluorescence silver nanoclusters. Baskakov and his co-workers⁴⁵⁹ have presented the first imaging application of silver nanoclusters in combination with a fluorophore, thioflavin T (ThT). Dickson and co-workers investigated the staining of living cells using peptide encapsulated fluorescent Ag NCs. These ultrasmall Ag NCs has found to distribute within the cells, and this causes weak staining. These fluorescent Ag NCs have short lifetimes (220 ps (33%) and 1760 ps (67%)).³³⁵ The same group has also reported the application of DNA templated fluorescent Ag NCs for biological imaging in a more specific way using surface labeling of live cells (Figure 1.81). These templated fluorescent Ag NCs have been easily conjugated with proteins (including avidin) as these AgNCs have ultrasmall size.³³⁶

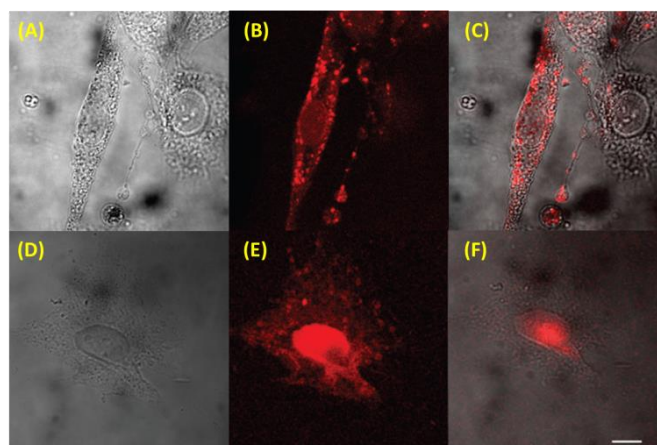


Figure 1.81. Fluorescence images of live NIH 3T3 cells stained with anti-HS-C24-Ag. Live cells incubated with anti-HS-C24-Ag at 4 °C for 20 min (A) bright field; (B) silver clusters; (C) merge or at 37 °C for 6 min (D) bright field; (E) silver clusters; (F) merge. Images (A)–(F) were recorded on Zeiss LSM 10 confocal microscope. The fluorescence images were taken at 543 nm excitation. Scale bar 25 μ m (adapted from, J. Yu, S. Choi, C. I. Richards, Y. Antoku and R. M. Dickson, *Photochem. Photobiol.*, 2008, **84**, 1435–14390).

Cu-Nanoclusters as Imaging Tools: Apart from gold quantum clusters, copper quantum clusters have also been used for imaging purposes.

However, the number of reports is limited to few due to the inherent lower stability of the Cu(0) state. Chattopadhyay and co-workers have synthesized lysozyme protected CuQCs that possess high fluorescence quantum yield of 18%. Mass spectrometric analysis indicated presence of Cu₂ to Cu₉ species in the clusters. These highly photostable CuQCs have been successfully utilized to label cervical cancer HeLa cells (Figure 1.82).⁴⁶⁰

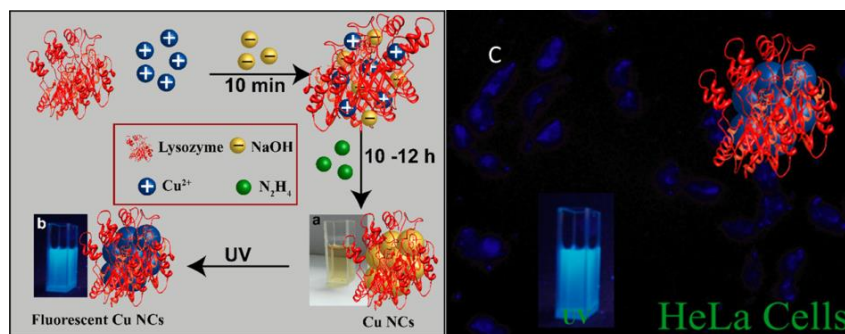


Figure 1.82. Reaction scheme for the synthesis of CuNCs in presence of Lysozyme, photograph of the clusters in (a) daylight, (b) UV light and labeling of the HeLa cells (adapted from, R. Ghosh, A. K. Sahoo, S. S. Ghosh, A. Paul and A. Chattopadhyay, *ACS Appl. Mater. Interfaces*, 2014, **6**, 3822-3828).

Mukherjee and co-workers have synthesized blue emitting CuNCs using a bioactive tripeptide glutathione as a stabilizing agent. Cell-imaging studies reveal that CuNCs primarily localize in nuclear membranes of the different cancerous cells. The corresponding cell viability studies conclusively proved that our synthesized CuNCs are not detrimental for normal cell growth morphology in different cancerous cell lines and possess excellent potential to be used as a next-generation nontoxic and biomedical luminescent probe.⁴⁶¹

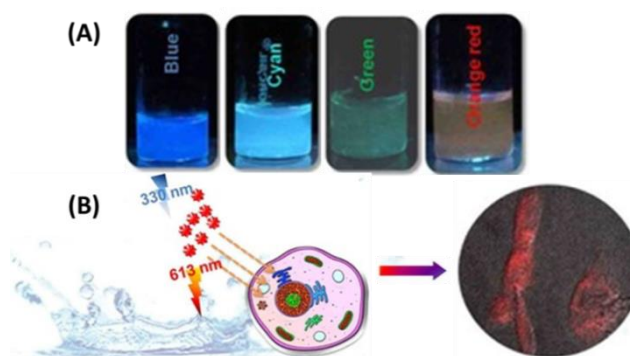


Figure 1.83. (A) Four different colors emitting CuNCs. (B) Confocal microscopic images of the cells treated with orange-red emitting CuNCs at a concentration of 20 µg/ml (adapted from, K. Basu, K. Gayen, T. Mitra, A. Baral, S. S. Roy and A. Banerjee, *ChemNanoMat.*, 2017, **3**, 808-814).

Recently, our group has reported different colors emitting four different CuNCs in an eco-friendly water medium using bioactive peptide as a stabilizing agent. Later, they found that the orange-red emitting CuNCs show very high Stokes shift and non-cytotoxicity towards the cancer cells during the bio-imaging time (Figure 1.83).⁴⁶²

1.16.3. Metals (Au, Ag, Cu) Nanoclusters as Catalysts

For a long time scientists from both chemistry and engineering are using nano-particles for catalyzing various synthetic and energy producing reactions using nanoparticles as catalyst. The main advantage of nano-materials is their high surface to volume ratio. For metal nanoclusters this ratio is increased to the highest level.

Au and Ag Nanoclusters as Catalyst: The gold and silver quantum clusters utilized as catalyst for several reactions. For example, Jin and co-workers has used TiO_2 , CeO_2 or Fe_2O_3 supported thiolate-protected $\text{Au}_{25}(\text{SR})_{18}$ ($\text{R} = \text{CH}_2\text{CH}_2\text{Ph}$) for catalytic oxidation of CO. Out of all the supports, $\text{Au}_{25}(\text{SR})_{18}/\text{CeO}_2$ catalyst was found to be more efficient than others (Figure 1.84).

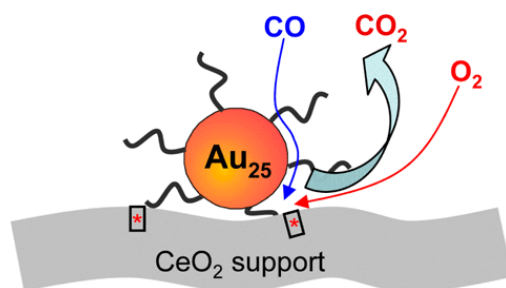


Figure 1.84. Proposed model for CO oxidation at the perimeter sites of $\text{Au}_{25}(\text{SR})_{18}/\text{CeO}_2$ catalyst (adapted from, X. Nie, H. Qian, Q. Ge, H. Xu and R. Jin, *ACS Nano*, 2012, **6**, 6014–6022).

Interestingly, O_2 pretreatment of the catalyst at $150\text{ }^\circ\text{C}$ for 1.5 h significantly enhanced the catalytic activity. These results contrast the common thought that surface thiolates must be removed before the catalyst can exert high catalytic activity. At $150\text{ }^\circ\text{C}$ O_2 -pretreated $\text{Au}_{25}(\text{SR})_{18}/\text{CeO}_2$ catalyst offers $\sim 94\%$ conversion of CO to CO_2 at $80\text{ }^\circ\text{C}$ and $\sim 100\%$ conversion at $100\text{ }^\circ\text{C}$.⁴⁶³ Zhu *et al.*³⁴⁶ has investigated solution-phase styrene oxidation with O_2 , catalyzed by $\text{Au}_{25}(\text{SR})_{18}$ quantum clusters (in the form of free clusters in solution or being

supported on oxides). The reaction was performed at 80-100 °C for 12-24 h using toluene as solvent (Figure 1.85). In this produces benzaldehyde is obtained as the major product (selectivity ~70%) and styrene epoxide (less, selectivity~25%) and minor byproduct acetophenone (selectivity ~5%).³⁴⁶

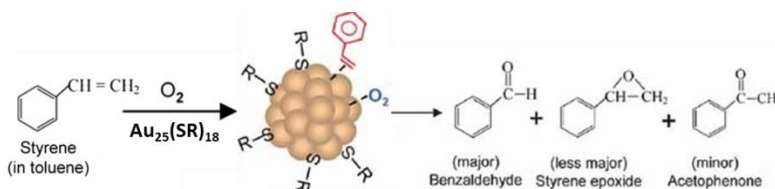


Figure 1.85. Selective oxidation of styrene by gold-cluster catalysts (adapted from, Y. Zhu, H. Qian, M. Zh and R. Jin, *Adv. Mater.*, 2010, **22**, 1915–1920).

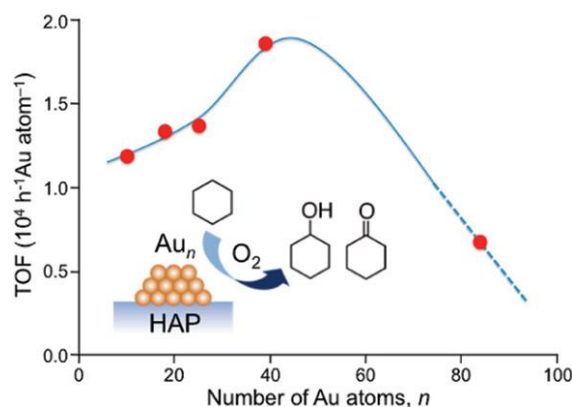


Figure 1.86. TOF (turnover frequency) values as a function of the cluster size n (Au atom number). The curve is a guide for the eye (adapted from, Y. Liu, H. Tsunoyama, T. Akita, S. Xie and T. Tsukuda, *ACS Catal.*, 2011, **1**, 2-6).

Tsukuda and co-workers³⁴⁵ made HAP (hydroxyapatite) supported $\text{Au}_{10}(\text{SG})_{10}$, $\text{Au}_{18}(\text{SG})_{14}$, $\text{Au}_{25}(\text{SG})_{18}$ and $\text{Au}_{39}(\text{SG})_{24}$ nanocluster catalysts with 0.2 wt% loading of clusters (SG = glutathione). Optical reflectance spectroscopy and TEM measurements confirmed that the Au clusters adsorbed on HAP were intact. Subsequent thermal calcination at 300 °C for 2 h in vacuo completely removed the glutathione ligands on the clusters. TEM analysis showed no growth of the clusters without ligands into large plasmonic nanoparticles. This happens due to the excellent protecting role of HAP (its relatively strong interaction with clusters via the PO_4^{3-} moiety) (Figure 1.86).⁴⁶⁴ Besides the oxidation reactions, $\text{Au}_n(\text{SR})_m$ quantum cluster catalysts were also demonstrated to be capable of catalyzing hydrogenation reactions in solution phase,^{346, 347} such as chemoselective hydrogenation of α,β -unsaturated ketones to α,β -unsaturated alcohols under mild conditions (60 °C, in mixed solvents (1:1

toluene/acetonitrile)).³⁴⁶ It has been observed that the $\text{Au}_{25}(\text{SR})_{18}$ clusters were found to hydrogenate preferentially the $\text{C}=\text{O}$ bond of benzalacetone against the $\text{C}=\text{C}$ bond, and the $\text{C}=\text{O}$ hydrogenated product (i.e. unsaturated alcohol) was obtained with 76% selectivity, with 14% selectivity for saturated ketone and 10% for saturated alcohol.³⁴⁶ A nearly complete selectivity for α,β -unsaturated alcohol was further obtained in a mixed toluene/ethanol (1:1) solvent after optimization (Figure 1.87).³⁴⁷

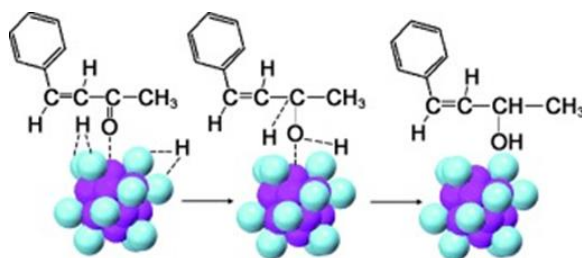


Figure 1.87. The proposed mechanism of the chemoselective hydrogenation of α,β -unsaturated ketone to unsaturated alcohol catalyzed by $\text{Au}_{25}(\text{SR})_{18}$ nanoparticles. For clarity, the thiolate ligands are not shown. Dark grey: Au atoms of the core; light gray: Au atoms of the shell (adapted from, Y. Zhu, H. Qian, B. A. Drake and R. Jin, *Angew. Chem, Int. Ed.*, 2010, **49**, 1295–129).

Li and co-workers designed atomically precise metal quantum cluster catalysts to understand the essence of the catalytic reactions at the atomic level. In this work, Au_{25}^- quantum clusters were employed as electron transfer (via Au_{25}^0 catalysts to induce an intramolecular cascade reaction at ambient conditions and gave rise to high conversion (87%) and selectivity (96%) (Figure 1.87).⁴⁶⁵ Electron spin-resonance spectra confirmed the consecutive electron transfer process and the formation of N radical. UV-vis absorption spectra also verified that Au_{25}^z was intact after the catalytic circle.⁴⁶⁵

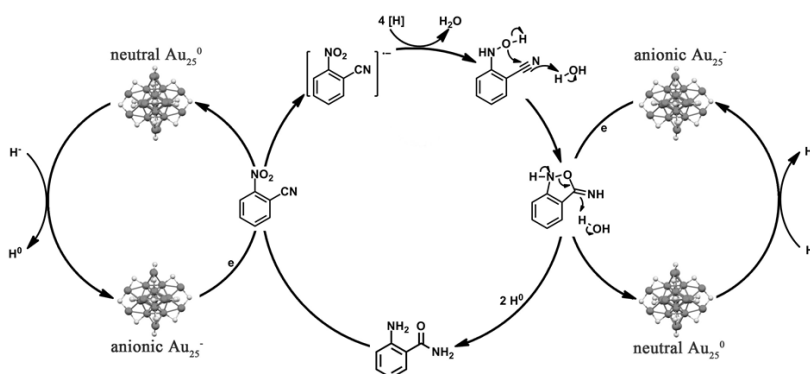


Figure 1.88. The proposed mechanism of Au_{25}^z catalyzed intramolecular cascade reaction (adapted from, H. Chong, P. Li, S. Wang, F. Fu, J. Xiang, M. Zhu and Y. Li, *Sci. Rep.*, 2013, **3**, 3214).

Similarly, Ag nanocluster can be used as a catalyst as both Au and Ag NCs have very high stability which makes them suitable for a catalytic reaction. Pradeep and co-workers synthesized silver nanoclusters (Ag_{7-8}) by the interfacial etching of Ag nanoparticle precursors. Then the AgNCs were loaded on metal oxide supports to prepare active catalysts. The synthesized metal-supported nanoclusters were utilized for the reduction of various nitro groups to amine, such as 3-nitrophenol, 4-nitrophenol, 3-nitroaniline, and 4-nitroaniline.⁴⁶⁶

Cu-Nanoclusters as Catalyst: Unlike Au and Ag, less number of Cu-nanoclusters have been used as catalyst. Kou and co-workers in 2008 first reported an efficient copper nanocluster catalyst for the synthesis of methyl formate from carbonmonoxide and methanol.⁴⁶⁷ López-Quintela and his group checked size dependent activity of Cu(0) nanoclusters for electrolytic degradation of methylene blue (MB) to leucomethylene blue (LMB) in presence of hydrazine (Figure 1.89).⁴⁶⁸

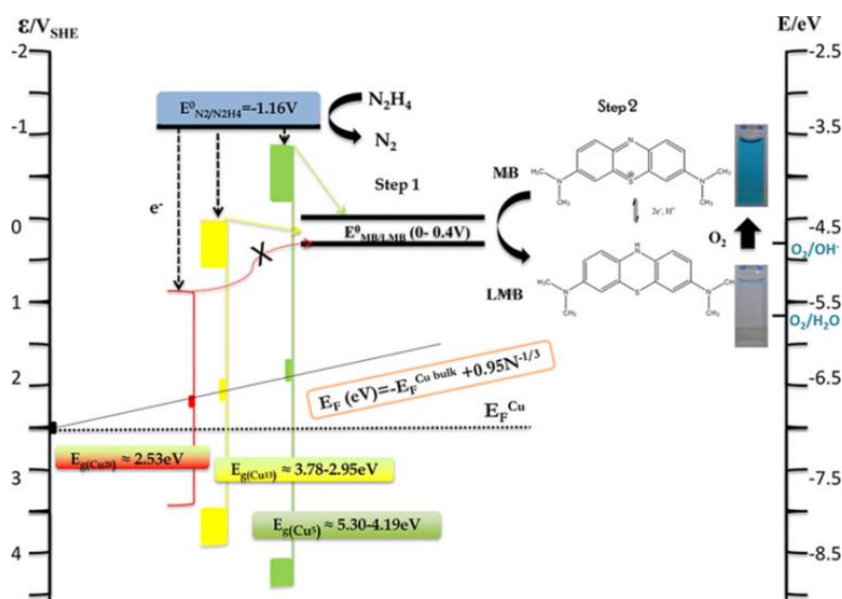


Figure 1.89. Schematic Energy Diagram Showing the Catalytic Activity of Different CuNCs (Cu_5 , Cu_{13} and Cu_{20}) Used for the MB Reduction by N_2H_4 (adapted from, N. Vilar-Vidal, J. Rivas and M. A. López-Quintela, *ACS Catal.*, 2012, **2**, 1693-1697).

Recently, Banerjee and co-workers reported a bulk scale synthesis of CuNCs which show is a very good catalytic property during the reduction of nitro group.⁴⁶⁹ Corma and co-workers synthesized copper nanoclusters having the size Cu_{2-7} used in C–N, C–C, C–O, C–S, and C–P bond

formation reactions with a high yield up to 91% of products (Figure 1.90).⁴⁷⁰

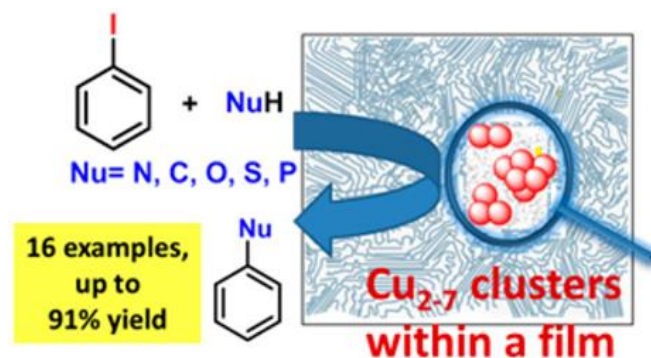


Figure 1.90. Copper nanoclusters (Cu_{2.7} clusters) within a polymeric film catalyze C–N, C–C, C–O, C–S and C–P bond forming reaction (adapted from, J. Oliver-Messeguer, L. Liu, S. García-García, C. Canós-Giménez, I. Domínguez, R. Gavara, Doménech-Carbó, A.; Concepción, P.; A. Leyva-Pérez and A. Corma, *J. Am. Chem. Soc.*, 2015, **137**, 3894–3900).

Future Perspective: The next generation technology is looking for a cheap and facile synthesis of metal nanoclusters with multiple uses. In this context, scientists are still trying to get insight of the structural details of metal nanoclusters in order to develop them to make advanced materials.

From the point of stability, obviously Au and Ag nanoclusters have higher applicability; however, chemists are trying to synthesizing stable cheap functional copper nanoclusters by replacing costly Au and Ag-nanoclusters.

1.17. References

- (1) J.-M. Lehn, *Supramolecular Chemistry*, 1995.
- (2) H. -J. Schneider and A. Yatsimirsky, *Principles and Methods in Supramolecular Chemistry*, 2000.
- (3) J. W. Steed and J. L. Atwood, *Supramolecular Chemistry*, 2000.
- (4) G. M. Whiteside and B. Grzybowski, *Science*, 2012, **295**, 2418–2421.
- (5) E. Hanssen, B. Reinboth and M. A. Gibson, *J. Biol. Chem.*, 2003, **278**, 24334–24341.
- (6) C. R. Martinez and B. L. Iverson, *Chem. Sci.*, 2012, **3**, 2191–2201.
- (7) J. -M. Lehn *Proc. Natl. Acad. Sci. U. S. A.*, 2002, **99**, 4763–4768.
- (8) J. -M. Lehn, *Supramolecular Science: Where It Is and Where It Is Going*, 1999, 287–304.

- (9) F. Tantakitti, J. Boekhoven, X. Wang, R. V. Kazantsev, T. Yu, J. Li, E. Zhuang, R. Zandi, J. H. Ortony, C. J. Newcomb, L. C. Palmer, G. S. Shekhawat, M. Olvera de la Cruz, G. C. Schatz and S. I. Stupp, *Nature Materials*, 2016, **15**, 469–478.
- (10) H. Sirringhaus, T. Kawase, R. H. Friend, T. Shimoda, M. Inbasekaran, W. Wu and E. P. Woo, *Science*, 2000, **290**, 2123–2126.
- (11) J. A. Rogers, Z. Bao, K. Baldwin, A. Dodabalapur, B. Crone, V. R. Raju, V. Kuck, H. Katz, K. Amundson, J. Ewing and P. Drzaic, *Proc. Natl. Acad. Sci. USA*, 2001, **98**, 4835–4840.
- (12) S. A. Jenekhe and L. X. Chen, *Science*, 1999, **283**, 372–375.
- (13) Y. Xia, B. Gates, Y. Yin and Y. Lu, *Adv. Mater.*, 2000, **12**, 693–713.
- (14) M. H. Wu and G. M. Whitesides, *Appl. Phys. Lett.*, 2001, **78**, 2273–2275.
- (15) S. Maiti, I. Fortunati, C. Ferrante, P. Scrimin and L. J. Prins, *Nature* **2016**, **8**, 725–731.
- (16) D. Voet and J. G. Voet, *Biochemistry*, J. Wiley and Sons, 3rd edition (ISBN 0-471-25090-2), 2004, 1–1591.
- (17) A. J. Barrett, N. D. Rawlings and J. F. Woessner, *The Handbook of Proteolytic Enzymes*, Academic Press, 2nd edition, 2003.
- (18) E. H. Man and J. L. Bada, *Annu. Rev. Nutr.*, 1987, **7**, 209–225.
- (19) G. Liang, Z. Yang, R. Zhang, L. Li, Y. Fan, Y. Kuang, Y. Gao, T. Wang, W. W. Lu and B. Xu, *Langmuir*, 2009, **25**, 8419–8422.
- (20) I. L. Karle, A. Pramanik, A. Banerjee, S. Bhattacharjya and P. Balaram, *J. Am. Chem. Soc.*, 1997, **119**, 9087–9095.
- (21) M. Goodman and S. Ro, *In Burger's Medicinal Chemistry and Drug Discovery*; 1995, ed. M. E. Wolff, John Wiley & Sons, New York, 1995; **1**, 803.
- (22) Y. Barrans and M. Cortrait, *J. Appl. Cryst.*, 1978, **11**, 288.
- (23) M. Sandberg and I. Jacobson, *J. Neurochem.*, 1981, **37**, 1353–1356.
- (24) S. J. McGlone and P. D. Godfrey, *J. Am. Chem. Soc.*, 1995, **117**, 1043–1048.
- (25) H. Itoh, T. Yamane and T. Ashida, *Acta Crystallogr., Sect. B*, 1977, **33**, 2959–2961.
- (26) L. Bonfanti, P. Peretto, S. de Marchis and A. Fasolo, *Progr. Neurobiol.*, 1999, **59**, 333–353.

- (27) J. Awapara, A. J. Landua, R. Fuerst and B. Scale, *J. Biol. Chem.*, 1950, **187**, 35–39.
- (28) E. Roberts and S. Frankels, *J. Biol. Chem.*, 1950, **187**, 55–63.
- (29) W. Tsutumi, R. Onodera and H. Kandastu, *Agric. Biol. Chem. Jpn.*, 1975, **39**, 711–716.
- (30) C. Groeger, H. R. Wenzel and H. Tschesche, *Angew. Chem. Int. Ed.*, 1993, **32**, 898–900.
- (31) B. Fiser, B. Jójárt, M. Szőri, G. Lendvay, I. G. Csizmadia and B. Viskolcz, *J. Phys. Chem. B*, 2015, **119**, 3940–3947.
- (32) D. Ganguly, C. V. Srikanth, C. Kumar, P. Vats and A. K. Bachhawat, *IUBMB Life*, 2003, **55**, 553–554.
- (33) J. Nanda and A. Banerjee, *Soft Matter*, 2012, **8**, 3380–3386.
- (34) S. Roy, A. Baral and A. Banerjee, *Chem. Eur. J.*, 2013, **19**, 14950–14957.
- (35) P. J. Artymiuk and C. C. F. Blake, *J. Mol. Biol.*, 1981, **152**, 737–762.
- (36) D. J. Barlow and J. M. Thornton, *J. Mol. Biol.*, 1988, **201**, 601–619.
- (37) G. N. Ramachandran, C. Ramakrishnan and V. Sasisekaran, *J. Mol. Biol.*, 1963, **7**, 95–99.
- (38) R. Diaz-Avalos, C. Long, E. Fontano, M. Balbirnie, R. Grothe, D. Eisenberg and D. L. D. Caspar, *J. Mol. Biol.*, 2003, **330**, 1165–1175.
- (39) M. R. Sawaya, S. Sambashivan, R. Nelson, M. I. Ivanova, S. A. Sievers, M. I. Apostol, M. J. Thompson, M. Balbirnie, J. J. W. Wiltzius, H. T. McFarlane, A. Ø. Madsen, C. Riek and D. Eisenberg, *Nature*, 2007, **447**, 453–457.
- (40) I. W. Hamley, *Angew. Chem. Int. Ed.*, 2007, **46**, 8128–8147.
- (41) J. S. Nowick, J. H. Tsai, Q.-C. D. Bui and S. Maitra, *J. Am. Chem. Soc.*, 1999, **121**, 8409–8410.
- (42) D. S. Kemp, B. R. Bowen and C. C. Muendel, *J. Org. Chem.*, 1990, **55**, 4650–4657.
- (43) S. K. Maji, M. G. B. Drew and A. Banerjee, *Chem. Commun.*, 2001, 1946–1947.
- (44) A. Banerjee, S. K. Maji, M. G. B. Drew, D. Haldar, A. K. Das and A. Banerjee, *Tetrahedron*, 2004, **60**, 5935–5944.

- (45) A. Banerjee, A. K. Das, M. G. B. Drew and A. Banerjee, *Tetrahedron*, 2005, **61**, 5906–5914.
- (46) J. A. Fallas, L. E. R. O’Leary and J. D. Hartgerink, *Chem. Soc. Rev.*, 2010, **39**, 3510–3527.
- (47) J. F. Almine, D. V. Bax, S. M. Mithieux, L. Nivison-Smith, J. Rnjak, A. Waterhouse, S. G. Wise and A. S. Weiss, *Chem. Soc. Rev.*, 2010, **39**, 3371–3379.
- (48) M. Krejchi, E. Atkins, A. Waddon, M. Fournier, T. Mason and D. Tirrell, *Science*, 1994, **265**, 1427–1432.
- (49) D. N. Woolfson and Z. N. Mahmoud, *Chem. Soc. Rev.*, 2010, **39**, 3464–3479.
- (50) E. Krieg, M. M. C. Bastings, P. Besenius and B. Rybtchinski, *Chem. Rev.*, 2016, **116**, 2414–2477.
- (51) D. W. P. M. Löwik, E. H. P. Leunissen, M. van den Heuvel, M. B. Hansen and J. C. M. van Hest, *Chem. Soc. Rev.*, 2010, **39**, 3394–3412.
- (52) X. Zhao, F. Pan, H. Xu, M. Yaseen, H. Shan, C. A. E. Hauser, S. Zhang and J. R. Lu, *Chem. Soc. Rev.*, 2010, **39**, 3480–3498.
- (53) Q. Cheng, D. R. Benson, M. Rivera and K. Kuczera, *Biopolymers*, 2006, **83**, 297–312.
- (54) M. R. Ghadiri, J. R. Granja, R. A. Milligan, D. E. McRee and N. Khazanovich, *Nature*, 1993, **366**, 324–327.
- (55) N. Khazanovich, J. R. Granja, D. E. McRee, R. A. Milligan and M. R. Ghadiri, *J. Am. Chem. Soc.*, 1994, **116**, 6011–6012.
- (56) K. Kobayashi, J. R. Granja and M. R. Ghadiri, *Angew. Chem., Int. Ed. Engl.*, 1995, **34**, 95–98.
- (57) D. T. Bong, T. D. Clark, J. R. Granja and M. R. Ghadiri, *Angew. Chem., Int. Ed.*, 2001, **40**, 988–1011.
- (58) J. D. Hartgerink, J. R. Granja, R. A. Milligan and M. R. Ghadiri, *J. Am. Chem. Soc.*, 1996, **118**, 43–50.
- (59) W. S. Horne, C. D. Stout and M. R. Ghadiri, *J. Am. Chem. Soc.*, 2003, **125**, 9372–9376.
- (60) J. Montenegro, M. R. Ghadiri and J. R. Granja, *Acc. Chem. Res.*, 2013, **46**, 2955–2965.
- (61) R. J. Brea, C. Reiriz and J. R. Granja, *Chem. Soc. Rev.*, 2010, **39**, 1448–1456.

- (62) R. Chapman, M. Danial, M. L. Koh, K. A. Jolliffe and S. Perrier, *Chem. Soc. Rev.*, 2012, **41**, 6023–6041.
- (63) J. Couet, J. D. J. S. Samuel, A. Kopyshev, S. Santer and M. Biesalski, *Angew. Chem., Int. Ed.*, 2005, **44**, 3297–3301.
- (64) M. G. J. ten Cate, N. Severin and H. G. Bö rner, *Macromolecules*, 2006, **39**, 7831–7838.
- (65) R. Chapman, K. A. Jolliffe and S. Perrier, *Polym. Chem.*, 2011, **2**, 1956–1963.
- (66) M. Danial, C. M. N. Tran, K. A. Jolliffe and S. Perrier, *J. Am. Chem. Soc.*, 2014, **136**, 8018–8026.
- (67) J. M. A. Carnall, C. A. Waudby, A. M. Belenguer, M. C. A. Stuart, J. J.-P. Peyralans and S. Otto, *Science*, 2010, **327**, 1502–1506.
- (68) N. Giuseppone, *Acc. Chem. Res.*, 2012, **45**, 2178–2188.
- (69) B. Rubinov, N. Wagner, H. Rapaport and G. Ashkenasy, *Angew. Chem., Int. Ed.*, 2009, **48**, 6683–6686.
- (70) M. Malakoutikhah, J. J. P. Peyralans, M. Colomb-Delsuc, H. Fanlo-Virgo s, M. C. A. Stuart and S. Otto, *J. Am. Chem. Soc.*, 2013, **135**, 18406–18417.
- (71) H. Cui, M. J. Webber and S. I. Stupp, *Biopolymers*, 2010, **94**, 1–18.
- (72) J. D. Hartgerink, E. Beniash and S. I. Stupp, *Science*, 2001, **294**, 1684–1688.
- (73) J. D. Hartgerink, E. Beniash and S. I. Stupp, *Proc. Natl. Acad. Sci. U. S. A.*, 2002, **99**, 5133–5138.
- (74) H. Jiang, M. O. Guler and S. I. Stupp, *Soft Matter*, 2007, **3**, 454–462.
- (75) S. E. Paramonov, H. -W. Jun and J. D. Hartgerink, *J. Am. Chem. Soc.*, 2006, **128**, 7291–7298.
- (76) H. A. Behanna, J. J. J. M. Donners, A. C. Gordon and S. I. Stupp, *J. Am. Chem. Soc.*, 2005, **127**, 1193–1200.
- (77) Y. S. Velichko, S. I. Stupp and M. O. de la Cruz, *J. Phys. Chem. B*, 2008, **112**, 2326–2334.
- (78) O.-S. Lee, S. I. Stupp and G. C. Schatz, *J. Am. Chem. Soc.*, 2011, **133**, 3677–3683.
- (79) P. A. Korevaar, C. J. Newcomb, E. W. Meijer and S. I. Stupp, *J. Am. Chem. Soc.*, 2014, **136**, 8540–8543.

- (80) T. J. Moyer, J. A. Finbloom, F. Chen, D. J. Toft, V. L. Cryns and S. I. Stupp, *J. Am. Chem. Soc.*, 2014, **136**, 14746–14752.
- (81) A. Baral, S. Basak, K. Basu, A. Dehsorkhi, I. W. Hamley and A. Banerjee, *Soft Matter*, 2015, **11**, 4944–4951.
- (82) A. Ghosh, M. Haverick, K. Stump, X. Yang, M. F. Tweedle and J. E. Goldberger, *J. Am. Chem. Soc.*, 2012, **134**, 3647–3650.
- (83) H. Dong, S. E. Paramonov, L. Aulisa, E. L. Bakota, and J. D. Hartgerink, *J. Am. Chem. Soc.*, 2007, **129**, 12468–12472.
- (84) M. Reches and E. Gazit, *Science*, 2003, **300**, 625–627.
- (85) L. Adler-Abramovich, M. Reches, V. L. Sedman, S. Allen, S. J. B. Tendler and E. Gazit, *Langmuir*, 2006, **22**, 1313–1320.
- (86) L. Adler-Abramovich and E. Gazit, *Chem. Soc. Rev.*, 2014, **43**, 6881–6893.
- (87) John D. Ferry, *Viscoelastic Properties of Polymers*. New York: Wiley, 1980, ISBN 0471048941.
- (88) D.M. Zurcher, and A.J. McNeil, *J. Org. Chem.*, 2015, **80**, 2473–2478.
- (89) Y. Lan, M.G. Corradini, R.G. Weiss, S. R. Raghavan, and M. A. Rogers, *Chem. Soc. Rev.*, 2015, **44**, 6035–6058.
- (90) P. Dastidar, *Chem. Soc. Rev.*, 2008, **37**, 2699–2715.
- (91) G.K. Veits, K.K. Carter, S. J. Cox, and A. J. McNeil, *J. Am. Chem. Soc.*, 2016, **138**, 12228–12233.
- (92) A.D. Martin, J. P. Wojciechowski, M. M. Bhadbhade and P. Thordarson, *Langmuir*, 2016, **32**, 2245–2250.
- (93) K. A. Houton, , K. L. Morris, L. Chen, M. Schmidtman, J. T. A. Jones, L. C. Serpell, G. O. Lloyd, and D . J. Adams, *Langmuir*, 2012, **28**, 9797–9806.
- (94) E. R. Draper, K. L. Morris, M. A. Little, J. Raeburn, C. Colquhoun, E. R. Cross, T. O. McDonald, L. C. Serpell, and D. J. Adams, *CrystEngComm.*, 2015, **17**, 8047–8057.
- (95) E. C. Barker, A. D. Martin, C. J. Garvey, C. Y. Goh, F. Jones, M. Mocerino, B. W. Skelton, M. I. Ogden and T. Becker, *Soft Matter*, 2017, **13**, 1006–1011.
- (96) E. Ostuni, P. Kamaras, and R. G. Weiss, *Angew. Chem. Int. Ed.*, 1996, **35**, 1324–1326.

- (97) S. Awhida, E. R. Draper, T. O. McDonald, and D. J. Adams, *J. Colloid Interface Sci.*, 2015, **455**, 24–31.
- (98) D. R. Trivedi, and P. Dastidar, *Chem. Mater.*, 2006, **18**, 1470–1478.
- (99) K. K. Carter, H. B. Rycenga, and A. J. McNeil, *Langmuir*, 2014, **30**, 3522–3527.
- (100) W. J. M. FrederixPim, G. G. Scott, Y. M. Abul-Haija, D. Kalafatovic, C. G. Pappas, N. Javid, N. T. Hunt, R. V. Ulijn, and T. Tuttle, *Nat. Chem.*, 2015, **7**, 30–37.
- (101) J. K. Gupta, D. J. Adams and N. G. Berry, *Chem. Sci.*, 2016, **7**, 4713–4719.
- (102) G. O. Lloyd, and J. W. Steed, *Nat. Chem.*, 2009, **1**, 437–442.
- (103) Y. J. Adhia, T. H. Schloemer, M. T. Perez, and A. J. McNeil, *Soft Matter*, 2012, **8**, 430–434.
- (104) V. J. Nebot, and D. K. Smith, B. Escuder and J.F. Miravet,, 2014 (The Royal Society of Chemistry), 30–66.
- (105) G. Yu, X. Yan, C. Han and F. Huang, *Chem. Soc. Rev.*, 2013, **42**, 6697–6722.
- (106) J. -B. Guilhaud and A. Saiani, *Chem. Soc. Rev.*, 2011, **40**, 1200–1210.
- (107) C. Yan, and D. J. Pochan, *Chem. Soc. Rev.*, 2010, **39**, 3528–3540.
- (108) S. R. Raghavan, and B. H. Cipriano, Gel formation: phase diagrams using tabletop rheology and calorimetry. In *Molecular Gels* R. G. Weiss and P. Terech, eds. 2005 (Springer), p. 233.
- (109) N. M. Sangeetha and U. Maitra, *Chem. Soc. Rev.*, 2005, **34**, 821–836.
- (110) P. Terech, J V. Rodriguez, J. D. Barnes and G. B. McKenna, *Langmuir*, 1994, **10**, 3406–3418.
- (111) K. Murata, M. Aoki, T. Nishi, A.. Ikeda and S. Shinkai, *J. Chem. Soc., Chem. Commun.*, 1991, 1715–1718.
- (112) U. Maitra, S. Mukhopadhyay, A. Sarkar, P. Rao and S. S. Indi, *Angew. Chem. Int. Ed.*, 2001, **40**, 2281–2283.
- (113) J. H. Jung, S. Shinkai and T. Shimizu, *Chem. Mater.*, 2003, **15**, 2141.
- (114) J. H. Jung, J. A. Rim, S. J. Lee and S. S. Lee, *Chem. Commun.*, 2005, 468.

- (115) S. Banerjee, R. Kandanelli, S. Bhowmik and U. Maitra, *Soft Matter*, 2011, **7**, 8207–8215.
- (116) H. Kobayashi, K. Koumoto, J. H. Junga and S. Shinkai, *J. Chem. Soc., Perkin Trans. 2*, 2002, 1930–1936.
- (117) J. J. D. D. Jong, L. N. Lucas, R. M. Kellogg, J. H. V. Esch and B. Feringa, *Science*, 2004, **304**, 278–281;
- (118) J. Eastoe, M. Sa´nchez-Dominguez, P. Wyatta and R. K. Heenan, *Chem. Commun.*, 2004, 2608.
- (119) D. Maiti and A. Banerjee, *Chem. Asian J.*, 2013, **8**, 113–120.
- (120) J. Sly, P. Kasák, E. Gomar-Nadal, C. Rovira, L. Górriz, P. Thordarson, D. B. Amabilino, A. E. Rowan and R. J. M. Nolte, *Chem. Commun.*, 2005, 1255–1257.
- (121) A. Ajayaghosh and S. J. George, *J. Am. Chem. Soc.*, 2001, **123**, 5148–5149.
- (122) Z. Brenzinger, *plzysiol. Chem.*, 1892, **16**, 537.
- (123) R. Gortner, W. F. Hoffman, *J. Am. Chem. Soc.*, 1921, **43**, 2199.
- (124) J. H. Van Esch, *Langmuir*, 2009, **25**, 8392–8394.
- (125) A. Dehsorkhi, V. Castelletto and I. W. Hamley, *J. Pept. Sci.*, 2014, **20**, 453–467.
- (126) M. Krysmann and V. Castelletto, *Biochemistry*, 2008, **47**, 4597–605.
- (127) M. Reches, *Science*, 2003, **300**, 625–627.
- (128) N. S. de Groot, T. Parella, F. X. Aviles, J. Vendrell and S. Ventura, *Biophys. J.*, 2007, **92**, 1732–1741.
- (129) C. K. Thota, N. Yadav and V. S. Chauhan, *Sci. Rep.*, 2016, **6**, 31167.
- (130) L. Jean, C. F. Lee, P. Hodder, N. Hawkins and D. J. Vaux, *Sci. Rep.*, **6**, 32124.
- (131) D. J. Porckop and K. I. Kivirikko, *Annu. Rev. Biochem.*, 1995, **64**, 403–434.
- (132) M. van der Rest and R. Garrone, *FASEB J.*, 1991, **5**, 2814–2823.
- (133) R. Parenteau-Bareil, R. Gauvin and F. Berthod, *Materials (Basel)*, 2010, **3**, 1863–1887.
- (134) C. M. Yamazaki, S. Asada, K. Kitagawa and T. Koide, *Biopolymers*, 2008, **90**, 816–823.

- (135) P. J. Skrzyszewska, F. A. de Wolf, M. W. T. Werten, A. P. H. A. Moers, M. A. C. Stuart and J. van der Gucht, *Soft Matter*, 2009, **5**, 2057.
- (136) L. E. R. O’Leary, J. A. Fallas, E. L. ak ta, . K. Kang and J. D. Hartgerink, *Nat. Chem.*, 2011, **3**, 821–828.
- (137) J. Naskar, G. Palui and A. Banerjee, *J. Phys. Chem. B*, 2009, **113**, 11787–11792.
- (138) S. Zhang, T. Holmes, C. Lockshin and a Rich, *Proc. Natl. Acad. Sci. U. S. A.*, 1993, **90**, 3334–3338.
- (139) M. A. Elsayy, A. M. Smith, N. Hodson, A. Squires, A. F. Miller and A. Saiani, *Langmuir*, 2016, **32**, 4917–4923.
- (140) C. Tang, A. F. Miller and A. Saiani, *Int. J. Pharm.*, 2014, **465**, 427–435.
- (141) J. P. Schneider, D. J. Pochan, B. Ozbas, K. Rajagopal, L. Pakstis and J. Kretsinger, *J. Am. Chem. Soc.*, 2002, **124**, 15030–15037.
- (142) C. Veerman, K. Rajagopal, C. S. Palla, D. J. Pochan, J. P. Schneider and E. M. Furst, *Macromolecules*, 2006, **39**, 6608–6614.
- (143) L. Haines-Butterick, K. Rajagopal, M. Branco, D. Salick, R. Rughani, M. Pilarz, M. S. Lamm, D. J. Pochan and J. P. Schneider, *Proc. Natl. Acad. Sci. U. S. A.*, 2007, **104**, 7791–7796.
- (144) R. P. Nagarkar, R. A. Hule, D. J. Pochan and J. P. Schneider, *J. Am. Chem. Soc.*, 2008, **130**, 4466–4474.
- (145) K. Hanabusa, J. Tange, Y. Taguchi, T. Koyama and H. Shirai, *J. Chem. Soc., Chem. Commun.*, 1993, 390–392.
- (146) K. Hanabma, R. Tanaka, M. Suzuki, M. Kimura and H. Shirai, *Adv. Mater.*, 1997, 1095–1097.
- (147) S. M. Hsu, Y. C. Lin, J. W. Chang, Y. H. Liu and H. C. Lin, *Angew. Chemie - Int. Ed.*, 2014, **53**, 1921–1927.
- (148) V. Zhang, Z. Yang, F. Yuan, H. Gu, P. Gao and B. Xu, *J. Am. Chem. Soc.*, 2004, **126**, 15028–15029.
- (149) D. Mandal, T. Kar and P. K. Das, *Chem. - A Eur. J.*, 2014, **20**, 1349–1358.
- (150) B. Adhikari, J. Nanda and A. Banerjee, *Chem. - A Eur. J.*, 2011, **17**, 11488–11496.
- (151) J. Nanda, A. Biswasa and A. Banerjee, *Soft Matter*, 2013, **9**, 4198–4208.

- (152) J. Nanda, A. Biswas, B. Adhikari and A. Banerjee, *Angew. Chemie - Int. Ed.*, 2013, **52**, 5041–5045.
- (153) S. Roy, A. Baral and A. Banerjee, *Chem. Eur. J.*, 2013, **19**, 14950–14957.
- (154) M. Ma, Y. Kuang, Yuan Gao, Y. Zhang, P. Gao and B. Xu, *J. Am. Chem. Soc.*, 2010, **132**, 2719–2728.
- (155) D. M. Ryan, S. B. Anderson and B. L. Nilsson, *Soft Matter*, 2010, **6**, 3220–3231.
- (156) D. M. Ryan, S. B. Anderson, F. T. Senguen, R. E. Youngman and B. L. Nilsson, *Soft Matter*, 2010, **6**, 475–479.
- (157) D. M. Ryan, T. M. Doran, S. B. Anderson and B. L. Nilsson, *Langmuir*, 2011, **27**, 4029–4039.
- (158) A. Mahler, M. Reches, M. Rechter, S. Cohen and E. Gazit, *Adv. Mater.*, 2006, **18**, 1365–1370.
- (159) S. Fleming, S. Debnath, P. W. J. M. Frederix, T. Tuttle and R. V. Ulijn, *Chem. Commun.*, 2013, **49**, 10587.
- (160) H. Wang, C. Yang, M. Tan, L. Wang, D. Kong and Z. Yang, *Soft Matter*, 2011, **7**, 3897.
- (161) Z. Yang, G. Liang, M. Ma, Y. Gao and B. Xu, *J. Mater. Chem.*, 2007, **17**, 850.
- (162) L. Chen, S. Revel, K. Morris, L. C. Serpell and D. J. Adams, *Langmuir*, 2010, **26**, 13466–13471.
- (163) L. Chen, S. Revel, K. Morris and D. J. Adams, *Chem. Commun.*, 2010, **46**, 4267.
- (164) S. K. M. Nalluri and R. V. Ulijn, *Chem. Sci.*, 2013, **4**, 3699–3705.
- (165) S. K. M. Nalluri, C. Berdugo, N. Javid, P. W. J. M. Frederix and R. V. Ulijn, *Angew. Chemie - Int. Ed.*, 2014, **53**, 5882–5887.
- (166) S. Fleming and R. V. Ulijn, *Chem. Soc. Rev.*, 2014, **43**, 8150–8177.
- (167) Y. Huang, Z. Qiu, Y. Xu, J. Shi, H. Lin and Y. Zhang, *Org. Biomol. Chem.*, 2011, **9**, 2149–2155.
- (168) X. Li, Y. Kuang, H. C. Lin, Y. Gao, J. Shi and B. Xu, *Angew. Chemie - Int. Ed.*, 2011, **50**, 9365–9369.
- (169) D. Yuan, X. Du, J. Shi, N. Zhou, J. Zhou and B. Xu, *Angew. Chemie - Int. Ed.*, 2015, **54**, 5705–5708.

- (170) J. Z , . O’Keeffe, . Lia , F. Z a , . Ter rst and . X , *Tetrahedron*, 2016, **72**, 6078-6083.
- (171) M. Mahato, V. Arora, R. Pathak, H. K. Gautam and A. K. Sharma, *Mol. Biosyst.*, 2012, **8**, 1742–1749.
- (172) X.-D. Xu, L. Liang, H. Cheng, X.-H. Wang, F.-G. Jiang, R.-X. Zhuo and X.-Z. Zhang, *J. Mater. Chem.*, 2012, **22**, 18164.
- (173) X. Li, Y. Kuang, J. Shi, Y. Gao, H. C. Lin and B. Xu, *J. Am. Chem. Soc.*, 2011, **133**, 17513–17518.
- (174) X. Li, Y. Kuang and B. Xu, *Soft Matter*, 2012, **8**, 2801–2806.
- (175) J. Raeburn, G. Pont, L. Chen, Y. Cesbron, R. Lévy and D. J. Adams, *Soft Matter*, 2012, **8**, 1168–1174.
- (176) A. L. Rodriguez, C. L. Parish, D. R. Nisbet and R. J. Williams, *Soft Matter*, 2013, **9**, 3915.
- (177) D. W. Urry, S. Q. Peng, T. M. Parker, D. C. Gowda and R. D. Harris, *Angew. Chemie Int. Ed. English*, 1993, **32**, 1440–1442.
- (178) C. Tang, A. M. Smith, R. F. Collins, R. V. Ulijn and A. Saiani, *Langmuir*, 2009, **25**, 9447–9453.
- (179) P. P. Bose, A. K. Das, R. P. Hegde, N. Shamala and B. A. Banerjee, *Chem. Mater.*, 2007, **19**, 6150–6157.
- (180) V. Jayawarna, M. Ali, T. A. Jowitt, A. F. Miller, A. Saiani, J. E. Gough and R. V. Ulijn, *Adv. Mater.*, 2006, **18**, 611–614.
- (181) D. J. Adams, M. F. Butler, W. J. Frith, M. Kirkland, L. Mullen and P. Sanderson, *Soft Matter*, 2009, **5**, 1856.
- (182) E. R. Draper, L. L. E. Mears, A. M. Castilla, S. M. King, T. O. McDonald, R. Akhtar and D. J. Adams, *RSC Adv.*, 2015, **5**, 95369–95378.
- (183) W. J. M. FrederixPim, G. G. Scott, Y. M. Abul-Haija, D. Kalafatovic, C. G. Pappas, N. Javid, N. T. Hunt, R. V. Ulijn, and T. Tuttle, *Nat. Chem.*, 2015, **7**, 30–37.
- (184) S. J. Marrink, H. J. Risselada, S. Yefimov, D. P. Tieleman and A. H. de Vries, *J. Phys. Chem. B*, 2007, **111**, 7812–7824.
- (185) H. Yu, H. A. Chokhawala, S. Huang and X. Chen, *Nat. Protoc.*, 2006, **1**, 2485–2492.
- (186) S. Toledano, R. J. Williams, V. Jayawarna and R. V. Ulijn, *J. Am. Chem. Soc.*, 2006, **128**, 1070–1071.

- (187) S. Dos Santos, A. Chandravarkar, B. Mandal, R. Mimna, K. Murat, L. Saucedo, P. Tella, G. Tuchscherer and M. Mutter, *J. Am. Chem. Soc.*, 2005, **127**, 11888–11889.
- (188) Z. M. Yang, G. L. Liang, L. Wang and B. Xu, *J. Am. Chem. Soc.*, 2006, **128**, 3038–3043.
- (189) M. R. Ghadiri, C. Soares and C. Choi, *J. Am. Chem. Soc.*, 1992, **114**, 825–831.
- (190) Y. Gao, Y. Kuang, Z. F. Guo, Z. Guo, I. J. Krauss and B. Xu, *J. Am. Chem. Soc.*, 2009, **131**, 13576–13577.
- (191) Y. Zhang, B. Zhang, Y. Kuang, Y. Gao, J. Shi, X. X. Zhang and B. Xu, *J. Am. Chem. Soc.*, 2013, **135**, 5008–5011.
- (192) S. Basak, J. Nanda and A. Banerjee, *Chem. Commun.*, 2014, **50**, 2356–2359.
- (193) D. L. Hern and J. A. Hubbell, *J. Biomed. Mater. Res.*, 1998, **39**, 266–276.
- (194) J. A. Burdick and K. S. Anseth, *Biomaterials*, 2002, **23**, 4315–4323.
- (195) Y. Gao, M. J. C. Long, J. Shi, L. Hedstrom and B. Xu, *Chem. Commun.*, 2012, **48**, 8404–8406.
- (196) Y. Kuang, D. Yuan, Y. Zhang, A. Kao, X. W. Du and B. Xu, *Nanoscale, RSC Adv.*, 2013, **3**, 7704–7707.
- (197) G. A. Silva, C. Czeisler, K. L. Niece, E. Beniash, D. A. Harrington, J. A. Kessler and S. I. Stupp, *Science*, 2004, **303**, 1352–1355.
- (198) V. M. Tysseling-Mattiace, V. Sahni, K. L. Niece, D. Birch, C. Czeisler, M. G. Fehlings, S. I. Stupp and J. A. Kessler, *J. Neurosci.*, 2008, **28**, 3814–3823.
- (199) K. Rajangam, H. A. Behanna, M. J. Hui, X. Han, J. F. Hulvat, J. W. Lomasney and S. I. Stupp, *Nano Lett.*, 2006, **6**, 2086–2090.
- (200) E. D. Spoerke, S. G. Anthony and S. I. Stupp, *Adv. Mater.*, 2009, **21**, 425–430.
- (201) A. Mata, Y. Geng, K. J. Henrikson, C. Aparicio, S. R. Stock, R. L. Satcher and S. I. Stupp, *Biomaterials*, 2010, **31**, 6004–6012.
- (202) M. J. Webber, J. Tongers, C. J. Newcomb, K.-T. Marquardt, J. Bauersachs, D. W. Losordo and S. I. Stupp, *Proc. Natl. Acad. Sci. U. S. A.*, 2011, **108**, 13438–13443.

- (203) Y. Lim, E. Lee, Y.-R. Yoon, M. S. Lee and M. Lee, *Angew. Chem. Int. Ed.*, 2008, **47**, 4525–4528.
- (204) K. Miyata, N. Nishiyama and K. Kataoka, *Chem. Soc. Rev.*, 2012, **41**, 2562–2574.
- (205) S. R. Morrone, T. Wang, L. M. Constantoulakis, R. M. Hooy, M. J. Delannoy and J. Sohn, *Proc. Natl. Acad. Sci. U. S. A.*, 2014, **111**, E62–E71.
- (206) X. Du, J. Zhou, L. Wu, S. Sun and B. Xu, *Bioconjugate Chem.*, 2014, **25**, 2129–2133.
- (207) X. Du, J. Zhou and B. Xu, *Colloid Interface Sci.* 2015, **447**, 273–277.
- (208) T. Liebmann, S. Rydholm, V. Akpe and H. Brismar, *BMC Biotechnol.*, 2007, **7**, 88.
- (209) W. Wang, G. Li, W. Zhang, J. Gao, J. Zhang, C. Li, D. Ding and D. Kong, *RSC Adv.*, 2014, **4**, 30168–30171.
- (210) K. M. Galler, L. Aulisa, K. R. Regan, R. N. D’Souza and J. D. Hartgerink, *J. Am. Chem. Soc.*, 2010, **132**, 3217–3223.
- (211) W.-N. Yin, F.-Y. Cao, K. Han, X. Zeng, R.-X. Zhuo and X.-Z. Zhang, *J. Mater. Chem. B*, 2014, **2**, 8434–8440.
- (212) M. Weerasekare, M. B. Taraban, X. F. Shi, E. K. Jeong, J. Trehwella and Y. H. B. Yu, *Biopolymers*, 2011, **96**, 734–743.
- (213) C. H. Ren, H. M. Wang, X. L. Zhang, D. Ding, L. Wang and Z. M. Yang, *Chem. Commun.*, 2014, **50**, 3473–3475.
- (214) S. Ray, A. K. Das and A. Banerjee, *Chem. Mater.*, 2007, **19**, 1633–1639.
- (215) C. Sonmez, K. J. Nagy and J. P. Schneider, *Biomaterials*, 2015, **37**, 62–72.
- (216) G. Laverty, A. P. McCloskey, B. F. Gilmore, D. S. Jones, J. Zhou and B. Xu, *Biomacromolecules*, 2014, **15**, 3429–3439.
- (217) R. N. Mitra, A. Shome, P. Paul and P. K. Das, *Org. Biomol. Chem.*, 2009, **7**, 94–102.
- (218) Y. Li, F. Zhou, Y. Wen, K. Liu, L. Chen, Y. Mao, S. Yang and T. Yi, *Soft Matter*, 2014, **10**, 3077–3085.
- (219) I. Irwansyah, Y.-Q. Li, W. Shi, D. Qi, W. R. Leow, M. B. Y. Tang, S. Li and X. Chen, *Adv. Mater.*, 2015, **27**, 648–654.

- (220) A. Baral, S. Roy, S. Ghosh, D. Hermida-Merino, I. W. Hamley and A. Banerjee, *Langmuir*, 2016, **32**, 1836–1845.
- (221) N. Nandi, K. Gayen, S. Ghosh, D. Bhunia, S. Kirkham, S. K. Sen, S. Ghosh, I. W. Hamley and A. Banerjee, *Biomacromolecules*, 2017, **18**, 3621–3629.
- (222) J. Naskar, S. Roy, A. Joardar, S. Das and A. Banerjee, *Org. Biomol. Chem.*, 2011, **9**, 6610–6615.
- (223) A. Mohanty and J. Dey, *Langmuir*, 2007, **23**, 1033–1040.
- (224) S. Kar, M. G. B. Drew and A. Pramanik, *J. Mater Sci.*, 2012, **47**, 1825–1835.
- (225) A. Gupta, K. V. Krishna and S. Verma, *RSC Adv.*, 2015, **5**, 71785–71789.
- (226) X. Du, J. Zhou, J. Shi and B. Xu, *Chem. Rev.*, 2015, **115**, 13165–13307.
- (227) M. Casolaro, I. Casolaro, S. Bottari, B. Del Bello, E. Maellaro and K. D. Demadis, *Eur. J. Pharm. Biopharm.*, 2014, **88**, 424–433.
- (228) L. Liang, Q.-H. Li, K. Jin, T. Luo, Z.-A. Yang, X.-D. Xu and H. Cheng, *Asian J. Chem.*, 2014, **26**, 2977–2981.
- (229) M. C. Branco and J. P. Schneider, *Acta Biomater.* 2009, **5**, 817–831.
- (230) J. X. Zhang and P. X. Ma, *Adv. Drug Delivery Rev.*, 2013, **65**, 1215–1233.
- (231) S. R. Sirsi and M. A. Borden, *Adv. Drug Delivery Rev.*, 2014, **72**, 3–14.
- (232) A. Shome, S. Debnath and P. K. Das, *Langmuir*, 2008, **24**, 4280–4288.
- (233) M. C. Branco, D. J. Pochan, N. J. Wagner and J. P. Schneider, *Biomaterials*, 2010, **31**, 9527–9534.
- (234) M. C. Branco, D. J. Pochan, N. J. Wagner and J. P. Schneider, *Biomaterials*, 2009, **30**, 1339–1347.
- (235) S. Sutton, N. L. Campbell, A. I. Cooper, M. Kirkland, W. J. Frith and D. J. Adams, *Langmuir*, 2009, **25**, 10285–10291.
- (236) L. Qin, P. F. Duan, F. Xie, L. Zhang and M. Liu, *Chem. Commun.*, 2013, **49**, 10823–10825.

- (237) L. Qin, F. Xie, P. Duan and M. Liu, *Chem. - Eur. J.*, 2014, **20**, 15419–15425.
- (238) M. N. Rahaman, D. E. Day, B. S. Bal, Q. Fu, S. B. Jung, L. F. Bonewald and A. P. Tomsia, *Acta Biomater.* 2011, **7**, 2355–2373.
- (239) D. M. Ryan and B. L. Nilsson, *Polym. Chem.*, 2012, **3**, 18–33.
- (240) H. M. Wang and Z. M. Yang, *Nanoscale*, 2012, **4**, 5259–5267.
- (241) M. He and Y. Zhang, In *Engineering in Translational Medicine*; Cai, W., Ed.; Springer: New York, 2014.
- (242) K. J. Skilling, F. Citossi, T. D. Bradshaw, M. Ashford, B. Kellam and M. Marlow, *Soft Matter*, 2014, **10**, 237–256.
- (243) E. Arslan, I. C. Garip, G. Gulseren, A. B. Tekinay and M. O. Guler, *Adv. Healthcare Mater.*, 2014, **3**, 1357–1376.
- (244) Y. Q. Wang, Z. L. Zhang, L. Xu, X. Y. Li and H. Chen, *Colloids Surf., B*, 2013, **104**, 163–168.
- (245) B. F. Lin, K. A. Megley, N. Viswanathan, D. V. Krogstad, L. B. Drews, M. J. Kade, Y. C. Qian and M. V. Tirrell, *J. Mater. Chem.*, 2012, **22**, 19447–19454.
- (246) L. A. Castillo Diaz, M. Elsayy, A. Saiani, J. E. Gough, A. F. Miller, *J. Tissue Eng.*, 2016, **7**, 1–15.
- (247) L. A. Castillo Diaz, A. Saiani, J. E. Gough, A. F. Miller, Human osteoblasts within soft peptide hydrogels promote mineralisation in vitro, *J. Tissue Eng.*, 2014, **5**, 1–12.
- (248) L. Li, J. Y. Li, J. M. Guo, H. K. Zhang, X. Zhang, C. Y. Yin, L. M. Wang, Y. S. Zhu and Q. Q. Yao, *Adv. Funct. Mater.*, 2019, **29**, 1807356.
- (249) S. Babel and T. A. Kurniawan, *J. Hazard. Mater.*, 2003, **97**, 219–243.
- (250) V. K. Gupta and Suhas, *J. Environ. Manage.*, 2009, **90**, 2313–2342.
- (251) F. I. Hai, K. Yamamoto and K. Fukushi, *Crit. Rev. Environ. Sci. Technol.*, 2007, **37**, 315–377.
- (252) N. Zweep and J. H. van Esch, in *Functional Molecular Gels*, ed. B. Escuder and J. F. Miravet, RSC, Cambridge, 2014, pp. 1–2942.
- (253) S. Debnath, A. Shome, S. Dutta and P. K. Das, *Chem. -Eur. J.*, 2008, **14**, 6870–6881.
- (254) B. Adhikari, G. Palui and A. Banerjee, *Soft Matter*, 2009, **5**, 3452–3460.

- (255) P. J. Knerr, M. C. Branco, R. Nagarkar, D. J. Pochan and J. P. Schneider, *J. Mater. Chem.*, 2012, **22**, 1352–1357.
- (256) N. Nandi, A. Baral, K. Basu, S. Roy and A. Banerjee, *Peptide Science*, 2017, **108** : e22915.
- (257) S. Basak, N. Nandi, S. Paul, I. W. Hamley and A. Banerjee, *Chem. Commun.*, 2017, **53**, 43, 5910–5913.
- (258) Y. Gong, X. Zhao , Z. Cai, S. E. O'Reilly, X. Hao and D. Zhao, *Mar. Pollut. Bull.*, 2014, **79**, 16–33.
- (259) L. Guterman, *Science*, 2009, **323**, 1558–1559.
- (260) D. Dave and A. E. Ghaly, *Am. J. Environ. Sci.*, 2011, **7**, 423–440.
- (261) D. D. Prenderghast and P. M. Gschwend, *J. Cleaner Prod.*, 2014, **78**, 233–242.
- (262) USEPA-Water quality office, Gelling crude oils to reduce marine pollution from tanker oil spills, Water pollution control research series 15080DJN 1/71, U.S. government printing office, Washington D.C. 20402, 1971.
- (263) T. Saito, Y. Matsuzawa, S. Ninagawa, M. Honna, M. Takesada and M. Takehara, US Pat., 3969087 A, 1976.
- (264) S. Bhattacharya and Y. Krishnan-Ghosh, *Chem. Commun.*, 2001, 185–186.
- (265) S. Basak, J. Nanda and A. Banerjee, *J. Mater. Chem.*, 2012, **22**, 11658–11664.
- (266) S.-L. Yua, X. -Q. Doub, D. -H. Q. C. -L. Feng, *J. Mol. Liq.*, 2014, **190**, 94–98.
- (267) K. Basu, N. Nandi, B. Mondal, A. Dehsorkhi, I. W. Hamley and A. Banerjee, *Interface Focus*, 2017, **7**, 20160128.
- (268) B. D. Wall, S. R. Diegelmann, S. Zhang , T. J. Dawidczyk , W. L. Wilson , H. E. Katz , Hai-Quan Mao and J. D. Tovar, *Adv. Mater.* 2011, **23**, 5009–5014.
- (269) K. Akagawa and K. Kudo, *Acc. Chem. Res.* 2017, **50**, 2429–2439.
- (270) M. O. Guler and S. I. Stupp, *J. Am. Chem. Soc.* 2007, **129**, 12082–2083.
- (271) N. Singh and B. Escuder, *Chem. Eur.J.*, 2017, **23**, 9946–9951.
- (272) A. M. Garcia, M. Kurbasic, S. Kralj, M. Melchionna and S. Marchesan, *Chem. Commun.*, 2017, **53**, 8110–8113.

- (273) C. Zhang, X. Xue, Q. Luo, Y. Li, K. Yang, X. Zhuang, Y. Jiang, J. Zhang, J. Liu, G. Zou and X. -J. Liang, *ACS Nano*, 2014, **8**, 11715–11723.
- (274) N. Singh, M. P. Conte, R. V. Ulijn, J. F. Miravet and B. Escuder, *Chem. Commun.*, 2015, **51**, 13213–13216.
- (275) M. Tena-Solsona, J. Nanda, S. Díaz-Oltra, A. Chotera, G. Ashkenasy and B. Escuder, *Chem. Eur. J.*, 2016, **22**, 6687–6694.
- (276) K. Gayen, K. Basu, D. Bairagi, V. Castelletto, I. W. Hamley and A. Banerjee, *ACS Appl. Bio Mater.*, 2018, **1**, 1717–1724.
- (277) S. Pang, T. Yang and L. He, *TrAC Trends Anal. Chem.*, 2016, **85**, 73–82.
- (278) A. Mishra, J. Kumar and J.S. Melo, *Biosens. Bioelectron.*, 2017, **87**, 332–338.
- (279) X. Yan, H. Li, Y. Yan and X. Su, *Food Chem.*, 2015, **173**, 179–184.
- (280) K. Zhang, T. Yu, F. Liu, M. Sun, H. Yu and B. Liu, *Anal. Chem.*, 2014, **86**, 11727–11733.
- (281) C.G. Zambonin, M. Quinto, N. De Vietro and F. Palmisano, *Food Chem.*, 2004, **86**, 269–274.
- (282) R. Bala, M. Kumar, K. Bansal, R.K. Sharma and N. Wangoo, *Biosens. Bioelectron.*, 2016, **85**, 445–449.
- (283) S.C. Kamerlin, P.K. Sharma, R.B. Prasad and A. Warshel, *Q. Rev. Biophys.*, 2013, **46**, 1–132.
- (284) N. Fahimi-Kashani and M.R. Hormozi-Nezhad, *Anal. Chem.*, 2016, **88**, 8099–8106.
- (285) CORDIS, Peptide-based highly selective eco-friendly pest control, 2020, DOI: 10.3030/634361.
- (286) F. Haverkate, A. Tempel and A. J. Den Held, *Netherlands Journal of Plant Pathology*, 1969, **75**, 308–315.
- (287) M. Latijnhouwers, P. J. G. M. d. Wit and F. Govers, *Trends Microbiol.*, 2003, **11**, 462–469.
- (288) C. M. Hogan. *Encyclopedia of Earth*, 2011.
- (289) S. L. S. Velivelli, K. J. Czymmek, H. Li, J. B. Shaw, G. W. Buchko and D. M. Shah, *Proc. Natl. Acad. Sci.*, 2020, **117**, 16043–16054.
- (290) C. Lamberth, *Amino Acids.*, 2016, **48**, 929–940.

- (291) M. Faraday, *Philos. Trans. R. Soc. London*, 1857, **147**, 145–181.
- (292) J. Turkevich, P. C. Stevenson and J. Hillier, *Discuss. Faraday Soc.*, 1951, **11**, 55–75.
- (293) C. A. Mirkin, *Small*, 2005, **1**, 14–16.
- (294) G. Frens, *Colloid Polym. Sci.*, 1972, **250**, 736–741.
- (295) G. Frens, *Nature*, 1973, **241**, 20–22.
- (296) P. C. Lee and D. Meisel, *J. Phys. Chem.*, 1982, **86**, 3391–3395.
- (297) P. H. Hess and P. H. Parker, *J. Appl. Polym. Sci.*, 1966, **10**, 1915–1927.
- (298) C. H. Griffiths, M. P. O'Horo and T. W. Smith, *J. Appl. Phys.*, 1979, **50**, 7108–7115.
- (299) R. Rossetti and L. Brus, *J. Phys. Chem.*, 1982, **86**, 4470–4472.
- (300) A. J. Bard, *Science*, 1980, **207**, 139–144.
- (301) G. Schmid, R. Pfeil, R. Boese, F. Bandermann, S. Meyer, G. H. M. Calis and J. W. A. van der Velden, *Chem. Ber.*, 1981, **114**, 3634–3642.
- (302) C. D. Bain, J. Evall and G. M. Whitesides, *J. Am. Chem. Soc.*, 1989, **111**, 7155–7164.
- (303) C. D. Bain and G. M. Whitesides, *Angew. Chem. Int. Ed.*, 2003, **28**, 506–512.
- (304) L. H. Dubois and R. G. Nuzzo, *Annu. Rev. Phys. Chem.*, 1992, **43**, 437–463.
- (305) M. Brust, M. Walker, D. Bethell, D. J. Schiffrin and R. Whyman, *J. Chem. Soc.* 1994, 801–802.
- (306) M. Brust, J. Fink, D. Bethell, D. Schiffrin and C. Kiely, *J. Chem. Soc.*, 1995, 1655–1656.
- (307) M. Brust, D. J. Schiffrin, D. Bethell and C. Kiely, *J. Adv. Mater.* 2004, **7**, 795–797.
- (308) M. Alvarez, J. Khoury, T. Schaaff, M. Shafigullin, I. Vezmar and R. Whetten, *Chem. Phys. Lett.* 1997, **266**, 91–98.
- (309) M. M. Alvarez, J. T. Khoury, T. G. Schaaff, M. N. Shafigullin, I. Vezmar and R. L. Whetten, *J. Phys. Chem. B*, 1997, **101**, 3706–3712.
- (310) R. L. Whetten, M. N. Shafigullin, J. T. Khoury, T. G. Schaaff, I. Vezmar, M. M. Alvarez and A. Wilkinson, *Acc. Chem. Res.*, 1999, **32**, 397–406.

- (311) C. L. Cleveland, U. Landman, T. G. Schaaff, M. N. Shafigullin, P. W. Stephens and R. L. Whetten, *Phys. Rev. Lett.*, 1997, **79**, 1873–1876.
- (312) R. H. Terrill, T. A. Postlethwaite, C.-h. Chen, C.-D. Poon, A. Terzis, A. Chen, J. E. Hutchison, M. R. Clark, G. Wignall, J. D. Londono, R. Superfine, M. Falvo, C. S. Johnson Jr, E. T. Samulski and R. W. Murray, *J. Am. Chem. Soc.* 1995, **117**, 12537–12548.
- (313) S. Link and M. A. El-Sayed, *J. Phys. Chem. B*, 1999, **103**, 8410–8426.
- (314) W. T. Wallace and R. L. Whetten, *J. Am. Chem. Soc.*, 2002, **124**, 7499–7505.
- (315) C. T. Campbell, S. C. Parker and D. E. Starr, *Science*, 2002, **298**, 811–814.
- (316) A. Sanchez, S. Abbet, U. Heiz, W.-D. Schneider, H. Häkkinen, R. N. Barnett and U. Landman, *J. Phys. Chem. A*, 1999, **103**, 9573–9578.
- (317) L. A. Peyser, T. H. Lee and R. M. Dickson, *J. Phys. Chem. B*, 2002, **106**, 7725–7728.
- (318) W. Chen, A. G. Joly and J. Roark, *Phys. Rev. B*, 2002, **65**, 245404.
- (319) C. Félix, C. Sieber, W. Harbich J. Buttet, I. Rabin, W. Schulze and G. Ertl, *Phys. Rev. Lett.*, 2001, **86**, 2992–2995.
- (320) I. Rabin, W. Schulze, G. Ertl, C. Felix, C. Sieber, W. Harbich and J. Buttet, *Chem. Phys. Lett.*, 2000, **320**, 59–64.
- (321) W. Harbich, S. Fedrigo, J. Buttet and D. M. Lindsay, *Z. Phys. D-Atoms Mol. Clusters*, 1991, **19**, 157–159.
- (322) W. Harbich. S. Fedrigo, F. Meyer, D. M. Lindsay, J. Lignieres, J. C. Rivoal and D. Kreisler, *J. Chem. Phys.*, 1990, **93**, 8535–8543.
- (323) S. Chen, R. S. Ingram, M. J. Hostetler, J. J. Pietron, R. W. Murray, T. G. Schaaff, J. T. Khoury, M. M. Alvarez and R. L. Whetten, *Science*, 1998, **280**, 2098–2101.
- (324) J. P. Wilcoxon and B. L. Abrams, *Chem. Soc. Rev.*, 2006, **35**, 1162–1194.
- (325) J. Zheng, P. R. Nicovich and R. M. Dickson, *Annu. Rev. Phys. Chem.*, 2007, **58**, 409–431.
- (326) H. Xu and K. S. Suslick, *Adv. Mater.*, 2010, **22**, 1078–1082.
- (327) I. Díez and R. H. A. Ras, *Nanoscale*, 2011, **3**, 1963–1970.

- (328) C. Wang, L. Ling, Y. Yao and Q. Song, *Nano Res.*, 2015, **8**, 1975–1986.
- (329) P. Crespo, R. Litrán, T. C. Rojas, M. Multigner, J. M. de la Fuente, J. C. Sánchez-López, M. A. García, A. Hernando, S. Penadés and A. Fernández, *Phys. Rev. Lett.*, 2004, **93**, 087204.
- (330) G. Hodes, *Adv. Mater.*, 2007, **19**, 639–655.
- (331) J. Park, J. Joo, S. G. Kwon, Y. Jang and T. Hyeon, *Angew. Chem. Int. Ed.*, 2007, **46**, 4630–4360.
- (332) M. A. El-Sayed, *Acc. Chem. Res.*, 2004, **37**, 326–333.
- (333) Y.N. Xia, Y. J. Xiong, B. Lim and S. E. Skrabalak, *Angew. Chem. Int. Ed.*, 2009, **48**, 60–103.
- (334) C. J. Murphy, A. M. Gole, J. W. Stone, P. N. Sisco, A. M. Alkilany, E. C. Goldsmith and S. C. Baxter, *Acc. Chem. Res.*, 2008, **41**, 1721–1730.
- (335) J. Yu, S. A. Patel and R. M. Dickson, *Angew. Chem. Int. Ed.*, 2007, **46**, 2028–2030.
- (336) J. Yu, S. Choi, C.I. Richards, Y. Antoku and R.M. Dickson, *Photochem. Photobiol.*, 2008, **84**, 1435–1439.
- (337) R. C. Triulzi, M. Micic, S. Giordani, M. Serry, W. A. Chiou and R. M. Leblanc, *Chem. Commun.*, 2006, 5068–5070.
- (338) C. -A. J. Lin, T. -Y. Yang, C. -H. Lee, S. H. Huang, R. A. Sperling, M. Zanella, J. K. Li, J.-L. Shen, H. -H. Wang, H. -I. Yeh, W. J. Parak and W. H. Chang, *ACS Nano*, 2009, **3**, 395–401.
- (339) C. -C. Huang, Z. Yang, K. -H. Lee and H. -T. Chang, *Angew. Chem. Int. Ed.*, 2007, **46**, 6824–6828.
- (340) W. Guo, J. Yuan and E. Wang, *Chem. Commun.*, 2009, 3395–3397.
- (341) J. Xie, Y. Zheng and J. Y. Ying, *Chem. Commun.*, 2010, **46**, 961–963.
- (342) L. Shang and S. Dong, *J. Mater. Chem.*, 2008, **18**, 4636–4640.
- (343) B. Adhikari and A. Banerjee, *Chem. Mater.*, 2010, **22**, 4364–4371.
- (344) T. Vosch, Y. Antoku, J. C. Hsiang, C. I. Richards, J. I. Gonzalez and R. M. Dickson, *Proc. Natl. Acad. Sci. U.S.A.*, 2007, **104**, 12616–12621.
- (345) Y. Liu, H. Tsunoyama, T. Akita and T. Tsukuda, *Chem. Commun.*, 2010, **46**, 550–552.

- (346) Y. Zhu, H. Qian, M. Zhu and R. Jin, *Adv. Mater.*, 2010, **22**, 1915–1920.
- (347) Y. Zhu, H. Qian, B. A. Drake and R. Jin, *Angew. Chem., Int. Ed.*, 2010, **49**, 1295–1298.
- (348) H. Tsunoyama, N. Ichikuni, H. Sakurai and T. Tsukuda, *J. Am. Chem. Soc.*, 2009, **131**, 7086–7093.
- (349) Y. Lu, W. Wei and W. Chen, *Chin. Sci. Bull.*, 2012, **57**, 41–47.
- (350) Y. Guo, F. Cao, X. Lei, L. Mang, S. Cheng and J. Song, *Nanoscale*, 2016, **8**, 4852–4863.
- (351) R. Das, S. S. Nath and R. Bhattacharjee, *J. Fluoresc.*, 2011, **131**, 2703–2706.
- (352) Y. Lu and W. Chen, *Chem. Soc. Rev.*, 2012, **41**, 3594–3623.
- (353) A. Rotaru, S. Dutta, E. Jentzsch, K. Gothelf and A. Mokhir, *Angew. Chem., Int. Ed.*, 2010, **49**, 5665–5667.
- (354) Z. Qing, X. He, D. He, K. Wang, F. Xu, T. Qing and X. Yang, *Angew. Chem., Int. Ed.*, 2013, **52**, 9719–9722.
- (355) N. Goswami, A. Giri, M. Bootharaju, P. L. Xavier, T. Pradeep and S. K. Pal, *Anal. Chem.*, 2011, **83**, 9676–9680.
- (356) C. Wang, C. Wang, L. Xu, H. Cheng, Q. Lin and C. Zhang, *Nanoscale*, 2014, **6**, 1775–1781.
- (357) Q. Liu, B. Guo, Z. Rao, B. Zhang and J. R. Gong, *Nano Lett.*, 2013, **13**, 2436–2441.
- (358) Y. Wang, Y. Cui, R. Liu, Y. Wei, X. Jiang, H. Zhu, L. Gao, Y. Zhao, Z. Chai and X. Gao, *Chem. Commun.*, 2013, **49**, 10724–1072622.
- (359) Y. Hong, J. W. Y. Lam and B. Z. Tang, *Chem. Soc. Rev.*, 2011, **40**, 5361–5388.
- (360) X. Jia, J. Li and E. Wang, *Small*, 2013, **9**, 3873–3879.
- (361) X. Jia, X. Yang, J. Li, D. Li and E. Wang, *Chem. Commun.*, 2014, **50**, 237–239.
- (362) Z. Li, S. Guo and C. Lu, *Analyst*, 2015, **140**, 2719–2725.
- (363) A. Mathew and T. Pradeep, *Part. Part. Syst. Charact.*, 2014, **31**, 1017–1053.
- (364) Z. Xia-Hong, Z. Ting-Yao and C. Xi, *Chin. J. Anal. Chem.*, 2015, **43**, 1296–1305.

- (365) L.-Y. Chen, C.-W. Wang, Z. Yuan and H.-T. Chang, *Anal. Chem.*, 2015, **87**, 216–229.
- (366) Y. Negishi, K. Nobusada and T. Tsukuda, *J. Am. Chem. Soc.*, 2005, **127**, 5261–5270.
- (367) R. Ghosh, U. Goswami, S. S. Ghosh, A. Paul, A. Chattopadhyay, *ACS Appl. Mater. Interfaces*, 2015, **7**, 209–222.
- (368) Y. Negishi, Y. Takasugi, S. Sato, H. Yao, K. Kimura and T. Tsukuda, *J. Am. Chem. Soc.*, 2004, **126**, 6518–6519.
- (369) T. Huang and R. W. Murray, *J. Phys. Chem. B*, 2001, **105**, 12498–12502.
- (370) G. Wang, T. Huang, R. W. Murray, L. Menard and R. G. Nuzzo, *J. Am. Chem. Soc.*, 2004, **127**, 812–813.
- (371) F. Aldeek, M. A. H. Muhammed, G. Palui, N. Zhan and H. Mattoussi, *ACS Nano*, 2013, **7**, 2509–2521.
- (372) L. Rabara, M. Aranyosiova and D. Velic, *Appl. Surf. Sci.*, 2011, **257**, 1886–1892.
- (373) C. Zhou, C. Sun, M. Yu, Y. Qin, J. Wang, M. Kim and J. Zheng, *J. Phys. Chem. C*, 2010, **114**, 7727–7732.
- (374) Z. Luo, X. Yuan, Y. Yu, Q. Zhang, D. T. Leong, J. Y. Lee and J. Xie, *J. Am. Chem. Soc.*, 2012, **134**, 16662–16670.
- (375) J. Zheng, J. T. Petty and R. M. Dickson, *J. Am. Chem. Soc.*, 2003, **125**, 7780–7781.
- (376) J. Zheng, C. W. Zhang and R. M. Dickson, *Phys. Rev. Lett.*, 2004, **93**, 077402.
- (377) H. Kawasaki, H. Yamamoto, H. Fujimori, R. Arakawa, Y. Iwasaki and M. Inada, *Langmuir*, 2010, **26**, 5926–5933.
- (378) F. Aldeek, M. A. H. Muhammed, G. Palui, N. Zhan, and H. Mattoussi, *ACS Nano*, 2013, **7**, 2509–2521.
- (379) J. Xie, Y. Zheng and J. Y. Ying, *J. Am. Chem. Soc.*, 2009, **131**, 888–889.
- (380) H. Zhang, X. Huang, L. Li, G. Zhang, I. Hussain, Z. Li and B. Tan, *Chem. Commun.*, 2012, **48**, 567–569.
- (381) L. Li, Z. Li, H. Zhang, S. Zhang, I. Majeed and B. Tan, *Nanoscale*, 2013, **5**, 1986–1992.

- (382) C. -C. Huang, Y. -L. Hung, Y. -C. Shiang, T. -Y. Lin, Y. -S. Lin, C. -T. Chen and H. -T. Chang, *Chem. -Asian J.*, 2010, **5**, 334–341.
- (383) K. S. Jin, Y. Rho, J. Kim, H. Kim, I. J. Kim and M. Ree, *J. Phys. Chem. B*, 2008, **112**, 15821–15827.
- (384) P. L. Xavier, K. Chaudhari, P. K. Verma, S. K. Pal and T. Pradeep, *Nanoscale*, 2010, **2**, 2769–2776.
- (385) H. Kawasaki, K. Hamaguchi, I. Osaka and R. Arakawa, *Adv. Funct. Mater.*, 2011, **21**, 3508–3515.
- (386) T. -H. Chen and W. -L. Tseng, *Small*, 2012, **8**, 1912–1919.
- (387) P. -C. Chen, T. -Y. Yeh, C. -M. Ou, C. -C. Shih and H. -T. Chang, *Nanoscale*, 2013, **5**, 4691–4695.
- (388) C. -C. Huang, C. -K. Chiang, Z. -H. Lin, K. -H. Lee and H. -T. Chang, *Anal. Chem.*, 2008, **80**, 1497–1504.
- (389) Y. -C. Shiang, C. -A. Lin, C. -C. Huang and H. -T. Chang, *Analyst*, 2011, **136**, 1177–1182.
- (390) H. Duan and S. Nie, *J. Am. Chem. Soc.*, 2007, **129**, 2412–2413.
- (391) Y. Bao, H.-C. Yeh, C. Zhong, S. A. Ivanov, J. K. Sharma, M. L. Neidig, D. M. Vu, A. P. Shreve, R. B. Dyer, J. H. Werner and J. S. Martinez, *J. Phys. Chem. C*, 2010, **114**, 15879–15882.
- (392) M. A. H. Muhammed, S. Ramesh, S. S. Sinha, S. K. Pal and T. Pradeep, *Nano Res.*, 2008, **1**, 333–340.
- (393) H. Qian, Y. Zhu and R. Jin, *ACS Nano*, 2009, **3**, 3795–3803.
- (394) S. Roy, G. Palui and A. Banerjee, *Nanoscale*, 2012, **4**, 2734–2740.
- (395) E. S. Shibu, R. Radha, P. K. Verma, P. Bhyrappa, G. U. Kulkarni, S. K. Pal and T. Pradeep, *ACS Appl. Mater. Interfaces*, 2009, **1**, 2199–2210.
- (396) J. T. Petty, J. Zheng, N. V. Hud and R. M. Dickson, *Am. Chem. Soc.*, 2004, **126**, 5207–5212.
- (397) C. M. Ritchie, K. R. Johnsen, J. R. Kiser, Y. Antoku, R. M. Dickson and J. T. Petty, *J. Phys. Chem. C*, 2007, **111**, 175–181.
- (398) C. I. Richards, S. Choi, J. -C. Hsiang, Y. Antoku, T. Vosch, A. Bongiorno, Y. -L. Tzeng and R. M. Dickson, *J. Am. Chem. Soc.*, 2008, **130**, 5038–5039.
- (399) P. R. O'Neill, L. R. Velazquez, D. G. Dunn, E. G. Gwinn and D. K. Fygenson, *J. Phys. Chem. C*, 2009, **113**, 4229–4233.

- (400) X. Guo, L. Deng and J. Wang, *RSC Adv.*, 2013, **3**, 401–407.
- (401) B. Adhikari and A. Banerjee, *Chem. Mater.*, 2010, **22**, 4364–4371.
- (402) L. A. Peyser, A. E. Vinson, A. P. Bartko and R. M. Dickson, *Science*, 2001, **291**, 103.
- (403) J. Zheng and R. M. Dickson, *J. Am. Chem. Soc.*, 2002, **124**, 13982–13983.
- (404) J. Zhang, S. Xu and E. Kumacheva, *Adv. Mater.*, 2005, **17**, 2336.
- (405) T. U. B. Rao and T. Pradeep, *Angew. Chem. Int. Ed.*, 2010, **49**, 3925–3929.
- (406) X. Yang, Y. Feng, S. Zhu, Y. Luo, Y. Zhuo and Y. Dou, *Anal. Chim. Acta*, 2014, **847**, 49–54.
- (407) J.-S. Shen, Y.-L. Chen, Q.-P. Wang, T. Yu, X.-Y. Huang, Y. Yang and H.-W. Zhang, *J. Mater. Chem. C*, 2013, **1**, 2092–2096.
- (408) Y.-J. Lin, P.-C. Chen, Z. Yuan, J.-Y. Ma and H.-T. Chang, *Chem. Commun.*, 2015, **51**, 11983–11986.
- (409) Z. Wu, J. Liu, Y. Gao, H. Liu, T. Li, H. Zou, Z. Wang, K. Zhang, Y. Wang, H. Zhang and B. Yang, *J. Am. Chem. Soc.*, 2015, **137**, 12906–12913.
- (410) W. Wei, Y. Lu, W. Chen and S. Chen, *J. Am. Chem. Soc.*, 2011, **133**, 2060–2063.
- (411) R. Ghosh, U. Goswami, S. S. Ghosh, A. Paul and A. Chattopadhyay, *ACS Appl. Mater. Interfaces*, 2014, **7**, 209–222.
- (412) Y. Isomura, T. Narushima, H. Kawasaki, T. Yonezawa and Y. Obora, *Chem. Commun.*, 2012, **48**, 3784–3786.
- (413) X. J. Zhao and C. Z. Huang, *New J. Chem.*, 2014, **38**, 3673–3677.
- (414) H. Cao, Z. Chen, H. Zheng and Y. Huang, *Biosens. Bioelectron.*, 2014, **62**, 189–195.
- (415) R. Das, S. Nath and R. Bhattacharjee, *J. Fluoresc.*, 2011, **21**, 1165–1170.
- (416) M. Muniz-Miranda, C. Gellini, A. Simonelli, M. Tiberi, F. Giammanco and E. Giorgetti, *Appl. Phys. A: Mater. Sci. Process.*, 2013, **110**, 829–833.
- (417) M. Fernández-Ujados, L. Trapiella-Alfonso, J. M. Costa-Fernández, R. Pereiro and A. Sanz-Medel, *Nanotechnology*, 2013, **24**, 495601.

- (418) Y. Zhong, Q. Wang, Y. He, Y. Ge and G. Song, *Sens. Actuators, B*, 2015, **209**, 147–153.
- (419) J. Feng, Y. Ju, J. Liu, H. Zhang and X. Chen, *Anal. Chim. Acta*, 2015, **854**, 153–160.
- (420) K. Tanaka and F. Toda, *Chem. Rev.*, 2000, **100**, 1025–1074.
- (421) K. Kluchova, R. Zboril, J. Tucek, M. Pecova, L. Zajoncova, I. Safarik, M. Mashlan, I. Markova, D. Jancik and M. Sebel, *Biomaterials*, 2009, **30**, 2855–2863.
- (422) A. Ganguly, I. Chakraborty, T. Udayabhaskararao and T. Pradeep, *J. Nanopart. Res.*, 2013, **15**, 1–7.
- (423) X. Yuan, Z. Luo, Q. Zhang, X. Zhang, Y. Zheng, J. Y. Lee and J. Xie, *ACS Nano*, 2011, **5**, 8800–8808.
- (424) I. Bilecka and M. Niederberger, *Nanoscale*, 2010, **2**, 1358–1374.
- (425) M. B. Gawande, S. N. Shelke, R. Zboril and R. S. Varma, *Acc. Chem. Res.*, 2014, **47**, 1338–1348.
- (426) H. Kawasaki, Y. Kosaka, Y. Myoujin, T. Narushima, T. Yonezawa and R. Arakawa, *Chem. Commun.*, 2011, **47**, 7740–7742.
- (427) M. A. López-Quintela, C. Tojo, M. Blanco, L. G. A. Rio and J. Leis, *Curr. Opin. Colloid Interface Sci.*, 2004, **9**, 264–278.
- (428) C. Vázquez-Vázquez, M. Bañobre-López, A. Mitra, M. A. López-Quintela and J. Rivas, *Langmuir*, 2009, **25**, 8208–8216.
- (429) M. T. Reetz, M. Winter, R. Breinbauer, T. Thurn-Albrecht and W. Vogel, *Chem. -Eur. J.*, 2001, **7**, 1084–1094.
- (430) N. Vilar-Vidal, M. C. Blanco, M. A. López-Quintela, J. Rivas and C. Serra, *J. Phys. Chem. C*, 2010, **114**, 15924–15930.
- (431) X. Yuan, Y. Tay, X. Dou, Z. Luo, D. T. Leong, and J. Xie, *Anal. Chem.*, 2013, **85**, 1913–1919.
- (432) X. Yuan, T. J. Yeow, Q. Zhang, J. Y. Lee and J. Xie, *Nanoscale*, 2012, **4**, 1968–1971.
- (433) J. Fang, J. Li, B. Zhang, X. Yuan, H. Asakura, T. Tanaka, K. Teramura, J. Xie and N. Yan, *Nanoscale*, 2015, **7**, 6325–6333.
- (434) T. Yskatr, S. Yaaze, R. Takaata, J. -i. Nishigaki, A. Thivasasith, J. Limtrakul and T. Tsukuda, *ACS Catal.*, 2014, **4**, 3696–3700.
- (435) N. Goswami, K. Zhenga and J. Xie, *Nanoscale*, 2014, **6**, 13328–13347.

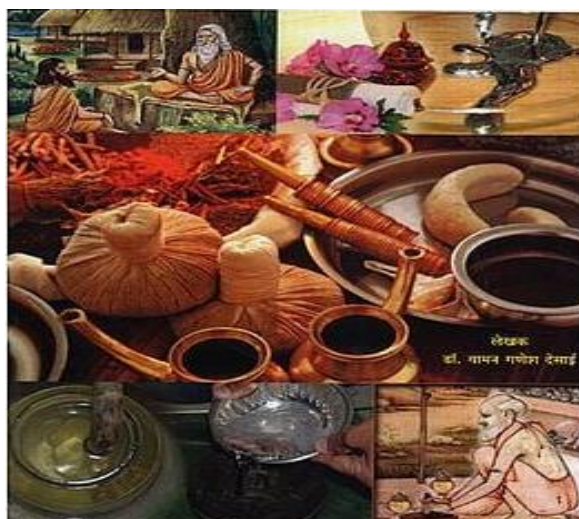
- (436) S. Choi, R. M. Dickson, J. Yu, *Chem. Soc. Rev.*, 2012, **41**, 1867–1891.
- (437) G. Schmid, *Chem. Soc. Rev.* 2008, **37**, 1909–1930.
- (438) L. Shang, S. Dong, G. U. Nienhaus, *Nano Today*, 2011, **6**, 401–418.
- (439) X. Tan, R. Jin, *Wiley Interdisciplinary Reviews: Nanomed. Nanobiotech.* 2013, **5**, 569–581.
- (440) A. Mathew and T. Pradeep, *Part. Part. Sys. Charact.*, 2014, **31**, 1017–1053.
- (441) X. Chen, Y. Zhou, X. Peng, J. Yoon, *Chem. Soc. Rev.*, 2010, **39**, 2120–2135.
- (442) K. Saha, S. S. Agasti, C. Kim, X. Li, V. M. Rotello, *Chem. Rev.* 2012, **112**, 2739–2779.
- (443) G. Guan, S.-Y. Zhang, Y. Cai, S. Liu, M. S. Bharathi, M. Low, Y. Yu, J. Xie, Y. Zheng, Y.-W. Zhang, M.-Y. Han, *Chem. Commun.*, 2014, **50**, 5703–5705.
- (444) E. S. Shibu, T. Pradeep, *Chem. Mater.*, 2011, **23**, 989–999.
- (445) A. George, E. S. Shibu, S. M. Maliyekkal, M. S. Bootharaju, T. Pradeep, *ACS Appl. Mater. Interfaces*, 2012, **4**, 639–644.
- (446) M. C. Paau, C. K. Lo, X. Yang, M. M. F. Choi, *J. Phys. Chem. C*, 2010, **114**, 15995–16003.
- (447) A. Baral, K. Basu, S. Roy and A. Banerjee, *ACS Sustainable Chem. Eng.* 2017, **5**, 1628–1637.
- (448) S. Liu, F. Lu, J. -J. Zhu, *Chem. Commun.* **2011**, 47, 2661.
- (449) P. -H. Li, J. -Y. Lin, C. -T. Chen, W. -Ru Ciou, P. -H. Chan, L. Luo, H. -Y. Hsu, E. W. -G. Diau and Y. -C. Chen, *Anal. Chem.* 2012, **84**, 5484–5488.
- (450) Z. Qing, T. Qing, Z. Mao, X. He, K. Wang, Z. Zou, H. Shi and D. He, *Chem. Commun.*, 2014, **50**, 12746–12748.
- (451) X. Jia, J. Li, L. Han, J. Ren, X. Yang and E. Wang, *ACS Nano*, 2012, **6**, 3311–3317.
- (452) P. L. Xavier, K. Chaudhari, A. Baksi and T. Pradeep, *Nano Rev.*, 2012, **3**, 14767.

- (453) C.-L. Liu, H.-T. Wu, Y.-H. Hsiao, C.-W. Lai, C.-W. Shih, Y.-K. Peng, K.-C. Tang, H.-W. Chang, Y.-C. Chien, J.-K. Hsiao, J.-T. Cheng and P.-T. Chou, *Angew. Chem., Int. Ed.*, 2011, **50**, 7056–7060.
- (454) X. Le Guével, N. Daum and M. Schneider, *Nanotechnology*, 2011, **22**, 275103.
- (455) J. W. Borst and A. Visser, *J. Meas. Sci. Technol.*, 2010, **21**, 102002.
- (456) L. Shang, N. Azadfar, F. Stockmar, W. Send, V. Trouillet, M. Bruns, D. Gerthsen and G. U. Nienhaus, *Small*, 2011, **7**, 2614–2620.
- (457) X. Wu, X. He, K. Wang, C. Xie, B. Zhou and Z. Qing, *Nanoscale*, 2010, **2**, 2244–2249.
- (458) D. -H. Hu, Z. -H. Sheng, P. -F. Zhang, D. -Z. Yang, S. -H. Liu, P. Gong, D. -Y. Gao, S. -T. Fang, Y. -F. Ma and L. -T. Cai, *Nanoscale*, 2013, **5**, 1624–1628.
- (459) N. Makarava, A. parfenov and I. V. Baskakov, *Biophys. J.*, 2005, **89**, 572.
- (460) R. Ghosh, A. K. Sahoo, S. S. Ghosh, A. Paul and A. Chattopadhyay, *ACS Appl. Mater. Interfaces*, 2014, **6**, 3822–3828.
- (461) N. K. Das, S. Ghosh, A. Priya, S. Datta and S. Mukherjee, *J. Phys. Chem. C*, 2015, **119**, 24657–24664.
- (462) K. Basu, K. Gayen, T. Mitra, A. Baral, S. S. Roy and A. Banerjee, *ChemNanoMat.*, 2017, **3**, 808–814.
- (463) X. Nie, H. Qian, Q. Ge, H. Xu and R. Jin, *ACS Nano*, 2012, **6**, 6014–6022.
- (464) Y. Liu, H. Tsunoyama, T. Akita, S. Xie and T. Tsukuda, *ACS Catal.*, 2011, **1**, 2–6.
- (465) H. Chong, P. Li, S. Wang, F. Fu, J. Xiang, M. Zhu and Y. Li, *Sci. Rep.*, 2013, **3**, 3214.
- (466) A. Leelavathi, T. Bhaskara Rao, T. Pradeep, *Nanoscale Res. Lett.*, 2011, **6**, 123.
- (467) L. He, H. Liu, C.-x. Xiao and Y. Kou, *Green Chem.*, 2008, **10**, 619–622.
- (468) N. Vilar-Vidal, J. Rivas and M. A. López-Quintela, *ACS Catal.*, 2012, **2**, 1693–1697.

- (469) K. Basu, S. Paul, R. Jana, A. Datta and A. Banerjee, *ACS Sustainable Chem. Eng.*, 2019, **7**, 1998–2007.
- (470) J. Oliver-Messeguer, L. Liu, S. García-García, C. Canós-Giménez, I. Domínguez, R. Gavara, Doménech-Carbó, A.; Concepción, P.; A. Leyva-Pérez, and A. Corma, *J. Am. Chem. Soc.*, 2015, **137**, 3894–3900.

Chapter 2

Materials and Methods



Chapter 2

Materials and Methods

2.1. Introduction

This chapter provides a detailed description of general synthetic procedures employed in this thesis for synthesis of amino acid and peptide derivatives by solution phase methods. It also provides details of all spectroscopic measurements, and many microscopic studies used in this work. The respective chapters described the specific synthetic procedures pertaining to sequences studied in this thesis.

2.2. Source of Chemicals

L-phenylalanine, L-tryptophan, myristic acid, glutathione (reduced), tert-butyl pyrocarbonate (Boc-anhydride), N,N'-dicyclohexylcarbodiimide (DCC), 1-hydroxy benzotriazole (HOBt), copper acetate monohydrate $[\text{Cu}(\text{OAc})_2 \cdot \text{H}_2\text{O}]_2$, cadmium chloride monohydrate ($\text{CdCl}_2 \cdot \text{H}_2\text{O}$), lead nitrate $\text{Pb}(\text{NO}_3)_2$, 4-mercaptobenzoic acid (4-MBA) and L-ascorbic acid were purchased from Sigma Chemical Company, St. Louis Missouri, U.S.A.; Aldrich, U.S.A.; E-Merck, Germany; Lancaster, England and SRL, India. Deuterated solvents for NMR studies, CDCl_3 and DMSO-d_6 were supplied by Sigma chemical company, St. Louis Missouri, U.S.A and Cambridge Isotopic Laboratories, Massachusetts. Silica gel for TLC was obtained from E-Merck, India. Silica gel (100–200 mesh) for column chromatography was supplied by SRL, India. All other chemicals used were obtained from local manufactures like Ranbaxy, SD Fine Chemicals Pvt. Ltd., Bengal Chemical and Pharmaceutical Ltd., SRL, India, E-Merck India etc.

2.3. Experimental Procedures

Purification of Solvents and Reagents: The solvents used during the course of synthesis were purified as follows: Ethyl acetate and chloroform were distilled and used. Dioxane was passed through basic alumina before use. Methanol was fractionally distilled and used. Absolute methanol was prepared from distilled methanol using magnesium and iodine.¹ Thionyl chloride was distilled from boiled linseed oil (20 mL/50 g SOCl_2).¹ Dimethyl formamide (DMF) was

fractionally distilled using condenser packed with fenske helices under reduced pressure over ninhydrin (3 g/L).

Preparation of Amino Acid Derivatives: All amino acid methyl ester hydrochlorides used in this work were prepared by thionyl chloride absolute methanol procedure² and Boc-amino acids used in this work were prepared using Schnabel's method.³

Solution Phase Peptide Synthesis: All peptides were synthesized by conventional solution-phase methods using racemization free fragment condensation strategy. The Boc group was used for N-terminal protection³ and the C-terminus was protected as a methyl ester.² Couplings were mediated by N,N'-dicyclohexylcarbodiimide/1-hydroxybenzotriazole (DCC/HOBt).⁴ Methyl ester deprotection was performed via the saponification method, and the Boc group was deprotected by 98% formic acid. The synthetic strategy was selected for most of the peptides keeping in mind that the racemization possibilities of other chiral residues in the sequence. Racemization in any step of the peptide synthesis leads to the formation of diastereomeric products. At each step of the synthesis the possibility of diastereomer formation was checked by NMR. Normally no diastereomers could be detected.

Characterization and Purification of Peptides: Peptide fragments were routinely checked for homogeneity by thin layer chromatography (TLC) on silica gel using ethyl acetate-pet ether as an eluent. All the intermediates were characterized by 400 and 500 MHz ¹H NMR spectroscopy, 100 and 125 MHz ¹³C NMR spectroscopy and mass spectrometry. All crude peptides were purified by column chromatography using silica gel (100–200 mesh size) as stationary phase ethyl acetate-pet ether mixture as eluent. The final compounds were fully characterized by 400 and 500 MHz ¹H NMR spectroscopy, 100 and 125 MHz ¹³C NMR spectroscopy and mass spectrometry.

2.4. Spectroscopic Measurements

NMR experiments: All 400 and 500 MHz NMR studies were carried out on a Brüker DPX spectrometer and. Coupling constants were calculated from one-dimensional experiments.

FT-IR spectrometer: Spectra were collected on a JASCO instrument, Model FT/IR-4200 type A. For the solution state in chloroform, NaCl cell was used. For the solution state in D₂O, CaF₂ cell was used.

Mass spectrometry: Mass spectra were recorded on a Q-ToF Micro™ YA263 high-resolution mass spectrometer.

MALDI-TOF MS study: The MALDI-TOF MS analyses were done using Bruker Daltonics flex Analysis mass spectrometer.

2.5. Microscopic Studies

Cryogenic Transmission Electron Microscopy (Cryo-TEM): Cryo-TEM images were recorded on a JEOL JEM-210 PLUS Cryogenic transmission electron microscope at an accelerating voltage of 200 KV.

Transmission Electron Microscopy: Transmission Electron Microscopy (TEM) was carried out to investigate the morphology of the nanostructures. Transmission electron microscopic (TEM) studies were carried out using a small amount of the solution of the corresponding compounds on a carbon coated copper grid (300 mesh) by slow evaporation and vacuum drying at 30 °C for 2 days. TEM images were recorded on a JEM 2010F electron microscope and JEOL 2100 Ultra High Resolution Field Emission Gun (UHR FEG at an accelerating voltage of 200 KV. STEM-HAADF image and EDS line scanning were recorded on a JEM 2010F electron microscope.

2.6. Rheological Study

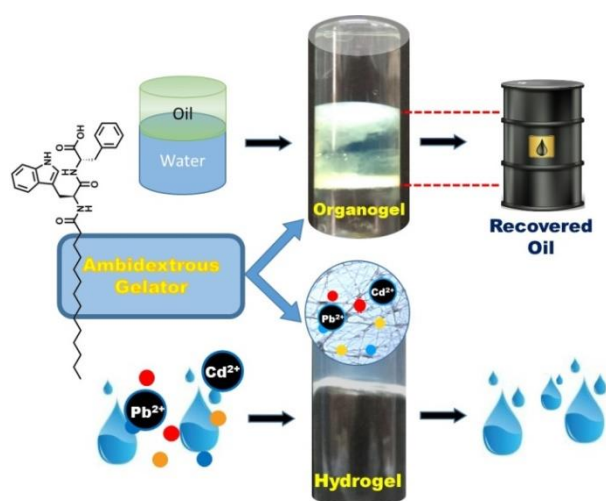
Rheological experiments were done using an Advanced Rheometer AR 2000 (TA Instruments) by cone and plate geometry in a peltier plate. The cone diameter was 40 mm, cone angle 1°59'50", and truncation 56 µm.

2.7. References

1. A. I. Vogel, A Text Book of Practical Organic Chemistry, 4th Eds. *ELBS, Longmans*, 19781.
2. M. Brenner and W. Hubber, *Helv. Chim. Acta.*, 1953, **36**, 1109–1115.
3. E. Schnabel, *Ann. Chem.*, 1967, **702**, 188–196.
4. M. Bodanszky and A. Bodanszky, The Practice of Peptide Synthesis, *Springer-Verlag*, Berlin, Heidelberg, New York, Tokyo, 1984, 1–282.

Chapter 3

Peptide-Based Gel in Environmental Remediation: Removal of Toxic Organic Dyes and Hazardous Pb^{2+} and Cd^{2+} Ions from Wastewater and Oil Spill Recovery



(Langmuir 2020, 36, 12942–12953)

Chapter 3

Peptide-Based Gel in Environmental Remediation: Removal of Toxic Organic Dyes and Hazardous Pb^{2+} and Cd^{2+} Ions from Wastewater and Oil Spill Recovery

3.1. Introduction

Supramolecular gels^{1–16} consisting of a variety of small organic molecules have attracted researchers' attention in the last few decades because of their various applications in chemical, material, and biological sciences.^{17–20} Among low-molecular weight gelators, peptide amphiphiles belong to a special category because they provide a distinctive opportunity to design soft materials with controllable structural features and specific secondary structures. The predictable structure-function relationships of the naturally occurring amino acids can thus be utilized to obtain materials with desirable properties.²¹ Under suitable physical conditions (solvent polarity, pH, and temperature), they can self-assemble via noncovalent interactions to form a nanofibrous network structure that can arrest a large amount of solvent molecules to form gels.^{22–25} Peptide hydrogels offer a variety of applications in biology and medicine including drug delivery,^{26–30} tissue engineering,³¹ 3D cell culture,^{32,33} antibacterial agents,^{16,34} and wound healing.^{35–37} Apart from the abovementioned applications, peptide hydrogels have been used for wastewater treatment,^{38–42} oil spill recovery,^{43–48} and templates for the synthesis of nanoparticles,^{49,50} nanoclusters,⁵¹ and catalysis.^{52,53} The toxicity of contaminated water is caused by heavy metals and organic dyes. They are most commonly found in the byproducts from the metallurgic industries and textile, printing, and other manufacturing sites that use the techniques of chemical precipitation, flocculation, bio-treatment, and so on.^{54–57} Highly toxic organic dyes and heavy metal ions such as Pb^{2+} , Cd^{2+} , Hg^{2+} , Cr^{6+} , and uranium pose a great threat to the environment and human health, and many organic dyes are also toxic and carcinogenic in nature. Untreated dye effluents from industry pollute water, leading to serious hazards for aquatic life and mankind.^{58–63} The presence of toxic dyes in water can be harmful to human beings and other living species even at low concentrations because these are generally nondegradable in nature. Toxic metal pollutants, such as lead and cadmium, exist widely in

industrial wastewater (from battery, electroplate, and dye industries), and exposure to high amounts of these pollutants can lead to accumulation in the human body and the environment for a long period of time.⁶⁴ Cadmium ions usually get accumulated in various human organs and therefore play a significant role in the food chain.⁶⁵ Lead ions, at very low concentrations ($<0.5 \mu\text{g/dL}$),⁶⁶ can damage nerve, immune, renal, and cardiovascular systems. Lead deposition in the bones, brain, kidneys, and muscles leads to severe developmental disorders, injuries, diseases, and even death.⁶⁷ Therefore, the need for a prompt and efficient approach for the removal of dye and heavy metal ions from wastewater is becoming a hot topic for research. The traditional techniques for wastewater management are membrane separation, flocculation, ion exchange, electrochemical treatment, and so forth.⁶⁸ However, there are limitations in terms of cost, efficiency, and complexity of these processes. The adsorption technique is most suitable in batch and continuous processes of industries. Some absorbents regularly used are carbon-based materials, polymers, clay minerals, and others.^{69–73} There are some materials and methods which are very effective toward oil spill and metal ion adsorption.^{74–81} In this context, it is notable that hydrogels, because of their interstitial void spaces, can absorb dyes and heavy metal ions. Hydrogels can also be very useful materials in many other fields apart from above mentioned applications.^{82–88} On the other hand, xerogels (dried gels) can be used in various fields, such as energy-storage devices, metacomposites, electromagnetic wave absorbing/shielding devices, and others.^{89–92} Xerogels having π -surfaces can perform similar water remediation, and hence these materials can be used as an attractive candidate for wastewater management.⁴⁵ Oil spills at sea and in river water pose a great threat to flora and fauna and mankind. Though there are different methods of oil spill recovery,^{43,44} gels are particularly successful in mopping up the spilled oil from the surface of water.^{43–48} Peptide amphiphile containing a long hydrophobic tail with an alkyl chain and a short peptide sequence with a hydrophilic head group can maintain a suitable balance between the hydrophobicity^{93,94} and hydrophilicity to form hydrogels under suitable conditions. Interestingly, this type of molecule with both lipophilic and hydrophilic parts can also be self-assembled in an organic medium under the suitable condition to form an organogel.⁴³ Therefore, this type of gelator molecule is termed as an “ambidextrous gelator”, as it is capable of forming gels in both aqueous medium and nonaqueous, organic solvents. The

ambidextrous nature of such gelator molecules can be utilized for some useful purposes. A prime need for the human society is to obtain clean and safe water for everyday use. Therefore, it is of great interest to construct and develop a new gelator molecule that can form a hydrogel which can be utilized for removing toxic organic dyes and hazardous metal ions from wastewater and also can form organogels that find applications in oil spill recovery.

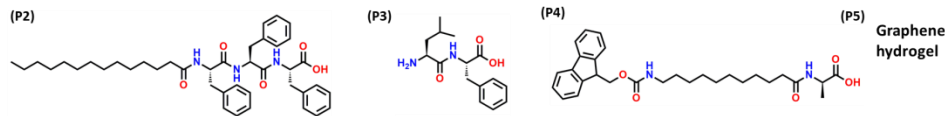
Short peptide-based gels from our group and other groups have been used for the removal of toxic organic dyes from wastewater, and these have also been applied for oil spill recovery.^{38,44–46,87} These are the examples of bifunctional peptide-based gels in environmental remediation. However, there are no examples of peptide-based trifunctional gels in the environmental remediation, to the best of our knowledge. This study vividly demonstrates a short peptide-based trifunctional hydrogel that has been used in environmental remediation: (a) scavenging of toxic organic dyes from wastewater, (b) removal of toxic metal ions including Pd^{2+} and Cd^{2+} from wastewater, and (c) oil spill recovery. Although, selective absorption of cationic/anionic dyes have never been reported previously for peptide-based gelators (to the best of our knowledge), it is noticed that a few nonpeptide-based small molecular hydrogels can be used for selective adsorption of cationic or anionic dyes.

Yu and co-workers reported an imidazole-based surfactant gelator which can selectively remove anionic dyes over cationic dyes with very high selectivity.⁹⁵ Bhattacharjee and Karan reported metallogels, which were found to show excellent selectivity for the adsorption of cationic dyes and their separation from anionic dyes.⁹⁶ The specialty of this result is that adsorption of cationic dyes by this hydrogel is relatively faster compared to the other peptide-based and nonpeptide-based hydrogels reported from our research group and others. Within only 2 h, the adsorption of two different cationic dyes [methylene blue (MB) and Bismarck brown (BB)] is about 80% (79.2 for MB and 78.4% for BB, respectively), and the adsorption of the mixture of dyes, either MB and MO (methyl orange) (Figure 3.21e) or MB and BB (Figure 3.21d), is even faster, that is, 87% approximately for each case. There is a previous report on the behavior of higher adsorption rate for the anionic dyes from a mixture of dyes; however, these dyes are a mixture of both cationic and anionic dyes unlike in this study.^{37,38,44,97} The detailed analysis of the performance of the peptide-based

hydrogel compared with two previous results is presented in Table 3.1. This indicates clearly the superiority of this peptide-based gel compared to our previous results and others' previous results. Moreover, this gel shows selectivity toward the adsorption of cationic dyes over anionic dyes in a mixture of dyes. Therefore, it can be stated that this study not only exemplifies the faster kinetics of adsorption of toxic organic dyes but also exhibits selectivity of cationic dyes over anionic dyes.

Table 3.1. Comparison of our peptide gelator with different kinds of peptide and non-peptide based gelators in environmental remediation. Here abbreviation used for different dyes are MB (methylene blue), CR (congo red), BB (bismark brown), MO (methyl orange), AB1 (acid black 1), RB (rhodamine B), DR-80 (direct red 80), and MG (malachite green).

| Dyes | Peptide Gelator | Non-peptide gelator | Absorption (Within 2 h) | Total Absorption | Total time | References |
|---------|-----------------|---------------------|-------------------------|------------------|------------|-------------|
| MB | P1 | | 79.2% | 98.9% \pm 0.2 | 12 h | This report |
| | P2 | | | 98.4% | 7 days | 37 |
| | | P5 | | 98% | 72 h | 97 |
| CR | P1 | | 64% | 97.1% \pm 0.2 | 12 h | This report |
| | P3 | | 45% | 92% | 48 h | 38 |
| | P4 | | 42% | 98% | 48 h | 44 |
| BB | P1 | | 78.4% | 98.1% \pm 0.1 | 12 h | This report |
| MB + MO | P1 | | 92.7% | 98.6% \pm 0.3 | 12 h | This report |
| MB + BB | P1 | | MB:86.98% BB: 86.86% | 97.6% \pm 0.5 | 12 h | This report |
| AB1 | P4 | | 32% | 82% | 48 h | 44 |
| RB | P3 | | 38% | 78% | 48 h | 38 |
| | P4 | | 32% | 71% | 48 h | 44 |
| DR-80 | P4 | | 39% | 93% | 48 h | 44 |
| MG | P3 | | 60% | 90% | 48 h | 38 |



In this study, our tripeptide-based gelator has been designed in such a way that it is able to attract cationic dyes in the presence of anionic dyes selectively. This happens because of the interplay of electrostatic interactions involving two oppositely charged species, as, for example, anionic xerogel matrix and cationic dyes. Another specialty of this result is that this is probably the first example of a

peptide-based hydrogel that can selectively absorb cationic dyes from a mixture of cationic and anionic dyes. Most probably, this is the first report of a small molecule based trifunctional supramolecular gel that has been successfully utilized for environmental remediation. Our previous results show the bifunctionality of peptide-based gels in environmental remediation. The functionality of peptide-based gels needs to be improved to get a clean and safe environment. To achieve this goal, this study vividly shows the formation of a trifunctional gel to remove different organic (toxic dyes) and inorganic (Pb^{2+} and Cd^{2+}) pollutants as well as spilled oil from the environment.

This report describes the discovery of a peptide-based ambidextrous trifunctional new gelator that has been used to remove toxic organic dyes (cationic and zwitterionic dyes) from wastewater and toxic heavy metal ions (lead and cadmium) also from wastewater using xerogels and hydrogels, respectively. The organogels formed by this gelator have further been used in oil spill recovery. Another interesting feature is that this gelator is economically viable and reusable several times without significant loss of its activity.

3.2. Experimental Section

3.2.1. Materials

L-tryptophan (Trp), L-phenylalanine (Phe) and myristic acid (C_{14}) were purchased from Sigma-Aldrich. HOBt (1-Hydroxybenzotriazole) and DCC (N, N'-Dicyclohexylcarbodiimide) were purchased from SRL, India. Sodium dihydrogen phosphate, and disodium hydrogen phosphate were purchased from Merck. KHSO_4 , Na_2CO_3 , NaOH, MeOH, CHCl_3 silica gel (100–200 mesh), Et_2O , petroleum ether, ethyl acetate, and DMF were purchased from SRL (India).

3.2.2. Methods

Dye Adsorption Study. For each dye adsorption study, 5 mg of gelator molecule was taken into a 5 mL screw cap vial. Then, it was heated on a hot plate by adding 1 mL of phosphate buffer solution (PBS) having pH 7.46. After dissolving all the gelator molecules into the PBS, the vial was cooled for a few minutes (10 min) to room temperature to make the hydrogel P1. Then, the gel was frozen in liquid nitrogen and lyophilized. After that, a pellet of dried gel (xerogel) was made by using a pelletizer instrument. The pellet was taken into a 5 mL screw cap vial, and 1 mL of aqueous dye solutions was carefully added to

the vial. During the dye adsorption study, the concentrations of MB, BB, and CR were 3.0, 2.0, and 2.0 mg/L, respectively. After that, at a definite time interval, 15, 30, 60, 120, 180, 360, and 720 min, dye adsorption data were collected by using UV-vis spectroscopy.

Metal Ions Removal Study. Atomic absorption spectroscopy (AAS) was performed to determine the efficiency of the hydrogel for Cd^{2+} ion absorption. An amount of 100 μL of 50 mM cadmium chloride monohydrate ($\text{CdCl}_2 \cdot \text{H}_2\text{O}$) solution was added to 5 mL of ultrapure water to prepare a stock solution. From this stock solution, 1 mL of $\text{CdCl}_2 \cdot \text{H}_2\text{O}$ was taken and added to 1 mL of hydrogel in the phosphate buffer (pH 7.5). The concentration of the Cd^{2+} ions in the initial solution was determined through AAS using a standard calibration curve. After 8 h, a 30 μL aliquot was taken from the solution which is in contact with the gel and this solution was diluted to 10 mL by mixing with Milli-Q water (pH 6.7) in order to examine the amount of Cd^{2+} ions retained after the absorption by the hydrogel. An aliquot of 10 μL of 50 mM solution of lead nitrate $\text{Pb}(\text{NO}_3)_2$ was added to a 1 mL of Milli-Q water. Then, this diluted lead nitrate solution was added to 1 mL of hydrogel. After 8 h, a 10 μL aliquot was taken out and it was diluted with 10 mL of Milli-Q water. The Pb^{2+} ion adsorption capacity was measured by inductively coupled plasma atomic emission spectroscopy, as it is a good technique for the determination of concentration of metal ions in different solutions.

Oil Spill Recovery. Gelator amphiphile (P1) was first dissolved in a minimum volume of ethyl acetate (5% v/v) and was injected (100 μL of the stock solution was used for injection in each set) into 2 mL of a 1:1 salt water (water containing NaCl , Na_2SO_4)-oil mixture.

Recovery and Reusability of the Gelator. The recovery of the gelator, from the hydrogel- and xerogel-mixed heavy metal ions and dye molecules, was simply done by extracting it in ethyl acetate, using a separating funnel. For the xerogel-adsorbed dye molecules, simple extraction with ethyl acetate was sufficient, as the dyes preferred to remain in aqueous medium, whereas in the case of hydrogels containing adsorbed metal ions, 1 mL of hydrogel was treated with 20 μL of 1 (N) hydrochloric acid before extraction of the gelator peptide amphiphile in ethyl acetate.

Recovery of Oil. The gelled oil part was taken out from the vial with the help of a spatula. Then, the gelled oil was taken into a round bottom flask and distilled

by using a low vacuum rotary evaporator to get the oil part into the collector. The gelator compound remained in the round bottom flask, and it was further used for the recovery of another set of oil spill.

3.2.3. Synthesis of Gelator Peptide P1

Synthesis of C₁₄-Trp-COOMe [H₃C-(CH₂)₁₂-CONH-Trp-COOMe]. Myristic acid (2.28 g, 10 mM) was taken in a 250 mL round bottom flask and 10 mL (dimethyl formamide) DMF was added to dissolve it. After that the mixture was cooled in an ice-water bath having temperature 0 °C–10 °C. H-Trp-COOMe was isolated from the corresponding methyl ester hydrochloride (3.054 g, 12 mM) by neutralization, subsequent extraction with ethyl acetate and concentration to 50 mL. Then it was added to the reaction mixture, followed immediately by DCC (2.472 g, 12 mM) and HOBt (1.62 g, 12 mM). The reaction mixture was stirred for 36 h in nitrogen atmosphere. The reaction mixture was filtered through a sintered glass crucible and the DCU (dicyclohexylurea) was filtered off. The organic layer was washed with brine (2×50 mL) and then dried over anhydrous sodium sulphate and evaporated in vacuum to yield peptide as a white solid. Purification was done using a silica gel column (100–200 mesh) using chloroform and ethyl acetate as eluents. Yield: 3.89 g, (9.09 mM, 90.89 %).

¹H NMR (500 MHz, CDCl₃, TMS, 25 °C): δ 8.57 (1H, s, NH), 7.53 (1H, d, J= 8.0 Hz, aromatic), 7.34 (1H, d, J= 8.0 Hz, aromatic), 7.19 (1H, t, J= 7.5 Hz, aromatic), 7.11 (1H, t, J= 7.5 Hz, aromatic), 6.95 (1H, d, J= 7.6 Hz, aromatic), 6.06 (1H, d, J= 8.0 Hz, NH of amide), 4.99–4.96 (1H, m, α –CH of Trp), 3.68 (3H, s, –OCH₃), 3.33–3.31 (2H, m, β –CH₂ of Trp), 2.14 (2H, t, J= 7.5 Hz, α –CH₂ of myristyl), 1.58–1.55 (2H, m, β –CH₂ of myristyl), 1.33–1.24 (20H, m, 10 –CH₂ of myristyl chain), 0.9 (3H, t, J= 6.5 Hz, –CH₃ of myristyl) (Figure 3.1).

¹³C NMR (125 MHz, CDCl₃, TMS, 25 °C): δ 173.09, 172.66, 136.31, 127.82, 122.89, 122.23, 119.66, 118.57, 111.45, 110.00, 53.06, 52.35, 36.66, 32.00, 29.77, 29.73, 29.70, 29.55, 29.43, 29.41, 29.31, 27.77, 25.57, 22.76, 14.18 (Figure 3.2). HRMS (m/z): Calculated for C₂₆H₄₀N₂O₃: 428.30 (M) Found: 429.3571 (M + H)⁺, 452.3448 (M + Na)⁺ (Figure 3.3).

Synthesis of C₁₄-Trp-COOH [H₃C-(CH₂)₁₂-CONH-Trp-COOH]. C₁₄-Trp-COOMe (3.78 g, 8.83 mM) was taken in a 250 mL round bottom flask. The solid was dissolved in MeOH (40 mL) and 1N NaOH (15 mL) was added to the mixture. The reaction mixture was stirred for 12 h in nitrogen atmosphere and the progress of saponification was monitored by thin layer chromatography (TLC).

After 12 h methanol was removed under vacuum, the residue was taken in 50 mL of water, washed with diethyl ether (2×50 mL). Then the pH of the aqueous layer was adjusted to 2 using 1(N) HCl and it was extracted with ethyl acetate (3×50 mL). The extracts were dried over anhydrous sodium sulphate, and evaporated in vacuum to yield as a white solid product. Purification was done using a silica gel column (100–200 mesh) using chloroform and methanol as eluents. Yield: 3.43 g, (8.36 mM, 94.68 %).

^1H NMR (500 MHz, DMSO- d_6 , TMS, 25 °C): δ 12.53 (1H, br, -COOH), 10.80 (1H, s, NH), 8.01 (1H, d, J = 8.0 Hz, NH), 7.52 (1H, d, J = 8.0 Hz, aromatic), 7.32 (1H, d, J = 8.5 Hz, aromatic), 7.11 (1H, s, aromatic), 7.05 (1H, t, J = 7.5 Hz, aromatic), 6.97 (1H, t, J = 7.5 Hz, aromatic), 4.49–4.45 (1H, m, α -CH), 3.17–2.96 (2H, m, β -CH₂ of Trp), 2.05 (2H, t, J = 7.5 Hz, α -CH₂ of myristyl), 1.42–1.38 (2H, m, β -CH₂ of myristyl), 1.28–1.14 (20H, m, 10 -CH₂ of myristyl chain), 0.85 (3H, t, J = 6.5 Hz, -CH₃ of myristyl) (Figure 3.4). ^{13}C NMR (125 MHz, DMSO- d_6 , TMS, 25 °C): δ 173.52, 172.12, 136.04, 127.19, 123.40, 120.79, 118.22, 118.11, 111.27, 110.00, 52.78, 35.06, 31.25, 29.00, 28.98, 28.87, 28.76, 28.67, 28.51, 27.11, 25.11, 22.04, 13.88 (Figure 3.5). HRMS (m/z): Calculated for C₂₅H₃₈N₂O₃: 414.29 (M) Found: 415.315 (M + H)⁺, 437.2995 (M + Na)⁺ (Figure 3.6).

Synthesis of C₁₄-Trp-Phe-COOMe [H₃C-(CH₂)₁₂-CONH-Trp-CONH-Phe-COOMe]. C₁₄-Trp-COOH (8 mM, 3.32 g) was taken in a 250 mL round bottom flask and 10 mL DMF was added to dissolve it. After that the mixture was cooled in an ice-water bath having temperature 0 °C–10 °C. H-Phe-COOMe was isolated from the corresponding methyl ester hydrochloride (2.16 g, 10 mM) by neutralization, subsequent extraction with ethyl acetate and concentration to 50 mL. Then it was added to the reaction mixture, followed immediately by DCC (2.06 g, 10 mM) and HOBt (1.35 g, 10 mM). The reaction mixture was stirred for 48h in nitrogen atmosphere. The reaction mixture was filtered through sintered glass crucible and the DCU (dicyclohexylurea) was filtered off. The organic layer was washed with brine (2×50 mL) and then dried over anhydrous sodium sulphate and evaporated in vacuum to yield peptide as a white solid. Purification was done using a silica gel column (100–200 mesh) using chloroform and methanol as eluents. Yield: 3.78 g, (8.83 mM, 88.32 %).

^1H NMR (400 MHz, CDCl₃, TMS, 25 °C): δ 8.28 (1H, s, NH), 7.73 (1H, d, J = 8 Hz, aromatic), 7.38–7.06 (8H, m, aromatic), 6.86 (1H, d, J = 6.8 Hz, aromatic),

6.25 (1H, d, J= 7.6 Hz, NH), 6.18 (1H, d, J= 7.6 Hz, NH), 4.78–4.68 (2H, m, 2 α –CH), 3.65 (3H, s, –OCH₃), 3.36–3.08 (2H, m, 2 β –CH₂), 3.03–2.9 (2H, m, 2 β –CH₂), 2.17 (2H, t, J= 7.5 Hz, α –CH₂ of myristyl), 1.562 (2H, m, β –CH₂ of myristyl), 1.36–1.26 (20H, m, 10 –CH₂ of myristyl chain), 0.91 (3H, t, J= 6.8 Hz, –CH₃ of myristyl) (Figure 3.7). ¹³C NMR (100MHz, CDCl₃, TMS, 25 °C): δ 173.21, 171.4, 171.12, 136.38, 135.7, 129.38, 129.22, 128.77, 128.71, 127.14, 123.55, 122.38, 119.94, 119.01, 111.37, 110.72, 53.72, 53.52, 53.52, 51.96, 38.00, 37.94, 36.78, 32.03, 29.80, 29.77, 29.75, 29.58, 29.46, 29.45, 29.34, 28.37, 26.07, 25.64, 25.64, 22.80, 14.22 (Figure 3.8). HRMS (m/z): Calculated for C₃₄H₄₇N₃O₄: 575.37 (M) Found: 576.5914 (M + H)⁺, 598.5812 (M + Na)⁺, 1174.2277 (2M + Na)⁺ (Figure 3.9).

Synthesis of C₁₄-Trp-Phe-COOH (P1) [H₃C-(CH₂)₁₂-CONH-Trp-CONH-Phe-COOH]. C₁₄-Trp-Phe-COOMe (3.78 g, 8.83 mM) was taken in a 250 mL round bottom flask. The solid was dissolved in MeOH (60 mL) and 1(N) NaOH (25 mL) was added to the mixture. The reaction mixture was stirred for 12 h in nitrogen atmosphere and the progress of reaction was monitored by thin layer chromatography (TLC). After 12 h methanol was removed under vacuum, the residue was taken in 50 mL of water. Then the pH of the aqueous layer was adjusted to 2 using 1(N) HCl and it was extracted with ethyl acetate (3×50 mL). The extracts were dried over anhydrous sodium sulphate, and evaporated in vacuum to yield as a white solid sample. Purification was done by silica gel column (100–200 mesh) using chloroform and methanol as eluents. Yield: 3.52 g, (93.12 %)

¹H NMR (400 MHz, DMSO-d₆, TMS, 25 °C): δ 12.79 (1H, br, –COOH), 10.77 (1H, s, –NH of indole), 8.15 (1H, d, J= 7.6Hz, NH), 7.85 (1H, d, J= 8.4Hz, NH), 7.58(1H, d, J= 7.6Hz, aromatic, ortho –CH of indole –NH), 7.32–6.94 (9H, m, aromatic), 4.6–4.54(1H, m, α –CH), 4.49–4.43 (1H, m, α –CH), 3.10–3.05 (2H, m, β –CH₂), 2.97–2.82 (2H, m, β –CH₂), 2.01–1.97 (2H, m, α –CH₂ of myristyl), 1.37–1.28 (22H, m, 11–CH₂ of myristyl chain), 0.86 (3H, t, J= 6.6 Hz, –CH₃ of myristyl) (Figure 3.10). ¹³C NMR (100MHz, DMSO-d₆, TMS, 25 °C): δ 172.63, 171.93, 171.68, 137.36, 135.98, 129.2, 129.09, 128.08, 127.32, 126.34, 123.39, 120.68, 118.33, 118.03, 111.14, 110.18, 53.32, 52.91, 36.64, 35.21, 31.23, 28.97, 28.81, 28.74, 28.64, 28.47, 27.53, 25.05, 22.03, 13.88 (Figure 3.11). HRMS (m/z): Calculated for C₃₄H₄₇N₃O₄: 561.36 (M) Found: 584.71 (M + Na)⁺ (Figure 3.12).

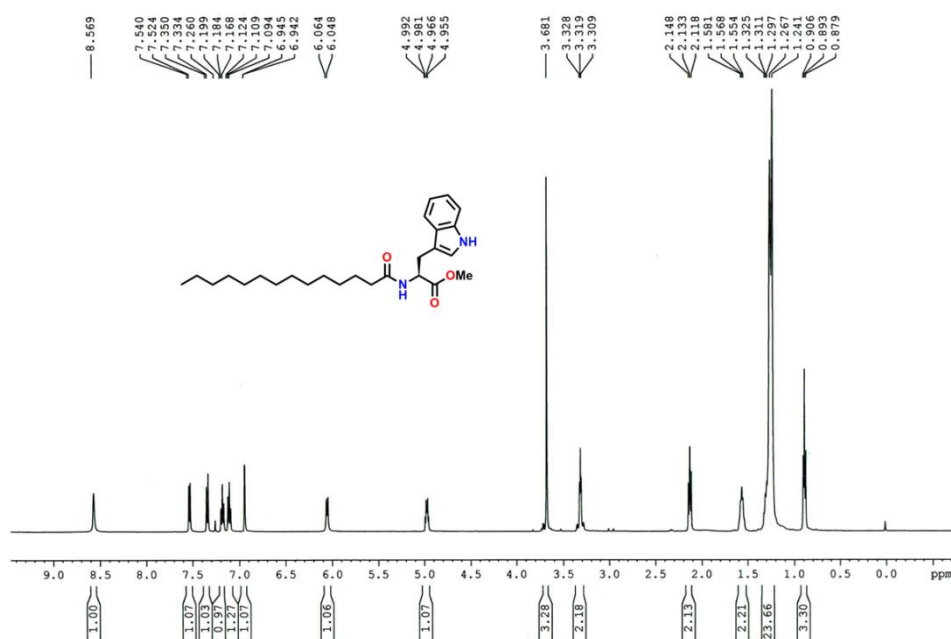


Figure 3.1. ^1H -NMR spectrum of C_{14} -Trp-OMe in CHCl_3 .

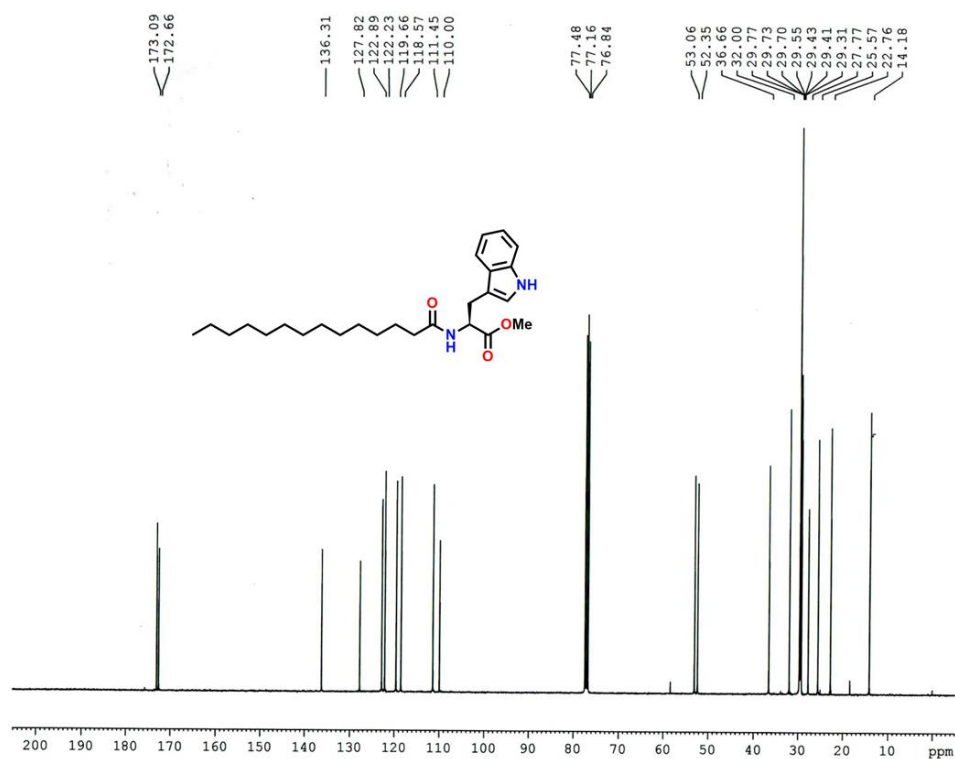


Figure 3.2. ^{13}C -NMR spectrum of C_{14} -Trp-OMe in CHCl_3 .

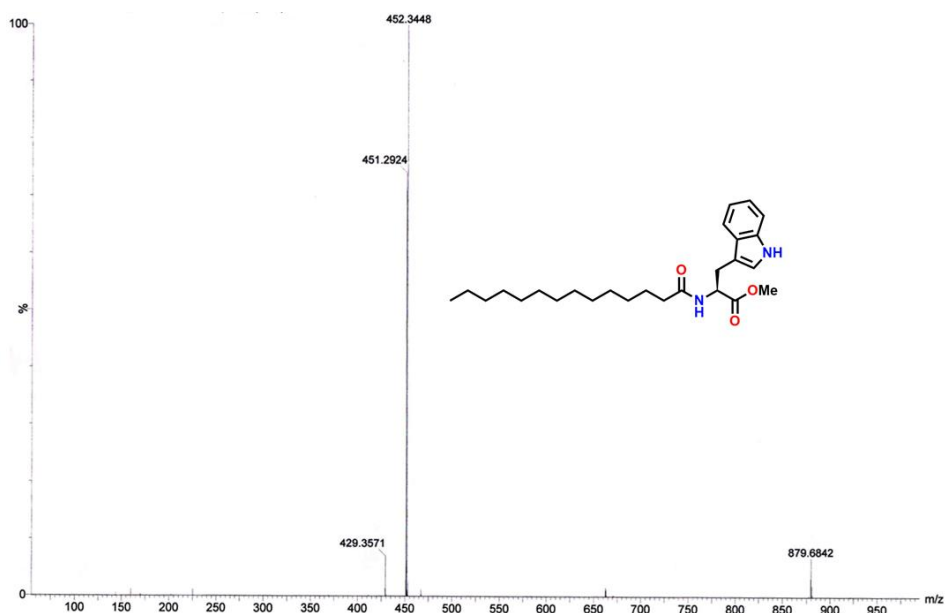


Figure 3.3. HR-MS spectrum of C_{14} -Trp-OMe.

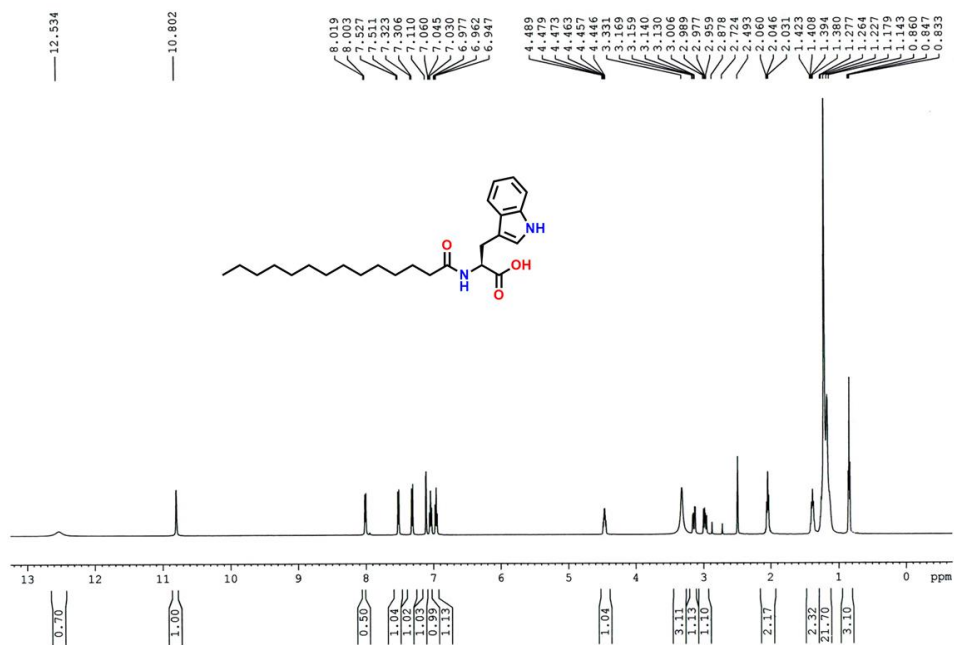


Figure 3.4. 1H -NMR spectrum of C_{14} -Trp-OH in $DMSO-d_6$.

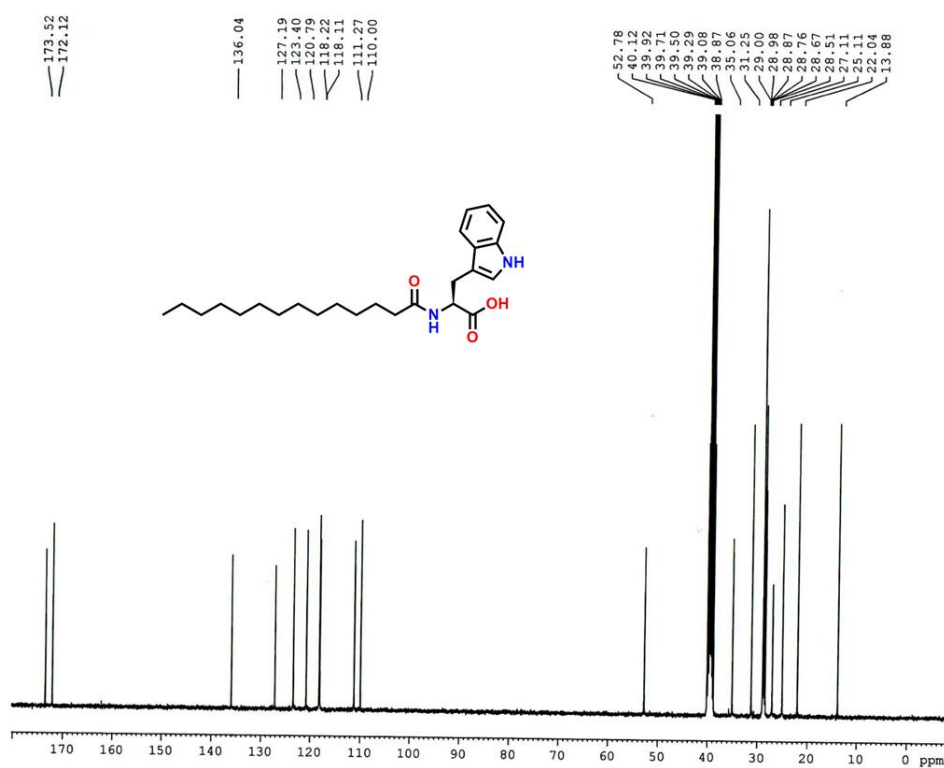


Figure 3.5. ^{13}C -NMR spectrum of C_{14} -Trp-OH in $\text{DMSO}-d_6$.

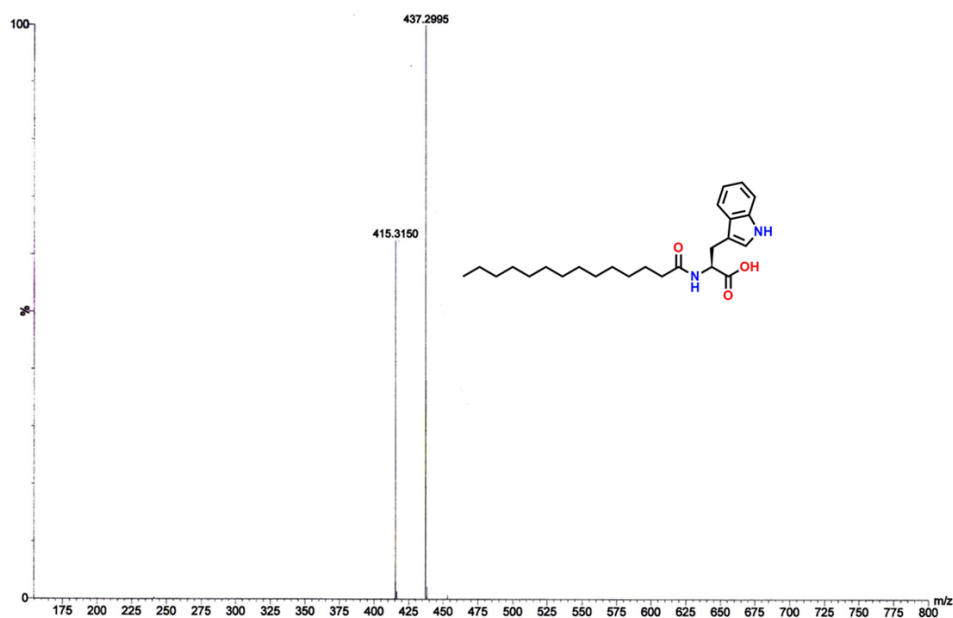


Figure 3.6. HR-MS spectrum of C_{14} -Trp-OH.

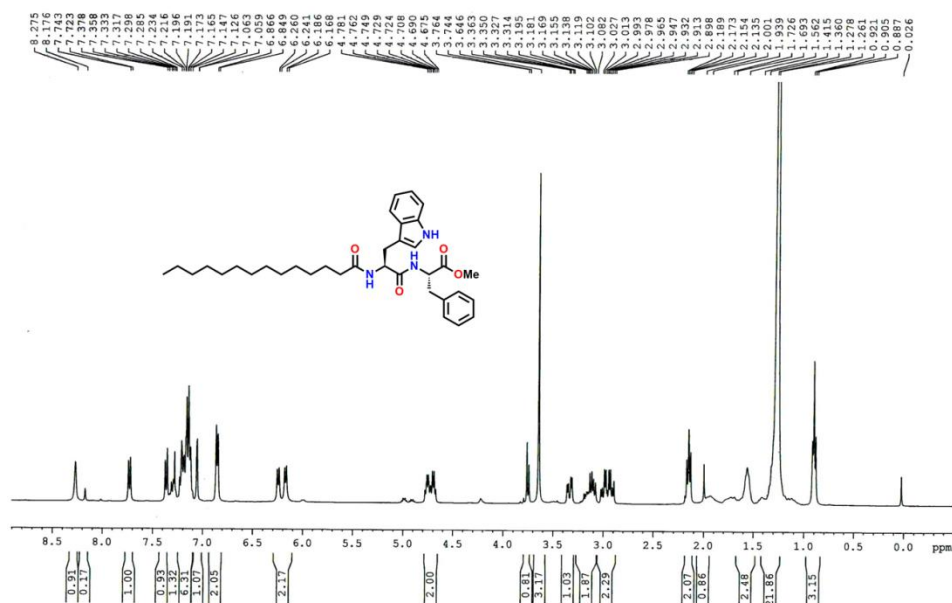


Figure 3.7. ^1H -NMR spectrum of C_{14} -Trp-Phe-OMe in CHCl_3 .

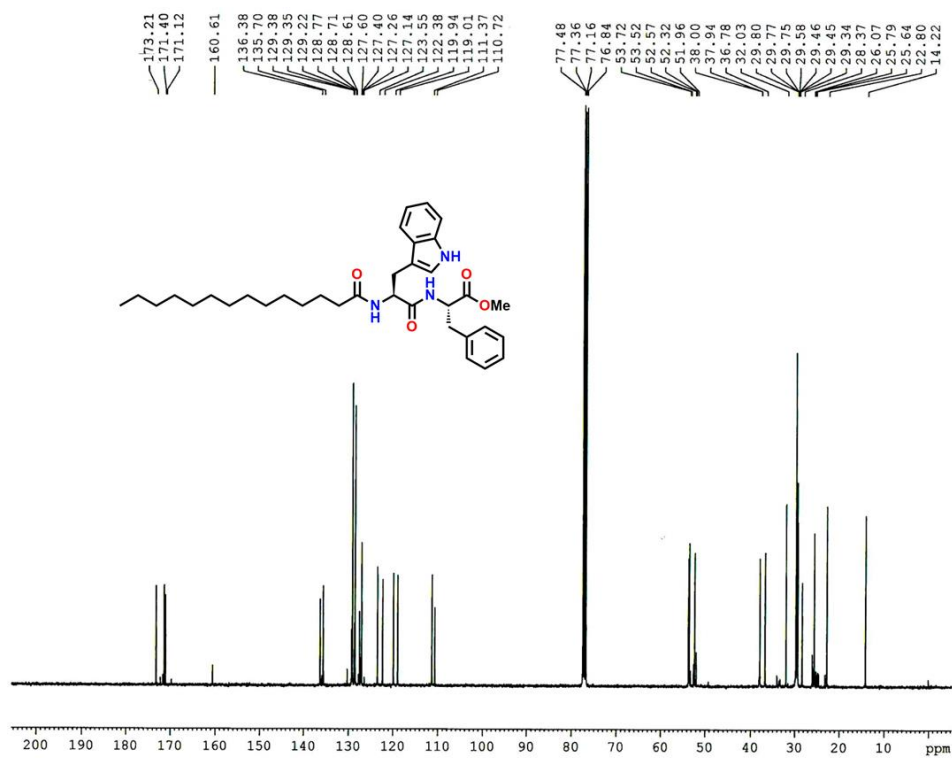


Figure 3.8. ^{13}C -NMR spectrum of C_{14} -Trp-Phe-OMe in CHCl_3 .

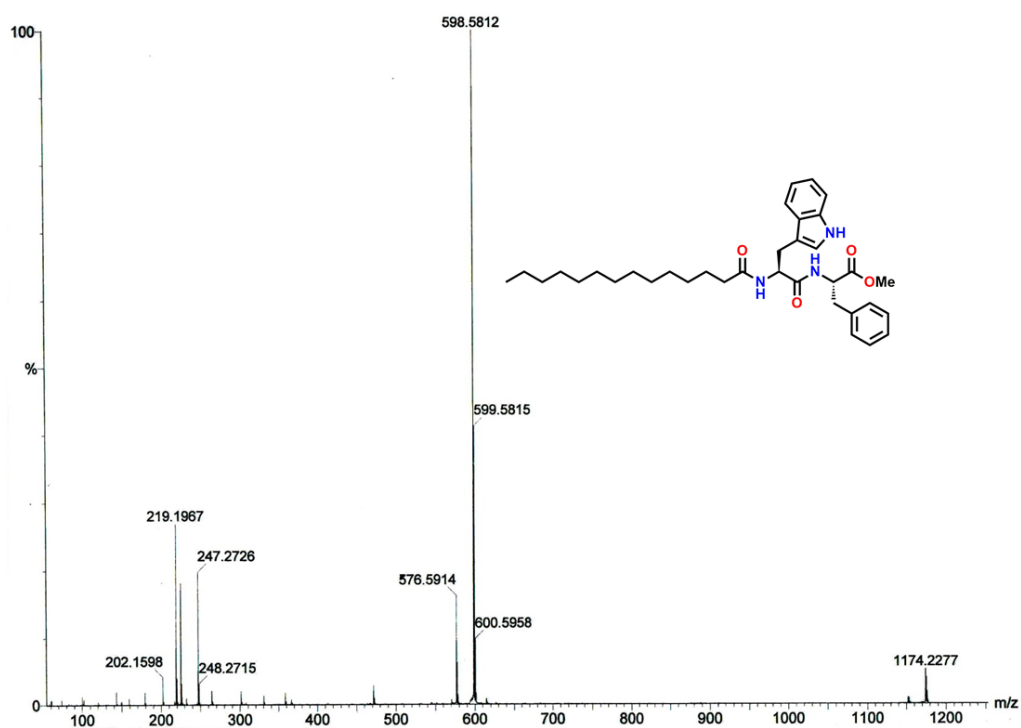


Figure 3.9. HR-MS spectrum of C_{14} -Trp-Phe-OMe.

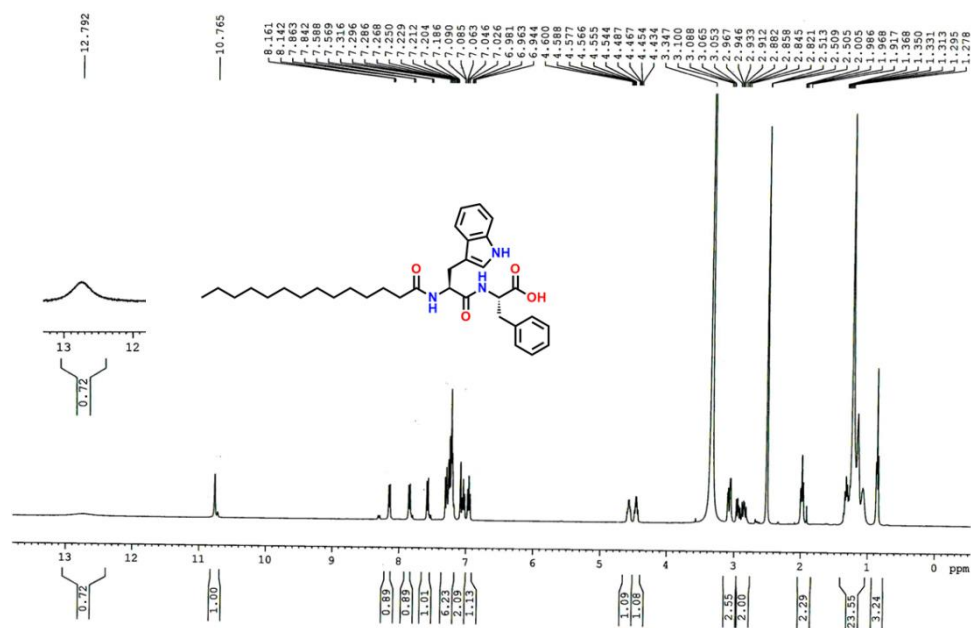


Figure 3.10. 1H -NMR spectrum of C_{14} -Trp-Phe-OH in $DMSO-d_6$.

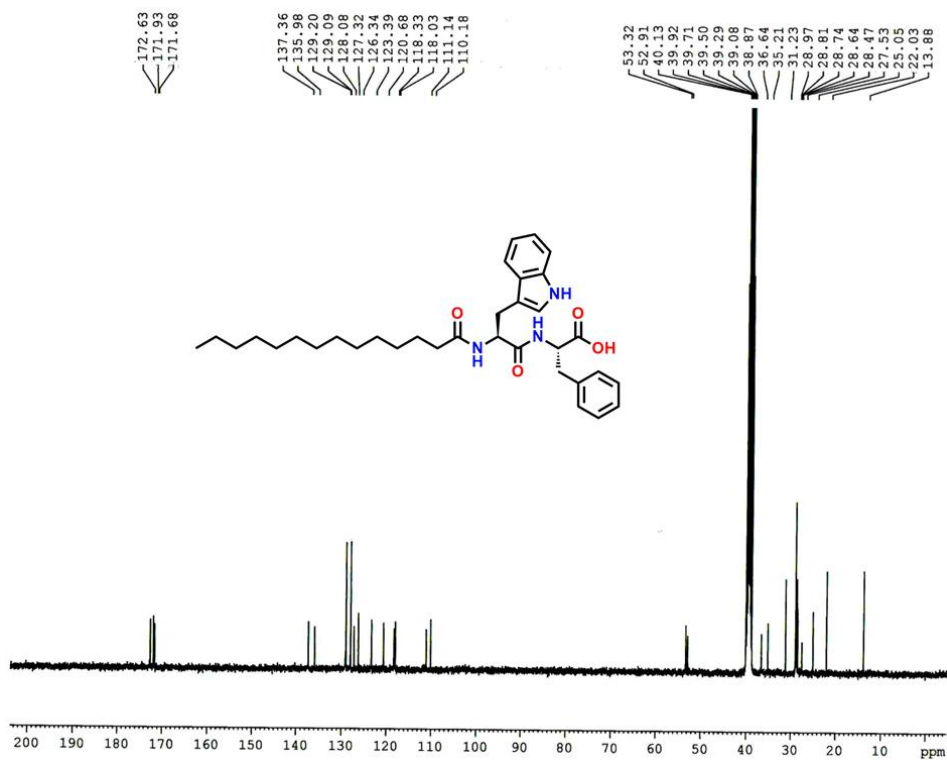


Figure 3.11. ^{13}C -NMR spectrum of C_{14} -Trp-Phe-OH in $\text{DMSO}-d_6$.

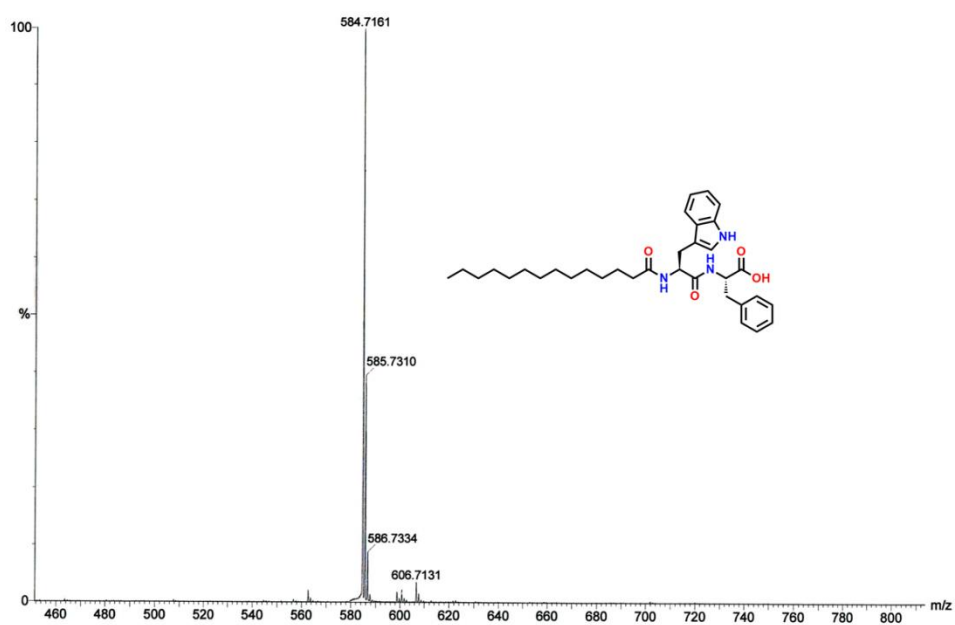


Figure 3.12. HR-MS spectrum of C_{14} -Trp-Phe-OH.

3.2.4. Instrumentation

NMR Experiments. All NMR studies were carried out on Bruker DPX 400 MHz and Bruker DPX 500 MHz spectrometers at 300 K. Compounds concentrations were in the range 1–10 mM in CDCl₃ or DMSO-d₆.

Mass Spectrometry. Mass spectra were recorded on a Q-ToF microTM (Waters Corporation) mass spectrometer using positive mode electrospray ionization.

FT-IR Spectroscopy. FTIR spectroscopy was performed using Nicolet 380 FT-IR spectrophotometer (Thermo Scientific). FTIR spectra were recorded using a cell with CaF₂ windows.

Transmission Electron Microscopy (TEM). TEM images were recorded on a JEM 2010 electron microscope at an accelerating voltage of 200 KV. During HR-TEM experiment, 20 µL of gel (concentration of gelator is 8.91 mM) was taken in a screw cap vial and diluted with 2 ml milli-Q water. Then, a drop of dilute solution was placed on carbon coated copper grids (300 mesh) and dried by slow evaporation. The grid was then allowed to dry in a vacuum for two days and then images were taken.

Small Angle X-Ray Scattering (SAXS). SAXS measurements on xerogels were performed using a Bruker Nanostar instrument using CuK α radiation and a Vantec 2000 detector. The sample-to-detector distance was 1.07 m. The $q = 4\pi\sin\theta/\lambda$ (scattering angle 2θ) scale was calibrated using silver behenate. Samples were mounted in quartz capillaries. In situ SAXS measurements on hydrogels were performed on beamline B21 at Diamond Light Source (Harwell, UK). Data was collected using a Dectris EIGER 4M detector at a fixed camera length of 3.9 m with a wavelength $\lambda = 1$ Å. Gels were mounted in a custom-designed enclosed gel cell holder⁹⁸ for gels and pastes. All measurements were performed at 20 °C.

Powder X-ray Diffraction. X-ray diffraction measurements on the xerogel were carried out by placing the sample on a glass plate. Experiments were carried out by using an X-ray diffractometer (Bruker D8 Advance) with a parallel beam optics attachment. The instrument was operated at 35 kV voltage and 30 mA current using Ni-filtered CuK α radiation and the instrument was calibrated with a standard silicon sample before use. Samples were scanned from 2° to 30° (2θ) in the step scan mode (step size 0.03°, preset time 2s) and diffraction patterns were recorded using a scintillation scan detector.

Atomic Absorption Spectroscopy (AAS). Atomic absorption spectroscopic measurements were carried out using a Shimadzu AA-6300AAS spectrometer fitted with a double beam monochromator. A Metrohm 861 Advanced Concept IC ion chromatograph was used for the determination of the concentrations of Cd^{2+} ions in expelled solution and in shrinkage gel.

Inductively Coupled Plasma Mass Spectrometry (ICP-OES). The quantitative chemical analyses of initial and final concentration of lead ions in solutions were carried out using a Perkin-Elmer Optima 2100 DV ICP-OES instrument.

UV/Vis Spectroscopy. UV/Vis absorption spectra were recorded on a UV/Vis spectrophotometer (Varian Cary 50.bio).

Rheological Study. Rheology experiments were performed in SDT Q Series Advanced Rheometer AR 2000.

3.3. Result and Discussion

3.3.1. Gelation Study. A peptide amphiphile (Figure 3.13) consisting of two aromatic amino acid residues (L-tryptophan and L-phenylalanine), a terminally placed polar head group ($-\text{COOH}$) and a long fatty acyl chain as a hydrophobic tail was designed. Specifically, aromatic amino acid residues were selected to promote π - π interactions, amide functionalities for hydrogen bonding interactions, hydrophobic long chain for van der Waals interactions and the terminally located carboxylic acid ($-\text{COOH}$) head group was chosen to increase the polarity of the peptide molecule. Moreover, the amphiphile was designed in such a way that it can easily form a hydrogel as well as organogels by using polar aqueous and nonpolar organic media respectively. To investigate the gelation behavior, 5 mg of the gelator was placed in a 5 mL screw capped glass vial with the addition of 1 mL of different types of solvent including water (phosphate buffer solution of pH 7.46). The glass vial was heated on a hot plate until the solute is dissolved into that particular solvent. After that, the glass vial was kept at room temperature (27°C) for a few minutes (depending upon the solvent) to form a stable gel (Figure 3.13). The compound was insoluble in *n*-hexane but soluble in ethyl acetate, an antisolvent-induced gelation study was performed to investigate the gelation behavior of peptide amphiphile. Only 5% ethyl acetate

(v/v) was used with respect to *n*-hexane to have rapid (approx. 30 s) gelation (Table 3.2).

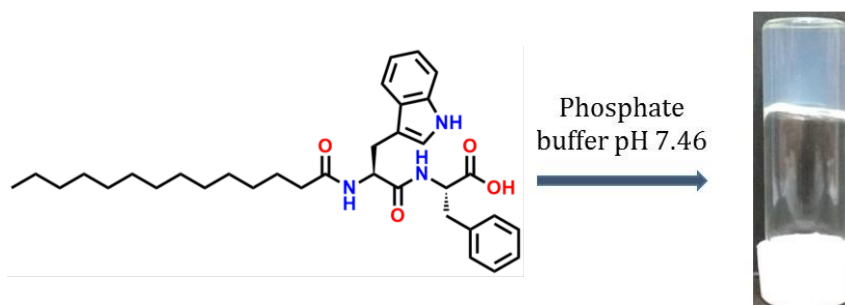


Figure 3.13. Structure of the peptide amphiphile that forms hydrogel at phosphate buffer solution of pH 7.46.

Table 3.2. Gelation behaviour of **P1**. G stands for gel, S stands for solution and M.G.C. means minimum gelation concentration.

| Solvent | Gelation activities |
|---|----------------------|
| Phosphate buffer solution (pH 7.46) | G (M.G.C. 0.25% w/v) |
| Petroleum ether (with 5% v/v ethyl acetate) | G (M.G.C. 0.45% w/v) |
| Diesel (with 5%v/v ethyl acetate) | G (M.G.C. 0.42% w/v) |
| Kerosene (with 5%v/v ethyl acetate) | G (M.G.C. 0.4% w/v) |
| Petrol (with 5% v/v ethyl acetate) | G (M.G.C. 0.4% w/v) |
| Dimethyl sulfoxide | S |
| Ethyl acetate | S |

3.3.2. Morphological Study. High resolution transmission electron microscopy (HR-TEM) imaging was performed in order to explore the morphological features of the peptide-based hydrogel. It is observed that the gelator molecule assembles to form a cross-linked nanofiber network structure in the gel state. These fibers are several micrometer (μm) in length, with width varying from 31.7 nm to 64.0 nm (Figure 3.14b). Whereas the organogel formed by using 5% ethyl acetate in *n*-hexane solution also shows a cross linked network structure in gel state. The width of the organogel was found 38.16 nm to 54.21 nm (Figure 3.14d). To understand the morphological change in hydrogel, HR-TEM images were taken at different pHs of 6.9, 7.46 and 8.5 respectively. Interestingly, at all these three pHs, only nanofibrous microstructure was observed (Figure 3.14a,b,c).

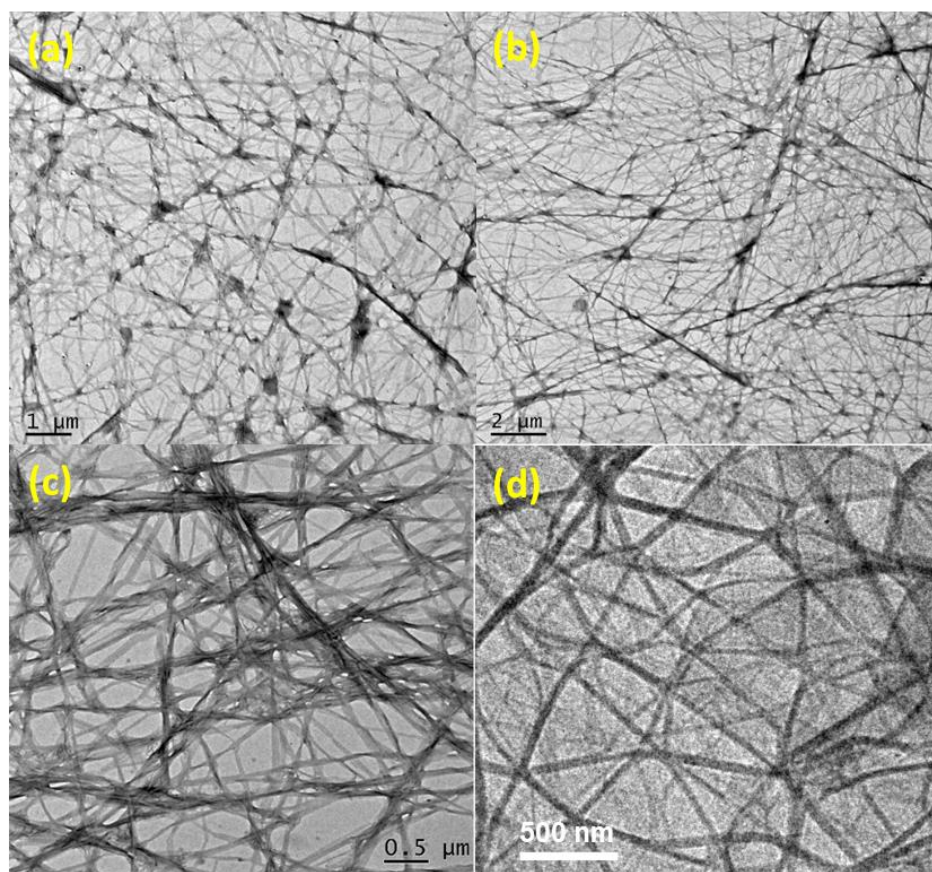


Figure 3.14. High Resolution Transmission Electron Microscopic (HR-TEM) images of hydrogel at pH (a) 6.90, (b) 7.46, (c) 8.5, and (d) organogel in *n*-hexane.

3.3.3. FTIR Analysis. Fourier-transform infrared spectroscopy (FTIR) experiments were conducted to provide structural insight on the packing of gelator molecule **P1** in dried gels (organogel or hydrogel) in their respective solvents. Figure 3.15 indicates that the dried gel obtained from the organogel and also from hydrogel show sharp signals at around 3320 cm^{-1} , 1646 cm^{-1} and 1547 cm^{-1}

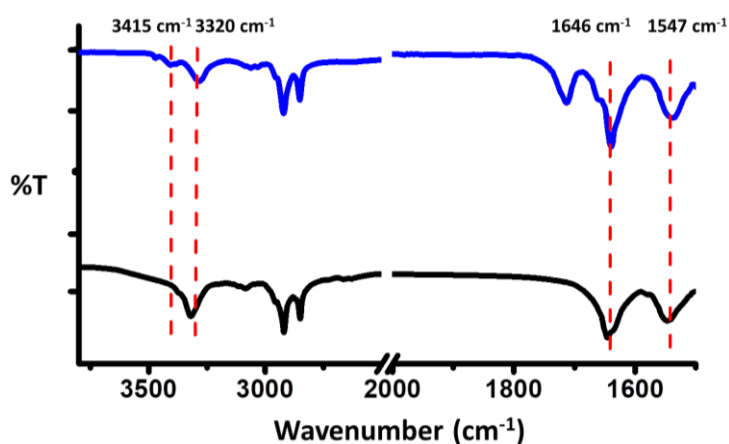


Figure 3.15. FTIR pattern for xerogel obtained from hydrogel (blue) and organogel (black) in *n*-hexane solvent.

cm^{-1} respectively. The strong signal at around 1646 cm^{-1} is due to the stretching of the amide C=O group of the aggregated gelator molecules. Two other peaks at 3320 cm^{-1} and 1547 cm^{-1} correspond to hydrogen-bonded N–H stretching and N–H bending frequencies respectively. The peak at around 3415 cm^{-1} for hydrogel indicates the non-hydrogen bonded stretching frequency of the N–H bond which is found to be very weak in intensity for the organogel. This observation indicates that unlike the hydrogel, almost all the N–Hs form hydrogen bonds inside the organogel (Figure 3.15).

3.3.4. Rheological Study. Rheological experiments were carried out at a constant gelator concentration 0.5 (w/v) (8.91 mM) to examine the viscoelastic characteristics of the gels obtained from the self-assembling peptide **P1** in aqueous medium (pH 7.46) as well as in organic solvent, n-hexane. All frequency sweep experiments were performed under a constant strain of 0.05% and it is observed that storage modulus (G') is almost independent of angular frequency within the tested frequency range and storage modulus (G') is always greater than loss modulus (G''), which indicates the characteristic feature of a gel phase material (Figure 3.16). At an angular frequency 10.5 rad/s, the storage modulus of the hydrogel is 920 Pa, whereas at the same angular frequency loss modulus is 305 Pa, i.e. the high storage modulus (G') value signifies the gel state of our materials (Figure 3.16a). Interestingly, the stiffness of the organogel obtained from the same gelator is much more than the hydrogel. Making comparison at a fixed frequency 10.5 rad/s, G' increases from 920 Pa for the hydrogel to 13494 Pa for the organogel in n-hexane (Figure 3.16b), a near 15-fold increase. These results show that the mechanical strength of the gel is enhanced significantly by the change of the solvent medium from water to an organic solvent (n-hexane). The change in solvent triggers a very significant increase of the gel storage modulus. The amplitude sweep experiments were done to determine the limits of linear viscoelastic region (LVE) of both gels. The hydrogel shows tolerance limit between 0.01% and 1.18% of shear strain (Figure 3.17a). Moreover, it was found that it showed a cross-over of storage modulus (G') and loss modulus (G'') when 6% shear strain was applied to the sample. Whereas, the tolerance limit of the organogel sample lies between 0.01% to 0.56% (Figure 3.17b) and the cross-over between G' and G'' took place, when 20% of shear strain was exerted on the sample. To confirm the thixotropic behavior of the hydrogel, time dependent step strain experiment was carried out with a time step 125s (Figure 3.17c,d). Initially

strain was increased from 0.05% to 30% at which the rupture of gel phase takes place, i.e. gel to sol conversion occurs. After that, when strain was reduced to 0.05%, reformation of gels were observed and this process was continued for 5 times to show the reproducibility of both gels (Figure 3.17c,d). It was observed from the FT-IR studies that both non-hydrogen and hydrogen bonded N–H stretching frequencies are present in the case of hydrogel, while in case of organogel almost all N–Hs of the gelator molecule are hydrogen bonded. The presence of extra H-bonding in the organogel can be attributed to greater stiffness of this gel which is reflected into this rheology data.

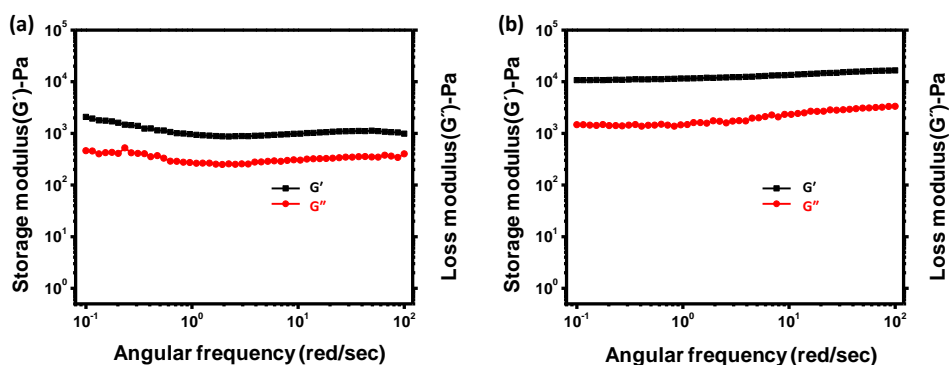


Figure 3.16. Frequency sweep analysis of (a) hydrogel and (b) organogel in *n*-hexane at a constant strain of 0.05%.

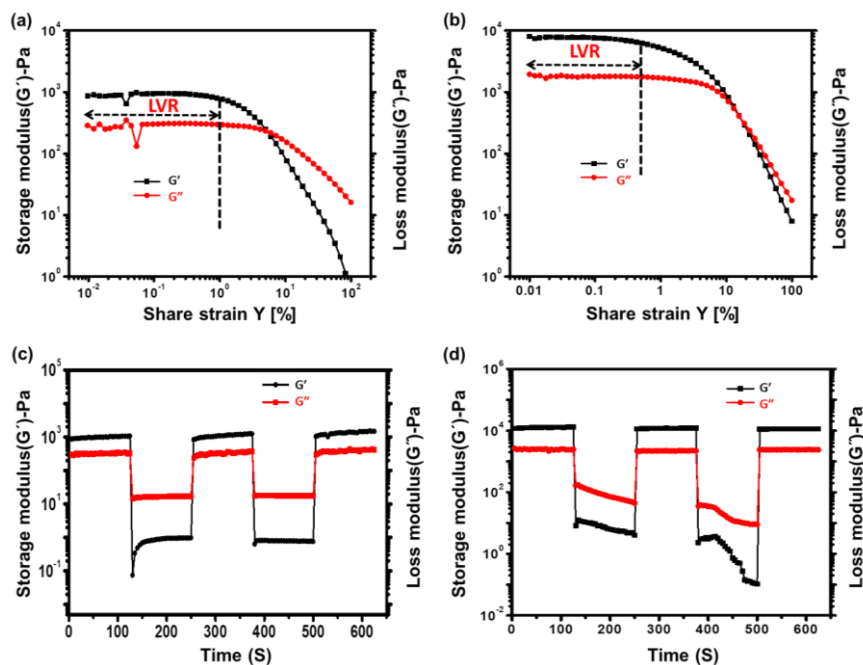


Figure 3.17. Amplitude sweep rheology data for (a) hydrogel and (b) organogel; step strain experiment for (c) hydrogel and (d) organogel with 125 s step length, showing thixotropic behaviour of both the gels.

3.3.5. XRD Analysis. The wide angle X-ray diffraction (XRD) data from xerogels obtained from the hydrogel, a peak at $2\theta = 18.45^\circ$ corresponds to a d -spacing value 4.68 \AA indicating the inter-planar distance between two β -strand. Peaks at $2\theta = 22.80^\circ$ and $2\theta = 23.58^\circ$ with d -spacing values 3.79 \AA and 3.67 \AA are due to π - π stacking, consistent with the presence of aromatic groups into the gelator molecule (Figure 3.18b).³⁷ In the small-angle XRD profile, the peak at $2\theta = 2.61^\circ$ ($d=33.57 \text{ \AA}$) arises from the gelator molecule in the gel state (Figure 3.18a). In the case of xerogel obtained from the organogel (in n -hexane), the peaks (Figure 3.18d) at $2\theta = 8.92^\circ$ ($d=9.64 \text{ \AA}$) and $2\theta = 18.61^\circ$ ($d = 4.64 \text{ \AA}$) are due respectively to the inter-sheet distance and the inter-planar distance between two β -strands of the aggregated peptide amphiphile **P1**. The peak at $2\theta = 21.99^\circ$ with d -spacing 3.90 \AA is due to aromatic stacking interactions between two gelator molecules (Figure 3.18d). In the small angle region, a peak at $2\theta = 3.14^\circ$ with d -spacing 28.09 \AA is also due to the intermolecular spacing in the gel (Figure 3.18c).

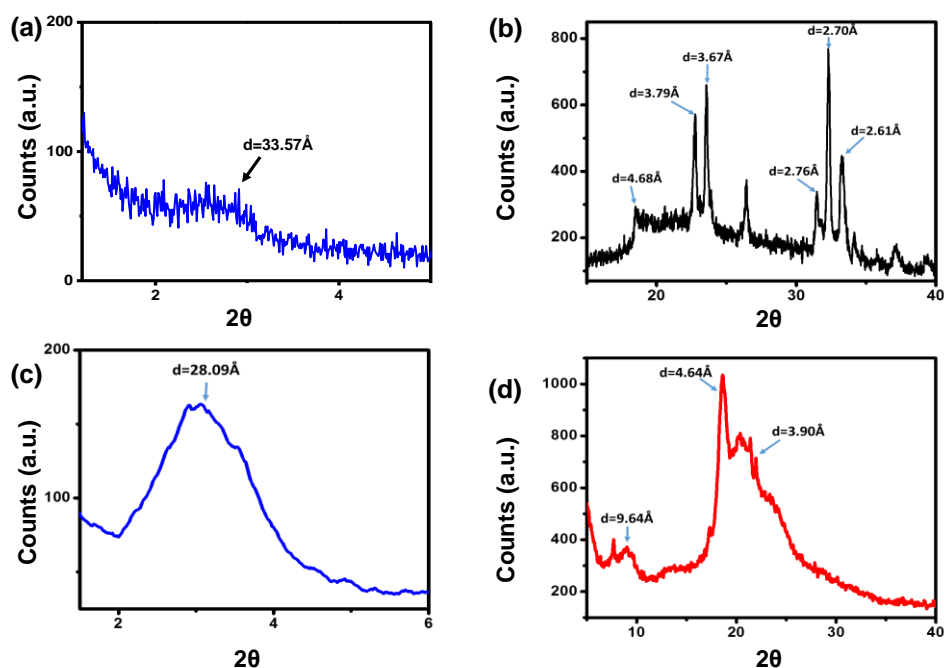


Figure 3.18. (a) Small-angle and (b) wide-angle X-ray diffraction pattern of xerogel obtained from hydrogel, (c) small-angle and (d) wide-angle X-ray diffraction pattern of xerogel obtained from organogel in n -hexane.

3.3.6. SAXS Analysis. To complement the small-angle XRD data obtained from xerogels, in situ SAXS measurements were performed on hydrogels. The intensity profile shown in Figure 3.19 for the **P1** hydrogel contains a broad Bragg peak with a d -spacing of 40 Å, which is longer than the length of a single molecule and also does not match with double the molecular length. Thus, this distance indicates end-to-end packing of peptide gelator molecules arranged in an interdigitated manner as shown in Figure 3.20. A tentative packing arrangement of the gelator molecules in the gel state is proposed based on Fourier-transform infrared spectroscopy (FTIR), small and wide angle powder X-ray diffraction (PXRD) and small angle X-ray scattering (SAXS) data (Figure 3.20).

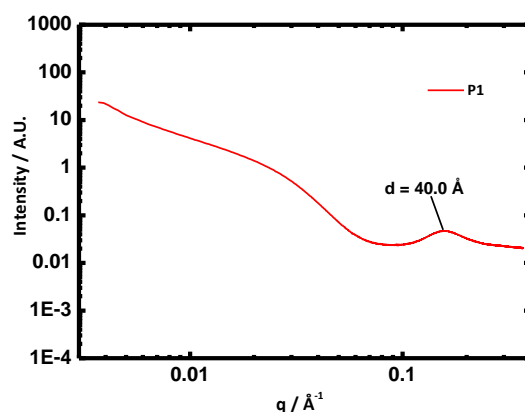


Figure 3.19. Small angle X-ray scattering (SAXS) data of hydrogel (**P1**).

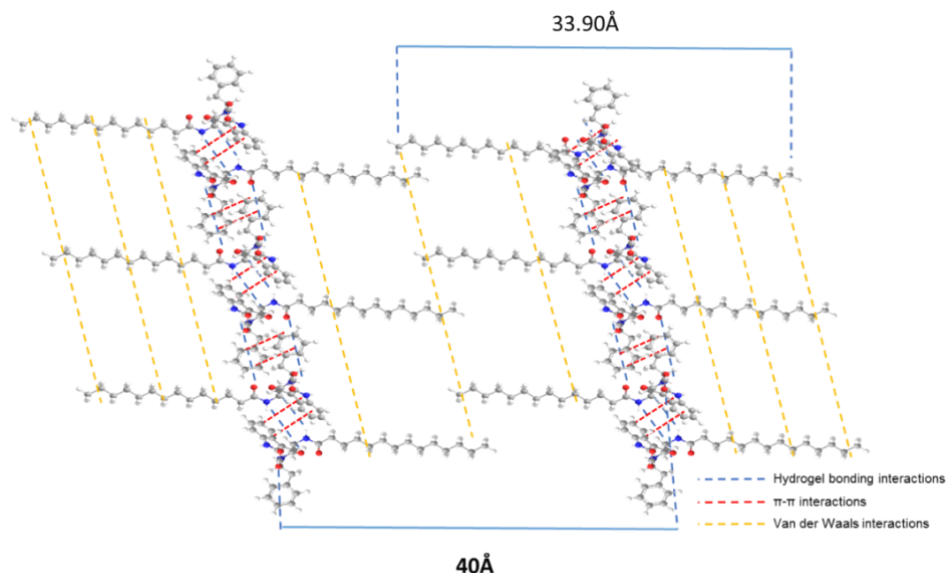


Figure 3.20. A tentative model of inter-molecular arrangements in the hydrogel derived from small angle X-ray scattering (SAXS), X-ray diffraction and FTIR data.

3.3.7. Dye Adsorption Study. Removal of toxic organic dyes from waste-water is a long-standing problem, as these dyes not only contaminate river and other water resources, but also endanger aquatic biota. So, it is important to explore new efficient methods for removal of these environmentally hazardous substances from waste-water.

Porous gels are potentially useful materials for removing toxic organic dyes from contaminated water. The hydrogel obtained from the peptide gelator **P1** has been used for removing cationic and neutral dyes effectively. Dyes like methylene blue (MB), bismarck brown (BB) and congo red (CR) are regularly used in textile industry. The hydrogel of **P1** is prepared in phosphate buffer solution of pH 7.46 and it was dried to get the xerogel. Adsorption studies were done by using the dried gel to nullify the effects of diffusion of dye from the solution to trapped water in the hydrogel network. Methylene blue and bismarck brown being cationic dyes, were adsorbed in the anionic xerogel network very fast. 90.3% of MB and 86.4% of BB of the dye solution were adsorbed in only three hours. It is found that the xerogel adsorb each of these dyes MB and BB separately more than 85% within only three hours and this result is better than the previous report.^{38, 44} Whereas, the neutral dye used in the experiment, congo red shows an adsorption of 65% in three hours. Almost complete adsorption of MB (98.9%) and BB (98.1%) has been observed within 24 hours. On the other hand, 97.1% adsorption of congo red has been observed within 48h (Table 3.3). Adsorption kinetics was studied with a mixture of dyes MB and BB. The dye adsorption kinetics of each dye is similar as it is evident from the experimental studies (Figure 3.21).

Our result shows the reusability of dried gel for several times (three times) without any significance loss of efficiency (Figure 3.25a). Moreover, this peptide based dried gel (xerogel) has been used for adsorption of more than one dyes (methylene blue and bismarck brown) from a mixture of dyes indicating its probable use in real life system for the waste water treatment, where more than one dyes are found in the contaminated water (Figure 3.22). It is found that the cationic dyes (methylene blue and basic brown) are strongly adsorbed compare to neutral dye (congo red), as it is evident from the Table 3.1 that per g of gelator molecules is able to adsorb 629 mg of methylene blue and 406 mg of bismarck brown, whereas same amount of gelator molecule is able to absorb 165 mg of

congo red. Dye adsorption kinetics was done by taking MB and BB separately and also the kinetics was done by taking their mixture (Figure 3.21a,b,d). To understand the mechanism of the adsorption of dyes on the xerogel matrix, dye solutions of different concentrations were charged on the absorbent xerogel and equilibrate for 12 hours. Both congo red and methylene blue showed good fitting in the Freundlich isotherm model which signifies the adsorption happened in multilayer mechanism (Figure 3.23a,b). Several anionic dyes have been used for adsorption by using self-assembled peptide based gels, none of these dyes were adsorbed by the xerogel indicating its selectiveness to adsorbing dyes towards basic (cationic) and neutral (non-ionic) dyes (Figure 3.21e). This can happen due to the fact that our peptide gelator is anionic at pH 7.46 at which it forms gel and all these adsorption studies were performed at this pH. Due to the electrostatic interaction between the gelator molecules and cationic dyes, the cationic dyes are adsorbed more and the non-ionic dyes are adsorbed to a lesser extent compared to the cationic dyes. However, the charge-charge repulsion between the gelator molecule and anionic dyes prevents the peptide gel (in this study) to adsorb any kind of anionic dyes. Reusability experiments were carried out in order to depict its large scale utility. The dye absorbed xerogels were recovered by using ethyl acetate-water interface, where the dye remained in water and the gelator **P1** was extracted from ethyl acetate. For the next cycle, hydrogels were reformed using those gelator **P1** molecules and it was freeze-dried before next set of absorption experiment. Table 3.5 clearly demonstrates the detailed reusability study including the percentage of loss of compound as well as the loss of activity for the removal of toxic dyes, metal ions and oil spill recovery in waste water treatment. From the Table, it can be clearly noted that **P1** can be recovered three times for reusing purpose without significant loss of its activity (Figure 3.25). This is because, after the third time, the amount of recovered gelator is not enough to form gel. However, the recycling can be done for another two times for the metal ion adsorption (Figure 3.25). After, the metal ion adsorption, no physical change is observed in the hydrogel. The recovery of gelators is done according to the previously mentioned procedure in the dye absorption section (Figure 3.25). In the case of reusability study for the oil spill recovery, oils were recovered from the organogel by vacuum distillation and gelator molecules were separated from the gel phase. During this study no physical change was observed in the organogel. The recovered gelator molecules were used for re-gelling of the

spilled oil. Finally, it was observed that the gelator amphiphile can be used three times (Figure 3.27) for the recovery of different sets of oil spill without any significant loss of the activity.

As we know, Freundlich adsorption isotherm model is expressed as-

$$\log q_e = \log K_f + \frac{1}{n} \log C_e \quad (a)$$

where, q_e is the equilibrium adsorption capacity of dye adsorbed on xerogel surface, C_e is the equilibrium concentration of the adsorbate (mg/L), K_f is the Freundlich constant and n is the heterogeneity factor of Freundlich adsorption isotherm. From methylene blue and congo red dyes data it is observed that the slope($1/n$) of Freundlich adsorption isotherm fitted plot Figure 3.23a and Figure 3.23b are 4.42 and 1.23 respectively. This data clearly matches with the rate of dye adsorption data showing in to the Figure 3.21a and Figure 3.21c.

Adsorption kinetics experiments have been done systematically. Kinetic study for the adsorption of methylene blue dye was done at different time intervals at a constant room temperature (22 °C) and these data were fitted against both pseudo-first order and pseudo-second order kinetics using the following equations⁹⁹ (Figure 3.24).

$$\log(q_e - q_t) = \log q_e - \frac{k_1 t}{2.303} \quad (b)$$

$$\frac{t}{q_t} = \frac{1}{k_2 q_e^2} + \frac{t}{q_e} \quad (c)$$

Where, q_e and q_t are the amount of adsorbed dye (mg of dye per g of the gelator) at equilibrium time and at the time t (min) respectively, k_1 is the pseudo-first order rate constant (min^{-1}) and k_2 (min^{-1}) is the pseudo-second-order rate constant. The coefficient of determination (R^2) for the pseudo-second-order kinetic model was much higher ($R^2 = 0.99986$) than that of the pseudo-first-order kinetic model ($R^2 = 0.72453$), which indicates the adsorption of methylene blue dye follows pseudo-second-order kinetics. The dye adsorption data for cationic dye methylene blue fits well with the pseudo-second order reaction kinetics than the pseudo first order kinetics.

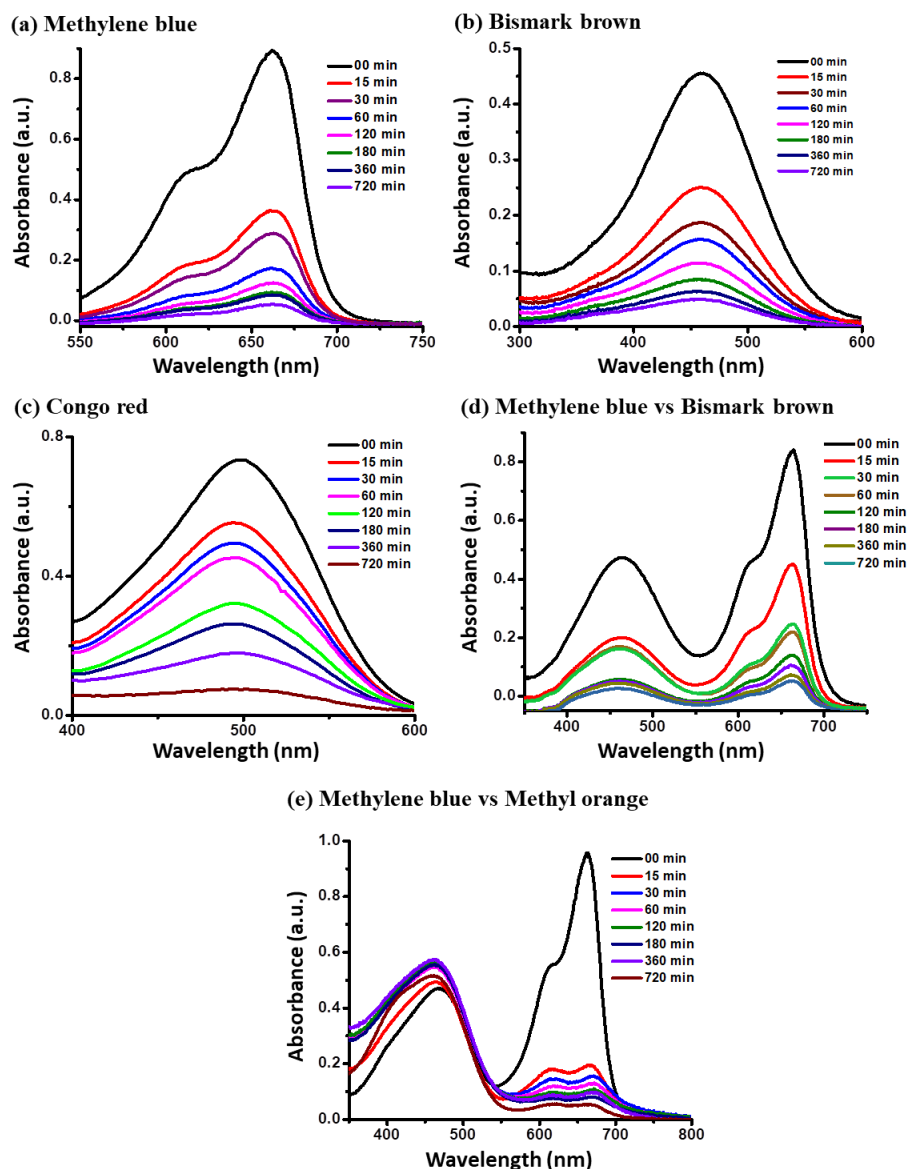


Figure 3.21. UV-vis spectroscopic study of dye adsorption of (a) methylene blue, (b) bismark brown, (c) congo red, (d) mixture of methylene blue and bismark brown and (e) mixture of methylene blue and methyl orange at 22 °C indicating the specific adsorption of methylene blue (cationic dye) from a mixture of both cationic and anionic dyes.

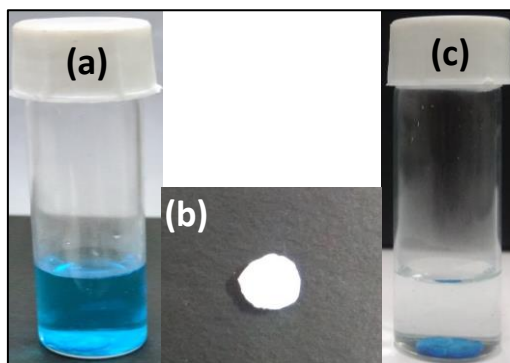


Figure 3.22. Photography (a) corresponds to the xerogel in methylene blue solution, (b) pellet of dried gelator molecule **P1** made by pelletizer and (c) methylene blue adsorbed xerogel and fresh water after 24h at 22°C.

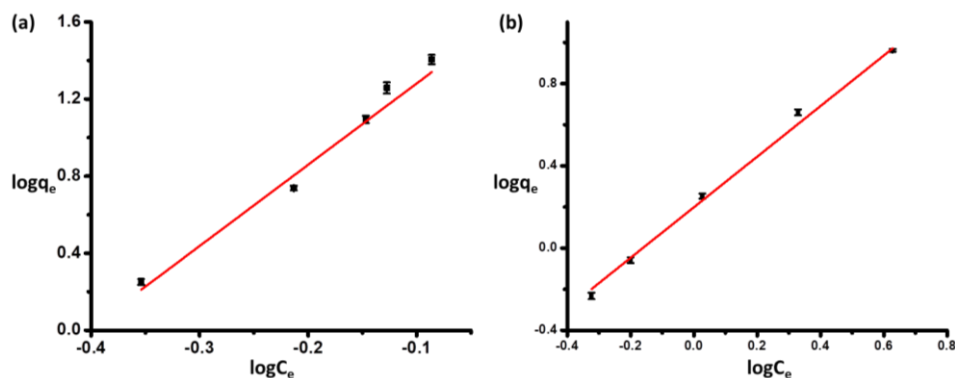


Figure 3.23. (a) Freundlich adsorption isotherm fitted dye adsorption data of methylene blue and (b) Freundlich adsorption isotherm fitted dye adsorption data of congo red with error bars at an average temperature 25 °C.

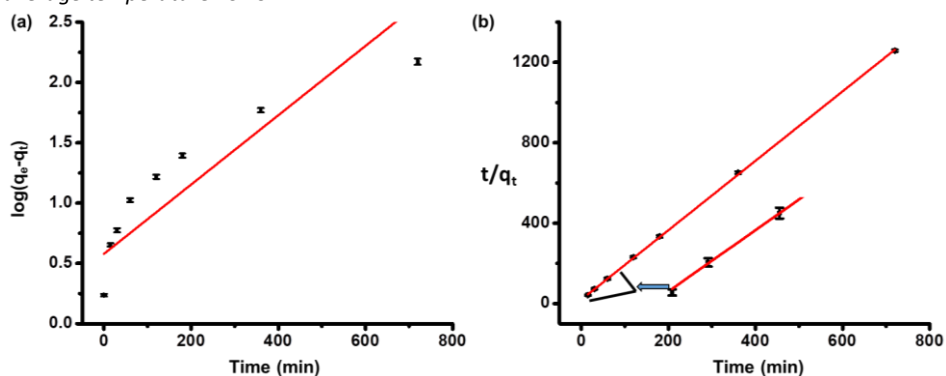


Figure 3.24. (a) Fit of kinetic data to pseudo-first-order model and (b) Fit of kinetic data to the pseudo-second-order model for methylene blue dye with error bars indicating the fact that it fits well with pseudo-second-order kinetics (First three data points are enlarged to show the error bars clearly).

Table 3.3. Dye adsorption by xerogel, obtained from UV-vis measurements at 22 °C.

| Dye | Nature | % removal | Amount of dye absorbed by per g of gelator (mg) |
|----------------|----------|----------------|---|
| Methylene blue | Cationic | 98.9 ± 0.2 | 629.3 ± 4.6 |
| Bismark brown | Cationic | 98.1 ± 0.1 | 406.0 ± 2.1 |
| Congo red | Neutral | 97.1 ± 0.2 | 165.7 ± 7.7 |

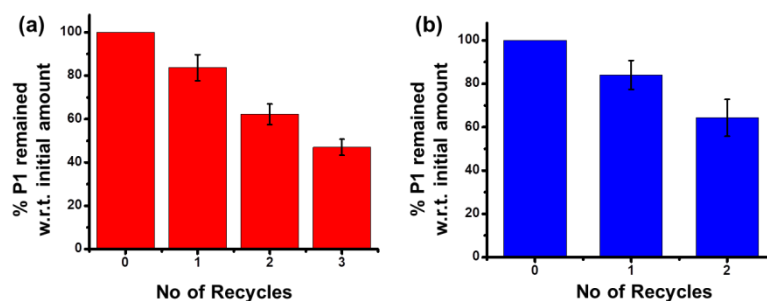


Figure 3.25. Plot showing reusability of peptide gelator during (a) dye absorption experiment and (b) metal ions (Pb^{2+}/Cd^{2+}) removal study.

3.3.8. Metal Ion Removal Studies. Toxic heavy metal pollutants, such as lead and cadmium are found in industrial waste-water and are hazardous towards the environment and have detrimental effects on human health causing cancer, bone damage, kidney damages and other fatal diseases.⁵¹ Thus, it is important to remove both Pb^{2+} and Cd^{2+} ions from contaminated water.

The initial concentrations of Cd^{2+} and Pb^{2+} ions were 2.54 ppm and 2.13 ppm for the freshly made metal ion solution respectively. After adsorption it was observed that the concentrations of Cd^{2+} metal ions were 0.054 ppm for hydrogel. As a result, it was found that the hydrogel removes 97.88% of Cd^{2+} ions (Table 3.4). Moreover, this gel is able to remove nearly all the toxic heavy metal ions from waste water. The maximum loading capacities of Cd^{2+} ions for the hydrogel was found to be 21.75 mg by per 1 mL of gel (5 mg gelator in 1mL buffer solution).

However, the concentration of Pb^{2+} was 0.024 ppm for the hydrogel after the adsorption of Pb^{2+} ions, corresponding to 98.8% adsorption for the hydrogel (Table 3.4). The adsorption of toxic Pb^{2+} ions using this hydrogel is comparable to that reported previously for a tripeptide-based gelator.³⁸ After the metal ion adsorption, no physical change is observed in the hydrogel. The recovery of gelators is done accordingly previously mentioned procedure in the dye adsorption section. While for metal ion adsorption, the recycling can be done twice (Figure 3.25).

Table 3.4. Details and amount of metal salt absorbed by the hydrogel.

| Metal salt | Gelator amount (mg) | Amount of metal salt removed by per g of gelator |
|--|---------------------|--|
| $\text{CdCl}_2 \cdot \text{H}_2\text{O}$ | 5 mg | 435 mg |
| $\text{Pb}(\text{NO}_3)_2$ | 5 mg | 382 mg |

3.3.9. Oil Spill Recovery. Peptide amphiphiles are potentially valuable in producing gels to recover oil spills from the ocean. In this regard, biphasic mixtures of salt water and oil were prepared with different types of oils including *n*-hexane, petroleum ether, diesel, petrol and kerosene. We investigated gelation using **P1** in a salt water/oil mixture. As shown in Figure 3.26, gelation of the oil

part was observed within 30 s after addition of the gelator solution. To the best of our knowledge, this is the first example of a tryptophan-based ambidextrous gelator which is able to selectively gel fuel oils from a salt water–oil mixture. Previous example of biphasic gelation from oil water mixtures includes the example of an amino acid containing amphiphile with a long fatty acid chain showing phase selective gelation for oil spill recovery and other examples include urea-based gelators and other low molecular weight gel-formers which gel fuel oils in oil-water biphasic mixture.⁴³⁻⁴⁸ There are several examples on TiO₂ based mechanically robust hybrid coatings,⁷⁸ nanocellulose based aerogels,¹⁰⁰ magnetic aerogels¹⁰¹ and nano-dimensional hydrophobic materials^{102, 103} for effective oil absorptions from biphasic oil-water mixtures, reported so far in literature. However, these methods have shortcomings, sometimes due to inherent toxicity, costly regeneration processing and sometimes due to difficulty in the recovery of oil from the separated substances. Gels are emerging materials for phase-selective oil spill recovery and these are very important materials to study as they are cost-effective systems with important application in waste remediation. The current gel material has high effectiveness with respect to oil spill. Our system can absorb or gelify fuel oil, kerosene, diesel, petrol in a biphasic mixture of salt water and oil within 30 sec and the absorption capacity of this gelator to gelify different fuel oils from waste water varies from 194 g to 205 g of fuel oils per g of the gelator.

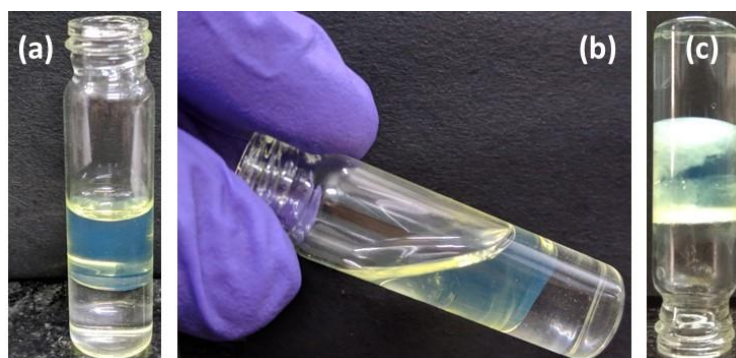


Figure 3.26. Images (a) biphasic oil-salt water, (b) liquid state of biphasic oil-salt water mixture, (c) self-supporting organogel formed after the addition of peptide amphiphile dissolved in 5% (v/v) ethyl acetate in the oil phase (diesel).

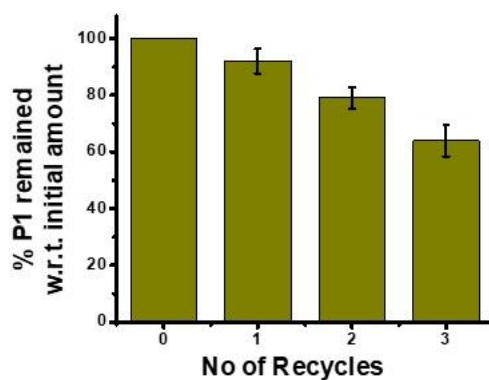


Figure 3.27. Plot showing reusability of peptide gelator during oil spill recovery experiment.

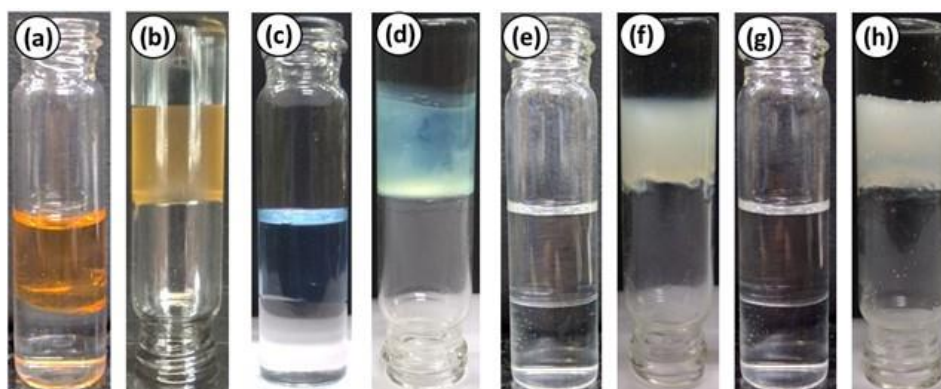


Figure 3.28. Gelation of oil from biphasic mixtures of different oils and salt water: (a) and (b) with petrol; (c) and (d) with kerosene; (e) and (f) with n-hexane; (g) and (h) with petroleum ether.

Table 3.5. Detail reusability study of toxic dyes, metal ions and oil spill in waste water treatment.

| Gelator amount | Adsorbed molecule/ions | Amount remaining after each of recycle | | | |
|----------------|--|--|-------------------|-------------------|-------------------|
| | | 0 | 1 | 2 | 3 |
| 5.0 mg | MB (4.69 mM) + BB (2.40 mM) in 1 mL Water | 5.00 mg | 4.19 mg ± 0.30 | 3.12 mg ± 0.24 | 2.35 mg ± 0.19 |
| 5.0 mg | Pb(NO ₃) ₂ + CdCl ₂ .H ₂ O 25 mM each in 1 mL water | 5.00 mg | 4.20 mg ± 0.34 | 3.21 mg ± 0.43 | - |
| 5.0 mg | Kerosene (0.5 mL) + Diesel (0.5 mL) in 1 mL salt water | 5.00 mg | 4.6 mg ± 0.22 | 4.0 mg ± 0.19 | 3.2 mg ± 0.28 |

Therefore, it can be stated that regarding oil-spill recovery from waste water, our peptide based ambidextrous gel material is comparable with previously mentioned studies. It is neither superior nor inferior to the previously mentioned gel based materials for oil-spill recovery. However, the efficiency of this gel to

selectively gelify fuel oils from a salt water–oil mixture is good and this gel is recyclable for further use. Moreover, this peptide based gelator shows three distinct activities for environmental remediation: oil-spill recovery, toxic organic dyes removal and heavy metal-ions removal from contaminated water. The main goal of our work is to project a tri-functional gelator, which can be used in multiple ways for the remediation of water pollution. From oil spill recovery and reusability study, oils have been recovered from organogel by vacuum distillation and gelator molecules were separated from the gel phase. During this study no physical change was observed in the organogel. The recovered gelator molecules were used for regelling of spilled oil. Finally, it was observed that the gelator amphiphile can be used three times (Figure 3.27, Table 3.5) for the recovery of different set of oil spill (Figure 3.28).

3. 4. Conclusions

A new peptide-based gelator is developed and is shown to form hydrogel within the pH range 6.9–8.5. It is able to effectively gel many organic solvents including petroleum ether, diesel, kerosene, petrol etc. from a biphasic mixture. The xerogels obtained from hydrogels have been successfully utilized to remove toxic organic dyes and hydrogels for hazardous heavy metal ions including lead and cadmium from waste water. Moreover, the peptide selectively gels fuel oil (forming an organogel phase) in a mixture with salt water-oil mixture including its probable use in oil spill recovery. The reusability of this peptide based gelator molecule without significant loss of activity is another notable feature of the peptide amphiphile. Thus, this peptide gelator shows three distinct activities for environmental remediation. Our results show, there is great future promise for self-assembling peptide amphiphile as novel smart soft materials for the removal of various pollutants from the environment.

3. 5. References

- (1) Cross, E. R.; Sproules, S.; Schweins, R.; Draper, E. R.; Adams, D. J. Controlled Tuning of the Properties in Optoelectronic Self-Sorted Gels. *J. Am. Chem. Soc.* **2018**, *140*, 8667–8670.
- (2) Kaufmann, L.; Kennedy, S. R.; Jones, C. D.; Steed, J. W. Cavity-Containing Supramolecular Gels as a Crystallization Tool for Hydrophobic Pharmaceuticals. *Chem. Commun.* **2016**, *52*, 10113–10116.

- (3) Du, X.; Zhou, J.; Shi, J.; Xu, B. Supramolecular Hydrogelators and Hydrogels: From Soft Matter to Molecular Biomaterials. *Chem. Rev.* **2015**, *115*, 13165–13307.
- (4) Das, S.; Okamura, N.; Yagi, S.; Ajayaghosh, A. Supramolecular Gel Phase Controlled [4 + 2] Diels-Alder Photocycloaddition for Electroplex Mediated White Electroluminescence. *J. Am. Chem. Soc.* **2019**, *141*, 5635–5639.
- (5) Liyanage, W.; Nilsson, B. L. Substituent Effects on the Self-Assembly/Coassembly and Hydrogelation of Phenylalanine Derivatives. *Langmuir* **2016**, *32*, 787–799.
- (6) Marti-Centelles, R.; Escuder, B. Morphology Diversity of L-Phenylalanine-Based Short Peptide Supramolecular Aggregates and Hydrogels. *ChemNanoMat* **2018**, *4*, 796–800.
- (7) Draper, E. R.; Adams, D. J. Controlling the Assembly and Properties of Low-Molecular-Weight Hydrogelators. *Langmuir* **2019**, *35*, 6506–6521.
- (8) Torres-Martinez, A.; Angulo-Pachon, C. A.; Galindo, F.; Miravet, J. F. In between Molecules and Self-Assembled Fibrillar Networks: Highly Stable Nanogel Particles from a Low Molecular Weight Hydrogelator. *Soft Matter* **2019**, *15*, 3565–3572.
- (9) Giano, M. C.; Ibrahim, Z.; Medina, S. H.; Sarhane, K. A.; Christensen, J. M.; Yamada, Y.; Brandacher, G.; Schneider, J. P. Injectable Bioadhesive Hydrogels with Innate Antibacterial Properties. *Nat. Commun.* **2014**, *5*, 1–9.
- (10) Kieffer, M.; Garcia, A. M.; Haynes, C. J. E.; Kralj, S.; Iglesias, D.; Nitschke, J. R.; Marchesan, S. Embedding and Positioning of Two Fe^{II}₄L₄ Cages in Supramolecular Tripeptide Gels for Selective Chemical Segregation. *Angew. Chemie - Int. Ed.* **2019**, *58*, 7982–7986.
- (11) Sajisha, V. S.; Maitra, U. Remarkable Isomer-Selective Gelation of Aromatic Solvents by a Polymorph of a Urea-Linked Bile Acid–amino Acid Conjugate. *RSC Adv.* **2014**, *4*, 43167–43171.
- (12) Marchesan, S.; Styan, K. E.; Easton, C. D.; Waddington, L.; Vargiu, A. V. Higher and Lower Supramolecular Orders for the Design of Self-Assembled Heterochiral Tripeptide Hydrogel Biomaterials. *J. Mater. Chem. B* **2015**, *3*, 8123–8132.
- (13) Vemula, P. K.; John, G. Smart Amphiphiles: Hydro/Organogelators for in Situ Reduction of Gold. *Chem. Commun.* **2006**, *21*, 2218–2220.

- (14) Beckers, S. J.; Parkinson, S.; Wheeldon, E.; Smith, D. K. In Situ Aldehyde-Modification of Self-Assembled Acyl Hydrazide Hydrogels and Dynamic Component Selection from Complex Aldehyde Mixtures. *Chem. Commun.* **2019**, 55, 1947–1950.
- (15) Pappas, C. G.; Shafi, R.; Sasselli, I. R.; Siccardi, H.; Wang, T.; Narang, V.; Abzalimov, R.; Wijerathne, N.; Ulijn, R. V. Dynamic Peptide Libraries for the Discovery of Supramolecular Nanomaterials. *Nat. Nanotechnol.* **2016**, 11, 960–967.
- (16) Edwards-Gayle, C. J. C.; Castelletto, V.; Hamley, I. W.; Barrett, G.; Greco, F.; Hermida-Merino, D.; Rambo, R. P.; Seitsonen, J.; Ruokolainen, J. Self-Assembly, Antimicrobial Activity, and Membrane Interactions of Arginine-Capped Peptide Bola-Amphiphiles. *ACS Appl. Bio Mater.* **2019**, 2, 2208–2218.
- (17) Abdallah, D. J.; Sirchio, S. A.; Weiss, R. G. Hexatriacontane Organogels. The First Determination of the Conformation and Molecular Packing of a Low-Molecular-Mass Organogelator in Its Gelled State. *Langmuir* **2000**, 16, 7558–7561.
- (18) Terech, P.; Weiss, R. G. Low Molecular Mass Gelators of Organic Liquids and the Properties of Their Gels. *Chem. Rev.* **2002**, 97, 3133–3160.
- (19) Sangeetha, N. M.; Maitra, U. Supramolecular Gels: Functions and Uses. *Chem. Soc. Rev.* **2005**, 34, 821–836.
- (20) Basu, K.; Mondal, B.; Das Mahapatra, A.; Nandi, N.; Basak, D.; Banerjee A. Modulation of Semiconducting Behavior and a Change in Morphology upon Gelation of a Peptide Appended Naphthalenediimide. *J. Phys. Chem. C* **2019**, 123, 20558–20566.
- (21) Lampel, A.; Ulijn, R. V.; Tuttle, T. Guiding Principles for Peptide Nanotechnology through Directed Discovery. *Chem. Soc. Rev.* **2018**, 47, 3737–3758.
- (22) Niu, D.; Jiang, Y.; Ji, L.; Ouyang, G.; Liu, M. Self-Assembly through Coordination and π -Stacking: Controlled Switching of Circularly Polarized Luminescence. *Angew. Chemie - Int. Ed.* **2019**, 58, 5946–5950.
- (23) Foster, J. A.; Damodaran, K. K.; Maurin, A.; Day, G. M.; Thompson, H. P. G.; Cameron, G. J.; Bernal, J. C.; Steed, J. W. Pharmaceutical Polymorph Control in a Drug-Mimetic Supramolecular Gel. *Chem. Sci.* **2016**, 8, 78–84.

- (24) Adler-Abramovich, L.; Gazit, E. The Physical Properties of Supramolecular Peptide Assemblies: From Building Block Association to Technological Applications. *Chem. Soc. Rev.* **2014**, *43*, 6881–6893.
- (25) Bera, S.; Mondal, S.; Xue, B.; Shimon, L. J. W.; Cao, Y.; Gazit, E. Rigid Helical-like Assemblies from a Self-Aggregating Tripeptide. *Nat. Mater.* **2019**, *18*, 503–509.
- (26) Baral, A.; Roy, S.; Dehsorkhi, A.; Hamley, I. W.; Mohapatra, S.; Ghosh, S.; Banerjee, A. Assembly of an Injectable Noncytotoxic Peptide-Based Hydrogelator for Sustained Release of Drugs. *Langmuir* **2014**, *30*, 929–936.
- (27) Sun, J. E. P.; Stewart, B.; Litan, A.; Lee, S. J.; Schneider, J. P.; Langhans, S. A.; Pochan, D. J. Sustained Release of Active Chemotherapeutics from Injectable-Solid β -Hairpin Peptide Hydrogel. *Biomater. Sci.* **2016**, *4*, 839–848.
- (28) Basu, K.; Baral, A.; Basak, S.; Dehsorkhi, A.; Nanda, J.; Bhunia, D.; Ghosh, S.; Castelletto, V.; Hamley, I. W.; Banerjee, A. Peptide Based Hydrogels for Cancer Drug Release: Modulation of Stiffness, Drug Release and Proteolytic Stability of Hydrogels by Incorporating d-Amino Acid Residue(s). *Chem. Commun.* **2016**, *52*, 5045–5048.
- (29) Mayr, J.; Saldias, C.; Diaz Diaz, D. Release of Small Bioactive Molecules from Physical Gels. *Chem. Soc. Rev.* **2018**, *47*, 1484–1515.
- (30) Qin, L.; Xie, F.; Duan, P.; Liu, M. A Peptide Dendron-Based Shrinkable Metallo-Hydrogel for Charged Species Separation and Stepwise Release of Drugs. *Chem. - A Eur. J.* **2014**, *20*, 15419–15425.
- (31) Miotto, M.; Gouveia, R. M.; Ionescu, A. M.; Figueiredo, F.; Hamley, I. W.; Cannon, C. J. 4D Corneal Tissue Engineering: Achieving Time-Dependent Tissue Self-Curvature through Localized Control of Cell Actuators. *Adv. Funct. Mater.* **2019**, *29*, 1807334.
- (32) Dou, X. Q.; Feng, C. L. Amino Acids and Peptide-Based Supramolecular Hydrogels for Three-Dimensional Cell Culture. *Adv. Mater.* **2017**, *29*, 1604062.
- (33) Chakraborty, P.; Guterman, T.; Adadi, N.; Yadid, M.; Brosh, T.; Adler-Abramovich, L.; Dvir, T.; Gazit, E. A Self-Healing, All-Organic, Conducting, Composite Peptide Hydrogel as Pressure Sensor and Electrogenic Cell Soft Substrate. *ACS Nano* **2019**, *13*, 163–175.
- (34) Nandi, N.; Gayen, K.; Ghosh, S.; Bhunia, D.; Kirkham, S.; Sen, S. K.; Ghosh, S.; Hamley, I. W.; Banerjee, A. Amphiphilic Peptide-Based

Supramolecular, Noncytotoxic, Stimuli-Responsive Hydrogels with Antibacterial Activity. *Biomacromolecules* **2017**, *18*, 3621–3629.

(35) Matson, J. B.; Stupp, S. I. Self-Assembling Peptide Scaffolds for Regenerative Medicine. *Chem. Commun.* **2012**, *48*, 26–33.

(36) Boekhoven, J.; Stupp, S. I. 25th Anniversary Article: Supramolecular Materials for Regenerative Medicine. *Adv. Mater.* **2014**, *26*, 1642–1659.

(37) Hirst, A. R.; Escuder, B.; Miravet, J. F.; Smith, D. K. High-Tech Applications of Self-Assembling Supramolecular Nanostructured Gel-Phase Materials: From Regenerative Medicine to Electronic Devices. *Angew. Chemie - Int. Ed.* **2008**, *47*, 8002–8018.

(38) Basak, S.; Nandi, N.; Paul, S.; Hamley, I. W.; Banerjee, A. A Tripeptide-Based Self-Shrinking Hydrogel for Waste-Water Treatment: Removal of Toxic Organic Dyes and Lead (Pb²⁺) Ions. *Chem. Commun.* **2017**, *53*, 5910–5913.

(39) Nandi, N.; Baral, A.; Basu, K.; Roy, S.; Banerjee, A. A Dipeptide-Based Superhydrogel: Removal of Toxic Dyes and Heavy Metal Ions from Waste Water. *Pept. Sci.* **2017**, *108*, e22915. doi:10.1002/bip.22915.

(40) Okesola, B. O.; Smith, D. K. Applying Low-Molecular Weight Supramolecular Gelators in an Environmental Setting-Self-Assembled Gels as Smart Materials for Pollutant Removal. *Chem. Soc. Rev.* **2016**, *45*, 4226–4251.

(41) Wood, D. M.; Acton, A. L.; Rodríguez-llansola, F.; Murray, C. A.; Cardin, C. J.; Miravet, J. F.; Escuder, B.; Hamley, I. W.; Hayes, W. pH-Tunable Hydrogelators for Water Purification: Structural Optimisation and Evaluation. *Chem. Eur. J.* **2012**, *18*, 2692–2699.

(42) Rodríguez-Llansola, F.; Escuder, B.; Miravet, J. F.; Hermida-merino, D.; Hamley, I. W.; Cardin, J.; Hayes, W. Selective and Highly Efficient Dye Scavenging by a pH-Responsive Molecular Hydrogelator. *Chem. Commun.* **2010**, *46*, 7960–7962.

(43) Bhattacharya, S.; Krishnan-Ghosh, Y. First Report of Phase Selective Gelation of Oil from Oil/Water Mixtures. Possible Implications toward Containing Oil Spills. *Chem. Commun.* **2001**, 185–186.

(44) Prathap, A.; Sureshan, K. M. Organogelator–Cellulose Composite for Practical and Eco-Friendly Marine Oil-Spill Recovery. *Angew. Chemie - Int. Ed.* **2017**, *56*, 9405–9409.

(45) Basu, K.; Nandi, N.; Mondal, B.; Dehsorkhi, A.; Hamley, I. W.; Banerjee, A. Peptide-Based Ambidextrous Bifunctional Gelator: Applications in Oil Spill

Recovery and Removal of Toxic Organic Dyes for Waste Water Management. *Interface Focus* **2017**, 7, 20160128.

(46) Jadhav, S. R.; Vemula, P. K.; Kumar, R.; Raghavan, S. R.; John, G. Sugar-Derived Phase-Selective Molecular Gelators as Model Solidifiers for Oil Spills. *Angew. Chemie - Int. Ed.* **2010**, 49, 7695–7698.

(47) Prathap, A.; Sureshan, K. M. Sugar-Based Organogelators for Various Applications. *Langmuir* **2019**, 35, 6005–6014.

(48) Basak, S.; Nanda, J.; Banerjee, A. A New Aromatic Amino Acid Based Organogel for Oil Spill Recovery. *J. Mater. Chem.* **2012**, 22, 11658–11664.

(49) Wu, J.; Tian, Q.; Hu, H.; Xia, Q.; Zou, Y.; Li, F.; Yi, T.; Huang, C. Self-Assembly of Peptide-Based Multi-Colour Gels Triggered by up-Conversion Rare Earth Nanoparticles. *Chem. Commun.* **2009**, 27, 4100–4102.

(50) Palui, G.; Nanda, J.; Ray, S.; Banerjee, A. Fabrication of Luminescent CdS Nanoparticles on Short-Peptide-Based Hydrogel Nanofibers: Tuning of Optoelectronic Properties. *Chem. - A Eur. J.* **2009**, 15, 6902–6909.

(51) Adhikari, B.; Banerjee, A. Short-Peptide-Based Hydrogel: A Template for the in Situ Synthesis of Fluorescent Silver Nanoclusters by Using Sunlight. *Chem. - A Eur. J.* **2010**, 16, 13698–13705.

(52) Slavik, P.; Kurka, D. W.; Smith, D. K. Palladium-Scavenging Self-Assembled Hybrid Hydrogels-Reusable Highly-Active Green Catalysts for Suzuki-Miyaura Cross-Coupling Reactions. *Chem. Sci.* **2018**, 9, 8673–8681.

(53) Gayen, K.; Basu, K.; Bairagi, D.; Castelletto, V.; Hamley, I. W.; Banerjee, A. Amino-Acid-Based Metallo-Hydrogel That Acts Like an Esterase. *ACS Appl. Bio Mater.* **2018**, 1, 1717–1724.

(54) Zhou, G.; Liu, C.; Tang, Y.; Luo, S.; Zeng, Z.; Liu, Y.; Xu, R.; Chu, L. Sponge-like Polysiloxane-Graphene Oxide Gel as a Highly Efficient and Renewable Adsorbent for Lead and Cadmium Metals Removal from Wastewater. *Chem. Eng. J.* **2015**, 280, 275–282.

(55) Miao, K.; Luo, X.; Wang, W.; Guo, J.; Guo, S.; Cao, F.; Hu, Y.; Chang, P.; Feng, G. One-Step Synthesis of Cu – SBA-15 under Neutral Condition and Its Oxidation Catalytic Performance. *Micropor. Mesopor. Mater.* **2019**, 289, 109640.

(56) Shi, X.; Wang, C.; Ma, Y.; Liu, H.; Wu, S.; Shao, Q.; He, Z.; Guo, L. Template-Free Microwave-Assisted Synthesis of FeTi Coordination Complex Yolk-Shell Microspheres for Superior Catalytic Removal of Arsenic and

Chemical Degradation of Methylene Blue from Polluted Water. *Powder Technol.* **2019**, 356, 726–734.

(57) Sun, L.; Shao, Q.; Zhang, Y.; Jiang, H.; Ge, S.; Lou, S.; Lin, J.; Zhang, J.; Wu, S.; Dong, M.; Guo, Z. N Self-Doped ZnO Derived from Microwave Hydrothermal Synthesized Zeolitic Imidazolate Framework-8 toward Enhanced Photocatalytic Degradation of Methylene Blue. *J. Colloid Interface Sci.* **2020**, 565, 142–155.

(58) WHO. Exposure to Mercury: A Major Public Health Concern. *Prev. Dis. Through Heal. Environ.* **2006**, 4.

(59) Gong, K.; Guo, S.; Zhao, Y.; Hu, Q.; Liu, H.; Sun, D.; Li, M.; Qiu, B.; Guo, Z. Bacteria Cell Templated Porous Polyaniline Facilitated Detoxi Fi Cation and Recovery of Hexavalent Chromium. *J. Mater. Chem. A* **2018**, 6, 16824–16832.

(60) Yuan, Y.; Yu, Q.; Wen, J.; Li, C.; Guo, Z.; Wang, X.; Wang, N. Uranium Extraction Ultrafast and Highly Selective Uranium Extraction from Seawater by Hydrogel-like Spidroin-Based Protein Fiber. *Angew. Chem. Int. Ed.* **2019**, 58, 11785–11790.

(61) Zhao, S.; Yuan, Y.; Yu, Q.; Niu, B.; Liao, J.; Guo, Z.; Wang, N. Uranium Extraction A Dual-Surface Amidoximated Halloysite Nanotube for High-Efficiency Economical Uranium Extraction from Seawater. *Angew. Chem. Int. Ed.* **2019**, 58, 14979–14985.

(62) Qian, Y.; Yuan, Y.; Wang, H.; Liu, H.; Zhang, J.; Shi, S.; Guo, Z.; Wang, N. Salicylaldoxime / Polydopamine Graphene Oxide. *J. Mater. Chem. A* **2018**, 6, 24676–24685.

(63) Wang, Y.; Zhou, P.; Luo, S.; Liao, X.; Wang, B.; Shao, Q.; Guo, X.; Guo, Z. Controllable Synthesis of Monolayer Poly(Acrylic Acid) on the Channel Surface of Mesoporous Alumina for Pb(II) Adsorption. *Langmuir* **2018**, 34, 7859–7868.

(64) Sankhla, M. S.; Kumari, M.; Nandan, M.; Kumar, R.; Agrawal, P. Heavy Metals Contamination in Water and Their Hazardous Effect on Human Health-A Review. *Int. J. Curr. Microbiol. Appl. Sci.* **2016**, 5, 759–766.

(65) Achary, M. S.; Satpathy, K. K.; Panigrahi, S.; Mohanty, A. K.; Padhi, R. K.; Biswas, S.; Prabhu, R. K.; Vijayalakshmi, S.; Panigrahy, R. C. Concentration of Heavy Metals in the Food Chain Components of the Nearshore Coastal Waters of Kalpakkam, Southeast Coast of India. *Food Control* **2017**, 72, 232–243.

(66) Merrill J.C., Morton J.J.P., Soileau S.D., Metals. In: Hayes A.W, editor. Principles and Methods of Toxicology. 5th ed. CRC Press; **2007**.

- (67) Jarup, L. Hazards of Heavy Metal Contamination. *Br. Med. Bull.* **2003**, 68, 167–182.
- (68) Van Der Bruggen, B.; Vandecasteele, C.; Van Gestel, T.; Doyen, W.; Leysen, R. A Review of Pressure-Driven Membrane Processes in Wastewater Treatment and Drinking Water Production. *Environ. Prog.* **2003**, 22, 46–56.
- (69) Chowdhury, A.; Khan, A. A.; Kumari, S.; Hussain, S. Superadsorbent Ni-Co-S/SDS Nanocomposites for Ultrahigh Removal of Cationic, Anionic Organic Dyes and Toxic Metal Ions: Kinetics, Isotherm and Adsorption Mechanism. *ACS Sustain. Chem. Eng.* **2019**, 7, 4165–4176.
- (70) Maiti, D.; Mukhopadhyay, S.; Devi, P. S. Evaluation of Mechanism on Selective, Rapid, and Superior Adsorption of Congo Red by Reusable Mesoporous α -Fe₂O₃ Nanorods. *ACS Sustain. Chem. Eng.* **2017**, 5, 11255–11267.
- (71) Ramalingam, B.; Parandhaman, T.; Choudhary, P.; Das, S. K. Biomaterial Functionalized Graphene-Magnetite Nanocomposite: A Novel Approach for Simultaneous Removal of Anionic Dyes and Heavy-Metal Ions. *ACS Sustain. Chem. Eng.* **2018**, 6, 6328–6341.
- (72) Ray, S.; Das, A. K.; Banerjee, A. pH-Responsive, Bolaamphiphile-Based Smart Metallo-Hydrogels as Potential Dye-Adsorbing Agents, Water Purifier, and Vitamin B₁₂ Carrier. *Chem. Mater* **2007**, 19, 1633–1639.
- (73) Minju, N.; Jobin, V.; Savithri, S.; Ananthakumar, S. Double-Silicate Derived Hybrid Foams for High-Capacity Adsorption of Textile Dye Effluent: Statistical Optimization and Adsorption Studies. *Langmuir* **2019**, 35, 9382–9395.
- (74) Zhang, X.; Pan, Y.; Zhao, J.; Hao, X.; Wang, Y.; Schubert, D. W.; Liu, C.; Shen, C.; Liu, X. Facile Construction of Copper Mesh Surface from Superhydrophilic to Superhydrophobic for Various Oil-Water Separations. *Eng. Sci.* **2019**, 7, 65–71.
- (75) Cai, J.; Tian, J.; Gu, H.; Guo, Z. Amino Carbon Nanotube Modified Reduced Graphene Oxide Aerogel for Oil/Water Separation. *ES Mater. Manuf.* **2019**, 6, 68–74.
- (76) Kayan, A. Inorganic-organic hybrid materials and their adsorbent properties. *Adv. Compos. Hybrid Mater.* **2019**, 2, 34–45.
- (77) Zhang, J.; Li, P.; Zhang, Z.; Wang, X.; Tang, J.; Liu, H.; Shao, Q.; Ding, T.; Umar, A.; Guo, Z. Solvent-Free Graphene Liquids: Promising Candidates for Lubricants without the Base Oil. *J. Colloid Interface Sci.* **2019**, 542, 159–167.

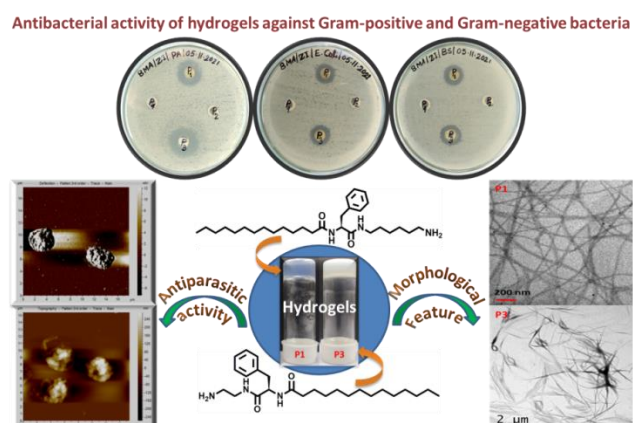
- (78) Hu, W.; Huang, J.; Zhang, X.; Zhao, S.; Pei, L.; Zhang, C.; Liu, Y.; Wang, Z. A Mechanically Robust and Reversibly Wetttable Benzoxazine/ Epoxy/ Mesoporous TiO₂ Coating for Oil/Water Separation. *Appl. Surf. Sci.* **2020**, *507*, 145168.
- (79) Wen, N.; Jiang, B.; Wang, X.; Shang, Z.; Jiang, D.; Zhang, L.; Sun, C.; Wu, Z.; Yan, H.; Liu, C.; Guo, Z. Overview of Polyvinyl Alcohol Nanocomposite Hydrogels for Electro-Skin, Actuator, Supercapacitor and Fuel cell. *Chem. Rec.* **2020**, *20*, 773–792.
- (80) Wei, H. G.; Wang, H.; Li, A.; Cui, D. P.; Zhao, Z. N.; Chu, L. Q.; Wei, X.; Wang, L.; Pan, D.; Fan, J. C.; Li, Y. C.; Zhang, J. X.; Liu, C. T.; Wei, S. Y.; Guo, Z. H. Multifunctions of Polymer Nanocomposites: Environmental Remediation, Electromagnetic Interference Shielding, And Sensing Applications. *ChemNanoMat* **2020**, *6*, 1–12.
- (81) Gu, H.; Zhang, H.; Gao, C.; Liang, C.; Gu, J.; Guo, Z. New Functions of Polyaniline. *ES Mater. Manuf.* **2018**, *1*, 3–12.
- (82) Xie, P.; Li, Y.; Hou, Q.; Sui, K.; Liu, C.; Fu, X.; Zhang, J.; Murugadoss, V.; Fan, J.; Wang, Y.; Fan, R.; Guo, Z. Tunneling-Induced Negative Permittivity in Ni/MnO Nanocomposites by a Bio-Gel Derived strategy. *J. Mater. Chem. C* **2020**, *8*, 3029–3039.
- (83) Zhang, L.; Jiang, D.; Dong, T.; Das, R.; Pan, D.; Sun, C.; Wu, Z.; Zhang, Q.; Liu, C.; Guo, Z. Overview of Ionogels in Flexible Electronics. *Chem. Rec.* **2020**, *20*, 1–21.
- (84) Zhou, N.; Wang, T.; Chen, S.; Hu, Q.; Cheng, X.; Sun, D.; Vupputuri, S.; Qiu, B.; Liu, H.; Guo, Z. Conductive Polyaniline Hydrogel Enhanced Methane Production from Anaerobic Wastewater Treatment. *J. Colloid Interface Sci.* **2021**, *581*, 314–322.
- (85) Zhang, Y.; Xie, S.; Zhang, D.; Ren, B.; Liu, Y.; Tang, L.; Chen, Q.; Yang, J.; Wu, J.; Tang, J.; Zheng, J. Thermo-Responsive and Shape-Adaptive Hydrogel Actuators from Fundamentals to Applications. *Eng. Sci.* **2019**, *6*, 1–11.
- (86) Li, S.; Jasim, A.; Zhao, W.; Fu, L.; Ullah, M. W.; Shi, Z.; Yang, G. Fabrication of pH-Electroactive Bacterial Cellulose / Polyaniline Hydrogel for the Development of a Controlled Drug Release System. *ES Mater. Manuf.* **2018**, *1*, 41–49.

- (87) Ul-Islam, M.; Ali, J.; Khan, W.; Haider, A.; Shah, N.; Ahmad, W.; Ullah, M. W.; Yang, G. Fast 4-Nitrophenol Reduction Using Gelatin Hydrogel Containing Silver Nanoparticles. *Eng. Sci.* **2019**, *8*, 19–24.
- (88) Huang, H.; Han, L.; Wang, Y.; Yang, Z.; Zhu, F.; Xu, M. Tunable Thermal-Response Shape Memory Bio-Polymer Hydrogels as Body Motion Sensors. *Eng. Sci.* **2020**, *9*, 60–67.
- (89) Sun, L.; Shi, Z.; Wang, H.; Zhang, K.; Dastan, D.; Sund, K.; Fand, R. Ultrahigh Discharge Efficiency and Improved Energy Density in Rationally Designed Bilayer Polyetherimide–BaTiO₃/P(VDF-HFP) Composites. *J. Mater. Chem. A* **2020**, *8*, 5750–5757.
- (90) Sun, K.; Wang, L.; Wang, Z.; Wu, X.; Fan, G.; Wang, Z.; Cheng, C.; Fan, R.; Dongef, M.; Guo, Z. Flexible Silver Nanowire/Carbon Fiber Felt Metacomposites with Weakly Negative Permittivity Behavior. *Phys. Chem. Chem. Phys.* **2020**, *22*, 5114–5122.
- (91) Wang, Z.; Sun, K.; Xie, P.; Liu, Y.; Gu, Q.; Fan, R. Permittivity Transition from Positive to Negative in Acrylic Polyurethane-Aluminum Composites. *Compos. Sci. Technol.* **2020**, *188*, 107969.
- (92) Sun, K.; Wang, Z.; Xin, J.; Wang, Z.; Xie, P.; Fan, G.; Murugadoss, V.; Fan, R.; Fan, J.; Guo, Z. Hydrosoluble Graphene/Polyvinyl Alcohol Membranous Composites with Negative Permittivity Behavior. *Macromol. Mater. Eng.* **2020**, *305*, 1900709.
- (93) Hu, J.; Lin, J.; Zhang, Y.; Lin, Z.; Qiao, Z.; Liu, Z.; Yang, W.; Liu, X.; Dong, M.; Guo, Z. A New Anti-Biofilm Strategy of Enabling Arbitrary Surfaces of Materials and Devices with Robust Bacterial Anti-Adhesion via a Spraying Modified Microsphere Method. *J. Mater. Chem. A* **2019**, *7*, 26039–26052.
- (94) Zheng, C.; Zhang, P.; Cheng, J.; Guo, Z.; Liu, H. Durably Antibacterial and Bacterially Antiadhesive Cotton Fabrics Coated by Cationic Fluorinated Polymers. *ACS Appl. Mater. Interfaces* **2018**, *10*, 6124–6136.
- (95) Cheng, N.; Hu, Q.; Guo, Y.; Wang, Y.; Yu, L. Efficient and Selective Removal of Dyes Using Imidazolium-Based Supramolecular Gels. *ACS Appl. Mater. Interfaces* **2015**, *7*, 10258–10265.
- (96) Karan, C. K.; Bhattacharjee, M. Self-Healing and Moldable Metallogels as the Recyclable Materials for Selective Dye Adsorption and Separation. *ACS Appl. Mater. Interfaces* **2016**, *8*, 5526–5535.

- (97) Zhang, X.; Liu, D.; Yang, L.; Zhou, L.; You, T. Self-assembled Three-Dimensional Graphene-Based Materials for Dye Adsorption and Catalysis. *J. Mater. Chem. A* **2015**, *3*, 10031–10037.
- (98) N. Khunti, C. J. C. Edwards-Gayle, N. Cowieson, I. W. Hamley and R. Rambo, *In preparation*, **2019**.
- (99) Li, D.; Li, Q.; Bai, N.; Dong, H.; Mao, D. One-Step Synthesis of Cationic Hydrogel for Efficient Dye Adsorption and Its Second Use for Emulsified Oil Separation. *ACS Sustainable Chem. Eng.* **2017**, *5*, 5598–5607.
- (100) Zhang, H.; Lyu, S.; Zhou, X.; Gu, H.; Ma, C.; Wang, C. Super Light 3D Hierarchical Nanocellulose Aerogel Foam with Superior Oil Adsorption. *J. Colloid Interface Sci.* **2019**, *536*, 245-251.
- (101) Gu, H.; Zhou, X.; Lyu, S.; Pan, D.; Dong, M.; Wu, S. Magnetic Nanocellulose-Magnetite Aerogel for Easy Oil Adsorption. *J. Colloid Interface Sci.* **2020**, *560*, 849–856.
- (102) Sun, S.; Zhu, L.; Liu, X.; Wu, L.; Dai, K.; Liu, C.; Shen, C.; Guo, X.; Zheng, G.; Guo, Z. Superhydrophobic Shish-Kebab Membrane with Self-Cleaning and Oil/Water Separation Properties. *ACS Sustainable Chem. Eng.* **2018**, *6*, 9866–9875.
- (103) Zhang, J.; Wang, Z.; Shen, C.; Guo, Z. Superhydrophobic/Superoleophilic Polycarbonate/Carbon Nanotubes Porous Monolith for Selective Oil Adsorption from Water. *ACS Sustainable Chem. Eng.* **2018**, *6*, 13747–13755.

Chapter 4

Amino Acid Containing Amphiphilic Hydrogelators with Antibacterial and Antiparasitic Activities



(*Soft Matter*, 2022, **18**, 7201–7216)

Chapter 4

Amino Acid Containing Amphiphilic Hydrogelators with Antibacterial and Antiparasitic Activities

4.1. Introduction

In recent years, low molecular weight gelators have been increasingly researched due to their interesting properties like self-association in a medium to form an inter-linked network structure for various applications.¹⁻⁷ These gelators can be assembled using various non-covalent interactions including hydrogen bonding, π - π stacking, van der Waals and other interactions to form gels under suitable conditions.⁸ The micro- and nano-network structure of hydrogels leads to a highly porous structure, so they can easily entrap numerous water molecules in the gel cavities.⁹ Natural amino acid-based hydrogels have attracted interest not only for the formation of hydrogels via non-covalent interactions but also for their uses in different fields of research work.¹⁰⁻¹⁴ They have a wide variety of applications in tissue engineering,¹⁵ cell culture,^{16,17} sustained release of drugs and biomolecules,^{18,19} drug delivery,²⁰ vaccine development,²¹ wastewater treatment,^{14,22,23} wound healing,²⁴ antimicrobial,²⁵⁻³² and others.^{22,23,33,34} Peptides and natural amino acid-based supramolecular hydrogels are desirable candidates to prepare biomaterials due to their biocompatibility and biodegradability.²⁴ In recent times, the increasing prevalence of bacterial strains with resistance to conventional antibiotics has been emerging as a significant threat to modern society.²⁷ Therefore, new types of antibiotics are required to combat such bacteria. The biocompatibility of the natural amino acid-based hydrogels makes them suitable starting materials to develop new antibiotics or biologically active molecules.^{25,27} Polycationic peptides containing lysine or arginine moieties can act as antibacterial agents due to their ability to disrupt bacterial membranes.³⁵⁻³⁷ Peptides containing hydrophobic and/or cationic residues can be used as molecular building blocks to create antibacterial hydrogels as such peptides can mimic the structure of natural antibiotics.^{38,39} In this context, peptide-based amphiphiles are attractive materials for developing peptide therapeutics as they can be synthesized easily at an affordable cost.⁴⁰ Leishmaniasis holds the second largest position among all parasitic infections after malaria. Recent reports in

2016 by the World Health Organisation suggest that 200 000–400 000 new cases occur every year by visceral leishmaniasis (VL) in 65 countries. Also, visceral leishmaniasis or kala-azar has been found to be endemic, having a 95% mortality rate if kept untreated.⁴¹ Among the new cases, 90% of the cases have been found in India, Brazil, Somalia, Sudan, South Sudan, and Ethiopia.⁴² Specifically, the spread of VL is highly alarming in India and Brazil. In India, annually 100 000 new cases have been reported; among which, 90% of the cases are found in Bihar. On the other hand, VL has been observed in 21 states out of 27 in Brazil. Unfortunately, until now, chemotherapy has been the only choice to combat this disease. Visceral leishmaniasis is characterized by irregular bouts of fever, weight loss, enlargement of the spleen and liver and anaemia. VL is endemic in more than 80 countries.⁴³ If left untreated it is fatal in more than 95% of cases within 2 years after the onset of the disease. To date, there has been no effective vaccine against any form of human leishmaniasis. The problem is even more difficult because of the cases of HIV co-infection.⁴⁴ The solutions to overcome these problems include improved chemotherapy and the development of novel drugs specific to these resistant and pathogenic strains. Some drugs such as amphotericin B⁴⁵ and its lipid formulations, pentavalent antimonials,⁴⁶ pentamidine, miltefosine, paromomycin, and sitamaquine⁴⁷ have been used to treat patients. However, the toxicity, side effects, and high cost restrict the use of these drugs. A plausible solution to these issues is the use of chemotherapy⁴⁸ and concurrently probing for novel targets showing specificity towards the parasites. There are reports that amino acid containing peptides and amphiphiles exhibit biologically important applications in antibacterials,^{25–31} cell culture,^{16,17} and drug release.^{18,19,49} Many of these molecules contain aromatic amino acid residues like L-phenylalanine²⁷ and L-tryptophan.¹² However, the development of aromatic amino acid containing amphiphilic gelators with antiparasitic activity is unprecedented to the best of our knowledge. The previous reports also suggest that organic heterocyclic compounds, such as oxindoles, can be excellent materials against the parasite *L. donovani*. Thus, we chose L-tryptophan (and for reference L-phenylalanine) as components of our gelator amphiphiles. We have synthesized four amphiphiles containing proteinaceous aromatic amino acids L-phenylalanine and L-tryptophan with a varying chain length of the cationic –NH₂ containing a polar head group, and with a fatty acyl chain of fourteen carbon atoms at the C-terminus. Firstly, gelator amphiphiles **P1**, **P2**, **P3** and **P4**

containing L-phenylalanine or L-tryptophan (Figure 4.1a) were synthesised and studied for antiparasitic and antibacterial activities. However, it was observed that only **P1** and **P3** are active towards the parasite *L. donovani* and also against Gram-positive and -negative bacteria. Thus, L-phenylalanine has a role in antiparasitic and antibacterial activities. Our results also show that methylene units (CH_2) attached to the terminal amino groups do not have any role in either antiparasitic or antibacterial properties. From the comprehensive experimental data, it was evident that both molecules **P2** and **P4** containing L-tryptophan are unable to kill the protozoan parasite *Leishmania donovani* and Gram-positive and Gram-negative bacteria.

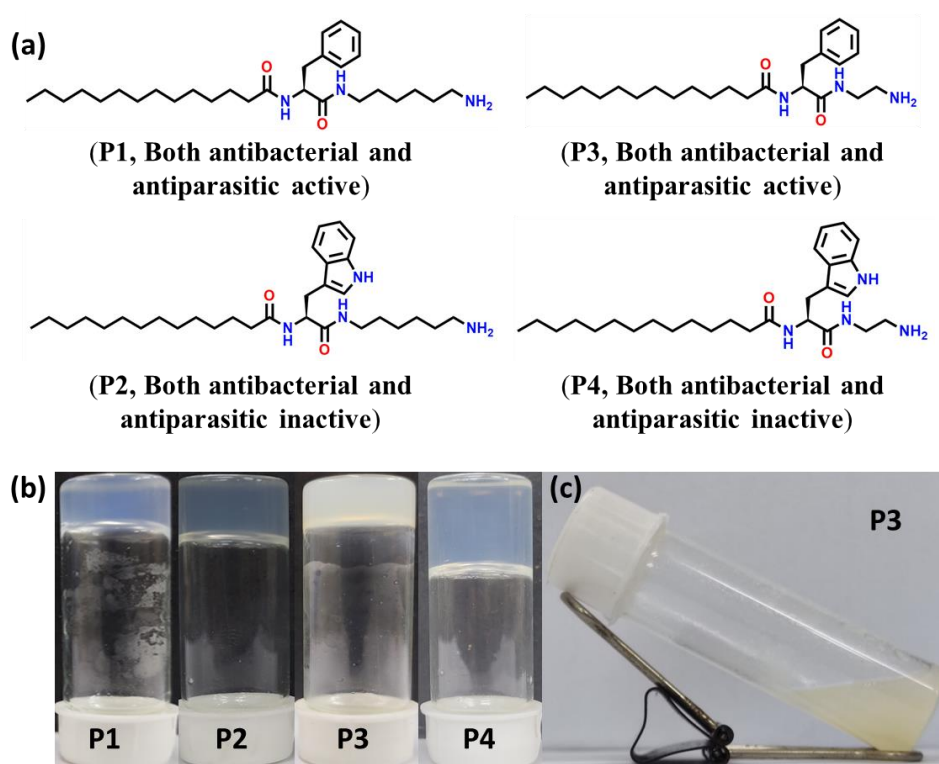


Figure 4.1. (a) Chemical structures and the activity of amphiphilic gelators **P1**, **P2**, **P3** and **P4** used in antibacterial and antiprotozoal study, (b) hydrogels obtained from amphiphilic gelators (**P1**, **P2** and **P4**) in ultrapure water and in 2% DMSO (v/v) mixed in ultrapure water for **P3** respectively, (c) viscous solution of **P3** in only ultrapure water.

4.2. Experimental Section

4.2.1. Materials

L-phenylalanine (Phe), L-tryptophan (Trp), myristic acid (C_{14}), HOBt (1-hydroxybenzotriazole), DCC (N,N'-dicyclohexylcarbodiimide), di-tert-butyl dicarbonate (BOC Anhydride, DiBOC), silica gel (100–200 mesh), and aluminium oxide (basic) were purchased from SRL, India. N,N'-

Dimethylformamide (DMF), trifluoroacetic acid (TFA), ethylenediamine, hexamethylenediamine, sodium dihydrogen phosphate, and disodium hydrogen phosphate were purchased from Merck. Millipore milli-Q grade water was used for all experiments. Dimethyl sulfoxide (DMSO), camptothecin and penicillin–streptomycin solution were purchased from Sigma Chemicals (St. Louis, MO, USA). 3-(4, 5-Dimethyl-2-thiazolyl)-2, 5-diphenyl-2H-tetrazolium bromide (MTT) was purchased from Invitrogen Life Technologies (Carlsbad, CA, USA). All drugs were dissolved in 100% DMSO at a concentration of 25 mM and stored at -20 °C. MitoSOX red (M36008), MitoTracker green (M7514), TMRM (T668), CM-H2DCFDA (C6827), and FITC Annexin V/Dead Cell Apoptosis kit (V13242) were obtained from Molecular Probes.

4.2.2. Methods

Synthesis and Characterisation. The amino acid containing gelator amphiphiles were synthesized by conventional solution phase coupling methods using a racemization-free fragment condensation strategy. The characterisation of the synthesis products was performed using mass spectrometry, ¹H NMR spectroscopy and ¹³C NMR spectroscopy. All NMR studies were carried out using a Bruker DPX 400 MHz or a Bruker DPX 500 MHz spectrometer at 300 K. Concentrations were in the range of 5–10 mM in CDCl₃ or DMSO-d₆. Mass spectra were recorded using a Q-ToF micro (Waters Corporation) mass spectrometer by the positive mode electrospray ionization process.

Preparation of Gels. 15 mg of **P1**, 10 mg of **P2**, and 10 mg of **P4** gelator amphiphiles were weighed into three different sets of 5 mL screw-capped glass vials with the addition of 1 mL of ultrapure water (milli-Q) in each one. Then, the glass vials were heated on a hot plate till the gelator molecules were dissolved completely. After this, the heated glass vials were cooled in a water bath for 5 min. Later, these solutions obtained from the gelator molecule **P1** showed instant gelation within 1 min of resting after cooling, whereas **P2** and **P4** showed a longer gelation time of 6 h and 24 h, respectively. On the other hand, the co-solvent-induced gelator **P3** formed a gel after 30 min of resting at 28 °C, room temperature (Table 4.1). Initially, the gelation time was determined by the glass vial inversion technique.

Table 4.1. Comparison of minimum gelation concentration, gel forming kinetics and thermal stability of freshly prepared hydrogel in presence of ultrapure water.

| Amphiphilic gelators | MGC (wt% /V) | Gel forming time after cooling | T _{gel} (°C) |
|----------------------|--------------|--------------------------------|-----------------------|
| P1 | 1.20 ± 0.01 | 1 min | 43 ± 0.4 |
| P2 | 0.65 ± 0.01 | 6 h | 59 ± 0.8 |
| P3 | - | - | - |
| P4 | 0.78 ± 0.01 | 24 h | 52 ± 0.8 |

*All gelator concentrations were 31.68 mM for all cases during the T_{gel} (°C) measurement.

For the gelator amphiphile **P3**, 10 mg of amphiphile was added to 980 mL of milli-Q water and heated on a hot plate until the solute gelator amphiphile was dissolved. Then 20 mL of DMSO was added to the heated solution before cooling it in a water bath and at room temperature (at 28 °C). The formation of stable co-solvent-induced gelation was observed within one hour.

Loading of Hydrogels onto a Rheometer. Firstly, hydrogels were removed from the 5 mL glass vial using a Scoopula. These hydrogels were further loaded onto a Peltier plate without any air or bubbles in the hydrogels. Then these hydrogels were placed at the centre of the Peltier plate. After this, a program was used to set the height of the cone to a 27 µm height gap. When, the gap height is reached, trim the edges of the hydrogel with a pipet tip so that the hydrogel correctly fills the geometry.

Then, the solvent trap was placed over the geometry and onto the Peltier plate and it surrounded the outer edges of the solvent trap with water to keep the hydrogel hydrated during the data acquisition.

General Procedure for the Antibacterial Study. A well-established agar well cut-diffusion method was employed to analyze the antibacterial activity of amphiphilic gelators against four pathogenic strains of Gram-positive (*S. aureus* and *B. subtilis*) and Gram-negative (*E. coli* and *P. aeruginosa*) bacteria. A measurable quantity of HiMedia agar (HA) was liquefied in ultra-pure deionized water and stirred vigorously to obtain a homogenous mixture. The homogeneous solution was autoclaved for about 30 min, after which 20 mL of the autoclaved mixture was trickled in each of the sterilized Petri plates and allowed to form gel for 30 min. The gel plates were placed in an incubator for 12 h at 37 °C to

identify the presence of any adventitious bacteria. After this, four known bacteria were spread on the fresh agar gel medium one by one. The gel well was cut to introduce the gel samples. The gel samples of **P1** to **P4** were placed at that position to identify the antibacterial properties of the gelator amphiphiles. The sample-charged plates were gently positioned for incubation at 37 °C temperature for 24 h to enhance the complete diffusion of the gelator amphiphiles. The inhibition zones of each plate were measured and recorded in millimeter (mm) units.

Parasite Maintenance and Culture. Five strains of *Leishmania donovani* were used: (i) the sodium antimony gluconate (SAG)-sensitive (SAG^S) MHOM/IN/1983/AG83, (ii) the multidrug resistant field isolate MHOM/IN/2009/BHU575/0 (BHU-575),⁵⁰ (iii) laboratory grown miltefosineresistant (MIL^R) strains, (iv) camptothecin resistant (CPT^R) strain, and (v) *Leishmania major* were used in the study. Amastigotes obtained from the spleens of infected hamsters were cultured at 22 °C to obtain promastigotes.⁵¹ Promastigotes were cultured in M199 medium containing 20% (v/v) heat-inactivated fetal bovine serum (FBS-Gibco Life Technologies, Carlsbad, California, USA) supplemented with 100 IU per mL penicillin and 100 mg mL⁻¹ streptomycin solution at 22 °C. Promastigotes were further grown in 10% (v/v) heat-inactivated FBS for 5–6 days at 22 °C before use. To observe the ultrastructure alterations of the parasites, 1×10^6 cells were treated with different concentrations of amphiphilic gelators for 12 h and observed under a microscope. DMSO was used as a vehicle control.

***Leishmania* Promastigotes Cell Viability Measurement.** The *L. donovani* AG83 wild type strain, multidrug resistant (BHU-575), laboratory grown MIL^R cells, CPT^R cells and *L. major* strain were individually incubated with different concentrations of amphiphilic gelators for 24 h, following which the viability was assessed using a MTT assay.⁵² Yellow MTT (3-(4,5-dimethyl-2-thiazolyl)-2,5-diphenyl-2H-tetrazolium bromide) was reduced to purple formazan in the mitochondria of the living cells. The formazan was then solubilised by adding isopropanol and 6(N) HCl and the concentration was determined by taking OD at 595 nm. The living cells actively converted MTT to formazan, thereby generating a quantitative measure of viability and cytotoxicity.

All IC₅₀ and IC₉₀ values were calculated using a variable slope model to find EC₅₀ using prism (version 5.0, GraphPad software, San Diego, CA, USA). We

further investigated the effect of drugs on the survivability of *Leishmania* promastigotes using a light microscope by direct microscopic counting in a haemocytometer. The cells of the exponential phase of the growth curve were used in the study. Briefly, cells were collected and transferred onto a 24-well tissue culture plate (2×10^6 cells per well). The cells were then incubated at various concentrations of amphiphilic gelators (1.0, 2.5, 5.0, 10.0 and 20.0 μM) for 12 h at 22 °C. After incubation, the cells were collected and centrifuged and the pellet was washed with $1 \times \text{PBS}$ twice and finally resuspended in $1 \times \text{PBS}$. Aliquots of 50 μL were mixed with a 0.4% solution of trypan blue and incubated for 3 min at 22 °C. About 5–7 μL of the mixture was carefully transferred to a haemocytometer and the blue (dead) and clear (live) cells were counted. The total number of viable cells in the mixture was measured by multiplying the total number of viable cells by 2 (the dilution factor for trypan blue). Percentages of viable cells were calculated using the formula:

$$\text{Percentage Viability} = \left(\frac{\text{Live cell count}}{\text{Total cell count}} \right) \times 100$$

Measurement of ROS. The level of intracellular reactive oxygen species (ROS) was measured using a cell-permeable, non-polar probe H2DCFDA (molecular probes, Eugene, USA). For the measurement of ROS in treated and untreated parasites, 2×10^6 cells were treated with amphiphilic gelators (0.5, 1.0, 2.5 and 5.0 μM) for 12 h. Promastigotes treated with 0.2% DMSO served as controls. After incubation, parasites were washed with phosphate buffer saline and resuspended in 500 mL of PBS (without phenol red) and stained with the cell-permeant dye H2DCFDA for 15–20 min.⁵³ In another set of reactions, the parasites were incubated with N-acetyl cysteine (NAC) prior to treatment with amphiphilic gelators. The green fluorescence of 2',7'-dichlorofluorescein (DCF) was measured at 530 nm using a flow cytometer. All the fluorometric measurements were performed in triplicate, and the results were expressed as the mean fluorescence intensity per 10^6 cells.

Atomic Force Microscopy

The AFM studies were performed to observe any morphological changes in the *Leishmania donovani* promastigotes after treatment with the amphiphilic gelators **P1** and **P3**. The *Leishmania donovani* promastigotes (1×10^6 cells per mL) were incubated with medium M199 containing 1.25 μM of amphiphilic gelators (IC_{50}

value of both the amphiphilic gelators) for 12 h. Then the cells were again washed (1100g for 15 min at room temperature) and fixed in 4% (w/v) paraformaldehyde. The fixed cells were then diluted 1:10 with milli Q water. Aliquots 10 μ L of diluted sample were then deposited on a freshly cleaved muscovite Ruby mica sheet (ASTM V1 Grade Ruby Mica from MICAFAFAB, Chennai, India) and kept for 5–10 min for air drying. Mica sheets are negatively charged so samples bind strongly to the mica surface. After drying, the samples were gently washed with 0.5 mL milli-Q water and again kept for drying. The images of the samples were captured at a scan rate of 0.5 lines per s.

4.2.3. Synthesis Details of Peptide Amphiphiles (P1–P4)

Synthesis of Gelator P1:

Synthesis of C₁₄-Phe-COOMe [H₃C-(CH₂)₁₂-CONH-Phe-COOMe]: Myristic acid (1.14 g, 5 mM) was taken in a 250 mL round bottom flask and 8 mL (N,N'-Dimethylformamide) DMF was added to dissolve it. After that the mixture was cooled in an ice-water bath having temperature 0 °C–10 °C. H-Phe-COOMe was isolated from the corresponding methyl ester hydrochloride (1.186 g, 5.5 mM) by neutralization, subsequent extraction with ethyl acetate and concentration to 50 mL. Then it was added to the reaction mixture, followed immediately by DCC (1.133 g, 5.5 mM) and HOBt (0.697 g, 5.5 mM). The reaction mixture was stirred for 48 h. The reaction mixture was filtered through a sintered glass crucible and the DCU (dicyclohexyl urea) was filtered off. The organic layer was washed with brine (2 \times 50 mL) and then dried over anhydrous sodium sulphate and evaporated in vacuum to yield peptide as a white solid. Purification was done using a silica gel column (100–200 mesh) using chloroform and ethyl acetate as eluents.

Yield: 1.46 g (3.75 mM, 74.90%).

¹H NMR (500 MHz, CDCl₃, TMS, 25 °C): δ 7.27 (m, 3H, aromatic), 7.09 (d, 2H, J=6.5 Hz, aromatic) 5.89 (d, J= 7.5 Hz, 1H, NH of amide), 4.90 (m, 1H, α -CH of Phe), 3.73 (s, 3H, -OCH₃), 3.12 (m, 2H, β -CH₂ of Phe), 2.17 (t, 2H, J= 7.5 Hz, α -CH₂ of myristyl C=O), 1.58 (m, 2H, β -CH₂ of myristyl C=O), 1.25 (m, 20H, 10-CH₂ of myristyl chain), 0.88 (t, 3H, J= 6.75 Hz, -CH₃ of myristyl) (Figure 4.2). ¹³C NMR (125 MHz, CDCl₃, TMS, 25 °C): δ 172.8, 172.3, 136.0, 129.4, 128.7, 127.2, 53.0, 36.7, 32.1, 29.8, 29.8, 29.7, 29.6, 29.5, 29.5, 29.3, 25.7, 22.8, 14.2 (Figure 4.3). MALDI-TOF MS (m/z): Calculated for C₂₄H₃₉NO₃ (M):

412.283 (M + Na)⁺, 428.256 (M + K)⁺ Found: 412.920 (M + Na)⁺, 428.919 (M + K)⁺ (Figure 4.4).

Synthesis of C₁₄-Phe-COOH [H₃C-(CH₂)₁₂-CONH-Phe-COOH]: C₁₄-Phe-COOMe (1.4 g, 3.6 mM) was taken in a 250 mL round bottom flask. The solid was dissolved in MeOH (40 mL) and 1N NaOH (15 mL) was added to the mixture. The reaction mixture was stirred for 12 h and the progress of saponification was monitored by thin layer chromatography (TLC). After 12 h methanol was removed under vacuum, the residue was taken in 50 mL of water, washed with diethyl ether (2 × 50 mL). Then the pH of the aqueous layer was adjusted to 2 using 1N HCl and it was extracted with ethyl acetate (3 × 50 mL). The extracts were dried over anhydrous sodium sulphate, and evaporated in vacuum to yield as a white solid product. Purification was done using a silica gel column (100–200 mesh) using chloroform and methanol as eluents.

Yield: 1.28 g (3.41 mM, 95%).

¹H NMR (400 MHz, DMSO-d₆, TMS, 25 °C): δ 12.63 (1H, br, -COOH), 8.08 (d, J=7.6 Hz, 1H, NH), 7.23 (m, 5H, aromatic), 4.43 (m, 1H, α-CH of Phe), 2.95 (m, 2H, β-CH₂ of Phe), 2.03 (t, J= 7.2 Hz, 2H, α -CH₂ of myristyl C=O), 1.38 (m, 2H, β -CH₂ of myristyl C=O), 1.18 (m, 20H, 10-CH₂ of myristyl chain), 0.86 (t, J= 6.8 Hz, 3H, -CH₃ of myristyl) (Figure 4.5). ¹³C NMR (100 MHz, DMSO-d₆, TMS, 25 °C): δ 173.1, 172.0, 137.7, 129.0, 128.0, 126.2, 53.1, 36.7, 35.0, 31.2, 29.0, 28.9, 28.8, 28.7, 28.6, 28.4, 25.1, 22.0, 13.8 (Figure 4.6). MALDI-TOF (m/z): Calculated for C₂₃H₃₇NO₃ (M): 376.285 (M + H)⁺, 398.267 (M + Na)⁺, 414.241 (M + K)⁺ Found: 376.864 (M + H)⁺, 398.857 (M + Na)⁺, 414.890 (M + K)⁺ (Figure 4.7).

Synthesis of C₁₄-Phe-CO-Hex-Boc [H₃C-(CH₂)₁₂-CONH-Phe-CONH-Hex-Boc]: C₁₄-Phe-COOH (1.25 g, 3.33 mM) was taken in a 250 mL round bottom flask and 8 mL (dimethylformamide) DMF was added to dissolve it. After that the mixture was cooled in an ice-water bath having temperature 0 °C–10 °C. NH₂-Hex-Boc (mono-Boc protected hexamethylene diamine) (0.86 g, 4.0 mM) was added to this reaction mixture, followed immediately by DCC (0.84 g, 4.0 mM) and HOBt (0.61 g, 4.5 mM). The reaction mixture was stirred for 48 h. The reaction mixture was filtered through a sintered glass crucible and the DCU (dicyclohexyl urea) was filtered off. The organic layer was washed with brine (2×50 mL) and then dried over anhydrous sodium sulphate and evaporated in

vacuum to yield peptide as a white solid. Purification was done using a silica gel column (100–200 mesh) using chloroform and ethyl acetate as eluents.

Yield: 1.47 g (2.57 mM, 77.10%).

^1H NMR (400 MHz, CDCl_3 , TMS, 25 °C): δ 7.25 (m, 5H, aromatic), 6.36 (br, m, 1H, NH), 6.02 (br, m, 1H, NH), 4.62 (m, 2H, NH of amide and α -CH of Phe), 3.07 (m, 6H, β -CH₂ and 2α -CH₂ of hexamethylenediamine) 2.16 (t, 2H, J= 6.6 Hz, α -CH₂ of myristyl C=O), 1.56 (m, 2H, β -CH₂ of myristyl C=O), 1.44 (s, 9H, 3-Me of Boc), 1.28 (m, 28H, 10-CH₂ of myristyl chain and 4-CH₂ of hexamethylenediamine), 0.88 (t, J= 6.5 Hz, 3H, -CH₃ of myristyl) (Figure 4.8). ^{13}C NMR (100 MHz, CDCl_3 , TMS, 25 °C): δ 173.3, 171.0, 156.2, 137.0, 129.4, 128.7, 127.0, 79.2, 55.7, 40.4, 39.3, 38.8, 36.7, 32.0, 31.0, 30.0, 29.8, 29.8, 29.7, 29.6, 29.5, 29.3, 29.2, 28.6, 26.8, 26.2, 25.7, 22.8, 14.2 (Figure 4.9). HRMS (m/z): Calculated for $\text{C}_{34}\text{H}_{59}\text{N}_3\text{O}_4$ (M): 573.458 (M + H)⁺, 596.440 (M + Na)⁺, 612.414 (M + K)⁺ Found: 574.553 (M + H)⁺, 596.544 (M + Na)⁺, 612.515 (M + K)⁺ (Figure 4.10).

Synthesis of P1 (C_{14} -Phe-CO-Hex-NH₂) [$\text{H}_3\text{C}-(\text{CH}_2)_{12}-\text{CONH-Phe-CONH-Hex-NH}_2$]: C_{14} -Phe-CO-Hex-Boc (1.2 g, 2.10 mM), 4 mL of trifluoroacetic acid (TFA) was added and removal of Boc group was monitored by TLC. After 3 h, TFA was removed under vacuum. The residue was taken in water (20 mL) and covered with ethyl acetate (about 50 mL) and basified with a solution of NaHCO_3 . The aqueous phase was extracted with ethyl acetate and this operation was done repeatedly. The ethyl acetate extracts were pooled, washed with water and dried over anhydrous Na_2SO_4 and evaporated in vacuum. A white solid material was obtained.

Yield: 1.47 g (2.57 mM, 77.10%).

^1H NMR (400 MHz, DMSO-d_6 , TMS, 25 °C): δ 8.44 (br, 2H, free -NH₂), 8.07 (d, J=7.6 Hz, 1H, NH), 7.97 (m, 1H, NH), 7.21 (m, 5H, aromatic), 4.45 (m, 1H, α -CH of Phe), 3.34 (m, 4H, 2α -CH₂ of hexamethylenediamine), 2.74 (m, 2H, β -CH₂ of Phe), 2.02 (m, 2H, α -CH₂ of myristyl C=O), 1.49 (2H, m, β -CH₂ of myristyl C=O), 1.34 (4H, m, 2β -CH₂ of hexamethylenediamine), 1.16 (24H, m, 10-CH₂ of myristyl chain and 2γ -CH₂ of hexamethylenediamine), 0.86 (3H, t, J= 6.5 Hz, -CH₃ of myristyl) (Figure 4.11). ^{13}C NMR (100 MHz, DMSO-d_6 , TMS, 25 °C): δ 172.4, 171.5, 138.5, 129.6, 128.4, 126.6, 79.7, 54.4, 38.8, 38.4, 35.7, 31.8, 31.1, 29.5, 29.5, 29.4, 29.3, 29.2, 28.9, 28.3, 26.3, 26.1, 25.7, 22.6, 14.4

(Figure 4.12). HRMS (m/z): Calculated for $C_{29}H_{51}N_3O_2$ (M): 473.398 (M)⁺, 474.406 (M + H)⁺ Found: 473.9274 (M)⁺, 474.9582 (M + H)⁺ (Figure 4.13).

Synthesis of gelator P2:

Synthesis of C_{14} -Trp-COOMe [$H_3C-(CH_2)_{12}-CONH-Trp-COOMe$]: It was prepared by maintaining the previous procedure as mentioned during the synthesis of C_{14} -Trp-Phe-COOH in Chapter 3 (Page No. 155).

Synthesis of C_{14} -Trp-COOH [$H_3C-(CH_2)_{12}-CONH-Trp-COOH$]: It was prepared by maintaining the previous procedure as mentioned during the synthesis of C_{14} -Trp-Phe-COOMe in Chapter 3 (Page No. 155–156).

Synthesis of C_{14} -Trp-CO-Hex-Boc [$H_3C-(CH_2)_{12}-CONH-Trp-CONH-Hex-Boc$]: C_{14} -Trp-COOH (1.45 g, 3.50 mM) was taken in a 250 mL round bottom flask and 8 mL (dimethylformamide) DMF was added to dissolve it. After that the mixture was cooled in an ice-water bath having temperature 0 °C–10 °C. NH_2 -Hex-Boc (0.86 g, 4.0 mM) was added to this reaction mixture, followed immediately by DCC (0.84 g, 4.0 mM) and HOBt (0.61 g, 4.5 mM). The reaction mixture was stirred for 48 h at nitrogen atmosphere. The reaction mixture was filtered through a sintered glass crucible and the DCU (dicyclohexyl urea) was filtered off. The organic layer was washed with brine (2 × 50 mL) and then dried over anhydrous sodium sulphate and evaporated in vacuum to yield peptide as a white solid. Purification was done using a silica gel column (100–200 mesh) using chloroform and methanol as eluents.

Yield: 1.72 g (2.81 mM, 80.30%).

¹H NMR (400 MHz, $CDCl_3$, TMS, 25 °C): δ 9.16 (s, 1H, aromatic –NH), 7.78 (d, J= 8.0 Hz, 1H, aromatic), 7.37 (d, J= 8.0 Hz, 1H, aromatic), 7.19 (t, J= 7.2 Hz, 1H, aromatic), 7.13 (t, J= 7.0 Hz, 1H, aromatic) 7.06 (s, 1H, aromatic), 6.39 (d, J=7.2 Hz, 1H, NH of amide), 5.42 (s, br, 1H, –NH), 4.71 (m, 1H, α -CH of Trp), 4.66 (br, s, 1H, –NH of amide), 3.16 (m, 6H, β -CH₂ of Trp and 2 α -CH₂ of –Hex–), 2.20 (t, J= 7.5 Hz, 2H, α -CH₂ of myristyl –C=O), 1.63 (m, 2H, β -CH₂ of myristyl C=O), 1.47 (s, 9H, –Boc), 1.42 (m, 4H, 2 β -CH₂ of –Hex– near Trp), 1.19 (m, 24H, 10-CH₂ of myristyl chain and 2 γ -CH₂ of –Hex–), 0.88 (t, J= 6.5 Hz, 3H, –CH₃ of myristyl) (Figure 4.14). ¹³C NMR (100 MHz, $CDCl_3$, TMS, 25 °C): δ 173.1, 171.3, 156.5, 136.6, 127.4, 123.4, 122.3, 119.8, 119.1, 119.0, 111.5, 110.8, 79.7, 54.1, 40.7, 39.3, 36.9, 32.1, 29.9, 29.8, 29.8, 29.8, 29.6, 28.5, 29.4, 29.2, 28.9, 28.6, 26.2, 25.9, 25.7, 22.8, 14.2 (Figure 4.15). HRMS (m/z): Calculated for $C_{36}H_{60}N_4O_4$ (M): 613.469 (M + H)⁺, 614.477 (M + 2H)⁺, 636.459

(M + H + Na)⁺ Found: 613.407 (M + H)⁺, 614.465 (M + 2H)⁺, 636.445 (M + H + Na)⁺ (Figure 4.16).

Synthesis of P2 (C₁₄-Trp-CO-Hex-NH₂) [H₃C-(CH₂)₁₂-CONH-Trp-CONH-Hex-NH₂]: C₁₄-Trp-CO-Hex-Boc (1.5 g, 2.45 mM), 5 mL of trifluoroacetic acid (TFA) was added at nitrogen atmosphere and removal of Boc group was monitored by TLC. After 3 h, TFA was removed under vacuum. The residue was taken in water (20 mL) and covered with ethyl acetate (about 50 mL) and basified with a solution of NaHCO₃. The aqueous phase was extracted with ethyl acetate and this operation was done repeatedly. The ethyl acetate extracts were pooled, washed with water and dried over anhydrous Na₂SO₄ and evaporated in vacuum. A white solid material was obtained.

Yield: 1.08 g (2.11 mM, 84.40%).

¹H NMR (400 MHz, DMSO-d₆, TMS, 25 °C): δ 10.80 (br, s, 1H, aromatic -NH), 7.90 (d, J= 8.0 Hz, 1H, NH of amide), 7.85 (m, 1H, NH of amide), 7.58 (d, J= 8.0 Hz, 1H, aromatic), 7.31 (d, J= 8.0 Hz, 1H, aromatic), 7.09 (s, 1H, aromatic), 7.05 (t, J= 7.6 Hz, 1H, aromatic), 6.96 (t, J= 7.6 Hz, 1H, aromatic), 4.49 (m, 1H, α - CH of Trp), 2.96 (m, 4H, α-CH₂ of -NH-Hex-NH-), 2.05 (t, 3H, α-CH₂ of myristyl C=O), 1.39 (m, 2H, β-CH₂ of myristyl C=O), 1.27 (m, 28H, 10-CH₂ of myristyl chain and 4-CH₂ of hexamethylene diamine), 0.86 (t, J= 6.6 Hz, 3H, -CH₃ of myristyl) (Figure 4.17). ¹³C NMR (125 MHz, DMSO-d₆, TMS, 25 °C): δ 171.8, 171.3, 136.0, 127.3, 123.3, 120.7, 118.4, 118.0, 111.1, 110.2, 53.3, 41.5, 38.4, 35.2, 33.3, 31.2, 29.0, 29.0, 28.8, 28.7, 28.6, 28.5, 28.0, 26.2, 26.1, 25.1, 22.0, 13.9 (Figure 4.18). HRMS (m/z): Calculated for C₃₁H₅₂N₄O₂ (M): 513.417 (M + H)⁺, 514.425 (M + 2H)⁺ Found: 513.397 (M + H)⁺, 514.399 (M + 2H)⁺ (Figure 4.19).

Synthesis of gelator P3:

Synthesis of C₁₄-Phe-COOH: It was prepared by maintaining the previous procedure as mentioned during the synthesis of P1.

Synthesis of C₁₄-Phe-CO-En-Boc [H₃C-(CH₂)₁₂-CONH-Phe-CONH-En-Boc]: C₁₄-Phe-COOH (1.20 g, 3.20 mM) was taken in a 250 mL round bottom flask and 8 mL (dimethylformamide) DMF was added to dissolve it. After that the mixture was cooled in an ice-water bath having temperature 0 °C–10 °C. NH₂-En-Boc (mono-Boc protected ethylene diamine) (0.64 g, 4.0 mM) was added to this reaction mixture, followed immediately by DCC (0.84 g, 4.0 mM) and HOBt (0.61 g, 4.5 mM). The reaction mixture was stirred for 48 h. The reaction mixture

was filtered through a sintered glass crucible and the DCU (dicyclohexyl urea) was filtered off. The organic layer was washed with brine (2×50 mL) and then dried over anhydrous sodium sulphate and evaporated in vacuum to yield peptide as a white solid. Purification was done using a silica gel column (100–200 mesh) using chloroform and ethyl acetate as eluents.

Yield: 1.27 g (2.46 mM, 76.87%).

^1H NMR (400 MHz, CDCl_3 , TMS, 25 °C): δ 7.25 (m, 5H, aromatic), 6.36 (m, 1H, NH), 6.07 (m, 1H, NH), 4.62 (m, 1H, α -CH of Phe), 4.60 (m, 1H, α -CH of –Trp), 3.15 (m, 6H, β -CH₂ of Phe and α -CH₂ of Hex-Boc), 2.16 (2H, m, α -CH₂ of myristyl C=O), 1.57 (m, 2H, β -CH₂ of myristyl C=O), 1.42 (s, 9H, 3Me- of Boc), 1.28 (m, 20H, 10-CH₂ of myristyl chain), 0.88 (t, J = 6.6Hz, 3H, -CH₃ of myristyl) (Figure 4.20). ^{13}C NMR (100 MHz, CDCl_3 , TMS, 25 °C): δ 173.3, 171.5, 136.9, 129.4, 128.9, 127.3, 54.7, 38.8, 36.8, 32.1, 29.8, 29.8, 29.8, 29.6, 29.5, 29.5, 29.4, 28.5, 25.7, 22.8, 14.2 (Figure 4.21). HRMS (m/z): Calculated for $\text{C}_{30}\text{H}_{51}\text{N}_3\text{O}_4$ (M): 540.378 (M + Na)⁺, 541.386 (M + H + Na)⁺ Found: 539.888 (M + Na)⁺, 540.912 (M + H + Na)⁺ (Figure 4.22).

Synthesis of P3 (C_{14} -Phe-CO-En-NH₂) [$\text{H}_3\text{C}-(\text{CH}_2)_{12}$ -CONH-Phe-CONH-En-NH₂]: C_{14} -Phe-CO-En-Boc (1.00 g, 1.93 mM), 4 mL of trifluoroacetic acid (TFA) was added and removal of Boc group was monitored by TLC. After 3 h, TFA was removed under vacuum. The residue was taken in water (20 mL) and covered with ethyl acetate (about 50 mL) and basified with a solution of NaHCO_3 . The aqueous phase was extracted with ethyl acetate and this operation was done repeatedly. The ethyl acetate extracts were pooled, washed with water and dried over anhydrous Na_2SO_4 and evaporated in vacuum. A white solid material was obtained.

Yield: 0.67 g (1.61 mM, 83.40%).

^1H NMR (400 MHz, $\text{DMSO}-d_6$, TMS, 25 °C): δ 8.00 (d, J = 7.6 Hz, 1H, NH), 7.91 (m, 1H, NH), 7.21 (m, 5H, aromatic), 4.46 (m, 1H, α -CH of Trp), 2.90 (m, 6H, 2 β -CH₂ of Trp and 4 α -CH₂ of En-Boc), 2.02 (m, 2H, α -CH₂myristyl C=O), 1.35 (m, 2H, β -CH₂ of myristyl C=O), 1.17 (m, 20H, 10-CH₂ of myristyl chain), 0.86 (t, 3H, J = 6.5 Hz, -CH₃ of myristyl) (Figure 4.23). ^{13}C NMR (100 MHz, $\text{DMSO}-d_6$, TMS, 25 °C): δ 171.9, 171.2, 138.0, 129.1, 127.9, 126.0, 53.9, 42.1, 41.0, 37.8, 35.1, 31.2, 29.0, 29.0, 28.8, 28.7, 28.7, 28.4, 25.1, 22.0, 13.9 (Figure 4.24). HRMS (m/z): Calculated for $\text{C}_{25}\text{H}_{43}\text{N}_3\text{O}_2$ (M): 418.343 (M + H)⁺, 419.351 (M + 2H)⁺ Found: 418.054 (M + H)⁺, 419.120 (M + 2H)⁺ (Figure 4.25).

Synthesis of gelator P4:

Synthesis of C₁₄-Trp-COOH: It was prepared by maintaining the previous procedure as mentioned during the synthesis of **P2**.

Synthesis of C₁₄-Trp-CO-En-Boc [H₃C-(CH₂)₁₂-CONH-Trp-CONH-En-Boc]: C₁₄-Trp-COOH (1.45 g, 3.50 mM) was taken in a 250 mL round bottom flask and 8 mL (dimethylformamide) DMF was added to dissolve it. After that the mixture was cooled in an ice-water bath having temperature 0 °C–10 °C. NH₂-En-Boc (0.64 g, 4.0 mM) was added to this reaction mixture, followed immediately by DCC (0.84 g, 4.0 mM) and HOBt (0.61 g, 4.5 mM). The reaction mixture was stirred for 48 h at nitrogen atmosphere. The reaction mixture was filtered through a sintered glass crucible and the DCU (dicyclohexyl urea) was filtered off. The organic layer was washed with brine (2 × 50 mL) and then dried over anhydrous sodium sulphate and evaporated in vacuum to yield peptide as a white solid. Purification was done using a silica gel column (100–200 mesh) using chloroform and methanol as eluents.

Yield: 1.60 g (2.88 mM, 82.29%).

¹H NMR (400 MHz, CDCl₃, TMS, 25 °C): δ 8.44 (s, br, 1H, aromatic NH), 7.67 (d, J = 8.0 Hz, 1H, aromatic), 7.35 (d, J = 8.0 Hz, 1H, aromatic), 7.18 (t, J = 7.4 Hz, 1H, aromatic), 7.11 (t, J = 7.4 Hz, 1H, aromatic), 7.03 (1H, m, aromatic), 6.38 (m, 1H, NH), 6.30 (m, 1H, -NH), 4.69 (m, 2H, -NH of ethylene diamine and α-CH of Trp), 3.25 (m, 6H, 2β-CH₂ of Trp and 4α-CH₂ of En-Boc) 3.00 (m, 4H, α-CH₂ of -En-), 2.16 (t, 2H, α-CH₂ of myristyl C=O), 1.56 (m, 2H, β-CH₂ of myristyl C=O), 1.40 (s, 9H, 3-Me of Boc), 1.27 (m, 20H, 10-CH₂ of myristyl chain), 0.87 (t, 3H, J = 6.6 Hz, -CH₃ of myristyl) (Figure 4.26). ¹³C NMR (100 MHz, CDCl₃, TMS, 25 °C): δ 173.4, 172.1, 156.5, 136.3, 127.5, 123.3, 122.5, 119.9, 118.9, 111.5, 110.9, 89.7, 54.2, 40.1, 36.8, 36.7, 32.1, 29.8, 29.8, 29.8, 29.6, 28.5, 29.5, 29.4, 28.8, 28.5, 25.6, 22.8, 14.2 (Figure 4.27). HRMS (m/z): Calculated for C₃₂H₅₂N₄O₄ (M): 557.407 (M + H)⁺, 558.415 (M + 2H)⁺ Found: 557.639 (M + H)⁺, 558.681 (M + 2H)⁺ (Figure 4.28).

Synthesis of P4 (C₁₄-Trp-CO-En-NH₂) [H₃C-(CH₂)₁₂-CONH-Trp-CONH-En-NH₂]: C₁₄-Trp-CO-En-Boc (1.20 g, 2.16 mM), 4 mL of trifluoroacetic acid (TFA) was added at nitrogen atmosphere and removal of Boc group was monitored by TLC. After 3 h, TFA was removed under vacuum. The residue was taken in water (20 mL) and covered with ethyl acetate (about 50 mL) and basified with a solution of NaHCO₃. The aqueous phase was extracted with ethyl

acetate and this operation was done repeatedly. The ethyl acetate extracts were pooled, washed with water and dried over anhydrous Na_2SO_4 and evaporated in vacuum. A white solid material was obtained.

Yield: 0.84 g (1.84 mM, 85.19%).

^1H NMR (500 MHz, DMSO-d_6 , TMS, 25 °C): δ 10.77 (s, br, 1H, $-\text{NH}$), 7.90 (d, $J=8.5$ Hz, 1H, aromatic), 7.84 (m, 1H, NH), 7.57 (d, $J=7.5$ Hz, 1H, aromatic), 7.30 (d, $J=8.0$ Hz, 1H, aromatic), 7.09 (br, 1H, NH), 7.04 (m, 1H, aromatic), 6.96 (m, 1H, aromatic), 4.48 (m, 1H, α $-\text{CH}$ of Trp), 2.97 (m, 6H, 2β $-\text{CH}_2$ of Trp and 4α $-\text{CH}_2$ of En-Boc), 2.04 (t, 3H, α $-\text{CH}_2$ of myristyl $\text{C}=\text{O}$), 1.36 (m, 2H, β $-\text{CH}_2$ of myristyl $\text{C}=\text{O}$), 1.20 (m, 20H, 10 $-\text{CH}_2$ of myristyl chain), 0.85 (t, $J=6.5$ Hz, 3H, $-\text{CH}_3$ of myristyl) (Figure 4.29). ^{13}C NMR (100 MHz, DMSO-d_6 , TMS, 25 °C): δ 172.5, 172.1, 136.5, 127.8, 123.9, 121.2, 118.9, 118.6, 111.7, 110.7, 53.9, 42.8, 41.6, 35.7, 31.7, 29.5, 29.5, 29.4, 29.3, 29.2, 29.0, 28.5, 25.6, 22.5, 14.4 (Figure 4.30). HRMS (m/z): Calculated for $\text{C}_{27}\text{H}_{44}\text{N}_4\text{O}_2$ (M): 457.354 (M + H) $^+$, 479.336 (M + Na) $^+$ Found: 456.911 (M + H) $^+$, 478.873 (M + Na) $^+$ (Figure 4.31).

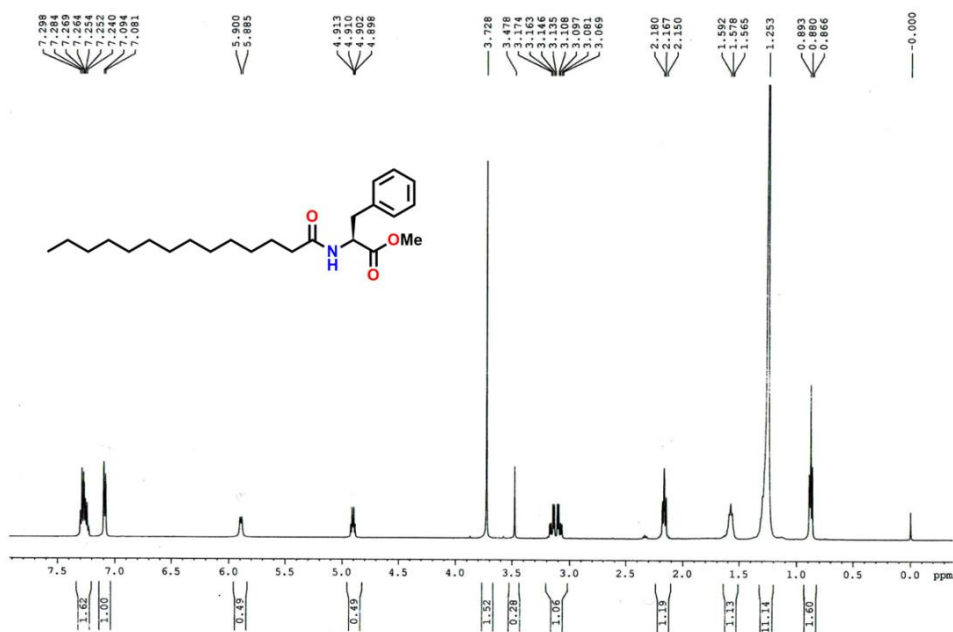


Figure 4.2. ¹H NMR spectrum of C₁₄-Phe-COOMe in CDCl₃.

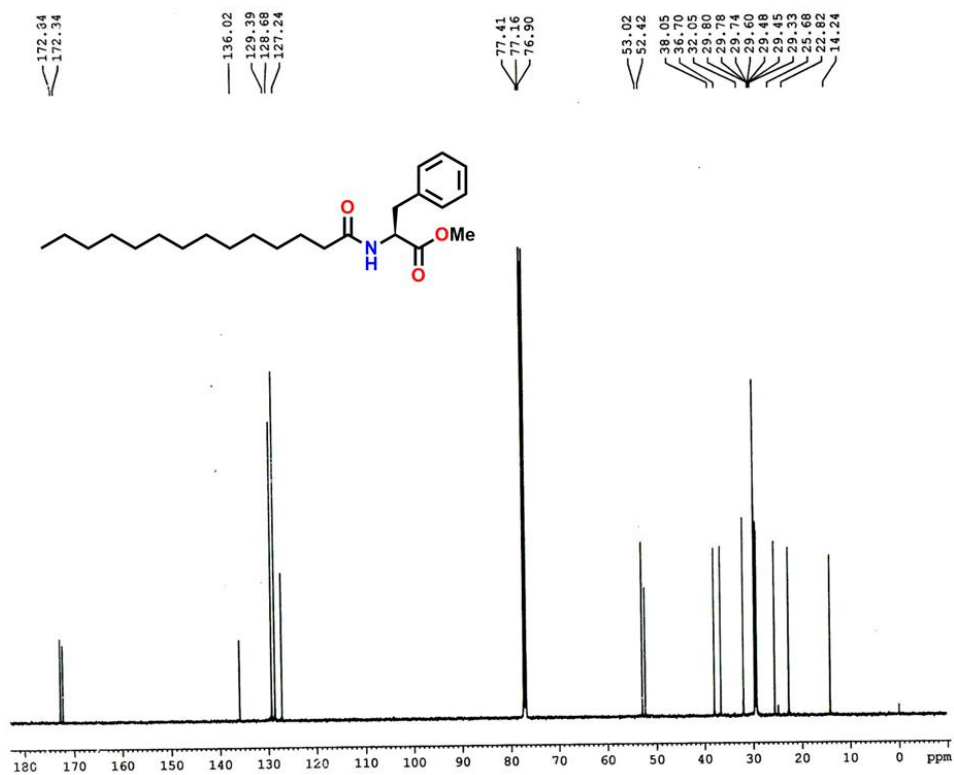


Figure 4.3. ¹³C NMR spectrum of C₁₄-Phe-COOMe in CDCl₃.

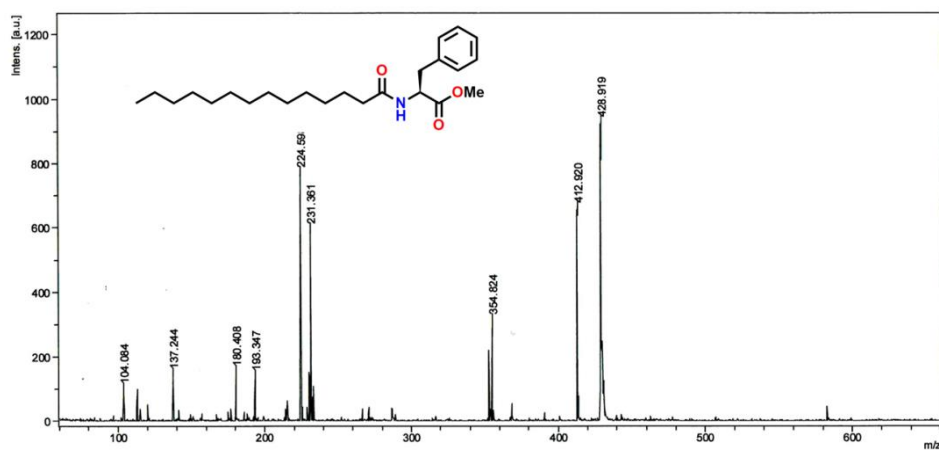


Figure 4.4. MALDI-TOF MS spectrum of C_{14} -Phe-COOMe.

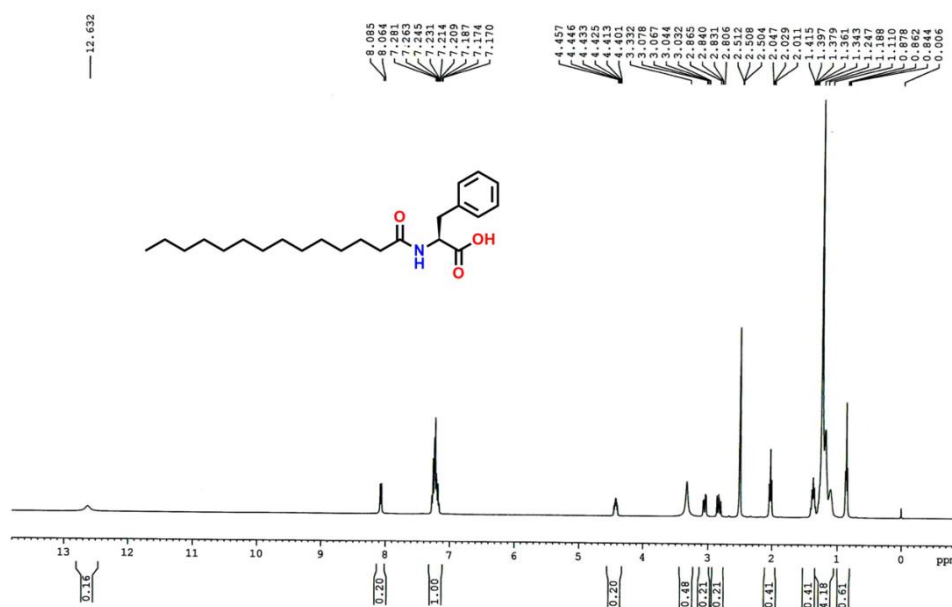


Figure 4.5. ^1H NMR spectrum of C_{14} -Phe-COOH in $\text{DMSO}-d_6$.

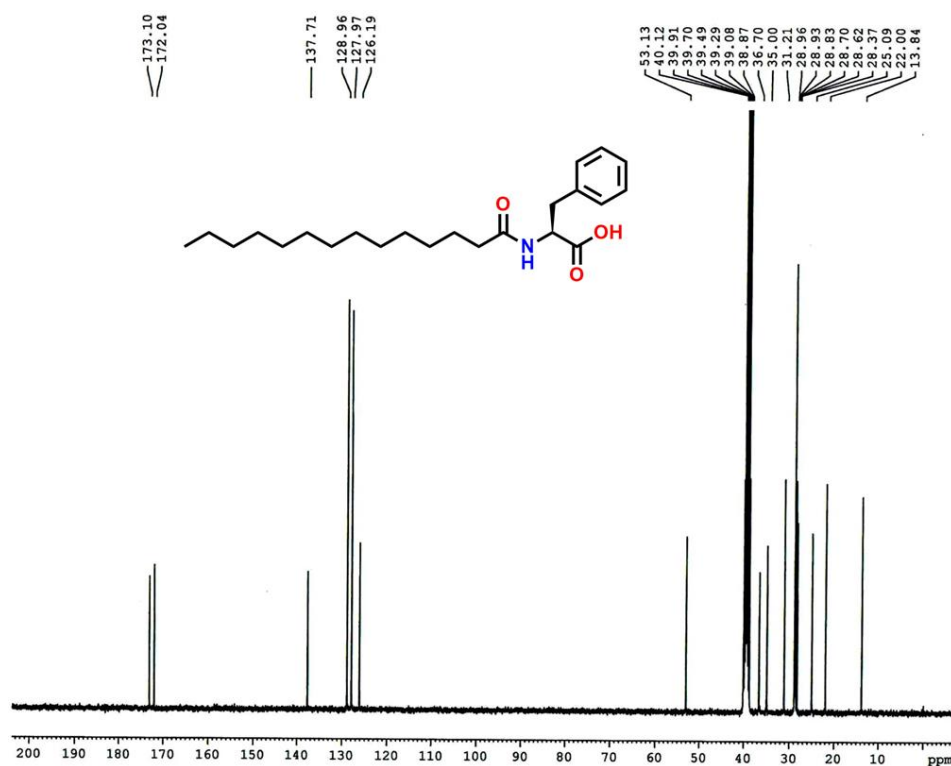


Figure 4.6. ^{13}C NMR spectrum of C_{14} -Phe-COOH in $\text{DMSO-}d_6$.

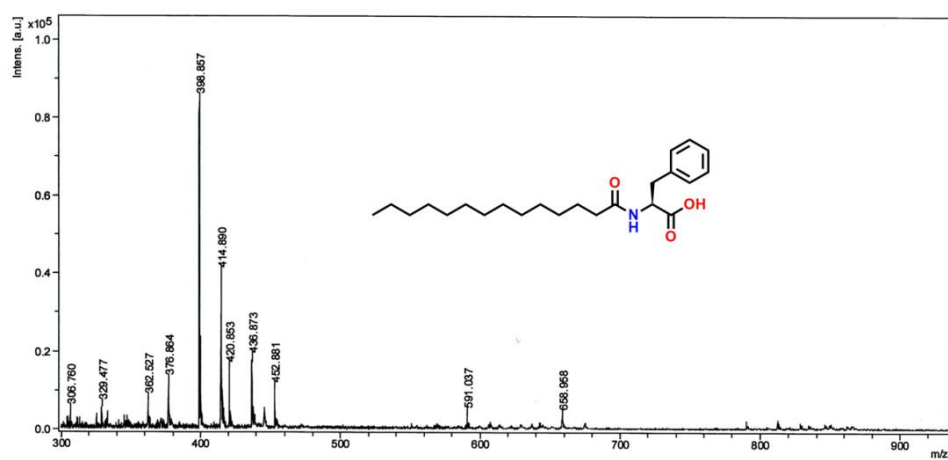


Figure 4.7. MALDI-TOF MS spectrum of C_{14} -Phe-COOH.

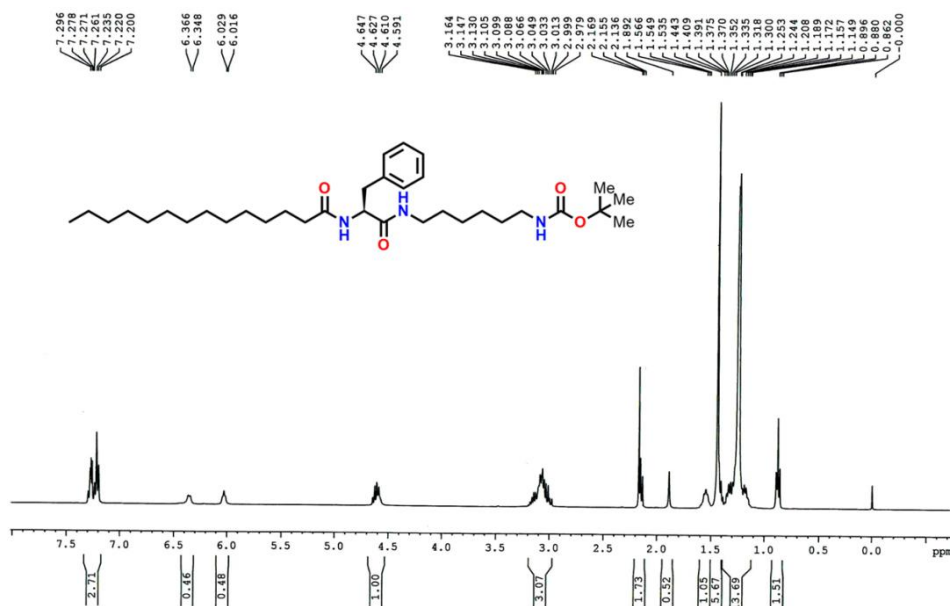


Figure 4.8. 1H NMR spectrum of C_{14} -Phe-Hex-Boc in $CDCl_3$.

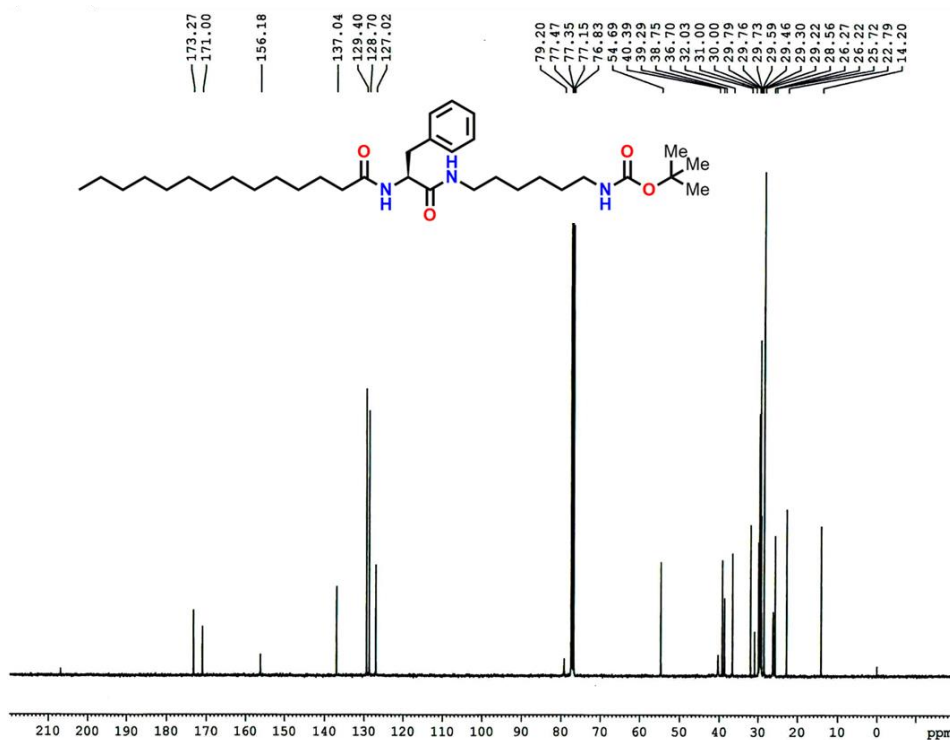


Figure 4.9. ^{13}C NMR spectrum of C_{14} -Phe-Hex-Boc in $CDCl_3$.

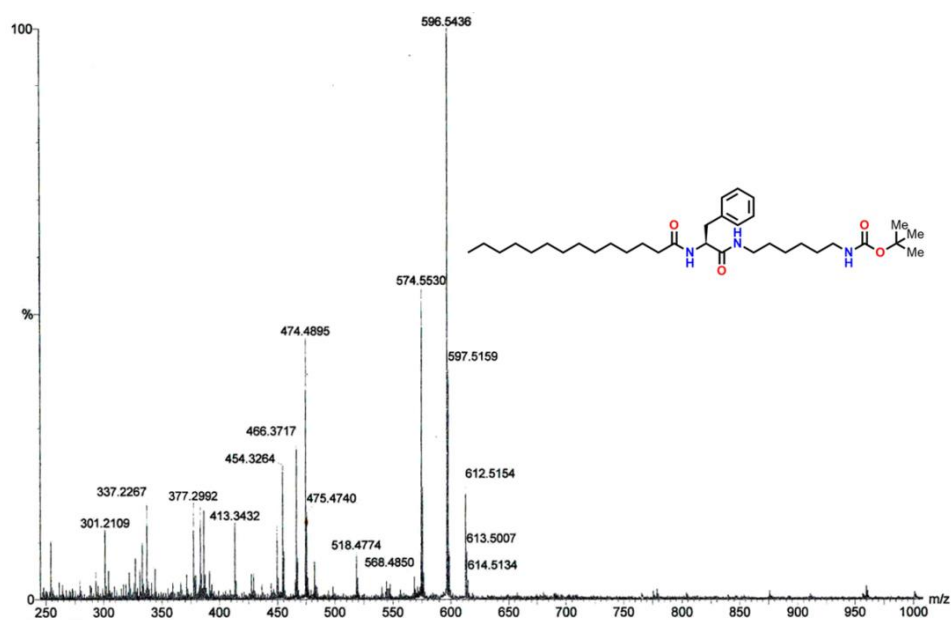


Figure 4.10. HR-MS spectrum of C_{14} -Phe-Hex-Boc.

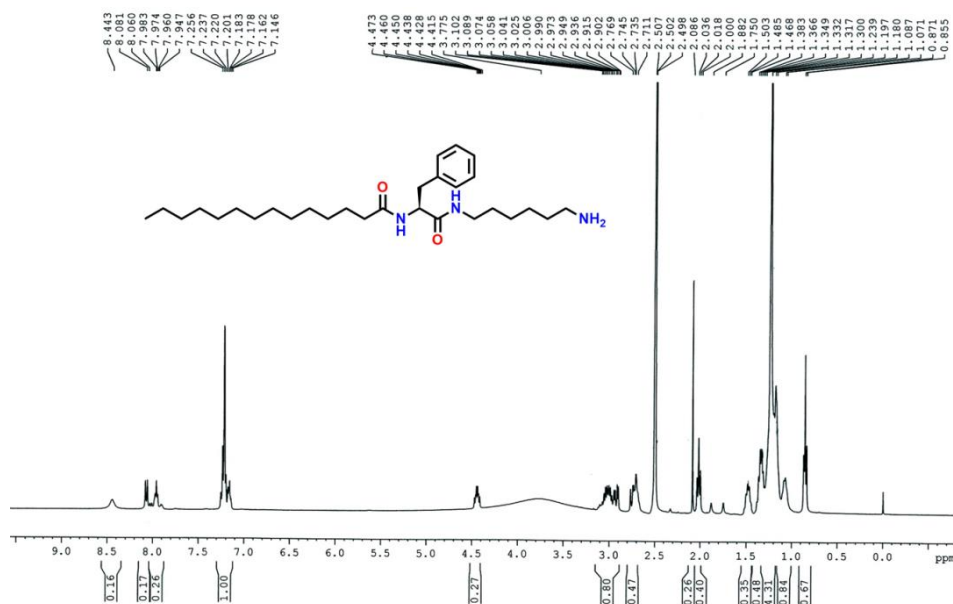


Figure 4.11. 1H NMR spectrum of **P1** in $DMSO-d_6$.

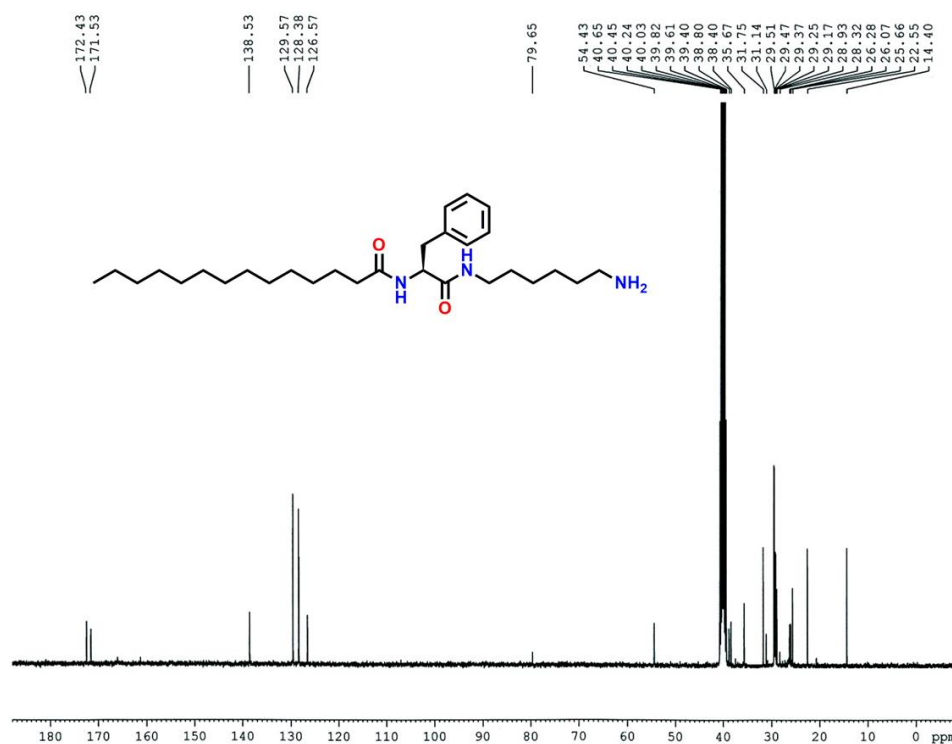


Figure 4.12. ¹³C NMR spectrum of P1 in DMSO-d₆.

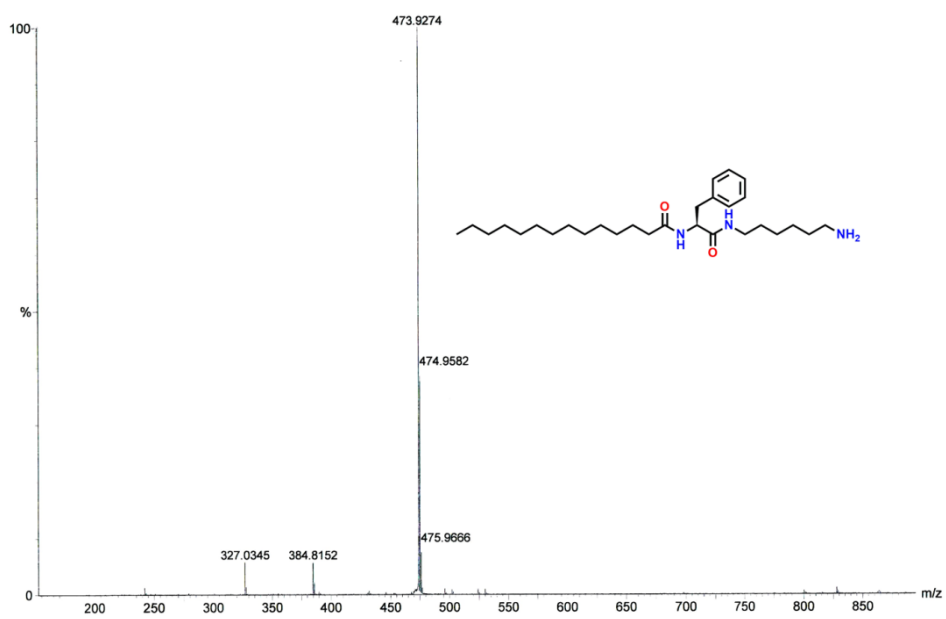
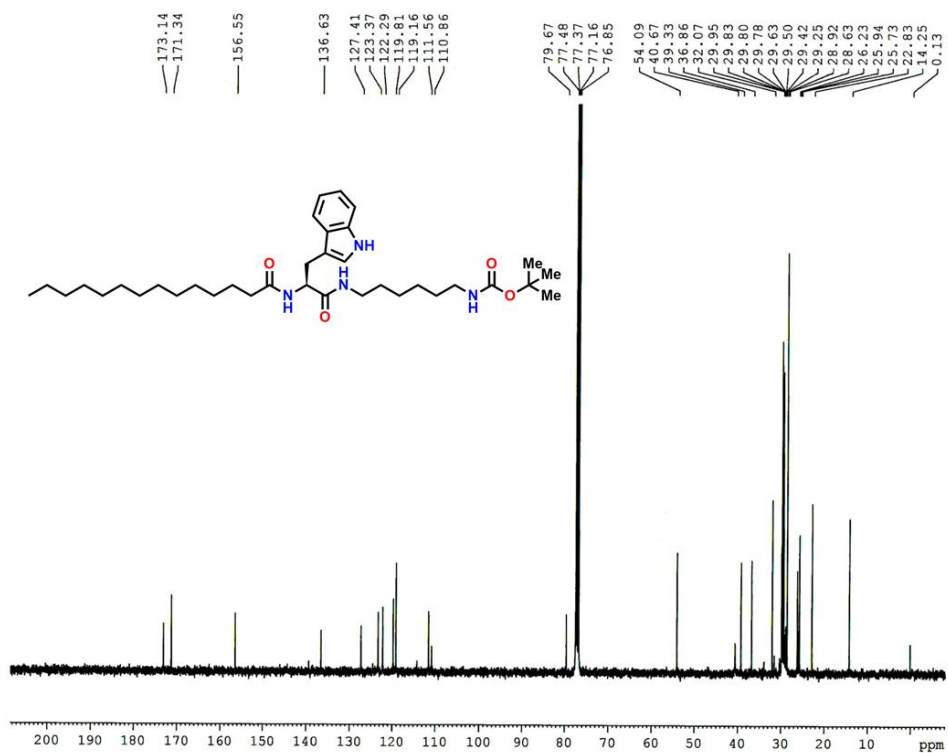
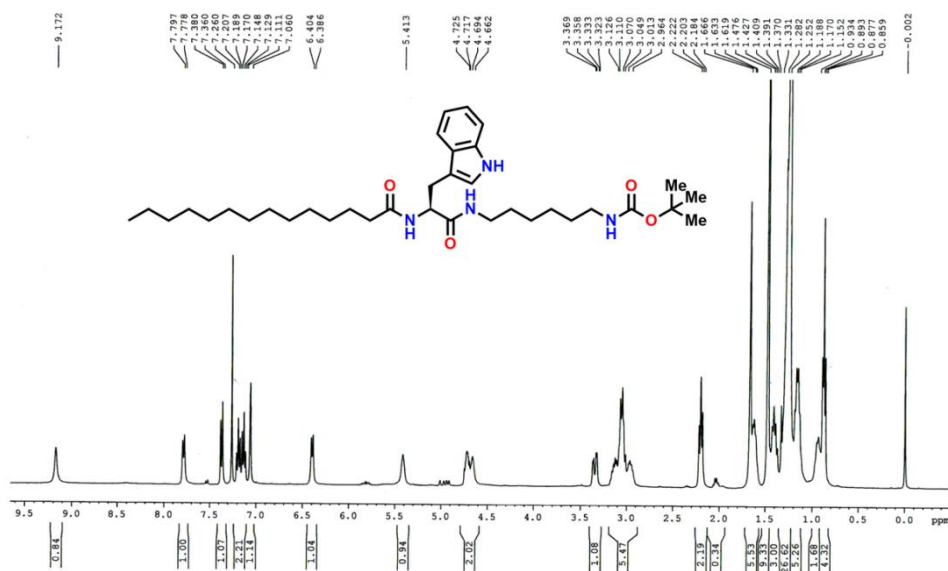


Figure 4.13. HR-MS spectrum of P1.



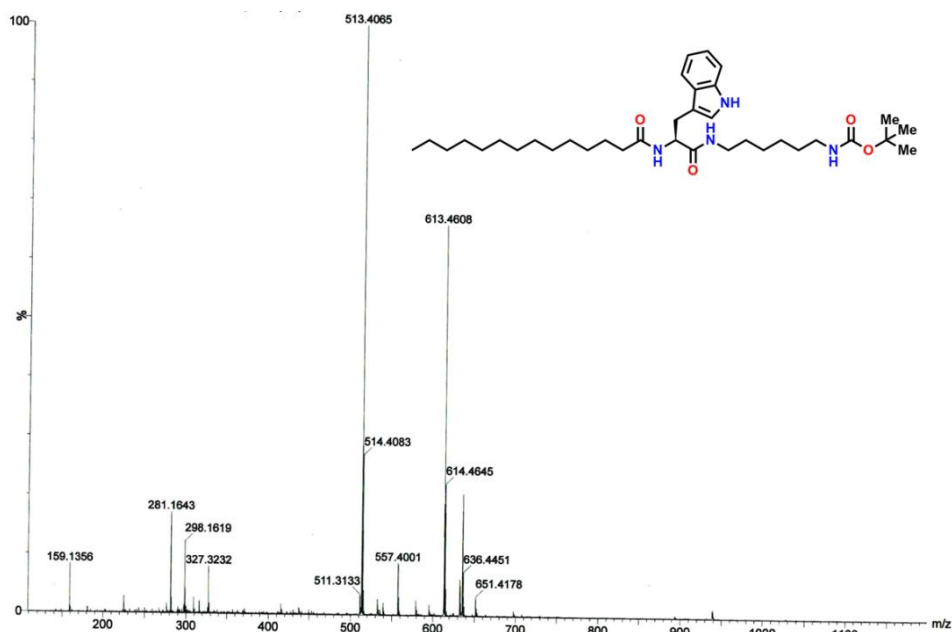


Figure 4.16. HR-MS spectrum of C_{14} -Trp-Hex-Boc.

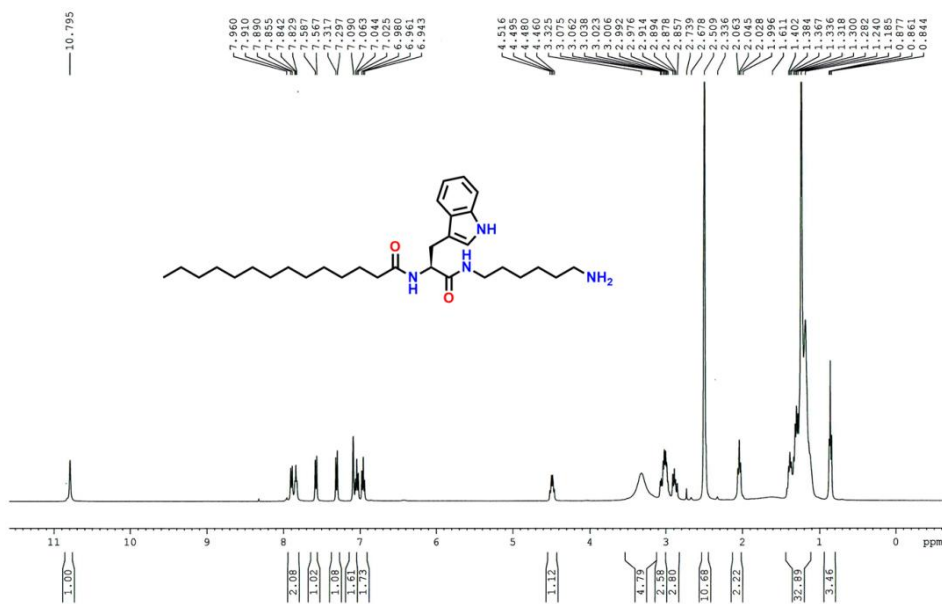
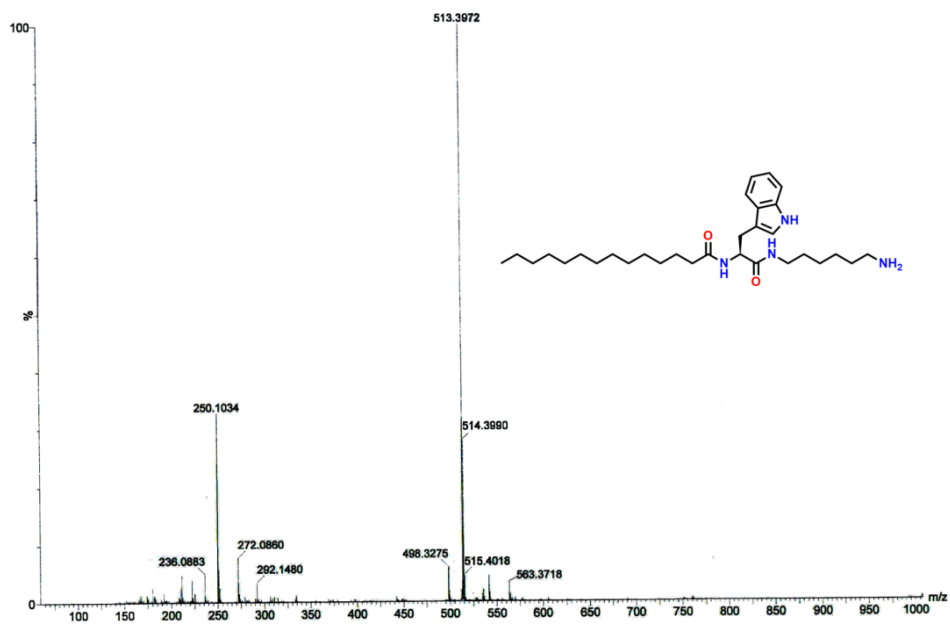


Figure 4.17. ^1H NMR spectrum of P2 in DMSO-d_6 .



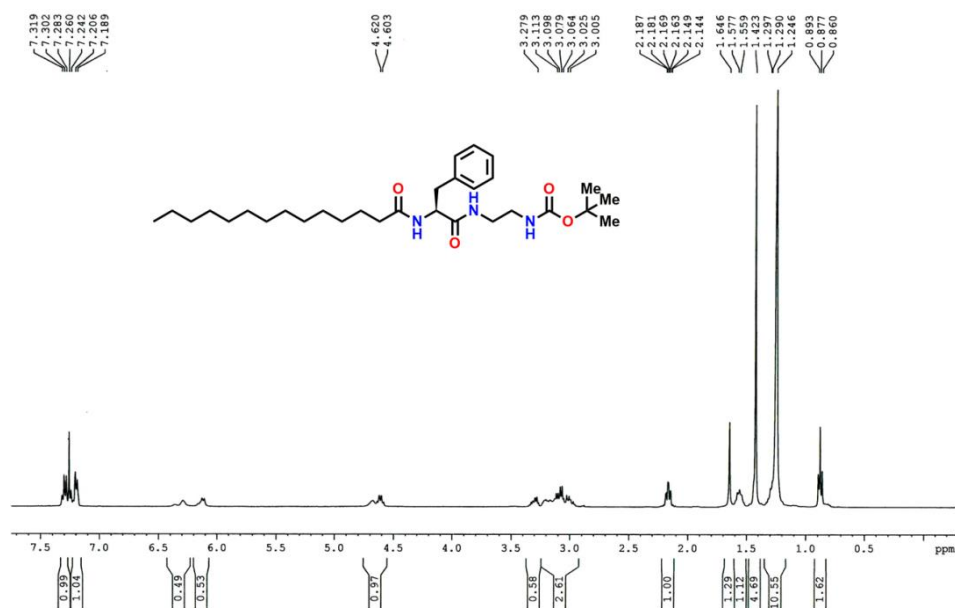


Figure 4.20. ¹H NMR spectrum of **C₁₄-Phe-En-Boc** in CDCl₃.

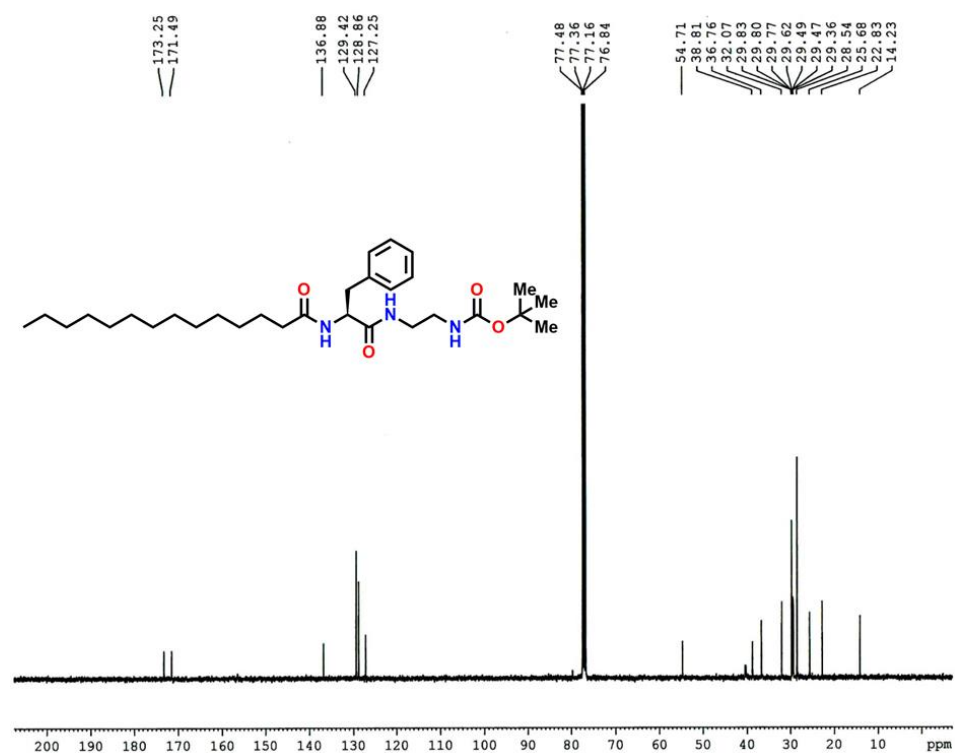
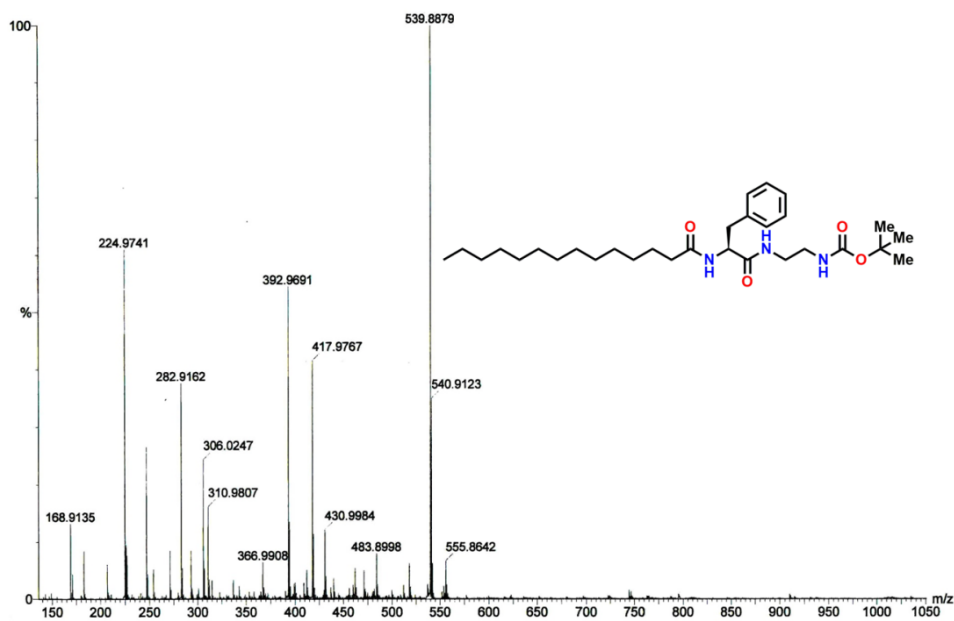
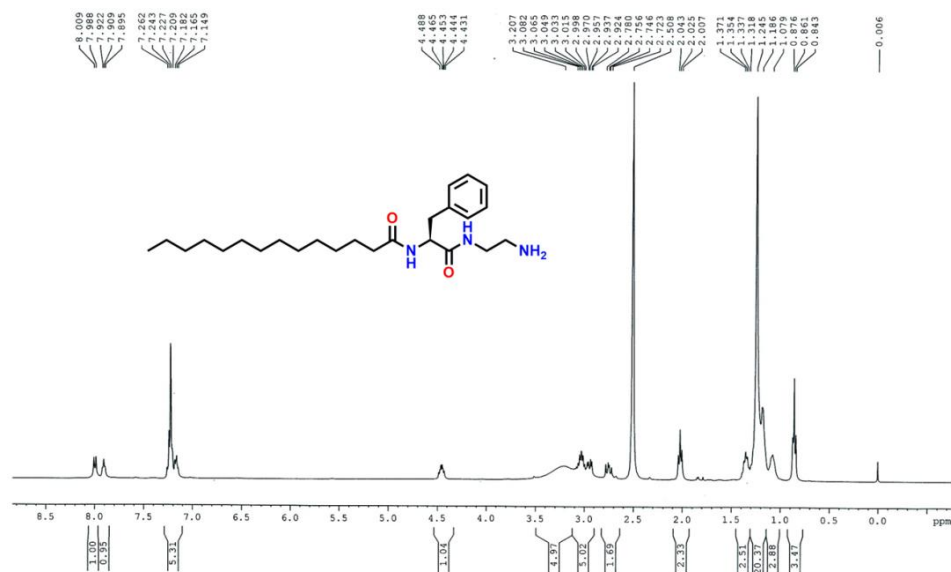


Figure 4.21. ¹³C NMR spectrum of **C₁₄-Phe-En-Boc** in CDCl₃.

Figure 4.22. HR-MS spectrum of C_{14} -Phe-En-Boc.Figure 4.23. 1H NMR spectrum of **P3** in $DMSO-d_6$.

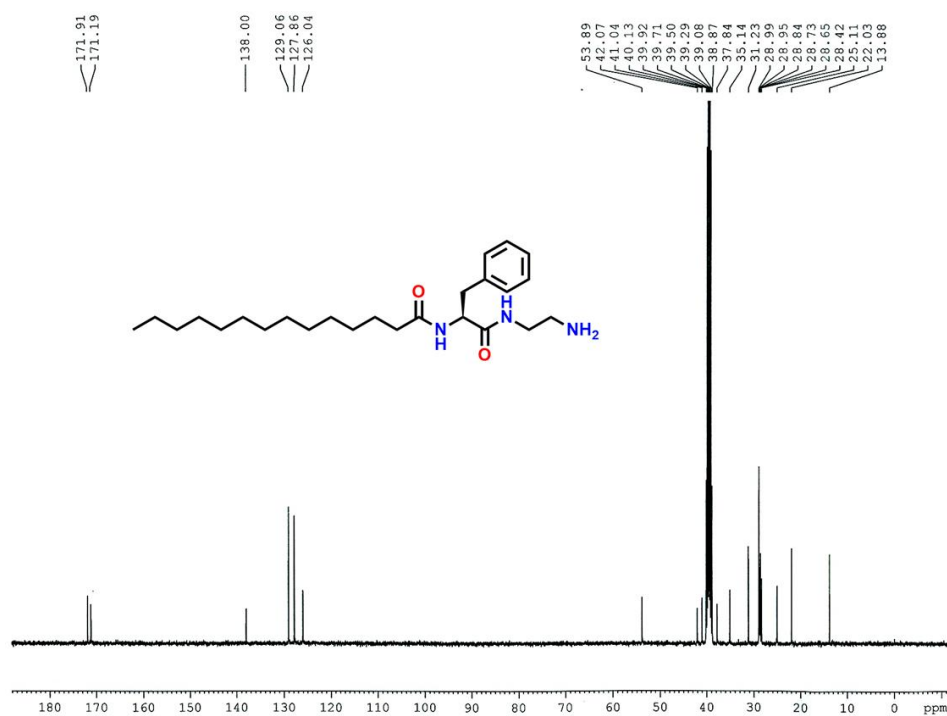


Figure 4.24. ¹³C NMR spectrum of P3 in DMSO-d₆.

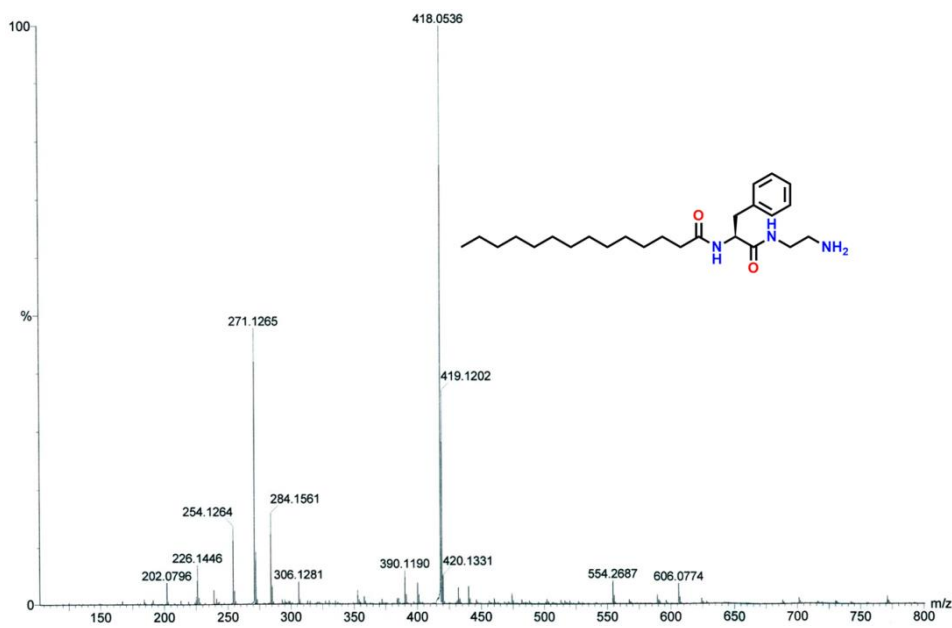


Figure 4.25. HR-MS spectrum of P3.

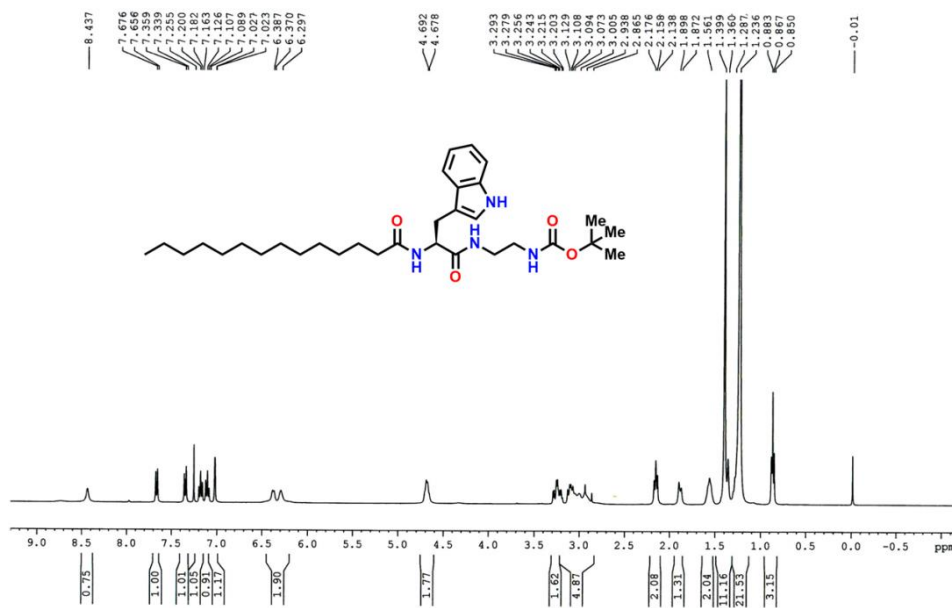


Figure 4.26. ¹H NMR spectrum of *C*₁₄-Trp-En-Boc in CDCl₃.

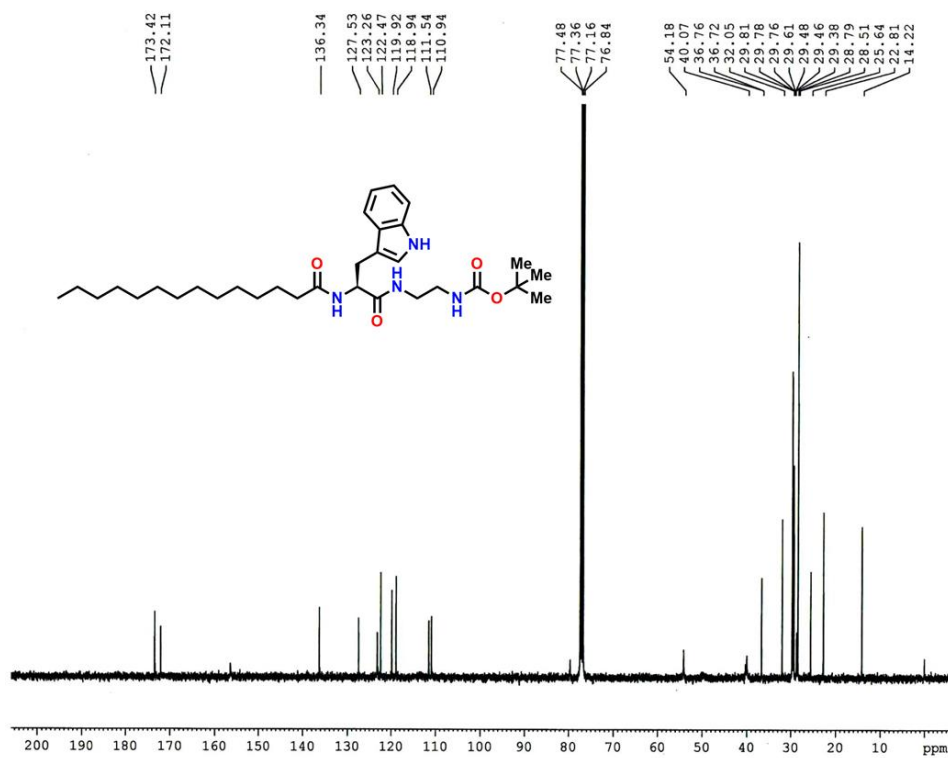


Figure 4.27. ¹³C NMR spectrum of *C*₁₄-Trp-En-Boc in CDCl₃.

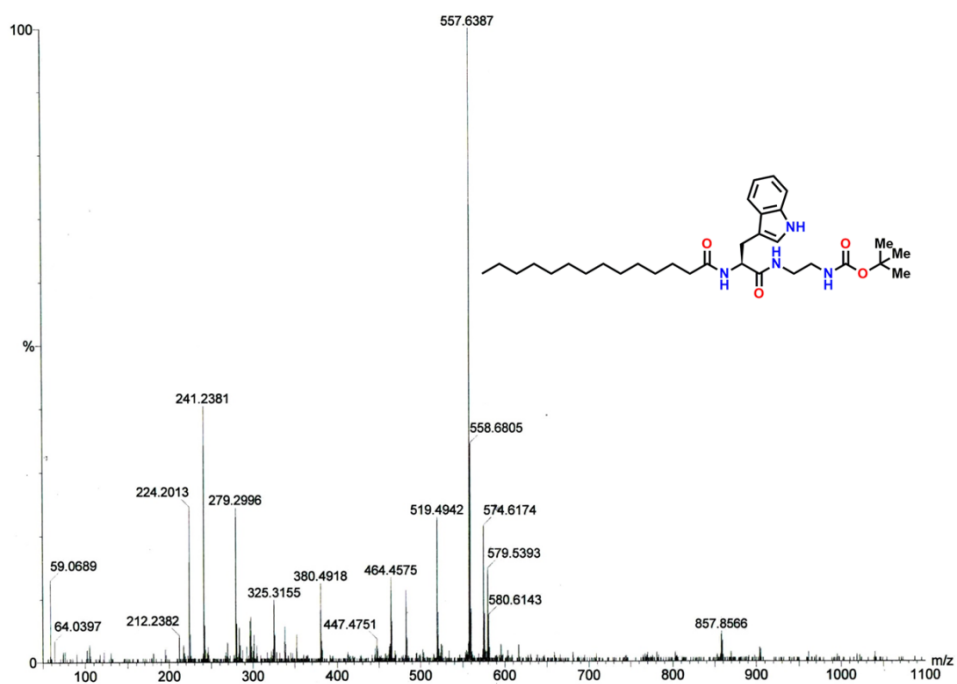


Figure 4.28. HR-MS spectrum of C_{14} -Trp-En-Boc.

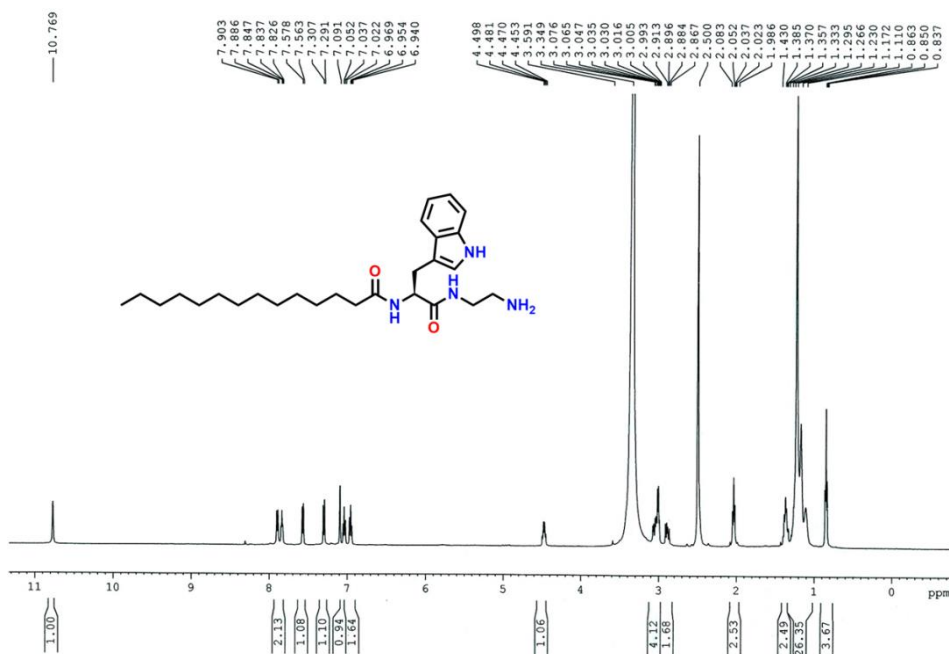


Figure 4.29. 1H NMR spectrum of $P4$ in $DMSO-d_6$.

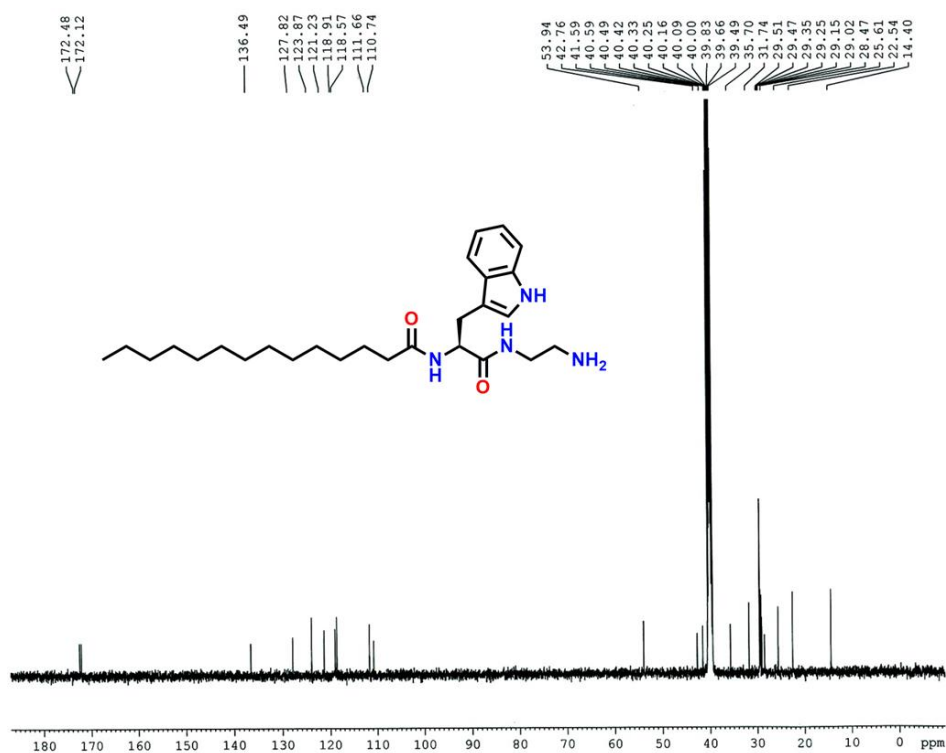


Figure 4.30. ¹³C NMR spectrum of P4 in DMSO-d₆.

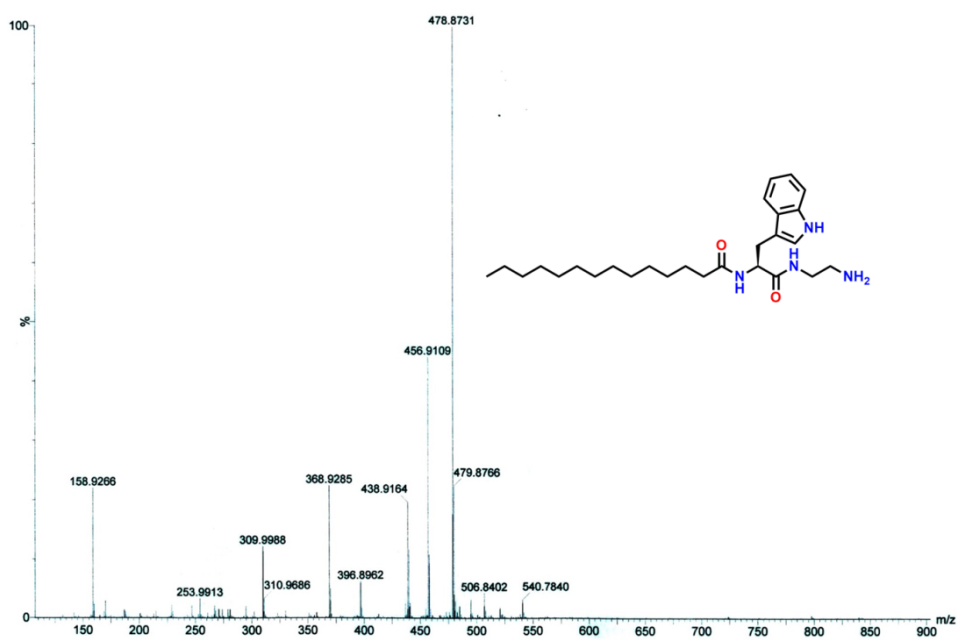


Figure 4.31. HR-MS spectrum of P4.

4.2.4. Instrumentations

NMR Experiments. All NMR studies were carried out on Bruker DPX 400 MHz and Bruker DPX 500MHz spectrometers at 300 K. Compounds concentrations were in the range 1–10 mM in CDCl₃ or DMSO-d₆.

Mass Spectrometry. Mass spectra were recorded on a Q-ToF microTM (Waters Corporation) mass spectrometer by positive mode electro spray ionisation process.

MALDI-TOF MS Study. The MALDI-TOF MS analyses were done using Bruker Daltonics flex Analysis mass spectrometer.

FT-IR Spectroscopy. FTIR spectroscopy was performed using Nicolet 380 FT-IR spectrophotometer (Thermo Scientific). FTIR spectra were recorded using a cell with CaF₂ windows.

Transmission Electron Microscopy (TEM). TEM images were recorded on a JEM 2010 electron microscope at an accelerating voltage of 200 KV. During HR-TEM experiment, 20 µL of gel (concentration of gelator is 31.68 mM) was taken in a screw cap vial and diluted with 2 mL milli-Q water. Then, a drop of dilute solution was placed on a carbon coated copper grid (300 mesh) and dried by slow evaporation. The grid was then allowed to dry in a vacuum for two days and then images were taken.

Cryogenic Transmission Electron Microscopy (Cryo-TEM). Cryo-TEM images were recorded on a JEOL JEM-210 PLUS Cryogenic transmission electron microscope at an accelerating voltage of 200 KV.

Atomic Force Microscopy (AFM). An Agilent Technologies 5500 ILM Pico plus AFM system with a piezo scanner maximum range of 100 µm was used for this experiment. All the images were obtained in contact mode by using micro-fabricated silicon cantilevers of 450 µm length with a nominal spring force constant of 0.02–0.77 N/m from Nano sensors (Neuchatel, Switzerland). The cantilever oscillation frequency was tuned to resonance frequency, 6–21 kHz. Images were processed by using Pico view 1.12 version software (Agilent Technologies, Santa Clara, CA, USA). Image manipulation was done through Pico Image Advanced version software (Agilent Technologies).

Small Angle X-Ray Scattering (SAXS). SAXS measurements on xerogels were performed using a Bruker Nanostar instrument using CuKα radiation and a Vantec 2000 detector. The sample-to-detector distance was 1.07 m. The $q=4\pi\sin\theta/\lambda$ (scattering angle 2θ) scale was calibrated using silver behenate.

Samples were mounted in quartz capillaries. In situ SAXS measurements on hydrogels were performed on beamline B21 at Diamond Light Source (Harwell, UK). Data was collected using a Dectris EIGER 4M detector at a fixed camera length of 3.9 m with a wavelength $\lambda = 1 \text{ \AA}$. Gels were mounted in a custom-designed enclosed gel cell holder for gels and pastes. All measurements were performed at 20 °C.

Powder X-ray Diffraction. X-ray diffraction measurements on the xerogel were carried out by placing the sample on a glass plate. Experiments were carried out using an X-ray diffractometer (Bruker D8 Advance) with a parallel beam optics attachment. The instrument was operated at 35 kV voltages and 30 mA current using Ni-filtered $\text{CuK}\alpha$ radiation and the instrument was calibrated with a standard silicon sample before use. Samples were scanned from 2° to 30° (2 θ) in the step scan mode (step size 0.03°, present time 2s) and diffraction patterns were recorded using a scintillation scan detector.

Rheological Study. Rheology experiments were performed with a SDT Q Series AR 2000 advanced rheometer (TA Instruments) using cone-plate geometry in a Peltier plate.

4.3. Results and discussion

4.3.1. Gelation Study. The amphiphilic gelators consist of a natural aromatic amino acid residue such as L-phenylalanine or L-tryptophan, long fatty acyl hydrophobic chain, and a terminally placed polar head, containing $-\text{NH}_2$ as a functional group. In this regard, four amphiphiles, **P1**, **P2**, **P3**, and **P4**, (Figure 4.1a), were synthesized by introducing two different amino acids L-phenylalanine or L-tryptophan with the variation of the polar $-\text{NH}_2$ head containing a diamine derivative. Figure 4.1a shows the chemical structures of these gelator molecules. The aromatic amino acid, L-phenylalanine or L-tryptophan, was selected to promote the π - π stacking interaction between the gelator molecules. The hydrophobic fatty acyl chains were introduced to promote van der Waals and hydrophobic interactions, and the terminally located polar amine ($-\text{NH}_2$) group as a head group was used to increase the polarity of the gelator amphiphile. Moreover, the gelator molecules were designed in a way so that they can quickly form a stable hydrogel in the presence of a polar aqueous solvent. It was found that the gelators **P1**, **P2**, and **P4** form stable hydrogels in the presence of ultrapure water (milli-Q)(pH 6.67) at a concentration of 0.65–

1.20% w/v of the gelator molecule (Figure 4.1). The gelator molecule **P3** does not form a hydrogel in ultrapure water alone, but it exhibits a viscous aggregated solution. However, **P3** forms a hydrogel in 2% v/v DMSO mixed in water (Figure 4.1b and c). During the experimental analysis, the viscous solution of the gelator **P3** has been used for further experiments to keep the environment same for all these gelator amphiphiles.

4.3.2. Thermal Stability of Gels. Gel-to-sol transition temperatures (T_{gel}) of these hydrogels (**P1**, **P2**, and **P4**) were measured to determine the thermal stability of these hydrogels. The gel transition temperature (T_{gel}) was highest for **P2** and lowest for **P1**, keeping the gelator concentration 31.68 mM fixed. As mentioned above, the amphiphile **P3** does not form a hydrogel in ultrapure water but forms a viscous solution. However, **P1** with a longer terminal diamine unit did form a hydrogel. The L-tryptophan-based amphiphilic gelators **P2** and **P4** show higher thermal stability than **P1**. The gel-to-sol transition temperature shows the following trend: **P2** > **P4** > **P1** (Table 4.1). It is evident that the gelator **P2** with the highest van der Waals interaction and strong π - π interaction shows the best-ordered packing structure compared to **P1** and **P4**. The gelator **P4** forms a more robust hydrogel than that of **P1**. This may be due to the fact that the L-tryptophan residue shows better π - π interactions than that of the L-phenylalanine containing amphiphiles (**P1** and **P3**) as L-tryptophan has a greater π -electron containing surface area than L-phenylalanine.

4.3.3. Rheological Study. Rheological experiments were carried out at a constant concentration of 31.68 mM of gelators. The frequency sweep experiment was performed at a fixed strain of 0.1% for all the amphiphile gelators. The two moduli, storage modulus (G') and loss modulus (G''), have been plotted against the angular frequency (ω) ranging from 0.05 to 100 rad s^{-1} . The storage modulus (G') is always greater than that of the loss modulus (G''), indicating a stable gel formation. Rheological studies have been performed for gelators **P1**, **P2** and **P4** at a fixed concentration of 31.68 mM for all cases (**P3** does not form a hydrogel). As discussed above, the stability order of gels is **P2** > **P4** > **P1** corroborated with T_{gel} values, which is also reflected in the moduli measured in the frequency sweep experiments. The storage moduli of **P1**, **P2**, and **P4** are 0.28×10^2 Pa, 2.34×10^4 Pa and 1.31×10^4 Pa, respectively, at a constant strains of 0.1% and at a fixed concentration 31.68 mM of the individual gelator (Figure 4.32). The amplitude sweep experiments also show the linear viscoelastic region (LVE)

limits of gels. The hydrogels formed by the gelator amphiphiles **P1**, **P2**, and **P4** show a tolerance limit from 0.01% to 0.72%, 0.01% to 0.98%, and 0.01% to 2.18% of the shear strain (Figure 4.33), respectively. The cross-over between G' and G'' took place when 20%, 3.48%, and 7.85% of the shear strain were applied to the **P1**, **P2**, and **P4** hydrogels, respectively. Thus, the mechanical stability follows the thermal stability of these hydrogels in the order **P2** > **P4** > **P1**.

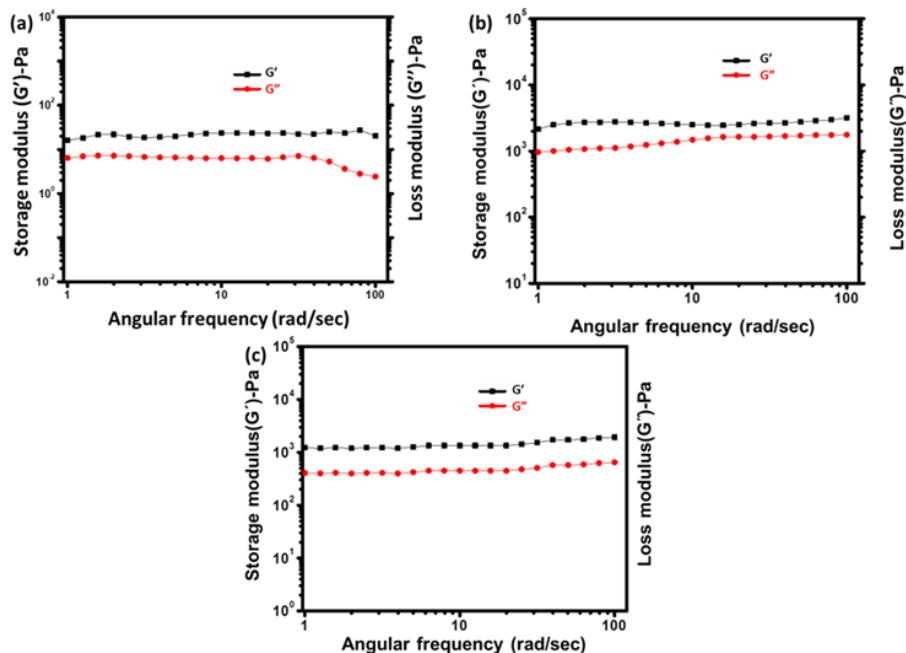


Figure 4.32. Frequency sweep analysis of hydrogels obtained from (a) **P1**, (b) **P2** and (c) **P4** amphiphilic gelators.

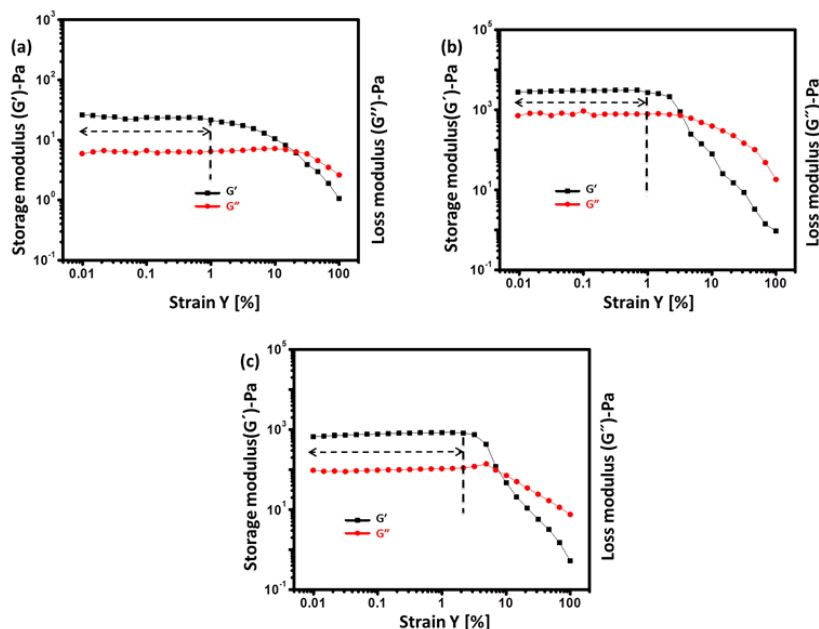


Figure 4.33. Amplitude sweep analysis of hydrogels obtained from (a) **P1**, (b) **P2** and (c) **P4** amphiphilic gelators.

4.3.4. Morphological Study. High-resolution transmission electron microscopy (HR-TEM) imaging was used to probe the morphological features of these hydrogels (Figure 4.34). The L-phenylalanine-containing gelator **P1** forms a nano-fibrous network structure in the gel, whereas **P3** forms a sheet-like morphology in the viscous solution. The morphologies differ due to the distinct states of the solutions. The morphologies differ due to the distinct states of the solutions. The L-tryptophan-containing amphiphilic gelators **P2** and **P4** form hydrogels and the morphology comprises twisted nano-fibres (Figure 4.34). HR-TEM images show the cross-linked nano-fibrous network structure in the hydrogels. The fibres are several nanometres in length, and the width varies from 17.10 nm to 30.67 nm, with an average width of 23.24 nm. However, the majority of these nano-fibres have a width between 20 nm and 25 nm (Figure 4.34). Even the Cryo-TEM (Cryogenic transmission electron microscopic) images have been taken for the amphiphiles **P2** hydrogel and **P3** viscous solution, to know whether any change in morphology takes place in HR-TEM in the dry state or not. However, the Cryo-TEM images show that **P2** and **P3** have similar morphological features (Figure 4.34) compared to their respective dried state morphological HR-TEM images (Figure 4.34b and c).

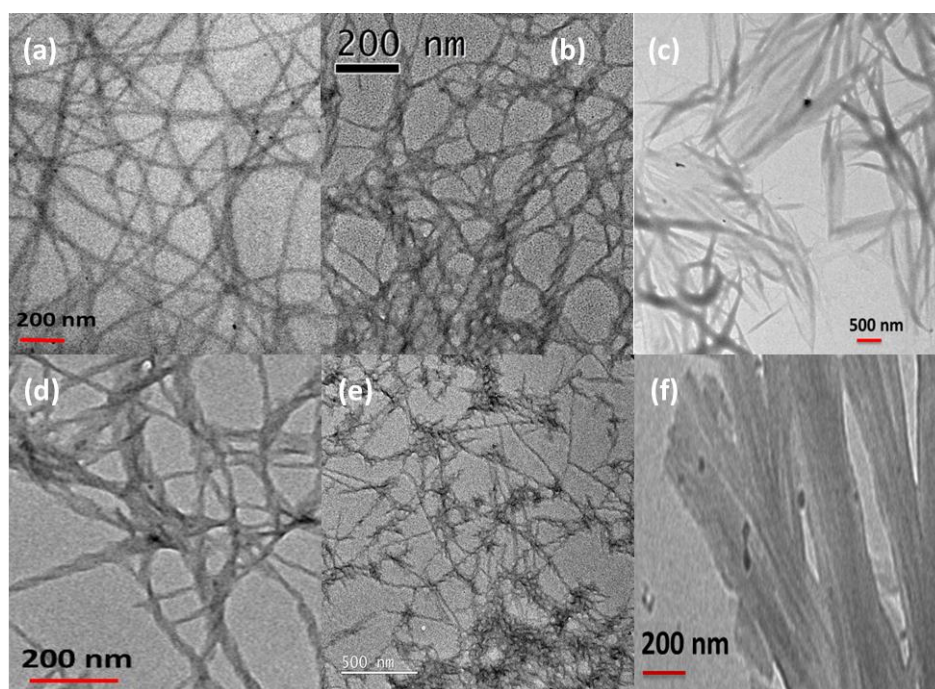


Figure 4.34. HR-TEM images of dried (a) hydrogel of amphiphile **P1**, (b) hydrogel of amphiphile **P2**, (c) viscous solution of amphiphile **P3**, and (d) hydrogel of amphiphile **P4** in presence of ultrapure water. Cryo-TEM image of (e) hydrogel obtained from the **P2** amphiphile, and (f) aggregated viscous solution obtained from amphiphile **P3** in presence of ultrapure water.

4.3.5. FTIR Analysis. Fourier transform infrared (FT-IR) spectroscopy was used to understand non-covalent interactions among the gelator molecules in the gel state during self-assembly. The FTIR spectra of dried gels and the aggregated solution for amphiphilic gelators contain four signature peaks at 3466 cm^{-1} , 3298 cm^{-1} , 1648 cm^{-1} , and 1556 cm^{-1} (Figure 4.35). The peaks at 3298 cm^{-1} and 1556 cm^{-1} correspond to the hydrogen bonding N–H stretching and bending frequencies, respectively. The strong signal at around 1648 cm^{-1} is due to the amide C=O stretching frequency of the aggregated gelator molecules. Lastly, the peak at 3466 cm^{-1} is due to the non-hydrogen bonded N–H stretching frequency of the gelator molecules. The broad peak at 3466 cm^{-1} with the highest intensity indicates the presence of mainly free N–H in the aggregated state of **P3**. Moreover, the minimum intensity of the 3466 cm^{-1} peak for **P2** indicates that most N–H units are involved in the H-bond formation in the gel state. These data are consistent with the thermal stability measurement data, as the hydrogel formed by the **P2** gelator was the strongest one. The FTIR data reveal that hydrogen bonding is consistent with a sheet-like structure during the self-assembly of gelator molecules in the gel state (Figure 4.35).

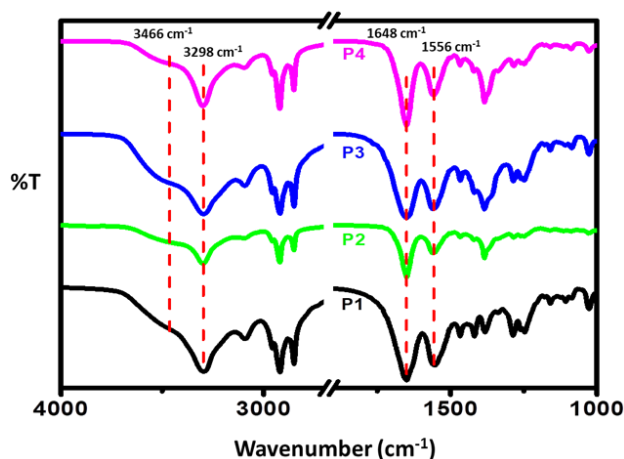


Figure 4.35. FTIR spectra of dried hydrogels (**P1**, **P2**, and **P4**) and viscous aggregated solution (**P3**).

4.3.6. XRD Analysis. The wide-angle X-ray diffraction (XRD) study was performed for dried gels (**P1**, **P2**, and **P4**) and a dried sol (**P3**), respectively, to understand the non-covalent interactions between the amphiphilic gelator molecules. This study also helps us to understand the inter-sheet and inter-planer distances between the amphiphilic gelators. The d-spacing values between 3.69 and 3.78 Å peaks are due to the π – π stacking interactions between the aromatic residues present in the respective amphiphiles in their gel and viscous solution

states.²³ The peaks corresponding to 2θ in the range 18.20° – 17.62° ($d = 4.74$ – 4.90 Å) are due to the formation of a β -sheet-like structure by the amphiphilic gelators in their aggregated states (Figure 4.36).²⁷ A peak with a d -spacing of 9.12 – 9.20 Å ($2\theta = 9.43$ – 9.35°) suggests the formation of a β -sheet-like alignment of these gelators in their respective gel state. The d -spacing values in the range 4.74 – 4.90 Å correspond to the distance between the peptide chains formed by the gelator molecules within a β -sheet-like backbone structure, while the peaks in the range 9.12 – 9.20 Å can be attributed to the distance between two β -sheet layers formed in the gel state (Figure 4.37).²⁵

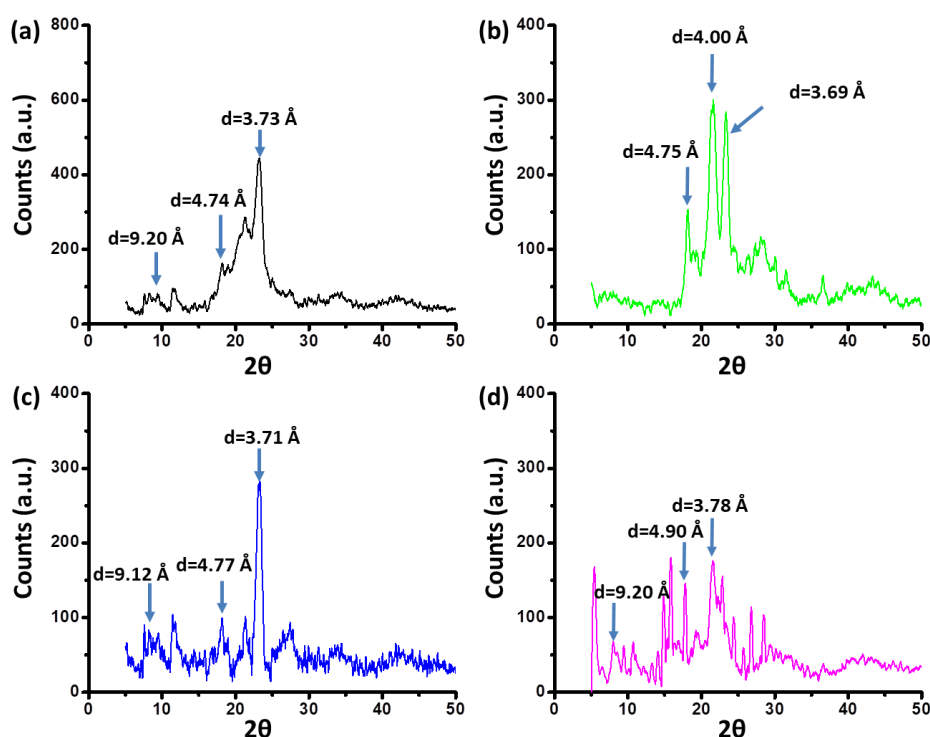


Figure 4.36. Wide angle XRD pattern of xerogels obtained from (a) hydrogel of **P1**, (b) hydrogel of **P2**, and (d) hydrogel of **P4** and (c) dried viscous aggregated solution of **P3**.

4.3.7. SAXS Analysis. Small-angle X-ray scattering (SAXS) has been used to obtain more insight into the supramolecular network structure formed by the gelator molecules in their respective gel states or aggregated states. Similar SAXS patterns for **P1**, **P2**, and **P4** gelator amphiphile in their gel state and the **P3** amphiphile in its aggregated form (Figure 4.38) indicate the formation of a similar type of morphology in their respective gel/aggregated state. The d -spacing values of **P1**, **P2**, and **P4** amphiphilic gelators in their gel state are 35.81 Å, 40.28 Å, and 34.95 Å, respectively (Figure 4.39). At the same time, **P3** shows a d -spacing value of 38.85 Å in its aggregated state (Figure 4.39b).

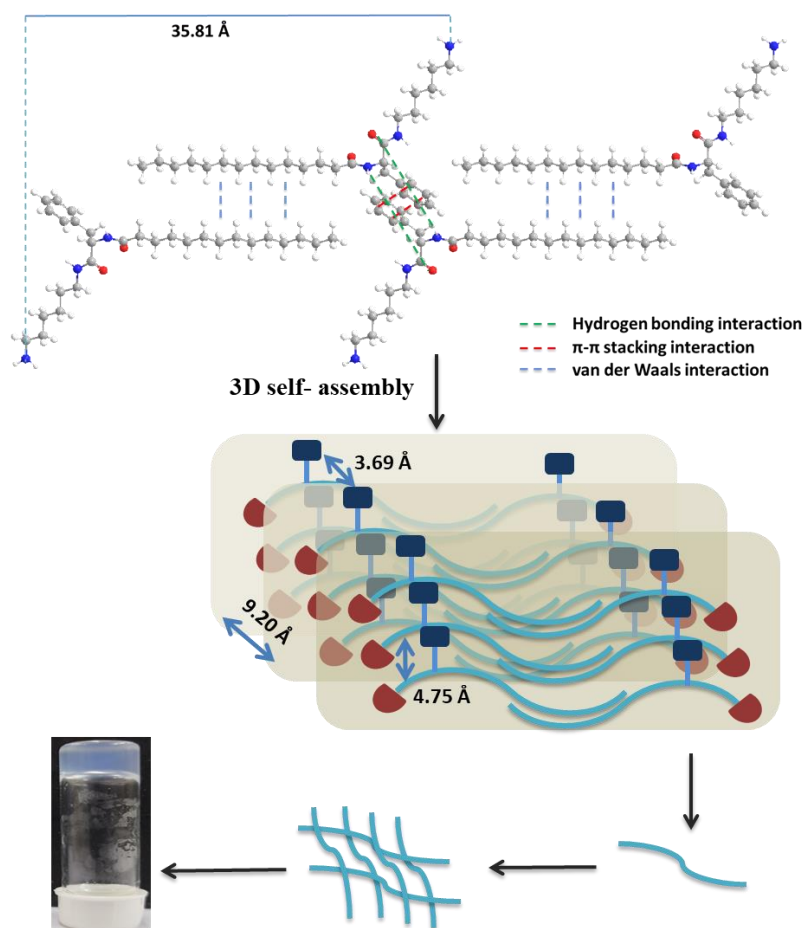


Figure 4.37. A tentative model of intermolecular arrangements in the hydrogel obtained from **P1** derived from FTIR, XRD, and SAXS data.

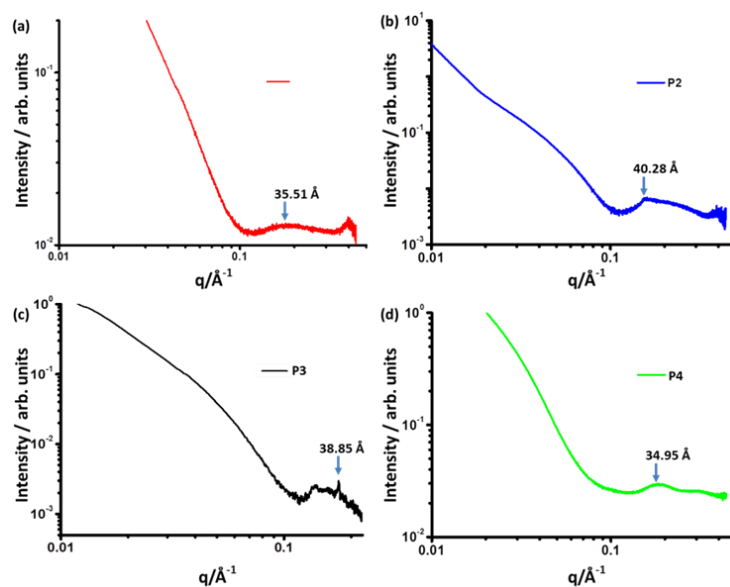


Figure 4.38. SAXS data of (a) **P1**, (b) **P2**, and (d) **P4** hydrogelators in their respective gel states and (c) **P3** amphiphile in its aggregated state.

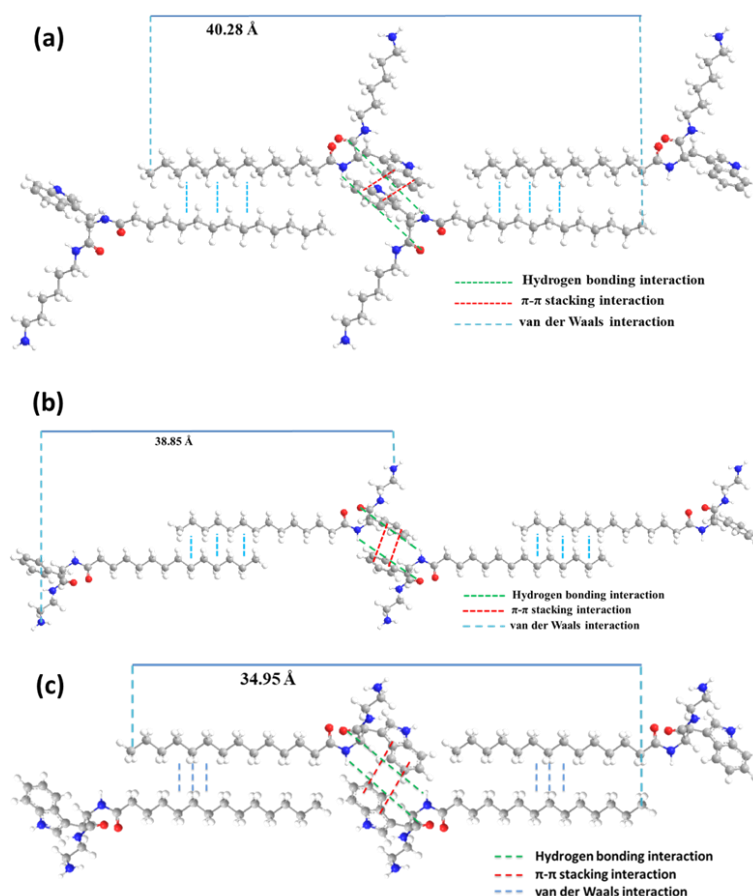


Figure 4.39. A tentative model of intermolecular arrangements in the hydrogel obtained from (a) **P2**, (b) **P3**, and (c) **P4** hydrogelator derived from SAXS, FTIR, and XRD data.

The amphiphilic gelator **P2** shows a d-spacing value of 40.28 Å (Figure 4.39), which is higher than a molecular length of 26.75 Å but smaller than twice this value, 53.50 Å (Figure 4.38), indicating that the molecules are interdigitated. Thus, a tentative molecular model has been constructed based on the FTIR, XRD, and SAXS data (Figure 4.37).

4.3.8. Antibacterial Study. Most of the reported natural peptide antibiotics generally contain N-terminal L-lysine and/or L-arginine.²⁹ Reports also demonstrate the antibacterial activity of cyclicpeptides.^{35,36} Li and co-workers report that the L-tryptophan-based self-assembling peptide shows a strong interaction with the lipid membrane of bacteria, which led to the death of *E. coli* and *S. aureus* bacteria.¹² Also, L-tryptophan is present in various classes of antimicrobial peptides.⁵⁴ But, in this report, the lack of the antibacterial activity of L-tryptophan-based amphiphilic gelators makes this paper more exciting. Interestingly, some of the amphiphilic gelators, **P1** and **P3**, were highly active against both Gram-positive and Gram-negative bacteria. Antibacterial activities

for the viscous solution of the amphiphile **P3** and hydrogels **P1**, **P2**, and **P4** were investigated for different kinds of pathogenic bacteria, such as Gram-positive *B. subtilis* and *S. aureus* and Gram-negative *E. coli* and *P. aeruginosa* using the agar well diffusion method. As shown in Figure 4.40, L-phenylalanine gelators show very high activity against both bacteria. Both of these amphiphiles (**P1** and **P3**) were highly active against Gram-positive bacteria *B. subtilis* and Gram-negative bacteria *E. coli* and *P. aeruginosa*. Both **P2** and **P4** amphiphiles were dormant against all four bacteria used in this experiment (Figure 4.40). **P2** and **P4** were inactive even at higher 650 mg mL^{-1} concentrations. The inhibition zone formed by the amphiphiles **P1** and **P3** in the screening test proves the antibacterial activities of the **P1** hydrogel and **P3** for the viscous solution. The zone of inhibition studies using amphiphiles **P1** and **P3** indicate sufficient inhibition zones for these compounds to be classed as antibiotics. The zone of inhibition diameters for **P1** against *B. subtilis*, *P. aeruginosa*, and *E. coli* were 22 mm, 26 mm, and 20 mm, respectively (Table 4.2). For **P3**, the zone of inhibition diameters against *B. subtilis*, *P. aeruginosa*, and *E. coli* were 22 mm, 28 mm,

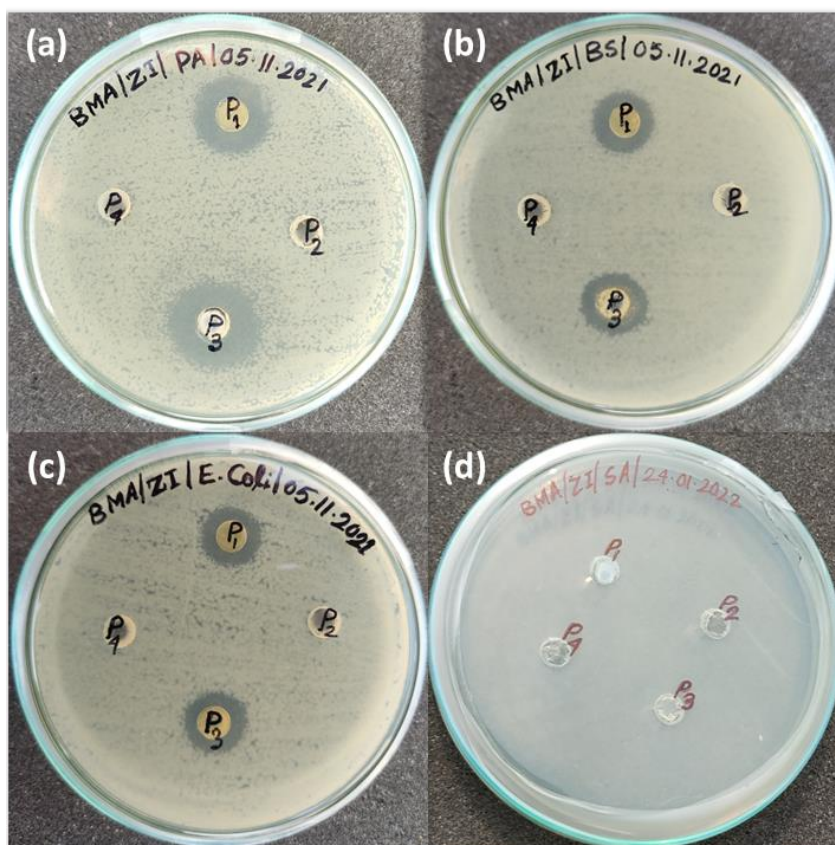


Figure 4.40. Effects of hydrogels on Gram-negative and Gram-positive bacteria by the agar well diffusion method against: (a) *P. aeruginosa*, (b) *B. subtilis*, (c) *E. coli* and (d) *S. aureus*. The concentrations of the hydrogels were 320 mg mL^{-1} in all cases.

Table 4.2. List of bacterial zone of inhibition (ZOI) diameter in mm by agar-well diffusion method and minimum inhibitory concentration (MIC) by **P1** and **P3** amphiphile on Gram-negative and Gram-positive bacteria.

| Bacteria | P1 | | P3 | |
|----------------------|-----------|-------------------------------|-----------|-------------------------------|
| | ZOI (mm) | MIC ($\mu\text{g mL}^{-1}$) | ZOI (mm) | MIC ($\mu\text{g mL}^{-1}$) |
| <i>P. aeruginosa</i> | 26 | 80–130 | 28 | 70–140 |
| <i>B. subtilis</i> | 22 | 40–80 | 22 | 40–120 |
| <i>E. coli</i> | 20 | 100–200 | 18 | 100–200 |
| <i>S. aureus</i> | — | — | — | — |

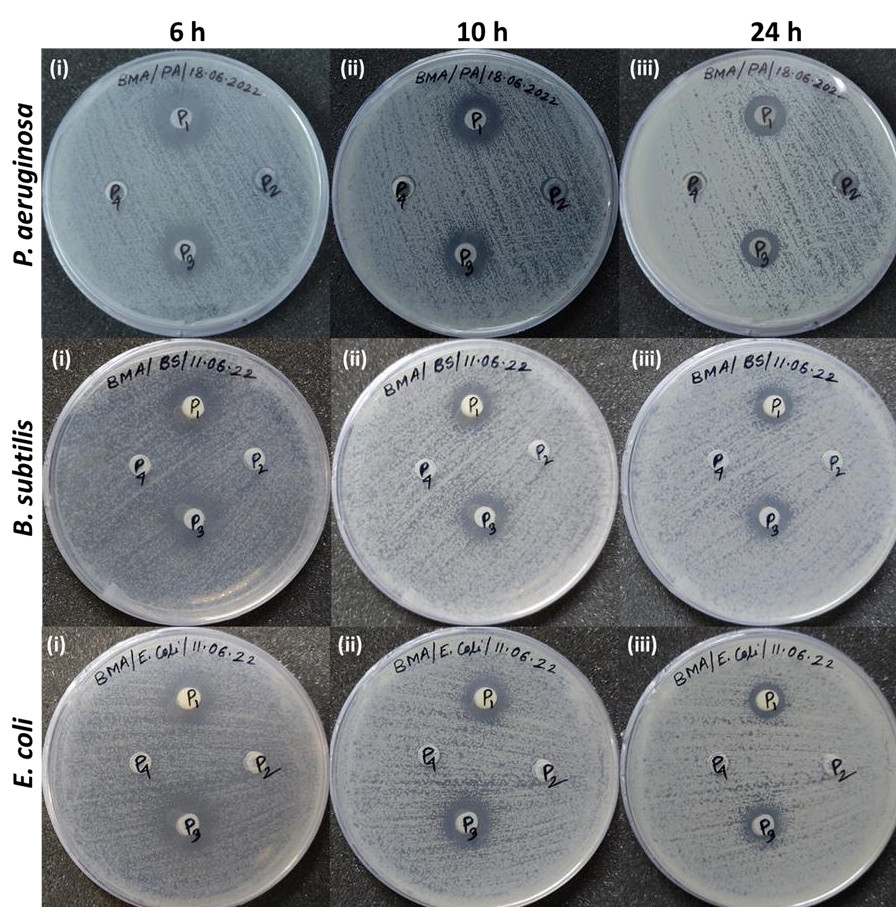


Figure 4.41. Monitoring the zone of inhibition with different time interval (6 h, 10 h, and 24 h) using (a) *P. aeruginosa*, (b) *B. subtilis*, and (c) *E. coli* bacteria.

and 18 mm, respectively (Table 4.2). The minimum inhibitory concentration (MIC) values of the gelator amphiphiles (**P1** and **P3**) against Gram-positive bacteria (*B. subtilis*) and Gram-negative bacteria (*P. aeruginosa* and *E. coli*) were determined by using the microdilution technique.

Gram-positive bacteria *B. subtilis* show a similar zone of an inhibition diameter of 22 mm for both **P1** and **P3** at a fixed concentration of 320 mg mL⁻¹, whereas

their MIC values are 40–80 mg mL⁻¹ and 40–120 mg mL⁻¹, respectively. The MIC value for *E. coli* was 100–200 mg mL⁻¹ of **P1** and **P3**. The amphiphilic gelators **P1** and **P3** show MIC values of 80–130 mg mL⁻¹ and 70–140 mg mL⁻¹ respectively for the bacteria *P. aeruginosa*. Both gelators **P2** and **P4** were inactive against all the bacteria used throughout the antibacterial study, even up to a concentration of 650 mg mL⁻¹. Moreover, the time growth inhibition study using different bacterial populations upon the lead hydrogels was performed to establish the stability of the hydrogelators for a longer duration of time (Figure 4.41).

4.3.9. MTT Assay Study. Both amphiphilic gelators **P1** and **P3** show cytotoxicity against the wild type AG83 and drug resistant *L. donovani* promastigotes. The cytotoxic potential of four different amphiphilic gelators on *Leishmania* promastigotes was checked using the MTT assay. SAG-sensitive *L. donovani* AG83 parasites (2×10^6 cells per mL) were incubated with these four amphiphilic gelators (25 mM for 12 h). Data showed that only **P1** and **P3** have cytotoxicity against *Leishmania* promastigotes. Treatments of the *L. donovani* wild type AG83 strain, *Leishmania major*, multidrug resistant (BHU-575) strain, miltefosine resistant (MIL^R) strain and camptothecin resistant (CPT^R) strain (2×10^6 cells per mL) with seven different concentrations of amphiphilic gelators **P1** and **P3** (0.25 μ M, 0.5 μ M, 1.00 μ M, 2.50 μ M, 5.00 μ M, 7.50 μ M and 10.00 μ M) for 12 h were evaluated using the MTT assay. This study demonstrated a dose-dependent cytotoxic effect towards the parasitic growth. Promastigotes treated with amphiphilic gelators **P1** and **P3** showed that, at 12 h, 94% and 99% of the total number of AG83 promastigotes were killed by 7.5 μ M and 10.0 μ M concentrations, respectively (Figure 4.42a). In the case of the *Leishmania major* parasite growth study, only 1% cells were viable after treatment with a 10 μ M concentration of amphiphilic gelators (Figure 4.42b). On the other hand, for the multidrug resistant (BHU-575) parasite, only 2% and less than 1% of the total number of parasites were viable after treatments with a 10 μ M concentration of amphiphilic gelators **P1** and **P3** (Figure 4.42c). Moreover, MIL^R parasites treated with amphiphilic gelators **P1** and **P3** with a concentration of 10 μ M showed that only 1.0 to 1.5% viability after 12 h of treatment (Figure 4.42d). Similar results were seen with CPT^R parasites, where only less than 1.0% and 1.5% parasites were viable after treatments with amphiphilic gelators **P1** and **P3**, respectively (Figure 4.42e). Controls containing 0.2% DMSO were incubated

Table 4.3. EC_{50} and EC_{90} values for the effects of **P1** and **P3** on the *Leishmania promastigote* growth measured using the MTT assay.

| Drug | Promastigotes | EC_{50} (μ M) | EC_{90} (μ M) | Miltefosine EC_{50} (μ M) |
|-----------|------------------|----------------------|----------------------|----------------------------------|
| P1 | AG83 | 1.148 ± 0.0012 | 7.237 ± 0.0016 | 19.827 ± 0.0009 |
| | <i>L. Major</i> | 1.045 ± 0.0013 | 7.068 ± 0.0014 | 15.362 ± 0.0017 |
| | BHU-575 | 2.376 ± 0.0011 | 7.402 ± 0.0016 | 20.235 ± 0.0013 |
| | MIL ^R | 3.420 ± 0.0011 | 8.560 ± 0.0014 | >100 |
| | CPT ^R | 4.193 ± 0.0012 | 8.243 ± 0.0015 | 19.713 ± 0.0012 |
| P3 | AG83 | 1.153 ± 0.0012 | 7.145 ± 0.0016 | 19.827 ± 0.0009 |
| | <i>L. Major</i> | 1.071 ± 0.0013 | 7.054 ± 0.0014 | 15.362 ± 0.0017 |
| | BHU-575 | 2.218 ± 0.0011 | 7.329 ± 0.0016 | 20.235 ± 0.0013 |
| | MIL ^R | 3.832 ± 0.0011 | 8.776 ± 0.0014 | >100 |
| | CPT ^R | 5.364 ± 0.0012 | 8.138 ± 0.0015 | 19.713 ± 0.0012 |

Table 4.4. EC_{50} and EC_{90} values for the effect of **P1** and **P3** on the *Leishmania promastigotes* growth obtained by the trypan blue exclusion method.

| Drug | Promastigotes | EC_{50} (μ M) | EC_{90} (μ M) | Miltefosine EC_{50} (μ M) |
|-----------|------------------|----------------------|----------------------|----------------------------------|
| P1 | AG83 | 0.972 ± 0.0010 | 6.952 ± 0.0014 | 19.627 ± 0.0011 |
| | <i>L. Major</i> | 1.037 ± 0.0014 | 7.281 ± 0.0011 | 14.971 ± 0.0009 |
| | BHU-575 | 1.982 ± 0.0013 | 6.994 ± 0.0013 | 19.826 ± 0.0010 |
| | MIL ^R | 2.967 ± 0.0011 | 7.956 ± 0.0011 | >100 |
| | CPT ^R | 4.233 ± 0.0010 | 8.817 ± 0.0014 | 19.544 ± 0.0007 |
| P3 | AG83 | 1.042 ± 0.0011 | 7.145 ± 0.0016 | 19.627 ± 0.0011 |
| | <i>L. Major</i> | 0.931 ± 0.0012 | 7.054 ± 0.0014 | 14.971 ± 0.0009 |
| | BHU-575 | 2.121 ± 0.0013 | 7.329 ± 0.0016 | 19.826 ± 0.0010 |
| | MIL ^R | 3.672 ± 0.0013 | 8.776 ± 0.0014 | >100 |
| | CPT ^R | 4.984 ± 0.0010 | 8.138 ± 0.0015 | 19.544 ± 0.0007 |

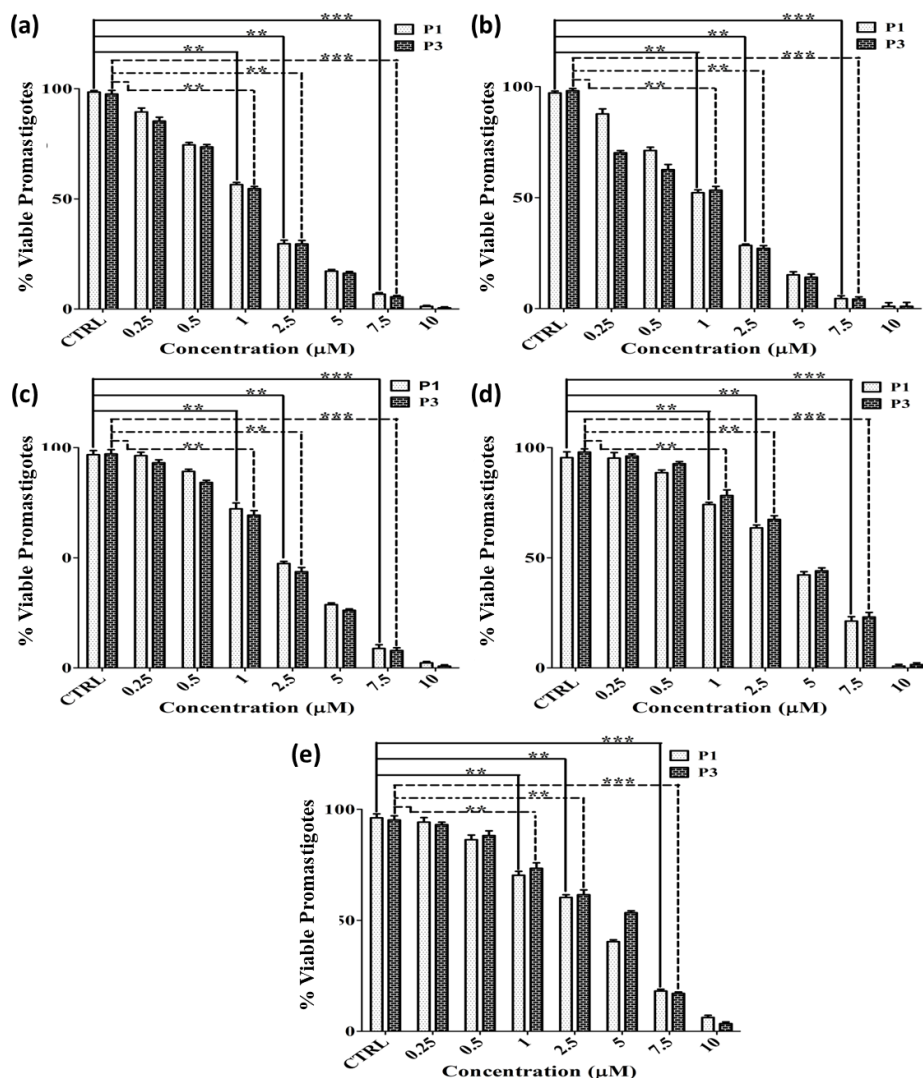


Figure 4.42. Cytotoxic effects of aromatic amino acid containing amphiphilic gelators **P1** and **P3** on *Leishmania* promastigotes. Analysis of the *in vitro* dose-dependent cytotoxicity of **P1** and **P3** using the MTT assay. Log phase (a) AG83 promastigotes cells, (b) *L. major* promastigote cells, (c) BHU-575 promastigotes cells, (d) MIL^R promastigote cells and (e) CPT^R promastigote cells were cultured for 12 h in M199 media. Percentages of viable promastigotes were measured using the MTT assay. All data were expressed as the percentage of live promastigotes and represent mean \pm S.D. from three independent experiments. * $P < 0.01$, ** $P < 0.001$, *** $P < 0.0001$ compared with the control, by the Student's *t*-test (a–e).

separately in the experiment and data showed no adverse effect on the parasite viability. The EC_{50} and EC_{90} values of amphiphilic gelators **P1** and **P3** against all strains (AG83, *L. major*, BHU-575, MIL^R and CPT^R) of *L. donovani* were calculated using the variable slope model (Prism, GraphPad Software, Version 5.0, San Diego, CA) and these data are presented in Table 4.3. Miltefosine was used as a positive control. We also measured the viability of the AG83 promastigote along with BHU-575 and MIL^R parasites by direct microscopic counting using the trypan blue exclusion method and obtained similar results to

the MTT assay. The EC₅₀ and EC₉₀ values obtained using this method are presented in Table 4.4.

4.3.10. ROS Generation Study. It has been reported that, unlike in other mammalian cells, camptothecin (CPT) induces oxidative stress in *Leishmania donovani* cells.⁵⁵ It was reported that, during oxidative phosphorylation, the release of ROS inside the cells in the form of superoxide anions occurs to the extent of 4–6% of the total O₂ consumed.⁵⁶ However, sometimes under certain conditions when drugs inhibit oxidative phosphorylation, there is an increase in the production of ROS.⁵⁶ To identify the effect of these amphiphilic gelators on intracellular ROS generation, *Leishmania* promastigotes were separately treated with **P1** and **P3** at four different concentrations (0.5, 1.0, 2.5 and 5.0 µM) for 12 h (Figure 4.43a). In another set of experiments, the time course effect of amphiphilic gelators on ROS generation was measured. Promastigotes were treated with an anti-oxidant NAC (10 mM for 2 h) prior to the treatment with both the amphiphilic gelators (5 µM). Intracellular ROS generations were measured fluorometrically by the conversion of CM-H₂DCFDA to highly fluorescent 2',7'-dichlorofluorescein after treatment with these amphiphilic gelators in *L. donovani* promastigotes. The level of peroxide radicals gradually increased inside the cell with the increase in time in a dose dependent manner of **P1** and **P3**. Briefly, the fluorescence intensity was significantly increased at a 5.0 µM concentration in comparison to 1.0 and 2.5 µM concentrations (Figure 4.43b). When promastigotes were treated with NAC prior to treatment with amphiphilic gelators, the ROS generation decreased. The above experimental data lead to the conclusion that the generation of the total cellular ROS at 12 h primarily induces the downstream progress of the programmed cell death (PCD). We have performed the FACs analysis on mammalian fibroblast cells to check the levels of reactive oxygen species (ROS) generated before and after the treatment with the hydrogelators amphiphiles. We treated the cells with amphiphiles **P1** and **P3** (25, 50, 75 and 100 µM) for 48 h and checked the levels of ROS production using a flow cytometer. The result shows that at a 100 µM concentration of amphiphiles **P1** and **P3** only 3–4% ROS are generated, which is considered as a negligible amount.

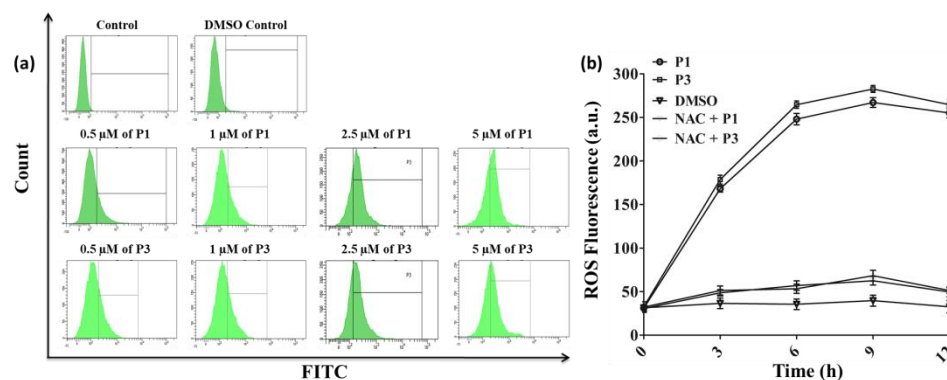


Figure 4.43. Flow cytometric analysis of ROS generation inside *L. donovani* promastigotes induced by **P1** and **P3**. Measurements of the induced ROS generation. (a) Generation of peroxide radicals within the *L. donovani* promastigotes was measured after treatment with 0.2% DMSO, peptide **P1** (0.5, 1.0, 2.5 and 5.0 μM) and **P3** (0.5, 1.0, 2.5 and 5.0 μM) as described in the Materials and methods section. After incubation with H₂DCFDA, the fluorescence intensity was measured at 530 nm by flow cytometry. (b) Formation of peroxide radicals within the leishmanial promastigotes was measured after treatment with 0.2% DMSO, **P1** (5 μM), **P3** (5 μM), and NAC (10 mM) treatment prior to the treatment with **P1** and **P3** for 3, 6, 9 and 12 h.

Some other experiments such as- “*measurement of the mitochondrial membrane potential (ψ_m), determination of mitochondrial superoxide levels, double staining with annexin V and PI, isolation of gDNA, DNA fragmentation assay, culture of *Leishmania donovani* axenic amastigotes, measurement of the dose-dependent cytotoxic effect of these amphiphilic gelators on cultured murine peritoneal macrophages by the MTT assay, statistical analysis*” are also performed and the related results are given into the literature (Soft Matter, 2022, 18, 7201–7216) for antiparasitic study. Some discussion about these experiments will be given after the “**4.2.11. AFM Image Analysis for Antiparasitic Study**” section of anti-parasitic activity.

4.2.11. AFM Image Analysis for Antiparasitic Study. The AFM imaging analysis shows the ultrastructure disruption of the *Leishmania* promastigote architecture. This imaging analysis revealed the topographical differences in the cell shape, size, etc. between normal untreated and treated leishmanial cells. So far we observed that these amphiphilic gelators could induce the progression of PCD, these processes being detrimental to cells. AG83 promastigotes treated with **P1** and **P3** at 1.0, 2.5 and 5.0 μM concentrations for 12 h showed an altered cell architecture. Untreated or control parasites possessed typical slender cell bodies with a smooth cell surface and the presence of an elongated flagellum confirmed the normal design of the cell (Figure 4.44a). Treated promastigotes show the shrunken morphology which is a sign of the possible loss of the cell volume (Figure 4.44c and f) when treated with 1.0 μM of **P1** and **P3**. At a 2.5

μM concentration of amphiphilic gelators, the outer membrane got ruptured showing a typical phenotype of such cell morphology (Figure 4.44d and g). After increasing the concentration up to $5.0 \mu\text{M}$ for 12 h treatment, the complete disruption of the cell morphology was observed and they were also devoid of any flagella (Figure 4.44e and h).

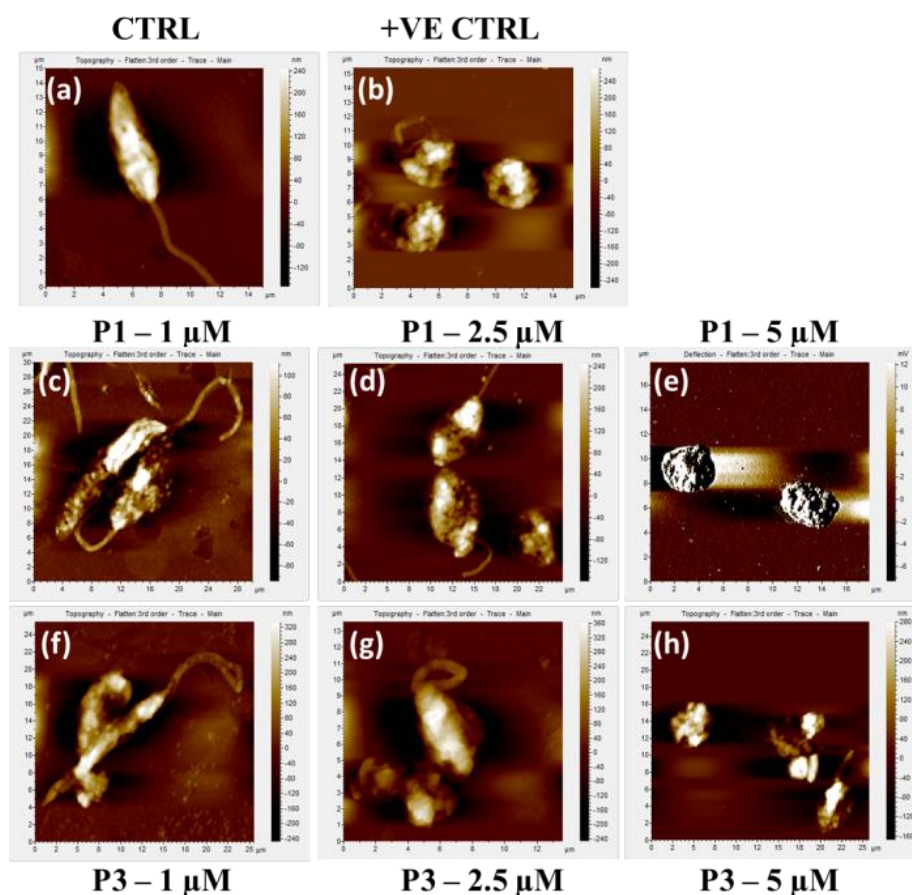


Figure 4.44. (a) Atomic force microscopy (AFM) micrograph of the intact promastigote. (b) Promastigotes treated with $10 \mu\text{M}$ CPT. (c-e) Promastigotes treated with 1.0 , 2.5 and $5.0 \mu\text{M}$ of **P1** and (f-h) Promastigotes treated with 1.0 , 2.5 and $5.0 \mu\text{M}$ of **P3**.

Due to the emergence of drug resistant parasites, there is a need to develop new drugs to diagnose this deadly disease. Moreover, due to the unavailability of effective vaccines and chemotherapy, the treatment of leishmaniasis is unsatisfactory. Thus, there is a crucial need to develop new drugs and newer therapeutic strategies. The main rationale to synthesize gelator amphiphiles and to initiate the study was the fact that they have antibacterial properties. Self-assembling amphiphilic molecules are an intriguing platform for the development of functional biomolecular actives against pathogens due to their ability to disrupt bacterial membranes and function as drug carriers. In an earlier study, it was reported that oxindoles, a heterocyclic organic compound, which have a

tryptophan like structure have great potential to kill *Leishmania*.⁵⁶ Oxindoles constitute a large array of natural products and other compounds that have a great pharmaceutical value.^{57–59} Oxindoles have a broad spectrum of biological activity and have been reported to have antitumour, antibacterial, and insecticidal activities and are also used for the treatment of hyponatremia.^{56,60,61} Based on these relevant data we synthesize L-phenylalanine and L-tryptophan based gelator amphiphiles with variable chain length of $-NH_2$ containing cationic head groups. There are reports that L-tryptophan-containing peptides can be used as a class of antibacterial peptides.^{12,54} But, in this report, thus the lack of the antibacterial activity of L-tryptophan makes the results very noticeable.

In the present study, we have investigated the effects of these gelator amphiphiles on *Leishmania donovani* AG83 promastigotes *in vitro*. To the best of our knowledge, this study provides the first evidence that amino acid containing amphiphiles can exhibit anti-leishmanial activity. Moreover, these molecules were effective against different drug-resistant strains of *L. donovani*. Our report showed that amphiphilic **P1** and **P3** effectively kill both the wild type and drug resistance parasites in both time and concentration dependent manners. The introduction of these amphiphilic gelators causes an increase in intracellular and mitochondrial ROS production. However, following pretreatment with NAC, there is an inhibition in the formation of ROS. This study indicates that amphiphilic gelators **P1** and **P3** are effective inducers of apoptosis in *Leishmania donovani* cells, and this is confirmed by the externalization of phosphatidyl serine. Moreover, gDNA fragmentation is observed which is a hallmark of apoptosis. These data together indicate the initiation of apoptosis-like cell death in response to treatment with amphiphilic gelators. The parasite ultra-structure studies by atomic force microscopy analysis also led to some interesting observations. We observed the disruption of the cell architecture, shortening of flagella and atypical cell phenotype. This investigation also provides a meticulous insight into the parasite ultra-structure alteration caused by these gelator amphiphiles. To our knowledge, this report is the first of this kind. The apoptotic pathway that initiates inside the parasite after exposure to these amphiphilic gelators was revealed, and we have shown that these compounds have promise as chemotherapeutic tools against several forms of human leishmaniasis. Microscopic studies shed light on the events occurring at the

cellular level. Interestingly, the effect was more or less similar in all the strains (wild type and drug resistance) of trypanosomatid parasites tested here.

To confirm the accessibility of these gelator amphiphiles as a drug candidate, their effect upon human macrophage cells was evaluated. The amphiphilic gelators showed the minimal cytotoxic effect on uninfected cultured murine peritoneal macrophages up to a 200 μM concentration. The IC_{50} value of uninfected cultured murine peritoneal macrophages was also very high compared to those of amastigotes and promastigotes. Further *in vitro* studies were performed with infected murine peritoneal macrophage cells. Interestingly, the parasitic burden gradually decreased after treatment with these amphiphilic gelators up to a 5.0 μM concentration. Thus, for the first time, we have shown that amino acid-based gelator amphiphiles are effective against a large array of trypanosomatid parasites. In the current time, when parasites are emerging resistance to available classical drugs, the very fact that these compounds work with equal potency against the wild type *Leishmania donovani* AG83 strain, multidrug resistant BHU-575 strain, CPT^R strain and MIL^R strain of the parasite and finds a way towards the development of new pharmaceutical approach against this deadly disease in near future. The amphiphilic gelators **P1** and **P3** serve as lead candidate compounds for anti-leishmanial chemotherapy to combat this dreadful disease.

4.4. Conclusions

This study demonstrates the formation of hydrogels based on β -sheet fibril networks from a series of amino acid-containing amphiphilic molecules. Interestingly, two of these gels show antibacterial activity against both Gram-positive bacteria (*B. subtilis*) and Gram-negative bacteria (*P. aeruginosa* and *E. coli*). Moreover, the two gelators containing L-phenylalanine exhibit antiparasitic activity against several strains of *L. donovani*, including a drug resistant strain. Interestingly, it is evident from the results that ROS generation inside the parasite and mitochondrial membrane depolarisation are the main cause of antiparasitic activity. Additionally, these gelator-based amphiphiles are minimally toxic to host macrophage cells, indicating the potential application of these gels as a therapeutic agent for leishmaniasis in the near future. The gels were comprehensively characterized by using various techniques such as thermal stability, rheology, HR-TEM, FTIR, wide-angle X-ray diffraction, and small-

SAXS. Unexpectedly, L-tryptophan-containing amphiphiles show neither antibacterial nor antiparasitic activity against any type of leishmaniasis. However, remarkable activity was observed for L-phenylalanine-based amphiphiles in terms of both antibacterial and antiparasitic activities against leishmaniasis.

4.5. References

- (1) M. Tena-Solsona, D. Marson, A. C. Rodrigo, S. M. Bromfield, B. Escuder, J. F. Miravet, N. Apostolova, E. Laurini, S. Pricl and D. K. Smith, *Biomater. Sci.*, 2019, **7**, 3812–3820.
- (2) A. Pettignano, S. Grijalvo, M. Häring, R. Eritja, N. Tanchoux, F. Quignard and D. Díaz Díaz, *Chem. Commun.*, 2017, **53**, 3350–3353.
- (3) W. Ji, Y. Tang, P. Makam, Y. Yao, R. Jiao, K. Cai, G. Wei and E. Gazit, *J. Am. Chem. Soc.*, 2021, **143**, 17633–17645.
- (4) M. Samateh, S. S. Sagiri, R. Sanni, C. A. Chee, S. Satapathy and G. John, *J. Agric. Food Chem.*, 2020, **68**, 13282–13290.
- (5) A. S. Pina, L. Morgado, K. L. Duncan, S. Carvalho, H. F. Carvalho, A. J. M. Barbosa, B. de P. Mariz, I. P. Moreira, D. Kalafatovic, B. M. Morais Faustino, V. Narang, T. Wang, C. G. Pappas, I. Ferreira, A. C. A. Roque and R. V. Uljin, *Chem. Sci.*, 2022, **13**, 210–217.
- (6) G. Grover and R. G. Weiss, *Gels*, 2021, **7**, 19.
- (7) S. Panja, B. Dietrich and D. J. Adams, *Angew. Chemie - Int. Ed.*, 2022, **61**, 1–6.
- (8) N. Singh, M. Kumar, J. F. Miravet, R. V. Uljin and B. Escuder, *Chem. - A Eur. J.*, 2017, **23**, 981–993.
- (9) D. B. Amabilino, D. K. Smith and J. W. Steed, *Chem. Soc. Rev.*, 2017, **46**, 2404–2420.
- (10) W. Liyanage, K. Vats, A. Rajbhandary, D. S. W. Benoit and B. L. Nilsson, *Chem. Commun.*, 2015, **51**, 11260–11263.
- (11) V. Castelletto and I. W. Hamley, *ACS Nano*, 2022, **16**, 1857–1867.
- (12) J. Zhang, S. Liu, H. Li, X. Tian and X. Li, *Langmuir*, 2020, **36**, 11316–11323.
- (13) A. D'Souza, J. H. Yoon, H. Beaman, P. Gosavi, Z. Lengyel-Zhand, A. Sternisha, G. Centola, L. R. Marshall, M. D. Wehrman, K. M. Schultz, M. B.

- Monroe and O. V. Makhlynets, *ACS Appl. Mater. Interfaces*, 2020, **12**, 17091–17099.
- (14) S. Basak, N. Nandi, S. Paul, I. W. Hamley and A. Banerjee, *Chem. Commun.*, 2017, **53**, 5910–5913.
- (15) S. S. Lee, E. L. Hsu, M. Mendoza, J. Ghodasra, M. S. Nickoli, A. Ashtekar, M. Polavarapu, J. Babu, R. M. Riaz, J. D. Nicolas, D. Nelson, S. Z. Hashmi, S. R. Kaltz, J. S. Earhart, B. R. Merk, J. S. McKee, S. F. Bairstow, R. N. Shah, W. K. Hsu and S. I. Stupp, *Adv. Healthcare Mater.*, 2015, **4**, 131–141.
- (16) D. Bairagi, P. Biswas, K. Basu, S. Hazra, D. Hermida-Merino, D. K. Sinha, I. W. Hamley and A. Banerjee, *ACS Appl. Bio Mater.*, 2019, **2**, 5235–5244.
- (17) C. Ligorio, A. Vijayaraghavan, J. A. Hoyland and A. Saiani, *Acta Biomater.*, 2022, **143**, 145–158.
- (18) K. Basu, A. Baral, S. Basak, A. Dehsorkhi, J. Nanda, D. Bhunia, S. Ghosh, V. Castelletto, I. W. Hamley and A. Banerjee, *Chem. Commun.*, 2016, **52**, 5045–5048.
- (19) L. Qin, F. Xie, P. Duan and M. Liu, *Chem. - A Eur. J.*, 2014, **20**, 15419–15425.
- (20) R. Martí-Centelles, I. Dolz-Pérez, J. De la O, I. Ontoria-Oviedo, P. Sepúlveda, V. J. Nebot, M. J. Vicent and B. Escuder, *ACS Appl. Bio Mater.*, 2021, **4**, 935–944.
- (21) I. W. Hamley, *ACS Appl. Bio Mater.*, 2022, **5**, 905–944.
- (22) K. Basu, N. Nandi, B. Mondal, A. Dehsorkhi, I. W. Hamley and A. Banerjee, *Interface Focus*, 2017, **7**, 20160128.
- (23) B. Mondal, D. Bairagi, N. Nandi, B. Hansda, K. S. Das, C. J. C. Edwards-Gayle, V. Castelletto, I. W. Hamley and A. Banerjee, *Langmuir*, 2020, **36**, 12942–12953.
- (24) Z. Yang, G. Liang, M. Ma, A. S. Abbah, W. W. Lu and B. Xu, *Chem. Commun.*, 2007, 843–845.
- (25) A. Baral, S. Roy, S. Ghosh, D. Hermida-Merino, I. W. Hamley and A. Banerjee, *Langmuir*, 2016, **32**, 1836–1845.
- (26) E. R. Cross, S. M. Coulter, A. M. Fuentes-Caparrós, K. McAulay, R. Schweins, G. Lavery and D. J. Adams, *Chem. Commun.*, 2020, **56**, 8135–8138.
- (27) N. Nandi, K. Gayen, S. Ghosh, D. Bhunia, S. Kirkham, S. K. Sen, S. Ghosh, I. W. Hamley and A. Banerjee, *Biomacromolecules*, 2017, **18**, 3621–3629.
- (28) A. S. Veiga and J. P. Schneider, *Biopolymers*, 2013, **100**, 637–644.

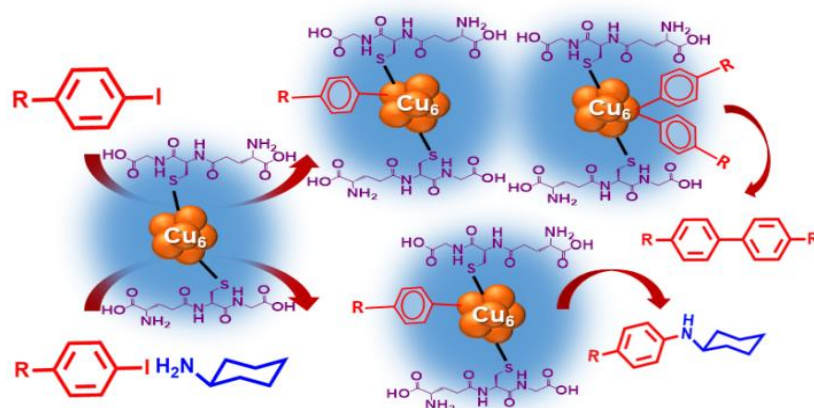
- (29) E. Ji, A. Parthasarathy, T. S. Corbitt, K. S. Schanze and D. G. Whitten, *Langmuir*, 2011, **27**, 10763–10769.
- (30) E. Pazos, E. Sleep, C. M. R. Pérez, S. S. Lee, F. Tantakitti and S. I. Stupp, *J. Am. Chem. Soc.*, 2016, **138**, 5507–5510.
- (31) V. Castelletto, C. J. C. Edwards-Gayle, I. W. Hamley, G. Barrett, J. Seitsonen and J. Ruokolainen, *ACS Appl. Mater. Interfaces*, 2019, **11**, 9893–9903.
- (32) N. Mukherjee, A. Adak and S. Ghosh, *Soft Matter*, 2020, **16**, 10046–10064.
- (33) S. Basak, J. Nanda, A. Banerjee, *J. Mater. Chem.* 2012, **22**, 11658–11664.
- (34) A. Adak, S. Ghosh, V. Gupta and S. Ghosh, *Biomacromolecules*, 2019, **20**, 1889–1898.
- (35) D. S. S. M. Uppu, S. Samaddar, J. Hoque, M. M. Konai, P. Krishnamoorthy, B. R. Shome and J. Haldar, *Biomacromolecules*, 2016, **17**, 3094–3102.
- (36) C. J. C. Edwards-Gayle, V. Castelletto, I. W. Hamley, G. Barrett, F. Greco, D. Hermida-Merino, R. Rambo, J. Seitsonen and J. Ruokolainen, *ACS Appl. Bio Mater.* 2019, **2**, 2208–2218.
- (37) C. J. C. Edwards-Gayle, G. Barrett, S. Roy, V. Castelletto, J. Seitsonen, J. Ruokolainen and I. W. Hamley, *ACS Appl. Bio Mater.* 2020, **3**, 1165–1175.
- (38) S. Fernandez-Lopez, H. S. Kim, E. C. Choi, M. Delgado, J. R. Granja, A. Khasanov, K. Kraehenbuehl, G. Long, D. A. Weinberger, K. M. Wilcoxon and M. R. Ghadiri, *Nature*, 2001, **412**, 452–455.
- (39) H. Hashizume, R. Sawa, K. Yamashita, Y. Nishimura and M. Igarashi, *J. Antibiot.*, 2017, **70**, 699–704.
- (40) O. Bellotto, S. Kralj, M. Melchionna, P. Pengo, M. Kisovec, M. Podobnik, R. De Zorzi and S. Marchesan, *ChemBioChem*, 2022, **23**, e202100518.
- (41) P. Sriwongpan, S. Nedsuwan, J. Manomat, S. Charoensakulchai, K. Lacharojana, J. Sankwan, N. Kobpungton, T. Sriwongpun, S. Leelayoova, M. Mungthin, S. Siripattanapipong, T. Ruang-Areerate, T. Naaglor, T. Eamchotchawalit and P. Piyaraj, *PLoS Negl. Trop. Dis.*, 2021, **15**, e0009545.
- (42) F. Chappuis, S. Sundar, A. Hailu, H. Ghalib, S. Rijal, R. W. Peeling, J. Alvar and M. Boelaert, *Nat. Rev. Microbiol.*, 2007, **5**, 873–882.
- (43) E. Torres-Guerrero, M. R. Quintanilla-Cedillo, J. Ruiz-Esmenjaud and R. Arenas, *F1000Research*, 2017, **6**, 750.

- (44) M. A. Cunha, B. J. Celeste, N. Kesper, M. Fugimori, M. M. Lago, A. S. Ibanes, L. M. Ouki, E. A. S. Neto, F. F. Fonseca, M. A. L. Silva, W. L. B. Júnior and J. A. L. Lindoso, *BMC Infect. Dis.*, 2020, **20**, 885.
- (45) S. Sundar and J. Jaya, *J. Glob. Infect. Dis.*, 2010, **2**, 159–166.
- (46) T. R. N. Berbert, T. F. P. De Mello, P. Wolf Nassif, C. A. Mota, A. V. Silveira, G. C. Duarte, I. G. Demarchi, S. M. A. Aristides, M. V. C. Lonardoni, J. J. Vieira Teixeira and T. G. V. Silveira, *Dermatol. Res. Pract.*, 2018, **2018**, 1–21.
- (47) J. Chakravarty and S. Sundar, *J. Glob. Infect. Dis.*, 2010, **2**, 167–176.
- (48) N. Shakya, P. Bajpai and S. Gupta, *J. Parasit. Dis.*, 2011, **35**, 104–112.
- (49) V. Castelletto, C. J. C. Edwards-Gayle, F. Greco, I. W. Hamley, J. Seitsonen and J. Ruokolainen, *ACS Appl. Mater. Interfaces* 2019, **11**, 33573–33580.
- (50) K. K. Banoth, Faheem, K. V. G. ChandraSekhar, N. Adinarayana and S. Murugesan, *Heliyon*, 2020, **6**, e04916.
- (51) R. Basu, S. Bhaumik, J. M. Basu, K. Naskar, T. De and S. Roy, *J. Immunol.*, 2005, **174**, 7160–7171.
- (52) S. Chowdhury, T. Mukherjee, S. R. Chowdhury, S. Sengupta, S. Mukhopadhyay, P. Jaisankar and H. K. Majumder, *Antimicrob. Agents Chemother.*, 2014, **58**, 2186–2201.
- (53) A. Roy, B. B. Das, A. Ganguly, S. Bose Dasgupta, N. V. M. Khalkho, C. Pal, S. Dey, V. S. Giri, P. Jaisankar, S. Dey and H. K. Majumder, *Biochem. J.*, 2008, **409**, 611–622.
- (54) D. I. Chan, E. J. Prenner and H. J. Vogel, *Biochim. Biophys. Acta – Biomembranes*, 2006, **1758**, 1184–1202.
- (55) N. Sen, B. B. Das, A. Ganguly, T. Mukherjee, G. Tripathi, S. Bandyopadhyay, S. Rakshit, T. Sen and H. K. Majumder, *Cell Death Differ.* **2004**, **11**, 924–936.
- (56) M. Mattiazzi, C. Vijayvergiya, C. D. Gajewski, D. C. DeVivo, G. Lenaz, M. Wiedmann and G. Manfredi, *Hum. Mol. Genet.*, 2004, **13**, 869–879.
- (57) S. Saha, C. Acharya, U. Pal, S. R. Chowdhury, K. Sarkar, N. C. Maiti, P. Jaisankar and H. K. Majumder, *Antimicrob. Agents Chemother.*, 2016, **60**, 6281–6293.
- (58) J. Li, N. Wang, C. Li and X. Jia, *Chem. - A Eur. J.*, 2012, **18**, 9645–9650.
- (59) N. Lashgari and G. M. Ziarani, *Arkivoc*, 2012, **1**, 277–320.
- (60) H. Venkatesan, M. C. Davis, Y. Altas, J. P. Snyder and D. C. Liotta, *J. Org. Chem.*, 2001, **66**, 3653–3661.

(61) Â. Monteiro, L. M. Gonçalves and M. M. M. Santos, *Eur. J. Med. Chem.*, 2014, **79**, 266–272.

Chapter 5

Copper Nanoclusters for Catalytic Carbon–Carbon and Carbon–Nitrogen Bond Formations



(ACS Appl. Nano Mater. **2022**, 5, 7932–7943)

Chapter 5

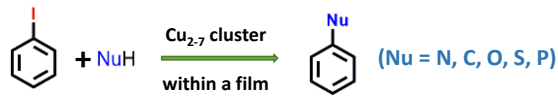
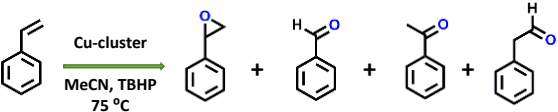
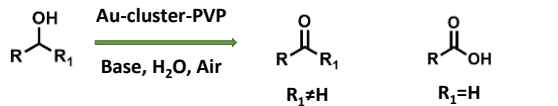
Copper Nanoclusters for Catalytic Carbon–Carbon and Carbon–Nitrogen Bond Formations**5.1. Introduction**

Fluorescent metal nanoclusters¹⁻⁶ have been an expanding area of current research for the last several years. The recent advancement of nanoscience and technology is not only restricted to the nanoparticles⁷ but also expands to control the size of the nanomaterials³ at the atomic level to make nanoclusters with exciting properties, including fluorescent behavior,^{1,2} semiconducting nature,⁸ very high photostability,^{4,9} and others.¹⁰⁻¹⁶ So, the noble metal nanoclusters have found many applications in bio-imaging,¹⁰⁻¹² optoelectronics,⁸ toxic-metal ion sensor,^{13,14} and catalysis.^{15,16} However, most of the properties and applications mentioned above have been reported for Au and Ag-nanoclusters.

Synthesis and detailed study of Cu-nanoclusters are relatively much less than its other congeners.¹⁷ The prime challenge to make and stabilize copper nanoclusters (CuNCs) is their instability under ambient conditions due to very easy oxidation of the Cu(0) to Cu(II) state compared to Ag(0) to Ag(I) and Au(0) to Au(I).¹⁸ Moreover, Cu is much cheaper than Au and Ag, and so, it will be interesting to make, stabilize and find various applications of these Cu-nanoclusters.^{16,19} Among various applications of nanoparticles and nanoclusters, catalyzing organic reactions is one of the most important applications in organic synthesis. There are many examples of using Cu, Au, Pd, Ru based catalysts for C–C²⁰⁻²² and C–N bond formation.²³ However, there are very less reports of aryl-aryl and aryl-nitrogen bond formation by a few atom metal nanoclusters.²⁴ Along with a few organic group transformations are known by using noble metal nanoclusters.²⁵⁻²⁷ Corma and co-workers synthesized copper nanoclusters having the size Cu₂₋₇ used in C–N, C–C, C–O, C–S, and C–P bond formation reactions with a high yield up to 91% of products.²⁴ Zhang and co-workers synthesized protein stabilized Cu-nanoclusters, which can be used for catalytic oxidation of styrene to form styrene epoxide, benzaldehyde, acetophenone, and 2-phenylacetaldehyde derivatives.²⁶ There is also a report of Au-nanoclusters stabilized by PVP for alcohol oxidation reaction in aerobic conditions (Table 5.1).²⁷ The use of nanoparticles or nanoclusters in organic synthesis is exciting because the

efficiency of transforming a substrate to products is more in nanoparticles and nanoclusters than that in their bulk counterpart due to the high surface area associated with these nanoclusters and nanoparticles.²⁸ Moreover, metal nanoclusters have the advantage of precise super-atomic nature, which further increases the surface area in the atomic scale.²⁹

Table 5.1. Reported schemes for catalytic transformation of C–N, C–C, C–O, C–S, and C–P bonds and catalytic oxidation reaction by copper nanoclusters.

| SL. No. | Schemes | References |
|---------|--|------------|
| 1 |  | 24 |
| 2 |  | 26 |
| 3 |  | 27 |

Aromatic C–C bond formation is the most important and mostly encountered topic for the synthesis of organic compounds, because it forms the backbone of many kinds of natural products.³⁰ Synthesis of biphenyl compounds is essential due to various applications of these molecules as antimicrobials, antifungals, antidiabetics, immunosuppressants, antihypertensive, and analgesics.^{31–34} For example, biphenyl moiety is an active functional group in a broad spectrum antibiotic oritavancin.³⁵ Biphenyl moiety can also serve as an essential intermediate in the synthesis of a larger bioactive molecule like an antipsychotic drug biphenyl-indanone A (BINA).³⁶ On the other side, among various C–hetero atom bonds, C–N bond formation is also important as it is associated with the synthesis of a large number of natural aromatic amines and alkaloids.^{37, 38} Ullmann’s coupling is an important reaction in organic chemistry which exploits a cheap metal, bulk Cu for the formation of both C–C/ C–N bonds.²⁹ The existing metal-based catalysts which are routinely being used for C–N and C–C bond formation are generally costly, and they are not environment friendly.³⁹ Use of CuNCs can serve these prepose in a more efficient and eco-friendly way. Various examples of Cu/CuO-nanoparticles based on Ullmann’s coupling are reported in the literature.^{40, 41} However, to the best of our knowledge, there is no report for fluorescent a few atom copper nanoclusters with an application of catalyzing C–

C and C–N bond formation. So, there is a genuine need for the investigation of cheap nanomaterial based on fluorescent metal nanoclusters that can be used for C–C and C–N bond coupling.

In this study, we have reported a cheap and facile synthesis of copper nanoclusters (CuNCs) from a cheap precursor copper acetate monohydrate, a bioactive peptide ligand glutathione as a stabilizing agent and ascorbic acid as a reducing agent in dimethylsulfoxide at 120 °C and the wonderful application of these nanoclusters as a nanocatalyst for C–C and C–N bond formation. These CuNCs emit blue light with emission peak at 450 nm for an excitation at 374 nm. MALDI-TOF analysis vividly demonstrates that the composition of the cluster is $\text{Cu}_6(\text{GS})_2$. Also, the time-dependent MALDI-TOF analysis shows the formation of different intermediates in C–C and C–N bond formation reactions in the presence of substrate molecules. Since the last few years, the identification of reaction intermediates using mass spectrometry has been a new field of research work. This type of recent development in mass spectrometry study can suggest a proper reaction pathway for a reaction. These reaction intermediates are operative by reactions catalyzed by the cationic metal complexes of silver, copper, gold, palladium, rhodium, ruthenium, etc., with their counter anions.⁴²

The ESI-MS characterization for the intermediates is possible if the fragmentation energy and the energy of the transition structure for the rearrangement to the product complex are almost similar. This type of unique approach requires controlled experiments. Roglans and co-workers detected rhodacyclic intermediates and identified them by ESI-MS. The detection of intermediate is possible due to the homolytic cleavage of the tosyl group in the intermediate step.⁴³ Wedd and co-workers investigated the reaction intermediates even further for the gas-phase reaction by using the ESI-MS method. They identified the whole catalytic cycle for the oxidation of methanol to formaldehyde.⁴⁴ Catalytic C–C and C–N bond formation using metal nanoclusters is a new entry for catalyzing C–C and C–N bond formation. They can potentially replace conventional catalysts based on metal complexes or bulk metal (Cu, Pd, Ru).

5.2. Experimental Section

5.2.1. Materials

Copper acetate monohydrate, dimethyl sulphoxide (DMSO), potassium hydroxide and ascorbic acid were brought from Merck, Germany. Stabilizing agent reduced glutathione was purchased from SRL India. Reagents related to catalysis such as iodobenzene, 4-iodoacetophenone, 4-iodotoluene, 4-iodophenol and 4-iodoanisole were purchased from Sigma Aldrich, USA. Primary amine (cyclohexylamine) was purchased from SRL India. Two NMR solvents CDCl_3 and DMSO-d_6 were purchased from Sigma Aldrich, USA and SRL India respectively.

5.2.2. Methods

Synthetic method of blue CuNCs. 4 mg (0.02 mM) of copper acetate monohydrate, 5 mg (0.016 mM) of glutathione ($\text{GSH} = \text{C}_{10}\text{H}_{16}\text{N}_3\text{O}_6\text{SH}$), and 5 mg of ascorbic acid (0.028 mM) were dissolved in 2 mL, 2 mL, and 1 mL of dimethylsulphoxide (DMSO) respectively. Then copper acetate monohydrate and GSH dissolved in DMSO were taken in a 25 mL round bottom flask and stirred on a magnetic stirrer for 5 min at room temperature. The round bottom flask was then fitted with the bulb condenser at nitrogen atmosphere and heated at 120 °C. After 5 min of heating, 1 mL of ascorbic acid solution in DMSO was added and kept for 7 h. A pale yellow-colored solution was formed after 7 h, showing blue fluorescence on UV lamp irradiation at 365 nm.

5.2.3. Synthesis Details

C–C (aryl-aryl) coupling:

General procedure for C-C coupling reactions. 1 mM of aryl iodide, 2 mM of potassium hydroxide, and 5 mL of CuNCs dispersed in DMSO (2 mol% CuNCs) were heated at 160 °C temperature in an oil bath for 15 h under nitrogen atmosphere. After 15 h, the completion of the reaction was checked by thin-layer chromatography (TLC), and DMSO was discarded from the reaction mixture under a high vacuum. The solid crude product was then extracted with ethyl acetate and washed thoroughly by distilled water. The desired product was purified using column chromatography, using EtOAc/ hexanes as the eluting solvent.

Characterization of compound 1. ^1H NMR (CDCl_3 , 400 MHz) δ 7.63–7.61 (m, 4H, 2, 6, 2', 6' aromatic CH protons), 7.48–7.44 (m, 4H, 3, 5, 3', 5' aromatic CH protons), 7.38–7.35 (m, 2H, 4, 4' aromatic CH protons) (Figure 5.1). ^{13}C NMR (CDCl_3 , 100 MHz) δ 141.43, 128.89, 127.39, 127.32 (Figure 5.2). HRMS (m/z): Calculated for $\text{C}_{12}\text{H}_{10}$: 154.0783, Found: 177.1090 ($\text{M} + \text{Na}$) $^+$ (Figure 5.3). C, H, N analysis: %C calculated 93.46, found 93.07; %H calculated 6.54, found 6.92. Melting point: Reported 68–69 $^\circ\text{C}$, found 70 $^\circ\text{C}$.^{56, 57}

Characterization of compound 2. ^1H NMR (CDCl_3 , 400 MHz) δ 7.52–7.50 (d, $J_{\text{ortho}} = 8.0$ Hz, 4H, 2, 6, 2', 6' aromatic CH protons of biphenyl system), 7.27–7.25 (d, $J_{\text{ortho}} = 8.0$ Hz, 4H, 3, 5, 3', 5' aromatic CH protons of biphenyl system), 2.42 (s, 6H, $-\text{CH}_3$) (Figure 5.4). ^{13}C NMR (CDCl_3 , 100 MHz) δ 138.44, 136.82, 129.56, 126.94, 21.20 (Figure 5.5). HRMS (m/z): Calculated for $\text{C}_{14}\text{H}_{14}$: 182.1096, Found: 205.0715 ($\text{M} + \text{Na}$) $^+$ (Figure 5.6). C, H, N analysis: %C calculated 92.26, found 91.92; %H calculated 7.74, found 8.06. Melting point: Reported 118–120 $^\circ\text{C}$, found 118 $^\circ\text{C}$.⁵⁶

Characterization of compound 3. ^1H NMR (CDCl_3 , 500 MHz) δ 7.49–7.48 (m, 4H, 2, 6, 2', 6' aromatic CH protons of biphenyl system), 6.97–6.96 (q, $J_{\text{ortho}} = 6.5$ Hz, $J_{\text{meta}} = 2.0$ Hz, 4H, 3, 5, 3', 5' aromatic CH protons of biphenyl system), 3.85 (s, 6H, $-\text{OCH}_3$) (Figure 5.7). ^{13}C NMR (CDCl_3 , 100 MHz) δ 158.88, 133.66, 127.87, 114.33, 55.48 (Figure 5.8). HRMS (m/z): Calculated for $\text{C}_{14}\text{H}_{14}\text{O}_2$: 214.0994, Found: 214.6317 ($\text{M} + \text{H}$) $^+$ (Figure 5.9). C, H, N analysis: %C calculated 78.48, found 78.01, %H calculated 6.59, found 6.78. Melting point: Reported 179–180 $^\circ\text{C}$, found 178 $^\circ\text{C}$.⁵⁷

Characterization of compound 4. ^1H NMR (CDCl_3 , 500 MHz) δ 8.07–8.05 (m, 4H, 3, 5, 3', 5' aromatic CH protons of biphenyl system), 7.73–7.71 (m, 4H, 2, 6, 2', 6' aromatic CH protons of biphenyl system), 2.65 (s, 6H, $-\text{COCH}_3$) (Figure 5.10). ^{13}C NMR (CDCl_3 , 100 MHz) δ 197.70, 144.50, 136.76, 129.15, 127.59, 26.81 (Figure 5.11). HRMS (m/z): Calculated for $\text{C}_{16}\text{H}_{14}\text{O}_2$: 238.0994, Found: 239.0715 ($\text{M} + \text{H}$) $^+$, 240.0754 ($\text{M} + 2\text{H}$) $^+$ (Figure 5.12). C, H, N analysis: %C calculated 80.65, found 80.20; %H calculated 5.92, found 5.97. Melting point: Reported 193–195 $^\circ\text{C}$, found 193 $^\circ\text{C}$.⁵⁷

Characterization of compound 5. ^1H NMR ($\text{DMSO}-d_6$, 400 MHz) δ 9.35 (s, 2H, $-\text{OH}$), 7.38–7.36 (d, $J_{\text{ortho}} = 8.4$ Hz, 4H, 2, 6, 2', 6' aromatic CH protons of biphenyl system), 6.81–6.79 (d, $J_{\text{ortho}} = 8.0$ Hz, 4H, 3, 5, 3', 5' aromatic CH

protons of biphenyl system) (Figure 5.13). ^{13}C NMR (DMSO- D_6 , 100 MHz) δ 156.17, 149.69, 131.13, 126.94, 115.60, 115.52 (Figure 5.14). HRMS (m/z): Calculated for $\text{C}_{12}\text{H}_{10}\text{O}_2$: 186.0681, Found: 186.0587 (M^+), 187.0620 ($\text{M} + \text{H}^+$) (Figure 5.15). C, H, N analysis: %C calculated 77.40, found 76.90; %H calculated 5.41, found 5.51. Melting point: Reported 283 °C, found 280 °C.⁵⁶

C–N (aryl-nitrogen) coupling:

General procedure for C–N coupling reactions. 0.5 mM of aryl iodide, 0.6 mM of cyclohexylamine, 0.6 mM of potassium hydroxide, and 5 mL DMSO copper nanocluster (2 mol% CuNCs) was heated at 120 °C for 7–15 h under nitrogen atmosphere. After 7–15 h, the completion of the reaction was checked by thin-layer chromatography (TLC), and DMSO was evaporated from the reaction mixture under a high vacuum. The yellow color oily crude was then extracted with ethyl acetate and washed thoroughly with distilled water. The desired product was purified using column chromatography, using EtOAc/hexanes as the eluting solvent.

Characterization of compound 6. ^1H NMR (CDCl_3 , 400 MHz) δ 7.21–7.14 (m, $J_{\text{meta}} = 7.6$ Hz, 2H, aromatic CH (meta) protons), 6.72–6.68 (m, $J_{\text{para}} = 7.2$ Hz, 1H, aromatic CH (para protons), 6.64–6.62 (m, $J_{\text{ortho}} = 8.0$ Hz, 2H, aromatic CH (ortho) protons), 3.54 (s, 1H), 3.33–3.26 (m, 1H), 2.11–2.08 (m, 2H), 1.83–1.78 (m, 2H), 1.71–1.67 (m, 1H), 1.46–1.36 (m, 2H), 1.31–1.14 (m, 3H) (Figure 5.16). ^{13}C NMR (CDCl_3 , 100 MHz) δ 147.54, 137.60, 129.36, 116.93, 113.26, 51.79, 33.61, 26.07, 25.14 (Figure 5.17). HRMS (m/z): Calculated for $\text{C}_{12}\text{H}_{17}\text{N}$ = 175.1361, Found: 176.0941 ($\text{M} + \text{H}^+$) (Figure 5.18). C, H, N analysis: %C calculated 82.23, found 81.99, %H calculated 9.78, found 9.90, %N calculated 7.99, found 8.10.⁵⁸

Characterization of compound 7. ^1H NMR (CDCl_3 , 500 MHz) δ 6.97–6.95 (d, $J_{\text{meta}} = 8.5$ Hz, 2H), 6.52–6.51 (d, $J_{\text{ortho}} = 8.0$ Hz, 2H), 3.38 (br, 1H), 3.24–3.18 (m, 1H), 2.25 (s, 3H), 2.10–2.03 (m, 2H), 1.76–1.62 (m, 3H), 1.40–1.08 (m, 5H) (Figure 5.19). ^{13}C NMR (CDCl_3 , 100 MHz) δ 145.26, 129.85, 126.20, 113.61, 52.17, 33.86, 32.06, 26.12, 25.18, 20.47 (Figure 5.20). HRMS (m/z): Calculated for $\text{C}_{13}\text{H}_{19}\text{N}$ = 189.1517, Found: 190.1678 ($\text{M} + \text{H}^+$), 202.0854 ($\text{M} + \text{Na}^+$) (Figure 5.21). C, H, N analysis: %C calculated 82.48, found 82.09, %H calculated 10.12, found 10.41, %N calculated 7.40, found 7.30.⁵⁸

Characterization of compound 8. ^1H NMR (CDCl_3 , 500 MHz) δ 6.78–6.76 (d, $J_{\text{meta}} = 8.8$ Hz, 2H), 6.59–6.57 (d, $J_{\text{ortho}} = 8.8$ Hz, 2H), 3.75 (s, 3H), 3.22 (s, 1H),

3.20–3.14 (m, 1H), 2.06–2.04 (m, 2H), 1.77–1.74 (m, 2H), 1.67–1.63 (m, 1H), 1.37–1.10 (m, 5H) (Figure 5.22). ^{13}C NMR (CDCl_3 , 100 MHz) δ 152, 141.77, 115.06, 114.96, 55.95, 52.92, 33.77, 26.12, 25.20 (Figure 5.23). HRMS (m/z): Calculated for $\text{C}_{13}\text{H}_{19}\text{NO}$ = 205.1467, Found: 205.1468 (M) $^+$, 206.1567 ($\text{M} + \text{H}$) $^+$, 207.1614 ($\text{M} + 2\text{H}$) $^+$ (Figure 5.24). C, H, N analysis: %C calculated 76.06, found 76.19, %H calculated 9.33, found 9.04, %N calculated 6.82, found 7.00.⁵⁸

Characterization of compound 9. ^1H NMR (CDCl_3 , 400 MHz) 7.81–7.79 (d, J_{meta} = 8.8 Hz, 2H), 6.53–6.51 (d, J_{ortho} = 8.0 Hz, 2H), 4.13 (br, s, 1H), 3.38–3.31 (m, 1H), 2.48 (s, 3H), 2.07–2.03 (m, 2H), 1.80–1.75 (m, 2H), 1.69–1.64 (m, 1H), 1.44–0.88 (m, 6H) (Figure 5.25). ^{13}C NMR (CDCl_3 , 100 MHz) δ 196.29, 151.45, 131.02, 126.36, 111.67, 51.39, 33.61, 33.26, 29.82, 26.05, 25.85, 24.96 (Figure 5.26). HRMS (m/z): Calculated for $\text{C}_{13}\text{H}_{19}\text{NO}$ = 217.1467, Found: 218.0865, 218.1681, ($\text{M} + \text{H}$) $^+$ 219.1301 ($\text{M} + 2\text{H}$) $^+$ (Figure 5.27). C, H, N analysis: %C calculated 77.38, found 77.01, %H calculated 8.81, found 8.49, %N calculated 6.39, found 6.50.

Characterization of compound-10. ^1H NMR (CDCl_3 , 400 MHz) δ 6.78–6.76 (d, J_{meta} = 8.8 Hz, 2H), 6.58–6.56 (d, J_{ortho} = 6.8 Hz, 2H), 3.22 (s, 1H), 3.20–3.14 (m, 1H), 2.06–2.04 (m, 2H), 1.77–1.74 (m, 2H), 1.67–1.63 (m, 1H), 1.37–1.10 (m, 5H) (Figure 5.28). ^{13}C NMR (CDCl_3 , 100 MHz) δ 152, 141.77, 115.06, 114.96, 55.95, 52.92, 33.77, 26.12, 25.20 (Figure 5.29). HRMS (m/z): Calculated for $\text{C}_{12}\text{H}_{17}\text{NO}$ = 191.1310, Found: 192.1607 ($\text{M} + \text{H}$) $^+$ (Figure 5.30). C, H, N analysis: %C calculated 75.35, found 74.89, %H calculated 8.96, found 9.18, %N calculated 7.32, found 6.99.

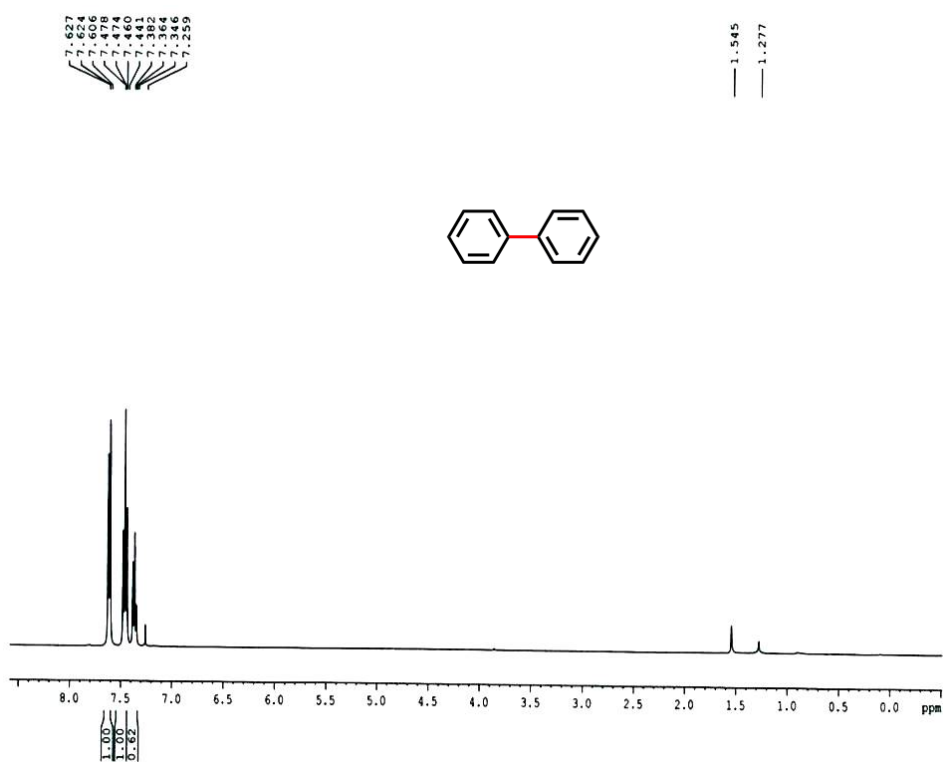


Figure 5.1. ¹H NMR spectrum of biphenyl.

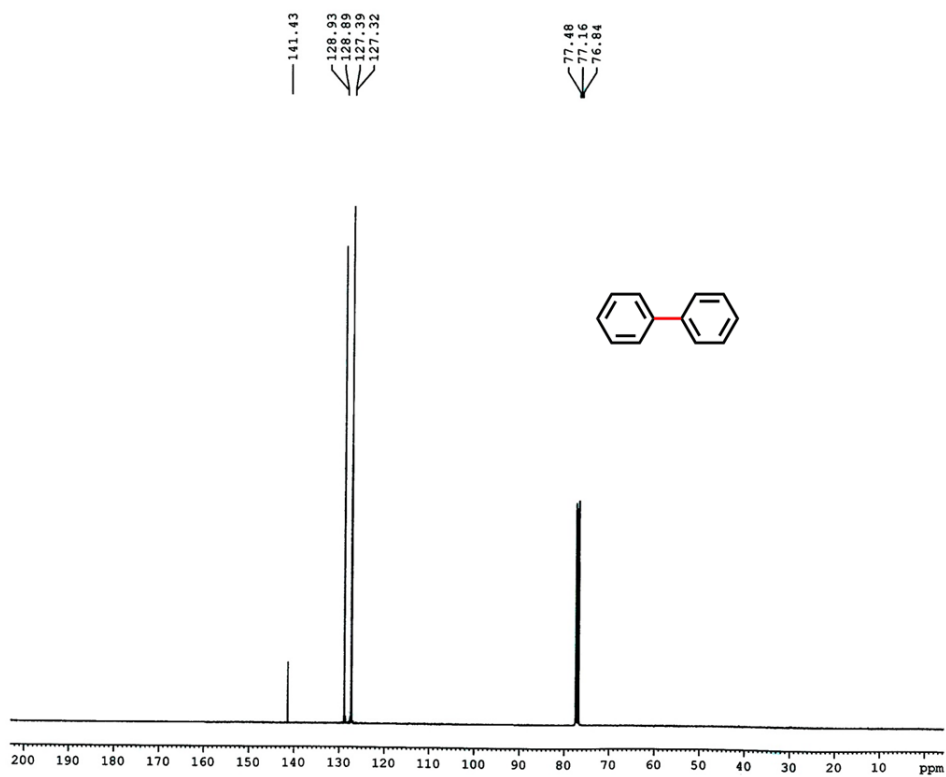


Figure 5.2. ¹³C NMR spectrum of biphenyl.

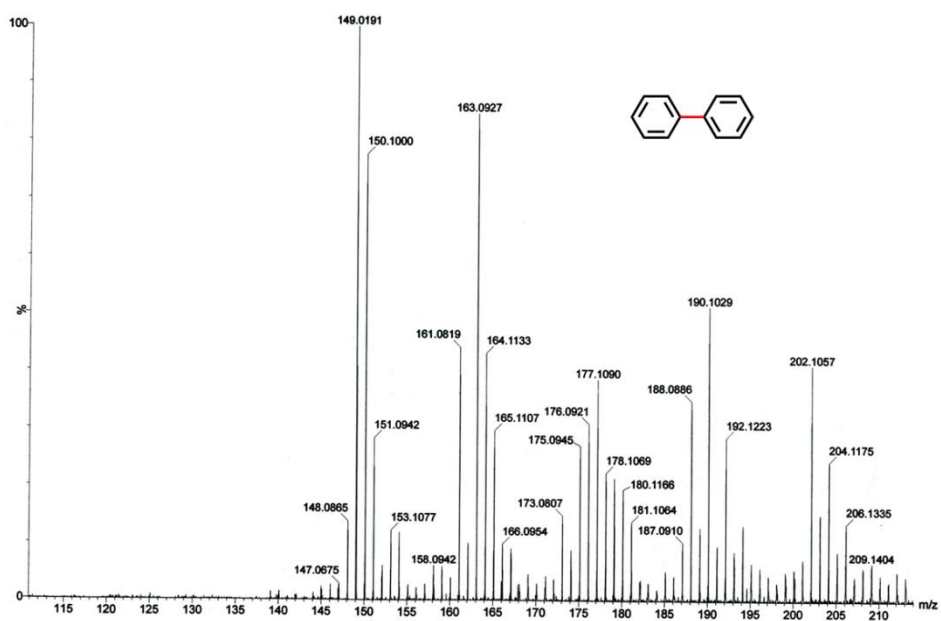


Figure 5.3. HRMS spectrum of biphenyl.

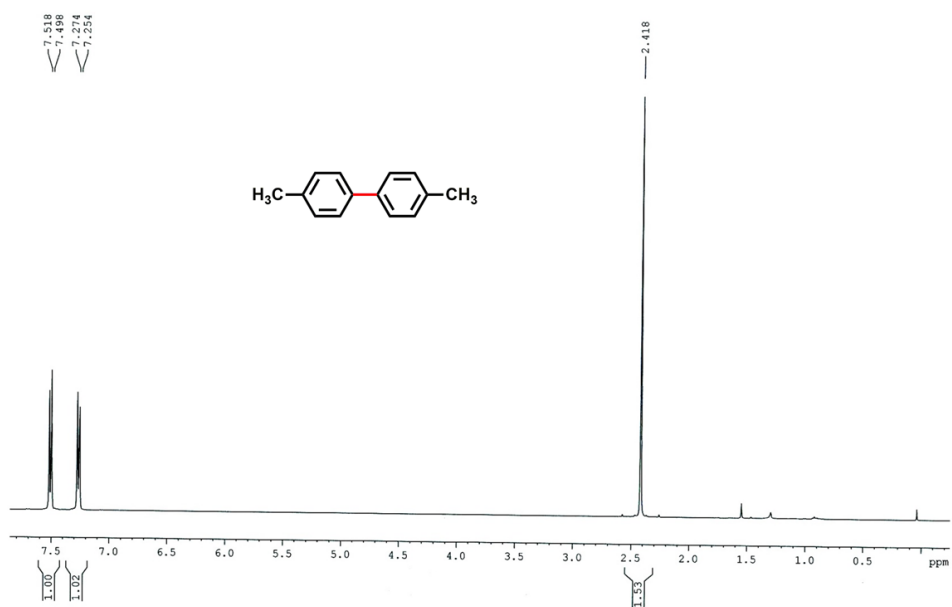


Figure 5.4. ^1H NMR spectrum of 4, 4'-Dimethylbiphenyl.



Figure 5.5. ¹³C NMR spectrum of 4, 4'-Dimethylbiphenyl.

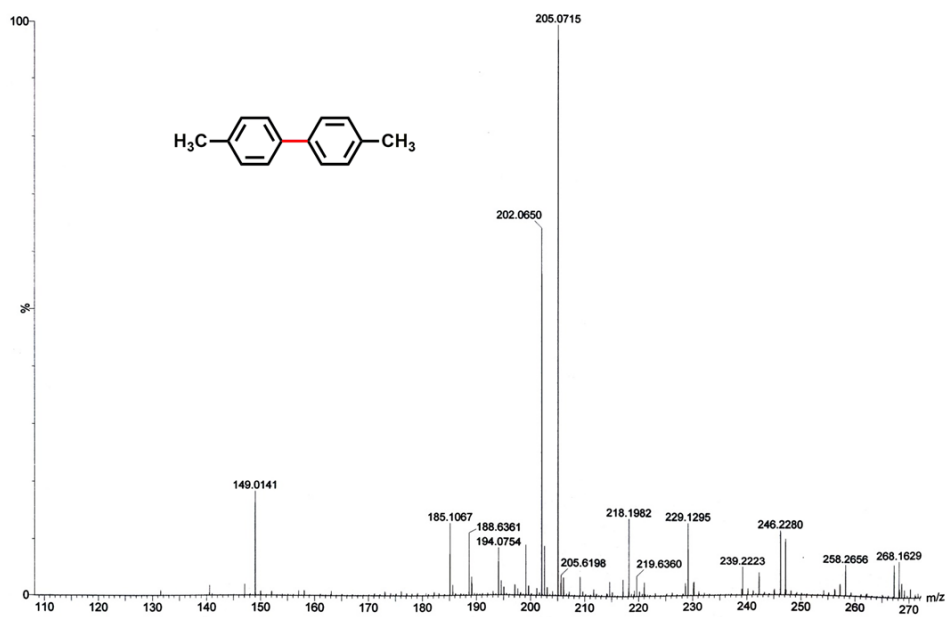


Figure 5.6. HRMS spectrum of 4, 4'-Dimethylbiphenyl.

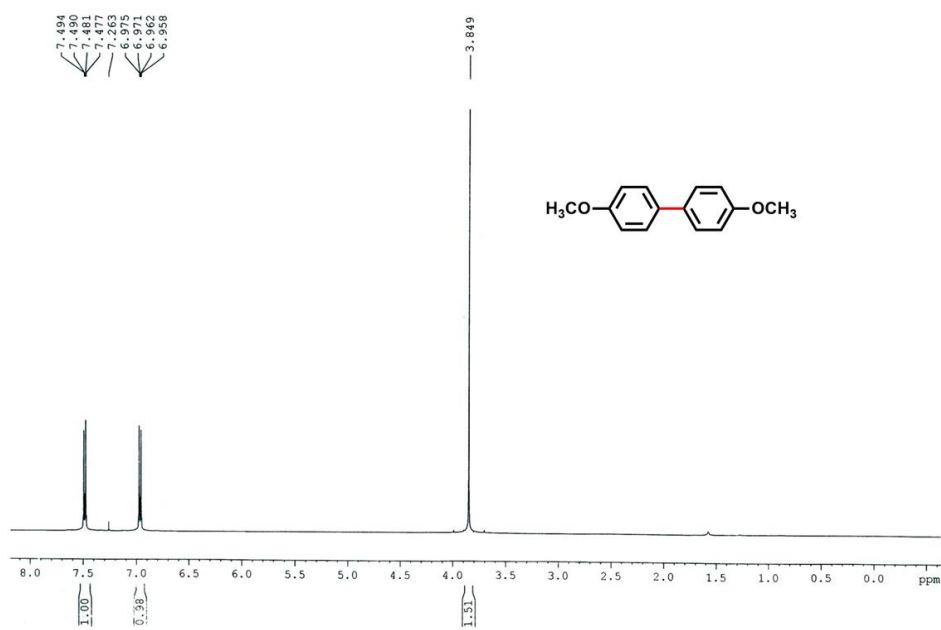


Figure 5.7. ¹H NMR spectrum of 4, 4'-Dimethoxybiphenyl.

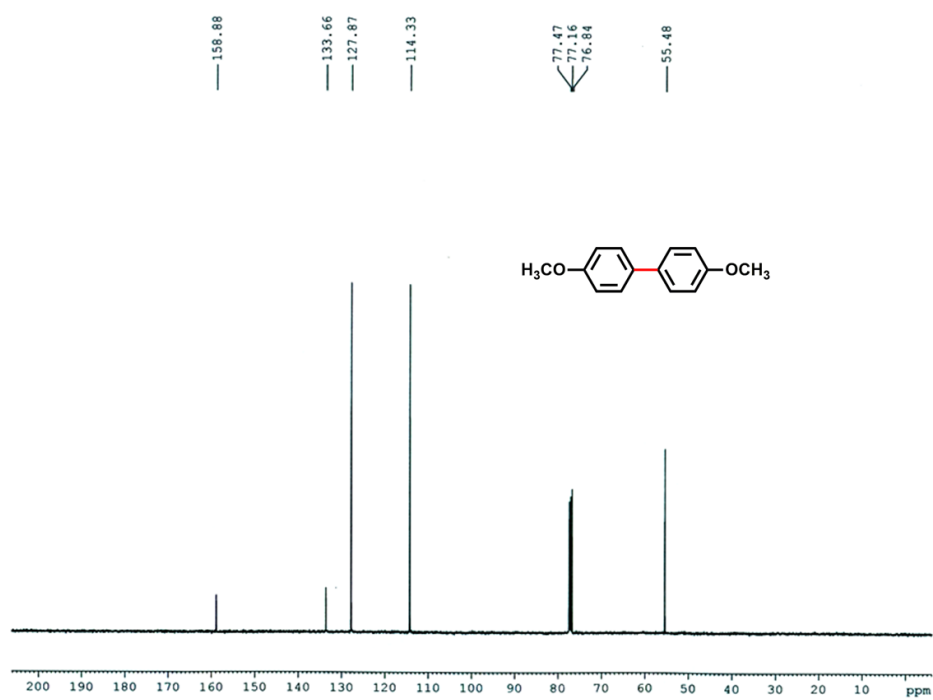


Figure 5.8. ¹³C NMR spectrum of 4, 4'-Dimethoxybiphenyl.

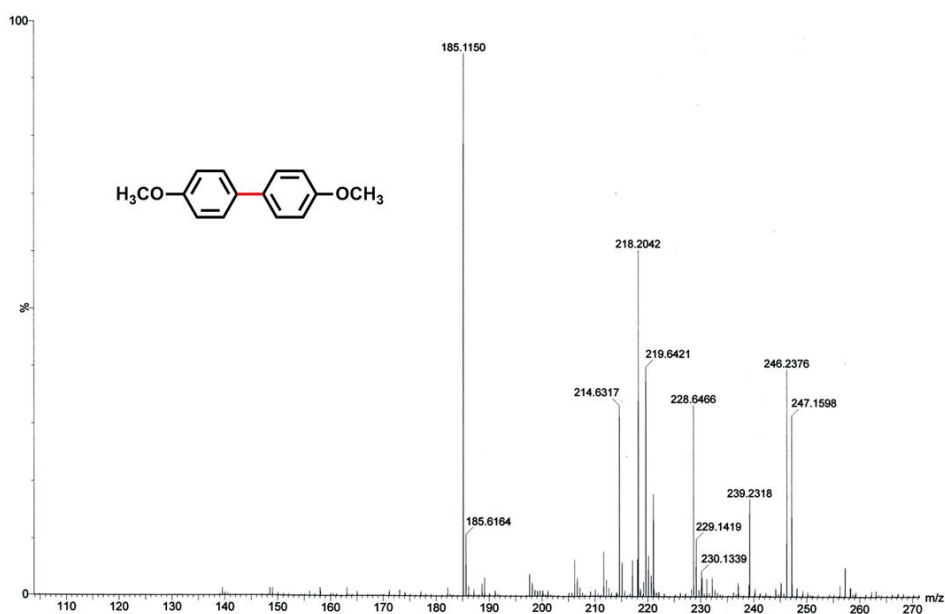


Figure 5.9. HRMS spectrum of 4,4'-Dimethoxybiphenyl.

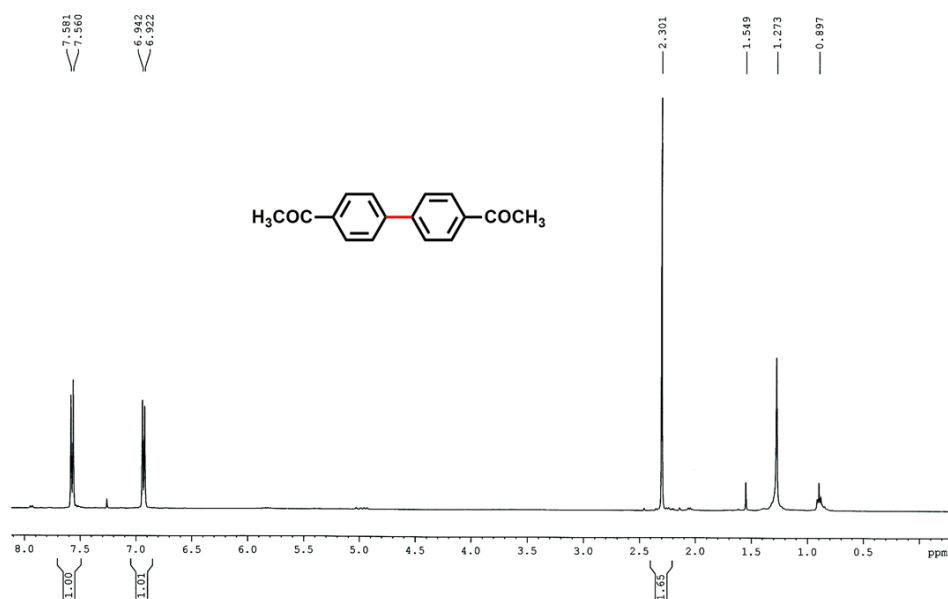


Figure 5.10. ^1H NMR spectrum of Biphenyl 4,4'-diacetyl.

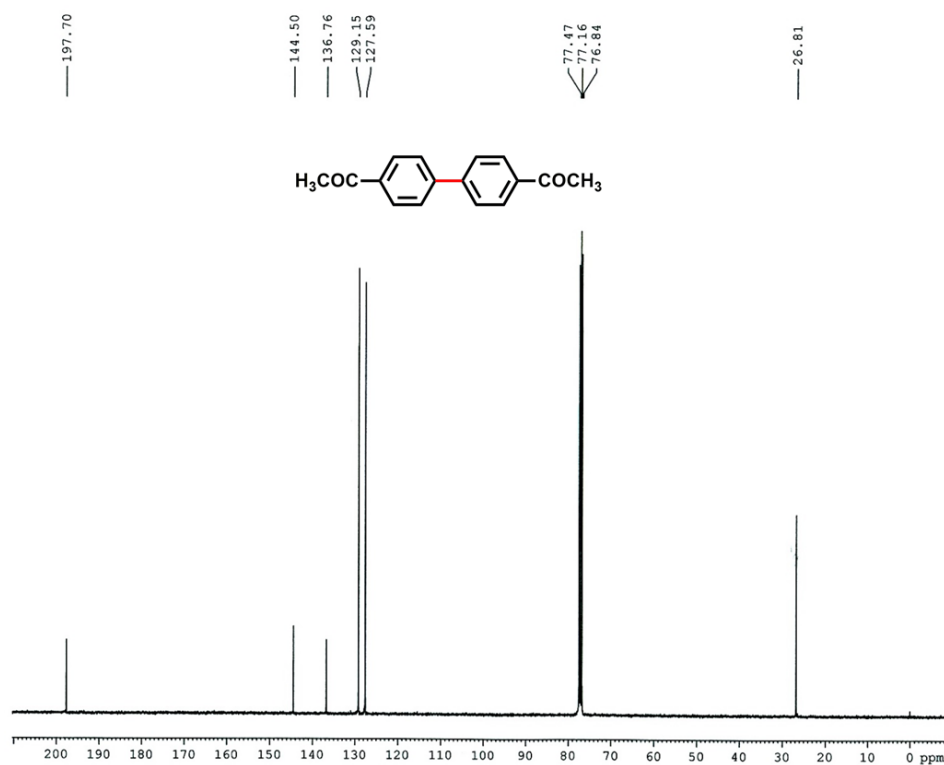


Figure 5.11. ¹³C-NMR spectrum of Biphenyl 4, 4'-diacetylphenyl.

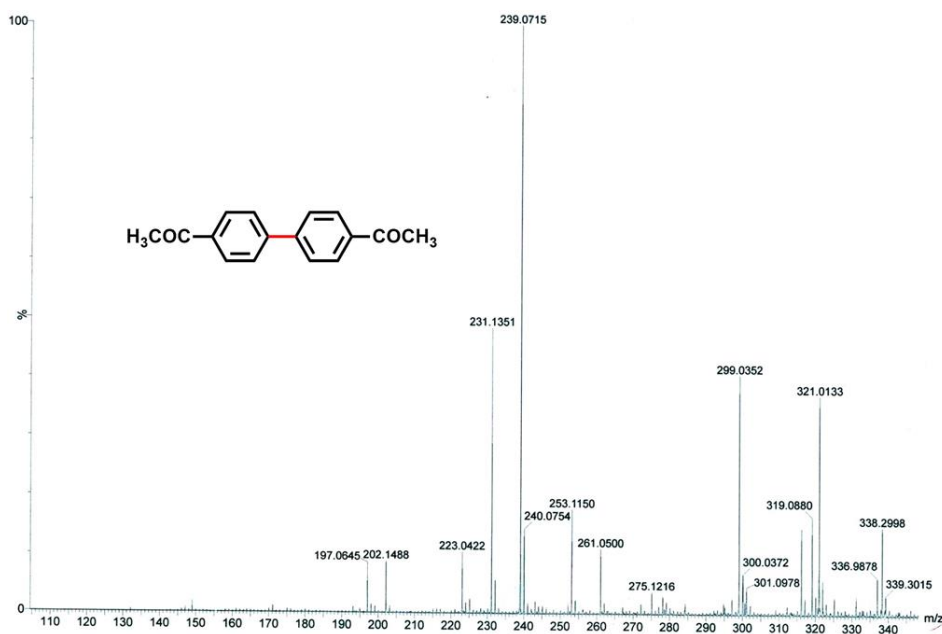


Figure 5.12. HRMS spectrum of Biphenyl 4, 4'-diacetylphenyl.

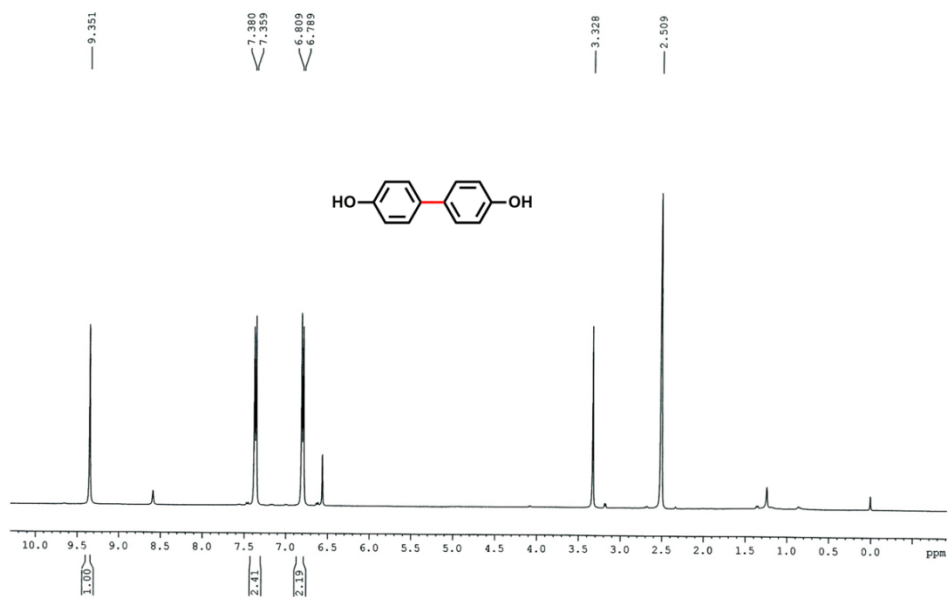


Figure 5.13. ¹H NMR spectrum of 4, 4'-Biphenol.

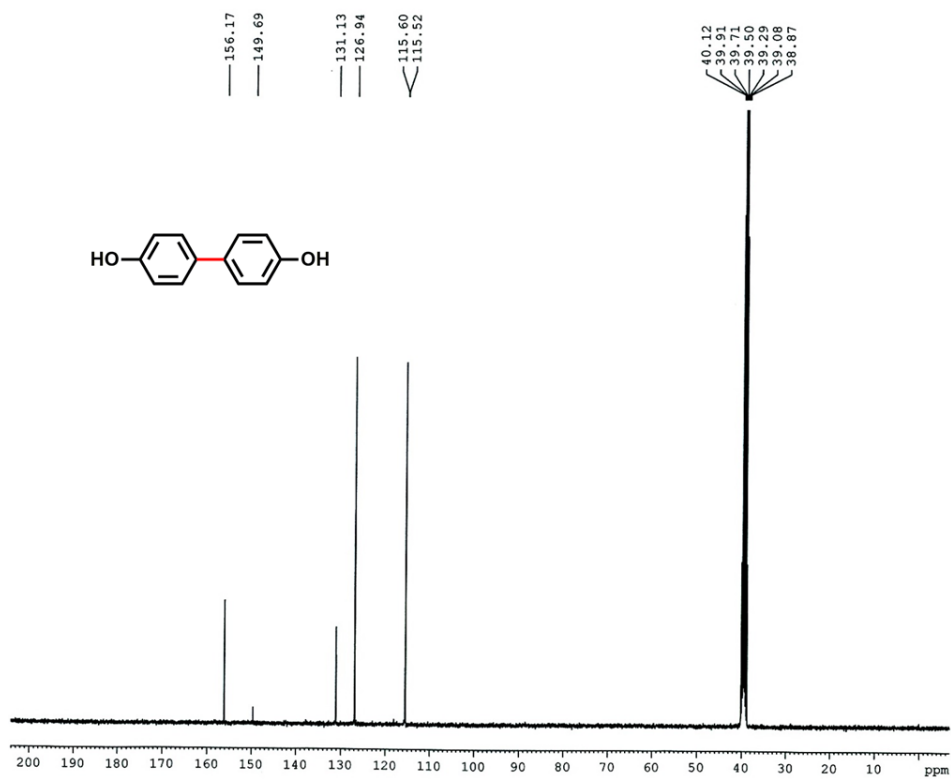


Figure 5.14. ¹³C NMR spectrum of 4, 4'-Biphenol.

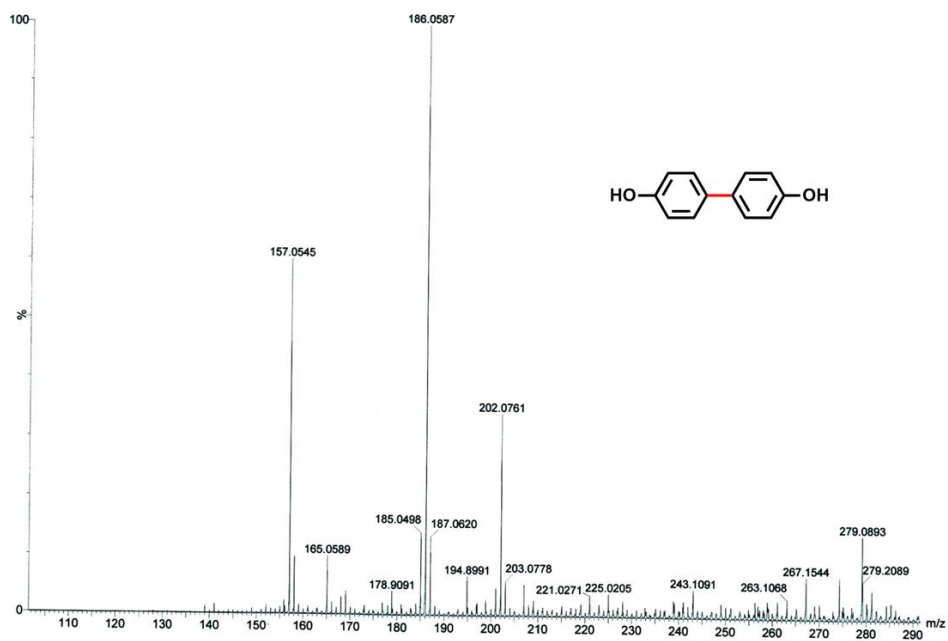


Figure 5.15. HRMS spectrum of 4,4'-Biphenol.

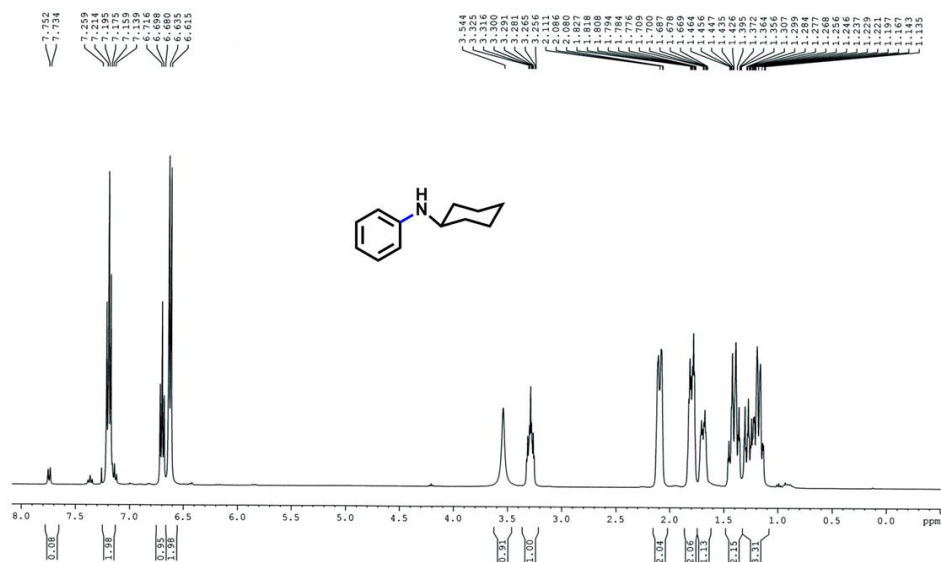


Figure 5.16. ^1H NMR spectrum of N-Cyclohexylaniline.

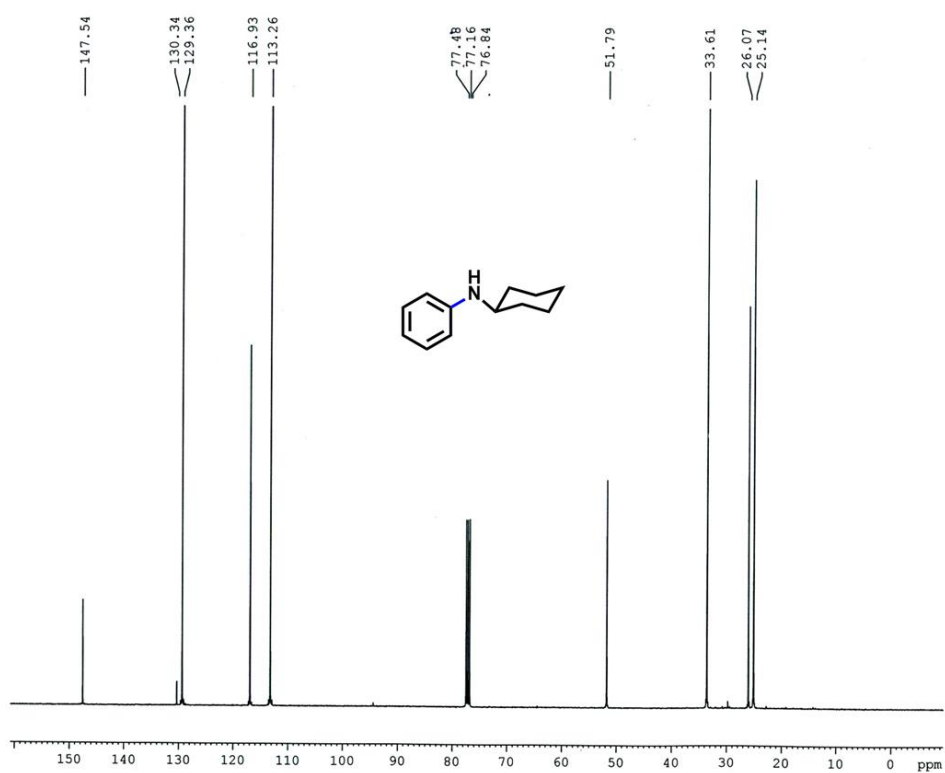


Figure 5.17. ¹³C NMR spectrum of N-Cyclohexylaniline.

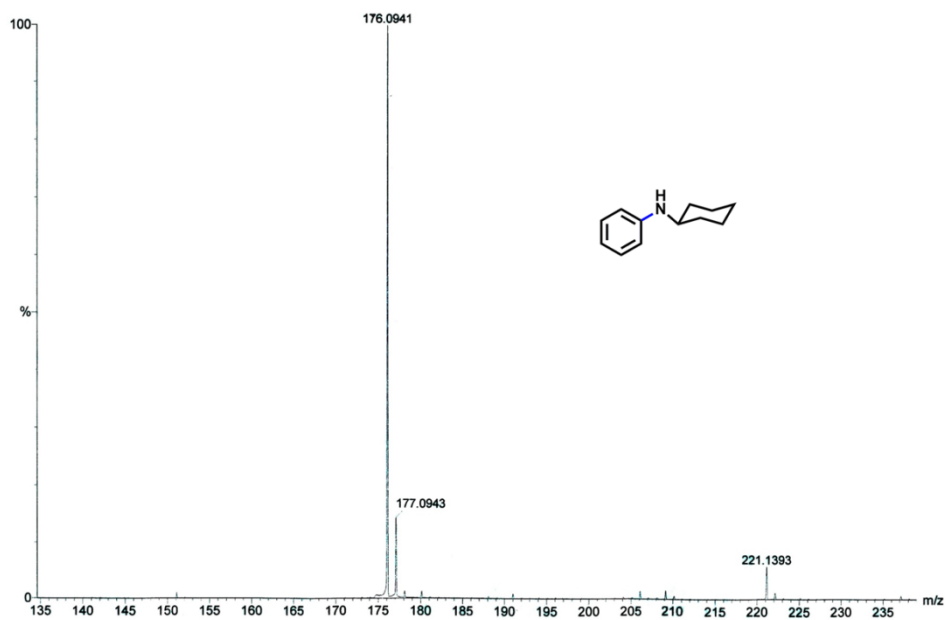


Figure 5.18. HRMS spectrum of N-Cyclohexylaniline.

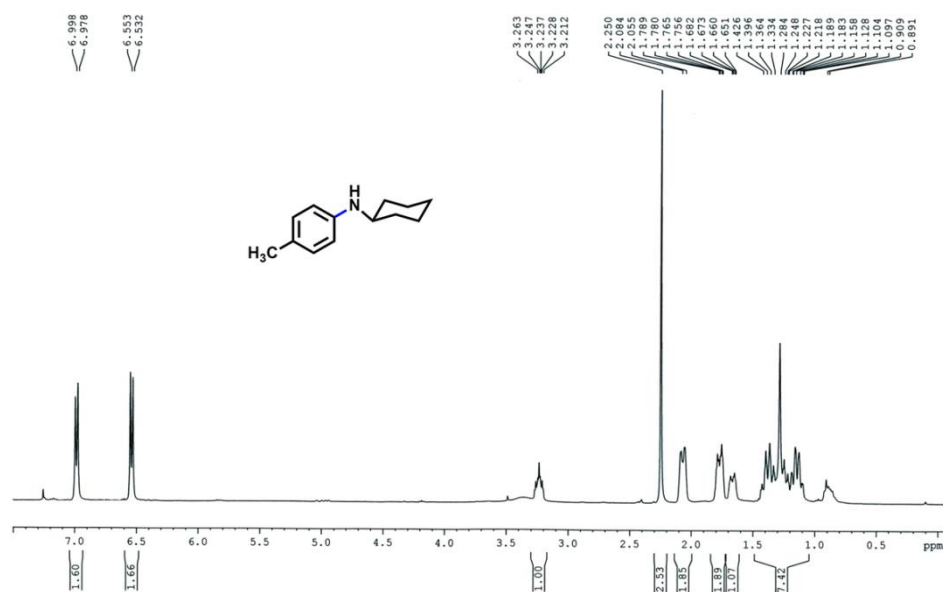


Figure 5.19. ¹H NMR spectrum of N-Cyclohexyl-4-methylaniline.

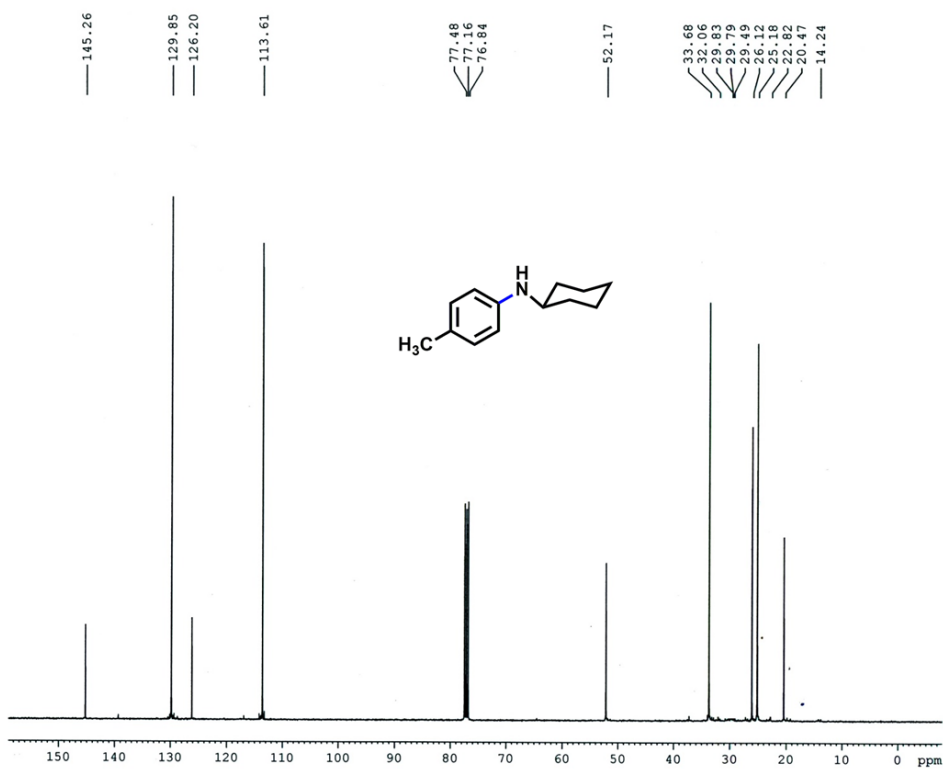


Figure 5.20. ¹³C NMR spectrum of N-Cyclohexyl-4-methylaniline.

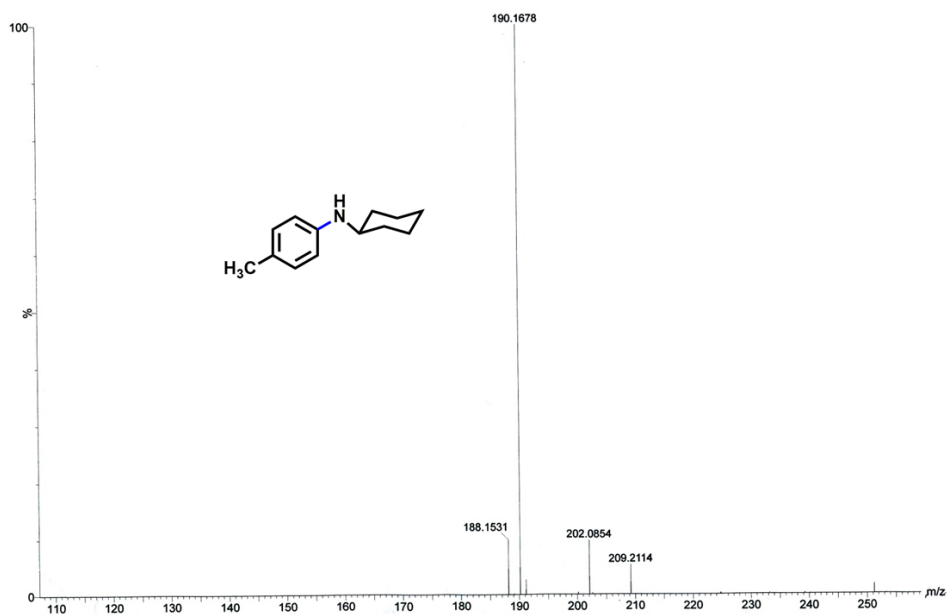


Figure 5.21. HRMS spectrum of N-Cyclohexyl-4-methylaniline.

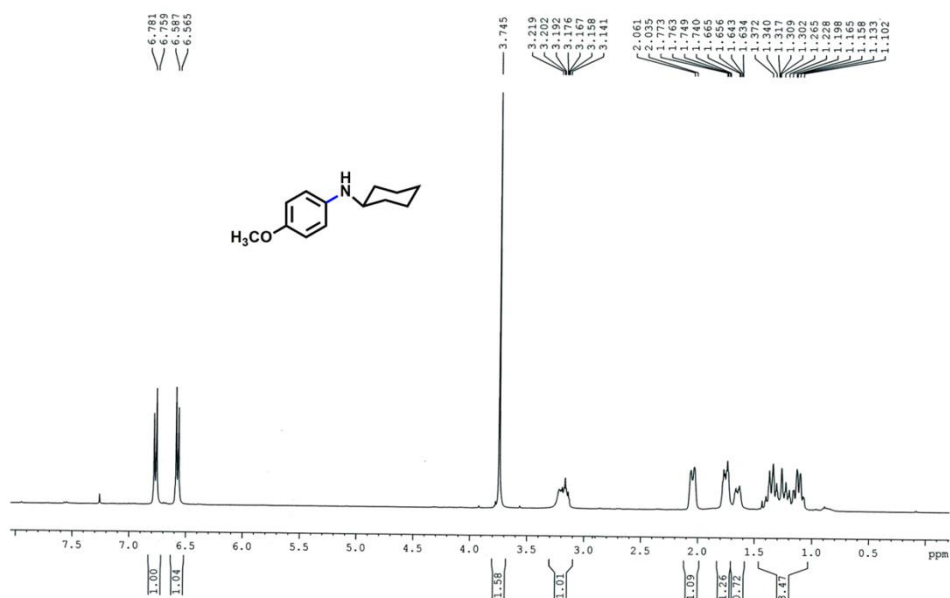


Figure 5.22. ^1H NMR spectrum of N-Cyclohexyl-4-methoxyaniline.

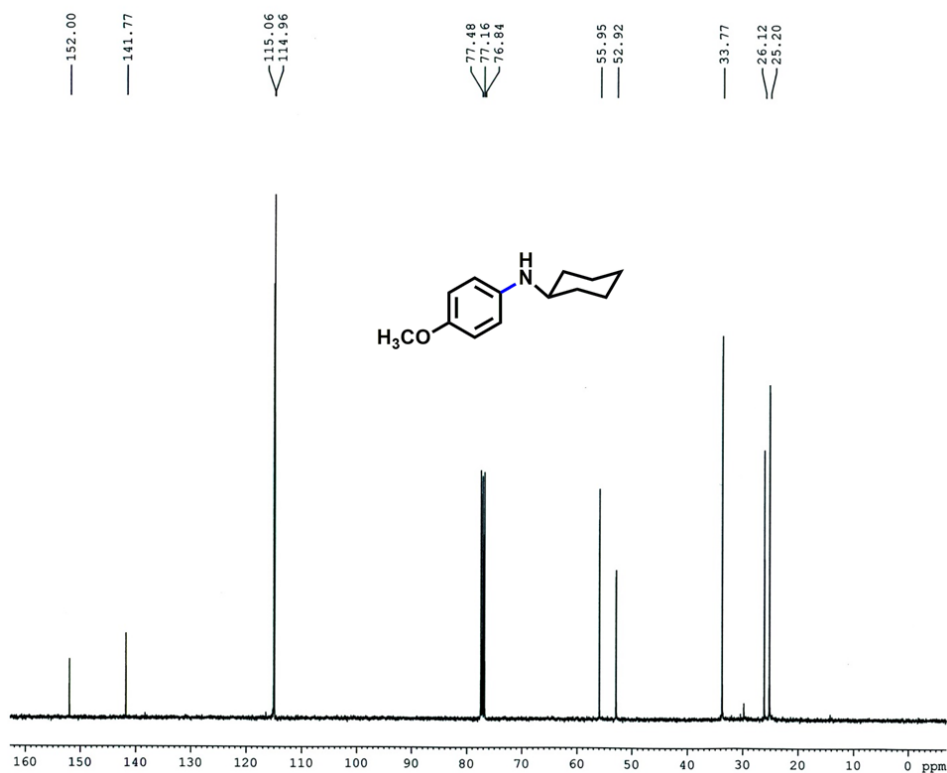


Figure 5.23. ¹³C NMR spectrum of N-Cyclohexyl-4-methoxyaniline.

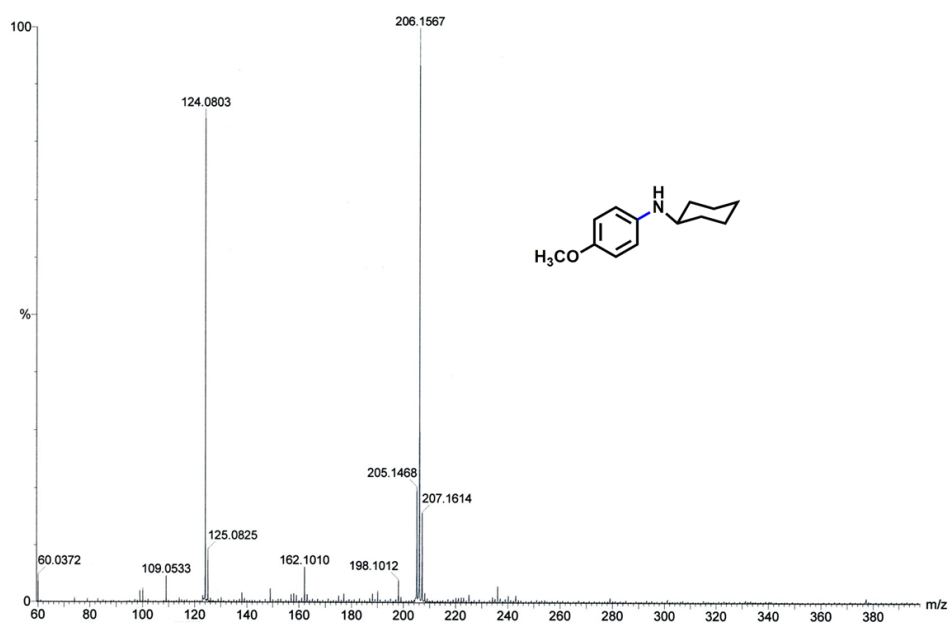


Figure 5.24. HRMS spectrum of N-Cyclohexyl-4-methoxyaniline.

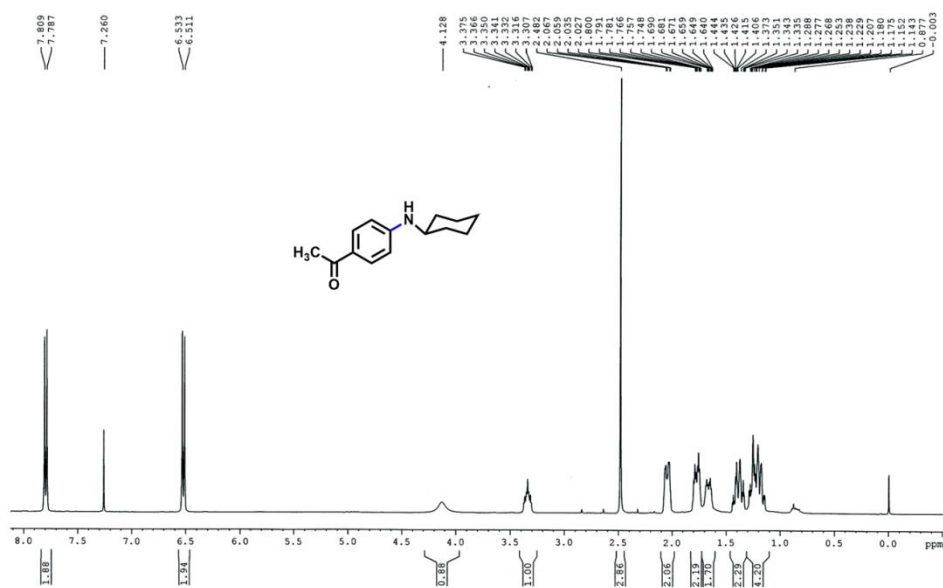


Figure 5.25. ¹H NMR spectrum of 4-(Cyclohexylamino)-acetophenone.

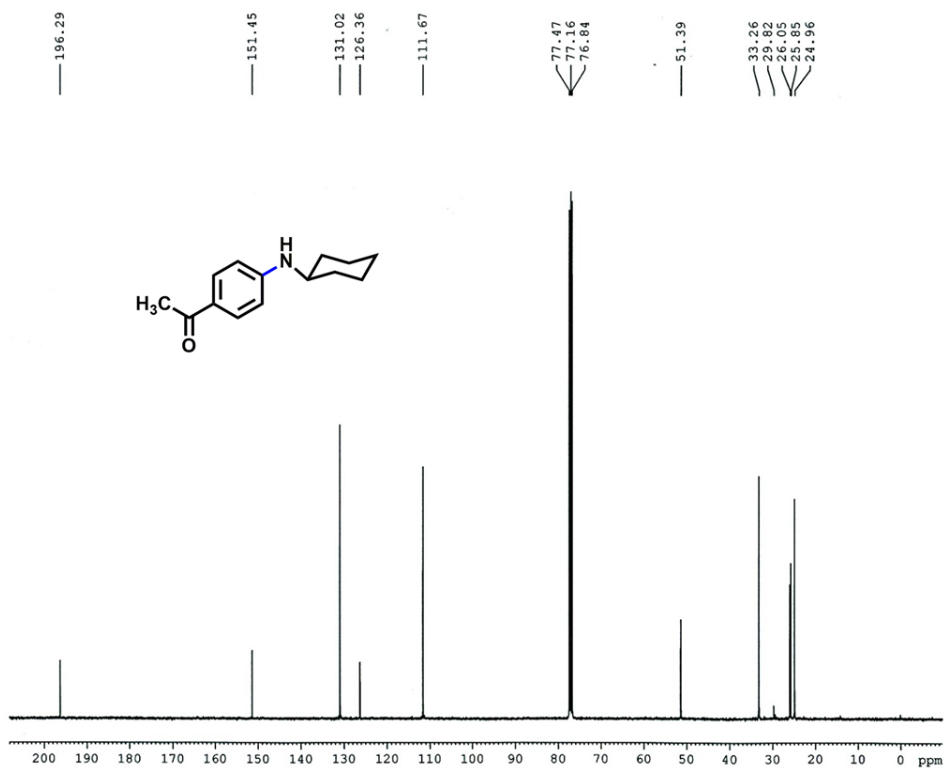


Figure 5.26. ¹³C NMR spectrum of 4-(Cyclohexylamino)-acetophenone.

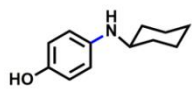
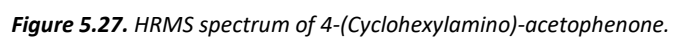


Figure 5.28. ^1H NMR spectrum of 4-(Cyclohexylamino)-phenol.

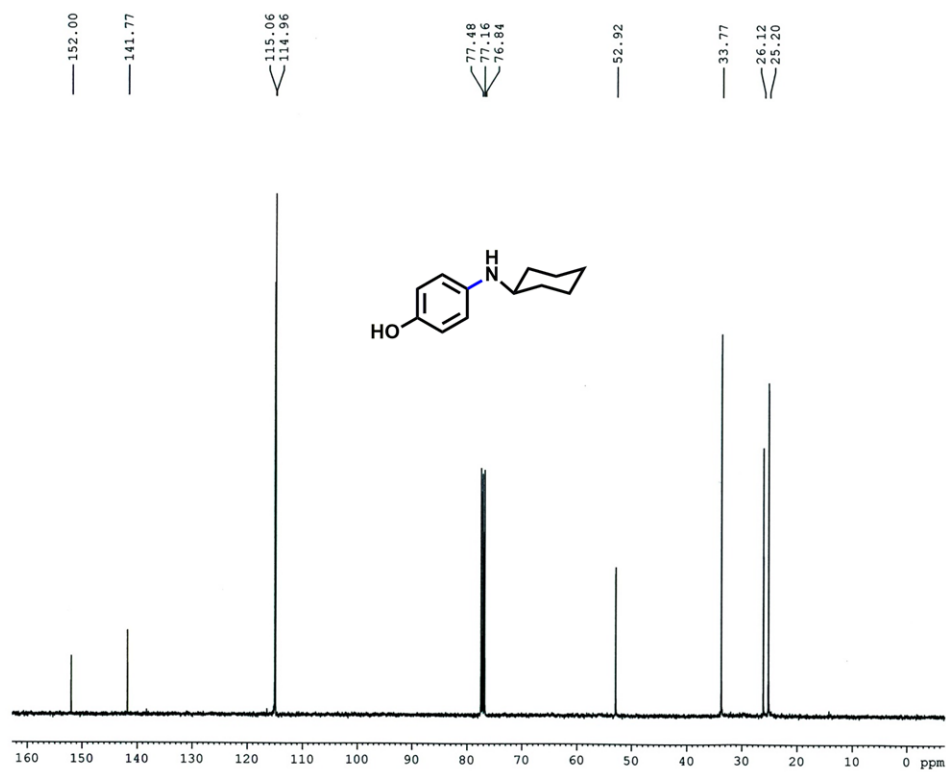


Figure 5.29. ¹³C NMR spectrum of 4-(Cyclohexylamino)-phenol.

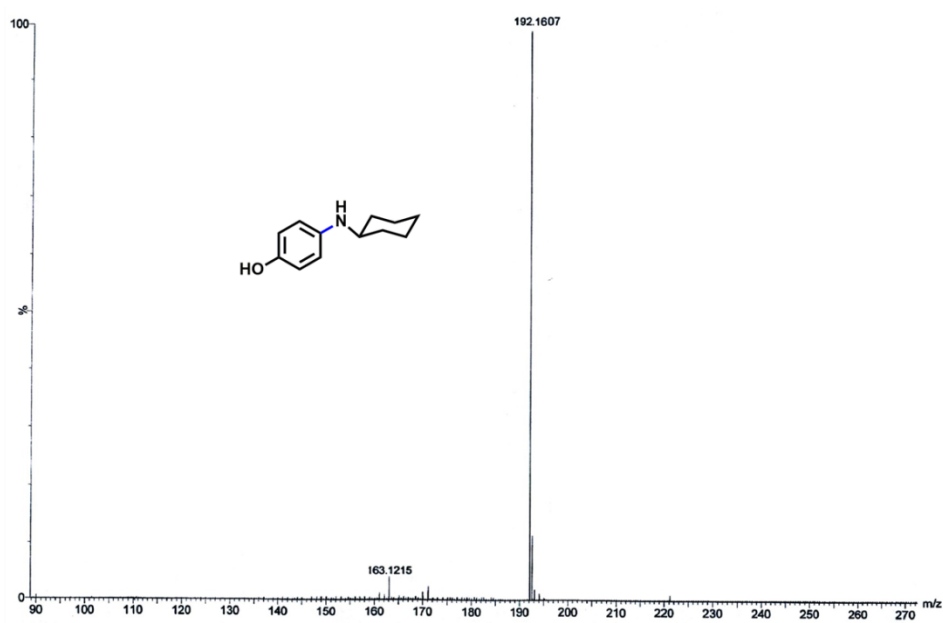


Figure 5.30. HRMS spectrum of 4-(Cyclohexylamino)-phenol.

5.2.4. Computational Details. All the DFT calculations were performed using Gaussian 16 suite of electronic structure programs.⁴⁵ The studied structures were optimized in the gas phase employing hybrid DFT functional namely B3LYP^{46, 47} in combination with the relativistic effective core potential (ECP),⁴⁸ LANL2DZ basis set for Cu and I atoms⁴⁹, while the Pople's split basis set 6-31G(d), was used for all other anchoring C, N, O, S and H atoms (Figure 5.45). Moreover, single-point energy calculations with M06-L functional⁵⁰ and larger basis set: SDD⁵¹ for the Cu and I atoms and 6-31++G(d,p) for other atoms were also performed to obtain more accurate energies (Figure 5.46). We have examined by analytical harmonic vibrational frequency analysis that all the minima structures have zero imaginary vibrational frequencies while transition state structures have one imaginary frequency. Some of the low-lying vibrational frequencies which can potentially be a source of error while calculating thermochemical parameter were treated using the quasi-harmonic approximation (QHA). In QHA, the contribution from low vibrational frequencies to the entropy is replaced by corresponding rotational entropy (i.e. low frequencies are treated as free rotors).⁵² Connection of TS to the reactant and/or product was also been verified by performing intrinsic reaction coordinate (IRC) calculations.⁵³ To mimic experimental condition, we employed single-point SMD solvation model (version SM5.2R)^{54, 55} calculations using Dimethyl sulfoxide as solvent ($\epsilon = 46.83$) with the SMD/M06-L/SDD (for Cu and I) and 6-31++G(d, p) (for all other atoms) level of theory, and their relative free energies are reported in kcal/mol.

Cartesian coordinates of all the intermediates, reactants, products and transition states

| | | |
|---|--|-------------------------------------|
| A1 | Sum of electronic and thermal Energies= | - |
| | 3985.617462 | |
| No of negative frequencies= 0 | Sum of electronic and thermal Enthalpies= | - |
| | 3985.616518 | |
| Electronic Energy : -3986.2487148 au | Sum of electronic and thermal Free Energies= | - |
| | 3985.779136 | |
| Zero-point correction= 0.574631 | | |
| (Hartree/Particle) | | |
| Thermal correction to Energy= 0.631252 | | |
| Thermal correction to Enthalpy= 0.632197 | | |
| Thermal correction to Gibbs Free Energy= 0.469579 | | |
| Sum of electronic and zero-point Energies= - | | |
| 3985.674084 | | |
| | Cu | -0.18055600 -1.53448800 2.04522600 |
| | Cu | 1.25767800 -2.75679200 0.53142900 |
| | Cu | 1.02754500 -3.48129700 -2.12960500 |
| | Cu | -1.19840800 -2.75543500 0.25477300 |
| | Cu | 0.25494400 -1.34944100 -1.36757500 |
| | Cu | -1.36512000 -2.98013000 -2.25717500 |

Chapter 5

| | | | |
|---|-------------|-------------|-------------|
| S | 3.07798100 | -3.31231200 | -0.86332600 |
| C | 3.67346300 | -1.70014900 | -1.56957000 |
| C | 3.80907800 | -0.54322600 | -0.56565800 |
| H | 3.03227400 | -1.39359100 | -2.40164100 |
| H | 4.67005400 | -1.91343900 | -1.96788400 |
| H | 4.08141800 | -0.93625600 | 0.41974100 |
| N | 4.90445100 | 0.34763200 | -0.98837800 |
| C | 2.52229800 | 0.30753900 | -0.39589700 |
| O | 1.53433300 | 0.24046900 | -1.15895600 |
| N | 2.56882900 | 1.19665400 | 0.60739300 |
| H | 3.43881700 | 1.25186500 | 1.14261800 |
| C | 1.50067200 | 2.15157300 | 0.82405900 |
| H | 1.19742300 | 2.60841400 | -0.12159800 |
| H | 1.87569300 | 2.94273700 | 1.48132500 |
| C | 0.27111400 | 1.52659100 | 1.48604600 |
| O | 0.34252200 | 0.59410700 | 2.27513300 |
| O | -0.84950900 | 2.12841800 | 1.11729300 |
| H | -1.65438100 | 1.69230700 | 1.55306000 |
| S | -3.35357700 | -2.93873700 | -0.78164400 |
| C | -3.92010300 | -1.17373700 | -0.96746000 |
| C | -3.14615500 | -0.11029800 | -0.15764500 |
| H | -3.82319900 | -0.89462000 | -2.01899200 |
| H | -2.07606800 | -0.27111900 | -0.34367000 |
| N | -3.44453200 | 1.23561200 | -0.63931700 |
| H | -2.66264300 | 1.81821500 | -0.90688200 |
| C | -3.29765700 | -0.13583000 | 1.38089200 |
| O | -2.95723000 | 0.84295400 | 2.07003700 |
| N | -3.75730400 | -1.25688500 | 1.96625500 |
| H | -3.88796800 | -2.09146500 | 1.39516200 |
| C | -3.92799200 | -1.32030800 | 3.39576700 |
| H | -4.45012500 | -2.24920600 | 3.64721400 |
| H | -4.55079200 | -0.49066400 | 3.74427300 |
| C | -2.63384700 | -1.28651600 | 4.20397200 |
| O | -1.49552000 | -1.42911300 | 3.80079500 |
| O | -2.91122500 | -1.10618400 | 5.50462700 |
| H | -2.05994900 | -1.11118800 | 5.98342200 |
| H | -4.98046000 | -1.12927500 | -0.71100600 |
| H | 5.19511900 | 0.29701200 | -1.95566000 |
| C | -4.64207500 | 1.84107400 | -0.35164100 |
| O | -5.55784800 | 1.22757900 | 0.18656900 |
| C | -4.73735600 | 3.31229700 | -0.73538900 |
| C | -6.17530700 | 3.73100300 | -1.05112800 |
| H | -4.07282200 | 3.53067800 | -1.58182600 |
| H | -4.37644600 | 3.90833300 | 0.11281700 |
| C | -6.32263800 | 5.26400500 | -1.17469500 |
| H | -6.51519600 | 3.25991800 | -1.97961000 |
| H | -6.82956800 | 3.36379300 | -0.25204400 |
| H | -5.65075400 | 5.61464900 | -1.96878900 |
| N | -5.94342400 | 5.91876400 | 0.07217100 |

| | | | |
|---|-------------|------------|-------------|
| C | -7.75178400 | 5.60128400 | -1.60794900 |
| H | -5.92980400 | 6.92849800 | -0.06345000 |
| H | -6.68026200 | 5.75288700 | 0.75838400 |
| O | -8.59258000 | 6.10694900 | -0.89663600 |
| O | -7.99236600 | 5.25408700 | -2.89517400 |
| H | -8.92759500 | 5.47412700 | -3.06970700 |
| C | 5.65740500 | 1.06910800 | -0.11131900 |
| O | 5.34519900 | 1.17649000 | 1.08001500 |
| C | 6.91357900 | 1.70806000 | -0.68224200 |
| C | 7.24311400 | 3.04482700 | -0.01119400 |
| H | 6.82435700 | 1.82904100 | -1.76998500 |
| H | 7.75095200 | 1.01991900 | -0.50894500 |
| C | 8.65381700 | 3.54821600 | -0.39291200 |
| H | 6.50270600 | 3.80529600 | -0.28270900 |
| H | 7.18540700 | 2.91324700 | 1.07536200 |
| H | 8.69727900 | 3.66480800 | -1.48333800 |
| N | 9.66687900 | 2.58044900 | 0.00913000 |
| C | 8.87872300 | 4.93248900 | 0.22215700 |
| H | 10.56751800 | 2.83963700 | -0.38992700 |
| H | 9.79262600 | 2.64500100 | 1.01969500 |
| O | 9.61786300 | 5.16574400 | 1.15296800 |
| O | 8.13440500 | 5.88849200 | -0.38388800 |
| H | 8.32082300 | 6.72362100 | 0.08686300 |

Ph-I

No of negative frequencies= 0

Electronic Energy : -243.0215899 au

Zero-point correction= 0.090302

(Hartree/Particle)

Thermal correction to Energy= 0.096192

Thermal correction to Enthalpy= 0.097137

Thermal correction to Gibbs Free Energy= 0.058536

Sum of electronic and zero-point Energies= -242.931288

Sum of electronic and thermal Energies= -242.925398

Sum of electronic and thermal Enthalpies= -242.924453
Sum of electronic and thermal Free Energies= -242.963054

| | | | |
|---|------------|-------------|-------------|
| C | 3.36164500 | 0.00000100 | 0.00000000 |
| C | 2.66127700 | 1.20725000 | 0.00000200 |
| C | 1.26374400 | 1.21566900 | -0.00000100 |
| C | 0.58098300 | 0.00000100 | 0.00000000 |
| C | 1.26374600 | -1.21567000 | 0.00000200 |

| | | | |
|---|-------------|-------------|-------------|
| C | 2.66127600 | -1.20725100 | -0.00000200 |
| H | 4.44792300 | 0.00000000 | 0.00000000 |
| H | 3.19855300 | 2.15184700 | -0.00000100 |
| H | 0.72220600 | 2.15529400 | -0.00000200 |
| H | 0.72220500 | -2.15529500 | 0.00000400 |
| H | 3.19855400 | -2.15184500 | -0.00000200 |
| I | -1.56689600 | 0.00000000 | 0.00000000 |

A2

No of negative frequencies= 0

Electronic Energy : -4229.2649548 au

Zero-point correction= 0.665430
(Hartree/Particle)

Thermal correction to Energy= 0.730468

Thermal correction to Enthalpy= 0.731412

Thermal correction to Gibbs Free Energy= 0.545268

Sum of electronic and zero-point Energies= -
4228.599525

Sum of electronic and thermal Energies= -
4228.534487

Sum of electronic and thermal Enthalpies= -
4228.533543

Sum of electronic and thermal Free Energies= -
4228.719687

| | | | |
|----|-------------|-------------|-------------|
| C | 0.19900100 | 4.70999500 | -1.53714300 |
| C | -0.54930500 | 4.21691500 | -0.46962700 |
| C | -1.87050300 | 3.79760100 | -0.69567000 |
| C | -2.41683600 | 3.79295900 | -1.98817900 |
| C | -1.64851900 | 4.29745500 | -3.04678400 |
| C | -0.34959500 | 4.75416300 | -2.82269100 |
| H | 1.21790900 | 5.04985900 | -1.34895000 |
| H | -0.12092300 | 4.16319800 | 0.52300700 |
| H | -3.43857000 | 3.45987800 | -2.15114800 |
| H | -2.08038800 | 4.33068600 | -4.04429400 |
| H | 0.23345400 | 5.14528400 | -3.65149900 |
| I | -3.17934000 | 3.51948100 | 1.00723900 |
| Cu | -1.67416500 | 1.42253600 | -0.47908800 |
| Cu | -1.65563300 | -1.10163500 | -3.76611700 |
| Cu | -0.07120600 | -0.44773800 | -0.96742500 |
| Cu | -3.54835400 | -0.05695000 | -4.71521700 |
| Cu | -2.52827900 | -0.87067200 | -0.28297100 |
| Cu | -2.99493100 | 0.34354100 | -2.31833100 |
| S | 0.14403000 | -1.97806600 | -2.63744500 |
| C | -0.54710000 | -3.45632600 | -1.75521700 |

| | | | |
|---|-------------|-------------|-------------|
| C | -0.11314500 | -3.54405300 | -0.27334200 |
| H | -0.23093500 | -4.34802200 | -2.30384200 |
| H | -1.64112800 | -3.40706400 | -1.79104200 |
| H | -0.10658500 | -2.52950400 | 0.14839400 |
| N | -1.04548400 | -4.33683500 | 0.50861000 |
| C | 1.27647600 | -4.17227700 | -0.05915600 |
| O | 1.39724700 | -5.24361400 | 0.54654100 |
| N | 2.32227500 | -3.47936400 | -0.55227200 |
| H | 2.19055500 | -2.61979000 | -1.07328000 |
| C | 3.68505000 | -3.92216100 | -0.34895900 |
| H | 3.90138100 | -4.83950200 | -0.91418800 |
| H | 3.86252000 | -4.16498300 | 0.70503700 |
| C | 4.66751800 | -2.84236800 | -0.78414500 |
| O | 4.32493800 | -1.78098000 | -1.28781700 |
| O | 5.91381000 | -3.22299500 | -0.56097100 |
| H | 6.57391100 | -2.51017100 | -0.86058300 |
| H | -0.66076200 | -5.21815600 | 0.85050000 |
| C | -2.20755100 | -3.85316200 | 0.98919600 |
| O | -2.61933000 | -2.69994200 | 0.73618100 |
| C | -3.02954300 | -4.79839500 | 1.84189000 |
| C | -3.57113200 | -4.11618200 | 3.10993600 |
| H | -2.44754600 | -5.68898700 | 2.10013000 |
| H | -3.88907000 | -5.13273700 | 1.24473600 |
| C | -4.59896000 | -5.01136400 | 3.84520700 |
| H | -2.74952600 | -3.86914700 | 3.78820100 |
| H | -4.05462600 | -3.17512100 | 2.82675700 |
| H | -4.11212400 | -5.95490100 | 4.11664600 |
| N | -5.73496300 | -5.30113300 | 2.97746300 |
| C | -5.00803400 | -4.30407100 | 5.14030600 |
| H | -6.30773400 | -6.03377900 | 3.39492900 |
| H | -6.33230900 | -4.47312400 | 2.94394000 |
| O | -6.02766900 | -3.65866100 | 5.28281500 |
| O | -4.07569500 | -4.45516100 | 6.11920600 |
| H | -4.39699300 | -3.93537500 | 6.88354400 |
| S | 0.36665200 | 0.93217700 | 0.84488000 |
| C | 2.05180500 | 1.43996900 | 0.23499200 |
| C | 2.95402000 | 2.01544100 | 1.35449600 |
| H | 1.96293500 | 2.17130000 | -0.57279800 |
| H | 2.55755700 | 0.55206500 | -0.14908900 |
| H | 2.87188700 | 1.38915400 | 2.24806500 |
| N | 4.34607400 | 1.97413400 | 0.92372300 |
| C | 2.59989200 | 3.47406800 | 1.63579000 |
| O | 2.88950700 | 4.36413700 | 0.83115000 |
| N | 1.94615800 | 3.72928200 | 2.79453300 |
| H | 1.63863300 | 2.97598400 | 3.39995900 |
| C | 1.48176100 | 5.05839000 | 3.12380900 |
| H | 0.93699400 | 5.50718000 | 2.28335900 |
| H | 2.32181900 | 5.73777600 | 3.34070700 |

Chapter 5

| | | | |
|---|-------------|-------------|-------------|
| C | 0.57455800 | 4.98337800 | 4.33746000 |
| O | 0.29619700 | 3.96643400 | 4.93824200 |
| O | 0.11245800 | 6.20335800 | 4.67666000 |
| H | -0.46720100 | 6.07824000 | 5.45338900 |
| H | 4.60997400 | 2.68428200 | 0.24668700 |
| C | 5.06679300 | 0.81388700 | 1.02112300 |
| O | 4.72390700 | -0.12037600 | 1.73481900 |
| C | 6.29769500 | 0.73449100 | 0.11629500 |
| C | 7.39173500 | -0.15172100 | 0.71101800 |
| H | 6.67929000 | 1.73345200 | -0.12256900 |
| H | 5.91983000 | 0.29042300 | -0.81640400 |
| C | 8.43864600 | -0.57971800 | -0.33288000 |
| H | 7.90001600 | 0.37180900 | 1.53109700 |
| H | 6.92475600 | -1.04689800 | 1.13834300 |
| H | 8.89055700 | 0.32546800 | -0.77374900 |
| N | 7.84075200 | -1.43771600 | -1.37364900 |
| C | 9.60841800 | -1.34668400 | 0.27304500 |
| H | 7.45387400 | -0.88058000 | -2.12965500 |
| H | 8.57372300 | -2.03884000 | -1.76163300 |
| O | 10.08026800 | -2.36178700 | -0.18940300 |
| O | 10.10551300 | -0.73779000 | 1.37199900 |
| H | 10.86167300 | -1.28188600 | 1.67109700 |

TS1

No of negative frequencies= 1

Imaginary Frequency = -207.184 cm⁻¹

Electronic Energy: -4229.2489315 au

Zero-point correction= 0.664618

(Hartree/Particle)

Thermal correction to Energy= 0.729298

Thermal correction to Enthalpy= 0.730242

Thermal correction to Gibbs Free Energy= 0.545117

Sum of electronic and zero-point Energies= -4228.584314

Sum of electronic and thermal Energies= -4228.519634

Sum of electronic and thermal Enthalpies= -4228.518689

Sum of electronic and thermal Free Energies= -4228.703814

| | | | |
|---|-------------|-------------|-------------|
| C | -2.46920500 | -5.40122600 | -0.33681500 |
| C | -1.33377500 | -4.67661100 | 0.06233600 |
| C | -0.24083600 | -4.59646400 | -0.81175100 |
| C | -0.18895400 | -5.36011500 | -1.98838000 |

| | | | |
|----|-------------|-------------|-------------|
| C | -1.30910700 | -6.10337800 | -2.34420700 |
| C | -2.45647500 | -6.11347400 | -1.53167600 |
| H | -3.33948000 | -5.40575200 | 0.31292400 |
| H | -1.32554200 | -4.17020500 | 1.02184200 |
| H | 0.68739600 | -5.33596300 | -2.62539900 |
| H | -1.29699700 | -6.66741300 | -3.27348100 |
| H | -3.32391100 | -6.69593700 | -1.82822500 |
| I | 1.97539600 | -4.36954300 | 0.41547800 |
| Cu | -0.06306700 | -2.57095800 | -0.59604700 |
| Cu | 2.29070600 | -0.00649900 | -2.67653200 |
| Cu | 0.33464700 | 0.05736300 | -1.17806600 |
| Cu | 0.49741200 | -1.91669600 | -2.89071600 |
| Cu | 3.42568700 | 0.21495800 | -0.52144300 |
| Cu | 2.48853400 | -1.92101300 | -1.22981500 |
| S | 0.77028800 | 1.80949100 | -2.75934500 |
| C | 1.76665700 | 3.03827500 | -1.78215900 |
| C | 1.43040200 | 3.07924400 | -0.27021500 |
| H | 1.60793000 | 4.02448800 | -2.23098400 |
| H | 2.82547100 | 2.79245100 | -1.88671700 |
| H | 1.23775600 | 2.05611500 | 0.07724100 |
| N | 2.52674800 | 3.64222200 | 0.50881200 |
| C | 0.20842700 | 3.97096000 | 0.05418000 |
| O | 0.35197500 | 4.99631800 | 0.72718600 |
| N | -0.98310000 | 3.57535500 | -0.43217700 |
| H | -1.06802000 | 2.75548100 | -1.02746100 |
| C | -2.17610400 | 4.36098700 | -0.18139100 |
| H | -2.03339500 | 5.40121600 | -0.49236200 |
| H | -2.41032100 | 4.38016200 | 0.89037800 |
| C | -3.37601000 | 3.77311300 | -0.90113500 |
| O | -3.38029100 | 2.67764100 | -1.44086500 |
| O | -4.40538700 | 4.60820800 | -0.84721500 |
| H | -5.24544000 | 4.18811000 | -1.23067500 |
| H | 2.29445600 | 4.55134600 | 0.90832800 |
| C | 3.62891100 | 2.99465800 | 0.90841100 |
| O | 3.92201800 | 1.82366100 | 0.57466800 |
| C | 4.56421400 | 3.76114200 | 1.82727900 |
| C | 6.01547800 | 3.71391900 | 1.32884000 |
| H | 4.50488600 | 3.28206100 | 2.81452300 |
| H | 4.24604800 | 4.79985700 | 1.94943200 |
| C | 6.97366300 | 4.47328100 | 2.27281600 |
| H | 6.33733500 | 2.67331200 | 1.23413400 |
| H | 6.07803500 | 4.16583900 | 0.32869000 |
| H | 6.88951900 | 4.02928200 | 3.27257900 |
| N | 6.60626300 | 5.88251300 | 2.35636200 |
| C | 8.41414500 | 4.26546400 | 1.79636600 |
| H | 7.11600400 | 6.32412900 | 3.11994500 |
| H | 6.93657500 | 6.34943500 | 1.51106300 |
| O | 9.09083400 | 5.11015100 | 1.25108300 |
| O | 8.85465500 | 3.00737600 | 2.03063000 |

Copper Nanoclusters for.....

| | | | |
|---|-------------|-------------|-------------|
| H | 9.75872700 | 2.95620100 | 1.66499100 |
| S | -0.59389600 | -0.73735500 | 0.78012000 |
| C | -2.38720800 | -0.44582500 | 0.40126000 |
| C | -3.28468600 | -0.52444800 | 1.65562900 |
| H | -2.73725800 | -1.17729100 | -0.33229100 |
| H | -2.49793300 | 0.55296600 | -0.02480600 |
| H | -2.92758400 | 0.18306600 | 2.40737400 |
| N | -4.63870400 | -0.13059200 | 1.28556200 |
| C | -3.35840100 | -1.94978700 | 2.21107100 |
| O | -4.02830300 | -2.81801200 | 1.64797600 |
| N | -2.65778800 | -2.18361700 | 3.34481400 |
| H | -2.04861300 | -1.47734800 | 3.74167200 |
| C | -2.60434600 | -3.49448100 | 3.94867700 |
| H | -2.19959800 | -4.24834200 | 3.26047600 |
| H | -3.60586300 | -3.84300500 | 4.22920100 |
| C | -1.72422100 | -3.43633400 | 5.18006000 |
| O | -1.13965700 | -2.44853100 | 5.56691100 |
| O | -1.66616000 | -4.63249600 | 5.79595600 |
| H | -1.07416700 | -4.52348600 | 6.56456700 |
| H | -5.17225900 | -0.84272600 | 0.80101500 |
| C | -4.98031200 | 1.18662000 | 1.15981300 |
| O | -4.31557000 | 2.09294900 | 1.65268900 |
| C | -6.20355000 | 1.45072500 | 0.28253400 |
| C | -6.90896700 | 2.76719000 | 0.62410800 |
| H | -6.90047000 | 0.60308200 | 0.31024600 |
| H | -5.78985500 | 1.49591200 | -0.73441700 |
| C | -7.72011600 | 3.31888400 | -0.56526000 |
| H | -7.57540900 | 2.62707800 | 1.48037800 |
| H | -6.15204200 | 3.50202800 | 0.91280300 |
| H | -8.47466800 | 2.56831200 | -0.85593200 |
| N | -6.84476000 | 3.66683800 | -1.70215700 |
| C | -8.52002900 | 4.56619200 | -0.20084500 |
| H | -6.75273800 | 2.88734300 | -2.34835600 |
| H | -7.26305500 | 4.44937300 | -2.20679000 |
| O | -8.56626900 | 5.57239700 | -0.87596200 |
| O | -9.21512400 | 4.41483100 | 0.94332800 |
| H | -9.70736000 | 5.24686300 | 1.08039800 |

A3

No of negative frequencies= 0

Electronic Energy: -4229.3602614 au

Zero-point correction= 0.665625

(Hartree/Particle)

Thermal correction to Energy= 0.730441

Thermal correction to Enthalpy= 0.731386

Thermal correction to Gibbs Free Energy= 0.545497

Sum of electronic and zero-point Energies= -4228.694637

Sum of electronic and thermal Energies= -4228.629820

Sum of electronic and thermal Enthalpies= -4228.628876

Sum of electronic and thermal Free Energies= -4228.814765

| | | | |
|----|-------------|-------------|-------------|
| C | 0.44116200 | -5.33951300 | -4.33875900 |
| C | 0.76848900 | -4.17406400 | -3.63966400 |
| C | 1.44867100 | -4.21107100 | -2.39403300 |
| C | 1.75486700 | -5.50094400 | -1.88401400 |
| C | 1.42787900 | -6.67024700 | -2.57716500 |
| C | 0.77385100 | -6.58900800 | -3.80923900 |
| H | -0.07004200 | -5.27262300 | -5.29613400 |
| H | 0.49547900 | -3.21513100 | -4.07469700 |
| H | 2.27795600 | -5.59148300 | -0.93322800 |
| H | 1.68823000 | -7.64129100 | -2.16212700 |
| H | 0.52061800 | -7.49624700 | -4.35227300 |
| I | -2.57113700 | -2.87487300 | 2.81195800 |
| Cu | 0.12206900 | -3.29525800 | -0.98057500 |
| Cu | 0.69848100 | -1.05969600 | 0.01705200 |
| Cu | -0.89920700 | -1.27014000 | -1.99117400 |
| Cu | 2.43093900 | -2.63234700 | -1.66459700 |
| Cu | -1.80496200 | -1.92168000 | 0.21040300 |
| Cu | -0.12507900 | -2.89317300 | 1.59377400 |
| S | -1.73785300 | -0.22909100 | -3.75889900 |
| C | -3.44904300 | 0.14547800 | -3.16297200 |
| C | -3.48692900 | 1.24749500 | -2.10214600 |
| H | -3.93826500 | -0.75774700 | -2.78669400 |
| H | -4.00764900 | 0.50160600 | -4.03539900 |
| H | -2.84509300 | 2.07079900 | -2.42779600 |
| N | -4.83873200 | 1.79937700 | -1.94079600 |
| C | -2.98742900 | 0.77089000 | -0.72205200 |
| O | -3.10276400 | -0.41249800 | -0.34485100 |
| N | -2.48168000 | 1.75203400 | 0.04626300 |
| H | -2.63452800 | 2.70014600 | -0.30188100 |
| C | -2.03052800 | 1.57227800 | 1.40859400 |
| H | -2.44751700 | 0.63881700 | 1.80702500 |
| H | -2.38763200 | 2.39561400 | 2.03198000 |
| C | -0.51016700 | 1.48209300 | 1.52310100 |
| O | 0.21354100 | 0.95852000 | 0.68056200 |
| O | -0.06127300 | 2.00513200 | 2.65034700 |
| H | 0.93324600 | 1.90177500 | 2.69846600 |
| H | -5.62485100 | 1.22876500 | -2.22126900 |

Chapter 5

| | | | |
|---|-------------|-------------|-------------|
| C | -5.04679200 | 3.07736100 | -1.51460100 |
| O | -4.11632300 | 3.78936000 | -1.12097400 |
| C | -6.48009000 | 3.57991500 | -1.58845800 |
| C | -6.81673300 | 4.54662000 | -0.44907200 |
| H | -7.18363400 | 2.73709000 | -1.60484300 |
| H | -6.60255900 | 4.11276000 | -2.54005300 |
| C | -8.16706900 | 5.26222500 | -0.68044300 |
| H | -6.84896500 | 4.01597300 | 0.50887800 |
| H | -6.01718400 | 5.29286300 | -0.37696500 |
| H | -8.95298100 | 4.50089800 | -0.76475600 |
| N | -8.13243700 | 6.03021100 | -1.91909000 |
| C | -8.49659400 | 6.12379900 | 0.54173900 |
| H | -9.06906900 | 6.36175700 | -2.14374000 |
| H | -7.58043500 | 6.87359900 | -1.76025600 |
| O | -8.44882300 | 7.33401400 | 0.57031100 |
| O | -8.83636100 | 5.37546900 | 1.61837000 |
| H | -9.00017200 | 6.00136200 | 2.34990100 |
| S | 3.05488900 | -1.28614000 | 0.05035100 |
| C | 3.69067200 | 0.44452900 | -0.07378600 |
| C | 4.32893300 | 0.87808300 | 1.27302000 |
| H | 2.87634500 | 1.12526000 | -0.33269700 |
| H | 4.47041400 | 0.50578500 | -0.83540500 |
| H | 5.19253900 | 0.23296600 | 1.45942200 |
| N | 4.80898600 | 2.24532900 | 1.20253200 |
| C | 3.34181500 | 0.79726000 | 2.44514000 |
| O | 2.62218500 | 1.76764600 | 2.73092800 |
| N | 3.34708100 | -0.35433300 | 3.15927100 |
| H | 3.78947100 | -1.15842100 | 2.72623000 |
| C | 2.42113000 | -0.59886400 | 4.24658600 |
| H | 2.04899900 | 0.35902300 | 4.61101200 |
| H | 2.94275900 | -1.09507100 | 5.07476400 |
| C | 1.24909300 | -1.48541300 | 3.83623900 |
| O | 1.35806200 | -2.36027200 | 2.98007600 |
| O | 0.14308400 | -1.21195400 | 4.50519400 |
| H | -0.60311000 | -1.78854900 | 4.18930600 |
| H | 4.17498900 | 2.96922300 | 1.51457000 |
| C | 6.06865500 | 2.54516300 | 0.75821600 |
| O | 6.84449000 | 1.67791500 | 0.36913500 |
| C | 6.43728900 | 4.02406200 | 0.81028800 |
| C | 7.31307500 | 4.42788800 | -0.38004000 |
| H | 6.99474200 | 4.18701200 | 1.74438000 |
| H | 5.54975000 | 4.66232500 | 0.85936300 |
| C | 7.74976000 | 5.90674900 | -0.30684300 |
| H | 8.19171200 | 3.77843900 | -0.41944500 |
| H | 6.76003800 | 4.27021900 | -1.31633300 |
| H | 8.28996300 | 6.05874300 | 0.63610000 |
| N | 6.58708700 | 6.78984700 | -0.32329800 |
| C | 8.72650200 | 6.19937400 | -1.44872100 |
| H | 6.88276600 | 7.74399300 | -0.12129000 |

| | | | |
|---|-------------|------------|-------------|
| H | 6.22796900 | 6.82269500 | -1.27826700 |
| O | 8.45755600 | 6.83740800 | -2.44371000 |
| O | 9.94209200 | 5.64175400 | -1.23976800 |
| H | 10.47967600 | 5.84554100 | -2.02911200 |

A4

No of negative frequencies= 0

Electronic Energy: -4472.3707866 au

Zero-point correction= 0.755736
(Hartree/Particle) Thermal correction to Energy= 0.827870

Thermal correction to Enthalpy= 0.828815

Thermal correction to Gibbs Free Energy= 0.625785

Sum of electronic and zero-point Energies= -
4471.615051

Sum of electronic and thermal Energies= -
4471.542916

Sum of electronic and thermal Enthalpies= -
4471.541972

Sum of electronic and thermal Free Energies= -
4471.745002

| | | | |
|----|-------------|-------------|-------------|
| C | -2.81896100 | -2.54225200 | 4.92464300 |
| C | -2.44075200 | -1.90381300 | 3.73875400 |
| C | -2.06070200 | -2.63088100 | 2.57512200 |
| C | -2.05700400 | -4.05133900 | 2.70541500 |
| C | -2.41708300 | -4.68719100 | 3.89298900 |
| C | -2.80083700 | -3.93627100 | 5.00293500 |
| H | -3.11812800 | -1.95018400 | 5.78458100 |
| H | -2.44115400 | -0.81643000 | 3.70694000 |
| H | -1.77071000 | -4.65315800 | 1.84355700 |
| H | -2.38546600 | -5.78074100 | 3.94958100 |
| H | -3.08822700 | -4.42926300 | 5.92686900 |
| I | 1.98979600 | -3.23525400 | -2.01262800 |
| Cu | -0.30923900 | -1.95731900 | 1.70388400 |
| Cu | -0.03234700 | -0.00655100 | 0.11139800 |
| Cu | 1.53319500 | -0.45482200 | 2.28476200 |
| Cu | -2.57831000 | -1.67409400 | 0.87239300 |
| Cu | 1.89057900 | -1.66562100 | 0.20320000 |
| Cu | -0.26230400 | -2.36013900 | -0.78420800 |
| C | -6.22717500 | -2.49120500 | 0.69565500 |
| C | -5.06741900 | -3.16632900 | 0.29153700 |
| C | -4.42828700 | -2.76229900 | -0.89053000 |
| C | -4.95993100 | -1.73851900 | -1.69206900 |
| C | -6.11993800 | -1.07884700 | -1.27447800 |

| | | | | | | | |
|---|-------------|-------------|-------------|--|--------------------------|-------------|-------------|
| C | -6.75600700 | -1.45516400 | -0.08210000 | N | -3.63564300 | 3.80869700 | -1.24447200 |
| H | -6.70487000 | -2.79551600 | 1.62632000 | C | -1.81848300 | 2.73696000 | -2.43514600 |
| H | -4.66220100 | -3.98510300 | 0.89279200 | O | -1.05100000 | 3.67948700 | -2.16301800 |
| H | -4.46834000 | -1.44527800 | -2.60953000 | N | -1.63433900 | 1.84283400 | -3.43634600 |
| H | -6.53052000 | -0.26647900 | -1.87611600 | H | -2.23654500 | 1.03514800 | -3.42419600 |
| H | -7.66354800 | -0.95026600 | 0.22620800 | C | -0.37520300 | 1.61862600 | -4.13444700 |
| S | 2.80173800 | 0.14100700 | 4.00722800 | H | 0.38181100 | 2.31384700 | -3.78089700 |
| C | 4.47408900 | -0.21482100 | 3.31441400 | H | -0.48882800 | 1.78123400 | -5.21290900 |
| C | 4.86609500 | 0.78929400 | 2.22462400 | C | 0.03231600 | 0.17072300 | -3.91137100 |
| H | 4.52857500 | -1.23436900 | 2.92010000 | O | -0.76114300 | -0.74611100 | -3.98254600 |
| H | 5.19403200 | -0.12948000 | 4.13597400 | O | 1.33031600 | 0.01215600 | -3.60396100 |
| H | 4.66038300 | 1.79770900 | 2.58230700 | H | 1.48021100 | -0.94815500 | -3.42515600 |
| N | 6.29716800 | 0.73986400 | 1.89383500 | H | -2.96954200 | 4.57205600 | -1.13850400 |
| C | 4.06298700 | 0.58694700 | 0.91481500 | C | -4.97532600 | 3.98800100 | -1.02919700 |
| O | 3.72401200 | -0.54206800 | 0.50121800 | O | -5.77396500 | 3.06840900 | -1.12596300 |
| N | 3.83443800 | 1.72808100 | 0.22536400 | C | -5.39302900 | 5.42006900 | -0.68301700 |
| H | 4.33924200 | 2.54968100 | 0.55381700 | C | -6.57025400 | 5.44227400 | 0.29778700 |
| C | 3.20083500 | 1.76590700 | -1.08358800 | H | -5.69271800 | 5.90833300 | -1.62281000 |
| H | 3.13606100 | 0.73861700 | -1.45409000 | H | -4.55994100 | 6.00902000 | -0.28784400 |
| H | 3.80918900 | 2.34921700 | -1.77890400 | C | -7.06497100 | 6.87545100 | 0.59617900 |
| C | 1.78037000 | 2.32875800 | -1.04427900 | H | -7.38847200 | 4.83868200 | -0.10424400 |
| O | 0.87308200 | 1.88218400 | -0.35807100 | H | -6.27157800 | 4.96862600 | 1.24403900 |
| O | 1.61074200 | 3.35624000 | -1.86302900 | H | -7.37879900 | 7.33136300 | -0.35167400 |
| H | 0.63257000 | 3.59211900 | -1.89890600 | N | -5.98897300 | 7.68686500 | 1.16629600 |
| H | 6.80666100 | -0.11066300 | 2.10068600 | C | -8.29448700 | 6.79460900 | 1.50515500 |
| C | 6.95244800 | 1.83437400 | 1.41887200 | H | -6.30650000 | 8.65704500 | 1.23507200 |
| O | 6.34849400 | 2.87087800 | 1.12326500 | H | -5.85286900 | 7.39520600 | 2.13612400 |
| C | 8.46357100 | 1.70992200 | 1.30094200 | O | -8.30120200 | 7.07402200 | 2.68505300 |
| C | 9.02571500 | 2.49483700 | 0.11123300 | O | -9.39675600 | 6.35624200 | 0.85199000 |
| H | 8.76275200 | 0.65443000 | 1.24845200 | H | -10.11351400 | 6.30956700 | 1.51418400 |
| H | 8.90963100 | 2.11133500 | 2.22019800 | I | -2.62743800 | -3.77137000 | -1.53467200 |
| C | 10.56911200 | 2.58819400 | 0.15776100 | | | | |
| H | 8.71220800 | 2.03764600 | -0.83396500 | TS2 | | | |
| H | 8.59991900 | 3.50510800 | 0.12845300 | | | | |
| H | 10.97551100 | 1.56825700 | 0.16302600 | No of negative frequencies= | 1 | | |
| N | 11.01198100 | 3.26670100 | 1.37382800 | Imaginary Frequency = | -147.971cm ⁻¹ | | |
| C | 11.07850000 | 3.27115000 | -1.11832100 | | | | |
| H | 12.02703500 | 3.20461100 | 1.44965200 | Electronic Energy: -4472.3488371 au | | | |
| H | 10.82167000 | 4.26503400 | 1.27151400 | | | | |
| O | 11.53870900 | 4.39106200 | -1.17217900 | Zero-point correction= | 0.755371 | | |
| O | 10.93612800 | 2.48577600 | -2.21320400 | (Hartree/Particle) | | | |
| H | 11.25204200 | 3.00920800 | -2.97520300 | Thermal correction to Energy= | 0.828007 | | |
| S | -2.17309100 | -0.02429900 | -0.80457400 | Thermal correction to Enthalpy= | 0.828951 | | |
| C | -2.81458200 | 1.65092000 | -0.36125900 | Thermal correction to Gibbs Free Energy= | 0.624907 | | |
| C | -3.09655400 | 2.51766900 | -1.62605600 | | | | |
| H | -2.09489600 | 2.17661300 | 0.27359200 | Sum of electronic and zero-point Energies= | - | | |
| H | -3.75947100 | 1.55350700 | 0.17880800 | 4471.593466 | | | |
| H | -3.85775400 | 2.01139800 | -2.22869600 | | | | |

Chapter 5

| | | | | | | | | |
|--|-------------|-------------|-------------|---|-------------|-------------|-------------|-------------|
| Sum of electronic and thermal Energies= | | | | - | H | 2.92377600 | 0.61305500 | -1.98564600 |
| 4471.520830 | | | | | H | 3.51273700 | 2.25419500 | -2.34364000 |
| Sum of electronic and thermal Enthalpies= | | | | - | C | 1.58645100 | 2.16670400 | -1.38523300 |
| 4471.519886 | | | | | O | 0.77761600 | 1.66377300 | -0.60935600 |
| Sum of electronic and thermal Free Energies= | | | | - | O | 1.31736900 | 3.23033600 | -2.11954800 |
| 4471.723930 | | | | | H | 0.34661000 | 3.47774100 | -2.01705000 |
| | | | | | H | 6.86110500 | -0.13728100 | 1.32447500 |
| C | -1.71012600 | -2.57048600 | 5.00717900 | C | 6.93887500 | 1.77503200 | 0.55641500 | |
| C | -1.90002000 | -1.96512400 | 3.76193700 | O | 6.31571200 | 2.80674800 | 0.28420700 | |
| C | -1.84748400 | -2.71117200 | 2.55954800 | C | 8.41643000 | 1.61301400 | 0.23183700 | |
| C | -1.56638500 | -4.09362900 | 2.67448300 | C | 9.20956000 | 2.88026100 | 0.57431700 | |
| C | -1.35273600 | -4.69983500 | 3.91865000 | H | 8.49193600 | 1.41906200 | -0.84771100 | |
| C | -1.43621800 | -3.93946200 | 5.08676800 | H | 8.85425000 | 0.75007100 | 0.74213100 | |
| H | -1.77042800 | -1.97466600 | 5.91465900 | C | 10.70471900 | 2.73926800 | 0.21474900 | |
| H | -2.09697900 | -0.89565800 | 3.72661500 | H | 8.77569300 | 3.73464100 | 0.04779100 | |
| H | -1.53080400 | -4.71237000 | 1.77831600 | H | 9.12495100 | 3.09023600 | 1.64939600 | |
| H | -1.12818400 | -5.76256800 | 3.97426000 | H | 10.78004100 | 2.51447200 | -0.85645300 | |
| H | -1.28148700 | -4.40813300 | 6.05510200 | N | 11.31330400 | 1.64442800 | 0.96434100 | |
| I | 1.85646900 | -3.02650600 | -2.60671200 | C | 11.40635700 | 4.07862200 | 0.45555200 | |
| Cu | -0.13569000 | -2.15621800 | 1.48332600 | H | 12.23804300 | 1.44497500 | 0.58572900 | |
| Cu | -0.15851400 | -0.19905900 | -0.05226000 | H | 11.48205100 | 1.96792200 | 1.91767800 | |
| Cu | 1.61505400 | -0.51644100 | 1.93122700 | O | 12.15113800 | 4.31193600 | 1.38273700 | |
| Cu | -2.59475100 | -1.84521400 | 0.85170400 | O | 11.08354900 | 5.00195900 | -0.47975100 | |
| Cu | 1.86113200 | -1.69675300 | -0.22155200 | H | 11.54279300 | 5.82588100 | -0.22681800 | |
| Cu | -0.29488600 | -2.65831500 | -1.07638400 | S | -2.41005300 | 0.00322700 | -0.68286900 | |
| C | -6.12886600 | -3.90350500 | 1.88762900 | C | -2.83902100 | 1.68594200 | -0.03397400 | |
| C | -4.78066100 | -3.84252000 | 1.52253900 | C | -3.28659800 | 2.63170100 | -1.18121700 | |
| C | -4.39583600 | -2.84973200 | 0.62654300 | H | -1.98236200 | 2.12648000 | 0.48288100 | |
| C | -5.30617600 | -2.00867400 | -0.01090100 | H | -3.67512600 | 1.60530900 | 0.66398200 | |
| C | -6.64940400 | -2.08280600 | 0.38313800 | H | -4.17066600 | 2.19850700 | -1.65780000 | |
| C | -7.05996900 | -3.02421400 | 1.32672900 | N | -3.65494900 | 3.93641100 | -0.66665900 | |
| H | -6.44312600 | -4.64584600 | 2.61682700 | C | -2.15913000 | 2.82821100 | -2.19670900 | |
| H | -4.06053600 | -4.52127800 | 1.96076000 | O | -1.29964400 | 3.70686200 | -2.00494800 | |
| H | -4.98820700 | -1.30239200 | -0.76746500 | N | -2.17804000 | 2.00580400 | -3.26406300 | |
| H | -7.36762900 | -1.40721300 | -0.07394200 | H | -2.83132300 | 1.22867600 | -3.24029800 | |
| H | -8.10623600 | -3.08738000 | 1.61171800 | C | -1.06892600 | 1.84851100 | -4.19723300 | |
| I | -2.64483300 | -3.83759000 | -1.27431300 | H | -0.26662500 | 2.53216000 | -3.93094900 | |
| S | 3.00815100 | 0.14800100 | 3.53506000 | H | -1.40108300 | 2.07850200 | -5.21705600 | |
| C | 4.63294800 | -0.20459700 | 2.72198400 | C | -0.61448700 | 0.38883500 | -4.16490500 | |
| C | 4.93100300 | 0.76237900 | 1.57590200 | O | -1.38522100 | -0.53527800 | -4.28872700 | |
| H | 4.67472200 | -1.23868000 | 2.36645000 | O | 0.71014100 | 0.26182700 | -3.97470100 | |
| H | 5.40597200 | -0.07235900 | 3.48657000 | H | 0.91844200 | -0.69947000 | -3.90467700 | |
| H | 4.74559700 | 1.78159500 | 1.92487600 | H | -2.92479300 | 4.63673100 | -0.64311500 | |
| N | 6.33637600 | 0.71069000 | 1.15766000 | C | -4.90197800 | 4.18507600 | -0.16216700 | |
| C | 4.03745900 | 0.51097900 | 0.34406000 | O | -5.78178800 | 3.32826200 | -0.15558300 | |
| O | 3.65153500 | -0.63060700 | 0.02411500 | C | -5.10297500 | 5.58523300 | 0.40738100 | |
| N | 3.76705000 | 1.61939500 | -0.37005300 | C | -6.54875400 | 6.06388400 | 0.25101100 | |
| H | 4.32342500 | 2.43951300 | -0.12784900 | H | -4.40413400 | 6.29430000 | -0.05576900 | |
| C | 3.00288100 | 1.63479900 | -1.60290100 | H | -4.86154300 | 5.55597300 | 1.47759400 | |

| | | | |
|---|-------------|------------|-------------|
| C | -6.83245600 | 7.33903600 | 1.07667200 |
| H | -6.77613200 | 6.25821900 | -0.80279300 |
| H | -7.21851900 | 5.26020900 | 0.57788600 |
| H | -6.13913000 | 8.12522000 | 0.75123600 |
| N | -6.61324400 | 7.08937500 | 2.49658300 |
| C | -8.25062700 | 7.83040500 | 0.77538800 |
| H | -6.66779300 | 7.96714700 | 3.01085300 |
| H | -7.38840800 | 6.52586200 | 2.84700800 |
| O | -9.18945200 | 7.75412700 | 1.53780500 |
| O | -8.35745300 | 8.35722200 | -0.46850200 |
| H | -9.29374700 | 8.61119800 | -0.57989200 |

A5

No of negative frequencies= 0

Electronic Energy: -4472.420567 au

Zero-point correction= 0.756427
(Hartree/Particle)

Thermal correction to Energy= 0.829067

Thermal correction to Enthalpy= 0.830011

Thermal correction to Gibbs Free Energy= 0.627350

Sum of electronic and zero-point Energies= -
4471.664140Sum of electronic and thermal Energies= -
4471.591500Sum of electronic and thermal Enthalpies= -
4471.590556Sum of electronic and thermal Free Energies= -
4471.793217

| | | | |
|----|-------------|-------------|-------------|
| C | 1.17840200 | 5.46040000 | 0.27044500 |
| C | 0.33024100 | 4.51393700 | -0.32278900 |
| C | -0.29615800 | 3.51485300 | 0.45945600 |
| C | -0.05838500 | 3.51335100 | 1.85193900 |
| C | 0.77367900 | 4.46717600 | 2.43265500 |
| C | 1.39828600 | 5.44289400 | 1.64554000 |
| H | 1.63840600 | 6.22610500 | -0.34973300 |
| H | 0.11627000 | 4.59648500 | -1.38545700 |
| H | -0.54468400 | 2.77773200 | 2.48639900 |
| H | 0.93467300 | 4.45174800 | 3.50801700 |
| H | 2.04216800 | 6.18695900 | 2.10680000 |
| I | -2.45673700 | 0.03139600 | 2.75222500 |
| Cu | 0.70761400 | 2.07906300 | -0.70534700 |
| Cu | -1.11273800 | 0.43057500 | -1.74437800 |
| Cu | 1.37159700 | -0.49878700 | -2.09009400 |
| Cu | -1.88563800 | 2.55944500 | -0.29220600 |
| Cu | -0.63682500 | 0.49404900 | 0.71305200 |

| | | | |
|----|-------------|-------------|-------------|
| Cu | -3.03630700 | -0.31026200 | 0.12918600 |
| C | -4.44920700 | 5.38732500 | 1.61364700 |
| C | -3.59708300 | 4.30679300 | 1.35225200 |
| C | -2.96916000 | 4.17988500 | 0.10809800 |
| C | -3.18117400 | 5.16831400 | -0.85935600 |
| C | -4.02557100 | 6.25375500 | -0.59906100 |
| C | -4.66340100 | 6.36411400 | 0.63897800 |
| H | -4.94219200 | 5.46499400 | 2.58094500 |
| H | -3.43789400 | 3.56253600 | 2.13103400 |
| H | -2.70129700 | 5.10066300 | -1.83527900 |
| H | -4.18611500 | 7.01095500 | -1.36439200 |
| H | -5.31944200 | 7.20693100 | 0.84329000 |
| I | -3.76618400 | 1.31584100 | -1.85754300 |
| S | 2.22376900 | 1.63136100 | -2.40032600 |
| C | 3.90679100 | 1.92453100 | -1.68674800 |
| C | 4.36976300 | 0.84845400 | -0.70817400 |
| H | 3.90116700 | 2.90587500 | -1.20388600 |
| H | 4.59997300 | 1.94790500 | -2.53340500 |
| H | 4.14833800 | -0.13643800 | -1.12016300 |
| N | 5.82938900 | 0.89456100 | -0.52220600 |
| C | 3.65982200 | 0.95265900 | 0.65927000 |
| O | 2.98262900 | 1.91955200 | 0.99765600 |
| N | 3.86649000 | -0.11713100 | 1.47696200 |
| H | 4.34909500 | -0.92316200 | 1.09631500 |
| C | 3.17281700 | -0.21396100 | 2.73540900 |
| H | 3.37300000 | 0.66178300 | 3.36169600 |
| H | 3.52472600 | -1.09503000 | 3.28084700 |
| C | 1.65963100 | -0.31433200 | 2.56570700 |
| O | 1.11110100 | -0.50015600 | 1.48621900 |
| O | 1.02073100 | -0.17787500 | 3.71951600 |
| H | 0.04577000 | -0.22506100 | 3.55506400 |
| H | 6.28199900 | 1.79944800 | -0.53457700 |
| C | 6.58396800 | -0.20806900 | -0.32866900 |
| O | 6.07883900 | -1.34205000 | -0.21559500 |
| C | 8.08644900 | -0.00780800 | -0.26621100 |
| C | 8.74221400 | -0.84326000 | 0.84030200 |
| H | 8.33270500 | 1.05509900 | -0.14843300 |
| H | 8.50771300 | -0.32929200 | -1.22732000 |
| C | 10.28348800 | -0.84136600 | 0.71702100 |
| H | 8.45719100 | -0.46695400 | 1.82897700 |
| H | 8.37542300 | -1.87340000 | 0.76577400 |
| H | 10.63481800 | 0.19603600 | 0.78126900 |
| N | 10.69147000 | -1.39166600 | -0.56950700 |
| C | 10.88191000 | -1.60261000 | 1.90366200 |
| H | 11.67871800 | -1.19899200 | -0.72937100 |
| H | 10.61973900 | -2.40854400 | -0.52275800 |
| O | 11.38355300 | -2.70286900 | 1.83628900 |
| O | 10.76814700 | -0.91235100 | 3.06258800 |

Chapter 5

| | | | |
|---|-------------|-------------|-------------|
| H | 11.14689900 | -1.47851900 | 3.76259200 |
| S | -0.51173400 | -1.28303400 | -3.26602800 |
| C | -1.44529400 | -2.72140400 | -2.54003200 |
| C | -0.94324300 | -3.19305800 | -1.16048500 |
| H | -1.40639300 | -3.54224300 | -3.26353100 |
| H | -2.48267900 | -2.40391700 | -2.43914000 |
| H | -0.69406200 | -2.29505000 | -0.57387900 |
| N | -1.94079600 | -3.96650000 | -0.42448200 |
| C | 0.33086100 | -4.06069700 | -1.16842600 |
| O | 0.53265700 | -4.88047400 | -0.27527700 |
| N | 1.19269900 | -3.84793200 | -2.20147200 |
| H | 0.98517600 | -3.05707600 | -2.81086400 |
| C | 2.58022200 | -4.22196600 | -2.08081300 |
| H | 2.99232700 | -4.53442600 | -3.04683500 |
| H | 2.66357700 | -5.06786300 | -1.39376100 |
| C | 3.40937700 | -3.05989900 | -1.54565600 |
| O | 2.94409300 | -1.94673900 | -1.31610500 |
| O | 4.67746100 | -3.37754100 | -1.35724900 |
| H | 5.17550900 | -2.59364800 | -0.99663900 |
| H | -1.59237200 | -4.84378600 | -0.04855000 |
| C | -3.08173400 | -3.45118100 | 0.07042200 |
| O | -3.46699400 | -2.29664500 | -0.20206000 |
| C | -3.89939000 | -4.35089600 | 0.97699800 |
| C | -5.39867500 | -4.28245100 | 0.65892700 |
| H | -3.73027600 | -3.99331000 | 2.00333700 |
| H | -3.55383800 | -5.38754400 | 0.93276300 |
| C | -6.22679800 | -5.17205800 | 1.61152200 |
| H | -5.74149900 | -3.24677500 | 0.72739000 |
| H | -5.57399900 | -4.61425600 | -0.37390000 |
| H | -6.02739300 | -4.84789800 | 2.64047000 |
| N | -5.83690800 | -6.57252600 | 1.47914100 |
| C | -7.71641700 | -4.94644200 | 1.33736900 |
| H | -6.24212100 | -7.11196400 | 2.24268300 |
| H | -6.27182600 | -6.94379100 | 0.63355400 |
| O | -8.44246600 | -5.73790700 | 0.77549700 |
| O | -8.13879900 | -3.73855200 | 1.77439100 |
| H | -9.07980000 | -3.66215500 | 1.52478200 |

TS3

No of negative frequencies= 1

Imaginary Frequency = -172.099cm⁻¹

Electronic Energy: -4472.4176983 au

Zero-point correction= 0.756351

(Hartree/Particle)

Thermal correction to Energy= 0.828086

Thermal correction to Enthalpy= 0.829031

Thermal correction to Gibbs Free Energy = 0.630561

Sum of electronic and zero-point Energies = -4471.661348

Sum of electronic and thermal Energies = -4471.589612

Sum of electronic and thermal Enthalpies = -4471.588668

Sum of electronic and thermal Free Energies = -4471.787137

| | | | |
|----|-------------|-------------|-------------|
| C | 1.46465800 | 5.19957300 | 0.08416300 |
| C | 0.41269400 | 4.41369700 | -0.41506200 |
| C | -0.36078300 | 3.62057700 | 0.46173000 |
| C | -0.06359500 | 3.64912900 | 1.84295400 |
| C | 0.97565100 | 4.43818700 | 2.32148300 |
| C | 1.74611900 | 5.21929500 | 1.44639800 |
| H | 2.04294200 | 5.80818700 | -0.60694700 |
| H | 0.16748200 | 4.47025600 | -1.47189500 |
| H | -0.65644300 | 3.06149100 | 2.53738400 |
| H | 1.18639300 | 4.45009000 | 3.38820700 |
| H | 2.54851500 | 5.84207300 | 1.83240700 |
| I | -2.48385900 | 0.01084200 | 2.80141600 |
| Cu | 0.74914300 | 1.96148500 | -0.65773500 |
| Cu | -1.06711300 | 0.39150100 | -1.71506400 |
| Cu | 1.35707400 | -0.46670700 | -2.24377000 |
| Cu | -1.77114300 | 2.42774500 | -0.26602000 |
| Cu | -0.59219400 | 0.34676700 | 0.72838700 |
| Cu | -3.01036900 | -0.21448900 | 0.11969800 |
| C | -4.24561700 | 5.19865300 | 1.65160400 |
| C | -3.29530200 | 4.19595300 | 1.42711800 |
| C | -2.58095900 | 4.18053100 | 0.22769900 |
| C | -2.77044600 | 5.18471600 | -0.72207000 |
| C | -3.71630400 | 6.18725200 | -0.49004800 |
| C | -4.45601700 | 6.19498300 | 0.69593600 |
| H | -4.81695800 | 5.19858100 | 2.57698400 |
| H | -3.13742600 | 3.42967200 | 2.18214400 |
| H | -2.20131400 | 5.19054600 | -1.64834700 |
| H | -3.87384900 | 6.96189000 | -1.23703100 |
| H | -5.18644100 | 6.97902400 | 0.87735200 |
| I | -3.81506600 | 1.45098700 | -1.82823100 |
| S | 2.22365900 | 1.67512900 | -2.46805900 |
| C | 3.88151200 | 1.91478000 | -1.68594600 |
| C | 4.28768400 | 0.81843300 | -0.70223000 |
| H | 3.87969900 | 2.89080000 | -1.18981300 |
| H | 4.61560800 | 1.93458200 | -2.49790100 |
| H | 4.07872100 | -0.15839700 | -1.14137200 |
| N | 5.74046900 | 0.85983000 | -0.45720900 |
| C | 3.51025700 | 0.88737200 | 0.63045100 |

Copper Nanoclusters for.....

| | | | |
|---|-------------|-------------|-------------|
| O | 2.69197000 | 1.77057500 | 0.89480200 |
| N | 3.80708000 | -0.10859300 | 1.50497900 |
| H | 4.40143700 | -0.86611800 | 1.18236600 |
| C | 3.12952200 | -0.20300400 | 2.77476800 |
| H | 3.29142800 | 0.69847700 | 3.37539700 |
| H | 3.53684400 | -1.04905600 | 3.33698500 |
| C | 1.62238000 | -0.39046800 | 2.63086700 |
| O | 1.07604200 | -0.71375100 | 1.58394100 |
| O | 0.98574700 | -0.15977300 | 3.77155100 |
| H | 0.01077100 | -0.24688700 | 3.61742000 |
| H | 6.19974700 | 1.76038800 | -0.50278000 |
| C | 6.49246500 | -0.24124700 | -0.25115300 |
| O | 5.98092400 | -1.37155500 | -0.11936300 |
| C | 7.99552700 | -0.04584200 | -0.19176700 |
| C | 8.65294500 | -0.88393800 | 0.91152000 |
| H | 8.24481900 | 1.01646400 | -0.07461300 |
| H | 8.41301400 | -0.36753800 | -1.15465200 |
| C | 10.19348600 | -0.88980600 | 0.77954800 |
| H | 8.37555900 | -0.50579500 | 1.90166800 |
| H | 8.28039800 | -1.91218500 | 0.83961100 |
| H | 10.55041400 | 0.14581100 | 0.84259600 |
| N | 10.59112000 | -1.44068500 | -0.50986700 |
| C | 10.79548000 | -1.65470100 | 1.96209500 |
| H | 11.57873400 | -1.25425700 | -0.67472600 |
| H | 10.51294500 | -2.45715700 | -0.46472100 |
| O | 11.29640900 | -2.75489700 | 1.89005500 |
| O | 10.68628300 | -0.96728000 | 3.12326200 |
| H | 11.06753300 | -1.53543400 | 3.82030600 |
| S | -0.57562900 | -1.23799300 | -3.37090500 |
| C | -1.50070000 | -2.68365300 | -2.64481100 |
| C | -0.99963100 | -3.15620700 | -1.26449100 |
| H | -1.46375500 | -3.50466500 | -3.36828500 |
| H | -2.53770600 | -2.36538500 | -2.54137300 |
| H | -0.73016900 | -2.25892800 | -0.68547100 |
| N | -2.00651100 | -3.90391300 | -0.51537400 |
| C | 0.25801400 | -4.04434700 | -1.27594400 |
| O | 0.44147700 | -4.88316400 | -0.39641600 |
| N | 1.13374200 | -3.82360900 | -2.29668500 |
| H | 0.93916800 | -3.02153000 | -2.89639100 |
| C | 2.51620800 | -4.21191000 | -2.16114400 |
| H | 2.93866500 | -4.51912800 | -3.12484400 |
| H | 2.58233000 | -5.06430200 | -1.48086600 |
| C | 3.34795800 | -3.06038300 | -1.60811800 |
| O | 2.90698500 | -1.92683200 | -1.44552200 |
| O | 4.59274200 | -3.40823400 | -1.32860700 |
| H | 5.08494900 | -2.62915500 | -0.95406600 |
| H | -1.67481300 | -4.78883900 | -0.14215200 |
| C | -3.12153000 | -3.35279500 | 0.00098000 |

| | | | |
|---|-------------|-------------|-------------|
| O | -3.47762300 | -2.18894800 | -0.26977900 |
| C | -3.94492300 | -4.22348100 | 0.93085400 |
| C | -5.44843100 | -4.10719500 | 0.64963800 |
| H | -3.73895000 | -3.86664000 | 1.95073000 |
| H | -3.63320400 | -5.27067100 | 0.88311500 |
| C | -6.28291700 | -4.95749600 | 1.63188300 |
| H | -5.75306200 | -3.05954300 | 0.71563400 |
| H | -5.66132500 | -4.44240400 | -0.37505700 |
| H | -6.04527500 | -4.63112100 | 2.65199800 |
| N | -5.94731900 | -6.37249900 | 1.50443000 |
| C | -7.77005300 | -4.68098600 | 1.39416700 |
| H | -6.36010400 | -6.89067200 | 2.27862200 |
| H | -6.40955000 | -6.73353100 | 0.66898500 |
| O | -8.53939400 | -5.45092500 | 0.86034600 |
| O | -8.13786800 | -3.45438600 | 1.82905500 |
| H | -9.08144200 | -3.34725000 | 1.60166300 |

A6

No of negative frequencies= 0

Electronic Energy: -4472.5195609 au

Zero-point correction= 0.760252
(Hartree/Particle)

Thermal correction to Energy= 0.832214

Thermal correction to Enthalpy= 0.833158

Thermal correction to Gibbs Free Energy= 0.630799

Sum of electronic and zero-point Energies= -
4471.759308

Sum of electronic and thermal Energies= -
4471.687347

Sum of electronic and thermal Enthalpies= -
4471.686403

Sum of electronic and thermal Free Energies= -
4471.888761

| | | | |
|---|-------------|------------|------------|
| C | 2.62335300 | 3.88302300 | 2.90364400 |
| C | 2.11354300 | 3.68120300 | 1.62124400 |
| C | 1.10083900 | 4.51188800 | 1.11167400 |
| C | 0.61490000 | 5.55042500 | 1.92467300 |
| C | 1.12577800 | 5.75148400 | 3.20635600 |
| C | 2.13190300 | 4.91848500 | 3.70159800 |
| H | 3.40145900 | 3.21866800 | 3.26835500 |
| H | 2.49599500 | 2.85307000 | 1.03323400 |
| H | -0.15077100 | 6.21971400 | 1.54241200 |
| H | 0.74103900 | 6.56458700 | 3.81607600 |
| H | 2.52814200 | 5.07643200 | 4.70115500 |

Chapter 5

| | | | | | | | |
|----|-------------|-------------|-------------|---|-------------|-------------|-------------|
| I | -2.91739800 | 1.14866600 | 2.15959400 | H | 8.67066600 | -1.14230400 | -0.80690100 |
| Cu | 0.85809500 | 1.10222400 | -1.35666300 | H | 9.23420100 | 0.02473900 | 1.96077500 |
| Cu | -0.96374500 | -0.48594300 | -1.89455300 | N | 7.96041300 | 1.01469000 | 0.62156100 |
| Cu | 1.38625800 | -1.83096200 | -1.66574600 | C | 10.40105400 | 0.78495300 | 0.34054700 |
| Cu | -1.61959800 | 1.88482200 | -1.71094700 | H | 7.89009100 | 1.74143700 | 1.33142800 |
| Cu | -0.93020200 | 0.70065200 | 0.35891700 | H | 8.11916600 | 1.50328500 | -0.26160100 |
| Cu | -3.32272500 | 0.23642800 | -0.50999500 | O | 10.43064900 | 1.69058300 | -0.46367500 |
| C | -1.32465300 | 4.29443600 | -1.81621800 | O | 11.50935300 | 0.20265500 | 0.84504100 |
| C | -0.80874600 | 4.48582800 | -0.52651500 | H | 12.27531200 | 0.64178600 | 0.42710700 |
| C | 0.55719900 | 4.29287800 | -0.25200800 | S | -0.55020000 | -2.56768000 | -2.82675700 |
| C | 1.39455800 | 3.88342300 | -1.31086200 | C | -1.83731000 | -3.53195000 | -1.88599300 |
| C | 0.88335900 | 3.66139200 | -2.59354900 | C | -1.65600900 | -3.51400200 | -0.35351800 |
| C | -0.48117800 | 3.86715800 | -2.85702200 | H | -1.84364900 | -4.55899600 | -2.26507000 |
| H | -2.37434400 | 4.49083500 | -2.01236200 | H | -2.79509800 | -3.07393200 | -2.12838800 |
| H | -1.48187600 | 4.77245900 | 0.27522500 | H | -1.25164100 | -2.52860500 | -0.07566500 |
| H | 2.45907000 | 3.76163700 | -1.13354000 | N | -2.90969800 | -3.71306100 | 0.36252700 |
| H | 1.55039900 | 3.35124000 | -3.39266900 | C | -0.66187700 | -4.55221800 | 0.19661800 |
| H | -0.87609100 | 3.73012800 | -3.85949200 | O | -0.77873000 | -4.99940700 | 1.33439200 |
| I | -4.17648900 | 1.66577100 | -2.62004500 | N | 0.33553800 | -4.91696800 | -0.65937100 |
| S | 2.72702400 | -0.01532200 | -2.19195900 | H | 0.40702500 | -4.38276300 | -1.52276800 |
| C | 4.34419500 | 0.12109500 | -1.29161200 | C | 1.56191700 | -5.49569700 | -0.16926500 |
| C | 4.50126900 | -0.77798000 | -0.06039700 | H | 1.95083800 | -6.25366800 | -0.85703200 |
| H | 4.50083400 | 1.16632200 | -1.01205500 | H | 1.36019600 | -5.98658300 | 0.78780400 |
| H | 5.11057000 | -0.16067200 | -2.01915300 | C | 2.62334700 | -4.42103800 | 0.04255200 |
| H | 4.09450700 | -1.76370300 | -0.27389000 | O | 2.37000500 | -3.21534600 | -0.04530100 |
| N | 5.91713300 | -0.96255800 | 0.26693500 | O | 3.80518300 | -4.90836300 | 0.33062100 |
| C | 3.82901700 | -0.17570000 | 1.18873500 | H | 4.49502600 | -4.17845300 | 0.42113900 |
| O | 4.00606300 | 0.99663400 | 1.51220200 | H | -2.89139100 | -4.44141300 | 1.06876000 |
| N | 3.13306600 | -1.07029100 | 1.94905900 | C | -3.90879000 | -2.80342400 | 0.36208100 |
| H | 2.84428900 | -1.92574600 | 1.48367300 | O | -3.85348600 | -1.77686100 | -0.34015400 |
| C | 2.36529000 | -0.62677600 | 3.08680400 | C | -5.13470200 | -3.15377200 | 1.18596200 |
| H | 2.87446400 | 0.22196900 | 3.55076000 | C | -5.88015600 | -1.92358800 | 1.71012700 |
| H | 2.28743400 | -1.42170200 | 3.83669800 | H | -4.85297000 | -3.82118000 | 2.01098300 |
| C | 0.96206000 | -0.18738200 | 2.69022100 | H | -5.81758400 | -3.72312900 | 0.54147500 |
| O | 0.56607200 | -0.26646400 | 1.53327700 | C | -7.25125600 | -2.30422100 | 2.31258700 |
| O | 0.24473800 | 0.26156800 | 3.70631100 | H | -5.28110100 | -1.39931900 | 2.46076000 |
| H | -0.65346600 | 0.52704500 | 3.37827600 | H | -6.03746100 | -1.22140400 | 0.88336700 |
| H | 6.50551500 | -0.12388400 | 0.40954400 | H | -7.08663900 | -3.01407200 | 3.13350300 |
| C | 6.45253100 | -2.15966600 | 0.56310000 | N | -8.09089700 | -2.94569200 | 1.30685300 |
| O | 5.82824800 | -3.23536800 | 0.55385900 | C | -7.89775400 | -1.05253500 | 2.91242700 |
| C | 7.93041400 | -2.18952200 | 0.96500300 | H | -8.92664400 | -3.32408000 | 1.74995000 |
| C | 8.93612600 | -1.25699500 | 0.25178500 | H | -8.43131600 | -2.22539600 | 0.66882100 |
| H | 8.23368900 | -3.22773600 | 0.80657400 | O | -8.85246600 | -0.47392700 | 2.44149100 |
| H | 7.97678300 | -2.02576200 | 2.05147300 | O | -7.26626500 | -0.64146600 | 4.03640700 |
| C | 9.11582800 | 0.14931000 | 0.87830600 | H | -7.70459000 | 0.18527200 | 4.31539900 |
| H | 9.91227400 | -1.75251700 | 0.27661200 | | | | |

Form of SDD Basis sets used for Cu and I

Cu 0
 S 3 1.00 0.000000000000
 0.2769632000D+02 0.2311320967D+00
 0.1350535000D+02 -0.6568112749D+00
 0.8815355000D+01 -0.5458752285D+00
 S 1 1.00 0.000000000000
 0.2380805000D+01 0.1000000000D+01
 S 1 1.00 0.000000000000
 0.9526160000D+00 0.1000000000D+01
 S 1 1.00 0.000000000000
 0.1126620000D+00 0.1000000000D+01
 S 1 1.00 0.000000000000
 0.4048600000D-01 0.1000000000D+01
 S 1 1.00 0.000000000000
 0.1000000000D-01 0.1000000000D+01
 P 2 1.00 0.000000000000
 0.9350432700D+02 0.2282899946D-01
 0.1628546400D+02 -0.1009512976D+01
 P 2 1.00 0.000000000000
 0.5994236000D+01 0.2464500125D+00
 0.2536875000D+01 0.7920240403D+00
 P 1 1.00 0.000000000000
 0.8979340000D+00 0.1000000000D+01
 P 1 1.00 0.000000000000
 0.1317290000D+00 0.1000000000D+01
 P 1 1.00 0.000000000000
 0.3087800000D-01 0.1000000000D+01
 D 4 1.00 0.000000000000
 0.4122500600D+02 0.4469401381D-01
 0.1234325000D+02 0.2121060655D+00
 0.4201920000D+01 0.4534231401D+00
 0.1379825000D+01 0.5334651648D+00
 D 1 1.00 0.000000000000
 0.3834530000D+00 0.1000000000D+01
 D 1 1.00 0.000000000000
 0.1000000000D+00 0.1000000000D+01

 Cu 0
 Cu-ECP 3 10
 F component
 1
 2 1.0000000 0.00000000 0.00000000
 S-F projection
 2
 2 30.2200000 355.77015800 0.00000000
 2 13.1900000 70.86535700 0.00000000

P-F projection
 2
 2 33.1300000 233.89197600 0.00000000
 2 13.2200000 53.94729900 0.00000000
 D-F projection
 2
 2 38.4200000 -31.27216500 0.00000000
 2 13.2600000 -2.74110400 0.00000000

I 0
 S 3 1.00 0.000000000000
 0.2122765000D+01 0.2063429899D+01
 0.1770481000D+01 -0.2869526473D+01
 0.3130840000D+00 0.1404747074D+01
 S 1 1.00 0.000000000000
 0.1240710000D+00 0.1000000000D+01
 P 3 1.00 0.000000000000
 0.2432887000D+01 0.7732753148D+00
 0.2137249000D+01 -0.1020833156D+01
 0.3145460000D+00 0.1095666871D+01
 P 1 1.00 0.000000000000
 0.1049450000D+00 0.1000000000D+01
 P 1 1.00 0.000000000000
 0.3264100000D-01 0.1000000000D+01

I 0
 I-ECP 4 46
 G component
 1
 2 1.0000000 0.00000000 0.00000000
 S-G projection
 2
 2 3.5112000 83.11386300 0.00000000
 2 1.7556000 5.20187600 0.00000000
 P-G projection
 2
 2 2.9688000 82.81110900 0.00000000
 2 1.4844000 3.37968200 0.00000000
 D-G projection
 2
 2 1.9066000 10.30427700 0.00000000
 2 0.9533000 7.58803200 0.00000000
 F-G projection
 1
 2 2.3075000 -21.47793600 0.00000000

5.2.5. Instrumentation

UV-Vis spectroscopy. Cary Varian 50 scan UV/Vis optical spectrometer equipped with “Cary Win” UV software was used to elucidate the optical properties of CuNCs.

Fluorescence spectroscopy. Fluorescence studies of CuNCs in a sealed cuvette were carried out in a Perkin Elmer LS55 Fluorescence Spectrometer instrument. All the experiments were carried out with the excitation slit width 5 nm and emission slit width 5 nm.

MALDI-TOF MS spectrometer. The MALDI-TOF MS analyses were done using Bruker Daltonics flex Analysis mass spectrometer.

FEG-TEM study. TEM study of the blue clusters was carried out in a JEOL 2100 KeV Ultra High Resolution Field Emission Gun (UHR FEG) TEM with voltage 200 KeV, using carbon coated copper grids.

X-ray photoelectron spectroscopy (XPS). XPS analysis of dried orange-red emitting CuNCs was carried out by using an X-ray photoelectron spectroscopic (XPS, Omicron, model: 1712-62-11) method. Measurement was done by using an AlK α radiation source under 15 kV voltages and 5 mA current.

NMR. All NMR studies were carried out on a Bruker DPX 400 MHz and 500 MHz spectrometer at 300K. Concentration were in the range 5-10 mM in CDCl₃ or (CD₃)₂SO.

Mass spectrometry. Mass spectra were recorded on a Q-ToF microTM (Waters Corporation) mass spectrometer by positive mode electro spray ionisation process.

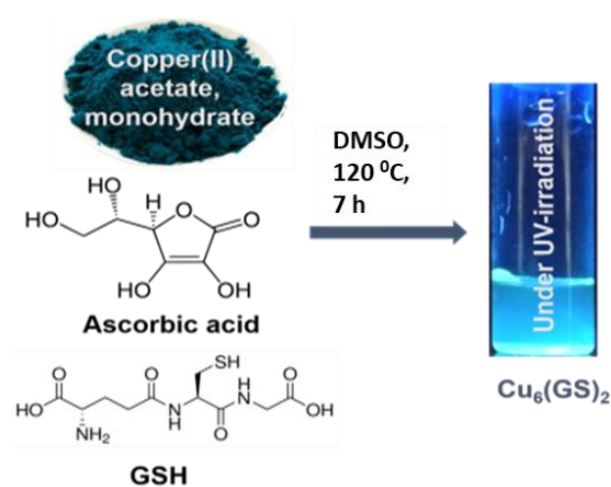
CHNS analyser. The elemental analysis was performed by Bruker Daltonics flex Analysis. The elemental analysis of C, H, and N were performed by CHN analyser after converting the sample elements to simple gases, CO₂, H₂O, and N₂ respectively by combustion (C, H, N).

C, H, N, S analysis procedure. The CHNS analyzer finds utility for the determination of the percentages of carbon, hydrogen, nitrogen, and sulphur elements in organic compounds, based on the principle of the “Dumas method,” which involves the complete and instantaneous oxidation of the sample by “flash combustion.” The CHNS analyzer is calibrated using the K-factors calculations from analyzing standard compounds. Thus the analyzer ensures maximum reliability of the results because the combustion gases are not split or diluted but directly carried to the GC system. The determination of CHNS can be done in

less than 10 min. This method finds the most significant utility in finding out percentages of C, H, N, and S elements in organic compounds, which are generally combustible at 1800 °C.

5.3. Results and Discussion

5.3.1. Synthesis Protocol of Copper Nanoclusters and UV-vis Studies. The amount of metal precursor, copper acetate monohydrate $[\text{Cu}(\text{CH}_3\text{COO})_2 \cdot \text{H}_2\text{O}]$, stabilizing agent (glutathione), and the reducing agent (L-ascorbic acid) were kept at a molar ratio of 5: 4: 7 to obtain the best reproducible result for the synthesis of Cu nanoclusters, and the reaction was carried out in DMSO at 120 °C for 7 h. The meticulous method for making CuNCs is given in the experimental section. The progress of the reaction was checked at different stages of reaction using UV-vis absorption spectroscopy. $\text{Cu}(\text{CH}_3\text{COO})_2 \cdot \text{H}_2\text{O}$ dissolved in DMSO shows a sharp absorption peak for Cu(II) with a λ_{max} 712 nm; however, after adding glutathione and heating it for 5 min, this peak has been vanished. This observation indicates that upon mixing with glutathione, the copper ions coordinate with the sulfur and amine groups of glutathione, and it causes a change in the UV-vis absorption pattern of the solution (Figure 5.31a of supporting information). Upon the formation of Cu nanoclusters, this pattern changes further, and a stiff increase in absorbance was found from the 600 nm range with a small hump at 460 nm (Figure 5.31b of supporting information). No peak was located at 560 nm, and this indicates the absence of bigger size nanoparticles (other than nanoclusters) in the mixture (Figure 5.31b).⁵⁹



Scheme 5.1. Schematic diagram showing the synthesis of blue-emitting Cu-nanoclusters at DMSO medium, using copper acetate monohydrate as a precursor, ascorbic acid as a reducing agent, and a thiol-containing bioactive peptide reduced glutathione as the stabilizing agent.

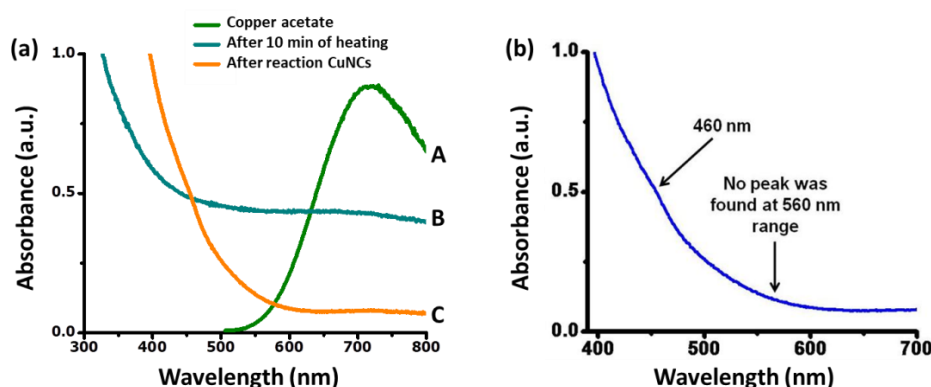


Figure 5.31. (a) UV-vis spectrum of copper acetate monohydrate in DMSO before heating without stabilizing agent (Curve A); copper acetate monohydrate in DMSO with the stabilizing agent, reduced glutathione after 5 min heating at 120 °C in an oil bath (Curve B); Copper acetate monohydrate in DMSO with stabilizing and reducing agent reduced glutathione, ascorbic acid respectively after 7 h heating at 120 °C on an oil bath (Curve C). (b) Extended UV-vis absorption spectrum of CuNCs.

5.3.2. Fluorescence Spectroscopic Study. The fluorescent nature of the metal nanoclusters makes them useful in a different way; at the same time, this observation proves their molecular nature. In our study, these above-stated CuNCs show blue emission upon irradiation with UV-torch (λ_{max} 365 nm) (Scheme 5.1), and the fluorescence spectrum reveals the exact position of emission band for the nanoclusters at 450 nm for excitation at 374 nm wavelength (Figure 5.32). This observation satisfies the basic requirement of atomically precise metal nanoclusters and their homogenous structural pattern with solubility in the corresponding media. At the same time, it casts light on the fact that it can be used as a homogenous catalyst.

We also studied the in-situ fluorescence spectra after CuNCs catalyzed Ullmann and Buchwald-Hartwig reaction. It was observed that the excitation maxima remained almost the same at 375 nm for C–N coupling reaction. Still, the emission maxima shifted towards a longer wavelength 465 nm with a 15 nm red shift with the broadening of the spectra (Figure 5.33). These may be due to organic molecules in the reaction mixture, which helps the Cu-nanoclusters form relatively larger particles. For C–C coupling reaction the excitation maxima and emission maxima shifted towards 374 nm to 455 nm and 465 nm to 538 nm respectively. This is due to the presence of organic molecules and under high temperature reaction.

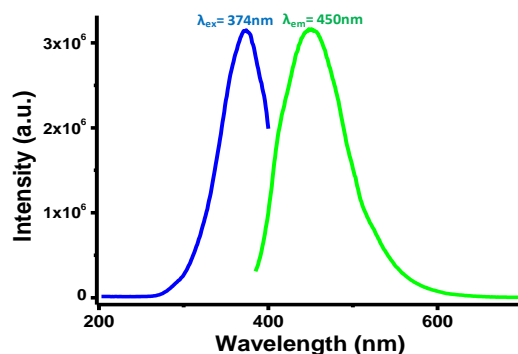


Figure 5.32. Fluorescence emission (green curve) and excitation (blue curve) spectra of copper nanoclusters showing an excitation maximum at 374 nm and an emission maximum at 450 nm with a Stoke's shift of 76 nm.

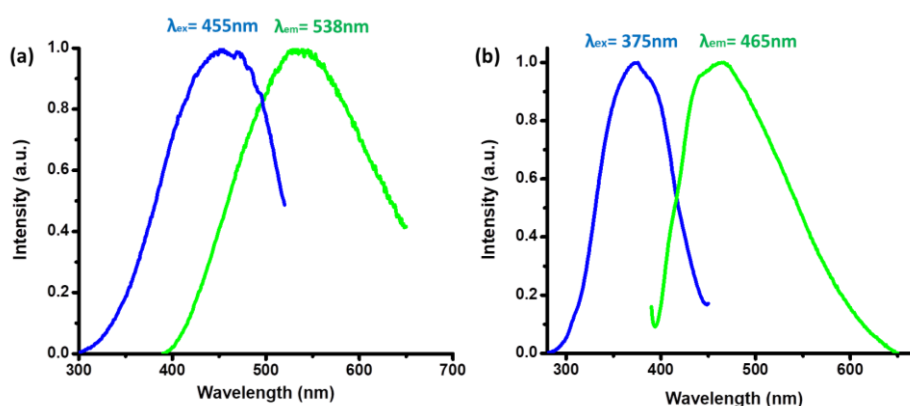


Figure 5.33. Fluorescence emission (green curve) and excitation (blue curve) spectra of copper nanoclusters for (a) C-C coupling reaction showing an excitation maximum at 455 nm and an emission maximum at 538 nm with a Stoke's shift of 83 nm, and (b) C-N coupling reaction showing an excitation maximum at 375 nm and an emission maximum at 465 nm with a Stoke's shift of 90 nm.

5.3.3. XPS Analysis. X-ray photoelectronic spectroscopic (XPS) study was performed with the CuNCs (Figure 5.34) to know the actual valence state of the metal ion present in the nanoclusters. X-ray photoelectronic spectrum shows two peaks at 933.7 eV and 953.5 eV, which can be assigned for Cu 2p_{3/2} and Cu 2p_{1/2} states. Due to the slight difference in the binding energy of Cu(0) and Cu(I) (~0.1 eV), it isn't easy to distinguish the valence state of Cu in our CuNCs in the XPS spectrum. The absence of any satellite peak at 942.0 eV cancels out the likelihood of the presence of Cu(II) species in the CuNCs sample. The observed binding energy of the sulfur (S) 2P state was 162.7 eV, which indicates the presence of chemisorbed S-atoms in the metal nanoclusters.¹⁵

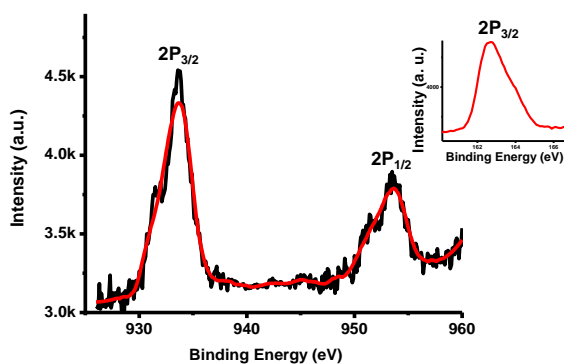


Figure 5.34. XPS spectra of copper nanoclusters, showing the Cu $2P_{3/2}$ and Cu $2P_{1/2}$ peaks at 933.7 and 953.5 eV respectively indicating the presence of Cu(0) or Cu(I) state. In the inset, binding energy of sulphur (S) 2P state was found to be 162.7 eV indicating the presence of chemisorbed S atoms.

5.3.4. MALDI-TOF MS Analysis. Matrix-assisted laser desorption ionization-time of flight (MALDI-TOF) mass spectrometry is one of the best techniques to characterize atomically precise metal nanoclusters. MALDI-TOF study of the CuNCs was done using sinapinic acid as a matrix, and the nanocluster to matrix ratio was kept at 1:6 for the best reproducible result. The exact mass for $\text{Cu}_6(\text{GS})_2$ nanoclusters are 989.73, with having a molecular weight of 993.91. The expected m/z value for $\text{Cu}_6(\text{GS})_2$ nanoclusters are 993.73 (100%) and 991.73 (89.3%). Positive mode mass peaks were found at $m/z = 992.79$, 1015.79, 1031.79, 1038.79 positions (Figure 5.35). Upon calculation of tentative empirical formula, it was found that the nanoclusters are $\text{Cu}_6(\text{GS})_2$ (where GS stands for deprotonated glutathione) species. The peaks can be assigned for the formation of $[\text{Cu}_6(\text{GS})_2 + \text{H}]^+$, $[\text{Cu}_6(\text{GS})_2 + \text{Na}]^+$, $[\text{Cu}_6(\text{GS})_2 + \text{K}]^+$, $[\text{Cu}_6(\text{GS})_2 + 2\text{Na}]^+$ species respectively in the corresponding ion beam (Figure 5.35). These observations indicate a common mechanistic pathway towards an Ullmann-type reaction. The formation of an activated complex of phenyl ring with the CuNCs promotes the further addition of another activated C or nucleophilic N atom to the aromatic ring. These observations also support the computational results showing the elaborate mechanistic pathway (*vide infra*).

5.3.5. MALDI-TOF Analysis for the Reaction Intermediates. Further MALDI-TOF studies were carried out to understand the mechanism of C–C and C–N bond formation reactions. Aliquots were collected from time to time and charged for MALDI analyses using sinapinic acid as a matrix. The analysis shows that only CuNCs were present in the reaction mixture of C–C and C–N coupling reactions before heating (Figure 5.36a and Figure 5.36a). For the C–C coupling reaction, after heating the reaction mixture for 5 min, intermediate $[\text{Cu}_6(\text{GS})_2\text{Ph}]^+$

$\text{Na}]^+$ (Figure 5.36b) was found along with the initial CuNCs, $[\text{Cu}_6(\text{GS})_2 + 2\text{Na}]^+$. When the reaction time was increased to 15 min, the intermediates were $[\text{Cu}_6(\text{GS})_2\text{Ph} + \text{Na}]^+$ and $[\text{Cu}_6(\text{GS})_2\text{Ph}_2 + \text{K}]^+$ (Figure 5.36c) with the initial CuNCs, but 60 min later, only intermediate $[\text{Cu}_6(\text{GS})_2\text{Ph}_2 + 2\text{Na}]^+$ (Figure 5.36d) was identified by MALDI-TOF analysis. In the case of C–N coupling reaction, CuNCs were present even after the completion of 60 min of reaction, and only intermediate $[\text{Cu}_6(\text{GS})_2\text{Ph} + \text{Na}]^+$ was identified by the analysis of MALDI-TOF data (Figure 5.37a-d).

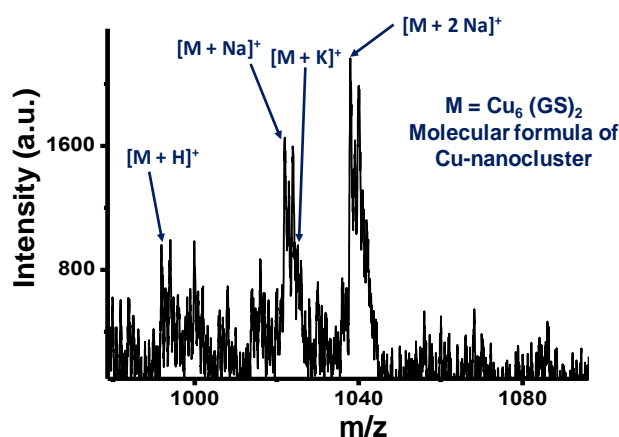


Figure 5.35. MALDI-TOF analysis of Cu-nanoclusters showing the presence of $\text{Cu}_6(\text{GS})_2$ species (GS = reduced glutathione).

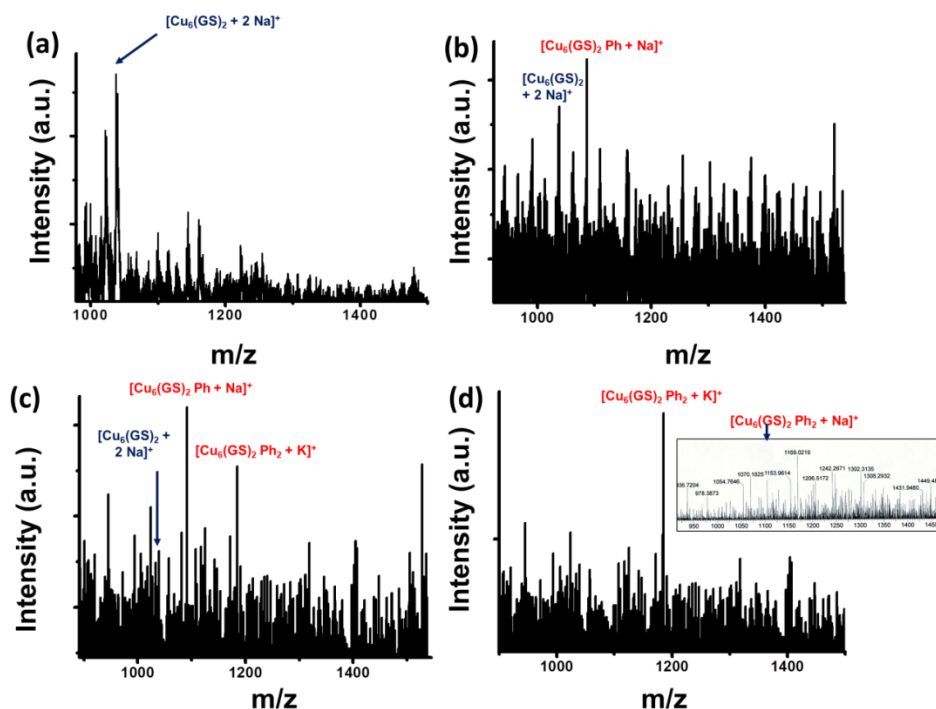


Figure 5.36. Intermediates formed by the CuNCs during the time interval of (a) 00 min, (b) 5 min, (c) 15 min, and (d) 60 min for the C–C coupling reaction.

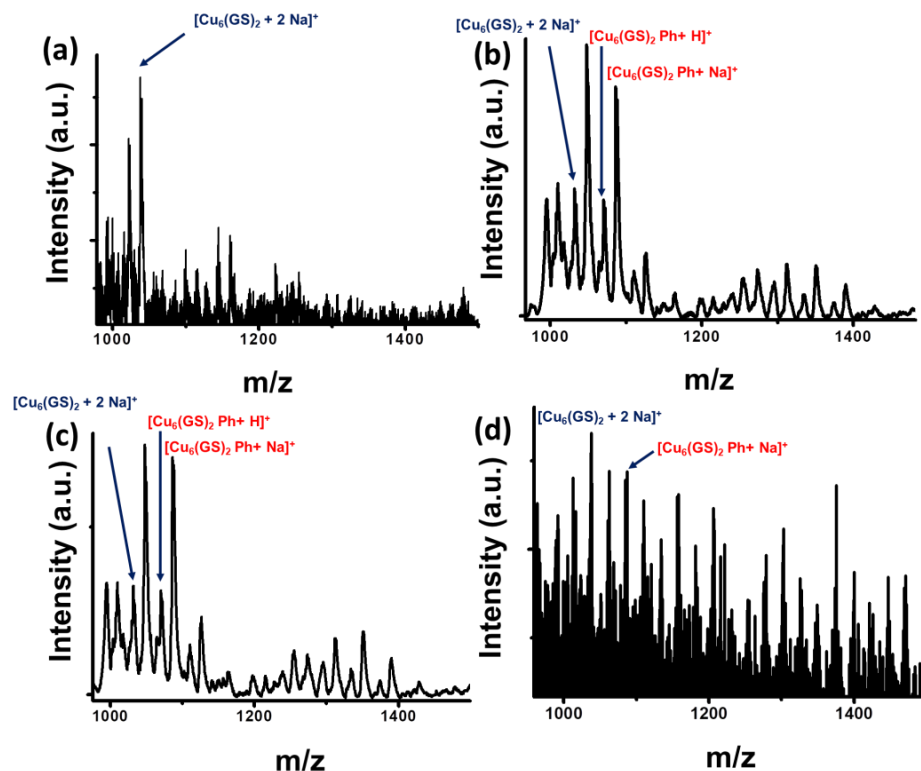


Figure 5.37. Intermediates formed by the CuNCs during the time interval of (a) 00 min, (b) 5 min, (c) 15 min, and (d) 60 min for the C–N coupling reaction.

5.3.6. UHR-FEG-TEM Study. An Ultra-High-Resolution Field-Emission Gun-Transmission Electron Microscopic (UHR-FEG-TEM) study was carried out to know the dimension and structural heterogeneity of this tiny nanoclusters species. The average size of Cu nanoclusters was 2.75 nm, with a size distribution ranging from 1.04 nm to 4.15 nm, where the most populated distribution range was 2.50–3.50 nm (Figure 5.38). This observation matches well with previous theoretical study showing the size of fluorescent copper nanoclusters have size limit of 1–6 nm.¹¹ The relatively larger particles with sizes ~ 3 nm are also present in the mixture due to the aggregation of nanoclusters to form relatively bigger-sized particles (Figure 5.39). This result agrees with the observation found by Pradeep and co-workers for the coagulation of metal nanoclusters under the high-energy electron beam irradiation during the TEM experiment.⁶⁰ However, on a gross scale, the nanoclusters are homogenous in terms of size and shape, which is an essential factor for regulated catalytic output.⁶¹

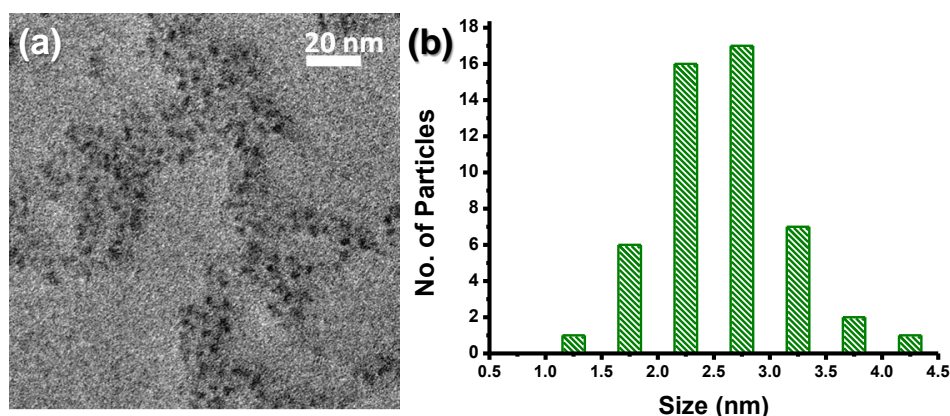


Figure 5.38. (a) FEG-TEM image of the Cu-nanoclusters; (b) size distribution histogram of Cu-nanoclusters showing most populated size 2.75 nm.

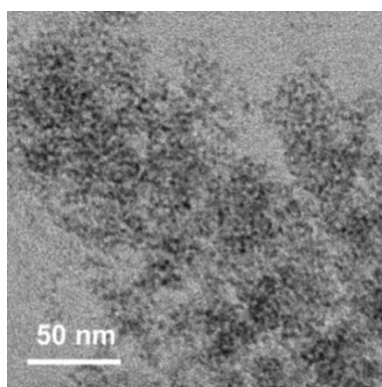


Figure 5.39. FEG-TEM picture of catalyst copper nanocluster after the completion of reaction.

5.3.7. Structural Investigation of CuNCs Using DFT. For a comprehensive understanding of synthesized CuNCs, geometry optimization of $\text{Cu}_6(\text{GS})_2$ cluster was performed using Gaussian 16 suite programs.⁴⁵ The optimized structure was shown in Figure 5.40. The calculated harmonic frequencies ensure the absence of any saddle point in the optimized structure. Distortion in planar geometry of bare Cu_6 cluster is observed after coordination with the S atoms of glutathione thiolate (GS) ligands. The average Cu–Cu distance is 2.43 Å in bare Cu_6 cluster⁶² while $\text{Cu}_6(\text{GS})_2$ cluster exhibits a relatively longer Cu–Cu average bond distance (2.51 Å). The average Cu–S bond distance between S atom of GS ligands and Cu atoms in $\text{Cu}_6(\text{GS})_2$ cluster is 2.38 Å (significantly lower than the sum of their van der Waals radii: $r_{\text{Cu}} = 1.40$ Å; $r_{\text{S}} = 1.80$ Å) indicating strong bonding interaction between Cu atoms and thiolate anchors.⁶³ Natural Bond Orbital (NBO) analysis exhibits charge delocalization among Cu_6 core and anchoring S atoms where S atoms possess small localized average charge $q = -0.39e$ while rest of the charge density is smeared out across Cu_6 core of the cluster. Interestingly, the optimized structure of $\text{Cu}_6(\text{GS})_2$ cluster attributes relatively short distances between Cu

atoms of Cu₆ core and oxygen centers of thiolate ligands. This predominant electrostatic, non-covalent interaction between Cu atoms and oxygen centers are known to stabilize thiolate-based Cu clusters.

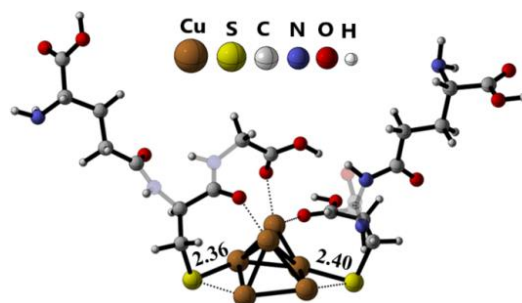
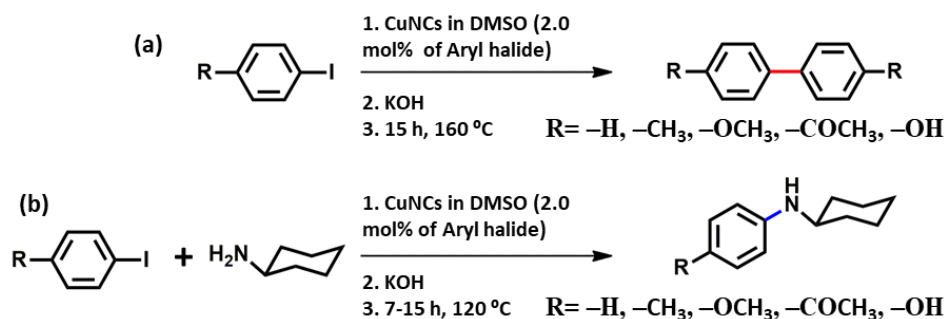


Figure 5.40. Structure of the optimized Cu₆(GS)₂ cluster with selected bond lengths (Å).

5.3.8. C–C and C–N Bond Formation Using CuNCs as a Catalyst. The current growth of organic industries demands cheap, easily processable, and stable catalysts for future green applications. Since the last few decades, researchers have discovered metal nanoparticles with catalytic properties much better than conventional metal complex or bulk metal catalysts.^{50, 51} However, various nanoparticles with toxic effects in the environment can be replaced by their less nontoxic and smaller counterpart, metal nanoclusters. Therefore, it is necessary to exploit the catalytic effect of metal nanoclusters to make clean, green, and safe catalytic materials. Interestingly the CuNCs discussed in the current study can efficiently catalyze C(sp²)–C(sp²) and C(sp²)–N(sp³) bond formation in an Ullmann's coupling reaction.

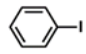
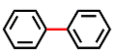
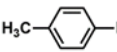
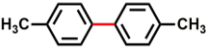
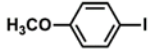
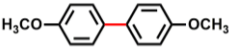


Scheme 5.2. (a) Ullmann's reactions catalyzed by copper nanoclusters, (b) Buchwald–Hartwig reactions catalyzed by copper nanoclusters.

In a C(sp²)–C(sp²) (aryl-aryl) bond formation reaction, aryl halides were found to undergo a C–C coupling reaction in the presence of measured amount copper nanoclusters in DMSO under nitrogenous atmosphere (see scheme 5.2 and for details see supporting information). After the completion of the reaction, the reaction mixtures were worked up with ethyl acetate (EtOAc)/ water mixture, and

biphenyl compounds were extracted in the EtOAc layer. Further purifications were done by column chromatography eluted with optimized solvent systems depending upon the polarity of the synthesized compounds. Characterization of these compounds was done by various spectroscopic techniques like ^1H NMR, ^{13}C NMR, and high-resolution mass spectrometric (HRMS) (see experimental section). The substrate scope, yield, and reaction conditions are summarized in table 5.2. As stated earlier, the Cu-nanoclusters can also catalyze $\text{C}(\text{sp}^2)\text{--N}(\text{sp}^3)$ (aryl- 1° amine) bond formation reaction between aryl halides and 1° amine (cyclohexylamine). These C–N bond formation reactions were carried out in the DMSO medium at an optimized 120°C temperature. Products were extracted with ethyl acetate, washed with water, purified using column chromatography, and characterized by ^1H NMR, ^{13}C NMR, high-resolution mass spectrometric (HRMS), and C, H, and N analyses (see experimental section). Details of substrate scope and reaction conditions are summarized in the table 5.3. A small number of Cu nanoclusters (2 mol%) are required for these reactions due to their advantages over the conventional metal catalyst since the amount of the catalyst used in this study is somewhat less than the traditional metal (in bulk form) catalyst used earlier for aryl-aryl and aryl-N coupling.^{23,40,41} In addition, no $\text{C}(\text{sp}^2)\text{--C}(\text{sp}^2)$ and $\text{C}(\text{sp}^2)\text{--N}(\text{sp}^3)$ bond forming reaction was observed in absence of the $\text{Cu}_6(\text{GS})_2$ cluster.

Table 5.2. Substrate scopes for $\text{C}(\text{sp}^2)\text{--C}(\text{sp}^2)$ bond formation reactions.

| Entry | Reactants | Reactants amount | Conditions | Products | Yield (%) |
|-------|--|------------------|----------------------------|---|-----------|
| 1 |  Iodobenzene | 204 mg (1 mM) | 160°C , 15 h |  Biphenyl | 88 |
| 2 |  4-Iodotoluene | 218 mg (1 mM) | 160°C , 15 h |  4, 4'-Dimethylbiphenyl | 96 |
| 3 |  4-Iodoanisole | 234 mg (1 mM) | 160°C , 15 h |  4, 4'-Dimethoxybiphenyl | 85 |

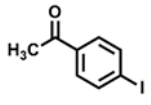
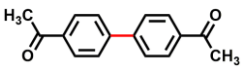
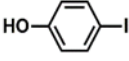
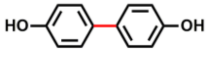
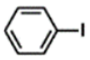
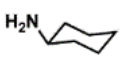
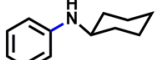
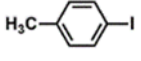
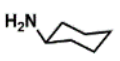
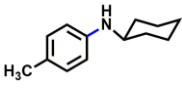
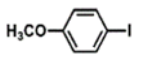
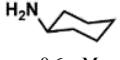
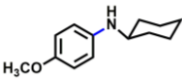
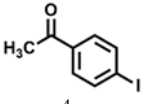
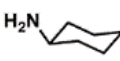
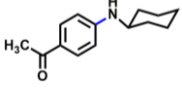
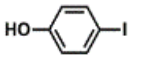

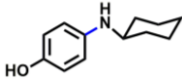
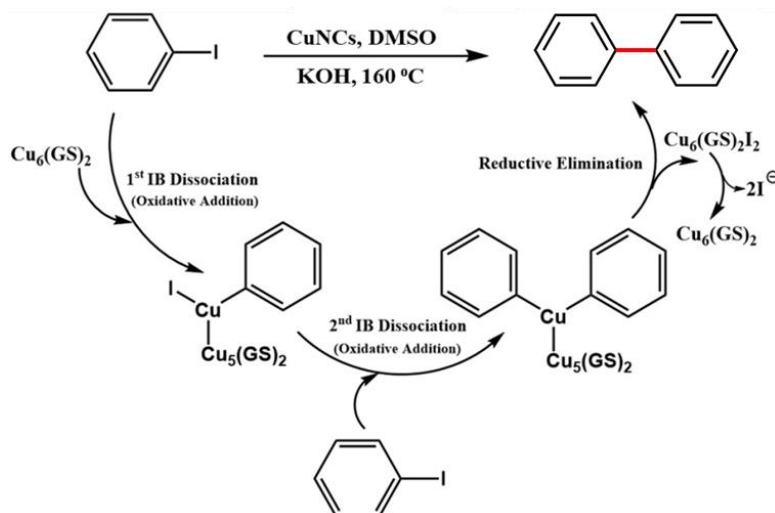
| | | | | | |
|---|---|------------------|--------------|--|----|
| 4 |  4-Iodoacetophenone | 246 mg (1 mM) | 160 °C, 15 h |  4, 4'-Diacylbiphenyl | 90 |
| 5 |  4-Iodophenol | 220 mg (1 mM) | 160 °C, 15 h |  4, 4'-Biphenol | 89 |

Table 5.3. Substrate scopes for $C(sp^2)-N(sp^3)$ bond formation reactions.

| Entry | Reactants | Aryl iodide amount | Cyclohexylamine | Conditions | Products | Yield (%) |
|-------|---|--------------------|---|--------------|--|-----------|
| 1 |  Iodobenzene | 102 mg (0.5 mM) |  0.6 mM | 120 °C, 7 h |  N-cyclohexylaniline | 95 |
| 2 |  4-Iodotoluene | 109 mg (0.5 mM) |  0.6 mM | 120 °C, 9 h |  N-cyclohexyl-4-methylaniline | 96 |
| 3 |  4-Iodoanisole | 117 mg (0.5 mM) |  0.6 mM | 120 °C, 9 h |  N-cyclohexyl-4-methoxyaniline | 95 |
| 4 |  4-Iodoacetophenone | 123 mg (0.5 mM) |  0.6 mM | 120 °C, 15 h |  4-(Cyclohexylamino)-acetophenone | 95 |
| 5 |  4-Iodophenol | 110 mg (0.5 mM) |  0.6 mM | 120 °C, 15 h |  4-(Cyclohexylamino)-phenol | 91 |

5.3.9. Mechanistic Elucidation Based on DFT Study. In order to gain insight into the mechanistic details of $Cu_6(GS)_2$ catalyzed Ullmann reaction, density functional theory study (DFT) was performed using Gaussian 16 suite of programs.⁴⁵ The proposed catalytic cycle for $C(sp^2)-C(sp^2)$ Ullmann coupling reaction (as shown in scheme 5.3) consists of first oxidative addition i.e.

iodobenzene dissociation (IB dissociation) followed by second oxidative addition of another IB and finally reductive elimination yielding biphenyl (BP), which is in accordance with the earlier studies.^{64, 65}



Scheme 5.3. Plausible mechanism for Cu₆(GS)₂ catalyzed C(sp²)-C(sp²) Ullmann coupling reaction.

To imitate the experimental condition, we have discussed the reaction mechanism based on solution phase results obtained at SMD/M06-L/SDD: Cu, I, 6-31++G(d, p):S, C, N, O, H level of theory (Figure 5.41) in DMSO solvent ($\epsilon = 46.83$). Cu₆(GS)₂ catalyzed Ullmann coupling reaction initiates through the abstraction of iodine atom from IB. The lone pair of iodine in IB interacts with Cu atom of Cu₆(GS)₂ cluster resulting the activation of IB which is evident from elongation of the C-I bond of IB from 2.10 to 2.17 Å forming intermediate complex (A2) (Figure 5.41 and Figure 5.43). A weak interaction between C atom of IB and Cu atom of Cu₆(GS)₂ cluster is also observed in A2. Subsequently, IB dissociates on Cu₆(GS)₂ cluster via TS1 (Figure 5.41). As shown in Figure 5.42, the structure of TS1 exhibits a three-membered transition state between C and I atom of IB and Cu atom of Cu₆(GS)₂ with extreme elongation of C-I bond with a bond length of 2.54 Å, leading to the breakage of C-I bond and formation of product (A3). Such a type of IB activation and dissociation has also been proposed by previous studies.⁶⁶ Moreover, Cu···C (2.05 Å) and Cu···I (2.90 Å) bond-forming interactions are also present in TS1. In the next step, another IB molecule interacts with A3 through lone pair of iodine with the Cu atoms resulting elongated C-I bond (2.16 Å) to form A4 complex (Figure 5.43). Subsequently, A4 undergoes oxidative addition of IB leading to the formation of

A5 intermediate. Here, it is noteworthy to mention that the oxidative addition of IB takes place at the same Cu center of the cluster where phenyl ring is already attached ensuring the effective C–C coupling product in the subsequent step. Attachment of two phenyl rings at the same Cu center of either Cu cluster or Cu surface to facilitate succeeding reductive elimination step is one of the important parameters in Ullmann coupling reaction and this phenomenon is in line with earlier studies.⁶⁷ However, the complex A4 undergoes oxidative addition via transition state TS2 to yield A5 complex. As shown in Figure 5.42, the TS2 structure exhibits lengthening of C–I bond from 2.16 to 2.77 Å along with bond-forming interactions of Cu···C (2.07 Å) and Cu···I (2.91 Å). However, the two phenyl rings reside in close proximity in complex A5 where the distance between two carbon atoms of the phenyl rings (coordinated to same Cu center) is 2.78 Å (Figure 5.43). We have also investigated the possibility of alternative pathway where second iodobenzene dissociation occurs on neighbouring Cu center instead of same Cu center which is already attached to phenyl ring (Figure 5.44 and Figure 5.47). As shown in free energy profile (Figure 5.47), the Gibbs activation barrier for the alternative path is higher (at SMD/M06-L/SDD: Cu, I, 6-31++G(d, p):S, C, N, O, H). Later, complex A5 rapidly undergoes reductive elimination to form biphenyl with a small local barrier and extrusion of C–C coupled product, BP takes place from the complex. A close look into the three-membered transition state structure (TS3) of reductive elimination step reveals crucial bond-forming C···C interaction with a distance of 2.3 Å (while C–C distance in A5 complex is 2.78 Å) toward the facile formation of BP (Figure 5.42). Similar results were obtained in gas phase DFT studies at B3LYP/LANL2DZ: Cu, I, 6-31G(d):S, C, N, O, H (Figure 5.45) and M06-L/SDD: Cu, I, 6-31++G(d, p):S, C, N, O, H level of theories (Figure 5.46). Interestingly, it can be observed that the transition states for oxidative addition steps (TS1 and TS2) get stabilized in presence of polar DMSO solvent due to the formation of two polar bonds in the transition states as polar solvent like DMSO will stabilize polar bonds. Based on the energy-span model for multi-step reactions as proposed by Kozuch and Shaik,⁶⁸ TS1 is the rate-limiting step with a Gibbs free energy of activation = 33.2 kcal/mol in DMSO (41.2 kcal/mol in gas-phase).

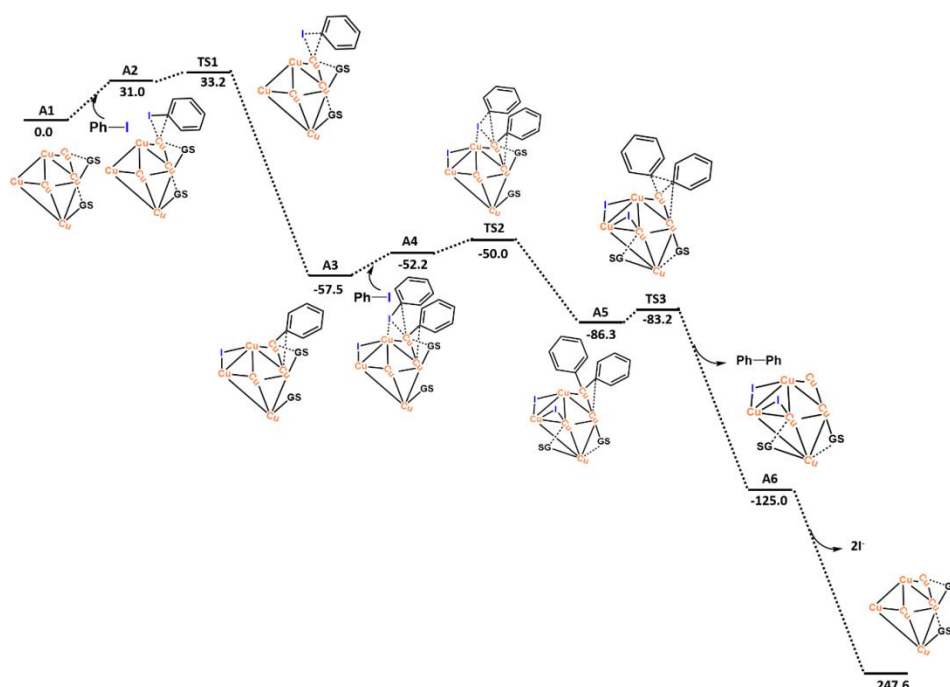


Figure 5.41. Free energy profile (kcal/mol) for $\text{Cu}_6(\text{GS})_2$ catalyzed $\text{C}(\text{sp}^2)\text{--C}(\text{sp}^2)$ Ullmann coupling reaction at SMD/M06-L/SDD: Cu, I, 6-31++G(d, p):S, C, N, O, H after applying quasi-harmonic approximation (QHA).

A similar trend of stabilization has also been noticed in the second oxidative addition step through TS2. The Gibbs activation energy reduces by 2.3 kcal/mol in DMSO with respect to the gas-phase. However, unlike oxidative addition, the final reductive elimination step exhibits increase in Gibbs activation energy as two polar bonds are converted to non-polar bond and polar solvent will destabilize the transition state. Hence, the Gibbs activation energy for TS3 is increased by 1.5 kcal/mol. Thus, computational studies reveal a detailed mechanistic pathway for $\text{Cu}_6(\text{GS})_2$ catalysed $\text{C}(\text{sp}^2)\text{--C}(\text{sp}^2)$ Ullmann coupling reaction and also establish the effect of polar solvent DMSO. Additionally, catalyst regeneration step is exothermic in nature indicating practical viability of the catalyst for $\text{C}(\text{sp}^2)\text{--C}(\text{sp}^2)$ Ullman coupling reaction (Figure 5.41 and Figure 5.45 and 5.46). Besides Cu clusters, Au clusters and surfaces are also well explored in the literature both experimentally and theoretically for catalyzing $\text{C}(\text{sp}^2)\text{--C}(\text{sp}^2)$ Ullman coupling reaction.⁶⁹ However, Au clusters and surfaces are reported to favour C–C coupling step while C–I bond cleavage in oxidative addition step is retarded due to much weaker bond strength of Au–C compared to C–C bond.⁶⁹ On the contrary, Cu analogues equally favours Cu–C and C–C bond formation due to comparable bond strength indicating facile progress of both the

oxidative addition and C–C coupling steps in $C(sp^2)–C(sp^2)$ Ullman coupling reaction.⁶⁹

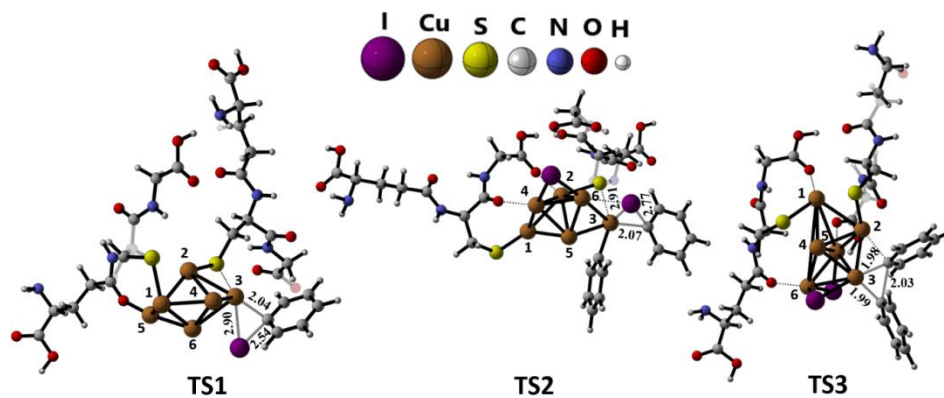


Figure 5.42. Optimized structures of **TS1**, **TS2** and **TS3** with selected bond lengths (Å) (Cu atoms of $Cu_6(GS)_2$ cluster are numbered).

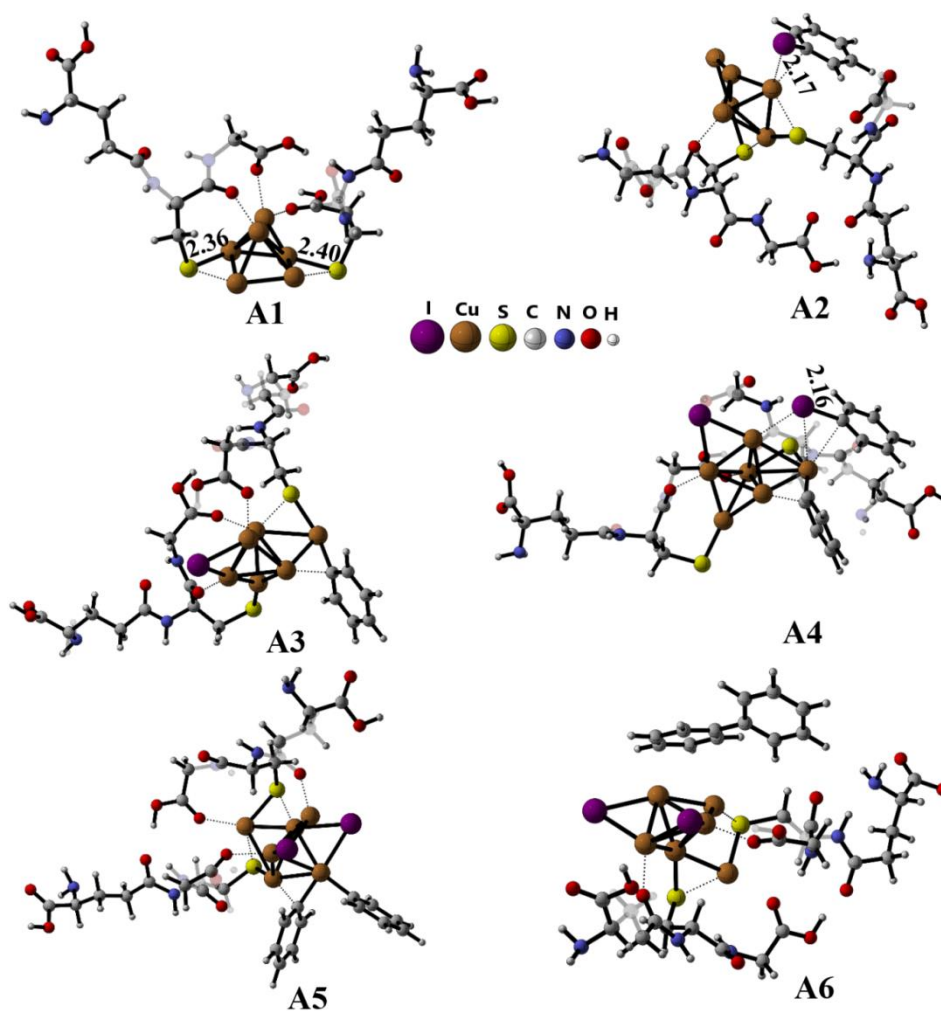


Figure 5.43. Optimized structures of all the reaction intermediates, reactants, products and catalyst for $Cu_6(GS)_2$ catalysed $C(sp^2)–C(sp^2)$ Ullmann coupling reaction.

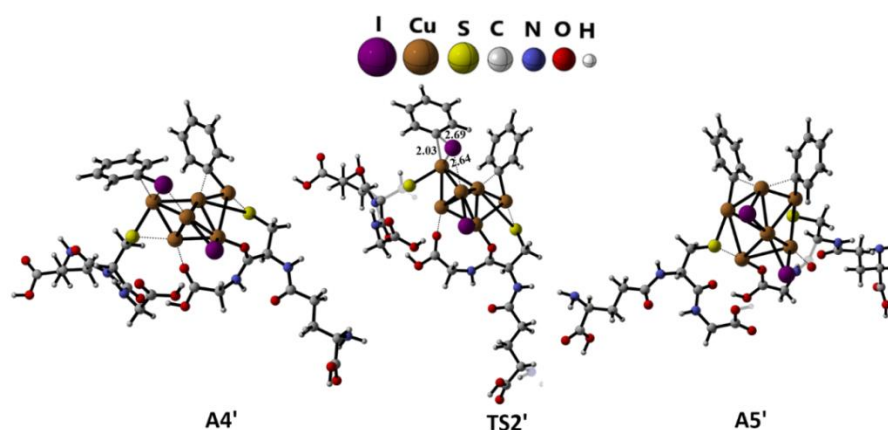


Figure 5.44. Optimized structures of the reactant (A4'), transition state (TS2') and product (A5') with selected bond lengths (Å) in the alternative oxidative addition path of second phenyl ring addition (at different Cu atom other than phenyl attached Cu) for $\text{Cu}_6(\text{GS})_2$ catalysed $\text{C}(\text{sp}^2)\text{--C}(\text{sp}^2)$ Ullmann coupling reaction.

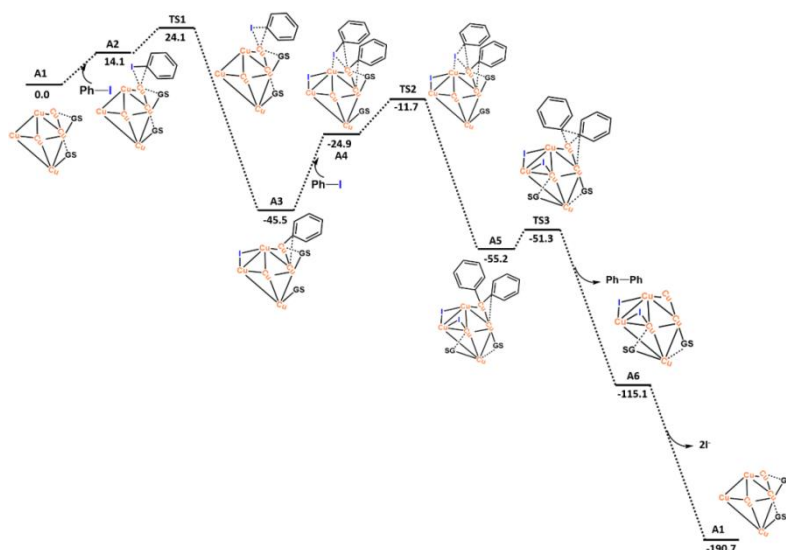


Figure 5.45. Free energy profile (kcal/mol) at B3LYP/LANL2DZ: I and Cu, 6-31G(d): S, C, N, O, and H.

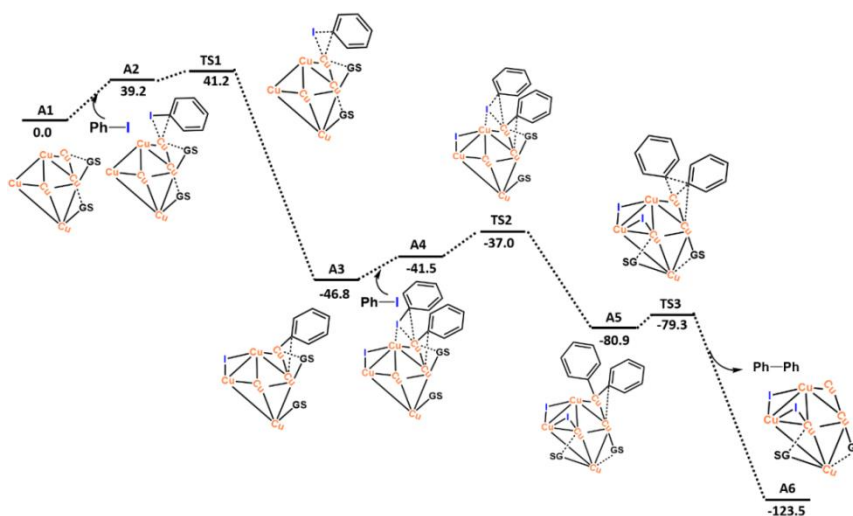


Figure 5.46. Free energy profile (kcal/mol) at M06-L/SDD: I and Cu, 6-31++G(d,p): S, C, N, O, and H.

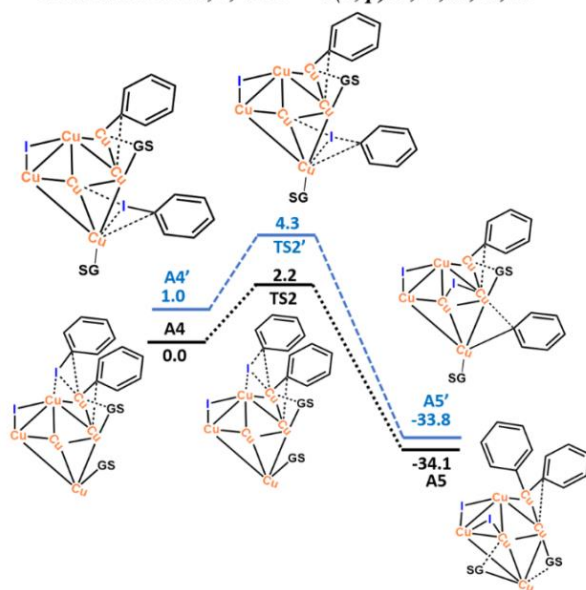
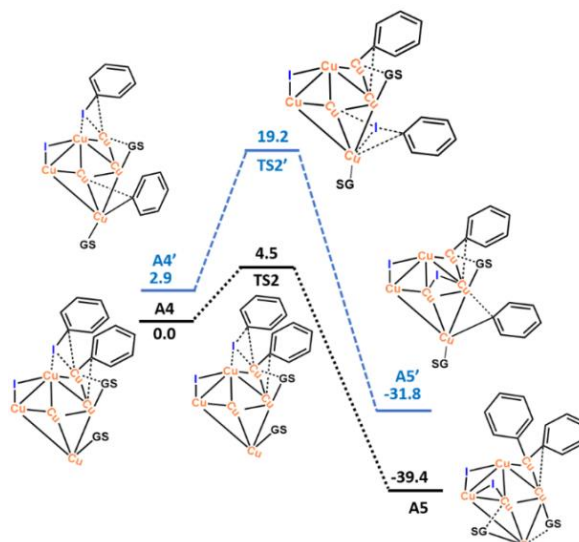
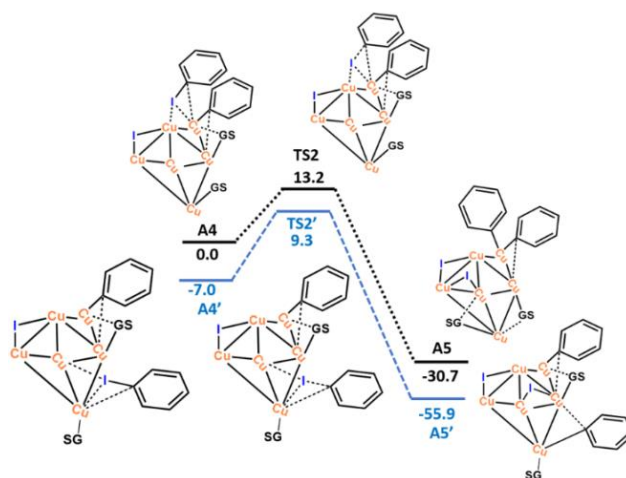


Figure 5.47. Free energy profiles at different level of theory for alternative oxidative addition path of second phenyl ring addition (at different Cu atom other than phenyl attached Cu).

4.4. Conclusion

This study vividly demonstrates the formation of newly synthesized fluorescent copper nanoclusters, which are thoroughly characterized by various techniques, including UV-vis absorption, fluorescence spectroscopy, matrix-assisted laser desorption ionization-time of flight (MALDI-TOF) spectrometry, transmission electron microscopy (TEM), and X-ray photoelectron spectroscopy (XPS). A detailed structural analysis based on the DFT study reveals the presence of strong Cu–S bonding interaction between Cu₆ core and anchoring thiolate ligands. This strong Cu–S bonding interaction, along with the preferential orientation of GS ligands, is responsible for stabilizing the copper nanocluster. Interestingly, these blue-emitting copper nanoclusters exhibit good catalytic activity for C(sp²)–C(sp²) and C(sp²)–N(sp³) bond coupling for making a series of substituted biphenyls and aromatic 2° amines in good yield at ambient conditions. Cheap, fluorescent, few atom Cu nanoclusters as a new catalyst for the C(sp²)–C(sp²) and C(sp²)–N(sp³) bond formation holds a future promise for the design and development of novel nanocatalyst in the organic synthesis. MALDI-TOF analysis shows the presence of mono and bi-phenyl substituted catalyst-substrate intermediates. The computational study also indicates the formation of various stable intermediates and transition states, namely TS1, TS2, and TS3 in C–C homoallylic bond coupling reactions. In the case of the C–N coupling reaction, the formation of only one intermediate [Cu₆(GS)₂Ph + Na]⁺ was observed from MALDI-TOF analysis may be due to the presence of a primary amine. This primary amine does not give the chance of the intermediate [Cu₆(GS)₂Ph + Na]⁺ for the formation of a more stable intermediate [Cu₆(GS)₂Ph₂ + Na]⁺, which immediately leads to the formation of the secondary amine as a product. The exploitation of a few atoms of copper nanoclusters for organic catalysis with probable mechanistic study holds future promise in next-generation green catalysis by a few atoms of metal clusters.

4.5. References

- (1) Diez, I.; Ras, R. H. A. Fluorescent Silver Nanoclusters. *Nanoscale* **2011**, *3*, 1963–1970.
- (2) Chakraborty, I.; Pradeep, T. Atomically Precise Clusters of Noble Metals: Emerging Link between Atoms and Nanoparticles. *Chem. Rev.* **2017**, *117*, 8208–8271.
- (3) Sakthivel, N. A.; Dass, A. Aromatic Thiolate-Protected Series of Gold Nanomolecules and a Contrary Structural Trend in Size Evolution. *Acc. Chem. Res.* **2018**, *51*, 1774–1783.
- (4) Kunwar, P.; Hassinen, J.; Bautista, G.; Ras, R. H. A.; Toivonen, J. Direct Laser Writing of Photostable Fluorescent Silver Nanoclusters in Polymer Films. *ACS Nano* **2014**, *8*, 11165–11171.
- (5) Jin, R.; Zeng, C.; Zhou, M.; Chen, Y. Atomically Precise Colloidal Metal Nanoclusters and Nanoparticles: Fundamentals and Opportunities. *Chem. Rev.* **2016**, *116*, 10346–10413.
- (6) Shichibu, Y.; Suzuki, K.; Konishi, K. Facile Synthesis and Optical Properties of Magic-Number Au₁₃ Clusters. *Nanoscale* **2012**, *4*, 4125–4129.
- (7) Suber, L.; Imperatori, P.; Pilloni, L.; Caschera, D.; Angelini, N.; Mezzi, A.; Kaciulis, S.; Iadecola, A.; Joseph, B.; Campi, G. Nanoclusters Superstructures or Nanoparticles? The Self-Consuming Scaffold Decides. *Nanoscale* **2018**, *10*, 7472–7483.
- (8) Baral, A.; Basu, K.; Ghosh, S.; Bhattacharyya, K.; Roy, S.; Datta, A.; Banerjee, A. Size Specific Emission in Peptide Capped Gold Quantum Clusters with Tunable Photoswitching Behavior. *Nanoscale* **2017**, *9*, 4419–4429.
- (9) Ghosh, S.; Das, N. K.; Anand, U.; Mukherjee, S. Photostable Copper Nanoclusters: Compatible Förster Resonance Energy-Transfer Assays and a Nanothermometer. *J. Phys. Chem. Lett.* **2015**, *6*, 1293–1298.
- (10) Das, N. K.; Ghosh, S.; Priya, A.; Datta, S.; Mukherjee, S. Luminescent Copper Nanoclusters as a Specific Cell-Imaging Probe and a Selective Metal Ion Sensor. *J. Phys. Chem. C* **2015**, *119*, 24657–24664.
- (11) Basu, K.; Gayen, K.; Mitra, T.; Baral, A.; Roy, S. S.; Banerjee, A. Different Color Emissive Copper Nanoclusters for Cancer Cell Imaging. *ChemNanoMat* **2017**, *3*, 808–814.

- (12) Chen, Y.-C.; Dickson, R. M. Improved Fluorescent Protein Contrast and Discrimination by Optically Controlling Dark State Lifetimes. *J. Phys. Chem. Lett.* **2017**, *8*, 733–736.
- (13) Baral, A.; Basu, K.; Roy, S.; Banerjee, A. Blue Emitting Gold Cluster Formation from Gold Nanorods: Selective and Sensitive Detection of Iron(III) Ions in Aqueous Medium. *ACS Sustain. Chem. Eng.* **2017**, *5*, 1628–1637.
- (14) Roy, S.; Palui, G.; Banerjee, A. The As-Prepared Gold Cluster-Based Fluorescent Sensor for the Selective Detection of As^{III} Ions in Aqueous Solution. *Nanoscale* **2012**, *4*, 2734–2740.
- (15) Basu, K.; Paul, S.; Jana, R.; Datta, A.; Banerjee, A. Red-Emitting Copper Nanoclusters: From Bulk-Scale Synthesis to Catalytic Reduction. *ACS Sustain. Chem. Eng.* **2019**, *7*, 1998–2007.
- (16) Jia, X.; Yang, X.; Li, J.; Li, D.; Wang, E. Stable Cu Nanoclusters: from an Aggregation-Induced Emission Mechanism to Biosensing and Catalytic Applications. *Chem. Commun.* **2014**, *50*, 237–239.
- (17) Lu, Y. Z., Wei, W. T., Chen, W. Copper Nanoclusters: Synthesis, Characterization and Properties. *Chin Sci Bull* **2012**, *57*, 41–47.
- (18) Ghosh, R.; Goswami, U.; Ghosh, S. S.; Paul, A.; Chattopadhyay, A. Synergistic Anticancer Activity of Fluorescent Copper Nanoclusters and Cisplatin Delivered through a Hydrogel Nanocarrier. *ACS Appl. Mater. Interfaces* **2015**, *7*, 209–222.
- (19) Borghei, Y. S., Hosseini, M., Khoobi, M., Ganjali, M. R. Novel Fluorometric Assay for Detection of Cysteine as a Reducing Agent and Template in Formation of Copper Nanoclusters. *J Fluoresc* **2017**, *27*, 529–536.
- (20) Schmidt, N. G.; Eger, E.; Kroutil, W. Building Bridges: Biocatalytic C–C–Bond Formation toward Multifunctional Products. *ACS Catal.* **2016**, *6*, 4286–4311.
- (21) Khan, F.; Dlugosch, M.; Liu, X.; Banwell, M. G. The Palladium-Catalyzed Ullmann Cross-Coupling Reaction: A Modern Variant on a Time-Honored Process. *Acc. Chem. Res.* **2018**, *51*, 1784–1795.
- (22) Nijamudheen, A.; Datta, A. Gold-Catalyzed Cross-Coupling Reactions: An Overview of Design Strategies, Mechanistic Studies, and Applications. *Chem. - A Eur. J.* **2020**, *26*, 1442–1487.
- (23) Ruiz-Castillo, P.; Buchwald, S. L. Applications of Palladium-Catalyzed C–N Cross-Coupling Reactions. *Chem. Rev.* **2016**, *116*, 12564–12649.

- (24) Oliver-Messeguer, J.; Liu, L.; García-García, S.; Canós-Giménez, C.; Domínguez, I.; Gavara, R.; Doménech-Carbó, A.; Concepción, P.; Leyva-Pérez, A.; Corma, A. Stabilized Naked Sub-Nanometric Cu Clusters within a Polymeric Film Catalyze C–N, C–C, C–O, C–S, and C–P Bond-Forming Reactions. *J. Am. Chem. Soc.* **2015**, *137*, 3894–3900.
- (25) Nasaruddin, R. R.; Yao, Q.; Chen, T.; Hülsey, M. J.; Yan, N.; Xie, J. Hydride-Induced Ligand Dynamic and Structural Transformation of Gold Nanoclusters During a Catalytic Reaction. *Nanoscale*, **2018**, *10*, 23113–23121.
- (26) Wang, C.; Wang, C.; Xu, L.; Cheng, H.; Lin, Q.; Zhang, C. Protein-Directed Synthesis of pH-Responsive Red Fluorescent Copper Nanoclusters and Their Applications in Cellular Imaging and Catalysis. *Nanoscale* **2014**, *6*, 1775–1781.
- (27) Tsunoyama, H.; Ichikuni, N.; Sakurai, H.; Tsukuda, T. Effect of Electronic Structures of Au Clusters Stabilized by Poly(N-Vinyl-2-Pyrrolidone) on Aerobic Oxidation Catalysis. *J. Am. Chem. Soc.* **2009**, *131*, 7086–7093.
- (28) Wilcoxon, J. P.; Abrams, B. L. Synthesis, Structure and Properties of Metal Nanoclusters. *Chem. Soc. Rev.* **2006**, *35*, 1162–1194.
- (29) Rong, H.; Ji, S.; Zhang, J.; Wang, D.; Li, Y. Synthetic Strategies of Supported Atomic Clusters for Heterogeneous Catalysis. *Nat. Commun.* **2020**, *11*, 5884.
- (30) Evano, G.; Blanchard, N.; Toumi, M. Copper-Mediated Coupling Reactions and Their Applications in Natural Products and Designed Biomolecules Synthesis. *Chem. Rev.* **2008**, *108*, 3054–3131.
- (31) Jain Z. J.; Gide P. S.; Kankate R. S. Biphenyls and Their Derivatives as Synthetically and Pharmacologically Important Aromatic Structural Moieties. *Arab. J. Chem.* **2017**, *10*, S2051–S2066.
- (32) Deep, A., Jain, S., Sharma, P.C., Verma, P., Kumar, M., Dora, C.P. Design and Biological Evaluation of Biphenyl-4-Carboxylic Acid Hydrazide-Hydrazone for Antimicrobial Activity. *Acta Pol. Pharm. Drug Res.* **2010**, *67*, 255–259.
- (33) Sachan, N., Thareja, S., Agarwal, R., Kadam, S.S., Kulkarni, V.M. Substituted Biphenyl Ethanones as Antidiabetic Agents: Synthesis and in-Vivo Screening. *Int. J. ChemTech Res.* **2009**, *1*, 1625–1631.
- (34) Kumar, J.R.; Jawahar, J.; Pathak, D.P. Synthesis of Benzimidazole Derivatives : As Anti-Hypertensive Agents. *E-J. Chem.* **2006**, *3*, 278–285.

- (35) Brade, K. D.; Rybak, J. M.; Rybak, M. J. Oritavancin: A New Lipoglycopeptide Antibiotic in the Treatment of Gram-Positive Infections. *Infect Dis Ther*, **2016**, *5*, 1–15.
- (36) Galici, R.; Jones, C. K.; Hemstapat, K.; Nong, Y.; Echemendia, N. G.; Williams, L. C.; Paulis, T. de.; Conn, P. J. Biphenyl-Indanone A, a Positive Allosteric Modulator of the Metabotropic Glutamate Receptor Subtype 2, Has Antipsychotic- and Anxiolytic-Like Effects in Mice. *J. Pharmacol. Exp. Ther.* **2006**, *318*, 173-185.
- (37) Okano, K.; Tokuyama, H.; Fukuyama, T. Copper-Mediated Aromatic Amination Reaction and Its Application to the Total Synthesis of Natural Products. *Chem. Commun.* **2014**, *50*, 13650–13663.
- (38) Chakraborti, G.; Paladhi, S.; Mandal, T.; Dash, J. “On Water” Promoted Ullmann-Type C-N Bond-Forming Reactions: Application to Carbazole Alkaloids by Selective N-Arylation of Aminophenols. *J. Org. Chem.* **2018**, *83*, 7347–7359.
- (39) Egorova, K. S.; Ananikov, V. P. Toxicity of Metal Compounds: Knowledge and Myths. *Organometallics* **2017**, *36*, 4071–4090.
- (40) Mitrofanov, A. Y.; Murashkina, A. V.; Martín-García, I.; Alonso, F.; Beletskaya, I. P. Formation of C-C, C-S and C-N Bonds Catalysed by Supported Copper Nanoparticles. *Catal. Sci. Technol.* **2017**, *7*, 4401–4412.
- (41) Jammi, S.; Sakthivel, S.; Rout, L.; Mukherjee, T.; Mandal, S.; Mitra, R.; Saha, P.; Punniyamurthy, T. CuO Nanoparticles Catalyzed C-N, C-O, and C-S Cross-Coupling Reactions: Scope and Mechanism. *J. Org. Chem.* **2009**, *74*, 1971–1976.
- (42) Mehara, J.; Roithová, J. Identifying Reactive Intermediates by Mass Spectrometry. *Chem. Sci.* **2020**, *11*, 11960–11972.
- (43) Parera, M.; Dachs, A.; Solà, M.; Pla-Quintana, A.; Roglans, A. Direct Detection of Key Intermediates in Rhodium(I)-Catalyzed [2+2+2] Cycloadditions of Alkynes by ESI-MS. *Chem. - A Eur. J.* **2012**, *18*, 13097–13107.
- (44) Waters, T.; O’Hair, R. A. J.; Wedd, A. G. Catalytic Gas Phase Oxidation of Methanol to Formaldehyde. *J. Am. Chem. Soc.* **2003**, *125*, 3384–3396.
- (45) Frisch, M. J.; Trucks, G. W.; Schlegel, H. B.; Scuseria, G. E.; Robb, M. A.; Cheeseman, J. R.; Scalmani, G.; Barone, V.; Petersson, G. A.; Nakatsuji, H.; Li, X.; Caricato, M.; Marenich, A. V.; Bloino, J.; Janesko, B. G.; Gomperts, R.;

Mennucci, B.; Hratchian, H. P.; Ortiz, J. V.; Izmaylov, A. F.; Sonnenberg, J. L.; Williams-Young, D.; Ding, F.; Lipparini, F.; Egidi, F.; Goings, J.; Peng, B.; Petrone, A.; Henderson, T.; Ranasinghe, D.; Zakrzewski, V. G.; Gao, J.; Rega, N.; Zheng, G.; Liang, W.; Hada, M.; Ehara, M.; Toyota, K.; Fukuda, R.; Hasegawa, J.; Ishida, M.; Nakajima, T.; Honda, Y.; Kitao, O.; Nakai, H.; Vreven, T.;Throssell, K.; Montgomery, J. A., Jr.; Peralta, J. E.; Ogliaro, F.; Bearpark, M. J.; Heyd, J. J.; Brothers, E. N.; Kudin, K. N.; Staroverov, V. N.; Keith, T. A.; Kobayashi, R.; Normand, J.; Raghavachari, K.; Rendell, A. P.; Burant, J. C.; Iyengar, S. S.; Tomasi, J.; Cossi, M.; Millam, J. M.; Klene, M.; Adamo, C.; Cammi, R.; Ochterski, J. W.; Martin, R. L.; Morokuma, K.; Farkas, O.; Foresman, J. B.; Fox, D. J. Gaussian 16, revision C.01; Gaussian, Inc.: Wallingford, CT, **2016**.

(46) Becke, A. D., Density-Functional Thermochemistry. III. The Role of Exact Exchange. *J. Chem. Phys.* **1993**, *98*, 5648-5652.

(47) Lee, C.; Yang, W.; Parr, R. G. Development of the Colle-Salvetti Correlation-Energy Formula into a Functional of the Electron Density. *Phys. Rev. B* **1988**, *37*, 785-789.

(48) Zhao, Y.; Truhlar, D. G. The M06 Suite of Density Functionals for Main Group Thermochemistry, Thermochemical Kinetics, Noncovalent Interactions, Excited States, and Transition Elements: Two New Functionals and Systematic Testing of Four Mo6-Class Functionals and 12 other Functionals. *Theor. Chem. Acc.* **2008**, *120*, 215–241.

(49) Hay, P. J.; Wadt, W. R. Ab Initio Effective Core Potentials for Molecular Calculations. Potentials for K to Au Including the Outermost Core Orbitals. *J. Chem. Phys.* **1985**, *82*, 299-310.

(50) Zhao, Y.; Truhlar, D. G. A New Local Density Functional for Main-group Thermochemistry, Transition Metal Bonding, Thermochemical Kinetics, and Noncovalent Interactions. *J. Chem. Phys.* **2006**, *125*, 194101-194118.

(51) Roy, L. E.; Hay, P. J.; Martin, R. L. Revised Basis Sets for the LANL Effective Core Potentials. *J. Chem. Theory Comput.* **2008**, *4*, 1029–1031.

(52) Funes-Ardoiz, I.; Paton, R. S. **2016**. <http://dx.doi.org/10.5281/zenodo.60811>.

(53) Fukui, K. The Path of Chemical Reactions-the IRC Approach. *Acc. Chem. Res.* **1981**, *14*, 368–375.

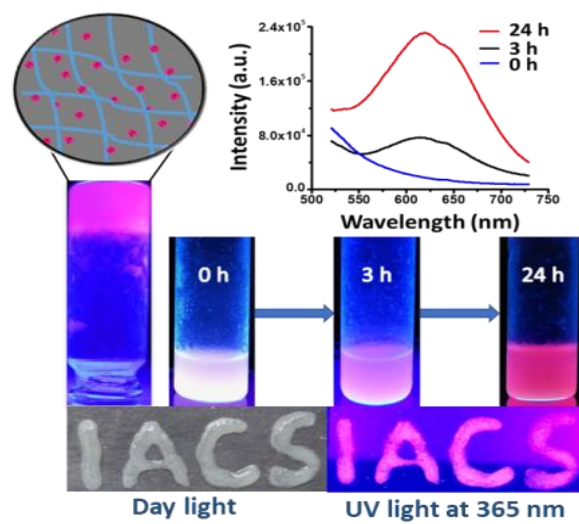
(54) Marenich, A. V.; Cramer, C. J.; Truhlar, D. G. Universal Solvation Model Based on Solute Electron Density and on a Continuum Model of the Solvent

- Defined by the Bulk Dielectric Constant and Atomic Surface Tensions. *J. Phys. Chem. B* **2009**, *113*, 6378-6396.
- (55) Hawkins, G. D.; Cramer, C. J.; Truhlar, D. G. Universal Quantum Mechanical Model for Solvation Free Energies Based on Gas-Phase Geometries. *J. Phys. Chem. B* **1998**, *102*, 3257-3271.
- (56) Matsumoto, H.; Inaba, S.; Rieke, R. D. Activated Metallic Nickel as a Reagent for the Dehalogenative Coupling of Halobenzenes. *J. Org. Chem.* **1983**, *48*, 840-843.
- (57) Du, F.; Zhou, Q.; Liu, D.; Fang, T.; Shi, Y.; Du, Y.; Chen, G. Dimerization of Aromatic Compounds Using Palladium-Carbon Catalyzed Suzuki-Miyaura Cross-Coupling by One-Pot. *Synlett* **2018**, *29*, 779–784.
- (58) He, W.-M.; Liu, K.-J.; Zeng, X.-L.; Zhang, Y.; Wang, Y.; Xiao, X.-S.; Yue, H.; Wang, M.; Tang, Z. Palladium-Catalyzed Reductive Coupling of Nitroarenes with Phenols leading to N-Cyclohexylamines. *Synthesis* **2018**, *50*, 4637–4644.
- (59) Li, G.; Liu, C.; Lei, Y.; Jin, R. Au₂₅ Nanocluster-Catalyzed Ullmann-Type Homocoupling Reaction of Aryl Iodides. *Chem. Commun.* **2012**, *48*, 12005–12007.
- (60) Ramasamy, P.; Guha, S.; Shibu, E. S.; Sreeprasad, T. S.; Bag, S.; Banerjee, A.; Pradeep, T. Size Tuning of Au Nanoparticles Formed by Electron Beam Irradiation of Au₂₅ Quantum Clusters Anchored within and Outside of Dipeptide Nanotubes. *J. Mater. Chem.*, **2009**, *19*, 8456–8462.
- (61) An, K.; Somorjai, G. A. Size and Shape Control of Metal Nanoparticles for Reaction Selectivity in Catalysis. *ChemCatChem* **2012**, *4*, 1512–1524.
- (62) Jaque, P.; Toro-Labbé, A. Polarizability of Neutral Copper Clusters. *J. Mol. Model.* **2014**, *20*, 1–8.
- (63) Andrew, C. R.; Loehr, T. M.; Sanders-Loehr, J.; Yeom, H.; Selverstone Valentine, J.; Göran Karlsson, B.; Bonander, N.; van Pouderoyen, G.; Canters, G. W. Raman Spectroscopy as an Indicator of Cu-S Bond Length in Type 1 and Type 2 Copper Cysteinate Proteins. *J. Am. Chem. Soc.* **1994**, *116*, 11489–11498.
- (64) Jones, G. O.; Liu, P.; Houk, K. N.; Buchwald, S. L. Computational Explorations of Mechanisms and Ligand-Directed Selectivities of Copper-Catalyzed Ullmann-Type Reactions. *J. Am. Chem. Soc.* **2010**, *132*, 6205–6213.
- (65) Monnier, F.; Taillefer, M. Catalytic C–C, C–N, and C–O Ullmann-Type Coupling Reactions. *Angew. Chemie Int. Ed.* **2009**, *48*, 6954–6971.

- (66) Nijamudheen, A.; Datta, A. Mechanism for C-I Bond Dissociation in Iodoethane, Iodobenzene, and Iodoethene for the C-C Cross Coupling Reactions over Gold Clusters. *J. Phys. Chem. C* **2013**, *117*, 21433–21440.
- (67) Zint, S.; Ebeling, D.; Schlöder, T.; Ahles, S.; Mollenhauer, D.; Wegner, H. A.; Schirmeisen, A. Imaging Successive Intermediate States of the On-Surface Ullmann Reaction on Cu(111): Role of the Metal Coordination. *ACS Nano* **2017**, *11*, 4183–4190.
- (68) Kozuch, S.; Shaik, S. How to Conceptualize Catalytic Cycles? The Energetic Span Model. *Acc. Chem. Res.* **2011**, *44*, 101–110.
- (69) Pham, T. A.; Song, F.; Nguyen, M. -T.; Li, Z.; Studener, F.; Stçhr, M. Comparing Ullmann Coupling on Noble Metal Surfaces: On-Surface Polymerization of 1,3,6,8-Tetrabromopyrene on Cu(111) and Au(111). *Chem. Eur. J.* **2016**, *22*, 5937–5944.

Chapter 6

Atomically Precise Red Emitting Copper Nanoclusters Containing Hydrogel as a Potential Fluorescent Ink



Chapter 6

Atomically Precise Red Emitting Copper Nanoclusters Containing Hydrogel as a Potential Fluorescent Ink**6.1. Introduction**

Metal nanoclusters¹⁻⁶ including Ag, Au, and Cu exhibit good and interesting fluorescent properties^{1,2} and other useful properties such as outstanding photostability,² and biocompatibility⁷⁻⁹. Due to this intense fluorescence property Cu-nanoclusters has been used for bio-imaging,⁷⁻⁹ sensing,⁹⁻¹¹ catalysis,¹¹⁻¹⁴ and others¹⁵⁻¹⁷ applications. Metal nanoclusters are mostly found to be synthesized from silver and gold due to the high stability of Ag(0) and Au(0) in silver and gold nanoclusters. The stabilization of copper as Cu(I) or Cu(0) in copper nanocluster is extremely difficult as the difference of reduction potential value between Cu(II)/Cu(I) and Cu(I)/Cu(0) is extremely low.¹⁸ The synthesis of copper nanoclusters involves the reduction of Cu(II) into Cu(I) or Cu(0) by using a stabilizing agent such as DNA,¹⁹ proteins,²⁰ peptides,^{12, 21} and thiols^{13, 22}. In compared to gold and silver NCs, the copper nanoclusters are less acknowledged, due to their less stability by easy oxidation and weakly fluorescent property in nature.¹⁸ However, it is still now challenging to synthesize and stabilize CuNCs for a long time (few months). This is due to their much less stability compared to Ag and Au nanoclusters. So, there is a genuine need for making and stabilizing a few atom fluorescent CuNCs for at least a few months.

Small organic molecules such as peptides²³⁻²⁷ and peptide amphiphiles²⁸⁻³¹ have attracted researchers' attention in various fields for their applications in chemicals,³² materials,^{33, 34} and biological sciences³⁵⁻⁴². Peptide-based hydrogels can also be used as a template for synthesizing nanomaterials such as nanoparticles or nanoclusters.⁴³⁻⁴⁵ There are very few reports in the literature on the synthesis of nanoclusters in the gel matrix; however, they are silver nanoclusters.^{43, 44} Banerjee and co-workers reported the synthesis of fluorescent silver nanoclusters (AgNCs) in the gel matrix. These fluorescent hydrogels were stable for 4–6 months but in a dark place at 4 °C temperature, as the silver nanomaterials are highly light-sensitive. These reports demonstrate that silver-based fluorescent NCs need some precursor to maintain the stability of noble silver nanoclusters, although their preparation is significantly an effortless task.⁴³

Chattopadhyay and co-workers reported the synthesis of red fluorescent CuNCs in a polymeric gel medium. They use hazardous inorganic reducing agent NaBH_4 for the reduction of the lipoic acid to form capping ligand dihydrolipoic acid. These CuNCs retain their optical property for a month; however, the use of toxic NaBH_4 makes this process environmentally harmful.¹⁸ So, there is a real need for synthesizing a few atom noble fluorescent copper nanoclusters, as they are very cheap compared to silver or gold. There are several reports on the synthesis of fluorescent CuNCs by using different DNA sequences as a template for synthesizing fluorescent CuNCs.¹⁹ But DNA-templated CuNCs have restricted applications due to the low stability of fluorescence. Hence researchers have paid significant attention to make the fluorescent CuNCs to enhance the fluorescence stability of CuNCs. Recently, Park and co-workers reported that a high concentration of fructose improves the stability of fluorescent CuNCs for a few minutes to several days.⁴⁶

In recent years the development of fluorescent materials has been explored for the anti-counterfeiting and security purposes.⁴⁷ Our synthesized CuNCs are highly stable for several months. The materials used for the synthesis of CuNCs are copper acetate monohydrate, stabilizing ligand 4-mercaptobenzoic acid, reducing agent L-ascorbic acid, and the amphiphilic gelator **G1** (Figure 6. 2). All of them are very low-cost materials. In this study copper-nanoclusters (CuNCs) have been synthesized in a controlled manner by using amphiphilic gelator **G1** as a hydrogel matrix with nano fibrillar network structure. These CuNCs exhibit a good emission at 621 nm with an excitation 420 nm. So, it has potential to be used as fluorescent ink. The gel medium synthesis of CuNCs has shown a very significant increase in stability (>700-fold) for the newly synthesized copper nanoclusters as compared to their synthesis in solution medium. The writing ability of this red emitting Cu-nanoclusters containing hydrogel and retaining of the solid state fluorescence property even after the evaporation of the water from the gel making a possibility to use as a good fluorescent ink for an anti-counterfeiting nano materials for authentication purpose.

6.2. Experimental Section

6.2.1. Materials

Myristic acid, L-Phenylalanine (Phe), 1-hydroxybenzotriazole (HOBt), DCC (N, N'-dicyclohexylcarbodiimide), di-tert-butylidicarbonate (BOC Anhydride, DiBOC), silica gel (100–200 mesh), and aluminium oxide (basic) were purchased from SRL, India. N, N'-dimethylformamide (DMF), dimethyl sulfoxide (DMSO) trifluoroacetic acid (TFA), hexamethylenediamine were purchased from Merck. Copper acetate monohydrate $[(\text{Cu}(\text{OAc})_2 \cdot \text{H}_2\text{O})_2]$, sodium dihydrogen phosphate, and disodium hydrogen phosphate were purchased from Sigma-Aldrich. 4-mercaptobenzoic acid was purchased from TCI, Japan. 300 mesh TEM grids were purchased from Ted Pella. Millipore milli-Q grade water was used for all experiments.

6.2.2. Methods

Synthesis and Characterisation. The amino acid containing gelator amphiphile (**G1**) was synthesized by conventional solution phase coupling methods using a racemization-free fragment condensation strategy. The characterisations of the synthesised products were done by using mass spectrometry, ^1H NMR spectroscopy and ^{13}C NMR spectroscopy. All NMR studies were carried out using a Bruker DPX 400 MHz or Bruker DPX 500 MHz spectrometer at 300 K. Concentrations were in the range 5–10 mM in CDCl_3 or DMSO-d_6 . Mass spectra were recorded on a Q-Tof micro (Waters Corporation) mass spectrometer by positive mode electrospray ionization process.

Preparation of Co-solvent Induced Two Component Hydrogel. The gelator amphiphile **G1** (10 mg) has been added to 950 μL of milli-Q water and heated on a hot plate until the solute gelator amphiphile get dissolved. Then 8 mg of 4-MBA was dissolved in 200 μL of DMF solvent, and 50 μL of DMF containing 4-MBA was transferred to the heated solution containing amphiphile gelator **G1**. The glass vial containing gelators **G1** and 4-MBA was then cooled at room temperature of 28 $^\circ\text{C}$. The formation of stable co-solvent-induced two-component gelation was observed after 1 h of its resting. When the 900 μL of milli-Q and 100 μL of DMF were used, i.e. the DMF amount was increased from 5% to 10 % very fast gel formation was observed even before the solution reached room temperature 28 $^\circ\text{C}$.

General Procedure for the Synthesis of Red Emitting CuNCs in Solution

Phase. 2 mg (0.01 mM) of copper acetate monohydrate and 8 mg (0.052 mM) of 4-mercaptobenzoic acid (MBA) dissolved in 1 mL of dimethylsulphoxide (DMSO) in each. Then both solution was transferred to a 10 mL of screw cap vial and stirred on a magnetic stirrer for 30 min at 5–10 °C temperature. After 10 min of stirring 2 mg (0.011 mM) of L-ascorbic acid was added to the solution. A pale yellow color solution was formed during the mixing of three components. From time to time, the formation of copper nanoclusters was confirmed by UV lamp irradiation at 365 nm, which shows the weak red fluorescence to intense red color fluorescence after the complete construction of maximum CuNCs.

The above experiment was repeated, and N, N-dimethylformamide (DMF) was used as a solvent instead of DMSO to prepare these above red CuNCs in a DMF solvent medium.

General Procedure for the Synthesis of Stable CuNCs in Gel Matrix.

10 mg **G1** was dissolved in 900 μ L of milli-Q and then 100 μ L of DMF containing Cu(OAc)₂, H₂O, 4-MBA and L-ascorbic acid was added to it. It can be noted that 100 μ L of DMF containing Cu(OAc)₂, H₂O and 4-MBA must be added before the milli-Q solution gets cooled. This condition must be maintained to get very much stable gel. After the addition of 100 μ L DMF very fast formation of gel was observed even before the solution reaches into the normal temperature. Initially, no fluorescent was observed under the UV-lamp at 365 nm.

Preparation of TEM Sample: TEM images were recorded on a JEM 2010 electron microscope at an accelerating voltage of 200 kV. During the TEM experiment, 20 μ L of gel containing Cu-nanoclusters was taken in a screw cap vial and diluted with a 2 mL solution containing 5% DMF in milli-Q water. Then, a drop of dilute solution was placed on carbon-coated copper grids (300 mesh) and dried by slow evaporation. The grid was then allowed to dry in a vacuum for two days, and then the images were taken.

Preparation of XPS Samples: The gel containing red emitting Cu-nanoclusters were coated on a Indium Tin oxide coated glass (ITO glass) and then dried the gel for overnight. Then the red emitted CuNCs coated ITO glass was used for the XPS measurement.

Detailed Quantum Yield Calculation: Relative Quantum Yield Φ_x of a substance x is given by the equation,

$$\Phi_x = \Phi_{St} (F_x \times f_{st}(\lambda_{ex}) \times \eta_x^2) / (F_{St} \times f_x(\lambda_{ex}) \times \eta_{St}^2)$$

Where, Φ_{St} is the absolute quantum yield of the standard fluorophore and F stands for the integral photon flux, f stands for the absorbance factor and η stands for the refractive indices of the respective solvents. The indices 'x' and 'St' stand for the sample under investigation and the standard reference. The absorbance factor $f(\lambda_{ex}) = 1 - 10^{-A(\lambda_{ex})}$, where $A(\lambda_{ex})$ is the absorbance value of the solutions at the excitation wavelength λ_{ex} . Quinine sulfate in 0.1 M sulfuric acid is taken as the reference. 0.1 M sulfuric acid and water both shows refractive index of 1.33 that is why refractive index is not taken under consideration. While collecting fluorescence spectra of copper nanocluster (Cu-NC), 420 nm was used as the excitation wavelength and for Quinine Sulfate (QS) excitation wavelength was 350 nm. Integration was done for the whole fluorescence spectra to calculate total photon flux for both Cu-NC and the reference.

$$A_{CuNC}(\lambda_{420}) = 0.06; A_{QS}(\lambda_{350}) = 0.65$$

$$\text{Hence, } f_{CuNC}(\lambda_{420}) = 1 - 10^{-0.06} = 0.13 \text{ and } f_{QS}(\lambda_{350}) = 1 - 10^{-0.65} = 0.78$$

Thus, the relative quantum yield of synthesized Cu-NC,

$$\Phi_{CuNC} = \Phi_{QS} (F_{CuNC} \times f_{QS}(\lambda_{350})) / (F_{QS} \times f_{CuNC}(\lambda_{420}))$$

$$= 0.546 \times (2.04 \times 10^6 \times 0.78) / (6.10 \times 10^8 \times 0.13)$$

$$= 0.01096 \text{ or } 1.1\%$$

6.2.3. Synthesis Gelator Peptide G1

The synthesis detail of amphiphilic based peptide gelator **G1** has been given into the Chapter 4, Synthesis and detail section as a synthesis of **P3** gelator (Page No. 204–205).

6.2.4. Instrumentation

UV-Vis spectroscopic analysis. We used a Cary Varian 50 scan UV-Vis optical spectrometer equipped with 'Cary Win' UV software to elucidate the optical properties of copper nanoclusters.

Fluorescence spectroscopy. Fluorescence studies of copper quantum clusters in a sealed cuvette were carried out in a Perkin Elmer LS55 Fluorescence

Spectrometer instrument. All the experiments were carried out with the excitation slit width 5 nm and emission slit width 5 nm.

MALDI-TOF MS study. The MALDI-TOF MS analyses were done using Bruker Daltonics flex Analysis mass spectrometer.

TEM study. TEM study of the NIR clusters were carried out in a JEOL 2100 Ultra High Resolution Field Emission Gun (UHR FEG) TEM with voltage 200 kV.

FTIR study. The FT-IR spectra were taken by using Shimadzu (Japan) model FT-IR spectrophotometer. In the solid state FT-IR studies, powdered were mixed with KBr for preparing thin films.

X-ray Photoelectron Spectroscopic (XPS) Study. XPS analysis of dried red emitting quantum cluster was carried out by using an X-ray photoelectron spectroscopic (XPS, Omicron, model: 1712–62–11) method. Measurement was done by using an Al-K α radiation source under 15 kV voltages and 5 mA current.

6.3. Results and Discussion

6.3.1. Synthesis of Stable Red Emitting CuNCs in the Hydrogel Matrix: Four different approaches have been taken to make stable red-emitting CuNCs. In the first approach, the synthesis of CuNCs was performed in DMSO solvent keeping the molar ratio of metal ion precursor (copper acetate monohydrate), stabilizing agent (4-MBA), and reducing agent (L-ascorbic acid) 1:5:1. The reaction was carried out at a temperature of 4–10 °C. The solution phase synthesis of CuNCs was mentioned in the experimental section. The progress of the reaction was checked by the UV-lamp irradiation at 365 nm (Figure 6. 1). In the second approach, the preparation of CuNCs was performed in DMF medium instead of DMSO keeping the reaction temperature (4–10 °C), conditions, and molar ratio of metal precursor, stabilizing ligand, and reducing agent constant. However, both of the Cu-nanoclusters were quite unstable in DMDO or DMF solvent medium. After 12 h, the slow reappearances of the blue color aggregates of the solution containing CuNCs indicate the decomposition of CuNCs. In this regard to synthesized stable NCs, the synthesis was performed in gel matrix. In the final two approach Cu(OAc)₂.H₂O, 4-MBA, and gelator amphiphile were dissolved into the DMSO or DMF solvent. The solution was further added to the milli-Q water to make a stable cluster. The polar co-solvent like DMSO or DMF was used to help the amphiphilic gelator **G1** to form a stable gel. It was observed that

DMSO-mediated **G1** gel shows fluorescent behavior very rapidly, within 4–6 h. Unfortunately, the gel was not also very much stable, and after 72 h, slowly disappearance of fluorescent intensity indicates the destabilization of CuNCs in DMSO-mediated (as a co-solvent) hydrogel.

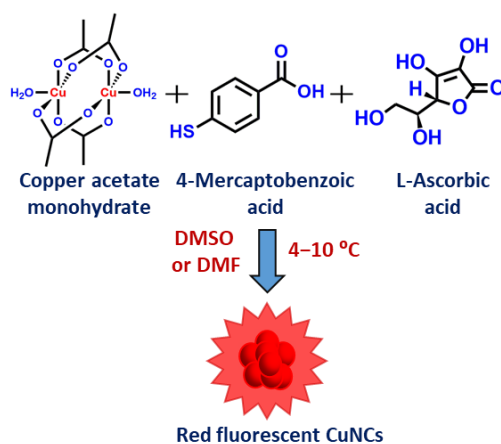


Figure 6.1. Schematic diagram showing the synthesis of red-emitting Cu-nanoclusters at DMSO or DMF medium, using copper acetate monohydrate as a precursor and a thiol-containing aromatic derivative as a stabilizing agent and L-ascorbic acid as a reducing agent.

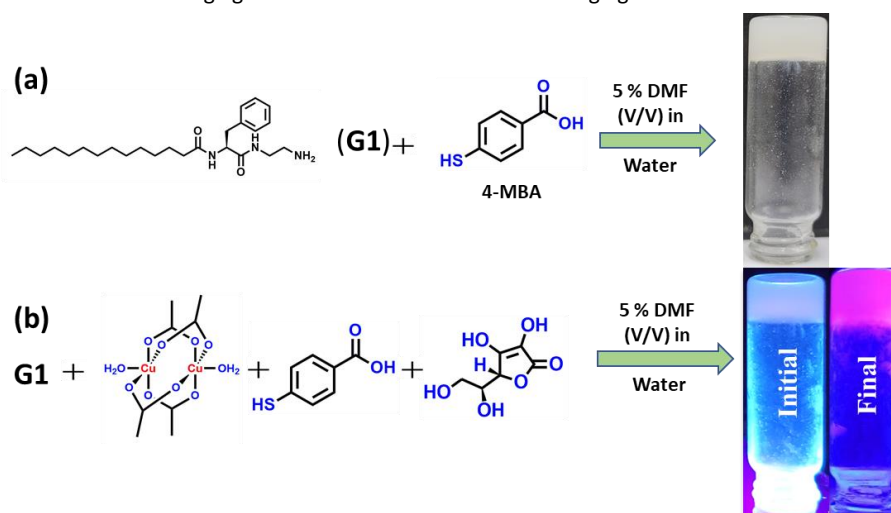


Figure 6.2. (a) Two-component co-solvent induced hydrogel formed by the gelator amphiphile **G1** and 4-MBA; (b) schematic diagram showing the synthesis of red-emitting Cu-nanoclusters at 5% DMF medium, where the initial image under UV-lamp 365 nm indicates that the gel before the formation of CuNCs and final image indicates the formation of CuNCs in gel medium.

Interestingly, in the case of DMF solvent-mediated hydrogel, slowly appearance of fluorescence indicates the controlled synthesis of stable CuNCs was observed. The high stabilization of CuNCs in DMF mediated gel medium suggests that the control synthesis is responsible for forming stable CuNCs (Figure 6.2). Once the cluster was formed, it did not undergo a rapid decomposition. In further addition, even the cluster was stable for twelve months in the solid-state and also in gel state.

6.3.2. UV-vis Spectroscopic Analysis. Copper acetate monohydrate shows a strong absorption band at 674 nm and 697 nm ranges due to the presence of Cu^{2+} ions in DMSO and DMF solvent respectively. With the addition of 4-mercaptobenzoic acid (4-MBA) into the copper acetate solution, the absorption band shifts to 340 nm due to the formation of the copper nanoclusters. The absence of surface plasmon resonance peak in the range 400-700 nm cancels out the presence of more significant larger-size nanoparticles in the reaction mixture (Figure 6.3).⁴⁸ Even after the formation of stable CuNCs in the gel medium, UV-vis spectroscopic data was taken, which also confirms the absence of bigger sized particles in the gel matrix. The UV-vis spectra of the DMF mediated cluster show a relatively intense sharper absorption shoulder at 340 nm than that of CuNCs formed in DMSO; this may be due to the formation of larger aggregates in the DMF medium (Figure 6.3b).²²

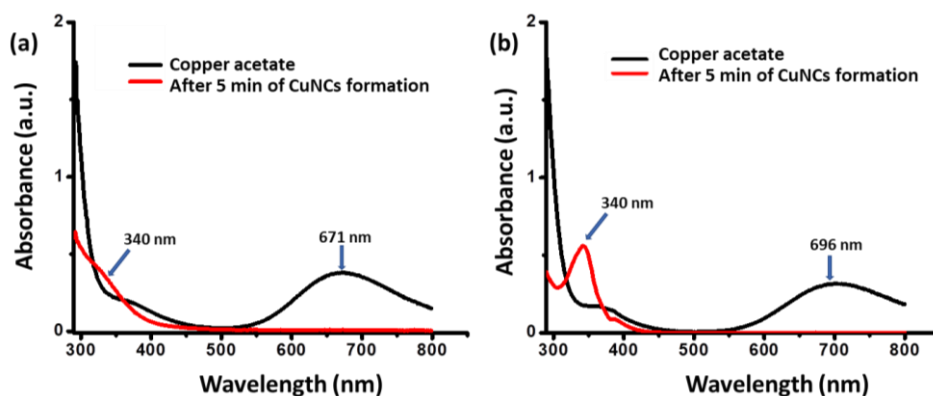


Figure 6.3. (a) Black curve is the UV-vis spectrum of copper acetate monohydrate in DMSO solvent without stabilizing agent and red with stabilizing agent 4-MBA after 5 min of CuNCs formation. (b) Black curve is the UV-vis spectrum of copper acetate monohydrate in DMF solvent without stabilizing agent and red with stabilizing agent 4-MBA after 5 min of CuNCs formation.

6.3.3. FTIR Analysis.

FTIR studies were performed for solid 4-MBA and dried CuNCs containing gel. The FTIR data of 4-MBA shows a strong peak at around 2115 cm^{-1} due to the presence of free S-H bond. The absence of a satellite peak at around 2115 cm^{-1} for dried gel-mediated CuNCs, confirms the formation of Cu-S bond during CuNCs formation in a gel medium. The strong signal at 1648 cm^{-1} is due to amide C=O in the gelator amphiphile. However, the FTIR data for dried aggregated solution of **G1** and dried CuNCs containing gel show similar FTIR spectra due to larger excess **G1** gelator with respect to the stabilizing ligand 4-MBA. The stretching frequency of C=O in 4-MBA is 1684 cm^{-1} , whereas in CuNCs was found to be 1648 cm^{-1} ; this may be due to the coordination of the acid group of 4-MBA with the copper ions or the formation of zwitter ionic

interaction between the acid group of 4-MBA and free -NH_2 of the **G1** gelator (Figure 6.4).

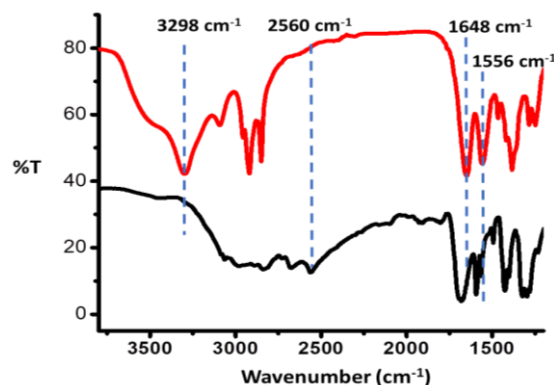


Figure 6.4. FTIR data of CuNCs containing dried gel formed by the gelator **G1** (red) and solid 4-MBA (black).

6.3.4. XPS Analysis. X-ray photoelectron spectroscopy (XPS) analysis was performed to identify whether the Cu atom in CuNCs is stabilized as a Cu(0) or Cu(I) or not. As, it is challenging to stabilize the CuNCs as Cu(0) or Cu(I) oxidation state due to their low reduction potential value of Cu(II) to Cu(0). It was observed that the two peaks at the binding energy values 932.80 eV and 952.58 eV for the Cu $2P_{3/2}$ and Cu $2P_{1/2}$ corresponding to the presence of Cu(0) state in our CuNCs. The absence of any peak at the binding energy value 942 eV indicates the absence of Cu(II) or any unreacted $\text{Cu(OAc)}_2 \cdot \text{H}_2\text{O}$. This result is consistent with our UV-vis spectroscopy data (Figure 6.3).

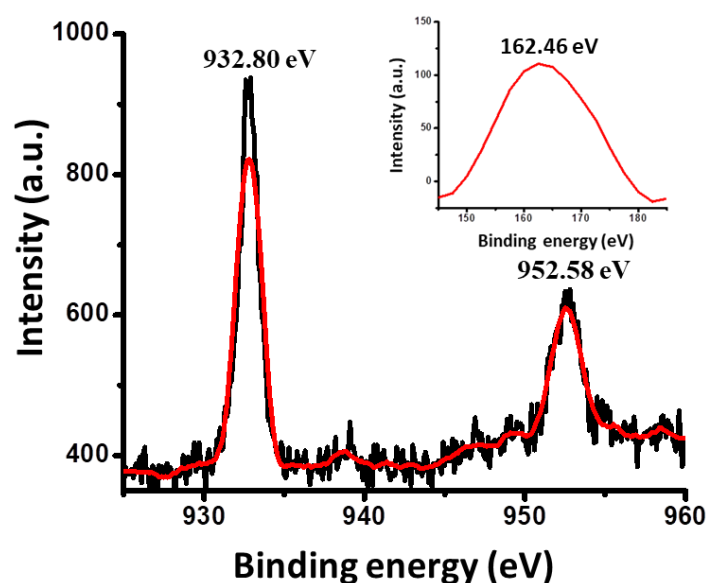


Figure 6.5. XPS spectra of copper nanoclusters, showing the Cu $2P_{3/2}$ and Cu $2P_{1/2}$ peaks at 932.80 and 952.58 eV respectively indicating the presence of Cu(0) or Cu(I) state. In the inset, binding energy of sulphur (S) 2P state was found to be 162.46 eV indicating the presence of chemisorbed S-atoms.

Moreover, the slight difference in binding energy between Cu(0) and Cu(I) (0.1 eV) indicates that it is challenging to distinguish between Cu(0) and Cu(I) states in the XPS spectrum. The peak at the binding energy value 162.46 eV is due to sulfur 2p orbital, which indicates the presence of Cu-S bond in the CuNCs (Figure 6.5).

6.3.5. MALDI-TOF MS Analysis. The matrix-assisted laser desorption/ionization-time-of-flight mass spectrometry (MALDI-TOF MS) analysis was performed to analyse the exact mass of the atomically precise few atoms CuNCs synthesised in the gel matrix. Negative mode MALDI-TOF MS data is taken by using a suitable matrix, sinapinic acid. The experimental analysis suggest that the highest mass peaks, $m/z = 1032.67$ $[\text{Cu}_8\text{L}_3 + \text{Na} + \text{K} + 4\text{H}]^+$, 1016.82 $[\text{Cu}_8\text{L}_3 + \text{Na} + \text{K} + 3\text{H}]^+$, 995.65 $[\text{Cu}_8\text{L}_3 + \text{Na} + \text{K} + 4\text{H}]^+$ ($\text{L} = \text{C}_7\text{H}_6\text{O}_2\text{S}$) confirms the formation of Cu_8L_3 copper nanoclusters in the co-solvent (DMF) induced gel mediated clusters. There are also some other peaks at the lower m/z values, 854.71 $[\text{Cu}_8\text{L}_2 + \text{K} + \text{H}]^+$, 837.53 $[\text{Cu}_8\text{L}_2 + \text{Na} + \text{H}]^+$, 815.35 $[\text{Cu}_8\text{L}_2 + 2\text{H}]^+$, 796.89 $[\text{Cu}_4\text{L}_3 + 2\text{Na} + \text{K}]^+$, 773.87 $[\text{Cu}_4\text{L}_3 + \text{Na} + \text{K}]^+$, 751.17 $[\text{Cu}_4\text{L}_3 + \text{K}]^+$,

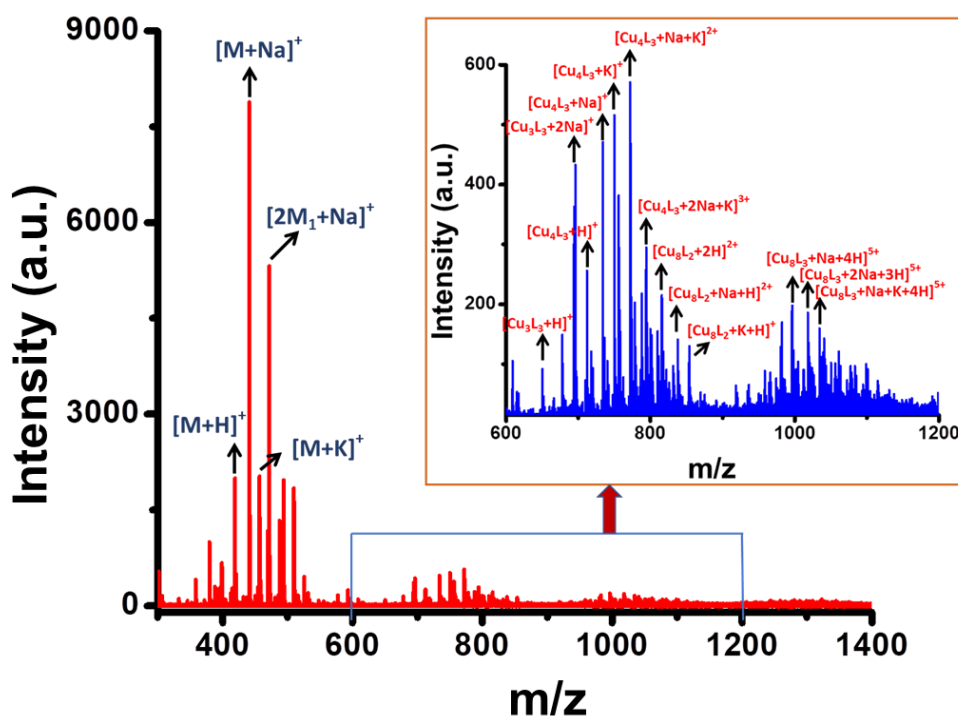


Figure 6.6. MALDI-TOF MS analysis showing the presence of amino acid containing amphiphile **G1** and Cu nanoclusters, Cu_8L_3 species ($\text{L} =$ reduced 4-mercaptobenzoic acid). Inset extended spectrum shows the exact nature of the mass spectrum of Cu_8L_3 nanocluster in MALDI-TOF MS analysis.

735.03 $[\text{Cu}_4\text{L}_3 + \text{Na}]^+$, 713.01 $[\text{Cu}_4\text{L}_3 + \text{H}]^+$, 696.07 $[\text{Cu}_3\text{L}_3 + 2\text{Na}]^+$, 650.13 $[\text{Cu}_3\text{L}_3 + \text{H}]^+$ may be due to the fragmentation of larger size copper nanoclusters Cu_8L_3 during the MALDI-TOF MS analysis (Figure 6.6).

As there was amino acid based gelator amphiphiles **G1**, the peaks for **G1** at m/z 418.95, 440.87, and 457.20 due to the formation of $[\text{M}+\text{H}]^+$, $[\text{M} + \text{Na}]^+$ and $[\text{M} + \text{K}]^+$ ions (M is the mass of **G1** gelator amphiphile). The peaks at 472.06 for $[2\text{M}_1 + \text{Na}]^+$ is also confirms that sinapinic acid (M_1 is the mass of sinapinic acid) has been used as a matrix during the MALDI-TOF MS analysis (Figure 6.6).

6.3.6. UHR-FEG-TEM Study. Ultra-high-resolution field-emission gun-transmission electron microscopic (UHR-FEG-TEM) studies were performed to investigate the exact size of CuNCs formed during the formation of CuNCs in DMF solvent and co-solvent induced gel medium. As the cluster formed in DMSO or DMF medium was very unstable and underwent decomposition within 12 h, they must be similar in size. So, only one of them, DMF-mediated CuNCs, was taken to study the TEM analysis. We have taken the CuNCs formed in the DMF solvent medium to investigate the exact size of the CuNCs formed during the synthesis of unstable copper nanoclusters. TEM study shows that the CuNCs formed in the DMF medium are relatively tiny, with a size of 1.67 nm. The gel-mediated copper nanoclusters were also further investigated to understand whether the CuNCs or CuNPs formed in this gel medium and their exact size. The size of the CuNCs produced in the gel medium lies between 2.20 nm to 5.12 nm, whereas the average size was 2.83 nm (Figure 6.7d,e). Relatively larger size clusters (> 3 nm) are also present; this may be due to the aggregation between the CuNCs or the aggregation between CuNCs and the gelator amphiphile. The appearance of relatively larger size particle can be formed due to the agglomeration of smaller size nanoclusters in presence of electron beam during the TEM experiment.⁴⁹ Figure 6.7c shows the presence of nanoclusters and nanofibre in a single image. The extended Figure 6.7c shows the coexistence of some nanoclusters with the nanofibrous network structure (Figure 6.7b). The gelator amphiphile **G1** and the stabilizing 4-MBA also form a two-component gel in a co-solvent-induced gelation study. In this regard, TEM experiments were performed for two-component gel and CuNCs gel to understand the difference between the network structures formed in two-component gel vs. CuNCs gel. But both gels show a similar nanofibrous network structure during the UHR-FEG-

TEM experiment (Figure 6.7a,b). It is apparent from the Figure 6.7e that there is a significant number of nanoclusters whose sizes are less than 2.50 nm.

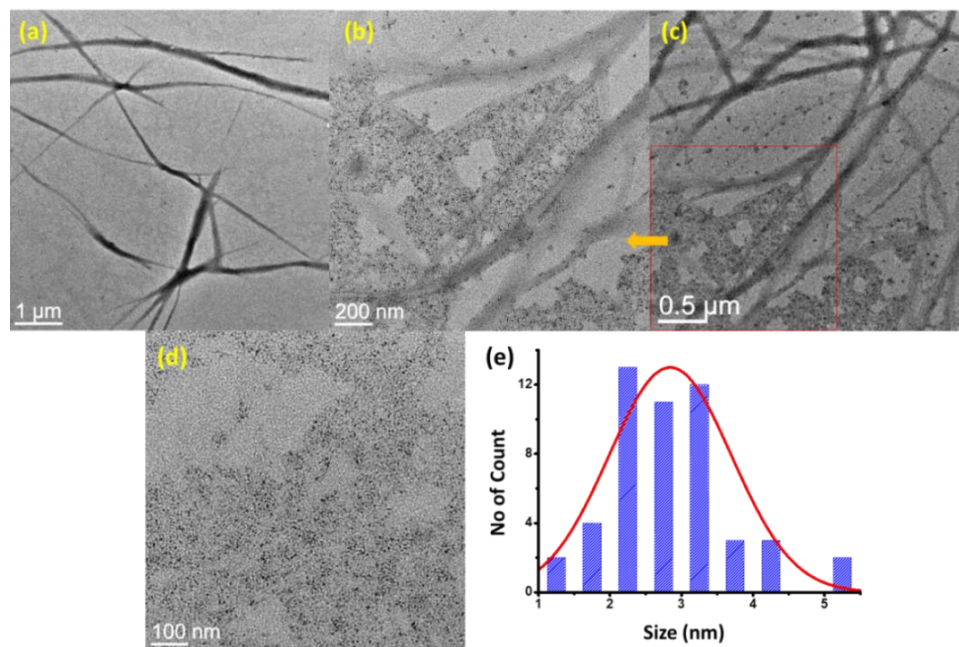


Figure 6.7. (a) FEG-TEM image shows the network structure formed during the two component gel formation; (b) and (c) images show both the copper nanoclusters and nanofibrous network structures are present indicating the formation of copper nanocluster within the hydrogel matrix; (d) More zoomed image where only Cu-nanoclusters are present; (e) size distribution histogram of Cu-nanoclusters showing most populated size 2.86 nm.

6.3.7. Fluorescence Spectroscopy Study. Few atoms nanoclusters are essential materials for their fluorescence properties. The above-stated synthesized Cu-nanoclusters show bright red fluorescence upon irradiation at UV-lamp with an excitation of 365 nm. The copper nanoclusters show an emission peak at 686 nm with an excitation of 396 nm in DMSO solvent (Figure 6.8). In comparison, the value of emission peak and excitation peak was at 340 nm and 681 nm in the presence of DMF solvent, respectively (Figure 6.9).

The red fluorescent nature of the solution and gel indicate the formation of CuNCs. The solution shows red emission upon irradiation under the UV lamp having an excitation wavelength 365 nm. The solid state quantum yield of gel mediated CuNCs was 1.1% taking quinine sulphate as a standard reference.

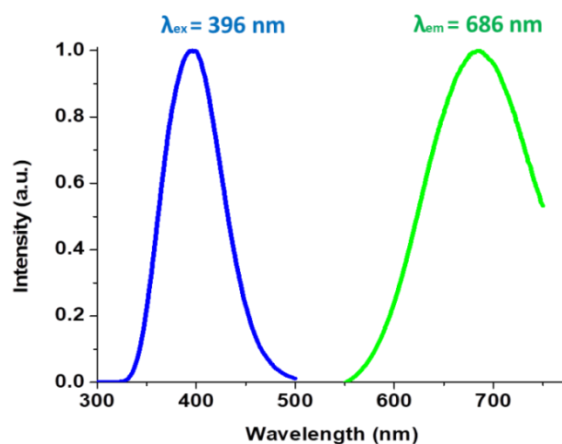


Figure 6.8. Fluorescence emission (green curve) and excitation (blue curve) spectra of red emitting CuNCs showing an excitation maximum at 396 nm and an emission maximum at 686 nm with a larger Stoke's shift of 290 nm.

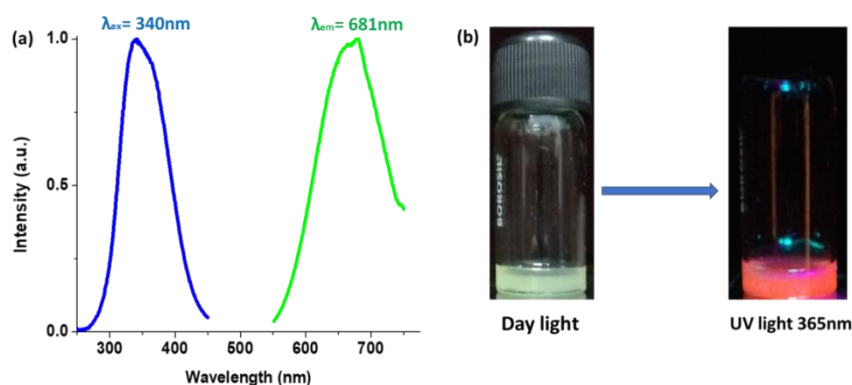


Figure 6.9. (a) Fluorescence emission (green curve) and excitation (blue curve) spectra of red emitting CuNCs in DMF medium shows an excitation maximum at 340 nm and an emission maximum at 681 nm with a larger Stoke's shift of 341 nm; (b) DMF mediated CuNCs under day light (pale yellow in color) and UV-light at 365 nm (red in color) respectively.

6.3.8. Time-Dependent Change in Fluorescence Study. The time-dependent photoluminescence spectra were taken during the formation of CuNCs in gel medium. The increase in the intensity of emission wavelength with time indicates the formation of more and more CuNCs in the gel medium with time. The gel-mediated CuNCs with a fixed excitation wavelength of 420 nm show emission of 621 nm (Figure 6.10b). The images of gel-mediated clusters are taken at a time interval of 3 h under the UV lamp having a fixed wavelength of 365 nm to understand the time-dependent fluorescent change by open eyes (Figure 6.10c). The emission peak position slowly shifts to the longer wavelength from 616 nm to 621 nm which indicates the H-aggregation between the CuNCs (Figure 6.10a).

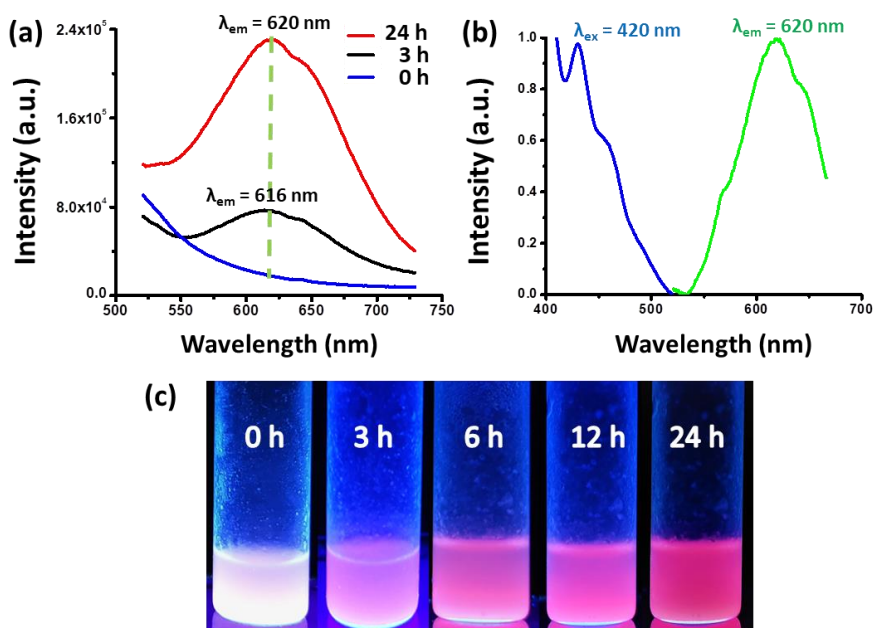


Figure 6.10. (a) Time dependent increase in fluorescence intensity during the formation of more and more Cu-nanocluster; (b) normalized fluorescence spectra of copper nanoclusters with excitation at 420 nm (blue curve) having an emission wavelength 620 nm (green curve) with a larger 200 nm Stoke's shift; (c) time dependent change in fluorescence intensity during the formation of CuNCs in gel matrix under UV-lamp having excitation wavelength 365 nm.

6.3.9. CuNCs Containing Gel as an Anti-counterfeiting Fluorescent Ink.

Anti-counterfeiting fluorescent ink shows its visibility under UV-light irradiation. The most practical use of fluorescent ink is in high-tech security technology including bank notes and bills. As we know, a material shows its fluorescence in the solid state to become an ideal fluorescent ink. In the case of our red-emitting copper nanocluster gel, the gel shows fluorescent behavior in both gels and the dried gel states. Figure 6.11 demonstrates that the gel state containing CuNCs in it shows red-emitting fluorescent behavior under UV-lamp irradiation at 365 nm. Even after the evaporation of water from the gel state, the dried gel (xerogel) also displays highly red fluorescent behavior; this makes our



Figure 6.11. Images of gel and dried gel under day light and under UV-light irradiation at 365 nm.

gel a potential candidate for high-tech security material or as a fluorescent ink in the future. Moreover, the high stability of this fluorescence permits to use this rewritable gel based red emitting fluorescent material containing Cu-nanoclusters for a long time.

6.4. Conclusion

This study clearly demonstrates the formation of a few atom CuNCs in the amino acid containing amphiphilic-based hydrogel medium and the stability of these red-emitting highly fluorescent eight-atom clusters for several months. Interestingly, the bright fluorescent is retained in the dried gel state (solid-state) just by using a portable UV-vis torch (excitation wavelength 365 nm), one can visualize the fluorescence of these CuNCs containing gel-based materials. So, this red emitting gel has been used as a potential fluorescent ink for anti-counterfeiting and security purposes. Moreover, the stability of CuNCs is increased by about >700 fold compared to its stability in the solution phase. This indicates a significant stability enhancement of CuNCs in the gel state and its utility as an invisible ink through the naked eye and a good fluorescent ink to use for security purposes in the future.

6.5. References

- (1) Jana, A.; Chakraborty, P.; Dar, W. A.; Chandra, S.; Khatun, E.; Kannan, M. P.; Ras, R. H. A.; Pradeep, T. Dual Emitting Ag₃₅ Nanocluster Protected by 2-Pyrene Imine Thiol. *Chem. Commun.* **2020**, 56, 12550–12553.
- (2) Zhou, S.; Peng, B.; Duan, Y.; Liu, K.; Ikkala, O.; Ras, R. H. A. Bright and Photostable Fluorescent Metal Nanocluster Supraparticles from Invert Emulsions. *Angew. Chemie Int. Ed.* **2022**, 61, 1–7.
- (3) Ghosh, A.; Hassinen, J.; Pulkkinen, P.; Tenhu, H.; Ras, R. H. A.; Pradeep, T. Simple and Efficient Separation of Atomically Precise Noble Metal Clusters. *Anal. Chem.* **2014**, 86, 12185–12190.
- (4) Rambukwella, M.; Dass, A. Synthesis of Au₃₈(SCH₂CH₂Ph)₂₄, Au₃₆(SPh-tBu)₂₄, and Au₃₀(S-tBu)₁₈ Nanomolecules from a Common Precursor Mixture. *Langmuir* **2017**, 33, 10958–10964.
- (5) Jin, R.; Zeng, C.; Zhou, M.; Chen, Y. Atomically Precise Colloidal Metal Nanoclusters and Nanoparticles: Fundamentals and Opportunities. *Chem. Rev.* **2016**, 116, 10346–10413.

- (6) Yao, Q.; Wu, Z.; Liu, Z.; Lin, Y.; Yuan, X.; Xie, J. Molecular Reactivity of Thiolate-Protected Noble Metal Nanoclusters: Synthesis, Self-Assembly, and Applications. *Chem. Sci.* **2021**, *12*, 99–127.
- (7) Roy, S.; Baral, A.; Bhattacharjee, R.; Jana, B.; Datta, A.; Ghosh, S.; Banerjee, A. Preparation of Multi-Coloured Different Sized Fluorescent Gold Clusters from Blue to NIR, Structural Analysis of the Blue Emitting Au₇ Cluster, and Cell-Imaging by the NIR Gold Cluster. *Nanoscale* **2015**, *7*, 1912–1920.
- (8) Basu, K.; Gayen, K.; Mitra, T.; Baral, A.; Roy, S. S.; Banerjee, A. Different Color Emissive Copper Nanoclusters for Cancer Cell Imaging. *ChemNanoMat* **2017**, *3*, 808–814.
- (9) Das, N. K.; Ghosh, S.; Priya, A.; Datta, S.; Mukherjee, S. Luminescent Copper Nanoclusters as a Specific Cell-Imaging Probe and a Selective Metal Ion Sensor. *J. Phys. Chem. C* **2015**, *119*, 24657–24664.
- (10) Kuppan, B.; Maitra, U. A p^H-Triggered Synthesis of Blue-Emitting Au Nanoclusters and Their Luminescence Enhancement in a Metallohydrogel: Selective Detection of Pb²⁺ through Luminescence Quenching. *ChemNanoMat* **2018**, *4*, 846–852.
- (11) Jia, X.; Yang, X.; Li, J.; Li, D.; Wang, E. Stable Cu Nanoclusters: From an Aggregation-Induced Emission Mechanism to Biosensing and Catalytic Applications. *Chem. Commun.* **2014**, *50*, 237–239.
- (12) Mondal, B.; Basu, K.; Jana, R.; Mondal, P.; Hansda, B.; Datta, A.; Banerjee, A. Copper Nanoclusters for Catalytic Carbon–Carbon and Carbon–Nitrogen Bond Formations. *ACS Appl. Nano Mater.* **2022**, *5*, 7932–7943.
- (13) Basu, K.; Paul, S.; Jana, R.; Datta, A.; Banerjee, A. Red-Emitting Copper Nanoclusters: From Bulk-Scale Synthesis to Catalytic Reduction. *ACS Sustain. Chem. Eng.* **2019**, *7*, 1998–2007.
- (14) Hirano, K.; Takano, S.; Tsukuda, T. Asymmetric Aerobic Oxidation of Secondary Alcohols Catalyzed by Poly(: N-Vinyl-2-Pyrrolidone)-Stabilized Gold Clusters Modified with Cyclodextrin Derivatives. *Chem. Commun.* **2019**, *55*, 15033–15036.
- (15) Sugiuchi, M.; Zhang, M.; Hakoishi, Y.; Shichibu, Y.; Horimoto, N. N.; Yamauchi, Y.; Ishida, Y.; Konishi, K. Aggregation-Mode-Dependent Optical Properties of Cationic Gold Clusters: Formation of Ordered Assemblies in Solution and Unique Optical Responses. *J. Phys. Chem. C* **2020**, *124*, 16209–16215.

- (16) Baral, A.; Basu, K.; Ghosh, S.; Bhattacharyya, K.; Roy, S.; Datta, A.; Banerjee, A. Size Specific Emission in Peptide Capped Gold Quantum Clusters with Tunable Photoswitching Behavior. *Nanoscale* **2017**, *9*, 4419–4429.
- (17) Chen, T.; Lin, H.; Cao, Y.; Yao, Q.; Xie, J. Interactions of Metal Nanoclusters with Light: Fundamentals and Applications. *Adv. Mater.* **2022**, *34*, 1–15.
- (18) Ghosh, R.; Goswami, U.; Ghosh, S. S.; Paul, A.; Chattopadhyay, A. Synergistic Anticancer Activity of Fluorescent Copper Nanoclusters and Cisplatin Delivered through a Hydrogel Nanocarrier. *ACS Appl. Mater. Interfaces* **2015**, *7*, 209–222.
- (19) Richards, C. I.; Choi, S.; Hsiang, J. C.; Antoku, Y.; Vosch, T.; Bongiorno, A.; Tzeng, Y. L.; Dickson, R. M. Oligonucleotide-Stabilized Ag Nanocluster Fluorophores. *J. Am. Chem. Soc.* **2008**, *130*, 5038–5039.
- (20) Chen, Y. C.; Dickson, R. M. Improved Fluorescent Protein Contrast and Discrimination by Optically Controlling Dark State Lifetimes. *J. Phys. Chem. Lett.* **2017**, *8*, 733–736.
- (21) Roy, S.; Baral, A.; Banerjee, A. Tuning of Silver Cluster Emission from Blue to Red Using a Bio-Active Peptide in Water. *ACS Appl. Mater. Interfaces* **2014**, *6*, 4050–4056.
- (22) Lin, Y.-J.; Chen, P.-C.; Yuan, Z.; Ma, J.-Y.; Chang, H.-T. The Isomeric Effect of Mercaptobenzoic Acids on the Preparation and Fluorescence Properties of Copper Nanoclusters. *Chem. Commun.* **2015**, *51*, 11983–11986.
- (23) Sheehan, F.; Sementa, D.; Jain, A.; Kumar, M.; Tayarani-Najjaran, M.; Kroiss, D.; Ulijn, R. V. Peptide-Based Supramolecular Systems Chemistry. *Chem. Rev.* **2021**, *121*, 13869–13914.
- (24) Kubota, R.; Nagao, K.; Tanaka, W.; Matsumura, R.; Aoyama, T.; Urayama, K.; Hamachi, I. Control of Seed Formation Allows Two Distinct Self-Sorting Patterns of Supramolecular Nanofibers. *Nat. Commun.* **2020**, *11*, 4100.
- (25) Okesola, B. O.; Smith, D. K. Applying Low-Molecular Weight Supramolecular Gelators in an Environmental Setting – Self-Assembled Gels as Smart Materials for Pollutant Removal. *Chem. Soc. Rev.* **2016**, *45*, 4226–4251.
- (26) Hirst, A. R.; Escuder, B.; Miravet, J. F.; Smith, D. K. High-Tech Applications of Self-Assembling Supramolecular Nanostructured Gel-Phase Materials: From Regenerative Medicine to Electronic Devices. *Angew. Chemie Int. Ed.* **2008**, *47*, 8002–8018.

- (27) Singh, N.; Kumar, M.; Miravet, J. F.; Ulijn, R. V.; Escuder, B. Peptide-Based Molecular Hydrogels as Supramolecular Protein Mimics. *Chem. - A Eur. J.* **2017**, *23*, 981–993.
- (28) Qin, L.; Duan, P.; Xie, F.; Zhang, L.; Liu, M. A Metal Ion Triggered Shrinkable Supramolecular Hydrogel and Controlled Release by an Amphiphilic Peptide Dendron. *Chem. Commun.* **2013**, *49*, 10823.
- (29) Dehsorkhi, A.; Castelletto, V.; Hamley, I. W. Self-assembling Amphiphilic Peptides. *J. Pept. Sci.* **2014**, *20*, 453–467.
- (30) Baral, A.; Roy, S.; Ghosh, S.; Hermida-Merino, D.; Hamley, I. W.; Banerjee, A. A Peptide-Based Mechano-Sensitive, Proteolytically Stable Hydrogel with Remarkable Antibacterial Properties. *Langmuir* **2016**, *32*, 1836–1845.
- (31) Nandi, N.; Gayen, K.; Ghosh, S.; Bhunia, D.; Kirkham, S.; Sen, S. K.; Ghosh, S.; Hamley, I. W.; Banerjee, A. Amphiphilic Peptide-Based Supramolecular, Noncytotoxic, Stimuli-Responsive Hydrogels with Antibacterial Activity. *Biomacromolecules* **2017**, *18*, 3621–3629.
- (32) Gayen, K.; Basu, K.; Bairagi, D.; Castelletto, V.; Hamley, I. W.; Banerjee, A. Amino-Acid-Based Metallo-Hydrogel That Acts Like an Esterase. *ACS Appl. Bio Mater.* **2018**, *1*, 1717–1724.
- (33) Basu, K.; Nandi, N.; Mondal, B.; Dehsorkhi, A.; Hamley, I. W.; Banerjee, A. Peptide-Based Ambidextrous Bifunctional Gelator: Applications in Oil Spill Recovery and Removal of Toxic Organic Dyes for Waste Water Management. *Interface Focus* **2017**, *7*, 20160128.
- (34) Mondal, B.; Bairagi, D.; Nandi, N.; Hansda, B.; Das, K. S.; Edwards-Gayle, C. J. C.; Castelletto, V.; Hamley, I. W.; Banerjee, A. Peptide-Based Gel in Environmental Remediation: Removal of Toxic Organic Dyes and Hazardous Pb²⁺ and Cd²⁺ Ions from Wastewater and Oil Spill Recovery. *Langmuir* **2020**, *36*, 12942–12953.
- (35) Ligorio, C.; Vijayaraghavan, A.; Hoyland, J. A.; Saiani, A. Acidic and Basic Self-Assembling Peptide and Peptide-Graphene Oxide Hydrogels: Characterisation and Effect on Encapsulated Nucleus Pulposus Cells. *Acta Biomater.* **2022**, *143*, 145–158.
- (36) Basu, K.; Baral, A.; Basak, S.; Dehsorkhi, A.; Nanda, J.; Bhunia, D.; Ghosh, S.; Castelletto, V.; Hamley, I. W.; Banerjee, A. Peptide Based Hydrogels for Cancer Drug Release: Modulation of Stiffness, Drug Release and Proteolytic

- Stability of Hydrogels by Incorporating D-Amino Acid Residue(s). *Chem. Commun.* **2016**, 52, 5045–5048.
- (37) Cross, E. R.; Coulter, S. M.; Fuentes-Caparrós, A. M.; McAulay, K.; Schweins, R.; Lavery, G.; Adams, D. J. Tuning the Antimicrobial Activity of Low Molecular Weight Hydrogels Using Dopamine Autoxidation. *Chem. Commun.* **2020**, 56, 8135–8138.
- (38) Salomé Veiga, A.; Schneider, J. P. Antimicrobial Hydrogels for the Treatment of Infection. *Biopolymers* **2013**, 100, 637–644.
- (39) Pazos, E.; Sleep, E.; Rubert Pérez, C. M.; Lee, S. S.; Tantakitti, F.; Stupp, S. I. Nucleation and Growth of Ordered Arrays of Silver Nanoparticles on Peptide Nanofibers: Hybrid Nanostructures with Antimicrobial Properties. *J. Am. Chem. Soc.* **2016**, 138, 5507–5510.
- (40) Elsayy, M. A.; Wychowaniec, J. K.; Castillo Díaz, L. A.; Smith, A. M.; Miller, A. F.; Saiani, A. Controlling Doxorubicin Release from a Peptide Hydrogel through Fine-Tuning of Drug–Peptide Fiber Interactions. *Biomacromolecules* **2022**, 23, 2624–2634.
- (41) Tan, W.; Zhang, Q.; Quiñones-Frías, M. C.; Hsu, A. Y.; Zhang, Y.; Rodal, A.; Hong, P.; Luo, H. R.; Xu, B. Enzyme-Responsive Peptide Thioesters for Targeting Golgi Apparatus. *J. Am. Chem. Soc.* **2022**, 144, 6709–6713.
- (42) Mukherjee, N.; Adak, A.; Ghosh, S. Recent Trends in the Development of Peptide and Protein-Based Hydrogel Therapeutics for the Healing of CNS Injury. *Soft Matter* **2020**, 16, 10046–10064.
- (43) Roy, S.; Banerjee, A. Amino Acid Based Smart Hydrogel: Formation, Characterization and Fluorescence Properties of Silver Nanoclusters within the Hydrogel Matrix. *Soft Matter* **2011**, 7, 5300.
- (44) Adhikari, B.; Banerjee, A. Short-Peptide-Based Hydrogel: A Template for the In Situ Synthesis of Fluorescent Silver Nanoclusters by Using Sunlight. *Chem. - A Eur. J.* **2010**, 16, 13698–13705.
- (45) Ray, S.; Das, A. K.; Banerjee, A. Smart Oligopeptide Gels: In Situ Formation and Stabilization of Gold and Silver Nanoparticles within Supramolecular Organogel Networks. *Chem. Commun.* **2006**, 26, 2816.
- (46) Kim, S.; Lee, E. S.; Cha, B. S.; Park, K. S. High Fructose Concentration Increases the Fluorescence Stability of DNA-Templated Copper Nanoclusters by Several Thousand Times. *Nano Lett.* **2022**, 22, 6121–6127.

- (47) Paul, S.; Gayen, K.; Nandi, N.; Banerjee, A. Carbon Nanodot-Induced Gelation of a Histidine-Based Amphiphile: Application as a Fluorescent Ink, and Modulation of Gel Stiffness. *Chem. Commun.* **2018**, 54, 4341–4344.
- (48) Li, G.; Liu, C.; Lei, Y.; Jin, R. Au₂₅ Nanocluster-Catalyzed Ullmann-Type Homocoupling Reaction of Aryl Iodides. *Chem. Commun.* **2012**, 48, 12005–12007.
- (49) Ramasamy, P.; Guha, S.; Shibu, E. S.; Sreeprasad, T. S.; Bag, S.; Banerjee, A.; Pradeep, T. Size Tuning of Au Nanoparticles Formed by Electron Beam Irradiation of Au₂₅ Quantum Clusters Anchored within and Outside of Dipeptide Nanotubes. *J. Mater. Chem.* **2009**, 19, 8456–8462.

List of Publications

1. **Amino Acid Containing Amphiphilic Hydrogelators with Antibacterial and Antiparasitic Activities.** Biplab Mondal, Vivek Kumar Gupta, Biswanath Hansda, Arpita Bhounmik, Tanushree Mondal, Hemanta K. Majumder, Charlotte J. C. Edwards-Gayle, Ian W. Hamley, Parasuraman Jaisankar and Arindam Banerjee, *Soft Matter*, 2022, **18**, 7201–7216.
2. **Copper Nanoclusters for Catalytic Carbon–Carbon and Carbon–Nitrogen Bond Formations.** Biplab Mondal, Kingshuk Basu, Rajkumar Jana, Partha Mondal, Biswanath Hansda, Ayan Datta, and Arindam Banerjee, *ACS Appl. Nano Mater.*, 2022, **5**, 7932–7943.
3. **Peptide-Based Gel in Environmental Remediation: Removal of Toxic Organic Dyes and Hazardous Pb²⁺ and Cd²⁺ Ions from Wastewater and Oil Spill Recovery.** Biplab Mondal, Dipayan Bairagi, Nibedita Nandi, Biswanath Hansda, Krishna Sundar Das, Charlotte J. C. Edwards-Gayle, Valeria Castelletto, Ian W. Hamley and Arindam Banerjee, *Langmuir*, 2020, **36**, 12942–12953.
4. **Modulation of Semiconducting Behavior and a Change in Morphology upon Gelation of a Peptide Appended Naphthalenediimide.** Kingshuk Basu, Biplab Mondal, Ayon Das Mahapatra, Nibedita Nandi, Durga Basak, and Arindam Banerjee, *J. Phys. Chem. C*, 2019, **123**, 20558–20566.
5. **Peptide-Based Ambidextrous Bifunctional Gelator: Applications in Oil Spill Recovery and Removal of Toxic Organic Dyes for Waste Water Management.** Kingshuk Basu, Nibedita Nandi, Biplab Mondal, Ashkan Dehsorkhi, Ian W. Hamley and Arindam Banerjee, *Interface Focus*, 2017, **7**: 20160128.

